

Deciphering the complexities in oncogenesis: An integrative approach to understand its adaptive phenotypes

by

Rupa Bhowmick
10BB17J26062

A thesis submitted to the
Academy of Scientific & Innovative Research
for the award of the degree of
DOCTOR OF PHILOSOPHY
in
SCIENCE

Under the supervision of
Dr. Ram Rup Sarkar



CSIR- National Chemical Laboratory, Pune



Academy of Scientific and Innovative Research
AcSIR Headquarters, CSIR-HRDC campus
Sector 19, Kamla Nehru Nagar,
Ghaziabad, U.P. – 201 002, India

July, 2021

Certificate

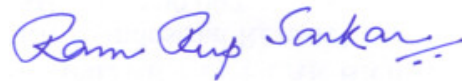
This is to certify that the work incorporated in this Ph.D. thesis entitled, “Deciphering the complexities in oncogenesis: An integrative approach to understand its adaptive phenotypes”, submitted by Ms. Rupa Bhowmick to the Academy of Scientific and Innovative Research (AcSIR) in fulfillment of the requirements for the award of the Degree of Doctor of Philosophy in Science, embodies original research work carried-out by the student. We, further certify that this work has not been submitted to any other University or Institution in part or full for the award of any degree or diploma. Research material(s) obtained from other source(s) and used in this research work has/have been duly acknowledged in the thesis. Image(s), illustration(s), figure(s), table(s) etc., used in the thesis from other source(s), have also been duly cited and acknowledged.



Rupa Bhowmick

(Student)

12th July, 2021



Dr. Ram Rup Sarkar

(Supervisor)

12th July, 2021

STATEMENTS OF ACADEMIC INTEGRITY

I, Ms. Rupa Bhowmick, a Ph.D. student of the Academy of Scientific and Innovative Research (AcSIR) with Registration No. 10BB17J26062 hereby undertake that, the thesis entitled “Deciphering the complexities in oncogenesis: An integrative approach to understand its adaptive phenotypes” has been prepared by me and that the document reports original work carried out by me and is free of any plagiarism in compliance with the UGC Regulations on “*Promotion of Academic Integrity and Prevention of Plagiarism in Higher Educational Institutions (2018)*” and the CSIR Guidelines for “*Ethics in Research and in Governance (2020)*”.



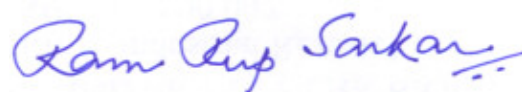
Signature of the Student

Name : Rupa Bhowmick

Date : 12th July, 2021

Place : Pune

It is hereby certified that the work done by the student, under my/our supervision, is plagiarism-free in accordance with the UGC Regulations on “*Promotion of Academic Integrity and Prevention of Plagiarism in Higher Educational Institutions (2018)*” and the CSIR Guidelines for “*Ethics in Research and in Governance (2020)*”.



Signature of the Supervisor

Name : Dr. Ram Rup Sarkar

Date : 12th July, 2021

Place : Pune

Dedicated to my Parents and Brother

Acknowledgement

I am fortunate enough to have come across some very special people, who have been inspirational and extremely supportive through my journey to Ph.D. I wish to express my sincere and heartfelt gratitude and acknowledgement to all of them who believed in me and encouraged to bring the best out of me throughout the different phases of this journey.

First and foremost, I express my sincere gratitude to my supervisor, Dr. Ram Rup Sarkar, who has not only been a mentor, but also a guardian, with his endless support and encouragement that helped me endure all the difficulties that I came across during my Ph.D. journey. His potential to guide through and visualize the brighter side of every problem has inspired me both academically and personally. I am obliged to him for his immense patience with me through my learning process, and putting his trust in me even in the most difficult of times. His quality as a teacher to explain even the most challenging topic in the most lucid way is both admirable and inspirational. My transition from a zoologist to a theoretical and computational biologist would not have been possible without his guidance. Over the years, he has instilled in me, the qualities of critical thinking, being more organized, and to seek perfection in work. I feel honoured to have had the chance to work under his guidance and learn from him.

I am grateful to my Doctoral Advisory Committee members Dr. Dhanasekaran Shanmugam, Dr. Durba Sengupta and Dr. Kiran Kulkarni for continuously evaluating my research work and offering insightful suggestions that helped me improvise my research work. Their continuous assessment and recommendations encouraged me to explore the greater details of my research topic with an interdisciplinary perspective. I offer my sincere gratitude to Prof. Sudip Kundu, Dr. Chetan Gadgil, Dr. Subhasis Mukhopadhyay, Dr. Sarmistha Raychaudhuri and Dr. Manika Pal Bhadra who have been inspirational and have encouraged me to continue my path as a researcher. I am also thankful to my other professors from University of Calcutta for their support, encouragement and guidance to shape my interest in research during my Masters.

I acknowledge the former Directors of NCL, Dr. Saurav Pal and Dr. Ashwini Kumar Nangia, the present Director, Dr. Ashish Lele, and the HOD of the CEPD Division, Dr. Sunil Joshi for providing the infrastructure to carry out my research at CSIR-National Chemical Laboratory and for being prompt and responsive to students' requirements. I sincerely

thank Mr. Hasso Raheja, who has been pro-actively helping us resolve and process our official works. I would like to thank Mr. P.K. Purushothaman, Ms. Komal, Mrs. Shubhangi and other members of the Student Academic Office and Administrative Section of CSIR-NCL who have patiently entertained and guided us through all our queries regarding AcSIR protocols, and fellowship and contingency disbursal. I am thankful to CSIR-HRDG for providing me the SRF fellowship to continue my research and AcSIR for providing me the platform to pursue the degree.

I am fortunate enough to have found a wonderful collegemate, roommate and lab mate, Ms. Piyali Ganguli who by now has become a part of my family. She has been there through all the ups and downs of my Ph.D. journey like a sister who has the most practical solution to any problem. I am also obliged to Dr. Saikat Chowdhury who has been a wonderful senior, lab mate and mentor and has always been there for me whenever I needed any help. I cannot thank them both enough for tolerating all my tantrums and still be there for me in a blink of an eye. They have adorned my Ph.D. journey with some priceless and beautiful memories.

I express my heartfelt love and gratitude towards my husband Dr. Samik Bose and my friend Ms. Sunanda Mandal for their everlasting encouragement, optimism and belief in me. Samik is a friend in a husband who constantly stands by my side boosting my morale to proceed with a positive outlook. His compassion, unbiased rationale of judgement, and immense patience with which he responds to my apprehensions have helped me calm down when I lost my composure. Sunanda's unconditional love and support has been the source of encouragement for me to keep proceeding with enthusiasm.

I am obliged to have the opportunity to work with some soulful and brilliant lab mates Dr. Noopur Sinha, Dr. Abhishek Subramanian, Mr. Sutanu Nandi and Dr. Swarnendu Banerjee who have enlightened me with their scientific merits and helped to overcome the obstacles I faced in both research and personal life. It was for them that I found a home in a place far away from my actual home. I would also like to thank the new members of our lab Mr. Anirudh Murali, Ms. Gauri Panditrao, Ms. Priyanka Gaware, Mr. Kshitij Patil, Dr. Chandrakala Meena and Ms. Bhagyashree Likhitkar for being such wonderful and joyous lab mates. I also had the opportunity to work with some brilliant and exceptional Project Assistants and Summer Interns that includes Nabiha, Shaswat, Mudita, Sandhya, Shomeek, Ritutama, Arpit, Rituparna, Varsha, Niviya, Souradeep, Apoorv, Swarnabha, Yogeshwari and many more. It was an absolute pleasure to work with them.

I express my deepest appreciation for some very caring and warm-hearted seniors and fellow mates that include Dr. Chayanika Das, Dr. Manoj Kumar Nandi, Dr. Monalisa Gangopadhyay, Dr. Atreyee Banerjee, Mr. Tushar Dubey, Mr. Ujjwal Kumar Nandi, Dr. Bipul Biswas, Ms. Vaishnavi Salunke, members of Dr. Kiran Kulkarni's lab, Dr. Anand Sukeerthi, Ms. Sneha Singh and Ms. Debopriya Roy and my Summer Internship mentors at IICT, Hyderabad, Dr. Dhananjaya Pal and Dr. Debasmita Mukherjee. In the last seven years, I have had the opportunity to nurture my cultural skills along with my academic career through the constant encouragement and support of my guide and his companion Mrs. Mousumi Sarkar, and a group of extremely talented people of the NCL Bangiya Samiti. I am thankful to all of them.

My acknowledgment would be incomplete without the mention of my teachers Mr. Shailesh Kumar Singh, Mr. Nisai Bangyang and Mr. Robin Kumar Dutta who believed in me from the very beginning of my academic journey and encouraged me to grow beyond the expected. Their faith has been the motivation that has driven me this far. I will remain forever indebted to them. I express thankfulness to my close friends Ms. Stuti Rai, Ms. Drishti, Mr. Rishov Goswami, Mrs. Rima Dutta, Mrs. Swati Mithia Haldar, Ms. Sanchari Debnath, Ms. Shraboni Dutta, Ms. Arpita Mishra, Dr. Deblina Basu, Mr. Ritaban Basu and Mr. Ameet Thakur for being there for me with their unconditional love and support.

Above all I am and will always remain indebted to my parents, Mr. Rajendra Nath Bhowmick and Mrs. Sudeshna Bhowmick, and my brother Mr. Subham Bhowmick for everything that I am and ever will be in my life. This thesis is the outcome of relentless struggles and innumerable sacrifices of my parents and my brother who stood like pillars to support me throughout the journey. I am fortunate enough to have them as a family that has always been liberal and extremely supportive of my choices knowing not where it will take me, and yet believing in me, guiding me through the pros and cons of my decisions that has helped me grow as a person. Words cannot express my gratitude towards my parents who have endured the toughest of situations with unabated tenacity and perseverance to provide me the opportunity to explore new heights in life. They have instilled in me the faith that hard-work and dedication can achieve success over the toughest of situations, and that, efforts can never be denied.

I express my sincere gratitude towards my grandparents, Mr. Mahadev Bhowmick and Mrs. Bhanumati Bhowmick, who have always encouraged me to pursue my dreams with their

ahead of time thinking and motivation. I am immensely grateful my Kaka Mr. Umesh Chandra Bhowmick and Mr. Ramesh Chandra Bhowmick, my Kaki Mrs. Anjana Bhowmick and Mrs. Sulekha Bhowmick, my Pisi Chayna Chaulia Bhowmick, my Pisemosai Mr. Amalendu Chaulia, and my cousins for persuading me to keep going. I am lucky to have found another equally supportive family as my in-laws. My father-in-law, Mr. Mihir Bose, mother-in-law, Mrs. Keka Bose, sister-in-law, Puja Bose and Dida, Mrs. Ashima Bose encourage me with their sense of pride in having me as their daughter-in-law and have always supported me in every possible way to ensure that I can pursue my career smoothly. Finally, I offer my sincere gratitude and reverence to the brilliant minds of the scientific community who understand no disparity between caste, creed, race or gender, working for Science, and the Almighty, both serving the same cause to bring the best for humanity. I believe Science and Faith, together, can do miracles.

-Rupa Bhowmick

Contents

CHAPTER 1 Introduction.....	1
1.1. Background	1
1.2. Cancer and its adaptive phenotypes	3
1.3. Metabolism as an enabling factor of phenotype switching	3
1.4. The origin of glioblastoma	6
1.4.1. Metabolic properties of astrocytes	7
1.4.2. Reprogrammed metabolism in glioblastoma.....	8
1.5. Regulation of metabolic reprogramming and its role in the development of oncogenic phenotypes in glioblastoma	10
1.5.1. Regulations imposed by upstream regulatory networks.....	10
1.5.2. Effect of microenvironmental stress.....	12
1.5.3. Signature metabolic regulations and their effect on glioblastoma	14
1.6. Computational strategies to address complexities of metabolic rewiring	18
1.7. Challenges created by metabolic reprogramming in glioblastoma	24
1.8. Scope and Specific Objectives of the Thesis.....	27
1.9. Organization and overview of the Thesis	29
CHAPTER 2 Methodologies	31
2.1. Systems-Level Analysis of deregulated metabolic pathways in Glioblastoma.....	31
2.1.1. Constraint-based model reconstruction	31
2.1.2. Flux Balance Analysis (FBA).....	34
2.1.3. The objective functions: defining objectives for energy and growth requirement.....	35
2.1.4. Creation of scenario-specific metabolic flux models.....	36
2.1.5. Validation of Constraint-based models	37
2.1.6. <i>In-silico</i> prediction of minimal essential metabolite for glioblastoma growth	38
2.1.7. Single and double reaction knockouts in glioblastoma	39
2.1.8. Identification of metabolic targets for therapeutic intervention.....	39
2.2. Dynamic analysis of important regulators of ROS generation and antioxidant machinery	40
2.2.1. Definition of model system.....	41
2.2.2. Model formulation.....	43
2.2.3. Model equations.....	44
2.2.4. Positivity and Boundedness	50
2.2.5. Numerical simulation and model calibration.....	53
2.2.6. Parameter estimation	53
2.2.7. Sensitivity analysis.....	55

2.2.8.	Parameter variation analysis	56
2.2.9.	Changing oxygen demand: creation of hypoxia scenario.....	56
2.2.10.	Creation of glioma scenario	56
2.2.11.	Identification of combination targets for ROS manipulation.....	57
2.3.	Network analysis of microRNA regulated metabolic genes, pathway and cellular phenotypes	57
2.3.1.	MicroRNA expression dataset	58
2.3.2.	Differential expression of miRNA	59
2.3.3.	Identification of predicted target genes	60
2.3.4.	Validation of differentially expressed miRNAs and predicted targets	60
2.3.5.	Differential expression analysis of gene expression data	60
2.3.6.	Integration of additional gene interactions in miRNA-target metabolic gene network	61
2.3.7.	Pathway enrichment analysis.....	61
2.3.8.	Network propagation using Diffusion algorithm	62
2.3.9.	Identification of miRNA regulated metabolic pathway.....	62
2.3.10.	Bipartite projection and backbone extraction of important miRNAs regulating metabolism.....	63
2.3.11.	Identification of miRNA-gene subnetwork for glioblastoma specific cellular phenotype	64
2.3.12.	Knockout analysis for identification of targetable miRNAs	65
CHAPTER 3 Anomalous behavior of metabolic pathways in glioblastoma and their effect on internal cellular mechanisms.....		67
3.1.	Rationale of the study	67
3.2.	Results	69
3.2.1.	Properties of the reconstructed metabolic network.....	69
3.2.2.	Validation of objective function for growth demand	71
3.2.3.	Analysis and validation of model properties for astrocyte and glioblastoma model.....	72
3.2.4.	Comparison with experimental data	75
3.2.5.	Opposing roles of glycine and glutamate uptake in astrocytes	76
3.2.6.	Difference of pathway responses in astrocyte and glioblastoma	78
3.2.7.	Essential uptake metabolites for glioblastoma growth	84
3.2.8.	Metabolic reactions crucial for maintaining glioblastoma growth	85
3.2.9.	Identification of reaction targets for therapeutic intervention	88
3.3.	Discussion	91
CHAPTER 4 Dynamics of anti-oxidant machinery and regulation of oxidants in gliomas.....		94
4.1.	Rationale of the study	94
4.2.	Results	97
4.2.1.	Dynamics of cells under normoxic conditions.....	97

4.2.2. Analyses of sensitive parameters.....	99
4.2.3. Dynamics of cells under high oxygen demand: induction of hypoxia.....	103
4.2.4. Redox and thiol status of the cell under glioma scenario.....	106
4.2.5. Identification of combinatory targets for pro and anti-oxidant therapy.....	110
4.3. Discussion.....	112
CHAPTER 5 Post-transcriptional regulation by micrnas on metabolism and cellular phenotypes in glioblastoma	117
5.1. Rationale of the study.....	117
5.2. Results	119
5.2.1. Differentially expressed miRNAs and target metabolic genes.....	119
5.2.2. Identification and analysis of hub miRNAs and metabolic genes.....	121
5.2.3. Metabolic pathway regulation by differentially expressed miRNA.....	125
5.2.4. Identification of miRNA regulated metabolic gene sub-network of cellular phenotypes	131
5.2.5. Prediction of miRNA targets for miRNA-based therapeutic approaches.....	134
5.2.6. Verification of miRNA targets using prior literature and experimental evidence.....	136
5.3. Discussion.....	137
CHAPTER 6 Conclusion and Future perspectives	140
6.1. Conclusion.....	140
6.2. Future perspectives	144
APPENDIX A.....	148
APPENDIX B.....	171
APPENDIX C.....	184
BIBLIOGRAPGHY	206
ABSTRACT	235
LIST OF PUBLICATIONS.....	236
THESIS RELATED PUBLICATIONS	238

List of Figures

Figure 1.1: Demonstration of frequently observed metabolic phenomena in cancer.	5
Figure 1.2: Difference in the role of astrocyte and glioblastoma towards maintaining neuronal function	6
Figure 1.3: Frequently reprogrammed metabolic pathways in glioblastoma.....	9
Figure 1.4: Communication between the cancer cells and the microenvironment	13
Figure 2.1: Schematic workflow of the constraint-based metabolic model using flux balance analysis.....	33
Figure 2.2: Diagrammatic representation of the metabolites belonging to different pathways directed towards the production of the glutathione along with the ROS generation machinery.	42
Figure 2.3: Predictive plot demonstration of model fitting with experimental data.	54
Figure 2.4: Parameter distribution and trace plot of estimated parameters.	54
Figure 2.5: Plots of sensitive parameters for different variables obtained for the three scenarios-normal, hypoxia, and glioma respectively.....	55
Figure 2.6: Flow diagram of the protocol followed for screening of potential miRNAs regulating metabolic genes and cellular phenotypes in glioblastoma.....	59
Figure 2.7: Illustration of methods.....	64
Figure 3.1: Classification of the properties of the reconstructed metabolic model.....	71
Figure 3.2: Change in flux through GBM_BM with increasing glucose uptake.....	72
Figure 3.3: Validation of Astrocyte model.....	74
Figure 3.4: Validation of Glioblastoma model.....	75
Figure 3.5: Effect of Glycine uptake on glutamate utilization by astrocyte.....	78
Figure 3.6: Pathway Response with maximization of ATPSyn as the objective function.....	81
Figure 3.7: Pathway Response with maximization of GBM_BM as the objective function.....	83
Figure 3.8: Essential input metabolites determining glioblastoma growth.....	85
Figure 3.9: Single and double reaction knockout classification	88
Figure 3.10: Therapeutic intervention scenarios and effective combination of target reactions.....	90
Figure 4.1: Model properties.	99
Figure 4.2: Parameter variation plot.....	101
Figure 4.3: Surface plots of two-parameter variation for the sensitive parameters on h_2o_2 level, $nadph/nadp^+$ ratio, and $gsh/gssg$ ratio.....	103
Figure 4.4: Temporal area plots of changing $nadph/nadp^+$ and $gsh/gssg$ ratios along with a change in h_2o_2 concentration.	108
Figure 4.5: Comparison of sensitive parameters in Normal, Hypoxia, and Gliomas for the variables gsh , $gssg$, and h_2o_2	109
Figure 5.1: Validation of differentially expressed miRNAs and network visualization.	121

Figure 5.2: Metabolic Pathways regulated by differentially expressed miRNAs	126
Figure 5.3: MicroRNA backbone of metabolic processes.....	130
Figure 5.4: MiRNA-metabolic gene subnetwork of cellular phenotypes in glioblastoma.....	133
Figure 5.5: MiRNAs involved in the regulation of genes associated with cellular phenotypes in glioblastoma.....	134
Figure 5.6: Radar plot representing percentage change in Katz centrality of key regulatory target genes upon miRNA knockout.....	136

List of Figures (Appendices)

Figure A. 1: Pathway Diagram of the reconstructed constraint-based metabolic network for Glioblastoma	166
Figure B. 1: Parameter estimation of glutamate exchange reaction.....	180
Figure B. 2: Change in external oxygen concentration with respect to changing $k_m^{O_2}$	181
Figure B. 3: Temporal plot of changes in nadph/nadp+ ratio with varying V_m^{GTHO} at $k_m^{O_2} = 1mM$	181
Figure B. 4: Temporal area plots of changing $nadph/nadp^+$ and $gsh/gssg$ ratios along with change in h_2o_2 concentration with combinatorial variation of parameters made in glioma scenario.	183
Figure C. 1: Volcano plot of data distribution for differentially expressed miRNA obtained from GEO datasets.....	184
Figure C. 2: Degree distribution in the directed graphs of upregulated and downregulated miRNA- target gene network with power law fit.	185

List of Tables

Table 1.1: Notable regulation of metabolic genes via gene regulatory factors in glioblastoma...	14
Table 1.2: Popular drugs and the resistance induced by metabolism in glioblastoma	17
Table 2.1: List of pathways selected pathway reconstruction of the constraint-based metabolic model for astrocyte and glioblastoma and their references.....	33
Table 3.1: Comparison of model prediction with the data available for enzyme expression in the young patient.....	76
Table 3.2: Total number of single and double lethal reactions obtained from the knockout analysis.....	85
Table 4.1: List of sensitive parameters for <i>gsh</i> , <i>gssg</i> , and h_2o_2 under normal, hypoxic, and glioma scenarios.....	109
Table 4.2: Values of parameters for which pro- and anti-oxidant effects could be induced in the glioma scenario.....	112

List of Tables (Appendices)

Table A. 1: Details of reactions and pathways considered in the constraint-based metabolic model	148
Table A. 2: Lethal Single Knockout Reactions.....	167
Table A. 3: Lethal Non-trivial Double Knockouts Reaction Combinations	167
Table A. 4: Identified combinations of therapeutic targets.....	168
Table A. 5: Percentage reduction of flux through combinatorial reaction targets	169
Table A. 6: List of available inhibitors for the predicted reaction targets.	170
Table B. 1: Parameter values and their units used for the dynamic model simulation and their references	171
Table B. 2: Initial values to all the variables considered in the model and their reported range in the biological systems.....	178
Table B. 3: Combinatorial effect of sensitive parameters on gliomas.....	182
Table C. 1: Upregulated miRNAs with downregulated target metabolic genes and enriched pathways.....	189
Table C. 2: Downregulated miRNAs with upregulated target metabolic genes and enriched pathways	192
Table C. 3: Details and statistics of the backbone analysis.....	197
Table C. 4: Key regulatory metabolic genes selected as seed sequence for network diffusion and identification of cellular phenotype subnetworks.....	199
Table C. 5: List of metabolic genes and miRNAs in the subnetworks of cellular phenotypes	201
Table C. 6: Significantly enriched metabolic pathways for the subnetworks of cellular phenotypes	202

List of Abbreviations

FBA	Flux Balance Analysis
ATPSyn	ATP Synthase
GBM_BM	Objective function for Glioblastoma growth
COBRA Toolbox	Constraint-Based Reconstruction and Analysis Toolbox
S-matrix	Stoichiometric matrix
GSMM	Genome Scale Metabolic Model
PPP	Pentose Phosphate Pathway
IDH	Isocitrate Dehydrogenase
IDO	Indoleamine-2,3-dioxygenase
ROS	Reactive Oxygen Species
GTHP	Glutathione Peroxidase
GTHO	Glutathione Oxidoreductase
NOX	NADPH Oxidase
SOD	Superoxide Dismutase
xCT	Cystine-glutamate antiporter
ODE	Ordinary Differential Equation
MCMC	Markov Chain Monte Carlo algorithm
DRAM	Delayed Rejection Adaptive Metropolis
eFAST	Extended Fourier Amplified Sensitivity Test
FDR	False Discovery Rate
GBM	Glioblastoma
miRNA	MicroRNA
hsa-miR	Human microRNA
LogFC	Log Fold Change
RPKM	Reads Per Kilobase of transcript, per Million mapped reads
PDI	Pairwise Disconnectivity Index
CNS	Central Nervous System
GCL	Glutamyl-Cysteine Ligase
GS	Glutathione Synthase

Summary

Reprogrammed cellular metabolism is a hallmark of cancer. It favours rapid growth, unregulated proliferation, anti-inflammatory responses and confers anti-tumoral immunity to the cancer cells. Glioblastoma are the most aggressive brain tumors that demonstrate complex metabolic rewiring in response to the intracellular and microenvironmental stress. Multiple factors determine the changes in the metabolic profile of these tumors that include the upstream regulation of metabolic genes by mutational, genetic, epigenetic or transcription factors, insults incurred within the mitochondria, or due to the nutritional, cytotoxic or oxidative stress generated in the microenvironment. The adaptability of the cellular metabolism facilitate phenotype switching in these tumors, which is manifested as the ability to switch between different cellular phenotypes as per growth condition. The plasticity of metabolism provides robustness to the cells against both random or deliberate perturbations. Additional challenges emerge over time with the disruption of redox and thiol balance of the tumors and development of complex oncogenic phenotypes that leads to poor prognosis of the glioblastoma. In order to address these challenges, we have considered to study the changes exhibited in the metabolism of glioblastoma at multiple biological scales starting from pathways to genes using computational and mathematical modelling.

In order to gain a holistic perspective of the pathway behavior and condition specific changes in the metabolic network of glioblastoma, we formulated and analyzed a constraint-based metabolic model. Analyses of the changes in the flux profiles of the model under normal and cancerous scenarios showed condition specific dependence of glioblastoma on glutamine and fatty acids as alternate energy sources and a considerable amount of flux re-routing towards glutathione production. By performing a knockout analysis of input metabolites, cystine and glucose were identified as the minimum essential input metabolites that could sustain glioblastoma growth under limited nutrient availability. Combinatorial therapeutic targets were also identified where the importance of enzymes belonging to glycine-serine biosynthesis pathway was highlighted.

To understand the changes in the redox and thiol status of the cells and the changes occurring in the oxidant-antioxidant balance during gliomagenesis, a dynamic ordinary

differential equation model was formulated. Model analyses established that the coordinated functioning of glutathione peroxidase (GTHP), glutathione oxidoreductase (GTHO) and NADPH oxidase (NOX) is crucial in determining cancerous transformation in gliomas. Further, we proposed that the puzzling duality of reactive oxygen species (ROS) in exhibiting varying cellular fates could be determined by considering simultaneous changes in *nadph/nadp⁺* and *gsh/gssg* that occur during the reprogramming of metabolic reactions. The model was further used to propose ROS manipulative strategies for designing effective pro-oxidant and/or antioxidant therapeutic approaches against gliomas.

To understand the genetic regulation of metabolic gene expression, the post-transcriptional regulation imposed by microRNAs on the metabolic genes was studied. We parallelly investigated the microRNA regulation of cellular metabolism and cellular phenotypes in order to identify miRNA targets that can regulate metabolic plasticity aided oncogenic phenotypes via miRNA-based therapeutic strategies. We explored the miRNA regulation of glioblastoma metabolism using graph theoretical approach. Differentially expressed miRNAs and metabolic gene expression data used for the analyses were obtained from glioblastoma patients-derived data. The effect of miRNA regulation on the metabolism associated with oncogenic phenotypes was analyzed to delineate the role of miRNAs in determining metabolic plasticity that aid phenotype switching in glioblastoma. Target miRNA combinations were identified for each phenotype that can be used for miRNA-based therapeutics. The strategies implemented in the study can be used to generate testable hypotheses and design context-specific miRNA-based therapy for individual patient and their usability can be extended to other gene regulatory networks as well.

With rationalized evaluation and computational analyses of the deregulated metabolic network, the present thesis provides explanations to some of the commonly observed but less understood phenomena in glioblastoma and generate testable hypotheses for potential therapeutic targets against the cancer. The outcomes of the thesis provide insightful understanding to both the researchers and the oncologists and find application in designing therapeutic strategy against glioblastoma that will help in better prognosis of the cancer.

CHAPTER 1

INTRODUCTION

1.1. Background

Cancer cells exhibit characteristic phenotypic plasticity that allows cellular reprogramming. Adaptive cellular reprogramming facilitates rapid proliferation, evading immunosurveillance and survival under stress. Reprogrammed cancer metabolism, a hallmark of cancer cells, is one such adaptation that exhibits distinctive phenotypic changes and has been considered as a signature for different cancer cells. In recent years, there has been a surge in research targeted to understand how these metabolic adaptations occur in cancer and how these can be ventured for therapeutic benefits. Many of the oncogenic signalling pathways directly regulate metabolic pathways that support cell growth. Additionally, metabolites are recognized to play important roles in regulating tumorigenesis in feedback and feed-forward manner. Besides providing the “food and fuel” for cell survival and growth, metabolites can influence stress response pathways, chromatin modifications, and gene expression directly or indirectly, which collectively drive tumor development.

Glioblastoma has been a subject of rigorous research in Cancer Biology. Identified as the most common and invasive tumors of the central nervous system, these brain tumors have a very low median survival time for patients suffering advanced malignancies. Tumor-free survival post-treatment is also impugned by their high recurrence rate. The capability of glioblastoma to exhibit surprising heterogeneity in their genotypic and phenotypic features has made them a suitable subject to study and understand cancer phenotypes. Like other cancers, glioblastoma displays metabolic remodelling to support the requirement of the highly proliferating cells. These cells exhibit profound metabolic alterations that allow them to fulfil the metabolic demands associated with rapid proliferation and additional features of malignancy. These metabolic transformations are supported by the gene regulatory events that drive tumorigenesis by activating oncogenes and/or the loss of onco-suppressor genes and further shaped by environmental cues, such as oxygen concentration, nutrient availability, cytotoxic

releases in the tumor microenvironment, etc. Pertaining to this, a mechanistic understanding of metabolic rewiring remains critical to address. Hence, in this thesis, we focus on the detailed study of the metabolic re-routing, quantitative evaluation of the critical mechanistic regulation and controls at the gene level that guides reprogramming in cancer, with particular reference to glioblastoma.

Metabolic phenomena like the Warburg effect and glutaminolysis have been repeatedly evaluated in the cancer cell and have been well established for their role in glioblastoma progression as well (1, 2). Strategies to target these phenomena have been developed and are popularly being used in treatment regimens. However, the high connectivity and robustness of metabolic networks protect the cells against random failure, and hence cells evolve and develop resistance against the therapeutic regimens. Hence, the study of metabolic pathway re-routing in glioblastoma is crucial to understand the alternate routes of therapeutic escape, opportunistic mode of nutrient acquisition, and evolving mechanisms to surpass oxidative stress and immune surveillance. The improper management of the redox balance and increased accumulation of reactive oxygen species (ROS) within the cells during hypoxia aid the development of oncogenic phenotypes. However, studies to delineate the role of ROS in cancer have shown that ROS have a double-edge sword property in regulating the apoptotic fate of cancer cells. This has left oncologists with the question of whether to increase or decrease it for therapeutic gains. A quantitative understanding of the mechanism of ROS management in cancer cells hence remains crucial to be addressed. The regulation of metabolic genes during cancer development is another important aspect of our study. The genetic regulations imposed due to mutation, methylation, and nucleotide polymorphism in glioblastoma have contributed to our understanding of metabolic regulations. Nevertheless, the recent understanding of the role of microRNAs in cancer metabolic regulation has been well appreciated and largely remains unexplored in glioblastoma. Hence, we attempt to delineate the metabolic gene and pathway regulations imposed by differentially expressed miRNAs in glioblastoma, concluding with their potential contribution in determining cellular phenotypes of glioblastoma.

1.2. Cancer and its adaptive phenotypes

One of the most critical phenomena of cancer cells is their ability to undergo phenotype switching. It facilitates adaptation to micro-environmental stress, immunosurveillance mechanisms, and loss of sensitivity to drugs and therapeutic regimens. Phenotype switching permits uncontrolled cell proliferation, cell migration, invasion, and development of stemness in tumor cells affecting the overall survival of the patients and eventually the evolution of resistant cancer cells. However, in doing so, the selfish requirements of the cancer cells are fulfilled at the cost of the cellular needs of normal cells. As a result, stress generated in the tumor micro-environment aggravates over time. Against all odds, the tumor cells sustain themselves by continuously adapting to the changing microenvironment.

In 2011, Hanahan and Weinberg proposed six well-established and two emerging hallmarks of cancer (3). These hallmarks include uncontrolled cell proliferation and growth, activation of invasion and metastasis, induction of angiogenesis in the tumor masses, stemness of tumor cells, and escaping programmed cell death by surpassing apoptotic signals. Capability to undergo spontaneous transitions between these cellular phenotypes help acquire transient resistant phenotype that helps tumor cells to temporarily evade stress responses and eventually attain permanent resistance mechanisms. The enabling characteristics behind these hallmarks are genome instability, mutation, metabolic plasticity, and the tumor-promoting inflammations. Hanahan and Weinberg registered metabolic reprogramming and evasion of immune surveillance as the two emerging hallmarks of cancer. Over the years, metabolic reprogramming has evolved as one of the most important hallmarks enabling phenotype switching in cancer cells. Initiated with the proposition of the Warburg effect, studies conducted to understand the altered metabolism of cancer cells have established their crucial role in meeting the survival and rapid proliferative requirements of these cells.

1.3. Metabolism as an enabling factor of phenotype switching

Emerging evidence indicates that impairment of cell metabolism is one of the most important defining characteristics of cancer cells, irrespective of their cell or tissue of

origin. In fact, this has led a group of the scientific community to believe that cancer is essentially a metabolic disease caused by the impairment of the energy metabolism, primarily due to mitochondrial dysfunction in the cancer cells, named the “*metabolic impairment theory*” (4). The theory is contradicted by “*gene theory*,” which states that mitochondrial dysfunction is a cause rather than an effect of cancer arising due to genetic mutation and chromosomal abnormalities. There is a continuing debate on the origin of cancer that includes a controversy between the gene theory and the metabolic impairment theory as well.

In 1924, Otto Warburg proposed that preference for aerobic glycolysis in cancer cells originates as a consequence of the faulty mitochondrial respiratory system (1). The phenomenon, popularly known as the “*Warburg effect*,” is considered an essential metabolic switch to compensate for the energy requirements of the rapidly proliferating tumor cells. As a result of the mitochondrial dysfunction, the ATP synthesis machinery of the tumor cells is compromised. As such, the cells switch their dependence on the alternate mechanism of ATP production. The glycolytic pathway tends to maximize ATP production by driving its glycolytic flux towards lactate formation. Although the mechanism of conversion of glucose to lactate yields only 4 ATPs per cycle as compared to the oxidative phosphorylation that yields 36 ATPs per cycle, the tumor cells rely on aerobic glycolysis as an alternative to maintain viability (**Figure 1.1A**). Although both aerobic and anaerobic glycolysis has the same end product, i.e., lactate, aerobic glycolysis is considered a signature of cancer cells as it originates due to damaged mitochondrial respiratory mechanism. Anaerobic glycolysis, on the other hand, arises due to the absence of oxygen and can be witnessed in normal cells.

Glutaminolysis is another compensatory mechanism in cancer cells that increases in response to mitochondrial dysfunction. Many cancer cells utilize glutamine as an alternate energy source and an anaplerotic substrate to produce TCA cycle intermediates required for macromolecular biosynthesis. Glutamine can stimulate glycolysis in the cytoplasm as well as induce substrate-level phosphorylation in the TCA cycle, both of which add up to the energy production of cancer cells. The preference of cancer cells to consume glutamine as an alternate energy source results in the switching of metabolic paths. Increased glutaminolysis in glutamine-dependent cancers is associated with an

increase in the activity of the enzymes glutaminase, which catalyzes the conversion of glutamine to glutamate and glutamate dehydrogenase that catalyzes the reversible conversion of α -ketoglutarate to glutamate and vice versa (**Figure 1.1B**). The flow of flux in these cancers is directed from glutamine to α -ketoglutarate to replenish the pool of TCA cycle intermediates and induce substrate-level phosphorylation rather than the usual flow of flux from α -ketoglutarate to glutamate and glutamine.

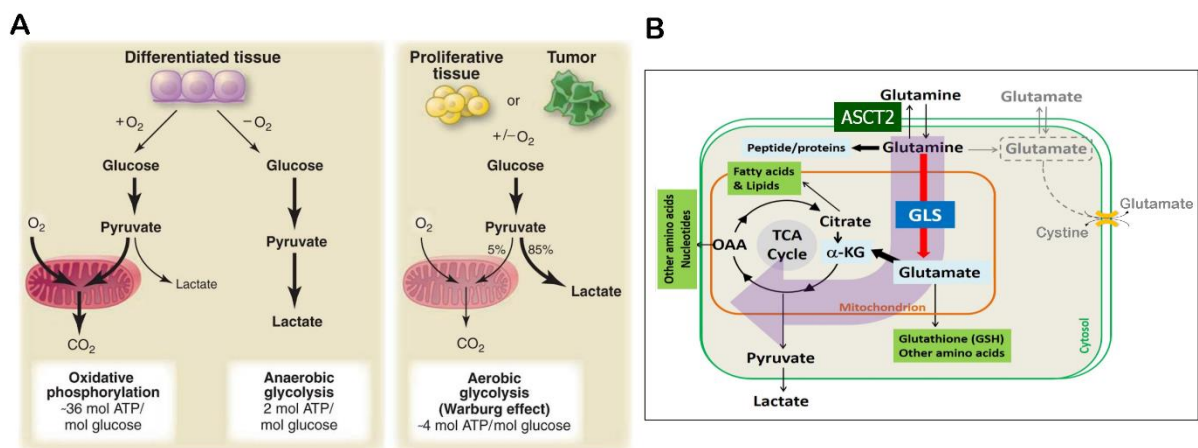


Figure 1.1: Demonstration of frequently observed metabolic phenomena in cancer. (A) The difference in the fate of glucose in normal differentiating tissues and tumor mass. Tumor masses and highly proliferating cells display the Warburg effect (Picture courtesy: Heiden *et al.*, 2009, Science (5)). (B) The fate of glutamine during glutaminolysis. Cells consume excess glutamine to produce glutamate and other cellular biosynthetic products (Adapted from www.pennmedicine.org).

A major difference in the normal and the cancer cell exists in their paths to procure energy substrates. Prolonged dependence on substrate-level phosphorylation for energy, damaged mitochondrial respiration along with a faulty DNA repair mechanism cause cellular malfunction, generation of oxidative stress and cytotoxic releases in the tumor microenvironment, and genomic instability within the cells. These factors contribute to the development of oncogenic phenotypes, and the process continues as a vicious circle, worsening the situation over time and eventually developing into aggressive malignant tumors. Metabolism also confers the ability to the cancer cells to evade immune-surveillance. Thus, to summarize the facts, metabolic reprogramming might be an epiphenomenon of a much more complex problem within the cancer cells, but the prevalence of a prolonged fault in metabolism can eventually promote the development of additional complexities of oncogenesis.

1.4. The origin of glioblastoma

Glioblastoma is a fast-growing aggressive tumor of the central nervous system, with a very low median survival time for patients suffering advanced malignancies. Tumor-free survival post-treatment is challenged by their high recurrence rate. These tumors are of glial origin. Glial cells support neurons by providing energy and nutrients and maintaining the blood-brain barrier. There are different types of glial cells, each with a different function: (i) astrocytes, (ii) oligodendrocytes, (iii) microglia, and (iv) ependymal cells. Astrocytes provide nutrients to the neurons and hold them in place; oligodendrocytes provide insulation; microglia digest the circulating pathogens and dead neurons from the neuronal microenvironment, and; ependymal cells form the epithelial lining of ventricles of the brain and the spinal cord and secrete the cerebrospinal fluid. The cancerous transformation of these glial cells is categorized under the umbrella term gliomas. Gliomas can be categorized into 4 categories based on aggressiveness: (i) Grade I: pilocytic astrocytoma, (ii) Grade II: Low-grade gliomas, (iii) Grade III: Malignant gliomas, and (iv) Grade IV: Glioblastoma. Glioblastoma is primarily an astrocytic tumor (**Figure 1.2**) (6). Owing to the morphology and high aggressiveness, these tumors can infiltrate across the brain as tentacular projections that make their surgical removal difficult (7).

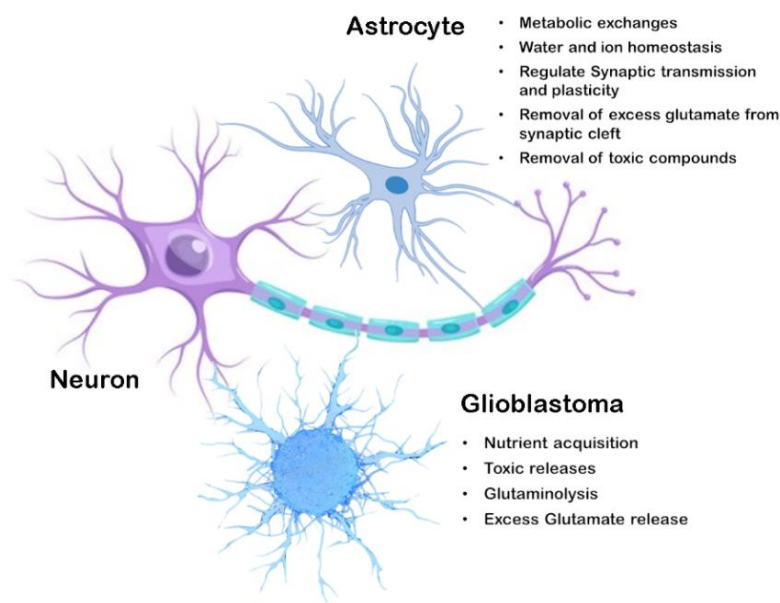


Figure 1.2: Difference in the role of astrocyte and glioblastoma towards maintaining neuronal function

1.4.1. Metabolic properties of astrocytes

Astrocytes are the most abundant glial cells accounting for about 20-40% of the brain cells (8). The origin of the word comes from the Latin words “*astra*” and “*cyte*,” meaning star-shaped cells. At the time of its discovery, it was postulated that there exists a link between the morphology and function of astrocytes, which was soon verified. The astrocytes establish interconnections between the blood vessels and parenchymal cells of the brain, hence responsible for the exchange of metabolites (9). They have additional roles of maintaining water and ion homeostasis and maintaining the blood-brain barrier (10). Astrocytes prefer a glucose-dependent metabolism where glucose is catabolized to pyruvate that enters the TCA cycle leading to ATP synthesis via the mitochondrial electron transport chain and partly to the formation of lactate so as to suffice the neuronal lactate requirement. The activation of neurons upon release of neurotransmitter glutamate stimulates glycolysis in astrocytes that is driven to produce lactate as fuel for the neuronal metabolism (11). The uptake of glucose increases with the rise in glutamate uptake in astrocytes, thus leading to amplified lactate production.

Another important metabolic function of astrocytes is the rapid uptake of glutamate released by neurons for neurotransmission at the junction of the synaptic cleft. This ensures instant termination of neurotransmission and also prevents accumulation of glutamate to excitotoxic levels. The excess glutamate released by the neurons is up-taken by the astrocytes and metabolized to glutamine via the glutamate-glutamine cycle. The cycle involves a series of conversions catalyzed by important enzymes like aspartate aminotransferase, alanine aminotransferase, glutamate decarboxylase, glutamate dehydrogenase, and most importantly, glutamine synthase. The enzyme glutamine synthase is responsible for the conversion of glutamate to glutamine and, as reported, is exclusively expressed in astrocytes. The glutamine thus produced is released for uptake by the glutamatergic neurons (12). In astrocytes, the uptake of glutamate from the synaptic cleft is mediated by the excitatory amino acid transporter (EAAT) 1 and EAAT2. However, in addition to the EAATs, glutamate transport is also maintained by the cystine-glutamate antiporters (xCT) in astrocyte, which releases glutamate out of the cell to antiport cystine. The regulation of xCT expression is thus important in astrocytes as its overexpression will release excess glutamate, causing excitotoxicity (13). The role of

astrocytes comprises of but is not confined to such signature metabolic functions towards maintaining proper neuronal function. However, with the onset of gliomagenesis, these supportive functions suffer detrimental consequences as a result of metabolic reprogramming in the tumor cells. This affects the neuronal function, thereby affecting the overall well-being of the patients. The well-studied changes in the tumor metabolism of glioblastoma have been discussed in the next subsection.

1.4.2. Reprogrammed metabolism in glioblastoma

The metabolic abnormalities incurred within the astrocytes lead to their phenotypic manifestation as glioblastoma (14). The concept of cancer as a metabolic disease can be debated with substantial evidence in the case of glioblastoma. The metabolic plasticity of the tumor cells enables them to thrive even in stressful conditions by switching phenotypes as per requirement. Reprogramming of the metabolic pathways in glioblastoma is exhibited in response to the gene expression regulation and stimulus generated by the microenvironment. Glioblastoma displays the Warburg Effect that enables reprogramming of energy metabolism to suffice their rapacious energy requirements (15). A schematic of frequently altered metabolic pathways in glioblastoma is provided in **Figure 1.3**. Additional discoveries have been made to delineate the phenomenal changes in the properties of glioblastoma as an effect of metabolic alterations in pathways like tryptophan metabolism (16), cysteine metabolism (17), glutamine, and glutamate metabolism (2). Phenomena like higher accumulation of glycine in the glioblastoma cells (18) and the disruption of primary brain tumor growth with the inhibition of cystine (19) have also been observed.

The energy acquisition in glioblastoma differs hugely from the astrocytes to sustain high proliferation and invasive phenotype. The reprogrammed energy metabolism puts neuronal function at stake. While the production of lactate via aerobic glycolysis is a feature of both astrocytes and glioblastoma, the defects in the mitochondrial respiration are the underlying cause that drives aerobic glycolysis in glioblastoma. The ATP synthase activity is severed, and the tumor cells depend heavily on the glycolytic pathway for ATP (15). Glioblastoma also displays glutaminolysis, which is characterized by the uptake and utilization of glutamine from the extracellular matrix, converted to glutamate for use within the tumor cells. Glutamine acts as an alternate energy source that allows

substrate-level phosphorylation in the TCA cycle and also replenishes pools of TCA cycle intermediates via anaplerosis. Overexpression of xCT antiporter in glioblastoma leads to excess release of glutamate in the microenvironment, inducing toxicity (2). Enhanced expression of xCT antiporter results in the excess uptake of cystine in glioblastoma (17). Enhanced β -oxidation of fatty acids is also an observable trait of glioblastoma that is linked with tumorigenesis. β -oxidation of fatty acids generates acetyl-CoA, NADH, and FADH₂ that create the electron gradient for oxidative phosphorylation required to drive ATP synthesis. The acetyl-CoA produced by the oxidation of fatty acids supplement the TCA cycle cataplerosis providing substrates for amino acid and nucleotide synthesis, as well as enhancing the redox potential of the tumor cells (20). Understanding the regulatory mechanisms that guide metabolic reprogramming and the role of these changes in regulating oncogenic phenotypes in glioblastoma will be conducive in the assessment of escape mechanisms and prognostic features of glioblastoma.

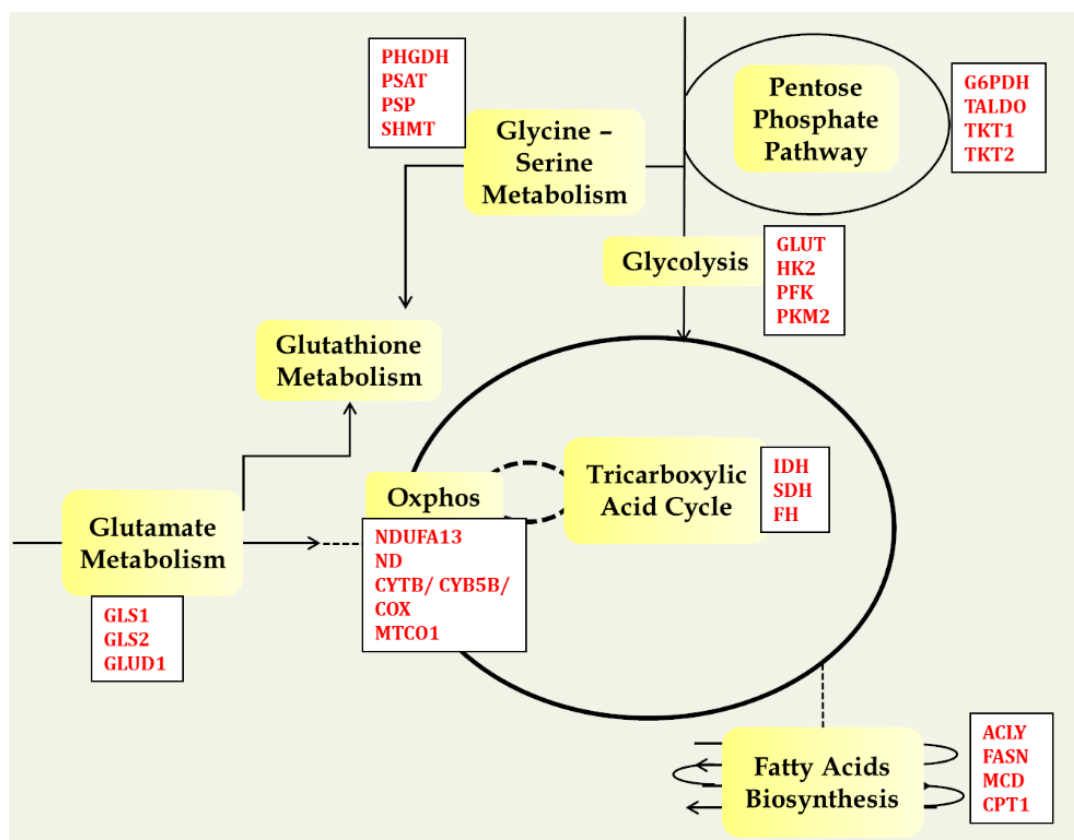


Figure 1.3: Frequently reprogrammed metabolic pathways in glioblastoma

1.5. Regulation of metabolic reprogramming and its role in the development of oncogenic phenotypes in glioblastoma

The gene regulatory networks can have a profound effect on the activity of metabolic pathways via enzyme gene regulation. The mutations, epigenetic modifications, and transcriptional regulations affecting metabolic genes have been explored in detail and contribute much to our understanding of the metabolic alterations in glioblastoma (21-24). In addition, the metabolic routes preferred in the tumors are also determined by the microenvironmental stress and availability of extracellular nutrients. Oxygen deprivation in the microenvironment is a vital stress factor responsible not only for metabolic reprogramming but many other hypoxia-induced oncogenic phenotypes as well. Increased demand for amino acids like cysteine, glutamine, aspartate, glycine, arginine, or methionine determines the metabolic dependency of the tumor cells, and the metabolism is reprogrammed accordingly. The probable factors determining metabolic reprogramming in glioblastoma are discussed in the subsequent subsections.

1.5.1. Regulations imposed by upstream regulatory networks

The increase in omics and high-throughput research has enabled the identification of genetic factors regulating the expression of metabolic genes. The mutational landscape of glioblastoma is very well studied. Somatic mutation of IDH1 and IDH2 is well established in this cancer (**Table 1.1**). The mutation results in the formation of 2-hydroxyglutarate (2-HG), which is a competitive inhibitor of α -ketoglutarate. 2-HG competitively binds and inhibits the α -ketoglutarate metabolizing enzymes resulting in DNA and histone hypermethylation and HIF degradation (25). Somatic mutation in Cytochrome C Oxidase (COX, complex IV), germline mutation in Ubiquinol-Cytochrome c reductase (Complex III), and mutation of ND6 subunit of Complex I are commonly observed mutations that deregulate the function of oxidative phosphorylation in glioblastoma. Genomic amplification of the PHGDH gene of the serine biosynthesis pathway and methylthioadenosine phosphorylase (MTAP) deletion are also characteristics of glioblastoma.

Epigenetic factors like DNA methylation and histone modification regulate the enzyme gene expression. Association of DNA methylation patterns with IDH mutation (26), hypomethylation in the intronic region of HK2 and PKM, and hypermethylation of glycolytic genes ENO1, HK3, GAPDH, and LDHA in IDH mutant glioblastoma are associated with the expression regulation of these genes (21). The methylation status of the MGMT gene has been used to stratify the glioblastoma patients into two categories: those with the methylation of MGMT have a comparatively longer survival period of 21.7 months as compared to those without it (12.7 months) (27). The modulation of HIF-1 α and Akt via histone modification, two key regulators of the genes associated with energy metabolism, have been noteworthy (21). Epigenetic regulation of the two key enzymes of the arginine biosynthetic pathway, ASS1, and ASL, via methylation, is also frequently witnessed in glioblastoma (28). The landscape of nucleotide polymorphism has been explored in-depth and conducive inferences on the regulation of metabolic gene expression by SNPs and CNVs have been captured via genome wide association studies (29, 30). Important findings include the association of copy number gain in EGFR and RNF139 with increased expression of carbonic anhydrase. Copy number gain of RNF19 also positively correlates with LDHA and MCT4 expression (31). Copy number deletion of PTEN and RB1 has been witnessed, the consequence of which is realized in the regulation of signalling and metabolic events (32).

The differential expression of transcription factors is also well studied in glioblastoma. HIF-1 α is a master regulator of the glycolytic genes and is often differentially regulated in glioblastoma. TFAM, p53, TIGAR, c-MYC, and PTEN have been found to be differentially expressed that regulate the expression of a range of genes, including those associated with metabolism (33). Additional regulatory mechanisms on metabolism are currently being explored to gain a better understanding of the metabolic plasticity. The role of microRNA as a regulator of metabolism has been discovered in the last one decade. Since its discovery, growing evidence of the microRNA-dependent regulation of metabolism has initiated research interest to explore their role in cancer metabolism (34). MicroRNAs (miRNAs) are 18-25 nucleotide long small non-coding RNAs produced endogenously within the cell. MiRNAs are post-transcriptional regulators that bind to the 3' UTR of the target genes via base complementarity between the seed sequences of the miRNAs and

the 3' UTR of the gene and regulate gene expression via gene silencing (35). The role of miRNAs is currently being explored for prospects of miRNA-based therapeutics in glioblastoma (36-38). Studying the effect of miRNA regulation on the metabolism associated with the oncogenic phenotypes in glioblastoma will delineate the role of miRNAs in metabolic plasticity that aid phenotype switching and will help identify targets for miRNA-based therapeutics.

1.5.2. Effect of microenvironmental stress

The reciprocal communication between the cancer cells and the microenvironment harbour collusive metabolic management that promote proliferation and metastasis. The tumor microenvironment participates actively in tumorigenesis via direct and indirect regulation of tumor cells. Oxidative and nutritional stress can be considered the secondary forces that drive metabolic rewiring in cancer cells. The oxygen availability in the tumor microenvironment is often depleted in order to meet the increased oxygen consumption of the tumors creating a hypoxic condition. The oxidative stress generated by hypoxia leads to the enhanced production of reactive oxygen species (ROS). Under normal physiology, ROS modulate various signalling and mitochondrial events favourable for normal cellular function. A balance of the ROS is maintained in the cells by the activity of anti-oxidants. However, under oxidative stress, the cells remain under the constant pressure of maintaining the balance between the ROS and anti-oxidants, failing which the cells are fated to generate stress response. The most recognized stress response generated by these cells is the enhanced expression of hypoxia-inducible factor (HIF) and the mitochondrial dysfunction due to disrupted redox balance.

The nutritional stress generated due to the reckless nutrient demands of the tumor cells is another important determinant of metabolic reprogramming. The immediate effect of mitochondrial dysfunction is the dependence of cells on aerobic glycolysis for energy requirements, thereby consuming excess glucose to drive higher flux through the glycolytic pathway. As the tumor cells sequester glucose from the microenvironment, the pool rapidly exhausts, thus creating a dependence on alternate energy sources. The cells seek glutamine and fatty acids as alternate energy sources and modify metabolic paths accordingly to metabolize them (**Figure 1.4**). The glioblastoma cells also show increased

demand for amino acids glycine, arginine, cysteine, and cystine, the disulfide form of cysteine. Cysteine is metabolized in the production of anti-oxidant glutathione, required to scavenge the excess ROS generated.

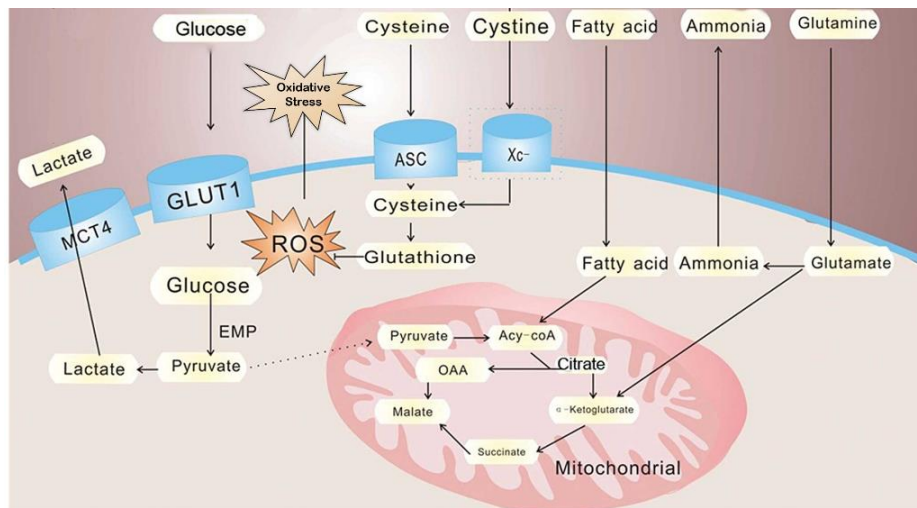


Figure 1.4: Communication between the cancer cells and the microenvironment (Adapted from Yuan *et al.*, 2016. *Oncology Reports* (39))

The lactate produced as a by-product of the enhanced aerobic glycolysis is released out, inducing acidic conditions and ROS generation in the microenvironment. The accumulation of lactate has an inhibitory effect on glycolysis and on tumor proliferation and growth. However, lactate is consumed as an energy substrate by the fibroblasts, epithelial, and other tumor cells in the microenvironment, inducing vascularization, angiogenesis, and rapid tumor growth. Glutamine, metabolized to produce glutamate and α -ketoglutarate in subsequent steps, releases ammonia as a by-product. Ammonia readily diffuses into the microenvironment and is consumed and metabolized by cancer-associated fibroblast (CAF) cells. The cascade of nutrient flow between the tumor cells and CAF cells induces autophagy of CAF cells. The exchange of metabolites between tumor cells and the microenvironment contributes to the proliferation, growth, differentiation, and stem-like properties of tumor cells. Thus, a systematic study of the changes inside and outside the tumor cells is important to understand the metabolic barriers contributing to the complexities in cancer and to identify the crack within the barrier that can be targeted for treatment.

1.5.3. Signature metabolic regulations and their effect on glioblastoma

In light of the advances made in the understanding of cancer metabolism, various signature metabolic changes have been identified in glioblastoma. A list of the important metabolic genes whose expression is altered by regulatory factors or mutations is provided in **Table 1.1**. The identification of these signatures in glioblastoma has helped classify the heterogeneity in the tumor population of glioblastoma, thereby assisting the development of tumor-specific treatment strategies. However, problems arise when the mutually cross-talking metabolic pathways re-structure their path to elude the effect of treatment response. The known effect of these changes on the cancer cell behavior is discussed in the subsequent sub-sections.

Table 1.1: Notable regulation of metabolic genes via gene regulatory factors in glioblastoma

Regulation	Target	Regulator	Mechanism of action	Ref.
Upregulation	GLUT1	VEGFA	Via AKT mediated regulation of PI3K/mTOR pathway	(40)
	G6PD	¹ PAK4, ² RHEB, ³ SREBP-1a, ⁴ HSPB1, ⁵ PLK1	¹ Mdm2-mediated p53 ubiquitination and degradation of G6PD by PAK4; ^{2,3} via enhanced mTORC1 expression; ⁴ Enhanced SIRT2-mediated G6PD activation; ⁵ PLK1 promote active dimerization of G6PD via direct phosphorylation	(41)
				(42)
				(43)
				(44)
SHMT2	H3K9	ATF4 dependent mono-methylation of H3K9 methyltransferase activates SHMT2	(45)	
GLS1	c-MYC	Via repression of microRNA-23A and microRNA-23B, that inhibit GLS1	(46)	
CPT1	PPAR	PGC-1 α , a potent activator and upregulator of PPARs, is activated by AMPK and sirtuin 1 (SIRT1). PPARs induce CPT1 gene expression	(47)	
Downregulation	GLUT1	STOM	via the TP53/PON2 pathway	(48)
	PDH	HIF1 α	Inhibitory phosphorylation of the pyruvate dehydrogenase α (PDH α) subunit by PDH1, a HIF-1 α regulated gene	(49)
Transcriptional Upregulation	GLUT1	HIF2 α	Preferential expression of HIF2 α under normoxia and hypoxia and transcriptional regulation of GLUT1	(50)
	HK2, LDHA	HIF1 α	HIF1 α enhances LDHA expression when cAMP binds to the cAMP response element (CRE) in the LDHA promoter region.	(51-53)
	G6PD	YY1	Direct activation of G6PD transcription by YY1	(54)

	MTHFD2	MYC	Overexpression in MYC is reflected in MTHFD2 expression	(55)
	SHMT2	NRF2	Transcriptional regulator	(56)
	CDO1	c-MYB	CDO1 promoter contains c-MYB responsive element.	(57)
Transcriptional Repression	GLUT1, HK2, LDHA	TP53	Transcriptional repression; negative regulation of AKT/mTOR and NF- κ B signalling pathways	(58)
Expression regulation	GLUD1, GLUD2	mTOR	mTORC1 promotes GLUD expression by repressing SIRT4 via promotion of proteasome-mediated destabilization of cAMP-responsive element-binding 2 (CREB2)	(59)
Expression regulation under Hypoxia	G6PD, RPIA, TALDO1, TKT, PGLS	IRE1	Inhibition of IRE1 under hypoxia increased sensitivity of G6PD, PGLS, RPIA, TALDO1, TKT gene expression to hypoxia	(60)
Co-expression	GSR	MGMT	GSR co-expresses with MGMT promoter and has a higher expression in unmethylated MGMT promoter.	(61)
Inhibition	G6PD	p53	p53 prevents active dimerization of G6PD	(62)
	PRMT5	MTA	MTAP deletion increases methylthioadenosine (MTA) that specifically binds and inhibits PRMT5	(63)
Mutation	¹ IDH1, ² IDH2, ³ Cytochrome C Oxidase (COX, complex IV)	Somatic mutation	¹ Mutation in the Arg132 codon (R132H). Associated with TP53 mutation, or with loss of heterozygosity of 1p/19q; ² Mutation in the Arg140 (R140Q) and Arg172 codon (R172K); ³ Somatic mutations in MT-CO1 and MT-CO3 subunits (G ₆₆₁₉ A and G ₉₆₅₅ A, respectively)	(64, 65, 66)
	Ubiquinol-Cytochrome c reductase (Complex III)	Germ-line mutations	The germline mutation in the MT-CYB subunit (T ₁₄₇₉₈ C and G ₁₅₅₀₀ A) causes potential genetic predisposition.	(66)
	NADH: ubiquinone oxidoreductase (Complex I)	Mutation of ND6 subunit	Mutation of ND6 subunit of Complex I (T ₁₄₆₃₄ C) renders the cells hypoxia-sensitivity. The mutation alters Complex I function as proton translocator, associated with cellular respiration.	(67)
	PHGDH	Genomic amplification	Genomic amplification of the PHGDH gene on chromosome 1p12. Associated with higher tumor grade and decreased overall survival.	(68)
	MTAP	Deletion	MTAP share genomic proximity to the commonly deleted tumor suppressor gene, CDKN2A	(63)
	Epigenetic regulation	ASS1, ASL	Methylation	Expression of ASS1 and ASL could be silenced by gene promoter methylation in glioblastoma
	MGMT	Promoter methylation of MGMT causes gene silencing and correlates with survival of patients.		(27)

Metabolic rewiring to support high proliferative requirement

The preference of metabolic routes in cancer cells is an optimization problem. The cancer cells optimize the metabolic flux distribution to maximize their ability to produce energy currencies and building blocks of cellular components (like lipid membrane, nucleic acids, proteins, and enzymes) to increase their proliferation rate. The management of energy metabolism serves a major part of these requirements. Gene regulation of glycolytic receptors and enzymes GLUT1, HK2, PKM2, PDH and LDHA, fatty acid metabolizing enzyme CPT1, and glutamine metabolizing enzymes GLUD1, GLUD2, and GLS are associated with energy production. The regulation of pentose phosphate pathway enzymes G6PD, RPIA, TALDO1, TKT, and PGLS are involved in the regulation of redox balance of the cell and generation of ribose units (*r5p*) for nucleotide biosynthesis. Changes in the expression of serine biosynthetic pathway enzymes PHGDH, SHMT2, MTHFD2 are associated with the production of anti-oxidants and changes in tryptophan degradation enzyme CDO1, and methionine and arginine catabolizing enzymes, MGMT, PRMT5, ASS1, and ASL confer stability against the cells own fail-check mechanism. The collusion of all these factors within a tumor cell guarantees an unhindered and high proliferation rate.

Altered metabolism helps cancer cells evade immune surveillance

The reduced expression of endogenous enzymes, ASS1 and ASL, of arginine metabolism makes it dependent on the external supply of arginine. As such, arginine depletion from the tumor micro-environment has been utilized as a therapeutic strategy for treating tumor cells, including gliomas (69). However, the applicability of this strategy is challenged by the downregulated antitumoral response of T-cells and macrophages. Exogenous arginine supply induces a metabolic switch from glycolysis to OxPhos during T-cell activation. T-cell sense arginine depletion in tumor-microenvironment (70). Moderate reduction in arginine uptake negatively impacts T-cell survival without affecting proliferation (71). The auxotrophic dependence of glioblastoma on arginine also generates a similar response towards T-cells, thus impeding the activation and differentiation of T-cells upon tumor initiation. Arginine also determines M1 and M2 polarized metabolism in macrophages. M1 macrophages engage in an anti-tumoral

response by metabolizing arginine to NO required for its cytotoxic activity via NO synthase (NOS). Whereas M2 macrophages, which have been described to possess anti-inflammatory responses, metabolize arginine to arginase, leading to ornithine and urea production, resulting in anti-tumoral immunity (72). Thus, arginine depletion in the tumor microenvironment can impede the generation of immunological responses allowing tumor cells the opportunity to evade immune-surveillance.

Metabolic changes serve drugs and therapeutic resistance

Metabolic rewiring during the administration of drugs or therapies makes the prognosis difficult. Cases of drug resistance and off-target responses induced by metabolic plasticity are frequently encountered. For e.g., the efficacy of alkylating agent prodrug temozolomide, popularly used for glioblastoma treatment, is often challenged by the presence of AP endonuclease-1 (APE-1) and deficiency of methylguanine methyltransferase (MGMT) or mismatch repair protein (MMR) (73). The anti-VEGF drug bevacizumab acquires resistance upon CXCL10, CXCL11, STAT3, or c-MET overexpression (74) and overexpression of hypoxic markers HIF-1 α and CAIX and glycolytic genes GLUT1, GLUT3, HK2, and LDHA following treatment (75). The tryptophan metabolism targeted drug navoximod that targets IDO/TDO has potential off-target effects on aryl hydrocarbon receptor (AhR) signalling that is anticipated to have detrimental effects on the treatment strategy (76). A list of resistant mechanisms against popular drugs induced by metabolic changes in glioblastoma are tabulated in **Table 1.2**.

Table 1.2: Popular drugs and the resistance induced by metabolism in glioblastoma

Drug/Therapy	Intervened by	Mechanism	Ref.
mTOR inhibition	GLS overexpression	Glutamine produced by GLS overexpression surpasses the effect of mTOR inhibition by compensating for the loss of TCA cycle intermediates	(77)
IDO inhibitors (Indoximod, Epacadostat, Navoximod, and Norharmine)	Off-target effects on aryl hydrocarbon receptor (AhR) that activates AhR signalling	AhR mediated transcription of IL-6 leads to STAT3 mediated activation of IDO, that is associated with poor prognosis in different cancer	(76)
Temozolomide (TMZ)	Resistance due to increased glucose uptake and enhanced glycolysis	-	(78)

	O-6-methylguanine-DNA-methyltransferase (MGMT) overexpression	Direct repair of O6-MeG adducts by MGMT. MGMT is an inducible DNA repair gene which can be up-regulated by alkylating agents, ionizing radiation, and glucocorticoids	(79-81)
	Resistance due to methionine	Low methionine has an impact on the MGMT levels that sensitizes the cells to TMZ	(78)
	Upregulation of APE-1	APE-1 is an endonuclease involved in base excision repair pathways that remove alkylation-induced abasic sites	(82, 83)
Bevacizumab	Off-target effect	Upon treatment, bevacizumab increases the expression of HIF-1 α and CAIX and the glycolytic enzymes GLUT1, GLUT3, HK2, LDHA, and also the enzymes of pentose phosphate pathway, thus reversing the effect of treatment	(75)
Xenobiotics/ anti-cancer drugs (in general)	Glutathione-S-transferases (GST) and MRP1 overexpression	GSTs detoxify xenobiotics and other endogenous toxic compounds by secreting them into the extracellular matrix. GSTs form a GST-GSH-drug conjugate that is excreted out of the cells via multiple resistance-associated proteins (MRP1) transporters	(84, 85)

1.6. Computational strategies to address complexities of metabolic rewiring

The use of *in-silico* approaches in understanding the biological systems has been instrumental in the post-genomic era (86). In the last few decades, the field has emerged and revolutionized the study of complex biological systems, especially allowing the study of large-scale systems-level and understanding the emergent properties. An integrative approach to understanding the system as a whole rather than going for the reductionist approach helps in narrowing down the wide range of search to a smaller subset of probable solutions. Emerging fields of bioinformatics, mathematical and computational biology have made it easier to analyze the big data. The use of bio-informatics tools has become indispensable in a few of the high-throughput studies and often are accompanied as combined packages for the analysis of the experiments. In recent years, the development of *in-silico* cancer models has been conducive in gaining significant results. The consecutive subsections provide an overview of the popularly used *in-silico* techniques to infer meaningful insights in the field of cancer metabolism.

Constraint-Based Approach

Constraint-based mathematical modelling is a popularly used systems-level modelling approach that assimilates biochemical, genetic, and genomic information within a single computational platform (87-91). It allows the study of the metabolic genotype-phenotype relationship of an organism. Genome-scale metabolic models (GSMM), that implements a constraint-based approach have been used in *in-silico* metabolic engineering for the design of studies like defining essentiality of the reaction/gene (92, 93), the influence of distant pathways (94), and overexpression or repressed expression of metabolites, reactions and metabolic pathways (95). These are efficient tools for the prediction of growth in living cells/tissues exposed to different external conditions (96). They have been used to predict the conditional and absolute essentiality of metabolites and reactions in metabolic networks. GSMM considerably contributes to deducing the metabolism of lower organisms. The construction of the Human RECON model and its recent update RECON3D has enabled scopes of whole-genome modelling of human metabolism as well. However, usage of this vast model has remained limited due to handling issues and is mostly used to develop context-specific models. Context-specific models allow systems-level understanding of the relevant part of the network while yielding results consistent with experimental findings (97).

Flux balance analysis (FBA) is the most popularly used constraint-based approach to model both genome-scale and context-specific systems-level metabolism that works on the basic principles of linear optimization (98). Linear Optimization in biological systems has been in use since the 1980s when Papoutsakis, in 1984, first used the technique to calculate the maximum fermentation yield of butyric acid-producing bacteria (99). In 1986, Fell and Small used linear optimization to analyze lipogenesis in adipose tissues (100). The technique was used by Majewski and Domach to study acetate overflow during aerobic growth in *E.coli* (101). The technique was later adapted by Savinell and Palsson to develop the FBA (102). In 1994, Varma and Palsson used the theory to describe the properties of *E.coli* (103). Further developments were made with the inclusion of the biomass concentration by Pramanik and Keasling (104) and elementary mode analysis by Pfeiffer *et al.*(105). Advanced features were eventually included in FBA like gene deletion, phase plane, and robustness analysis. The usability of the FBA models was

upgraded to another level with the inclusion of regulation imposed by gene expression by Covert *et al.*(106). Additional features of FBA like Minimization of metabolic adjustment (MOMA) (107) and Regulatory on/off minimization (ROOM) (108), the inclusion of 13C flux analysis (109), and Steady-State Regulatory FBA (SR-FBA) (110) were developed. The use of these techniques in Cancer Biology has started only lately in the last two decades and has been quite conducive. Prediction of selective drug target for Hereditary Leiomyomatosis and Renal-Cell Cancer (HLRCC) (111), multidimensional optimality (112) are some of its uses. Very recently, in a composite study by Mathias *et al.*, the transcriptome data of 17 different cancer types were analyzed by using a systems-level approach (113).

A further extension of the modelling technique has been done to incorporate dynamic regulation of metabolism popularly known as dynamic FBA (dFBA), where the optimization is done over a time period to obtain time-dependent changes in the flux profiles and metabolite levels (114). In yet another extension of FBA, the initial signalling response is analyzed using Boolean analysis. This is known as rFBA. The method which takes into account a combined FBA, boolean regulatory and ODE approach is known as integrative FBA (iFBA) (115).

There are various tools available for performing these analyses. COBRA Toolbox is the most widely used platform for flux balance analysis (116). This is a MATLAB extension that provides a user interface for ease of analysis. Other platforms are COBRAPy(117), PSAMM (118), OptFlux (119), FBASimVis (120), FluxViz (121), FlexFlux (122) and FAME (123).

Dynamic Approach

Unlike the constraint-based models that are discovered rather recently, dynamic modelling approaches to study biological phenomena have been in use for quite some time. Dynamic modelling of biological systems essentially involves converting the biological question into a mathematical problem using ordinary or partial differential equations. The approach requires to have information about the parameter used to define the biological system mathematically. Their benefits in the study of cancer phenomena have been realized in the early '70s. The initial use of dynamic models in cancer goes back

to 1976 when Greenspan used it to study the growth and stability of solid tumors (124). In 1982, Vaidya and Alexandro made a comparative study of then-existing exponential, Gompertz, Bertalanffy, and logistic models to best fit the experimental findings of human lung carcinoma and mice sarcoma. The logistic model for the human carcinoma and the Bertalanffy model for mice sarcoma generated the best fits (125). In later years, consideration of time factors in linear quadratic equations was reviewed by J.F. Fowler (126).

In 1993, Chaplain and Sleeman proposed a model for the growth of solid tumors using the membrane theory of shells and strain-energy function (127). A comparative work was performed by Marusic *et al.* in 1994, where they evaluated the efficiency of the then existing models to fit the spheroid growth hypothesis of tumors. Gompertz's model was found to best fit the hypothesis (128). Subsequently, models were built to capture the effect of chemotherapy on the spatiotemporal growth of gliomas which considered two domains: (i) geometry of the brain and (ii) its natural barriers to diffuse (129). A two-dimensional model on the effect of surgical re-sectioning on glioma growth was built by Woodward in 1996 (130), which was later extended by Burgess *et al.*, to include a third component of diffusion coefficients into gliomas growth (131). Another model developed by Orme and Chaplain on the tumor angiogenesis and anti-angiogenesis strategies were able to capture the role of hypotaxis and chemotaxis during the growth of neo-vasculature (132). In 2000, Swanson *et al.* developed a quantitative model for differential motility of gliomas in grey and white matter (133). Subsequently, they made advancements in the model and developed a model to quantify the spatio-temporal growth and invasion of gliomas and used it to quantify the efficacy of chemotherapy of brain tumors with homogenous and heterogeneous drug deliveries (134). In a similar period of time, an agent-based model of spatio-temporal growth and cell motility was developed by Mansury *et al.* (135).

Taking into consideration the effect of the microenvironment in tumorigenesis, Gatenby and Vincent developed an evolutionary model of carcinogenesis (136). Meanwhile, to take an account features like blood flow and vascular dynamics in tumors, Alarcon *et al.* developed a cellular automaton model for tumor growth and inhomogeneous environment (137). In 2004, Plank and Sleeman developed lattice and non-lattice models

of tumor angiogenesis, where the process of angiogenesis was simulated by the application of circular random walk, which allowed the cells to move independently (138). A three-way model was developed by Wu *et al.*, including tumor growth, replicate-competent virus, and immune response (139). A trend of *in-silico* modelling in cancer immune interactions and therapeutics developed around this time. Models for effective and less toxic therapies for breast cancer (140), immune response to tumor antigens (141), factors like tumor necrosis, neo-vasculature, tissue invasions (142), histopathological features of brain tumors (143), and multicellular patterns in brain tumors (144) were developed. Non-linear and multi-scale models of cancer considering both experimental and mathematical modelling approaches were developed by Lowergrub *et al.* (145). Hernandez *et al.* modelled cancer glycolysis and predicted therapeutic targets therefrom (146). In a recent advancement, Molina-Pena *et al.* developed a model based on the cancer stem cell hypothesis in which they considered that a small sub-population of cells within cancerous tissues exhibit stem-cell-like characteristics and is accountable for the maintenance and proliferation of cancer (147). Reviewing the different areas of oncology where dynamic modelling approaches have been applied helps us understand the diverse applicability of these models.

Graph Theoretical Approach

Graph theoretical approach has been applied in the metabolic network to determine the structural properties of these networks, their functional roles, identify hub nodes, and modularity between reactions. There are different methods of formulating the metabolic into a graph network (148). The classical way of representing a metabolic network is by considering the metabolites as nodes and edges represented by the reaction that converts one metabolite into another. One can also convert the information of metabolites and reactions into a reaction adjacency matrix, where the nodes are formed by the reactions, and the edge connectivity between two nodes is established if the product of the first reaction node is a substrate of the second reaction node. To determine the regulation of reaction on metabolites or vice-versa or the effect of a third regulator (transcription factors, signalling regulators, post-transcriptional regulators, etc.) on metabolism, one can formulate a bipartite network where both metabolites and reactions can be represented as nodes (149). The choice of the right graph-theoretical approach depends

on the biological question that needs to be addressed. This selection of a proper graph is a vital step as the conclusions drawn from the analyses depend on the structure of the network (150).

Two vital features of metabolic graph networks are: directionality and weight. Metabolic networks consist of both reversible and irreversible reactions that are capable of changing direction depending on cellular requirements. It is, therefore, essential to use directed graphs for metabolic networks (151). Yet another challenge in the construction of metabolic graph networks is the preferential selection of metabolic routes. The graph approach generally includes all possible reaction information in a single network providing a generic map of the whole network. Cellular metabolism, however, has a preference towards the selection of metabolic routes that are determined by the cellular requirement. Introducing the criteria to switch reactions on or off in a graph network is a challenge. The use of a weighted network is a probable choice that requires knowledge about the probability of flux distribution across the different paths in a metabolic network (152). The weight is generally introduced on the edges that determine the strength of information flow between two connected nodes. Weighted networks provide the opportunity to build context-specific graph models of the metabolic network that can be altered by changing the edge-weights. Information from gene or protein expression profiles, metabolomic analysis of metabolite concentration, flux flow distribution using ^{13}C analysis can be used as weights.

The selection of proper centrality measures to identify the central nodes in a graph network is important. The popularly used centralities are degree, betweenness, closeness centrality, eigenvector centrality, and eccentricity. Limitations in the usage of these centralities arise with the change in the structure of the network. The difference in the network structure and topology makes the selection of suitable centrality measures difficult. The universality of the “*centrality-lethality hypothesis*” (153) becomes questionable if the measures to identify central nodes in the network are not chosen wisely. To quantitatively evaluate the central nodes of the metabolic network, centrality measures like flux centrality have been developed (154). Nodes ranking based on the flux distribution through the network help identifies central nodes that are relevant in context to a particular growth condition. The application of network biology in metabolic

networks has gained momentum in the last one decade. New centralities and network measures are being developed to make use of graph theory in this direction.

1.7. Challenges created by metabolic reprogramming in glioblastoma

While metabolic plasticity is a boon to the cancer cells, it is a bane for the researchers seeking answers to the complex phenomena exhibited by these cells. The changing paths of preferred metabolic routes make the practical implementation of the understanding difficult. The flexibility of cancer cells to switch between phenotypes as and when required create additional challenges in the prognosis. The major challenges associated with metabolic reprogramming that need to be addressed are described below.

Robust mechanisms provide stability to perturbations

The scale-free nature of biological networks provides stability and protects these networks from random failures. However, cells under normal physiological conditions can be vulnerable to changes that induce severe cellular response breaking its symbiosis with the surrounding cells and microenvironmental factors. Cancer cells elude this response and continue to thrive with severe defects, causing a disruption of homeostasis with the cell as well as its microenvironment. Their ability to switch metabolism as per requirement provides a benefit over the cell's innate fail-check mechanisms. With the accumulation of genetic defects and differential regulation of metabolic genes in glioblastoma, as discussed in section 1.5.3, these tumor cells evolve into malignant and metastatic tumors with high invasive properties. The adjustments made in the metabolism of these cells confer robustness over the otherwise vulnerable changes and perturbations. The cell's innate machinery to identify lethal insults fails to guide the tumor cells to apoptosis. Owing to the devious metabolic changes, the cells manage to evade the immune-surveillance as well. Metabolic plasticity also confers stability to induced perturbations, as in the case of therapeutic interventions. The resistance mechanisms generated against drugs, as discussed in section 0 and the *gsh* dependent overexpression of glutathione-S-transferases (GST) inducing exocytosis of drugs and xenobiotics, protect the tumor cells from external perturbations. An additional level of complexities is added by the condition specificity of the metabolic changes exhibited by

these tumors. Simply understanding the preferred metabolic route in tumor cells is not sufficient to address the complexities associated with metabolic reprogramming. The knowledge about the environmental and growth condition under which the tumor cells exhibit a particular metabolic phenomenon is crucial for its implementation in therapies. The cancer cells can opt for a changing preference of metabolic routes under different growth conditions. As such, a major challenge is to understand the landscape of metabolic changes as an integrated systems-level network where the effectiveness and unintended consequences of a perturbation in the network can be anticipated.

Disruption of redox and thiol balance

Unregulated production of Reactive Oxygen Species (ROS) has been implicated in various disease conditions and is considered a crucial driving factor in the process of aging and carcinogenesis. ROS possess a double-edged sword property having both tumor-promoting and a tumor-suppressing function (155). An intricate balance between ROS and antioxidants and other ROS scavengers are maintained in a normal proliferating cell which is a prerequisite for maintaining redox balance and proper functioning of the cell. Human cells tend to function in a reduced state (e.g., by maintaining a high *gsh/gssg* ratio (156) and high *nadph/nadp⁺* ratio (157)). However, exceptions are made when the cells need to maintain a partial oxidative environment to aid various cellular processes like folding of nascent proteins in the endoplasmic reticulum, activation of gene transcription factors, etc. An increase in intracellular oxidative state induces apoptosis, although too much oxidation helps to evade apoptosis by oxidizing and inactivating the caspase enzymes (158). Thus, the balance between oxidant and antioxidant activity becomes crucial as a shift might facilitate apoptosis or might also suppress apoptosis rendering therapeutic approaches ineffective.

The changes in the thiol and redox ratios are important determinants of cellular response towards oxidative insults. These ratios are cumulative resultant of multiple changes in the metabolism and hence are considered as indicators of various diseased states. A conducive understanding of the cellular function can be obtained by considering changes in these ratios in light of other mutations considered together. Although, the effect of ROS manipulation on these ratios and how the metabolic switching of cells affects the redox

and thiol status of the cell are not clearly understood. Whether the redox and thiol status of the cell have any role in determining cellular fate during oxidative stress is another debatable topic of discussion. Within the cell, these changes are regulated by the metabolic processes, functioning as an orchestrated network that is rerouted during oxidative stress to maintain cell survival. However, changes in the metabolic network that govern the puzzling duality of ROS are yet not clearly understood. The role of the *gsh-gssg* cycle as a crucial regulator of the anti-oxidant machinery has been well studied, but whether it has any role in determining the paradox is yet to be explored. The changes in the metabolic network that affect the efficacy of pro-oxidant or anti-oxidant approaches in cancer therapeutic design are also an ongoing area of research and is yet to be understood.

Development of oncogenic phenotypes

Changed metabolism nurtures the tumor cells allowing the development of oncogenic phenotypes. Remodelled energy metabolism support proliferation and growth of tumor cells. Additional changes in the fatty acid metabolism and ROS production allow the development of invasion and metastasis. The energy metabolism also regulates the development of stem-like properties in these tumors. The stem cells have a strong dependence on the oxidative phosphorylation. However, the dependence can be easily bypassed by switching between metabolism. It has been observed that inhibition of both glycolysis and oxidative phosphorylation is necessary to target cancer stem cells. Yet another route available to the stem cells the fatty acid oxidation (159). The exchange of metabolites between tumor cells and microenvironment, as discussed in **Section 1.5.2**, allows nutrition to the cancer-associated fibroblasts and epithelial cells, thus promoting angiogenesis and vascularization. Glioblastoma is a highly vascularized tumor, and its growth depends on angiogenesis (160). Needless to say, the drug-resistant glioblastoma cells acquire resistance with changing metabolism over time. Understanding the role of metabolic pathways in the development of these oncogenic phenotypes and the underlying mechanism that could control the switching between phenotypes remains as a challenge.

Poor prognosis and recurrence

The cumulative effect of all the above-mentioned factors is realized during the prognosis of glioblastoma. Till date, glioblastoma remains to be the most challenging cancer, with a median overall survival time of only 12-15 months in primary glioblastoma patients. The 5-year survival rate of these patients is < 9.8% (161). Post-treatment tumor-free survival of the patients is also challenged by the high recurrence rate of this cancer. The morphology of glioblastoma cells has an added advantage on tumor invasiveness. Accumulation of metabolic insults within the cells is manifested as severe responses disrupting the homeostasis within the tumor cells and that of the nearby cells as well. In addition, the tentacular morphology of these tumor cells allows rapid infiltration into the nearby region of tumor origin that progresses to different areas of the brain. The web-like progression of tumor cells across the brain makes the complete surgical removal of these tumors very difficult, resulting in recurrent tumor formation. Current treatment protocols of cancer that consist of surgical resection of tumors followed by radio and chemotherapy is challenging in glioblastoma due to its dominant phenotypic plasticity.

Whether metabolic reprogramming is a cause of these challenges or an effect of an underlying factor that is manifested as oncogenic phenotypes via metabolic reprogramming remains debatable. Nonetheless, the complicity of metabolic changes in tumorigenesis is undeniable. Understanding the landscape of altered metabolism in glioblastoma can help address many of these challenges.

1.8. Scope and Specific Objectives of the Thesis

Metabolic phenomena like the Warburg effect and glutaminolysis have been repeatedly evaluated in the cancer cell and have been well established for their role in glioblastoma progression as well. Strategies to target these phenomena have been developed and are popularly being used in treatment regimens. However, high connectivity and robustness of metabolic networks protect the cells against random failure, and hence cells evolve and develop resistance against the therapeutic regimens. Hence, the study of metabolic pathway re-routing in glioblastoma is crucial to understand the alternate routes of therapeutic escape, opportunistic mode of nutrient acquisition, and evolving mechanisms

to surpass oxidative stress and immune surveillance. The improper management of the redox balance and increased accumulation of reactive oxygen species (ROS) within the cells during hypoxia aid the development of oncogenic phenotypes. However, studies to delineate the role of ROS in cancer have shown that ROS have a double-edge sword property in regulating the apoptotic fate of cancer cells. This has left the oncologists with the question of whether to increase or to decrease it for therapeutic gains. A quantitative understanding of the mechanism of ROS management in cancer cells hence remains crucial to be addressed. The regulation of metabolic genes during cancer development is another important aspect of our study. The genetic regulations imposed due to mutation, methylation, and nucleotide polymorphism in glioblastoma has contributed to our understanding of metabolic regulations. Nevertheless, the recent understanding of the role of microRNAs in cancer metabolic regulation has been well appreciated and largely remains unexplored in glioblastoma. Hence, we attempt to delineate the metabolic gene and pathway regulations imposed by differentially expressed miRNAs in glioblastoma, concluding with their probable contribution in determining cellular phenotypes of glioblastoma.

A reductionist approach aiming to annotate the vast expanse of biological data generated with the high-throughput technologies is currently being appreciated. However, simple analysis techniques become a limiting factor once the interacting components go beyond a certain number. In such scenarios, the employability of *in-silico* approaches provides a comprehensive insight into the resulting phenotypic behaviors. In similar lines, in the present thesis, the following biological objectives relating to glioblastoma metabolism have been addressed using *in-silico* techniques:

- Pathway-level analysis of the metabolic pathways deregulated in glioblastoma to understand its effect on internal cellular mechanism.
- To identify targets and mechanisms which could be used to develop therapeutics against glioblastoma.
- To understand the dynamics of glutathione (antioxidants) in determining paradoxical ROS-manipulation strategies in glioblastoma.
- To investigate the role of microRNAs in regulating the altered expression of metabolic genes, pathways, and cellular phenotypes in glioblastoma.

1.9. Organization and overview of the Thesis

The present thesis focusses on the detailed study of the metabolic re-routing, quantitative evaluation of the critical mechanistic regulation and controls at the gene expression level that guide metabolic reprogramming in cancer, with particular reference to glioblastoma. The composite picture of the metabolic reprogramming will be helpful in delineating the additional challenges posed by metabolic reprogramming in glioblastoma (**Section 1.7**). Hence, the objectives of the thesis have been defined with a top-down approach to understand the prevailing challenges in glioblastoma, by considering a systems-level analysis of large-scale metabolic network that has been subsequently narrowed down to a smaller module for detailed dynamic analysis. This part of the thesis addresses the “what” and “why” of glioblastoma metabolism. To further understand “how” these changes are regulated, a study of the gene regulatory changes has been done.

Systems approach to annotate the discrete and diverse landscape of glioblastoma metabolism using *in-silico* optimization methods like constraint-based modelling using linear programming, dynamic analysis using ordinary differential equations of reaction kinetics and network biology approaches have been employed to gain comprehensive insight into the resulting phenotypic behaviors.

Chapter 1 i.e., the present chapter provides an overview of the concepts, theories and understanding related to cancer metabolism. The previously studied metabolic changes in glioblastoma and related phenotypic changes are thoroughly reviewed. Based on the understanding, the biological questions that remain to be addressed, the challenges, and the objectives of the thesis are introduced.

Chapter 2 provides the details of methodologies applied to meet the objectives of the thesis. The chapter discusses the detailed working principles and rationale of the *in-silico* techniques used to formulate, analyze, and interpret the computational models used to address the different biological questions in the thesis.

Chapter 3 attempts to study the systems level changes in the flux flow through different metabolic pathways arising due to altered expression of important metabolic genes in glioblastoma. It focuses on a detailed comparison of metabolic routes chosen by

astrocytes vs glioblastoma, followed by the evaluation of the condition specificity of the observed phenomena and the identification of possible therapeutic targets.

Chapter 4 addresses the puzzling duality of ROS in gliomas and their manipulative strategies that could determine the apoptotic fate of the gliomas. It quantitatively evaluates the dynamic changes in the kinetics of reactions associated with generation of ROS and anti-oxidants during gliomagenesis using an ordinary differential equation model.

Chapter 5 investigates the microRNA regulation of metabolic gene expression and pathway regulation that results into metabolic reprogramming in glioblastoma. The study also focusses on the identification of miRNA targets to control and regulate oncogenic phenotypes in glioblastoma that can be used for miRNA-based therapeutic design.

Chapter 6 concludes the significant outcomes of the thesis. The chapter also discusses the prospects of the applied techniques and findings of the thesis that can embark new research avenues.

CHAPTER 2**METHODOLOGIES****2.1. Systems-Level Analysis of deregulated metabolic pathways in Glioblastoma**

The basic understanding of any disease pathology involves the identification of the underlying cause and understanding of the mechanism of its pathogenesis. The best way to begin with, is to study the normal and abnormal contrasts between the pathological and physiological conditions. This holds true for understanding the abnormalities at the molecular level too. Hence, to begin with, the work in **Chapter 3** takes into account a systems-level study of the metabolic differences between astrocyte and glioblastoma. To understand the differences in the metabolic behavior of astrocyte and glioblastoma at the pathway level, a context-specific constraint-based model for astrocyte and glioblastoma metabolism was reconstructed and analyzed using flux balance analysis (FBA). For specific comparison between the two scenarios, pathways that are known to get deregulated in glioblastoma when compared to the normal astrocyte were considered. The model comprises of a total of 13 deregulated metabolic pathways with 247 reactions (39 exchange reactions and 69 transport reactions) associated with 147 genes. By analyzing this network, the differences in preferred flux flow routes in astrocyte and glioblastoma under different scenarios were delineated. Model analyses further helped identification of metabolites essential for glioblastoma growth and to understand the differences in the uptake and utilization of metabolites (which can be categorized as essential and non-essential) and release of overflow metabolites in the two scenarios. Probable chemotherapeutic targets were identified through *in-silico* single and double reaction knockout analyses. The details of the methods used in this study are provided in the subsequent subsections.

2.1.1. Constraint-based model reconstruction

Constraint-based models are a convenient approach for modelling large-scale metabolic networks that work on the principle of linear optimization (**Section 1.6**). The approach involves multiple steps of formalizing various levels of metabolic information into a

reconstructed composite network. This is a crucial step in the modelling study as it involves careful scrutiny and verification of information regarding the association of enzymes to crucial metabolic reactions, their appropriate subcellular locations, transports, and exchanges compiled using a variety of data sources. The basis of this reconstruction is to identify the gene-protein-reaction (GPR) network along with appropriate transports and exchanges (**Figure 2.1**). In the present work, the GPR was reconstructed considering reactions that contribute to ATP synthesis and glioblastoma growth. The GPR relationship for 147 reactions out of the total 247 reactions was established.

The reactions considered in the model and their corresponding Enzyme Commission Numbers (EC Numbers) were curated from ExPasy Enzyme (162) and KEGG (163). The genes to the enzymatic reactions considered in the model were obtained from NCBI Gene (164). The molecular functions of these reactions were obtained from UniProt (165), KEGG, and through literature survey. Information regarding the subcellular localization of the reactions was compiled through extensive literature search, and for those reactions, for which literature support for subcellular localization was limited or not available, cytosol was taken to be the default compartment of the reaction. A list of reactions, their corresponding genes, and enzyme commission numbers were compiled with appropriate literature support to gather evidence related to the biological significance and subcellular localization of the reactions and have been provided in **APPENDIX A: Table A. 1**. Most of the internal reactions along with 12 transport reactions were associated with their corresponding genes, which accounted for 147 genes in the model. All the metabolites and the corresponding reactions in which they were involved were distributed into five different compartments: Extracellular space (e), Cytoplasm (c), Mitochondria (m), Mitochondrial intermembrane space (i), and Nucleus (n). All these information were organized in the rBioNet toolbox, a MATLAB extension of the COBRA Toolbox (166), to reconstruct the constraint-based metabolic model. The reconstructed metabolic network consisted of 13 pathways that are significantly affected during the tumorigenesis of glioblastoma (**Table 2.1**). The detailed pathway diagram has been drawn in Cell Designer version 4.3 and has been provided in **APPENDIX A: Figure A. 1**. Note that the abbreviations used for all the reactions specific to **Chapter 3** are explained

in **APPENDIX A: Table A. 1**. The abbreviations used for the metabolites in **Chapter 3** are elaborated within the text of the chapter, wherever necessary.

Table 2.1: List of pathways selected pathway reconstruction of the constraint-based metabolic model for astrocyte and glioblastoma and their references.

Sl. No.	Pathway	Reference
1	Alanine and Aspartate Metabolism	(167)
2	Beta Oxidation of Fatty acid	(168)
3	Cysteine Metabolism	(17)
4	Glutamate Metabolism	(2, 169)
5	Glutathione Metabolism	(170)
6	Glycine-Serine Metabolism	(18, 171)
7	Glycolysis	(14, 15, 172)
8	Methionine Metabolism	(173)
9	Oxidative Phosphorylation	(174)
10	Palmitic Acid Biosynthesis	(172)
11	Pentose Phosphate Pathway	(175)
12	TCA Cycle	(176)
13	Tryptophan Metabolism	(16)

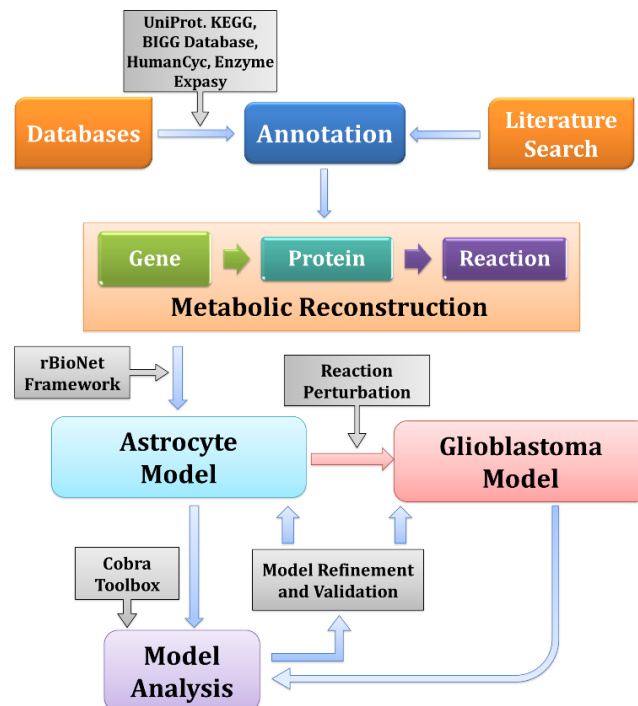


Figure 2.1: Schematic workflow of the constraint-based metabolic model using flux balance analysis

2.1.2. Flux Balance Analysis (FBA)

Flux Balance Analysis (FBA) is a mathematical approach to analyze the flow of metabolites through a metabolic network, where the metabolic reactions are represented in a matrix of metabolites and reactions composed of stoichiometric coefficients of each metabolite in each reaction (98). Flux balance analysis is the most popularly used constraint-based approach in systems-level metabolic modelling. The technique assumes a steady-state approach where all the metabolites of the network are considered to be in steady-state, i.e., the rate of change of metabolites over time remains zero. This ensures that the rate of formation of a metabolite in the network is always equal to the rate of its consumption and hence a net difference in the metabolite concentration over time always remains zero. All the reactions of the network work as constraints to the optimization problem. The reactions are bounded between a lower and an upper bound, which creates the constraint. The metabolites are connected to respective reactions in the form of a stoichiometric matrix, ' S ,' where the rows represent the metabolites (m), and the columns represent reactions (n). Thus, a ' $m \times n$ ' matrix is generated in which the involvement of a metabolite in a reaction is represented by its respective stoichiometry in that reaction. A positive stoichiometric value represents the formation of the metabolite, and a negative stoichiometric value represents consumption. The flux through the reactions is represented in a separate flux vector-matrix ' v ,' which is a ' $n \times 1$ ' matrix. The flux through the reactions could be adjusted manually by defining the bounds of the reactions: lower bound (v_{lb}) and upper bound (v_{ub}). This allows the flexibility to redefine model conditions as per different pathological and physiological scenarios. The outcome of optimization is obtained by matrix multiplication of $S \cdot v = 0$. The matrix multiplication results in an optimized ' v ' matrix which assigns an optimal flux to each of the reactions in the network. Generally, whole-genome models are large with a few hundred reactions and metabolites, which makes it a multi-dimensional optimization problem. An objective is assigned to the model, which depends on the biological question one wants to address. Thus, the model gets optimized as per the requirement of maximizing or minimizing the objective function.

In the present metabolic network, this relationship was established between the metabolites and the reactions in the form of an S-matrix, which comprised of 159

metabolites and 247 reactions, building up the S-matrix of dimension '159 x 247'. The score assigned to each element of the S-matrix, S_{xy} represented the stoichiometry of the metabolite 'x' in the reaction 'y'. A positive score signified the production of the metabolite, and a negative score implied its consumption in the reaction. The column vector v had 247 fluxes, including 39 exchange reactions and 69 transport reactions. FBA formalizes the flux distribution through the whole metabolic network as the dot product of the S-matrix and the vector v . All the reactions in the model were organized in the rBioNet extension of the Cobra Toolbox, where their fluxes were constrained between a lower bound v_{lb} and an upper bound v_{ub} . All the reversible reactions were bounded between $v_{lb} = -1000$ and $v_{ub} = 1000$. The irreversible reactions in the model were bounded either from 0 to 1000 or -1000 to 0 with respect to the substrate and products defined for that reaction as per available information from the literature. The bounds to the exchange reactions were fixed as per the requirement of the system for uptake or release of the exchange metabolites. Those exchanges which were known to be taken in were bounded between -1000 to 0, and those which were known to be released out were bounded between 0 to 1000. The rest of the exchanges was bounded between -1000 to 1000 to analyze their role in the metabolism by simulating the model using FBA.

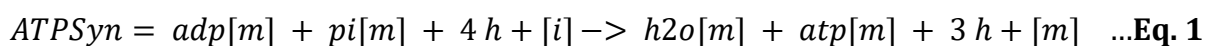
2.1.3. The objective functions: defining objectives for energy and growth requirement

The biological question to be addressed using the constraint-based model is defined with the help of an objective function. The model optimizes flux through all the reactions in the network to yield optimal flux through the objective function as per the requirement to maximize or minimize it. Multiple objective functions can be assigned to a single model to define different biological questions pertaining to the model. The metabolic requirement of the glioblastoma cells changes as per the growth condition. The proper functioning of energy metabolism in a normal cell ensures that the growth requirements of the cell are taken care of by generating by-products that are used in the biosynthesis of additional cellular components required for growth. However, due to the changed expression profile of glycolytic, pentose phosphate pathway and TCA cycle enzymes, and metabolic insults generated in the mitochondrial respiratory chain, this mutual fulfilment of energy and growth requirement is disrupted. An altered metabolic flux profile ensures

that both the energy requirement and metabolic requirement for the growth of the cancer cells are met. Hence, in the present work, two objective functions were defined to capture this difference in flux profiles of normal astrocytes and glioblastoma cells.

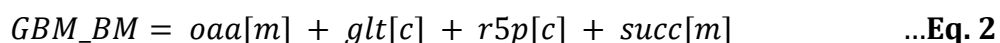
Objective function for energy demand

ATP synthesis through oxidative phosphorylation (ATPSyn) was considered as the objective function for energy demand. Cells under normal physiological conditions drive their glycolytic flux towards the production of ATP through the mitochondrial FOF1 ATP synthase. Hence, this reaction was chosen as the objective (**Eq. 1**) to understand the flux flow distribution in the model under normal astrocytic conditions as well as under the glioblastoma condition.



Objective function for growth demand

A metabolic demand reaction that will dually fulfil the requirements of growth and ATP (GBM_BM) was designed to capture the growth demands of glioblastoma. To define the growth requirement of the model, ribose-5-phosphate, $r5p(c)$, oxaloacetate, $oaa(m)$, succinate, $succ(m)$, and glutathione $glt(c)$ were included as components of the objective function, selected on the basis of their contribution as (a) precursor to the nucleotide biosynthesis and synthesis of amino acids like valine, lysine, methionine, threonine, etc. (106, 177), (b) intermediates for maintaining redox balance in different cellular compartments and biosynthesis of other cellular components required for cell growth (178), (c) preventing damage to cellular components caused by reactive oxygen species produced due to hypoxia or other cellular stress (19)



2.1.4. Creation of scenario-specific metabolic flux models

Flux models allow the flexibility to define model conditions by changing the bounds defined for each reaction. Different physiological and pathophysiological conditions could be defined in a model by adjusting the lower and upper bounds of reactions that generate different optimization conditions for the objective function. In this work, the

normal physiological and the pathological conditions were defined by the metabolic differences between astrocyte and glioblastoma, respectively. Bounds to the flux through a few enzymatic reactions which defined the differences between the two scenarios were assigned on the basis of literature support. Both the objective functions were optimized for the two scenarios. Limited bounds were assigned to a few reactions to create the astrocyte scenario. The rest of the reaction fluxes were allowed to vary between a wide range of [-1000 to 1000] or [0 to 1000] or [-1000 to 0] as per the reversibility or irreversibility of the reactions. The model was then simulated to obtain results that were in accordance with the experimentally available data defining the features of astrocytes (179-181). Bounds to the mitochondrial reactions- glutaminase [-50, 50], glutamate dehydrogenase [-150, 150], mitochondrial pyruvate carboxylase [-10, 10], and cytoplasmic reactions- acetyl-CoA carboxylase [0, 100], L-carnitine O-palmitoyltransferase [0, 20], and cytoplasmic malate dehydrogenase [-50, 50], were fixed and the model was analyzed using FBA to create the astrocytic scenario.

Perturbations were done to the same astrocytic model by varying the lower and upper bounds to a few reactions that were experimentally found to be deregulated in glioblastoma, and then the model was simulated to create the glioblastoma scenario. Bounds were released to a few reactions, which were imposed in the astrocytic scenario: glutaminase [-1000, 1000] and acetyl-CoA carboxylase [0, 1000]. New bounds were assigned to another set of reactions to generate the glioblastoma scenario: glutamate dehydrogenase [-200, 200], Cytochrome c Oxidase (complex IV) [-10, 10], Trans_Glutamate (ATP) [-90, 90] and glycine exchange [-500, 500]. This model was analyzed using both ATPSyn (**Eq. 1**) and GBM_BM (**Eq. 2**) as the objective function. This model was further validated with experimental data available for glioblastoma (2, 17, 182).

2.1.5. Validation of Constraint-based models

Validation is an important step in computational modelling that improves the credibility of results obtained from model analyses. In the case of biological models, verification of model properties with experimental observations made for the physiological and/or pathological conditions is a prerequisite for proceeding further with the model for

analyses. Hence, the reconstructed metabolic models in the present study were validated for both the astrocytic and the glioblastoma scenario. The mitochondrial ATPSyn (**Eq. 1**) was used as the objective function. The astrocytic and glioblastoma models were created as described in **Section 2.1.4**. Both the models were validated with experimentally verified observations made in astrocytes and glioblastoma.

Properties of astrocyte like the increase in glucose uptake driven towards both mitochondrial ATP synthesis and lactate production, increase in the activity of lactate dehydrogenase and pyruvate kinase in hypoxia conditions (180) and increase in glucose utilization and lactate production with increasing glutamate uptake (181) were validated for the astrocytic model. Similarly, the reduced mitochondrial ATP synthesis and increased glucose utilization (15) and reversal in glutamate and glutamine utilization, and increase in cystine uptake in glioblastoma cells (2) were validated for the glioblastoma model. The results are discussed in detail in **Section 3.2.3** of **Chapter 3**.

2.1.6. *In-silico* prediction of minimal essential metabolite for glioblastoma growth

Glioblastoma cells are grown in commercially available MEM or DMEM media (17, 183, 184). However, due to the lack of sufficient literature that reports the essential metabolites required for glioblastoma growth under nutrient-starved conditions, an *in-silico* simulation was performed to check the fate of some key metabolites that contribute to the growth in the glioblastoma. The model consisted of eight input metabolites: glucose, cystine, methionine, tryptophan, palmitate, glutamate, glutamine, and glycine. The entry of each of these input metabolites was allowed in the model, one at a time, and the corresponding flux through the GBM_BM, objective function for growth was computed. Further, the fate of the essential metabolite in combination with a second input metabolite within the model was checked, and the optimal solution of the GBM_BM objective was calculated. This was performed to identify the most important input metabolite required for enhancing glioblastoma growth.

2.1.7. Single and double reaction knockouts in glioblastoma

Reaction knockout analysis was performed to completely nullify the functional effect of a reaction in the network. Reaction knockout predictions allowed the identification of reactions that could be targeted for either completely inhibiting or reducing the glioblastoma growth. While transport reactions were considered for the knockout analysis, the 39 exchange reactions were eliminated. Each of the 208 reactions in the metabolic network was knocked down individually to predict the knockouts that could potentially reduce glioblastoma growth. For performing the knockout, flux through each individual reaction in the network was constrained to zero ($v_{lb} = v_{ub} = 0$) and the flux through the GBM_BM objective function was computed. Double reaction knockouts were also performed, with a combination of two reactions knocked out of the network simultaneously. The single and double knockouts were classified on the basis of percentage reduction of flux through the objective function, GBM_BM, from its optimal value. The optimal value of flux through the objective function in the astrocytic scenario corresponded to the normal growth rate ($v_{GBM_BM}^{Normal} = 240$).

2.1.8. Identification of metabolic targets for therapeutic intervention

The results of the double reaction knockout analysis were used to identify feasible therapeutic combinations to target glioblastoma growth. For performing *in-silico* therapeutic interventions, we divided the reactions into two broad categories: (i) essential ($v_{GBM_BM} = 0$) and (ii) growth reducing (GR) reaction pairs ($v_{GBM_BM}^{Max} > v_{GBM_BM}$) as per their essentiality in determining glioblastoma growth. Note that $v_{GBM_BM}^{Max} = 285$ that represented the maximum flux observed through the GBM_BM objective function in the glioblastoma model. The growth reducing pairs were further classified into partial growth reducing reactions ($v_{GBM_BM}^{Max} > GR > v_{GBM_BM}^{Normal}$) and normal growth reducing reactions ($GR = v_{GBM_BM}^{Normal}$). We further predicted the putative feasible ranges for each of these reaction combinations, in which therapeutics can effectively target glioblastoma growth either by complete inhibition of growth or by reducing the glioblastoma growth rate back to the normal astrocytic growth rate.

2.2. Dynamic analysis of important regulators of ROS generation and antioxidant machinery

The systems-level understanding of metabolic reprogramming in glioblastoma highlighted the role of glutathione metabolism in guiding the preferred flux routes through different pathways. Intrigued by this finding, a detailed evaluation of the glutathione metabolism in glioblastoma was performed. Glutathione is a thiol that acts as an antioxidant to protect the cells from oxidative stress-related responses by scavenging reactive oxygen species (ROS). The antioxidant machinery maintains the redox balance of the cells. Motivated by the observations of the previous work, the effect of changes in redox and thiol status and the role of antioxidants in managing the oxidative balance of glioma cell is analyzed in **Chapter 4**, using a dynamic ordinary differential equation model. Note that the dynamics of the antioxidant system and related properties are subject to changes upon changing oxidative stress in and around the tumor cells. The study has been initiated with the antioxidant properties observable in glial cells and astrocytes and eventually modified with changes that result in gliomagenesis. The dynamics observed through the study hold true for all grades of glioma, including glioblastoma, and hence, the term glioma has been used for this study. Hydrogen peroxide (h_2o_2) was considered as the stable ROS, scavenged by the antioxidant glutathione (*gsh*) in normal glial cells and gliomas. A set of sequential changes in metabolic events that determines the transformation from a normal glial to glioma condition were introduced in the model by tweaking the kinetic parameters of important reactions. Three scenarios: normal glial, hypoxic, and glioma scenarios, were created, and the dynamics of ROS generation and antioxidant machinery were compared between the scenarios. Simulations demonstrating the changes in redox ratio represented by $nadph/nadp^+$ and thiol ratio represented by $gsh/gssg$ with respect to the h_2o_2 levels in normal glial, hypoxic, and glioma conditions were performed. The effect of other enzymes that are re-routed towards antioxidant production during gliomagenesis for the management of ROS levels was analyzed. Changes in the activity of enzymes that could augment pro-oxidant and anti-oxidant therapeutic strategies in glioma were proposed. The details of methods used in this study are provided in the following subsections.

2.2.1. Definition of model system

The model (**Figure 2.2**) captured the dynamic changes in the metabolism regulating the interplay of glutathione and ROS (oxygen radicals and hydrogen peroxide) in normal glial cells and in gliomas. The model is biologically motivated by the previous work in which a subset of metabolic reactions has been observed to be directed towards *gsh* production in gliomas (185). A re-routing of the glycolytic, pentose phosphate, glycine-serine, glutamate, and cystine pathway was observed to be directed towards glutathione metabolism from the analysis. The present model was designed considering these pathways in order to understand the dynamics of this re-routing and their effect in determining the role of glutathione during ROS scavenging. ROS, which typically shows a paradoxical behavior in tumor progression and proliferation, is represented by hydrogen peroxide (h_2o_2) in the model, and the model includes the ROS production machinery. Glutathione (*gsh*) is a tri-peptide composed of cystine (*cys*), glycine (*gly*), and glutamate (*glut*) is the prime anti-oxidant involved in ROS scavenging. The model comprised of reactions required for the production of the components of tri-peptide units of *gsh*. A part of glycolytic pathways along with the glycine-serine metabolism has been included, which directs the glucose metabolism towards glycine production. Cystine metabolism and a part of the glutamate metabolism were incorporated to represent the metabolism of these two components into the complex- glutamyl-cysteine (*glucys*). The *gsh-gssg* cycle consisting of glutathione peroxidase (GTHP) and glutathione oxidoreductase (GTHO) were included along with the ROS production machinery comprising of NADPH Oxidase (NOX) and Superoxide Dismutase (SOD). Although these enzymes are present as multiple isoforms, all the isoforms were considered as one, as the basic mechanism and function of the isoforms remain the same. Other ROS scavenging machineries like the peroxiredoxin/thioredoxin systems, catalases, etc., were not considered in the model for the time being, as we intended to focus on the dynamics of glutathione during ROS scavenging and in determining the paradox. The scavenging of h_2o_2 by other mechanisms was represented by the parameter $d_{h_2o_2}$ which was defined as the decay of intracellular hydrogen peroxide in other cellular processes. The model was limited to two compartments only: extracellular matrix (e) and cytosol (c), and intracellular compartments were not considered as the availability of compartment-wise parameters

creates a limitation, and the introduction of intracellular compartments for such a large ODE model would make it complex. The details of abbreviations used for all the reaction parameters specific to **Chapter 4** are provided in **APPENDIX B: Table B. 1** and the abbreviations used for the metabolite variables are elaborated in **APPENDIX B: Table B. 2**.

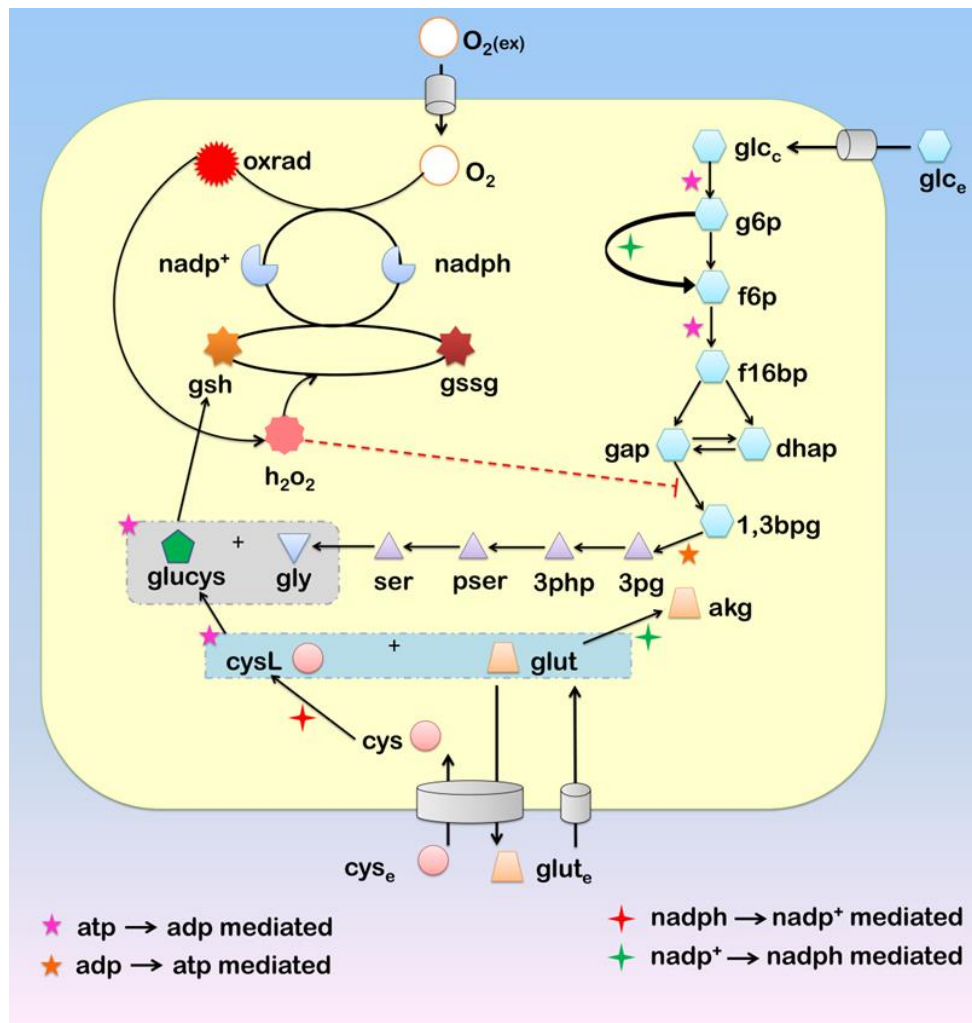


Figure 2.2: Diagrammatic representation of the metabolites belonging to different pathways directed towards the production of the glutathione along with the ROS generation machinery. The metabolites and the pathways to which they belong have been grouped into five groups viz.-(i) Central Carbon metabolism (glc_e , glc_c , $g6p$, $f6p$, $f16bp$, gap , $dhap$, $1,3bpg$, $3pg$, akg), (ii) Amino Acid metabolism ($3php$, $pser$, ser , gly , cys_e , cys , $cysL$, $glut_e$, $glut$), (iii) Thiol metabolism ($glucys$, gsh , $gssg$), (iv) h_2O_2 production and metabolism ($O_2(ex)$, O_2 , $oxrad$, h_2O_2) (v) Redox metabolism ($nadph$, $nadp^+$).

2.2.2. Model formulation

The model consisted of 35 metabolite variables involved in 25 reactions required for the production of *gsh* and ROS and for ROS scavenging. As per the available information of the reaction kinetics of these reactions, equations were formulated as forms of uni-uni, bi-bi, bi-uni, or ter-bi Michaelis-Menten kinetics. The equations were written in Cleland nomenclature. We considered initial reaction kinetics with first-order reaction rates. The values of all the parameters and initial values of all the parameters are provided in **APPENDIX B: Table B. 1 & Table B. 2.**

The general form of the initial kinetics of reaction equations considered in the model are given below:

$$\text{Uni-Uni / Uni-Bi: } \frac{V_m^R \cdot a}{K_m^R + a} \quad \dots \text{Eq. 3}$$

$$\text{Bi-Bi mechanism (Rapid equilibrium/ Ordered): } \frac{V_m^R \cdot (a \cdot b)}{(k_{i(a)}^R \cdot k_b^R + k_b^R \cdot a + k_a^R \cdot b + a \cdot b)} \quad \dots \text{Eq. 4}$$

$$\text{Partial Rapid Equilibrium Random Bi-Bi mechanism: } \frac{V_m^R \cdot (a \cdot b)}{(k_{i(a)}^R \cdot k_b^R + k_b^R \cdot a + a \cdot b)} \quad \dots \text{Eq. 5}$$

$$\text{Ordered Ter-Bi: } \frac{V_m^R \cdot (a \cdot b \cdot c)}{(k_{i(a)}^R \cdot k_{i(b)}^R \cdot k_c^R + k_{i(b)}^R \cdot k_c^R \cdot a + k_{i(a)}^R \cdot k_b^R \cdot c + k_c^R \cdot a \cdot b + k_b^R \cdot a \cdot c + k_a^R \cdot b \cdot c + a \cdot b \cdot c)} \quad \dots \text{Eq. 6}$$

Where R is the reaction, a , b and c represent the substrates, V_m^R represents the V_{max} of the reaction, k_i^R the rate constant for dissociation of enzyme-substrate complex and $k_a^R / k_b^R / k_c^R$ represent the rate constant for the association of a substrate with the enzyme.

The motivation behind considering a larger metabolic network for dynamic analysis comes from the observed metabolic re-routing of these pathways, which was directed towards glutathione production. In the model presented in **Chapter 4**, our main focus was to understand the strategies of h_2o_2 manipulation within cells and its effect on cell proliferation or death along with the effect of glutathione in scavenging h_2o_2 while considering the changes in the redox ratio represented by $nadph/nadp^+$ and thiol ratio represented by $gsh/gssg$.

2.2.3. Model equations

Initial kinetics with first-order reaction rates of the enzymatic reactions were considered for writing the equations. Since initial rates are usually measured in the presence of substrates only, there are no product terms present in the equations. Values of all the parameters are listed in **APPENDIX B: Table B. 1**, and initial values of all the variables are provided in **APPENDIX B: Table B. 2**.

Rate Equations

Glycolysis: Kinetic rate equations for the enzymes belonging to the first half of glycolysis, from where it branches to the glycine-serine pathway, were considered in the model. The kinetics is mostly represented by uni-uni and bi-bi mechanisms. The equation forms for most of the reactions were similar except for GAPDH and PGK. Competitive inhibition of GAPDH by h_2o_2 was considered. The rate kinetics of PGK follows a partial rapid equilibrium random bi-bi steady-state kinetics (186) where the binding of $1,3bpg$ with the enzyme is transient and hence was not considered in the denominator following the convention of partial rapid equilibrium random bi-bi mechanism.

$$v_{GLCT} = \frac{V_m^{GLCT} \cdot glc_e}{k_{glc_e}^{GLCT} + glc_e} \quad \dots \text{Eq. 7}$$

$$v_{HK} = \frac{V_m^{HK} \cdot (atp \cdot glc_c)}{(k_{i(atp)}^{HK} \cdot k_{glc_c}^{HK} + k_{glc_c}^{HK} \cdot atp + k_{atp}^{HK} \cdot glc_c + atp \cdot glc_c)} \quad \dots \text{Eq. 8}$$

$$v_{PGI} = \frac{V_m^{PGI} \cdot g6p}{k_{g6p}^{PGI} + g6p} \quad \dots \text{Eq. 9}$$

$$v_{PFK} = \frac{V_m^{PFK} \cdot (atp \cdot f6p)}{(k_{i(atp)}^{PFK} \cdot k_{f6p}^{PFK} + k_{f6p}^{PFK} \cdot atp + k_{atp}^{PFK} \cdot f6p + atp \cdot f6p)} \quad \dots \text{Eq. 10}$$

$$v_{FBA} = \frac{V_m^{FBA} \cdot f16bp}{k_{f16bp}^{FBA} + f16bp} \quad \dots \text{Eq. 11}$$

$$v_{TPI} = \frac{V_m^{TPI} \cdot dhap}{k_{dhap}^{TPI} + dhap} \quad \dots \text{Eq. 12}$$

$$v_{GAPDH} = \frac{V_m^{GAPDH} \cdot (gap.nad)}{(k_{i(gap)}^{GAPDH} \cdot k_{nad}^{GAPDH} + k_{gap}^{GAPDH} \cdot nad) \cdot \left(1 + \frac{h_2o_2}{k_{ii(h_2o_2)}^{GAPDH}}\right) + k_{nad}^{GAPDH} \cdot gap + gap.nad} \quad \dots \text{Eq. 13}$$

$$v_{PGK} = \frac{V_m^{PGK} \cdot (1,3bpg.adp)}{(k_{i(1,3bpg)}^{PGK} \cdot k_{adp}^{PGK} + k_{adp}^{PGK} \cdot 1,3bpg + 1,3bpg.adp)} \quad \dots \text{Eq. 14}$$

Pentose Phosphate Pathway: The pentose phosphate pathway was represented only partially by considering the enzymatic reaction G6PDH. The assumption here was that the final products of the pathway, i.e., fructose and glyceraldehyde 3-phosphate re-enter the glycolytic pathway. The whole pathway was reduced to a single equation, and the parameter values for the equation were determined by parameter estimation technique so as to represent the real biological situation focussing on the oxidant-antioxidant balance. Competitive inhibition of the pathway by *atp* was considered.

$$v_{G6PDH} = \frac{V_m^{G6PDH} \cdot (g6p.nadp)}{(k_{i(g6p)}^{G6PDH} \cdot k_{nadp}^{G6PDH} + k_{g6p}^{G6PDH} \cdot nadp) \cdot \left(1 + \frac{atp}{k_{ii(atp)}^{G6PDH}}\right) + k_{nadp}^{G6PDH} \cdot g6p + g6p.nadp} \quad \dots \text{Eq. 15}$$

Glutamate Metabolism: A part of the glutamate metabolism was considered, which included the transport of glutamate from the extracellular matrix to the cytoplasm where a part of it is utilized in the glutathione metabolism, and a part is converted into *akg* production by the activity of glutamate dehydrogenase, and the rest is utilized in other cellular processes.

$$v_{GLUTEX} = \frac{V_m^{GLUTEX} \cdot glut_e}{k_m^{GLUTEX} + glut_e} \quad \dots \text{Eq. 16}$$

$$v_{GLUD} = \frac{V_m^{GLUD} \cdot (glut.nadp)}{(k_{i(glut)}^{GLUD} \cdot k_{nadp}^{GLUD} + k_{nadp}^{GLUD} \cdot glut + k_{glut}^{GLUD} \cdot nadp + glut.nadp)} \quad \dots \text{Eq. 17}$$

Glutathione Metabolism: This pathway included the involvement of two important enzymes, glutamyl-cysteine ligase, and glutathione synthase. The former catalyzes the formation of glutamyl-cysteine, which is converted into the tripeptide complex of glutathione in the later reaction. Both the reactions involve the utilization of *atp* for the conversion and hence represented by three metabolites ordered ter-bi equation form.

$$v_{GCL} = \frac{V_m^{GCL} \cdot (atp.glut.cysL)}{(k_{i(atp)}^{GCL} \cdot k_{i(glut)}^{GCL} \cdot k_{cysL}^{GCL} + k_{i(glut)}^{GCL} \cdot k_{cysL}^{GCL} \cdot atp + k_{i(atp)}^{GCL} \cdot k_{glut}^{GCL} \cdot cysL + k_{cysL}^{GCL} \cdot atp \cdot glut + k_{glut}^{GCL} \cdot atp \cdot cysL + k_{atp}^{GCL} \cdot glut \cdot cysL + atp \cdot glut \cdot cysL)} \dots \text{Eq. 18}$$

$$v_{GS} = \frac{V_m^{GS} \cdot (atp.gly.glucys)}{(k_{i(atp)}^{GS} \cdot k_{i(gly)}^{GS} \cdot k_{glucys}^{GS} + k_{i(gly)}^{GS} \cdot k_{glucys}^{GS} \cdot atp + k_{i(atp)}^{GS} \cdot k_{gly}^{GS} \cdot glucys + k_{glucys}^{GS} \cdot atp \cdot gly + k_{gly}^{GS} \cdot atp \cdot glucys + k_{atp}^{GS} \cdot gly \cdot glucys + atp \cdot gly \cdot glucys)} \dots \text{Eq. 19}$$

Glycine Serine Metabolism: All the enzymatic reactions involved in the production of serine from *3pg* and conversion of serine to glycine were considered. Along with it, the exchange of glycine from the extracellular matrix was also considered.

$$v_{GLYex} = \frac{V_m^{GLYex} \cdot gly_e}{k_m^{GLYex} + gly_e} \dots \text{Eq. 20}$$

$$v_{PGCDH} = \frac{V_m^{PGCDH} \cdot (3pg.nad)}{(k_{i(3pg)}^{PGCDH} \cdot k_{nad}^{PGCDH} + k_{nad}^{PGCDH} \cdot 3pg + k_{3pg}^{PGCDH} \cdot nad + 3pg \cdot nad)} \dots \text{Eq. 21}$$

$$v_{PSP} = \frac{V_m^{PSP} \cdot pser}{k_m^{PSP} + pser} \dots \text{Eq. 22}$$

$$v_{GHMT} = \frac{V_m^{GHMT} \cdot (ser.thf)}{(k_{i(ser)}^{GHMT} \cdot k_{thf}^{GHMT} + k_{thf}^{GHMT} \cdot ser + k_{ser}^{GHMT} \cdot thf + ser \cdot thf)} \dots \text{Eq. 23}$$

$$v_{PST} = \frac{V_m^{PST} \cdot (glut.3php)}{(k_{i(glut)}^{PST} \cdot k_{3php}^{PST} + k_{3php}^{PST} \cdot glut + k_{glut}^{PST} \cdot 3php + glut \cdot 3php)} \dots \text{Eq. 24}$$

Cysteine metabolism: This was comprised of the transport of cystine from the extracellular matrix via the glutamate-cystine antiporter (xCT) and the conversion of cystine into cysteine, which is used as a component for building the tripeptide complex of glutathione.

$$v_{xCT} = \frac{V_m^{xCT} \cdot (cys_e \cdot glut)}{(k_i^{xCT}(cys_e) \cdot k_{glut}^{xCT} + k_{glut}^{xCT} \cdot cys_e + k_{cys_e}^{xCT} \cdot glut + cys_e \cdot glut)} \quad \dots \text{Eq. 25}$$

$$v_{CR} = \frac{V_m^{CR} \cdot (cys \cdot glut)}{(k_i^{CR}(cys) \cdot k_{nadph}^{CR} + k_{nadph}^{CR} \cdot cys + k_{cys}^{CR} \cdot nadph + cys \cdot nadph)} \quad \dots \text{Eq. 26}$$

GSH-GSSG cycle: This was represented by two enzymes, glutathione peroxidase, which catalyzes the conversion of *gsh* into *gssg* while neutralizing h_2o_2 to h_2o , and glutathione oxidoreductase, which replenishes *gsh* back into the system by converting *gssg* to *gsh* with the involvement of *nadph*. The equations for the reactions were formulated using ordered bi-bi mechanism.

$$v_{GTHP} = \frac{V_m^{GTHP} \cdot (h_2o_2 \cdot gsh)}{(k_i^{GTHP}(h_2o_2) \cdot k_{gsh}^{GTHP} + k_{gsh}^{GTHP} \cdot h_2o_2 + k_{h_2o_2}^{GTHP} \cdot gsh + h_2o_2 \cdot gsh)} \quad \dots \text{Eq. 27}$$

$$v_{GTHO} = \frac{V_m^{GTHO} \cdot (gssg \cdot nadph)}{(k_i^{GTHO}(gssg) \cdot k_{nadph}^{GTHO} + k_{nadph}^{GTHO} \cdot gssg + k_{gssg}^{GTHO} \cdot nadph + gssg \cdot nadph)} \quad \dots \text{Eq. 28}$$

ROS production machinery: This was represented by two enzymatic reactions: NADPH oxidase (NOX) that converts oxygen into oxygen free radicals, and superoxide dismutase (SOD) that converts the free radicals into h_2o_2 . The equation for the former reaction was represented by the ordered bi-bi mechanism and the latter by the uni-uni mechanism.

$$v_{NOX} = \frac{V_m^{NOX} \cdot (nadph \cdot O_2)}{(k_i^{NOX}(nadph) \cdot k_{O_2}^{NOX} + k_{O_2}^{NOX} \cdot nadph + k_{nadph}^{NOX} \cdot O_2 + nadph \cdot O_2)} \quad \dots \text{Eq. 29}$$

$$v_{SOD} = \frac{V_m^{SOD} \cdot oxrad}{k_{oxrad}^{SOD} + oxrad} \quad \dots \text{Eq. 30}$$

Oxygen Uptake: The uptake of oxygen was represented using simple Michaelis-Menten equation form. Here V_{max} represents the maximum rate of uptake of oxygen by the cell, and k_m represents the affinity of the cell for external oxygen. The lower the value of k_m , the higher is the affinity for external oxygen.

$$v_{O_2} = \frac{V_m^{O_2} \cdot O_2(ex)}{k_m^{O_2} + O_2(ex)} \quad \dots \text{Eq. 31}$$

Differential Equations

The differential equations for each of the 35 metabolite variables were formulated by considering reactions and parameters in which they were either produced or consumed.

$$\frac{d(glc_e)}{dt} = l_g - v_{GLCT} - d_g[glc_e] \quad \dots \text{Eq. 32}$$

$$\frac{d(glc_c)}{dt} = v_{GLCT} - v_{HK} \quad \dots \text{Eq. 33}$$

$$\frac{d(g6p)}{dt} = v_{HK} - v_{PGI} - v_{G6PDH} \quad \dots \text{Eq. 34}$$

$$\frac{d(f6p)}{dt} = v_{PGI} + v_{G6PDH} - v_{PFK} \quad \dots \text{Eq. 35}$$

$$\frac{d(f16bp)}{dt} = v_{PFK} - v_{FBA} \quad \dots \text{Eq. 36}$$

$$\frac{d(gap)}{dt} = v_{FBA} + v_{G6PDH} + v_{TPI} + v_{GAPDH} \quad \dots \text{Eq. 37}$$

$$\frac{d(dhap)}{dt} = v_{FBA} - v_{TPI} \quad \dots \text{Eq. 38}$$

$$\frac{d(1,3bpg)}{dt} = v_{GAPDH} - v_{PGK} \quad \dots \text{Eq. 39}$$

$$\frac{d(3pg)}{dt} = v_{PGK} - v_{PGCDH} - d_{3pg}[3pg] \quad \dots \text{Eq. 40}$$

$$\frac{d(atp)}{dt} = l_{atp} + v_{PGK} - v_{HK} - v_{PFK} - v_{GCL} - v_{GS} - d_{atp}[atp] \quad \dots \text{Eq. 41}$$

$$\frac{d(adp)}{dt} = l_{atp} + v_{HK} + v_{PFK} + v_{GCL} + v_{GS} - v_{PGK} - d_{adp}[adp] \quad \dots \text{Eq. 42}$$

$$\frac{d(\text{nadph})}{dt} = l_{\text{nadph}} + v_{\text{G6PDH}} + v_{\text{GLUD}} - v_{\text{GTHO}} - v_{\text{NOX}} - v_{\text{CR}} - d_{\text{nadph}}[\text{nadph}] \quad \dots\text{Eq. 43}$$

$$\frac{d(\text{nadp})}{dt} = l_{\text{nadp}} + v_{\text{GTHO}} + v_{\text{NOX}} + v_{\text{CR}} - v_{\text{G6PDH}} - v_{\text{GLUD}} - d_{\text{nadp}}[\text{nadp}] \quad \dots\text{Eq. 44}$$

$$\frac{d(\text{nadh})}{dt} = l_{\text{nadh}} + v_{\text{GAPDH}} + v_{\text{PGCDH}} - d_{\text{nadh}}[\text{nadh}] \quad \dots\text{Eq. 45}$$

$$\frac{d(\text{nad})}{dt} = l_{\text{nad}} - v_{\text{GAPDH}} - v_{\text{PGCDH}} - d_{\text{nad}}[\text{nad}] \quad \dots\text{Eq. 46}$$

$$\frac{d(\text{3php})}{dt} = v_{\text{PGCDH}} - v_{\text{PST}} \quad \dots\text{Eq. 47}$$

$$\frac{d(\text{glut})}{dt} = v_{\text{GLUTEX}} - v_{\text{GCL}} - v_{\text{PST}} - v_{\text{xCT}} - v_{\text{GLUD}} \quad \dots\text{Eq. 48}$$

$$\frac{d(\text{akg})}{dt} = v_{\text{PST}} + v_{\text{GLUD}} - d_{\text{akg}}[\text{akg}] \quad \dots\text{Eq. 49}$$

$$\frac{d(\text{pser})}{dt} = v_{\text{PST}} - v_{\text{PSP}} \quad \dots\text{Eq. 50}$$

$$\frac{d(\text{ser})}{dt} = v_{\text{PSP}} - v_{\text{GHMT}} \quad \dots\text{Eq. 51}$$

$$\frac{d(\text{thf})}{dt} = l_{\text{thf}} - v_{\text{GHMT}} - d_{\text{thf}}[\text{thf}] \quad \dots\text{Eq. 52}$$

$$\frac{d(\text{mlthf})}{dt} = l_{\text{mlthf}} + v_{\text{GHMT}} - d_{\text{mlthf}}[\text{mlthf}] \quad \dots\text{Eq. 53}$$

$$\frac{d(\text{gly})}{dt} = v_{\text{GLYex}} + v_{\text{GHMT}} - v_{\text{GS}} - d_{\text{gly}}[\text{gly}] \quad \dots\text{Eq. 54}$$

$$\frac{d(\text{cysL})}{dt} = v_{\text{CR}} - v_{\text{GCL}} \quad \dots\text{Eq. 55}$$

$$\frac{d(\text{glucys})}{dt} = v_{\text{GCL}} - v_{\text{GS}} - d_{\text{glucys}}[\text{glucys}] \quad \dots\text{Eq. 56}$$

$$\frac{d(\text{gsh})}{dt} = v_{\text{GS}} + v_{\text{GTHO}} - v_{\text{GTHP}} - d_{\text{gsh}}[\text{gsh}] \quad \dots\text{Eq. 57}$$

$$\frac{d(\text{cys})}{dt} = v_{\text{xCT}} - v_{\text{CR}} \quad \dots\text{Eq. 58}$$

$$\frac{d(h_2o_2)}{dt} = v_{SOD} - v_{GTHP} - d_{h_2o_2}[h_2o_2] \quad \dots\text{Eq. 59}$$

$$\frac{d(gssg)}{dt} = v_{GTHP} - v_{GTHO} - d_{gssg}[gssg] \quad \dots\text{Eq. 60}$$

$$\frac{d(glut_e)}{dt} = l_{gl} + v_{xCT} - v_{GLUTEX} - d_{gl}[glut_e] \quad \dots\text{Eq. 61}$$

$$\frac{d(cys_e)}{dt} = l_{cy} - v_{xCT} - d_{cy}[cys_e] \quad \dots\text{Eq. 62}$$

$$\frac{d(O_2(ex))}{dt} = L_{oxy} - v_{O_2} - d_{oxy}[O_2(ex)] \quad \dots\text{Eq. 63}$$

$$\frac{d(O_2)}{dt} = v_{O_2} + v_{SOD} - v_{NOX} - d_{in}[O_2] \quad \dots\text{Eq. 64}$$

$$\frac{d(oxrad)}{dt} = v_{NOX} - v_{SOD} \quad \dots\text{Eq. 65}$$

$$\frac{d(gly_e)}{dt} = l_{gly_e} - v_{GLYex} - d_{gly_e}[gly_e] \quad \dots\text{Eq. 66}$$

2.2.4. Positivity and Boundedness

Positivity: The system of equations described in the previous section (Eq. 32-Eq. 66) can be analyzed with the initial conditions (APPENDIX B: Table B. 2) defined in the thirty-five-dimensional variable space

$$R_+^{35} = [(glc_e, glc_c, g6p, f6p, f16bp, gap, dhap, 1,3bpg, 3pg, atp, adp, nadph, nadp, nadh, nad, 3php, glut, akg, pser, ser, thf, mlthf, gly, cysL, glucys, gsh, cys, h_2o_2, gssg, glut_e, cys_e, O_2(ex), oxrad, gly_e) \in \mathfrak{R}^{35} | (glc_e, glc_c, g6p, f6p, f16bp, gap, dhap, 1,3bpg, 3pg, atp, adp, nadph, nadp, nadh, nad, 3php, glut, akg, pser, ser, thf, mlthf, gly, cysL, glucys, gsh, cys, h_2o_2, gssg, glut_e, cys_e, O_2(ex), oxrad, gly_e) \geq 0]$$

It can be proven that all the solutions of the system in R_+^{35} remain in R_+^{35} . Hence, R_+^{35} is positively invariant, and it is appropriate to consider solutions only in R_+^{35} . The usual existence, uniqueness, and continuation of the results hold for the system-defined within this region. From our numerical simulations, we have observed the existence of positive solutions. The solution set we obtain for the set of ODEs represents the effective concentrations of the metabolites considered in the model at different time points during

the normal, hypoxia, and glioma development. The steady-state attained by all the variables of the model is a part of this positive solution space.

We observe that the right-hand side of **Eq. 32-Eq. 66** are smooth functions of the variables:

($glc_e, glc_c, g6p, f6p, f16bp, gap, dhap, 1,3bpg, 3pg, atp, adp, nadph, nadp, nadh, nad, 3php, glut, akp, pser, ser, thf, mlthf, gly, cysL, glucys, gsh, cys, h_2o_2, gssg, glut_e, cys_e, O_2(ex), oxrad, gly_e$)

Since all the parameters are non-negative, the local existence and uniqueness properties hold in R_+^{35} , if the following necessary conditions are satisfied,

1. $l_g > d_g[glc_e]$
2. $l_{atp} > d_{atp}[atp]$
3. $l_{adp} > d_{adp}[adp]$
4. $l_{nadph} > d_{nadph}[nadph]$
5. $l_{nadp} > d_{nadp}[nadp]$
6. $l_{nadh} > d_{nadh}[nadh]$
7. $l_{nad} > d_{nad}[nad]$
8. $l_{thf} > d_{thf}[thf]$
9. $l_{mlthf} > d_{mlthf}[mlthf]$
10. $v_{SOD} > d_{h_2o_2}[h_2o_2]$
11. $l_{gl} > d_{gl}[glut_e]$
12. $l_{cy} > d_{cy}[cys_e]$
13. $L_{oxy} > d_{oxy}[O_2(ex)]$
14. $l_{gly_e} > d_{gly_e}[gly_e]$

Boundedness:

Let, $W_1 = [glc_e] + [glc_c] + [g6p] + [f6p] + [f16bp] + [gap] + [dhap] + [1,3bpg] + [3pg] + [atp] + [adp] + [nadph] + [nadp] + [nadh] + [nad] + [3php] + [glut] +$

$$[akg] + [pser] + [ser] + [thf] + [mlthf] + [gly] + [cysL] + [glucys] + [gsh] + [cys] + [h_2o_2] + [gssg] + [glut_e] + [cys_e] + [O_2(ex)] + [oxrad] + [gly_e]$$

Then taking time derivative and using the above equation, we have

$$\frac{dW_1}{dt} \leq l_{wl} + v_{G6PDH} + v_{FBA} + v_{SOD} - v_{GCL} - v_{GS} - v_{GTHP} - d_{wl}W_1, \text{ where}$$

$$d_{wl} = \min \{d_g + d_{3pg} + d_{atp} + d_{adp} + d_{nadph} + d_{nadp} + d_{nadh} + d_{nad} + d_{akg} + d_{thf} + d_{mlthf} + d_{gly} + d_{glucys} + d_{gsh} + d_{h_2o_2} + d_{gssg} + d_{gl} + d_{cy} + d_{oxy} + d_{in} + d_{gly_e}\}, \text{ and}$$

$$l_{wl} = \max \{l_g + l_{atp} + l_{nadph} + l_{nadp} + l_{nad} + l_{thf} + l_{mlthf} + l_{gl} + l_{cy} + l_{oxy} + l_{gly_e}\}$$

Let $L_p = V_m^{G6PDH} + V_m^{FBA} + V_m^{SOD}$ and $L_n = V_m^{GCL} + V_m^{GS} + V_m^{GTHP}$, where

$v_{G6PDH} + v_{FBA} + v_{SOD} \leq L_p$ since $v_{G6PDH} \leq V_m^{G6PDH}$ and so on and $v_{GCL} + v_{GS} + v_{GTHP} \leq L_n$ since $v_{GCL} \leq V_m^{GCL}$ and so on. $L_n \leq L_p$, given the values of V_m of G6PDH, FBA, SOD, GCL, GS, and GTHP.

$$\Rightarrow \frac{dW_1}{dt} \leq l_{wl} + L_p - d_{wl}W_1$$

$$\Rightarrow \frac{dW_1}{dt} + d_{wl}W_1 \leq l_{wl} + L_p$$

$$\Rightarrow \frac{dW_1}{dt} + d_{wl}W_1 \leq \theta_1 \text{ where } \theta_1 = l_{wl} + L_p$$

From the theory of differential inequalities, we then obtain

$$0 < W_1([glc_e] + [glc_c] + [g6p] + [f6p] + [f16bp] + [gap] + [dhap] + [1,3bpg] + [3pg] + [atp] + [adp] + [nadph] + [nadp] + [nadh] + [nad] + [3php] + [glut] + [akg] + [pser] + [ser] + [thf] + [mlthf] + [gly] + [cysL] + [glucys] + [gsh] + [cys] + [h_2o_2] + [gssg] + [glut_e] + [cys_e] + [O_2(ex)] + [oxrad] + [gly_e]) < \frac{\theta_1}{d_{wl}} (1 - e^{-d_{wl}t}) + W_1([glc_e](0) + [glc_c](0) + [g6p](0) + [f6p](0) + [f16bp](0) + [gap](0) + [dhap](0) + [1,3bpg](0) + [3pg](0) + [atp](0) + [adp](0) + [nadph](0) + [nadp](0) + [nadh](0) + [nad](0) + [3php](0) + [glut](0) + [akg](0) + [pser](0) + [ser](0) + [thf](0) + [mlthf](0) + [gly](0) + [cysL](0) + [glucys](0) + [gsh](0) + [cys](0) + [h_2o_2](0) + [gssg](0) + [glut_e](0) + [cys_e](0) + [O_2(ex)](0) + [oxrad](0) + [gly_e](0)). e^{-d_{wl}t}$$

and for $t \rightarrow \infty$, it follows $0 < W_1 < \frac{\theta_1}{d_{wl}}$, hence all solutions of $W_1(t)$ that initiates at

$W_1(0) \in R^{35}$ are confined to the region: $G_1 = \{(W_1)^T \in R^{35}: W_1 = \frac{\theta_1}{d_{wl}} + \varepsilon_1 \text{ for any } \varepsilon_1 > 0$ for all $t \geq T^*$ where T^* depends on the initial value $(W_1(0))^T$.

2.2.5. Numerical simulation and model calibration

The system of differential equations (**Eq. 32 - Eq. 69**) was simulated using ODE15s in MATLAB 2017a. Calibration of the model was performed upon available experiment data on the change in *gsh* over a period of time in retinal Muller glial cells under normal and amino acid supplemented scenarios (187). This was used to create the normal glial scenario, to which changes were introduced to create the hypoxic and glioma scenario. The basal parameters and initial values to the variables were considered within a biologically feasible range as obtained through literature search and are provided in **APPENDIX B: Table B. 1 & Table B. 2**. Few of the parameters and initial values were assumed within biologically feasible range as had been reported in the literature. A set of 23 parameters remained unknown, which were determined using the parameter estimation technique. The model was ensured to reach a stable steady-state with the basal parameter states and initial values. Also, the simulations performed using the above parameters showed that at steady states, the basal extracellular glucose concentration and intracellular *gsh* concentration along with *nadph/nadp⁺* and *atp/adp* ratios resemble true biological concentrations as reported in the literature.

2.2.6. Parameter estimation

Parameter estimation of the 23 unknown parameters was performed using the Delayed Rejection Adaptive Metropolis (DRAM) algorithm of Markov Chain Monte Carlo (MCMC) Toolbox (188) in MATLAB 2017a. The algorithm generates posterior distribution calibrated using the sample path of the MCMC chain to estimate unknown parameters for a known experimental result. In the ODE model, parameter estimation was performed using experimental data on the change in *gsh* in retinal Muller glial cells (187), as has been specified in the previous section (**Figure 2.3A**). Distributions plots and trace plots of all the 23 estimated parameters have been provided in **Figure 2.4**. Values for the parameters V_m^{GLUTEX} and k_m^{GLUTEX} were estimated using available data on glutamate exchange in astrocytes (**Figure 2.3B**) (189).

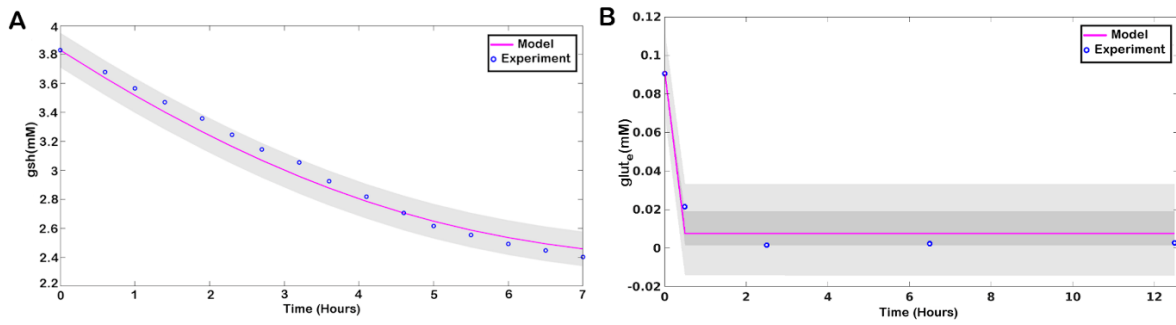


Figure 2.3: Predictive plot demonstration of model fitting with experimental data. (A) for reduced glutathione (gsh) and (B) for extracellular glutamate (glute). The blue circles represent the data points obtained from experiments, and the pink line represents the result obtained through model simulation.

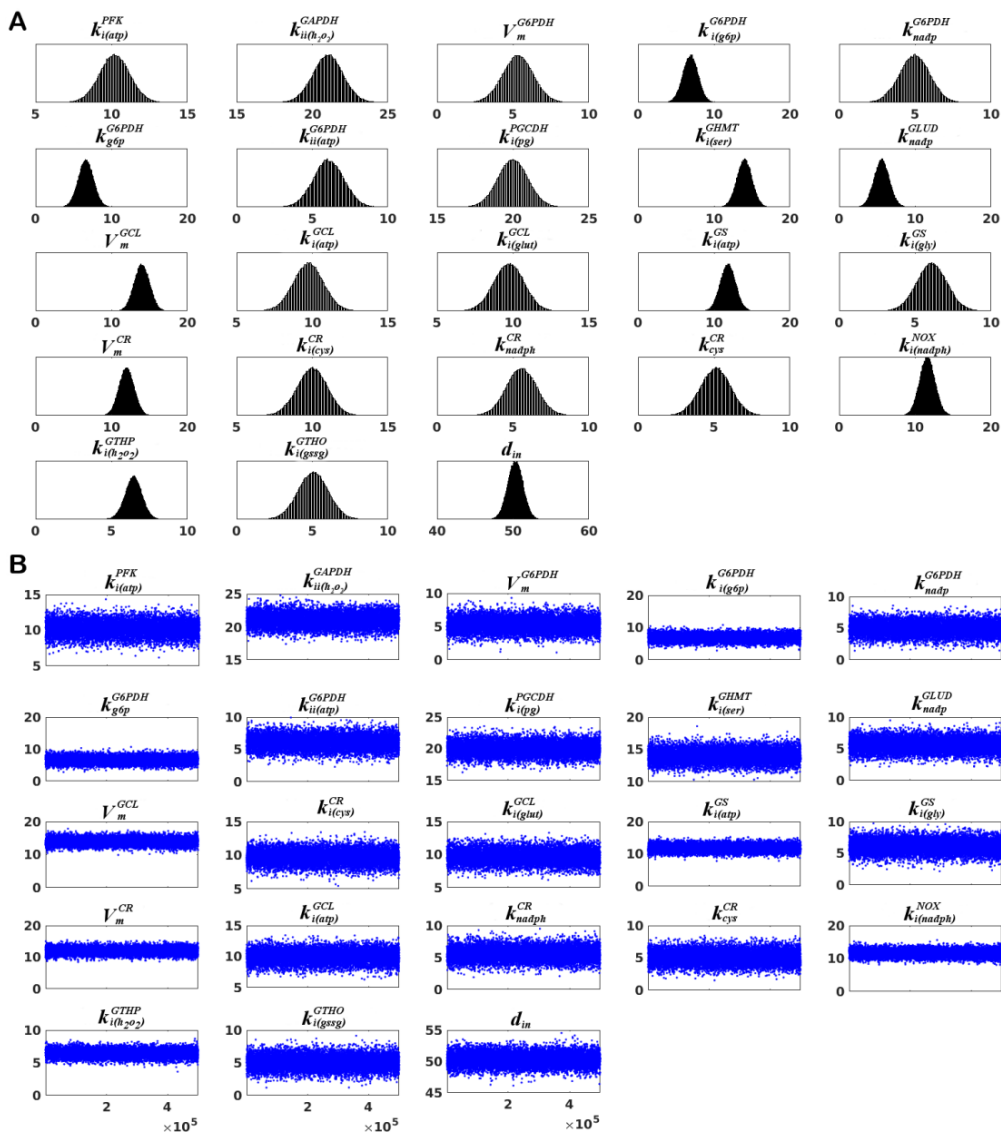


Figure 2.4: Parameter distribution and trace plot of estimated parameters. (A) Parameter distribution plot of the estimated parameters within the minimum and maximum range provided for the simulations, (B) Trace plots of the estimated parameters generated after 5 lakh chains of MCMC DRAM.

2.2.7. Sensitivity analysis

Extended Fourier Amplified Sensitivity Test (eFAST) algorithm was used for identifying sensitive parameters to the system (190). The algorithm makes use of the variance decomposition method to predict the sensitivity of parameters in a nonlinear non-monotonic system. The analysis was carried out using the whole set of parameters [k=123]. 150 samples were chosen per search curve, and the resampling of the search curves was carried out five times [$N_S = 150$, $N_R = 5$]. Hence, the total number of model simulations was $N=(k+1)*N_S*N_R=93000$. First-order sensitivity index S_i , and total order sensitivity index, S_{Ti} , were calculated for different transient time points and steady states of *gsh*, *gssg*, h_2o_2 , and *oxrad*. Plots of Sensitivity indices (S_i) of parameters with a p-value < 0.05 for *gsh* (reduced glutathione), *gssg* (oxidized glutathione), h_2o_2 (hydrogen peroxide), and *oxrad* (oxygen radical) are provided in **Figure 2.5**. The analysis was repeated for high intracellular oxygen demand (hypoxic) and glioma conditions to check the changes in sensitivity of parameters at different conditions.

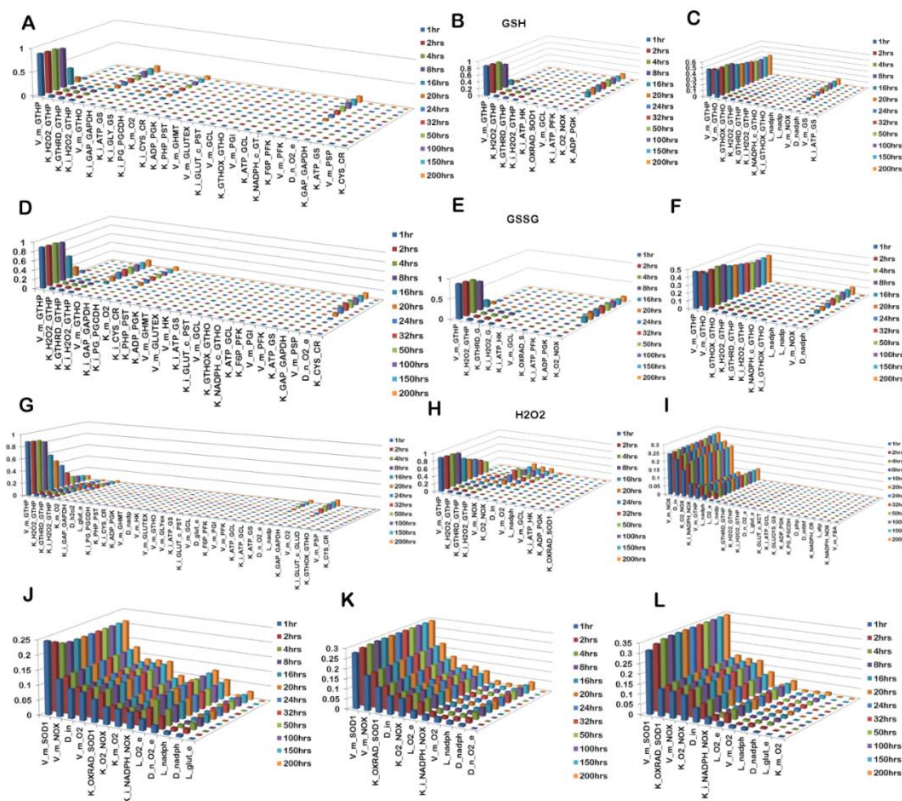


Figure 2.5: Plots of sensitive parameters for different variables obtained for the three scenarios- normal, hypoxia, and glioma respectively: (A-C) *gsh*; (D-F) *gssg*; (G-I) h_2o_2 ; (J-L) *oxrad*

2.2.8. Parameter variation analysis

Parameter variation analyses for a single parameter and two parameters were performed to understand the effect of sensitive parameters on the variables that govern the dynamics of oxidant-antioxidant balance. Parameters were varied over a feasible biological range at any given time point. For most of the instances, changes in the enzyme concentrations were introduced by varying the V_{max} of the enzyme, as V_{max} is determined by the enzyme concentration and substrate availability. For two-parameter variation analysis, two parameters were simultaneously varied, and the results were plotted as 3D surface plots to show their effect on the respective variable.

2.2.9. Changing oxygen demand: creation of hypoxia scenario

The oxygen uptake by cells was approximated by Michaelis-Menten kinetics (**Eq. 31**) in the model where V_{max} represents the rate of oxygen uptake by the cell and K_m represents the affinity of the cell for extracellular oxygen. Low K_m signifies a high affinity for oxygen. The value of K_m for extracellular oxygen was varied to create low to high intracellular oxygen demand. A low K_m value created high oxygen demand within the cell which was used to represent a hypoxic condition in the extracellular environment.

To create the hypoxic scenario, oxygen uptake rates of the cell was enhanced by reducing the K_m of Oxygen ($k_m^{O_2}$). The initial K_m value for oxygen uptake was 164mM for the normal condition. This was reduced down to a very low value of 1mM, which signifies a high affinity for the substrate, which in the present model is the external oxygen. The hypoxic condition that resulted was a consequence of the rapid uptake of oxygen by the cell. Hence, in the model, hypoxia was represented as a consequence of the high oxygen demand of the cell.

2.2.10. Creation of glioma scenario

In order to create a glioma-like scenario in the model, changes were introduced in the values of multiple parameters to induce the change in the activities of the respective enzymes. The selection of these parameters was based on literature evidence of their malfunctioning in gliomas and also from the analysis of sensitive parameters. Differential

regulation of the enzymes NADPH oxidase (NOX) (191, 192), glutathione peroxidase (GTHP) (193, 194), and glutathione oxidoreductase (GTHO) (195) were previously reported in the literature. The sensitivity analysis further added to the understanding of the parameters that govern these changes. These include V_m^{NOX} , V_m^{GTHO} , V_m^{GTHP} and $k_m^{O_2}$ where $k_m^{O_2}$ has been considered to alter the oxygen demand of the cell, thereby representing a hypoxic scenario as described in the previous section. An increase in h_2O_2 concentration was considered as a signature to ensure that the model represents a glioma-like situation (196, 197).

2.2.11. Identification of combination targets for ROS manipulation

The parameter sensitivity of the three different model conditions: normal glial, hypoxic, and glioma, were reassessed. Parameters exclusive for the h_2O_2 in the glioma scenario were obtained. 11 parameters including were found exclusive for the glioma scenario: d_{mlthf} , k_{3pg}^{PGCDH} , L_{oxy} , d_{php} , k_{glut}^{xCT} , $k_{i(nadph)}^{NOX}$, k_{nadph}^{NOX} , V_m^{FBA} , k_{glucys}^{GS} , k_{nadph}^{CR} , l_{atp} . A combination of 2 parameters from the 11 parameters was varied, and the effect of their variation on the h_2O_2 , $gsh/gssg$, and $nadph/nadp^+$ profiles were computed. The values of the parameters were varied between a wide range (0.0001 to 100 units), and the observed changes were proposed to augment the pro-oxidative or anti-oxidative therapeutic approach.

2.3. Network analysis of microRNA regulated metabolic genes, pathway and cellular phenotypes

Genomic insults are the primary cause of evolving landscape of cellular metabolism during tumorigenesis that build the foundation for phenotype switching in glioblastoma. Functional genomic studies correlating mutations, epigenetic modifications, and transcriptional regulations that affect metabolic genes with the observed phenotypic changes have contributed much to our understanding of the adaptive phenotypes exhibited by glioblastoma (**Section 1.5.3**). In the past decade, growing evidence of the microRNA-dependent regulation of metabolism has gained an appreciation and is being explored in cancer metabolism. MicroRNAs are potent post-transcriptional regulators of

gene expression that participate in almost all cellular processes. Parallel investigation of microRNA regulation of cellular metabolism and metabolic control on cellular phenotypes can provide the opportunity to identify miRNA targets that can regulate oncogenic phenotypes by taking control of cellular metabolism. Hence, the next work in **Chapter 5** is focussed on the post-transcriptional regulation imposed by microRNAs on the metabolic genes and their role in regulating cellular phenotypes in glioblastoma. Formal analyses of miRNA regulated metabolism were done using a graph-theoretical approach. Graph networks of miRNA - metabolic target gene and miRNA - metabolic pathway created using patient-derived differential expression data of miRNAs and metabolic genes were considered for the study. Functional annotation was done to identify the most frequently regulated metabolic pathways. Bipartite projection and backbone analysis were performed to identify important miRNAs that regulate important metabolism in glioblastoma. MiRNA - metabolic gene subnetworks were identified for various cellular phenotypes exhibited by glioblastoma. The identified subnetworks were further used to predict target combinations of miRNAs that could regulate the oncogenic phenotypes. MiRNA targets predicted were proposed as testable targets for *in-vivo* and *in-vitro* studies to test their feasibility as miRNA-based therapeutics in glioblastoma.

2.3.1. MicroRNA expression dataset

MicroRNA (miRNA) Expression data from Glioblastoma Multiforme (GBM) patient tumor samples and healthy brain tissue (partly from GBM patients) were obtained from the GEO dataset GSE90603 (198). The dataset was based on the GPL21572 (Affymetrix Multispecies miRNA-4 Array) platform and contained 16 fresh-frozen GBM samples, 3 fresh frozen healthy brain tissue samples from healthy volunteers, and 4 samples from healthy brain tissues of GBM patients. Differentially expressed miRNAs obtained from the dataset were used for further analyses. A flow diagram of the protocol followed for the present work has been provided in **Figure 2.6**.

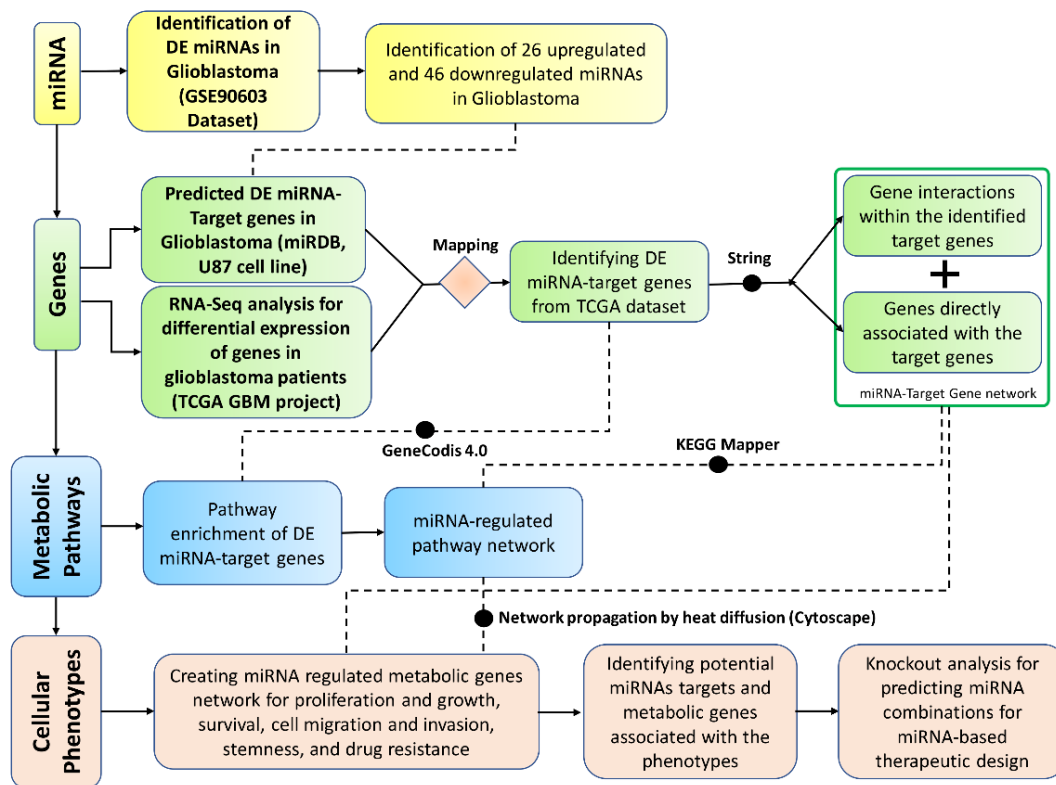


Figure 2.6: Flow diagram of the protocol followed for screening of potential miRNAs regulating metabolic genes and cellular phenotypes in glioblastoma.

2.3.2. Differential expression of miRNA

The differentially expressed miRNAs in GBM patients were identified by performing differential expression analysis using the GEO2R online tool. GEO2R is an R-based web application that allows users to analyze, identify and visualize the differential expression of transcriptomics data (199). The tool uses established R Bioconductor packages at the backend to transform and analyze GEO datasets and presents the results as a table ordered by the significance of differential expression (FDR). The processed data can be visualized with GEO Profile graphics. Three different groups, including GBM [GBM tumor tissue samples (n = 16)], Normal [normal brain tissue samples from healthy volunteer (n = 3)], and Normal from GBM [normal brain tissue samples from GBM patients (n = 4)] were defined. Two sets of differentially expressed miRNA were obtained by comparing GBM samples with Normal and Normal from GBM samples. We compared the differentially expressed miRNAs of the two sets to identify common miRNAs that are differentially expressed in both sets. A final set of 26 upregulated and 46 downregulated miRNAs were selected by considering $-1.5 > \log_{2}FC > 1.5$ and $FDR < 0.05$ as the threshold.

2.3.3. Identification of predicted target genes

The predicted target genes of the differentially expressed miRNAs were obtained from the miRDB database (200). The database allows the identification of miRNA target genes for specific cell lines of interest by determining target expression level through RNA-Seq using the RPKM method. The target genes for each of the 26 upregulated and 46 downregulated miRNAs that had detectable expression in the U87-MG glioblastoma cell lines were selected. The abbreviations used for the metabolic genes in **Chapter 5** are the conventional Uniprot gene symbols for *Homo sapiens*.

2.3.4. Validation of differentially expressed miRNAs and predicted targets

Additional datasets of miRNA expression were analyzed along with the GSE90603 dataset to validate the differential expression of miRNAs in glioblastoma. Dataset GSE65626, GSE25631, GSE165937, and GSE103229 were used for the validation. All the datasets were obtained from the GEO database. The distribution of data across the datasets was checked within the inbuilt platform of the GEO database that uses the R package “limma”. Volcano plots of the data distribution of all the five datasets have been provided in **APPENDIX C: Figure C. 1**. GSE90603, built on the GPL21572 platform, was the most stable dataset and hence chosen as the primary dataset for the analysis. While the rest of the datasets were used for validation of the upregulation or downregulation of the differentially expressed miRNAs obtained from GSE90603 as described in **Section 2.3.2**. The U87-MG specific predicted targets of the differentially expressed miRNAs obtained from miRDB were verified with the predicted target genes of a few additional glioblastoma cell lines. miRDB provides a repertoire of cell-line specific predicted targets of miRNAs. LN229, A172, SF126, and T98G were the additional cell line chosen for the verification of predicted targets and can be obtained from the miRDB database.

2.3.5. Differential expression analysis of gene expression data

Further filtering of the predicted target genes for the upregulated and downregulated set of miRNAs was done by mapping them with glioblastoma patient-derived gene expression data. RNA-Seq gene expression data for 169 glioblastoma patients and 5 normal individuals were obtained from the TCGA GBM project. Differential expression

analysis of the RNA-Seq data was performed using the “limma” and “edgeR” package of R Bioconductor version 3.10 (BiocManager 1.30.10) (201, 202). Significant differentially expressed genes were obtained considering FDR < 0.05 as the threshold. Genes involved in glioblastoma metabolism were filtered out for further analyses. Only the significantly downregulated target metabolic genes of upregulated miRNAs and significantly upregulated target metabolic genes of downregulated miRNAs were considered for network analysis.

2.3.6. Integration of additional gene interactions in miRNA-target metabolic gene network

The identified target metabolic genes were integrated into two miRNA-target gene networks for the upregulated and downregulated sets. In order to trace the effect of differentially expressed miRNA-target genes on the metabolic reaction network, additional genes were identified that work together with the target genes. These genes were considered on the basis of evidence of their involvement in the formation of protein complexes that catalyze a particular metabolic reaction or were involved in other coregulatory activities in the reaction network. Interactions within the target genes of each of the networks were obtained from the STRING database (203). Interactions with the highest confidence score (0.009) and active interaction sources from experiments, databases, co-expression, neighbourhood, and gene-fusion were considered to establish the interactions.

2.3.7. Pathway enrichment analysis

To identify the metabolic pathways that were regulated by the miRNA-target genes, pathway enrichment analysis was performed. The enrichment was done using GeneCodis 4.0 (204). The significantly enriched pathway entries ($p < 0.05$) from annotation against the KEGG and Reactome database were obtained and are tabulated in **APPENDIX C: Table C. 1 & Table C. 2.**

An extensive pathway search was done for each target metabolic gene of the miRNA-target gene networks using KEGG Mapper (205). KEGG Mapper allows mapping of molecular objects like genes, proteins, small molecules, etc., to molecular

interaction/reaction/relational networks like KEGG pathway maps, BRITE hierarchies, and KEGG modules. The search pathway query was used to map all the pathways regulated by the query genes. The output data was used to create a gene-pathway network that was further used to identify the specific pathways regulated by each miRNA.

2.3.8. Network propagation using Diffusion algorithm

Network propagation provides a robust estimate of the nodes proximal to a set of initial seed nodes by considering the overall connectivity of the network, shortest paths, and degree distribution of the seed nodes. The algorithm is widely used in biological network analysis for disease gene prioritization. We used the diffusion method of Cytoscape for network propagation (206) in both the miRNA-target gene network and the gene-pathway network to prioritize gene sets and corresponding pathways that were most proximal to each differentially expressed miRNA.

The diffusion method follows the heat diffusion algorithm (207). The calculation is given by:

$$d = h * \exp(-Lt) \quad \dots \text{Eq. 67}$$

where h is a vector representing the initial seed nodes, and d is the resultant vector of output nodes proximal to h . L is the graph Laplacian defined by $D - A$, where D is a diagonal matrix of the degree of each node and A is the graph adjacency matrix of the input network. t is a scalar parameter defined as the total time of diffusion that controls the extent to which the original signal is allowed to spread over the network. $\exp (*)$ is the exponential of the matrix.

The d was calculated repeatedly for each miRNA (h) in the miRNA-target gene network and a set of miRNA target genes in the gene-pathway network.

2.3.9. Identification of miRNA regulated metabolic pathway

The diffusion algorithm was used to identify a set of proximal genes for each miRNA of the miRNA-regulated target gene interaction network. The output genes were used as seed nodes for the gene-pathway network to extract pathways that were highly regulated by these gene sets. Nodes belonging to only the top 90th percentile of the diffusion output

rank were chosen as the output nodes to ensure only highly regulated genes and pathways were selected. Following the sequential network propagation, individual miRNAs were linked to the set of output pathways, and a network of miRNA-regulated metabolic pathways was obtained. The network integrated both upregulated and downregulated miRNAs and their target metabolic pathways. Gephi 0.9.2 was used for the visualization of the network (208).

2.3.10. Bipartite projection and backbone extraction of important miRNAs regulating metabolism

The miRNA-pathway network created was a true bipartite network defined by two mutually exclusive sets of nodes: top nodes formed by the miRNAs and bottom nodes formed by the pathways. The bipartite projection was used to compress the information of the network onto the top nodes. Bipartite projection allows compressing large bipartite graphs into unipartite network while retaining the information in the form of a weighted projected network (209). In the present work, the information of pathways was projected onto the miRNAs based on their connectivity to the pathways regulated by them. The final projected network of miRNAs contained edge weights that are defined by the number of common pathways targeted by a pair of connected miRNAs. R packages RCy3 and igraph were used for bipartite projection using the overlap count method (209, 210).

Further, backbone extraction was performed on the projected weighted miRNA network (**Figure 2.7A**). Ideally, backbone extraction yields a subgraph composed of the most significant nodes and edges in a network. The core miRNAs regulating different metabolic processes were obtained by filtering out all the redundant information. The extraction of the core component involves the use of a threshold. Edge weights exceeding the threshold value are retained in the backbone, while those weighing below the threshold value are eliminated. We used the unconditional threshold method (211) in the present work, where a single threshold was applied to all the edges, and edges with weights higher than the defined threshold were retained. R package backbone was used for the backbone extraction (212).

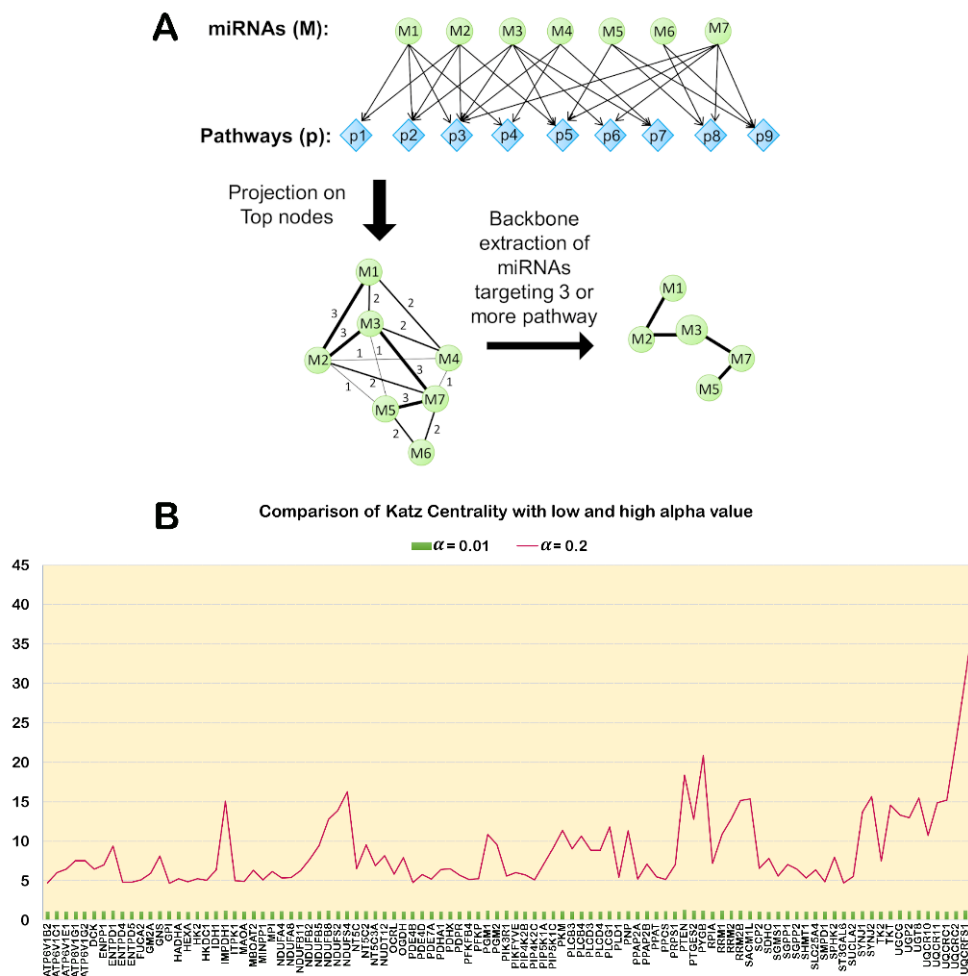


Figure 2.7: Illustration of methods. (A) Illustration of miRNA backbone extraction from miRNA-pathway bipartite network; (B) Comparison of the difference in Katz centrality with low and high α values.

2.3.11. Identification of miRNA-gene subnetwork for glioblastoma specific cellular phenotype

Cellular phenotypes that are dominantly regulated by metabolic changes in glioblastoma were considered for the analysis. These included proliferation and growth, survival, cell migration and invasion, stemness, and drug resistance. With an extensive literature search, a set of key regulatory metabolic genes associated with each of these cellular phenotypes were identified. Many of the key regulatory genes identified through literature were not essentially differentially regulated and were identified through experimental perturbations. Hence, to take into account all such genes, an integrated network of both upregulated and downregulated miRNAs and all the U87-MG specific predicted target metabolic genes from the miRDB database was used. We used the same

diffusion algorithm as discussed in **Section 2.3.8** to initiate network propagation, and the key regulatory genes were used as the seed nodes. Nodes belonging to the top 70th percentile of the diffusion output rank were chosen, and the group of highly connected nodes was selected as a subnetwork. Gephi 0.9.2 was used for the visualization of the network, and the R package tidyverse was used to generate the circular plot of miRNAs in the subnetworks (213).

2.3.12. Knockout analysis for identification of targetable miRNAs

A set of miRNAs for each of the cellular phenotypes was obtained from the respective miRNA-target gene subnetwork. These miRNAs were analyzed to identify targetable miRNAs for miRNA-based therapeutic approaches. Given the gene regulatory structure of the network, which was directed and partially bipartite, the network was studied as a two-mode graph, where the influence of the top nodes formed by the miRNAs over the bottom nodes formed by the target genes was studied. The usual network centrality measures face limitations in identifying the central nodes in such networks due to the partial connectivity of the nodes. Hence, the cruciality of the miRNAs in the subnetwork was determined by calculating their Pairwise Disconnectivity Index (PDI) in the subnetwork (214).

The PDI considers an ordered pair of nodes synonymously called vertices and mathematically represented as vertices $\{i, j\} | i \neq j \text{ and } i, j \in V$ of a directed graph $G(V, E)$ of the regulatory network formed by vertices $v \in V$ denoting biological entities, i.e., genes, proteins, transcription factors or miRNAs, and connected by directed edges $e \in E$. An ordered pair of vertices i and j in G are connected if they are linked by at least one path. PDI quantifies the importance of a node by measuring the effect of elimination of the vertex on the number of connected ordered pairs of vertices. It is mathematically defined as the fraction of initially connected pair of vertices of a network that become disconnected when the vertex v is deleted from the network

$$PDI(v) = 1 - \frac{N_{-v}}{N_0} \quad \dots \text{Eq. 68}$$

where N_0 is the initial number of connected ordered pairs of vertices in the network and N_{-v} is the number of ordered pairs that still remain connected after the deletion of the

vertex v from the network. PDI ranges between 0 to 1. The higher the value of $PDI(v)$, the more disconnected the network is upon deletion of the vertex v . Biologically, it quantifies the extent of regulation imposed by a regulatory node on the other connected pair of nodes in the network. The PDI of each miRNA in the subnetworks was calculated, and the miRNAs with high PDI were considered for knockout analysis.

The impact of miRNA regulation on the key regulatory genes of a subnetwork was determined by performing knockout analysis. The knockout analysis was performed on the integrated miRNA- metabolic target gene network (**Section 2.3.11**). MiRNAs with high PDI were knocked out from the network, individually and in combinations. Double and triple knockout combinations were designed to identify combinations that could target the maximum number of key regulatory genes in each subnetwork. Katz centrality (215, 216) of the genes were compared before and after the deletion of a miRNA to measure the impact of a miRNA deletion on these genes. Katz centrality (K) of a node i is computed as

$$K_i = \alpha \sum_j (A_{ij} * K_j) + \beta \quad \dots \text{Eq. 69}$$

where A is the adjacency matrix of graph G with eigenvalues λ . β is a bias constant used to avoid zero centrality values, and α is the attenuation factor and $\alpha < 1/\lambda_{max}$. Katz centrality measures the relative influence of a node i in a network by calculating the number of first-degree interactors of the node as well as all other nodes in the network that are connected to node i through the first-degree interacting nodes (217). The value of α is important in determining the local and global properties of the network using Katz centrality. Katz centrality with a low value of α measures the local influence of a node on the network, whereas a high α value close to $1/\lambda_{max}$ value measures the global influence of the node (217). The influence of the target gene nodes was computed using different α values. The difference in Katz centrality of the top 100 influential nodes in the network with $\alpha = 0.01$ and $\alpha = 0.2$ are shown in **Figure 2.7B**. $\alpha = 0.2$ was used for further analysis. This centrality was used to compute the change in the influence of a gene in the network before and after a miRNA deletion. The R package centiserve was used to compute both pairwise disconnectivity index and Katz centrality of the nodes (218).

CHAPTER 3

ANOMALOUS BEHAVIOR OF METABOLIC PATHWAYS IN GLIOBLASTOMA AND THEIR EFFECT ON INTERNAL CELLULAR MECHANISMS

3.1. Rationale of the study

Adaptive phenotype switching is a characteristic feature of cancer cells. The dynamic molecular crosstalk within the cell and a cumulative behavior of heterogenous tumor masses support phenotypic plasticity and rapid adaptation to stress in glioblastoma. Metabolic remodelling supports the high proliferative requirements of these cancer cells and is often associated with tumor cell plasticity. Heterogenous glioblastoma tumor masses exhibiting metabolic signatures like IDH mutation (64), IDO overexpression (219), MTAP deletion (63), accumulation of kynurenine, and cysteine sulfinic acid (57) act cumulatively to evade anti-cancer therapies. Deregulated expression of GLUT1, 3, and 4, phosphofructokinase, pyruvate kinase M2, glutathione oxidoreductase, glucose-6-phosphate dehydrogenase, phosphoglycerate dehydrogenase, glutaminase, and many other enzymes across different metabolic pathways are frequently observed in these tumors (**Section 1.5.3**), enabling metabolic plasticity. The study of the rewired metabolic network provides an understanding of the effect of metabolic regulations on the global outputs, manifested as phenotypes. The challenge, however, is to understand the condition-specificity of metabolic adaptations along with the overall picture of metabolic re-routing at a large-scale in these cancer cells. In this context, systems-level analysis of metabolic flux networks helps generate nonintuitive, testable hypotheses about metabolic reprogramming.

Several studies have been carried out to delineate the advantage of such metabolic modification in glioblastoma, enabling them to suffice their rapacious requirements (15). Several experimental and statistical analyses have been conducted to delineate the phenomenal changes in the properties of glioblastoma as an effect of metabolic alterations in different enzymes belonging to different pathways like tryptophan metabolism(16), cysteine metabolism(17), glutamine, and glutamate metabolism(2).

Properties of these individual metabolic pathways have been studied in both astrocytes and glioblastoma. A new arena of *in-silico* studies has also been employed in the past decade to get a large-scale network understanding of glioblastoma. Different types of dynamic modelling approaches, such as spatiotemporal modelling (129, 131), partial differential equation modelling (134), ordinary differential equations, have been used to detect the growth and invasion of glioblastoma cells (220). However, these studies have been mostly limited to understand the metabolism of glioblastoma in parts. These studies only provide a partial picture to the unaddressed questions, and further studies are required to address the same.

Hence, in line with the thesis objectives, in this chapter, we began with a systems-level analysis of a context-specific metabolic model of glioblastoma. The aim of this chapter is to understand what is the effect of change in metabolic flux through a deregulated pathway on the overall metabolic landscape of glioblastoma and what are the conditions under which the cell displays a particular change in flux route? It also aims to understand how this reprogramming favours the proliferation and growth of glioblastoma? The chapter partially fulfils the second objective by investigating the metabolic vulnerabilities that can be used as a potential therapeutic target.

The present work involves the specific comparison between the astrocyte and glioblastoma scenarios by taking into account those pathways which are known to get deregulated in glioblastoma when compared to the normal astrocytes. Our constraint-based model accommodates a total of 13 pathways, the abnormal functioning of which has been reported in glioblastoma. The model has 247 reactions, with 39 exchange reactions and 69 transport reactions associated with 147 genes (**Section 2.1.1**). By analyzing this large network using flux balance analysis, the differences in the individual pathway response as a part of a large metabolic network in astrocyte and glioblastoma scenarios were delineated (**Section 2.1.2**). Specific questions were addressed using the model, like how glioblastoma cells fuel their growth requirement? Is there an overlap between the energy and growth demand of these cells? Two objective functions: ATPSyn (**Eq. 1**) and GBM_BM (**Eq. 2**) were defined to capture the energy and growth demand of the model.

The model was validated for both astrocytic and glioblastoma scenarios with the experimentally available information to ensure that it generates results that are biologically reasonable (**Section 2.1.5**). By analyzing the steady-state flux profiles generated by the model, the fate of the input metabolites and their essentiality in glioblastoma growth was interpreted (**Section 2.1.6**). Single and double reaction knockouts analyses were performed to determine the essentiality of the reactions involved in the metabolic network in governing the growth properties of glioblastoma (**Section 2.1.7**). Potential drug targets were identified from those sets of essential reactions. To determine the extent of regulation that could be imposed on those drug targets and to analyze them quantitatively, they were further simulated for therapeutic intervention scenarios with the motive of either reducing the glioblastoma growth to zero or to reduce it to the growth rate of a normal astrocyte (**Section 2.1.8**). The classification of reaction knockouts combined with simulations of therapeutic interventions could predict reaction pairs as feasible drug targets, supporting the large-scale applicability of constraint-based models in predicting reasonable therapeutic target combinations.

3.2. Results

3.2.1. Properties of the reconstructed metabolic network

The present context-specific model for metabolism provides a composite understanding of metabolic re-routing in glioblastoma at the pathway level. The details of reactions involved in the thirteen frequently deregulated pathways in glioblastoma were collated and verified from multiple data sources, including databases and literature (**Section 2.1.1**). The reconstructed model comprised of a total of 247 reactions, with 39 exchange reactions and 69 transport reactions. Most of the internal reactions, along with a few transport reactions, were associated with their corresponding genes, which accounts for 147 genes in the model (**APPENDIX A: Table A. 1**).

The present model for glioblastoma metabolism could be classified on the basis of the following four categories: (i) enzyme commission number, (ii) gene non-gene association, (iii) sub-cellular locations, and (iv) metabolic processes (**Figure 3.1**). A large number of the reactions in the model belonged to the class 1 category of enzyme

classification, i.e., the oxidoreductases (22%). This set of enzymes catalyze the oxidation of one chemical species and the simultaneous reduction of the other by the transfer of electrons from one species to another. The other classes of enzymes in this classification scheme were the transferases (14%) followed by lyases (10%), hydrolases (4%), isomerases (2%), and ligases (2%). Another 28% of the reactions belonged to transport reactions and 16% to extracellular exchange reactions that occurred spontaneously in the system (**Figure 3.1A**).

The reactions were further classified on the basis of their association with genes to understand gene reaction associations (**Figure 3.1B**). 60% of the model reactions were gene-associated, out of which 6% are transport reactions. The rest of the reactions were classified as: Non-Gene associated Exchange Reactions (16%), Non-Gene associated Intracellular Reactions (2%), and Non-Gene associated Transport Reactions (22%).

The classification shown in **Figure 3.1C** depicts the subcellular localization of the reactions considered in the model. The cytosolic and mitochondrial reactions contributed to 54% of the total reactions in the model. 2% of the reactions belonged to the mitochondrial intermembrane space model compartment that specifically accounts for oxidative phosphorylation. The transport reactions were categorized according to the membrane where it is localized. Transports accounted for 30% of the total reactions: Mitochondrial membrane-spanning (11%), Nuclear membrane-spanning (2%), and Plasma membrane-spanning (17%).

In terms of metabolic processes, 23% of the reactions belonged to fatty acid metabolism, inclusive of both biosynthesis and beta-oxidation of palmitic acid. The rest of the pathways contributed to 30% of the total count of which 14% belong to Glycolytic, PPP, TCA cycle and Oxidative phosphorylation pathway and 2% is contributed each by Glycine-Serine Metabolism, Cysteine Metabolism, Methionine Metabolism, and Glutamate Metabolism, without taking into account the transport and exchange reactions. Another set of reactions, namely, cytosolic ATPase (ATPS), cytoplasmic malate dehydrogenase (MDH(Cyto)), Phosphoenolpyruvate carboxykinase (GTP) (PEP_CarbK_1), mitochondrial pyruvate carboxylase (Pyr_Carbm), which could not be assigned strictly under any particular pathway, were categorized as 'Others' which contributed to 2% of reactions to the (**Figure 3.1D**).

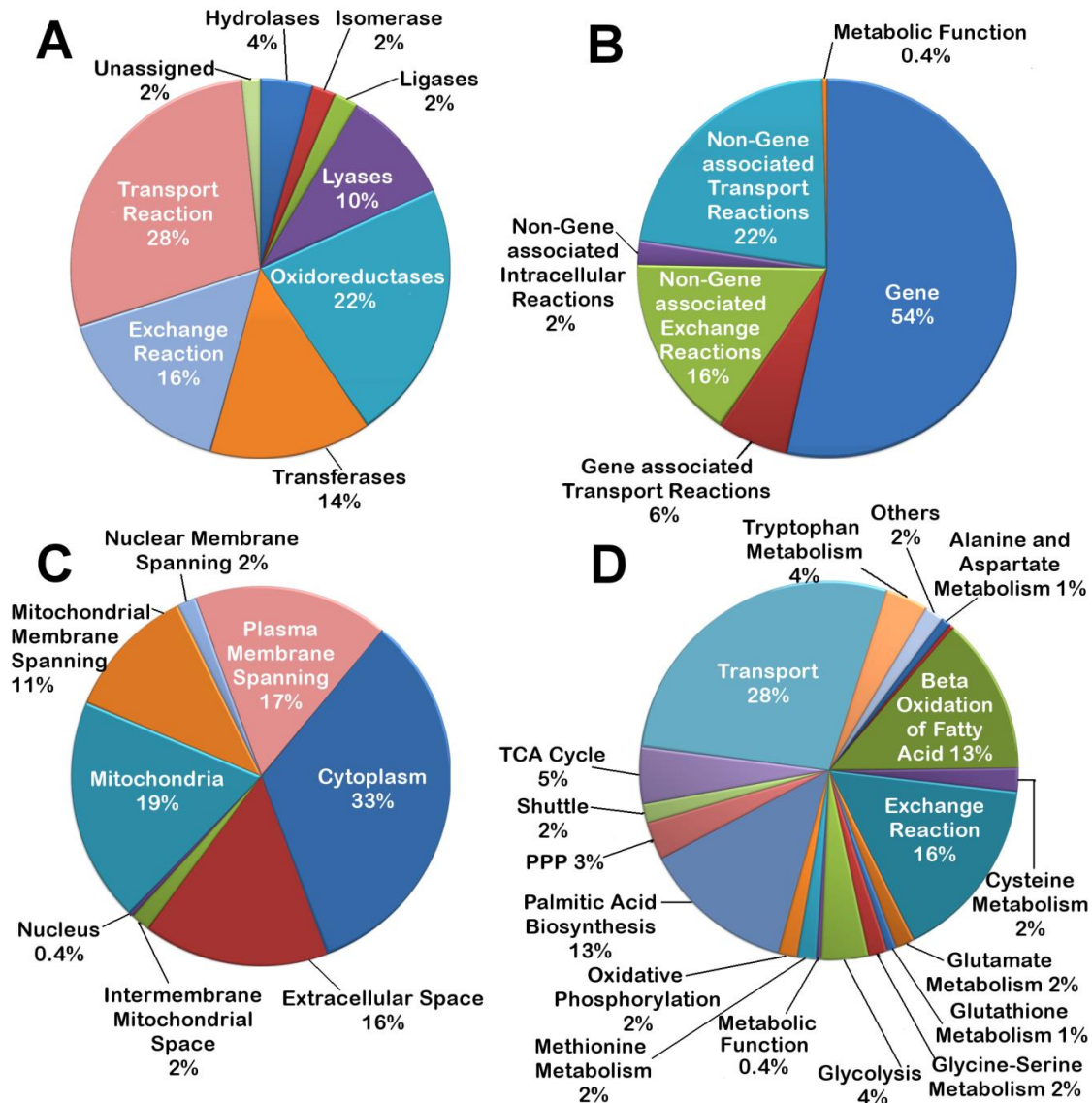


Figure 3.1: Classification of the properties of the reconstructed metabolic model. The model reconstruction has been classified on the basis of (A) Enzyme commission number or E.C. number, (B) Gene-Non gene association, (C) Cellular compartments, and (D) Metabolic processes, respectively.

3.2.2. Validation of objective function for growth demand

The cellular demands for ATP synthesis and growth were optimized separately so as to identify how the deregulation in mitochondrial ATP synthesis affects the flux flow through different pathways of the network while the cell manages to serve its energy and growth requirement (**Section 2.1.3**). The objective function that was designed to mimic the growth requirement of glioblastoma was validated with an experimentally observed

growth phenomenon. According to experimental evidence, excess glucose can retard the growth rate of glioblastoma cells, and high levels of glucose can even prove to be toxic due to excess accumulation of lactate (221). So, to check if the objective function for growth could display this growth property of glioblastoma, we observed the fate of GBM_BM with varying uptake of glucose (with glucose being taken as the carbon source along with cystine, and the uptake of glucose was varied). We found that GBM_BM limits to increase with excess glucose uptake, and after a point, the flux through it reduces to zero (**Figure 3.2**). Also, the lactate dehydrogenase activity increases rapidly with glucose uptake. This relationship of GBM_BM with the glucose uptake could account for the growth properties of glioblastoma and hence was considered to represent the growth demand of glioblastoma.

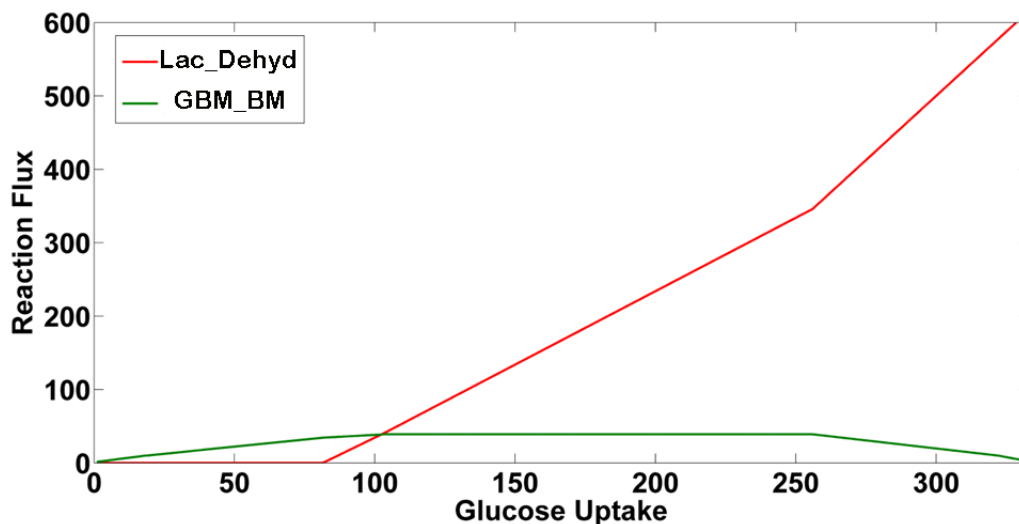


Figure 3.2: Change in flux through GBM_BM with increasing glucose uptake. Change in flux through the metabolic function GBM_BM and Lac_dehyd reaction with increasing uptake of glucose in the model glioblastoma scenario.

3.2.3. Analysis and validation of model properties for astrocyte and glioblastoma model

The reconstructed metabolic model was validated both for the astrocytic and the glioblastoma scenario, using mitochondrial ATPSyn (**Eq. 1**) as the objective function. The astrocytic scenario was created first by fixing the bounds of a few reactions. Few known perturbations from experiments were introduced to the astrocyte model so as to create the glioblastoma model (**Section 2.1.4**).

Validation of astrocyte model

Required changes were made to the bounds of certain reactions during simulation of the astrocyte model, and the optimal range of bounds within which it showed the properties of astrocyte was estimated. The astrocyte scenario was validated with experimental observations like pyruvate recycling, lactate production, and the effect of glutamate to ensure that the model mimics the properties of astrocytes.

Astrocytes prefer a glucose-dependent metabolism where glucose is catabolized to pyruvate that enters the TCA cycle, thereby leading to ATP synthesis(179) and partly to the formation of lactate so as to suffice the neuronal requirement. This property was examined in the model astrocytic scenario by performing a robustness analysis of glucose uptake with increasing oxygen uptake. The default flux balance analysis in the model astrocytic scenario suggested an optimal flux of -160 for oxygen uptake. The uptake of oxygen was thus, varied up to its optimal flux, and its effect on glucose uptake was observed. An increase in oxygen uptake led to a linearly proportional increase in glucose uptake (**Figure 3.3A**). The glucose was observed to produce lactate in the astrocytes without affecting the mitochondrial respiratory chain. Further, above an oxygen uptake of 130, a slight dip in the glucose uptake rate was observed without affecting the flux through mitochondrial ATP synthesis, which continued to increase. This was possibly because of the recycling of pyruvate from the TCA cycle intermediates. Reports suggest that TCA cycle intermediate, citrate may give rise to oxaloacetate, which is subsequently converted to pyruvate through the activity of malic enzyme or by the combined activity of PEP carboxykinase and pyruvate kinase (222).

Model simulations suggested that pyruvate was recycled from the TCA cycle via the conversion of oxaloacetate through PEP carboxykinase and pyruvate kinase reactions. This resulted in a reduced dependence of pyruvate production on glucose uptake. The pyruvate so formed was again catabolized into the TCA cycle and used for maintaining ATP production via the activity of the mitochondrial respiratory chain. The complex IV of the oxidative phosphorylation pathway consumes oxygen for its activity, and hence an increase in ATP Synthase activity proportional to oxygen uptake was observed.

The activity of lactate dehydrogenase and pyruvate kinase increases during anoxic conditions as compared to normoxic conditions in astrocytes (180). To verify this

property, normoxic and hypoxic conditions were created in the model by constraining the oxygen uptakes at the optimum (flux value=-120) and low (flux value=-2) values and ensuring sufficient glucose uptake in the model. It was observed qualitatively that the model is capable of capturing this feature of astrocytes (**Figure 3.3B**). Although the actual experimental result was generated by incubating the astrocyte cells in a completely oxygen-deprived anoxic condition for 6 hours, creating such a situation in the present *in-silico* model would lead to zero ATP synthesis due to its dependence on oxygen. Hence, the property was verified for hypoxic conditions represented by low oxygen uptake only.

In astrocytes, the uptake of glucose increases with an increase in glutamate uptake that leads to increased lactate production(181). This scenario was created in the model by regulating the exchanges of glucose, glutamate, and oxygen. By varying the glutamate uptake from 0 to 450, a corresponding increase in glucose uptake and hence, lactate production was observed during model simulations. Further, it was observed that the highest lactate production was at a glutamate uptake flux of 450 (**Figure 3.3C**).

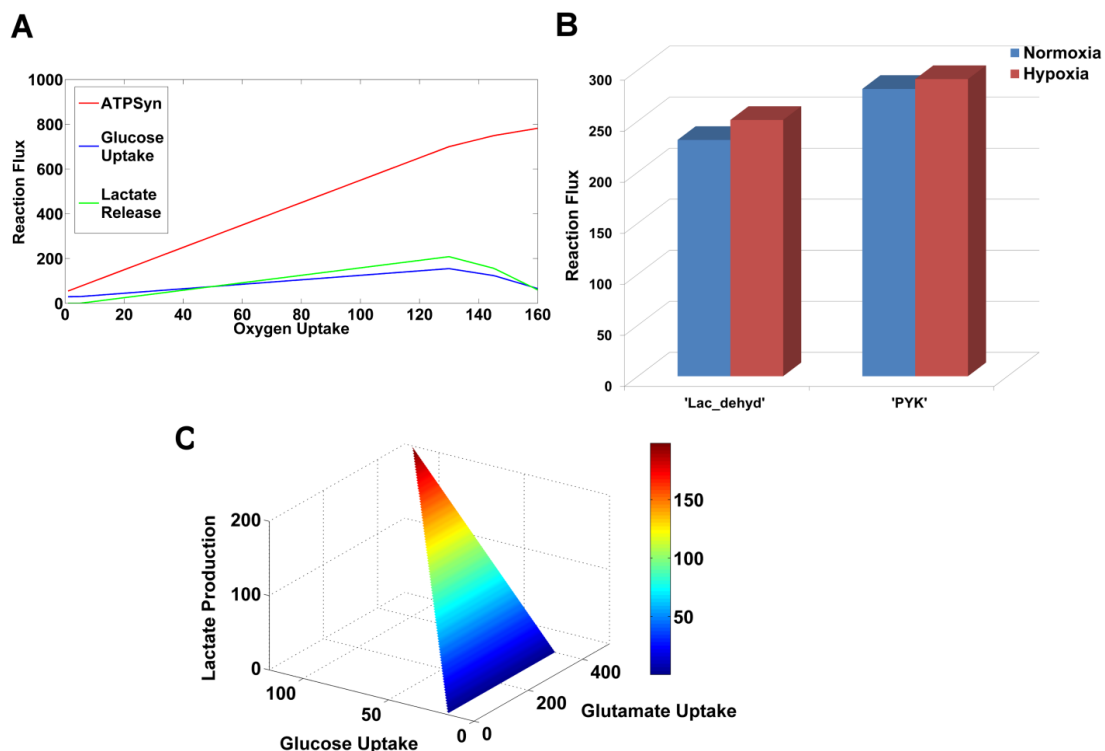


Figure 3.3: Validation of Astrocyte model. Properties of astrocyte have been depicted in figure (A) increase in glucose uptake driven towards mitochondrial ATP synthesis and lactate production, (B) increase in the activity of lactate dehydrogenase and pyruvate kinase in hypoxia conditions, (C) increase in glucose utilization and lactate production with increasing glutamate uptake.

Validation of glioblastoma model

The astrocyte model was further perturbed to create the glioblastoma scenario (**Section 2.1.4**). To validate the glioblastoma scenario, steady-state fluxes of certain reactions obtained by simulating for glioblastoma scenario were compared with that of the astrocyte scenario while keeping all the nine inputs open to the system. The Warburg effect, which states a reduction of ATP production through mitochondrial respiration and an increase in glucose utilization to increase the flux towards aerobic glycolysis (15), was observed in the glioblastoma scenario (**Figure 3.4A**).

For further validation of this scenario, few experimental observations were replicated from our model. Glutaminolysis is a known property of glioblastoma cells, where the uptake and utilization of glutamine is favoured over glutamate for compensating the loss of glutamate through cysteine-glutamate antiporter (2), which is a property that is exactly opposite to that of astrocytes (182). Also, uptake of cystine increases in the glioblastoma cells due to enhanced activity of cystine-glutamate antiporter (17). All these differences in the exchange properties of glioblastoma could be observed through our model when the entry of all the input metabolites was allowed (**Figure 3.4B**).

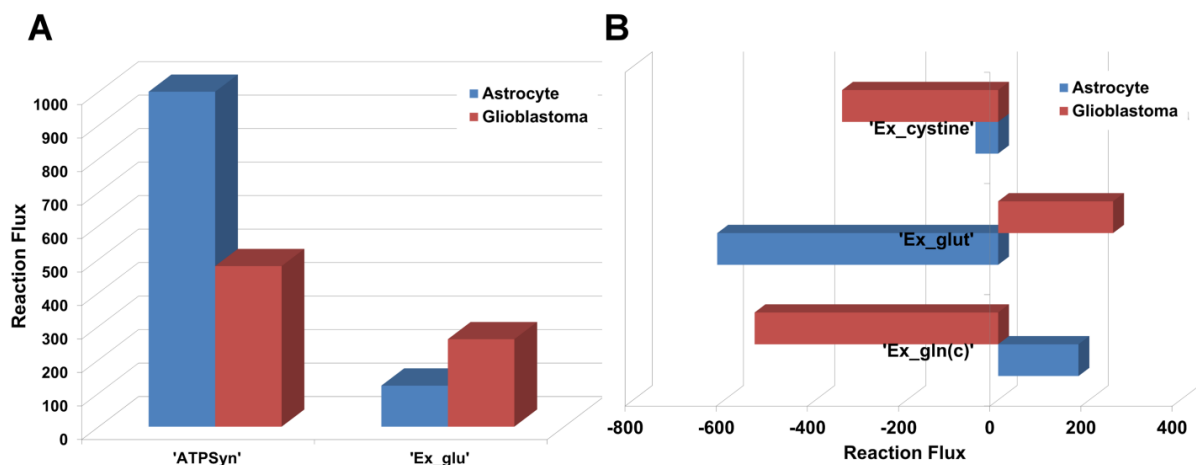


Figure 3.4: Validation of Glioblastoma model. Properties of glioblastoma have been depicted in (A) reduced mitochondrial ATP synthesis and increased glucose utilization in glioblastoma scenario (B) reversal in glutamate and glutamine utilization and increase in cystine uptake in glioblastoma scenario.

3.2.4. Comparison with experimental data

A separate objective function, GBM_BM (Eq. 2), was designed to understand the metabolic requirements associated with glioblastoma growth. Considering this reaction

as the cellular objective, the glioblastoma scenario was further evaluated for its metabolic properties. All the further analyses have been performed, keeping the GBM_BM as the objective function. Initial validation was done to ensure that the objective function represents the growth properties of glioblastoma (**Section 3.2.2**). Further verification of this objective function was done via a qualitative comparison of fold change in the flux values of few reactions with the fold change expression values of certain reported reactions in the astrocytic and glioblastoma scenario. The fold change in flux profiles of astrocytic to glioblastoma scenario as predicted from the model was compared to existing proteome data extracted from young glioblastoma patients (223). The results of this comparison are listed in **Table 3.1**. Fold change expression data for eight reactions could be matched with the model reactions. Out of the eight reactions, predicted activity for five reactions was qualitatively found to be in correspondence with the experimental observations.

Table 3.1: Comparison of model prediction with the data available for enzyme expression in the young patient.

Uniprot ID	Reaction name	Model abbr.	Fold Change	Model Prediction	Gene abbr.	Fold Change	Exp. Prediction
O43175	D-3-phosphoglycerate dehydrogenase	PGDH	0.9313	D	PHGDH	0.55	D
P04075	Fructose-bisphosphate aldolase A	FBA	0.9175	D	ALDOA	0.71	D
P50213	Isocitrate dehydrogenase [NAD] subunit alpha, mitochondrial	IDH	0.0000	D	IDH3A	0.48	D
P18669	Phosphoglycerate mutase 1	PGM	2.4046	U	PGAM1	1.6	U
Q9Y617	Phosphoserine aminotransferase	PST	0.9313	D	PSAT1	0.53	D
P00367	Glutamate dehydrogenase, mitochondrial	GlutDH	0.0000	D	GLUD1	1.4	U
P60174	Triosephosphate isomerase	TPI	0.7401	D	TPI1	2.1	U
P17174	Aspartate aminotransferase, cytoplasmic	ASPTc	1.0732	U	GOT1	0.53	D

*Regulation in enzymatic expression. Up-regulation is represented as 'U' and down-regulation is represented as 'D'.

3.2.5. Opposing roles of glycine and glutamate uptake in astrocytes

Evidence state that the glycine content of neuronal cells is higher than that of glial cells (224). Also, most of the CNS tissues suffice their glycine requirement via the internal

glycine-serine metabolism pathway derived from glucose via 3-phosphoglycerate (225), even though astrocyte cultures fed with glycine are capable of utilizing it by maintaining intracellular levels of glutathione, serine, and creatine (226). High uptake of glycine in astrocytes was observed to be tightly coupled with the high secretion of Na^+ and Cl^- (227). In the model, we have assumed a normal transport reaction of glycine that is not coupled with Na^+ and Cl^- . The effect of the ion-dependent exchange of glycine in astrocytes has been captured by changing the bounds of glycine transported in the astrocyte model scenario. Bounds on uptake of all the input metabolites were released so as to allow unrestricted flow of other input metabolites in the model. The model was analysed under this simulation condition to check the effect of excess glycine uptake on the astrocytes. It was observed that glycine uptake had a dominant influence on the glutamate/glutamate uptake cycle of astrocytes. Glutamate consumed by the cell is utilized in multiple metabolic processes. It is catabolized in the TCA cycle, metabolized into glutamine via the activity of glutamine synthase that is released out for neuronal consumption, and a part of it is released outside the cell through the cystine-glutamate antiporter. At low glycine uptake (flux value of glycine uptake < -60), most of the glutamate taken into the cell, produces glutamine that is released from the cell. This results in lower uptake of cystine and hence, less glutamate release through cysteine-glutamate antiporter (**Figure 3.5**). In contrast, increased glycine uptake is driven towards an increased synthesis of glutathione. For this to occur, an equally increased flux through cystine uptake (cystine-glutamate antiporter) is observed. Cystine is then catabolized for cysteine biosynthesis, which combines with glycine and glutamate to form glutathione. The increased uptake of cystine is coupled with an equal efflux of glutamate through the antiporter. Glutamate required for this efflux is provided by its uptake through glutamate-ATP transporter. To compensate for the amount of glutamate lost through efflux, glutamine uptake increases that is consumed in glutamate synthesis via the activity of glutaminase. This result suggests that lower uptake of glycine is preferred in astrocytes under normal physiological conditions when it needs to suffice the glutamine requirement of the neurons. However, under oxidative stress, it can easily switch metabolism towards the production of glutathione via a higher uptake of glycine uptake so as to combat oxidative stress. The rerouting also associates change in flux through glutamine and cystine metabolism.

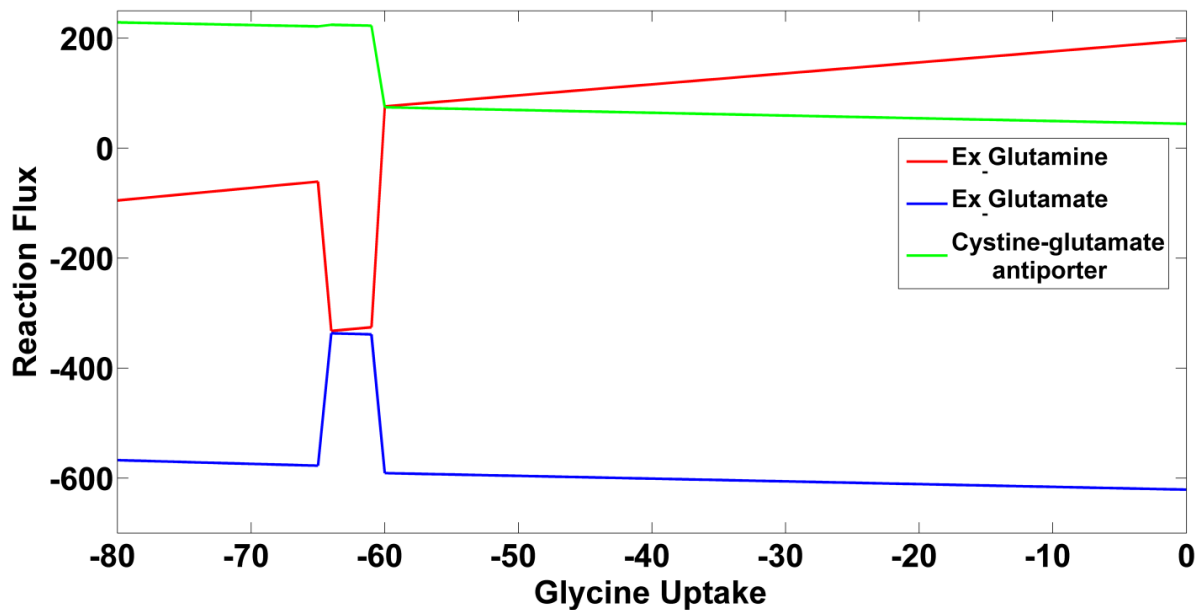


Figure 3.5: Effect of Glycine uptake on glutamate utilization by astrocyte. Change in the uptake and release of glutamate, glutamine, and cystine-glutamate antiporter with increasing uptake of glycine in the astrocyte scenario. The uptake of glutamate reduces with increasing uptake of glycine, and the glutamine exchange reverses its direction of flow of flux.

3.2.6. Difference of pathway responses in astrocyte and glioblastoma

The difference in the flux profiles of the astrocyte and glioblastoma models while the models were optimized for ATPSyn and GBM_BM were captured through model simulation and were analyzed. Distinct changes in the flux distribution of the two models were observed for the two objective functions. The details are provided in the following subsections.

A. Maximization of energy demand

FBA simulations for maximization of ATP synthesis revealed the difference in the flux through the glycolytic pathway, cystine uptake, glutamine metabolism, and glycine-serine biosynthetic pathways of the glioblastoma scenario.

Increase in glycolytic flux

Simulations for maximizing ATP synthesis as the objective function demonstrated a significant increase in the flux through the glycolytic and pentose phosphate pathways in the glioblastoma scenario as compared to the astrocyte but a corresponding decrease in

ATP synthesis (**Figure 3.6A and B**). To create the glioblastoma scenario, reduced activity of Complex IV of the electron transport chain was considered (228). ATP Synthase is largely dependent on the proper functioning of complexes of the electron transport chain that generate the proton gradient required to drive the F₀F₁ pump for ATP synthesis. Hence, with a low flux through Complex IV, a decreased ATP synthesis was observed. Under the reduced activity of Complex IV, the deficiency of electrons for ATP synthesis was partly met through Complex I and III of the electron transport chain. An increase in the synthesis of oxaloacetate was also observable as a consequence of the PEP carboxykinase-mediated catabolism of phosphoenolpyruvate. Hence, the increased flux through glycolysis in the glioblastoma was generated in response to the fault in the complex IV of oxidative phosphorylation pathway and the increased activity of PEP carboxykinase. The dependence on the glycolytic pathway for ATP synthesis is a characteristic feature of glioblastoma cells that could be captured from the model (5). However, constraining the availability of glucose showed an increase in flux through the β -oxidation of fatty acid metabolism represented by the palmitic acid in the glioblastoma model. Hence, it was inferred that glucose is the preferred energy substrate of glioblastoma, but under the limited availability of glucose, the cell can utilize fatty acids as secondary energy substrates.

Increase in cystine uptake

Simulations demonstrated increased uptake of cystine (**Figure 3.6C**). The total flux of cystine uptaken by glioblastoma was driven towards cysteine biosynthesis, which was then distributed towards glutathione biosynthesis in a relatively low amount (**Figure 3.6F**) and largely towards the production of pyruvate through the cysteine dioxygenase (CD), cysteine sulfinatase transaminase (CST), and the spontaneous 3snpyr (SPON1) reactions. The pyruvate so produced was utilized for acetyl CoA synthesis and ended with the biosynthesis of fatty acids, which were further released in the extracellular environment.

Increased catabolism of glutamine

Reactions belonging to glutamine-glutamate metabolism showed a higher activity due to the initiation of glutaminolysis in the glioblastoma scenario (2). Simulations

demonstrated the uptake of glutamine by the glioblastoma cells from the external medium, which was converted to glutamate within the cell via the activity of glutaminase (Glnase). A considerable amount of glutamate that was formed was released out through the cystine-glutamate antiporter (xCT) in order to uptake cystine. Cystine was then utilized in the cysteine metabolism pathway as discussed above (**Figure 3.6D**). A part of the glutamate entered the TCA anaplerotic cycle via the reversible conversion of glutamate to *akg* catalyzed by glutamate dehydrogenase (GlutDH), and a considerably smaller flux was directed towards the production of glutathione by the formation of its initial complex glutamyl-cysteine catalyzed by the reaction γ -glutamyl cysteine ligase (GCL). Constraining the flux through xCT increased the reverse flux through GlutDH producing more amount of *akg* that was utilized in the TCA cycle, thereby ascertaining the utilization of glutamate in the anaplerotic cycle. It was inferred from the observation that the glutamate produced in the process of glutaminolysis would normally enter the anaplerotic cycle in glioblastoma to replenish the TCA cycle intermediates. However, with an increase in demand for cystine or glutathione, the flux of glutamate redistributes itself among the reactions GlutDH, xCT, and GCL.

Decreased glycine-serine biosynthesis

Simulations further showed increased uptake of glycine in glioblastoma (**Figure 3.6E**). It could be observed that glycine was preferred to be taken from the external source as compared to being synthesized within the cell, as seen in the case of the astrocyte model. This was because the glycolytic flux, instead of getting distributed into the various branching metabolic paths including the glycine-serine biosynthesis pathway, was directed towards the faulty mitochondrial ATP synthesis machinery to maximize flux through the defined objective function ATPSyn. In biological conditions, a similar reduction through the glycine-serine biosynthetic pathway and increased dependence on external glycine source is observed in glioblastoma that can be explained by the increase in aerobic glycolysis that serves the ATP requirement of these cells.

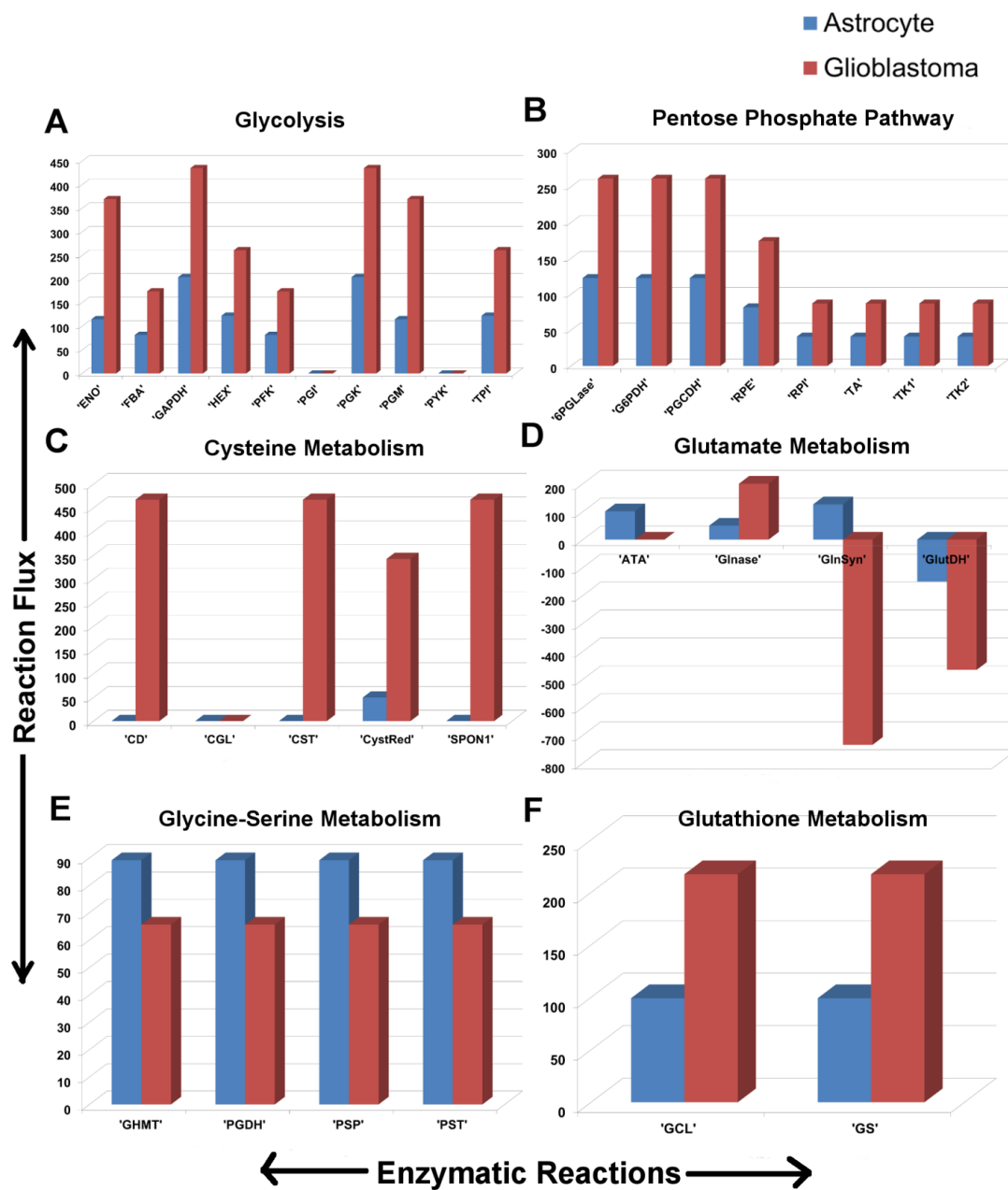


Figure 3.6: Pathway Response with maximization of ATPSyn as the objective function. The flow of flux through the different reactions of (A) Glycolysis, (B) Pentose phosphate pathway, (C) Cysteine metabolism, (D) Glutamate metabolism, (E) Glycine-serine metabolism, and (F) Glutathione metabolism pathway while maximizing mitochondrial ATP synthesis

B. Maximization of growth demand

Qualitatively, the same trend of pathway response was observed for the two scenarios while optimizing GBM_BM as the objective function. Although, a few differences in the underlying factors guiding the metabolic re-routing were observed in this case that are discussed below.

Rearranged flux through glycolysis and pentose-phosphate pathway

While maximizing the GBM_BM objective function, rearrangement of flux through the reactions of glycolytic and pentose-phosphate pathway (PPP) reactions were observed (**Figure 3.7A** and **B**). The lower part of glycolysis was observed to be more active as compared to the upper reactions as reported in a study where a low activity of hexokinase as has been reported in the literature (229). A probable explanation for this random arrangement of flux through the different reactions of the glycolytic and pentose phosphate pathway can be the requirement to maximize *r5p* production through the RPI reaction of PPP. Being a component of the objective function, with the maximization of GBM_BM, the production of *r5p* tends to maximize. It is to be mentioned here that *r5p* was considered a component of GBM_BM as a precursor of nucleotide biosynthesis and amino acids (**Section 2.1.3**). The non-oxidative part of the PPP shows a distinct rise in flux in the glioblastoma model and is directed towards RPI reaction to ensure high *r5p* production that will allow the cell to maintain its high growth requirements.

Increased cystine uptake in glioblastoma

Simulations demonstrated an increase in cystine uptake and its utilization in cysteine metabolism. In the model, cystine reductase (CystRed) is considered as the reaction that reduces the disulfide cystine into its monosulfide form, cysteine. When compared to the model simulations using ATPSyn as objective, the distribution of cysteine so formed is restricted, and the corresponding reactions of the cysteine catabolic pathway do not appear to drive a flux (**Figure 3.7C**). The probable explanation for the observation is the increased demand for cysteine in the production of glutathione. Glutathione is a tripeptide antioxidant composed of cysteine, glutamate, and glycine, that protects the cell from oxidative damage. Cysteine combines with glutamate in a reaction catalyzed by glutamyl-cysteine ligase (GCL) to form glutamyl-cysteine that is further converted to glutathione via the addition of glycine in the reaction glutathione synthase (GS). Both the reactions are observed to have increased flux in the glioblastoma model.

Reversal of flux through TCA cycle towards the production of malate and fumarate in both scenarios

A backward flow of flux in the TCA cycle, from oxaloacetate to fumarate, was also observed in experiments, in both cultured astrocytes and in *in-vivo* conditions, which was due to the activity of mitochondrial pyruvate carboxylase (230). Through the model simulation, similar properties in the glioblastoma model were observed (**Figure 3.7D**). The flux through the fumarate hydratase (FUMH) and malate dehydrogenase (MDH) reactions were reversed and enhanced in the glioblastoma model. The reason for this reversal was to maximize succinate production through the TCA cycle, which was an important component of the objective function for growth.

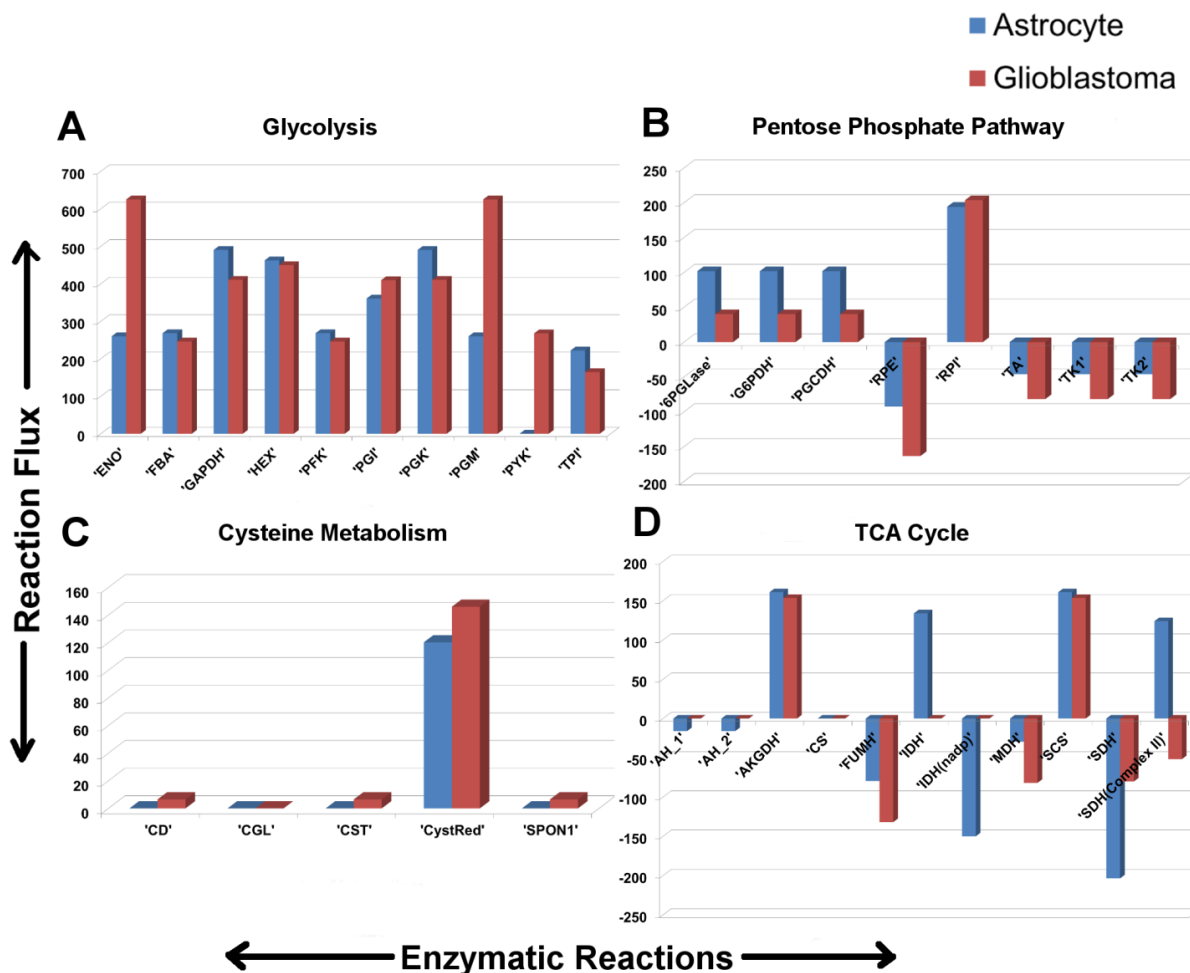


Figure 3.7: Pathway Response with maximization of GBM_BM as the objective function. The flow of flux through the different reactions of (A) Glycolysis, (B) Pentose phosphate pathway, (C) Cysteine metabolism, (D) TCA Cycle, and while maximizing GBM_BM for glioblastoma growth. A positive flux shows the progression of reaction in the forward direction, and a negative flux implies the flow of flux in the reverse direction.

3.2.7. Essential uptake metabolites for glioblastoma growth

Glioblastoma cell lines can show extremely long survival under glucose starved conditions by undergoing physiological adaptations to utilize alternatives and thus, bypass nutrient deprivation (229). In order to determine those metabolites which essentially contributed to glioblastoma survival, even at glucose starved conditions, the metabolic fate of eight carbon sources, namely, glucose (Glu), cystine (Cys), methionine (Met), tryptophan (Try), palmitate (PA), glutamate (Glut), glutamine (Gln), and glycine (Gly) in the network, was investigated (**Section 2.1.6**). GBM_BM was used as the objective function for this analysis. From the simulation results, cystine was found to be an essential metabolite for glioblastoma growth. As glucose is required to meet the glioblastoma growth demands, complete deprivation of glucose considerably reduced the flux through the objective function but did not lead to zero flux. Previous experimental findings have suggested a large reduction in cell growth due to glycolytic blockade by glucose starvation (231). In parity with the available experimental evidence, the model yielded that cystine was essential, and its deficiency might cause a disruption in the glioblastoma growth (19). Also, glucose uptake in combination with cystine could drive considerable flux through the objective function determining their contribution to glioblastoma growth instead of cystine alone as input (**Figure 3.8**). The simultaneous uptake and utilization of cystine and glucose served as the minimal metabolites that could maintain the growth requirement of glioblastoma by driving flux through necessary pathways that could generate the components of GBM_BM (**Eq. 2**). Cystine contributes to the production of glutathione that is required to combat oxidative stress. And glucose contributes to the production of ribulose-5-phosphate, oxaloacetate, and succinate through PPP and TCA cycle. Consequently, this minimal accounted for optimal glioblastoma growth. Restricting the uptake of either of these metabolites led to a highly reduced growth rate of glioblastoma (< 20% of the optimal value).

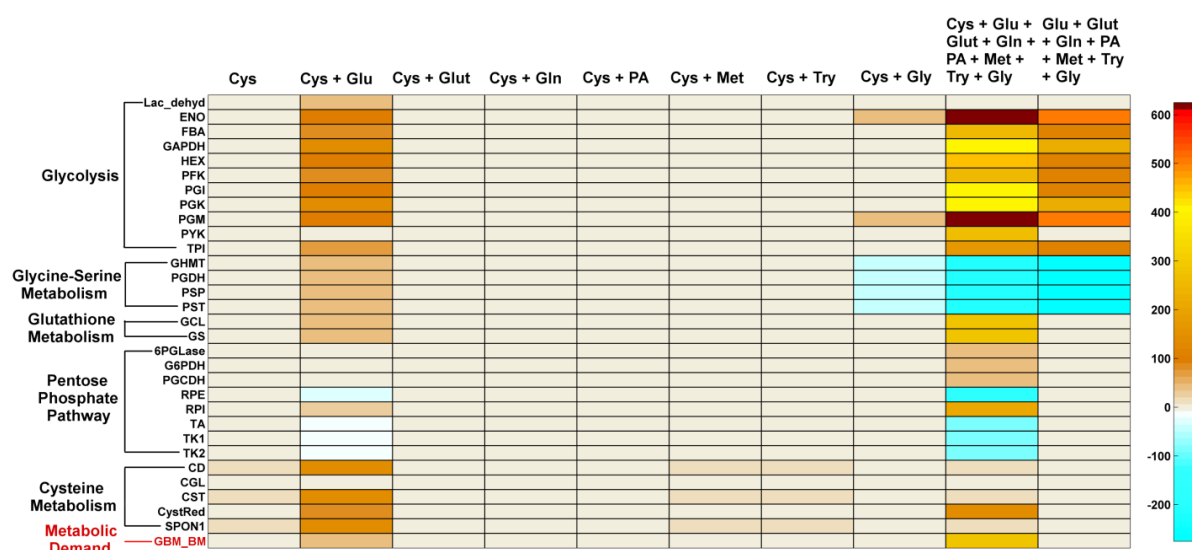


Figure 3.8: Essential input metabolites determining glioblastoma growth. Flux through different pathways and metabolic function in different input conditions to the glioblastoma scenario. Here flux through the different pathways and the metabolic function is maximum for cystine and glucose as input.

3.2.8. Metabolic reactions crucial for maintaining glioblastoma growth

To identify the essential reactions involved in maintaining glioblastoma growth, single and double reaction knockout analyses were performed (Section 2.1.7). All the single and double reaction knockout results were categorized as cases of lethal, trivial and non-trivial lethal and non-trivial solutions (Table 3.2). Knockout analysis was performed on the network using GBM_BM as the objective function. Those reactions whose knockout resulted in a zero flux through the objective function were considered “lethal” for glioblastoma growth.

Table 3.2: Total number of single and double lethal reactions obtained from the knockout analysis

Deletion	Lethal	Trivial Lethal	Non-trivial Lethal	Non-trivial Total	Total
Single	6	NA	6	208	208
Double	1268	1227	41	20301	21528

The lethal double reactions knockouts are categorized as trivial and non-trivial lethal. Those knockout combinations, of which at least one is a single lethal reaction, are considered to be “trivial”. Those combinations in which neither of the reactions is involved in single lethal reaction knockout are considered to be “non-trivial”.

NA – Not applicable

Glioblastoma cells can thrive on different metabolic pathways for survival and show great metabolic heterogeneity (231). In parity to this, it was observed that around 3% (6

reactions) (**APPENDIX A: Table A. 2**) of the total single knockouts (208 reactions) and 6% (1268 reactions) of the total double knockouts (21528) were lethal for the glioblastoma scenario. A low number of single lethal knockouts suggested the robustness of the metabolic network and sustenance of the glioblastoma growth through alternative routes.

Knockout analysis identified ribulose phosphate isomerase (RPI); a reaction of the pentose phosphate pathway, as lethal. In many types of cancers, it has been experimentally observed that PPP drives the glycolytic flux for the production of ribose-5-phosphate and NADPH that are used by cancers cells for maintaining redox balance and detoxification of reactive oxygen species (232). RPI is the rate-limiting step for ribose-5-phosphate production in the PPP pathway. As ribose-5-phosphate is essential to meet the cellular growth demand, RPI was predicted to govern a lethal phenotype in glioblastoma. Also, in different types of cancers, high levels of glutathione contents have been experimentally observed to protect the cells from oxidative stress (170). Glutamate-cysteine ligase (GCL), the rate-limiting step in the production of glutathione, was predicted to govern a lethal phenotype as it is the penultimate step for glutathione production. Similarly, glutathione synthase (GS), the ultimate step of glutathione synthesis, was also predicted to govern a lethal phenotype. The cystine-glutamate antiporter (Anti_cystine_glut) and cystine reductase (CystRed) reactions are involved in the production of cysteine. In the previous results, it was demonstrated that cystine was sufficient and important in maintaining the growth requirement of glioblastoma. Hence, both the reactions were predicted to demonstrate lethality when knocked out.

Of the 1268 lethal double knockout reactions, 41 were non-trivial (**APPENDIX A: Table A. 3**), which included reactions from glycolytic, pentose phosphate, TCA cycle, and glycine-serine metabolism pathway and a few transport reactions. The most typical observation of glioblastoma metabolism through experiments was the increased flux through glycolysis for high production of ATP and a corresponding reduction in glioblastoma growth under glucose starvation, even though the survival was maintained (231). Combinatorial targeting of the glycolytic pathway with the PPP, TCA cycle, and glycine-serine metabolic pathways was hence, found to be more effective in reducing glioblastoma growth. The knockdown of a glycolytic pathway reaction in combination

with a pentose phosphate pathway reaction or a TCA cycle reaction hindered the production of *r5p* or *oaa* or *succ*. Consequently, the double knockouts proved to be lethal to glioblastoma growth. The *in-silico* results also yielded reactions belonging to glycine-serine metabolism as good targets in combination with each other. Glycine was necessarily required for glutathione production. When the availability of glycine was blocked through the knockdown of both the internal glycine-serine metabolism and the external source of glycine uptake, this paired knockout led to the production of glutathione and hence proved lethal. Consequently, dual-targeting of the reactions of this pathway was effective in reducing the growth (**APPENDIX A: Table A. 4**).

The knockout reaction results were further classified as lethal, growth reducers, and null reducers on the basis of percentage inhibition in the growth demand reaction in the glioblastoma scenario (**Figure 3.9**). Knockouts that led to 100% inhibition of growth demand were considered to be “lethal”. Reaction knockouts that caused a flux reduction of greater than 80% of the flux through the objective function for growth were considered to be “Partial growth reducers”. Those set of reaction knockouts that reduced the flux through the objective function within 20% to 80% of the default value were considered as “Marginal growth reducers”. The class of ‘sub-marginal growth reducers’ was considered for those set of knockouts which could not bring effective reduction (0% to 20% inhibition) through the objective function. Analysis of the double knockout showed that 48% of the partial growth reducers belonged to the glycolytic pathway. The rest of the 52% were mostly constituted by the reactions of the TCA cycle, PPP, Oxidative phosphorylation, and Glycine-serine metabolism. The larger fraction of both single and double reaction knockouts belonged to sub-marginal growth reducers and null reducers, which were indicative of the robust and redundant reactions of the glioblastoma metabolic network.

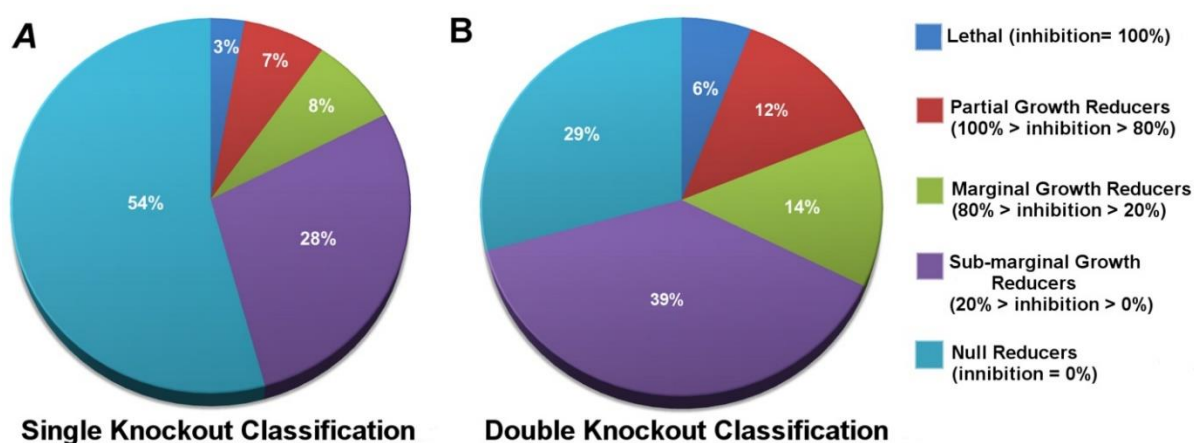


Figure 3.9: Single and double reaction knockout classification

3.2.9. Identification of reaction targets for therapeutic intervention

The reaction knockout analyses could predict a subset of reactions that were crucial in glioblastoma growth. To identify the feasibility of targeting these reactions and their effectiveness, these reactions were simulated for their effect as therapeutic targets for either inhibiting or reducing the growth rate of the glioblastoma cells to a normal range. For this analysis, the previously identified growth reducer reactions leading to reduced growth ($0 < \text{GBM_BM solution} < \text{glioblastoma optimum}$) were chosen (Section 2.1.8).

From the simulation, it was observed that in order to completely reduce the flux through the objective function, a complete reduction of flux through the lethal single knockout reactions is required. Whereas targeting the lethal double knockout reactions was more effective, as partial reduction of flux through those combinations brought a complete reduction in the flux through the objective function for growth. As such, combinations from non-trivial lethal knockout reactions were simulated, which could be targeted most effectively for efficient growth reduction.

Of the 41 non-trivial lethal double knockout predictions, 36 combinations were chosen for testing their growth intervening properties, which excluded a few transport reactions. Each reaction combination was simulated by varying the flux through individual reactions of the combination simultaneously to obtain the effective reduction of flux through both of these reactions, which reduced glioblastoma growth completely and to obtain a feasible flux range through both the reactions for which the growth was reduced to the normal level. The effective reduction of flux was depicted in percentage, which was

defined as the percentage reduction of flux through any particular reaction. The simulation results for the 10 most effective combinations have been shown as contour plots in **Figure 3.10**, and the rest of the 26 combinations have been listed in **APPENDIX A: Table A. 4**. The percentage reduction of flux value for complete reduction of growth and for Normal growth for each reaction of the combinations has been listed in **APPENDIX A: Table A. 5**.

Inhibitors for a few of these target reactions are already available (**APPENDIX A: Table A. 6**). *In-silico* study on the core metabolism in cancer cells showed that reactions of glycolytic, TCA cycle, oxidative phosphorylation, and pentose phosphate pathway could be good targets to check cancer cell progression (233). Our context-specific constraint-based metabolic model specific to glioblastoma interestingly could identify additional reactions belonging to the cysteine metabolism and reaction combinations belonging to the glycine-serine pathway as potential targets for controlling glioblastoma growth. These potent reaction pairs of the glycine-serine metabolism give way to the discovery/formulation of combinatorial drugs that can inhibit them. Therapeutic agents to target the glycine receptors are already known. Inhibitors like Picrotoxin targeted the neuronal γ -aminobutyric acid and homomeric glycine receptors (234), whereas strychnine hydrochloride was found to be a potent antagonist specific to the glycine receptor(235). These could be employed beneficially to understand the activity of the glycine transporters in glioblastoma, too, as evidence state a correlation between the glycine transporter activities with the distribution of its receptors(236). In recent years, many pharmaceutical companies have also developed potent and selective inhibitors for glycine transporters. SSR 504734 and SSR 103800 by researchers at Sanofi-Synthelabo Recherche, a series of *N*-(2-aryl-cyclohexyl) substituted spiropiperidines by researchers at F. Hoffmann-La Roche, Ltd. and ORG 25935 are a few compounds that showed promising results as inhibitors of glycine transporters (237). Our predictions can be further validated through experiments, thus providing testable targets to chemists and biologists for discovering small molecule inhibitors against glioblastoma.

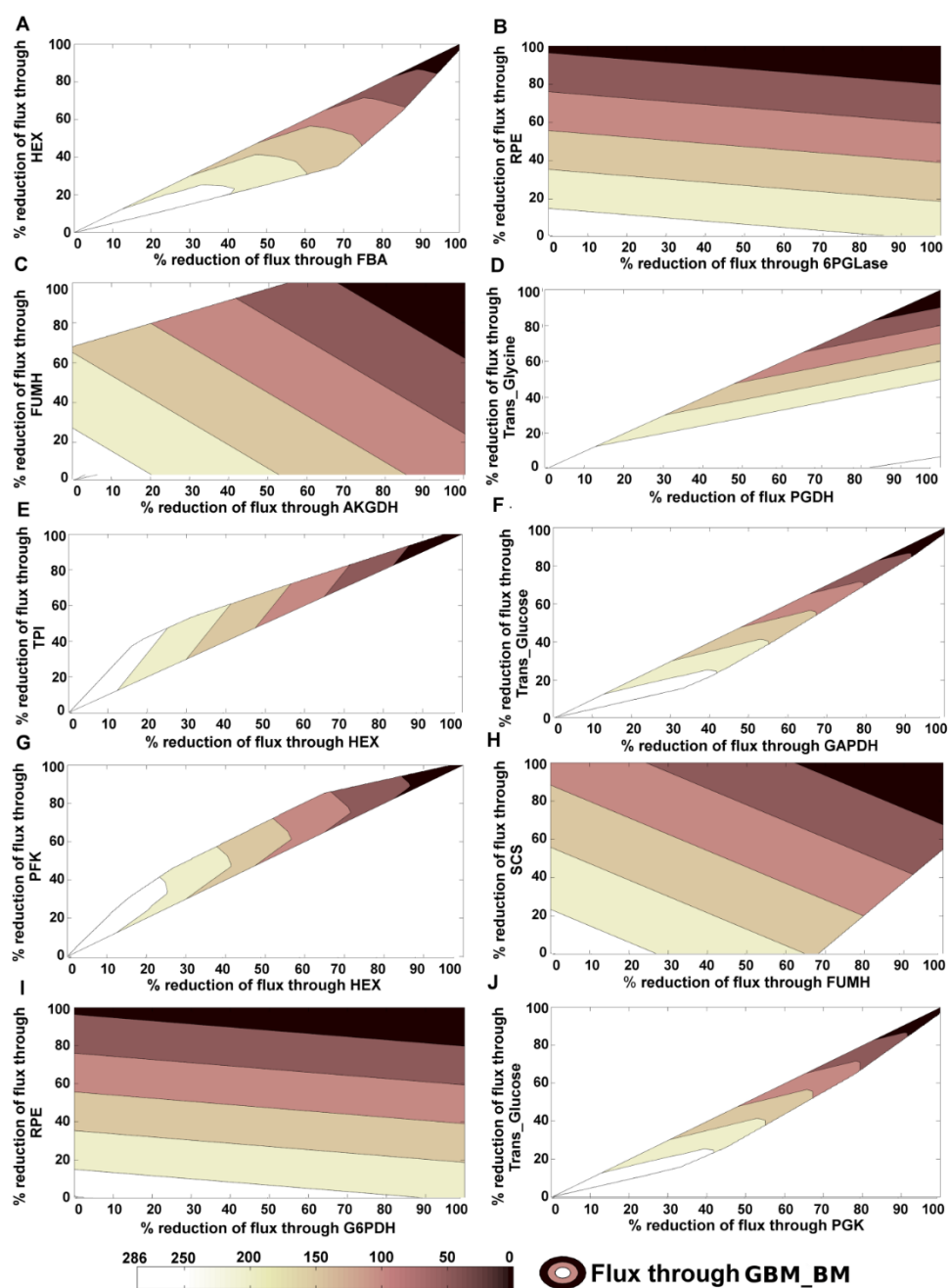


Figure 3.10: Therapeutic intervention scenarios and effective combination of target reactions. Percentage reduction of flux through the combination of essential double knockout reactions (A) Hexokinase (HEX) and fructose-1,6-bisphosphate aldolase (FBA), (B) ribulose phosphate-3 epimerase (RPE) and 6-phosphogluconolactonase (6PGLase), (C) fumarate hydratase (FUMH), and alpha-ketoglutarate dehydrogenase (AKGDH), (D) glycine transport (Trans_glycine) and Phosphoglycerate dehydrogenase (PGDH), (E) Hexokinase (HEX) and triosephosphate isomerase (TPI), (F) glucose transport (Trans_glucose) and glyceraldehyde-3-phosphate dehydrogenase (GAPDH), (G) phosphofruktokinase (PFK) and Hexokinase (HEX), (H) succinyl-CoA synthetase (SCS) and fumarate hydratase (FUMH), (I) ribulose phosphate-3 epimerase (RPE) and glucose-6-phosphate dehydrogenase (G6PDH) and (J) glucose transport (Trans_glucose) and phosphoglycerate kinase (PGK), and its effect on the flux through the metabolic function, GBM_BM (colored region of the contour plot).

3.3. Discussion

In the present work, a context-specific metabolic network for astrocyte and glioblastoma has been developed, which considers a biological context and a systems-level metabolic network to define a biological goal (238). The metabolic network for glioblastoma defines the biological context, and the interaction between the different pathways builds the physical structure of the network to ensure that the biological goal of ATP maximization and glioblastoma growth is achieved. Through this model, we tried to investigate the cumulative effect of a large-scale metabolism on the metabolic functioning of glioblastoma, the effect of the mutual connectivity of the individual pathways within the metabolic network, and the difference in response they show in the astrocytic and glioblastoma scenarios. Also, through the in-silico approach, we tried to gain some insight into the alternative metabolic routes and metabolites which contributed to the metabolic heterogeneity of glioblastoma. The present model was capable of yielding results that were in correspondence to the experimentally proved phenomena of both astrocytes and glioblastoma (2, 15, 179-181, 223)

Individual pathways interact mutually to propagate a network-level response. A cooperative effect of a few pathways could be contemplated in the present metabolic network, some of which have been observed experimentally, and a few were inferred through model predictions. Predictions of cooperative responses, which have been experimentally affirmed, include that of the cysteine metabolism pathway with the glutamate metabolism pathway in glioblastoma (17) and the glycolytic pathway with the glutamate metabolism pathway in astrocytes (11). A correlation of the glycine uptake with the glutamate and glutamine utilization in astrocytes was predicted from the model. The evidence stated that glycine content of neuronal cells was higher than that of glial cells (224), and most of the CNS tissues sufficed their glycine requirement via the internal glycine-serine metabolism pathway derived from glucose via 3-phosphoglycerate (225), even though astrocyte cultures fed with glycine were capable of utilizing it by maintaining intracellular levels of glutathione, serine, and creatine (226). Based on these literature evidence and predictions from the model, it was inferred that astrocytes' dependence on glycine uptake from external sources at a low, and most of its requirement is fulfilled by the internal glycine-serine biosynthesis pathway. Further, a higher uptake of glycine by

astrocytes from an external source resulted in a reduction in its glutamate uptake rate, and an excess of glycine caused glutaminolysis in the astrocytes. On the contrary, glioblastoma showed an increased glycine uptake which was driven towards the increased synthesis of glutathione. This increased production of glutathione was simultaneously accompanied by the increased uptake of cystine, which is taken in by the cystine-glutamate antiporter. Hence, a higher amount of glutamate was lost through efflux. This loss was compensated by glutamine uptake which is subsequently converted into glutamate within the cell.

Glioblastoma cell lines can show extremely long survival under glucose starved conditions, which are indicative of the fact that these cells undergo physiological adaptations to overcome nutrient deprivation (231). From the model, it was predicted that cystine could be one essential metabolite that could serve to glioblastoma survival and growth, even at glucose starved conditions. The utilization of glucose was found to be coupled to the cystine uptake in the model. This was perhaps because of the choice of the objective function. The objective function included ribulose-5-phosphate, oxaloacetate, succinate, and glutathione, which were generated by glycolysis and cysteine metabolism pathways. Consequently, a minimal combination of cystine and glucose could drive a considerable amount of flux through the objective function, as compared to any other minimal combination.

In-silico study on the core metabolism in cancer cells showed that reactions of glycolytic, TCA cycle, oxidative phosphorylation, and pentose phosphate pathway were good targets to check cancer cell progression (233), suggesting that the centrality-lethality hypothesis, which states that ‘The most highly connected proteins in the cell are the most important for its survival’ (239), also holds good for the metabolic networks. These pathways belonging to the central carbon metabolism essentially meet the energy requirements of the cell and hence are important. However, without disregarding the fact that central metabolism might be critical in complex networks but might not sufficiently predict lethality (153), reactions other than those belonging to the central carbon metabolism were also simulated for lethal responses. From the present context-specific constraint-based metabolic model for glioblastoma, it was observed that in addition to the above-mentioned pathways, targeting the reactions belonging to cysteine metabolism (Cystine

glutamate antiporter, Anti_cystine_glut, and cystine reductase, CystRed) and dual targeting of the reactions belonging to glycine-serine metabolism along with glycine transporter could potentially down-regulate the glioblastoma growth.

Thus, to summarize the present study, the constraint-based model could predict that most of the astrocytic glycine requirement was fulfilled by the internal glycine-serine metabolism pathway and excess glycine in the environment of growing astrocytes might have an effect on its glutamate metabolism. It could further demonstrate that cystine and glucose were two vital input metabolites, which could significantly contribute to glioblastoma growth. From model analysis for identification of therapeutic interventions, it was inferred that, reactions belonging to cysteine metabolism and combinatorial targeting of reactions belonging to glycine-serine metabolism could potentially reduce glioblastoma growth and hence can be proposed as prospective therapeutic targets. Our predictions can be further validated through experiments so as to enable the use of these targets in glioblastoma treatment. Thus, our study not only contributes to understanding the complexities, differences, and consequences of glioblastoma metabolic reprogramming but also provides an insight into the identification of important targets for therapeutic interventions.

CHAPTER 4

DYNAMICS OF ANTI-OXIDANT MACHINERY AND REGULATION OF OXIDANTS IN GLIOMAS

4.1. Rationale of the study

Reactive Oxygen Species (ROS) generation has been used as one of the non-surgical therapeutic approaches for cancer, as these are associated with the signalling cascade inducing cell death. Ironically, increased ROS production in cancer cells due to activation of oncogenes, reduced blood supply, and other factors cause progression and metastasis of cancer (240). ROS shows a paradoxical behavior, which can be stated as: increase in ROS to a certain non-lethal level serve normal biological processes, but a sustained high level for a long time might help in cancer progression (241). Antioxidants like glutathione (*gsh*), thioredoxin (*trx*), superoxide dismutase (SOD), etc., maintain a sustainable level of ROS within the cell. However, an increased redox capacity of *gsh* can cause chemoresistance in cancer (242). An intricate balance between the ROS and the antioxidants is maintained within the cell that ensures its proper functioning. Manipulative strategies of ROS in cancer are exhibited as changes in the redox and thiol ratio of the cells through regulations of various metabolic processes. However, the mechanism by which metabolic changes manage the ROS paradox in cancer remains poorly understood and debatable.

The differential suitability of ROS manipulation in tumor cells is explained by different theories. One of the most prevalent theories is the “*Threshold concept for cancer therapy*,” which states that as the level of ROS within the cancer cell increases, the ratio of ROS and antioxidants reaches a balance, beyond which any further increase in ROS or decrease in antioxidant activity will lead to cell death or increased sensitivity of tumor cells to cytotoxic treatments (243). According to an alternate threshold theory, when both tumor and normal cells are exposed to the equal intensity of exogenous ROS-producing or stimulating agents, the intracellular ROS levels of tumor cells increase more easily than the normal cells to reach a threshold and to trigger death due to higher basal level of ROS in tumors (240). While the validity of these theories in cancer has been proven with

increasing number of evidence, the quantifiable definition of ROS levels determining different cellular responses is subject to changes in the oxidant-antioxidant balance. The transformation of a cell from normal to tumor is governed by a sequence of events. Changes induced by these events are readily reflected as a change in the redox status of the cells mostly triggering ROS production. The applicability and effectiveness of ROS promotion or ROS depletion strategies in cancer therapeutics depend on where the cell is in the sequence of events. Change in the thiol ratio of the cell is another important determinant of the cellular response towards an oxidative insult. Reportedly, changes in the *nadph/nadp⁺* ratio and *gsh/gssg* ratio have been considered important in gaining a perspective towards the cellular response to such insults. The *nadph/nadp⁺* ratio is indicative of the reducing potential of the cell, which is required to be maintained high in order to keep the overall redox pool at a significantly reduced state for the proper functioning of the cell (244, 245). Changes in *gsh/gssg* ratio might induce the initiation of the induction phase of apoptosis (85, 246). A decrease in *gsh/gssg* ratio can induce apoptosis by causing Bcl-2 loss and activating caspase enzymes, whereas an increase in the ratio may have an effect otherwise (247).

The present chapter that fulfils the third objective of the thesis focuses on understanding the changing dynamics of oxidant-antioxidant balance and its effect on the redox and thiol status of the cell. Motivated by the findings of the previous chapter in which a subset of reactions belonging to different metabolic pathways was observed to be directed towards *gsh* production, we look deeper into the dynamics of this subset of reactions. The present ordinary differential equation model consists of 35 variables with 123 parameters (**APPENDIX B: Table B. 1 & Table B. 2**), capturing the dynamics of 25 reactions from 5 different metabolic processes (**Section 2.2.1 & 2.2.3**). The rationale behind considering these metabolic processes in understanding the oxidant-antioxidant dynamics is specified hereunder.

Central carbon metabolism: The glycolytic pathway branches out to various other pathways which are precursors to nucleotide, amino acid synthesis and other important biosynthesis pathways. A part of the glycolytic pathway which branches to serine metabolism has been considered, which allows the *de novo* synthesis of the amino acids, serine, and glycine within the cell (**Eq. 7 - Eq. 14**). Also, the pentose phosphate pathway

has been represented by the inclusion of glucose-6-phosphate dehydrogenase (G6PDH), which is a major source of *nadph* (Eq. 15).

Amino acid metabolism: A part of glutamate metabolism has been considered in the model. This forms another source of *nadph*, and glutamate supports the production of glutathione and also manages the uptake of cystine through the cystine-glutamate antiporter (Eq. 16 - Eq. 17). All the reactions belonging to serine and glycine metabolism have been considered in the model. This metabolism support generation of glutathione and maintains the redox status of the cell. Serine and glycine can be produced *de novo* from glycolytic intermediate *3pg*, and this part of the metabolism has been considered in the model (Eq. 20 - Eq. 24) (248). Cysteine metabolism has also been considered. The initiation of the metabolism has been considered with the uptake of cystine which is metabolized to cysteine (Eq. 25 - Eq. 26) (249). This reacts with glutamate to form glutamyl-cysteine (*glucys*), the precursor complex which reacts with glycine to produce glutathione (Eq. 18 - Eq. 19) (246).

Thiol metabolism: The thiol metabolism is represented by the glutathione metabolism itself. Two important enzymes which maintain glutathione homeostasis, i.e., glutathione peroxidase (Eq. 27) and glutathione oxidoreductase (Eq. 28), have been considered (85). Pertaining to the objective of looking into the glutathione and h_2o_2 dynamics, other thiol metabolisms like the peroxiredoxins, thioredoxins, and catalase systems have not been considered currently.

h_2o_2 production and metabolism: The model considers the activity of NADPH oxidase (250) and superoxide dismutase (193) as a part of h_2o_2 production. The formation of oxygen free radicals and their subsequent conversion into h_2o_2 is catalyzed by NADPH oxidase (Eq. 29) and superoxide dismutase (Eq. 30) respectively. The metabolism of h_2o_2 is linked to the thiol metabolism. Other mechanisms through which h_2o_2 are scavenged is represented by the parameter $d_{h_2o_2}$, which is defined as the decay of intracellular hydrogen peroxide in other cellular processes.

Redox metabolism: *nadph-nadp⁺* has been considered as the prime redox balancer in the model. The homeostasis and metabolism of *nadph-nadp⁺* have been considered in

reactions belonging to the earlier pathways where these function as cofactors to catalyze the reactions.

The oxygen uptake of the cell has been defined using the Michaelis-Menten equation (**Eq. 31**).

The model was calibrated using experimental data available for the temporal expression of *gsh* in retinal Muller glial cells under normal and amino acid supplemented scenarios (**Section 2.2.5**). Out of the 123 parameters, exact values of 31 parameters could be obtained from literature, and 69 parameters were assigned within the specified biologically ranges. 23 parameters remained unknown that were computed using the MCMC DRAM algorithm (**Section 2.2.6**). Using the model, we have demonstrated the role of the antioxidants in maintaining ROS levels under normal glial, hypoxic, and glioma conditions. Sensitive parameters associated with the regulation of metabolite variables that determine oxidant-antioxidant balance were identified using the eFAST algorithm (**Section 2.2.7**). Three different model conditions mimicking the normal glial, hypoxic, and glioma scenarios were simulated by introducing changes in the values of different parameters determined through parameter variation analyses (**Section 2.2.8, 2.2.9 & 2.2.10**). The model conditions were used to identify the changes in sensitivity of parameters in the three different scenarios. The parameters exclusive for the glioma scenario were used to identify the effect on the h_2o_2 level and to proposed therapeutic strategies of ROS manipulation in glioma (**Section 2.2.11**). Our hypothesis is the effectiveness of ROS manipulation as a therapeutic strategy depends on the ability to alter the redox and thiol status of the cell. Hence, throughout the study, the subsequent changes in the *nadph/nadp⁺* and the *gsh/gssg* ratio were continuously assessed.

4.2. Results

4.2.1. Dynamics of cells under normoxic conditions

The temporal behavior of reduced glutathione (*gsh*) (**Eq. 57**) and oxidized glutathione (*gssg*) (**Eq. 60**), hydrogen peroxide (h_2o_2) (**Eq. 59**) and oxygen radicals (*oxrad*) (**Eq. 65**) over time in the normal scenario were studied. The chemical kinetics of the enzyme GTHP have been included, which uses h_2o_2 and *gsh* as the substrates to yield *gssg*. From

simulations, we observe that the model was capable of maintaining h_2o_2 concentration within a biologically feasible range of $\sim 4\mu\text{M}$, which was initiated at a high h_2o_2 concentration of 1.5mM (**Figure 4.1A**), while there was a decrease in the gsh concentration (from 3.83mM to 2.33mM) and increase in the $gssg$ concentration (from 0.5mM to 2.09mM) at steady state. Meanwhile, the oxygen radicals ($oxrad$) generated as an action of NADPH oxidase (NOX) was readily metabolized into h_2o_2 due to the high activity of superoxide dismutase (SOD) as has been reported and was considered in the model ($V_m^{SOD} = 11.4 \cdot 10^3 \text{ mM hr}^{-1}$). Hence, a consistent reduced level of $oxrad$ was observed through our simulations.

As has been observed experimentally, a proliferating cell maintains a high $nadph/nadp^+$ ratio to maintain its redox balances and atp/adp ratio to suffice its proliferative requirements. In **Figure 4.1C**, we compared the experimentally reported values of $nadph/nadp^+$ (251) and average atp/adp (252, 253) ratios with the simulated values, which were comparable. The dynamics of the components of tripeptide that result in the formation of gsh were dictated by the $gsh-gssg$ cycle. **Figure 4.1B** shows the changes in the intracellular concentration of cystine (cys) (**Eq. 58**), glutamate ($glut$) (**Eq. 48**), glycine (gly) (**Eq. 54**) and glutamyl-cysteine ($glucys$) (**Eq. 56**) corresponding to changes in gsh and $gssg$ over time. Simulation results showed that in response to high oxidant (h_2o_2) concentration within the cell, available intracellular cystine and glutamate was used for the production of glutamyl-cysteine, which subsequently forms a complex with glycine to produce gsh . gsh then enters the $gsh-gssg$ cycle where gsh and h_2o_2 are used as substrate to produce $gssg$. As such, we observed a decline in the concentration of all other metabolites except for $gssg$, which was produced in response to nullify the high h_2o_2 concentration. Intracellular concentration of cystine and glutamate remained limiting in normal scenario.

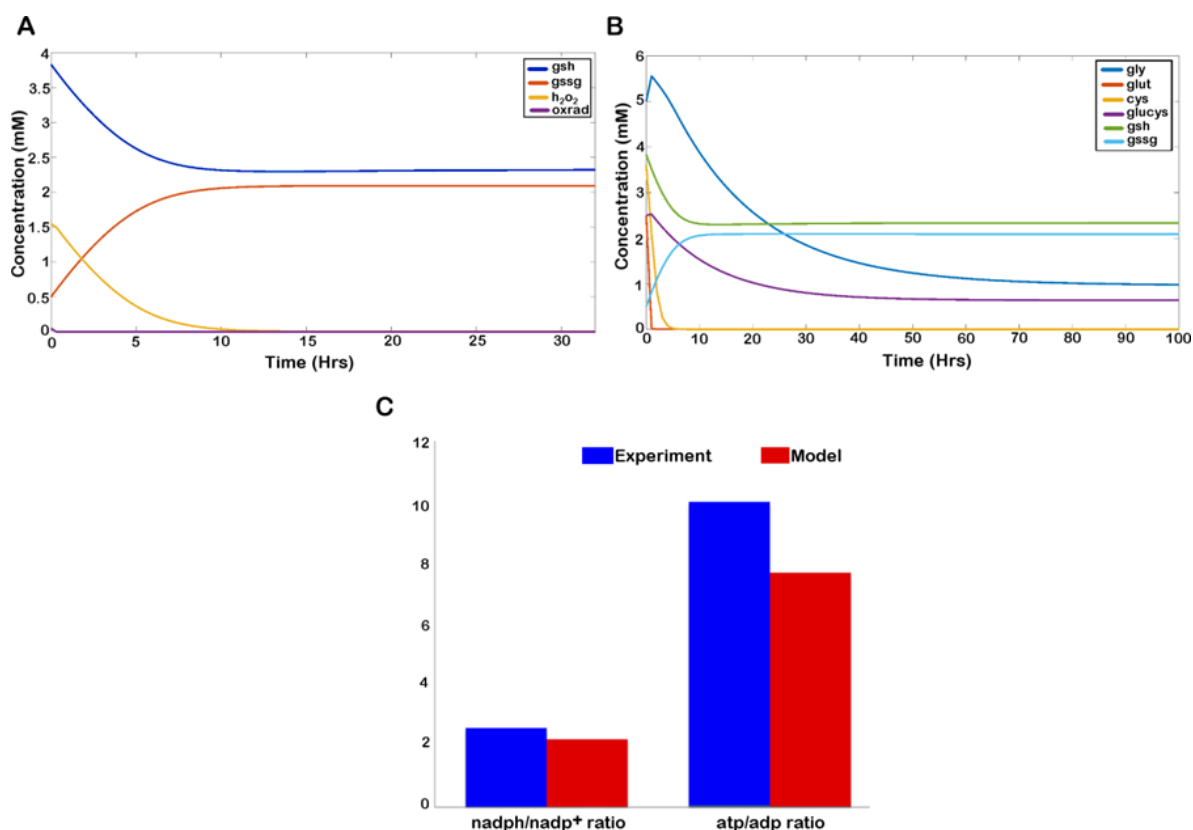


Figure 4.1: Model properties. (A) Temporal plot of *gsh*, *gssg*, h_2O_2 , and *oxrad*. (B) Temporal plot of the tri-peptides cystine (*cys*), glutamate (*glut*) and glycine (*gly*), and glutamyl-cysteine (*glucys*) along with changes in *gsh* and *gssg*. (C) Comparison of experimentally obtained range of $nadph/nadp^+$ and atp/adp ratio with values obtained through model simulation.

4.2.2. Analyses of sensitive parameters

Sensitivity analysis yielded a set of parameters crucial for determining the h_2O_2 level and the regulation of the *gsh-gssg* cycle. Enzymes GTHP, NOX, and GTHO were observed to be most sensitive in determining model properties. Changes in the uptake rate of oxygen also affected the model dynamics. Varying parameters for these enzymes showed interesting results, which are discussed in the subsequent subsections.

Effect of variation in V_{max} of Glutathione Peroxidase (GTHP)

The enzyme GTHP was crucial in neutralizing h_2O_2 with the help of *gsh*, which itself converted to *gssg*, converting h_2O_2 into H_2O . The V_{max} of the reaction is an important determinant of the rate of conversion of h_2O_2 . From our analysis, we could see that an increase in the V_m^{GTHP} (from 0.001 mM hr^{-1} to 1.5 mM hr^{-1}) resulted in a reduced level of

h_2o_2 . Simulations were performed at different time points (6hrs, 12hrs, 18hrs, 24hrs, and 32 hrs), and a similar trend was observed for all time points. A sharp decrease was observed at a V_{max} value between 0.1 mM hr⁻¹ to 0.3 mM hr⁻¹ when the h_2o_2 concentration was maintained at micromolar concentration, which initiated at a millimolar concentration (**Figure 4.2A**). However, the corresponding $nadph/nadp^+$ ratio remained unaltered, which suggests that the redox balance of the system largely remains unaffected by the change in V_m^{GTHP} although the $gsh/gssg$ ratio reduces significantly (**Figure 4.2B and C**). It is important to mention that the normal physiological expression of GTHP ranges between 0.2874 to 2.697 mM hr⁻¹ (**APPENDIX B: Table B. 1**), and interesting dynamics in h_2o_2 level, $nadph/nadp^+$, and $gsh/gssg$ ratios were only observable for a very low value of V_m^{GTHP} . By varying the value of V_m^{GTHP} from 0.001 mM hr⁻¹ to 1.5 mM hr⁻¹ we observed that high GTHP activity maintained a steady and low micromolar concentration of h_2o_2 , but h_2o_2 started accumulating as the activity lowered, which might induce oxidative damage to the cell. This observation could be compared with the diminished level of GTHP in brain tumors (254) and can be interpreted as a characteristic for gliomas with a very low expression of GTHP.

Effect of variation in V_{max} of NADPH Oxidase (NOX)

NADPH Oxidase catalyzes the production of oxygen free radicals from available oxygen using NADPH reduction. We could observe that an increase in the V_m^{NOX} (from 0.0001 mM hr⁻¹ to 1 mM hr⁻¹) resulted in an increase in the h_2o_2 concentration for the specified time points (6hrs, 12hrs, 18hrs, 24hrs, and 32 hrs). A marked decrease in the $nadph/nadp^+$ ratio and $gsh/gssg$ ratio was observed at later time points (24hrs and 32hrs) with the increase in V_{max} value (**Figure 4.2D, E, F**). This could be interpreted as one of the important factors determining the cancerous transformation of the glial cells.

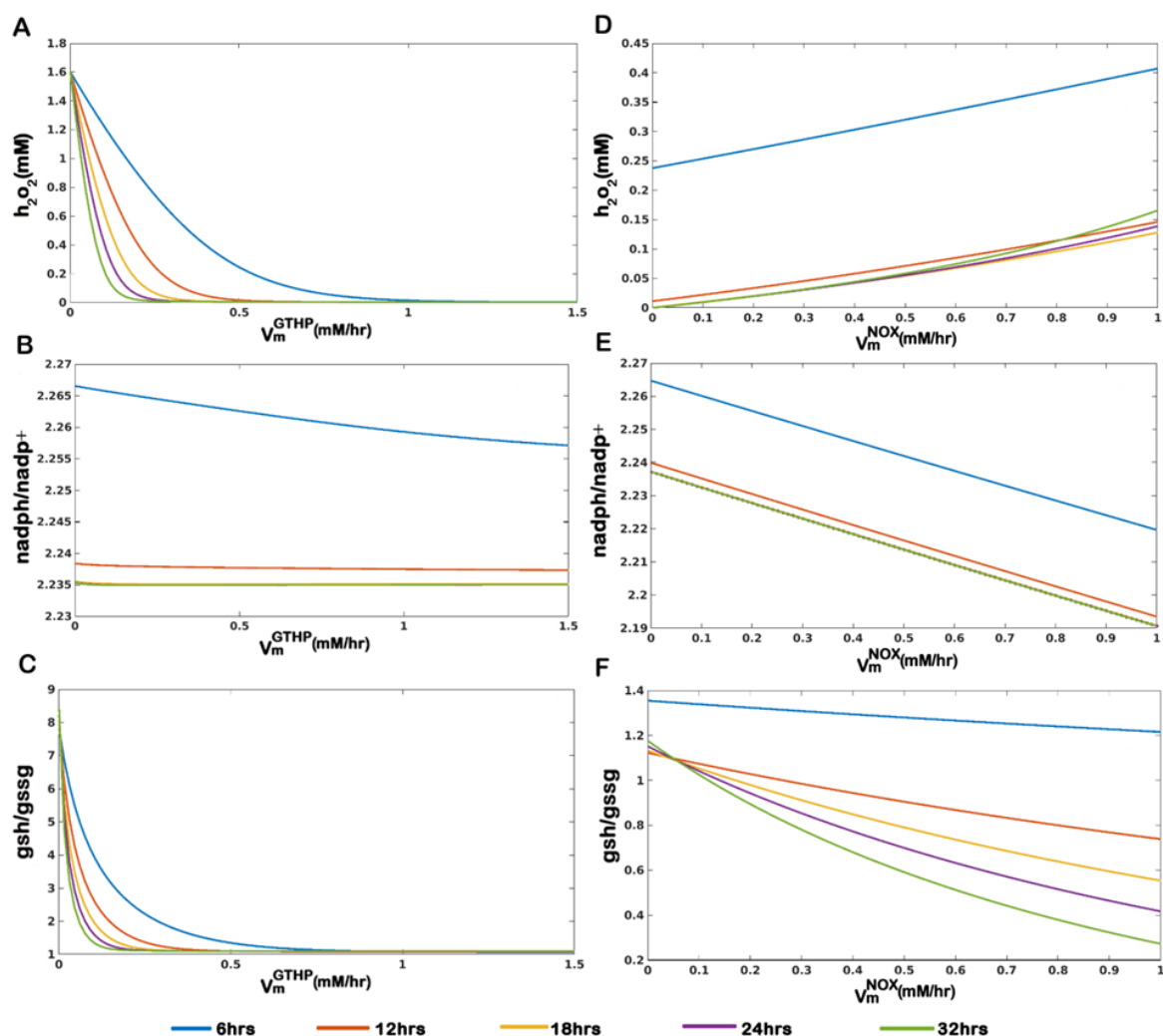


Figure 4.2: Parameter variation plot. (A-C) V_{max} of GTHP (V_m^{GTHP}) and (D-F) V_{max} of NOX (V_m^{NOX}) under the normal condition at different time points.

Effect of two-parameter variation of V_{max} of GTHP and V_{max} of GTHO

Figure 4.3 (A-C) illustrates the effect of simultaneous change in V_m^{GTHP} and V_m^{GTHO} on h_2O_2 level, $nadph/nadp^+$ and $gsh/gssg$ ratios. The h_2O_2 level reduced with increasing activity of V_m^{GTHP} , although change in the kinetics of GTHO did not have an effect (**Figure 4.3A**). When $nadph/nadp^+$ was taken into account, we observed that at a very low V_m^{GTHO} , the effect of V_m^{GTHP} remained minimum. With a gradual increase in the V_m^{GTHO} there was a reduction in the $nadph/nadp^+$ ratio, which furrowed deeper at a higher value of V_m^{GTHP} . The enzyme GTHO facilitates the reduction of $gssg$ into gsh in a $nadph-nadp^+$ dependent manner, and hence with an increasing enzyme availability and activity, the $nadph/nadp^+$ ratio was reduced. Here, we considered the dynamics of $nadph/nadp^+$ at 12hrs and could

observe that the initial dynamics were dependent on V_m^{GTHO} . At high V_m^{GTHP} , with increase in V_m^{GTHO} there was a decrease in the $nadph/nadp^+$ ratio (**Figure 4.3B**) which was due to the active involvement of the enzyme in nullifying the persistent levels of the substrate, h_2o_2 . We observed the decrease in the ratio till V_m^{GTHO} reached a value of 0.2 mM hr⁻¹ at 12 hours. However, the decrease was compensated back with further increase in the V_{max} . As a high level of h_2o_2 was metabolized to a non-toxic micromolar level, we observed from our model simulation that a V_{max} of 0.2 mM hr⁻¹ for the enzyme GTHO was sufficient to metabolize the persisting levels of h_2o_2 at 12 hours. At a V_{max} value lower than this, the enzyme became the limiting factor, and beyond this value, the activity of the enzyme was limited by the availability of the substrate (h_2o_2). Meanwhile, at lower values of V_m^{GTHP} (<0.5 mM hr⁻¹), persisting level of h_2o_2 at 12hrs was higher due to the slow activity of GTHP (**Figure 4.3A**). The substrate remained available for GTHO activity which continued to metabolize the conversion (at higher V_m^{GTHO} which was limited by substrate concentration in the earlier case) and $nadph$ pool diminished resulting into a reduction in $nadph/nadp^+$ ratio. The dip in the $nadph/nadp^+$ ratio was compensated by the action of other reactions that replenished the $nadph$ pools represented in the model as l_{nadph} . Trends were similar for $gsh/gssg$ ratio which was dependent on the substrate availability (h_2o_2) except at a very low value of V_m^{GTHP} (0.001 mM hr⁻¹) which limited the conversion of gsh to $gssg$ thereby resulting in an accumulation of gsh and leading to very high $gsh/gssg$ ratios. h_2o_2 level persisted in the sub-micromolar range (~0.045mM) at a V_{max} of 0.5 mM hr⁻¹ for GTHP, which was subsequently metabolized to micromolar levels (0.002mM) with further increase in V_{max} (**Figure 4.3A**). This governed the change in $gsh/gssg$ ratio and an increase in both V_m^{GTHP} and V_m^{GTHO} coordinated to metabolize h_2o_2 till it reached micromolar levels by cyclic production and consumption of gsh and $gssg$. As h_2o_2 reached a micromolar level, the activity of GTHP was limited due to h_2o_2 availability, whereas gsh production continued by the action of GTHO till $gssg$ reached a basal level. At this point, we observed an increase in the $gsh/gssg$ ratio (**Figure 4.3C**).

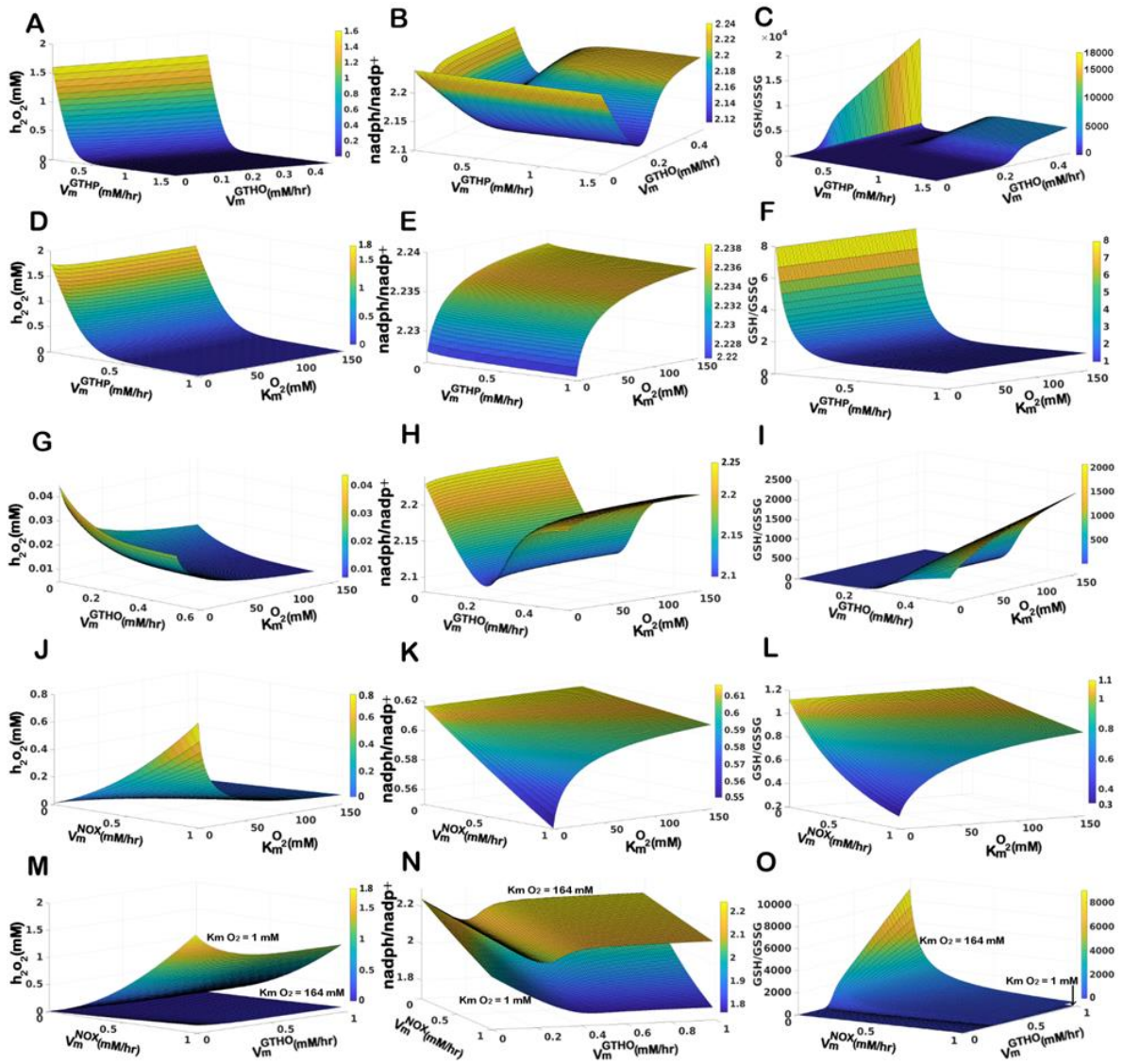


Figure 4.3: Surface plots of two-parameter variation for the sensitive parameters on h_2O_2 level, $nadph/nadp^+$ ratio, and $gsh/gssg$ ratio. (A-C) Effect of variations in V_m^{GTHP} and V_m^{GTHO} under normoxic conditions ($k_m^{O_2} = 164\text{mM}$). (D-F) Effect of variation in V_m^{GTHP} under changing oxygen demand ($164\text{mM} \geq k_m^{O_2} \geq 1\text{mM}$). (G-I) Effect of variation in V_m^{GTHO} under changing oxygen demand ($164\text{mM} \geq k_m^{O_2} \geq 1\text{mM}$). (J-L) Effect of variation in V_m^{NOX} under changing oxygen demand ($164\text{mM} \geq k_m^{O_2} \geq 1\text{mM}$). (M-O) Combined effect of simultaneous variation in V_m^{NOX} and V_m^{GTHO} under $k_m^{O_2} = 164\text{mM}$ and $k_m^{O_2} = 1\text{mM}$.

4.2.3. Dynamics of cells under high oxygen demand: induction of hypoxia

To mimic the changing oxygen demand of cells during cancerous transformation, we tuned the model parameter $k_m^{O_2}$ which determined the affinity for substrate (**Section 2.2.9**). A low K_m value implies an increase in the affinity for the substrate. To represent an increased affinity of the cell for oxygen, lowering values of K_m was tried ($k_m^{O_2} = 164, 50,$

10 and 1mM). As the value lowered, the cellular demand for oxygen increases, and the concentration of external oxygen reduced, creating a mild to severe hypoxic condition (**APPENDIX B: Figure B. 2**). Parameter variation of sensitive parameters was tried at $k_m^{O_2} = 1\text{mM}$ to investigate the changes in the reaction dynamics with induction of hypoxia and the results are discussed below.

Effect of changing Glutathione Peroxidase (GTHP) enzymatic activity

We observed a change in dynamics of h_2o_2 , $nadph/nadp^+$, and $gsh/gssg$ ratios with changing V_m^{GTHP} and $k_m^{O_2}$. Hydrogen peroxide (h_2o_2) concentration (**Figure 4.3D**) and $gsh/gssg$ ratio (**Figure 4.3F**) primarily depended on V_m^{GTHP} and remain unaffected by the change in $k_m^{O_2}$. The enzyme GTHP metabolized the conversion of h_2o_2 into water by oxidizing gsh to $gssg$, and hence the enzyme concentration directly affected the h_2o_2 concentration and $gsh/gssg$ ratio. Redox ratio ($nadph/nadp^+$) however, depended on $k_m^{O_2}$ and remained unaltered with change in the V_m^{GTHP} (**Figure 4.3E**). We inferred that high level of oxidants generated in response to increased uptake of oxygen (which eventually creates a hypoxic microenvironment for the cell) could be dealt with increased activity of GTHP within the cell but at the cost of reduced $nadph/nadp^+$ and $gsh/gssg$ ratios.

Effect of changing Glutathione Oxidoreductase (GTHO) enzymatic activity

At 12 hours, h_2o_2 was maintained between sub-micromolar to micromolar levels (0.045mM to 0.005mM) for changing values of V_m^{GTHO} and $k_m^{O_2}$. The concentration of h_2o_2 reduced with increasing V_m^{GTHO} . Simultaneously with increasing $k_m^{O_2}$, a further reduction in h_2o_2 level was observed (**Figure 4.3G**). The $nadph/nadp^+$ ratio showed a dip at the V_{max} value of 0.2 mM hr⁻¹ for GTHO, which was compensated back with a further increase in the V_{max} (**Figure 4.3H**). We plotted the temporal plots of varying V_m^{GTHO} at high oxygen demand ($k_m^{O_2}=1\text{mM}$) and checked the $nadph/nadp^+$ ratios at different time points (**APPENDIX B: Figure B. 3**). We inferred from our model simulations that the $nadph/nadp^+$ ratio in the model depends upon two factors: (i) concentration of the enzyme GTHO available to convert the $gssg$ into gsh in order to maintain the $gsh-gssg$ cycle necessary for neutralizing h_2o_2 levels (ii) the amount of oxidant (h_2o_2) concentration

persisting at any point of time. The $gsh/gssg$ ratio showed different patterns at different values of the two parameters (**Figure 4.3I**). At low values of V_m^{GTHO} , the enzymatic activity was limited and hence the conversion of $gssg$ to gsh was slower. With a low V_m^{GTHO} ($< 0.2mM$), $gssg$ accumulated and the difference in gsh and $gssg$ concentration reduced, resulting in a low $gsh/gssg$ ratio. As the V_{max} increased, the conversion of $gssg$ to gsh enhanced, which added to the gsh production pool, and the difference in gsh and $gssg$ concentration widened, giving high values of $gsh/gssg$ ratio. Adding to it was the effect of oxygen within the cell. As $k_m^{O_2}$ increased, the oxidant production was limited (due to limited substrate availability for NOX and SOD), and hence the conversion of gsh to $gssg$ was reduced, leading to a further increase in the $gsh/gssg$ ratio.

Effect of changing NADPH Oxidase (NOX) enzymatic activity

Characteristic changes in h_2o_2 , $nadph/nadp^+$ ratio, and $gsh/gssg$ ratio with changing V_m^{NOX} was observed under normoxic conditions. When we simulated the variation of the parameter over varying $k_m^{O_2}$, the concentration of h_2o_2 took a leap as V_m^{NOX} increased and $k_m^{O_2}$ decreased (**Figure 4.3J**). At smaller K_m value, cellular uptake of oxygen increased, and an increase in V_m^{NOX} ensured rapid metabolism of oxygen into free radicals. These free radicals were readily metabolized into h_2o_2 due to the high V_m^{SOD} which catalyzed the conversion. Hence, with the increasing activity of NOX, the free radicals so formed were directed towards the production of h_2o_2 . An inverse pattern of $nadph/nadp^+$ and $gsh/gssg$ ratio was observed in response to the changing h_2o_2 concentration (**Figure 4.3J**) due to the activity of the $gsh-gssg$ cycle (**Figure 4.3K-L**).

We inferred from the above simulations that GTHP is an important determinant of h_2o_2 levels in the cell. An increase in the activity of GTHP is helpful in reducing the h_2o_2 levels to a feasible range without affecting the $nadph/nadp^+$ ratio much, although it alters the $gsh/gssg$ ratio. The effect of changing affinity for oxygen was nullified with a change in V_m^{GTHP} . We attempted varying the activity of GTHP with other sensitive parameters only to observe a reduction in the h_2o_2 while maintaining the redox balance of the cell within a feasible range. As such, we propose here that an increase in the activity of GTHP is desirable for an antioxidant therapy as it reduces the h_2o_2 levels irrespective of oxygen

demand, simultaneously lowering the $gsh/gssg$ ratio, which is considered an initiation factor in the induction of apoptosis, thereby guiding the cell to an apoptotic fate in case of major oxidative damage.

While GTHP can be used for antioxidant therapy, analyses with NOX and GTHO suggested that they are favourable targets for pro-oxidant therapies. An increase in NOX activity at high oxygen demand clearly increased h_2o_2 production along with simultaneous lowering of $nadph/nadp^+$ and $gsh/gssg$ ratio, indicating cellular toxicity and initiation of apoptotic pathways. Changes in GTHO activity have differing patterns in brain tumors. A decrease in h_2o_2 concentration was observed with increasing GTHO activity in the model. However, $nadph/nadp^+$ and $gsh/gssg$ ratio at around a V_{max} value of 0.2 mM hr^{-1} of GTHO showed an ideal condition to initiate cellular toxicity. We further analyzed the effect of the two enzymes in reducing the redox potential and $gsh/gssg$ ratio of the cell at different oxygen demands of the cell.

An increase in NOX and GTHO activity had a synergistic effect in increasing the h_2o_2 concentration (**Figure 4.3M**) and lowering the $nadph/nadp^+$ ratio (**Figure 4.3N**) under high oxygen demand. Thiol ratio ($gsh/gssg$), however, lowered down with increasing activity of NOX, which otherwise increased with increasing GTHO activity at low NOX activity ($<0.3 \text{ mM hr}^{-1}$) (**Figure 4.3O**).

4.2.4. Redox and thiol status of the cell under glioma scenario

From the previous set of analyses, we observed that the system showed a characteristic change in its behavior for changes in sensitive parameters that were related to oxidant and antioxidant production. We used these parameters to create the glioma model scenario (**Section 2.2.10**). The system remained robust for most of the other parameter changes. The sensitivity of the h_2o_2 increased for GTHO during high oxygen demand which otherwise remained mostly unaffected in normoxic conditions. Also, the sensitivity of h_2o_2 increased for NOX during high oxygen demand. Parameter values to V_m^{NOX} , V_m^{GTHO} , V_m^{GTHP} and $k_m^{O_2}$ were changed to 1 mM hr^{-1} , 0.2 mM hr^{-1} , 0.19 mM hr^{-1} and 1 mM from $0.0468 \text{ mM hr}^{-1}$, 0.5 mM hr^{-1} , $0.00216 \text{ mM hr}^{-1}$ and 164 mM respectively to create the glioma scenario. Temporal plots generated for this model showed an excess increase in

h_2o_2 concentration due to limited regulation by *gsh* and *gssg*. A decline in $nadph/nadp^+$ and $gsh/gssg$ ratio was also observed.

With an observable difference in the cellular redox status and the ROS level, we tried to understand if the changes in $nadph/nadp^+$ and $gsh/gssg$ ratios associated with the changes in h_2o_2 level during the introduction of mutations in the model could be used to determine the pro-apoptotic or anti-apoptotic fates of the cell. Temporal dynamics of the changes in h_2o_2 level and the two ratios for normal, hypoxia, and glioma conditions for a duration of 48hrs are shown in **Figure 4.4**. Under normal conditions, the h_2o_2 level was readily reduced to micromolar concentration (4 μ M), and the resulting values of $nadph/nadp^+$ and $gsh/gssg$ ratios at steady state were 2.63 and 1.2 (**Figure 4.4A**). The values mostly remained unaltered during a shift to hypoxia except for a slight reduction in the $gsh/gssg$ ratio over time (**Figure 4.4B**). Changes were, however, distinct in the case of glioma. Reports suggest a difference in the expression of GTHO in gliomas: some show a high expression and some low (195). We created both the conditions in the model and observed a characteristic difference in the $gsh/gssg$ ratio and h_2o_2 level in the two scenarios. Under high GTHO expression ($V_m^{GTHO} = 0.19 \text{ mM hr}^{-1}$), the $gsh/gssg$ ratio remained higher than the normal (**Figure 4.4C**) whereas, under low GTHO expression ($V_m^{GTHO} = 0.001 \text{ mM hr}^{-1}$) the ratio diminished to a very low value of 0.01 with an abrupt increase in h_2o_2 level (**Figure 4.4D**). Through the simulations, we propose that at high values of V_m^{GTHO} , the increased level of $gsh/gssg$ ratio helps the cell to evade programmed cell death, which would otherwise lead to apoptosis by the induction of toxicity due to an uncontrolled increase in h_2o_2 levels. However, at lower values of V_m^{GTHO} , a sharp decline in the $gsh/gssg$ ratio drives the cell towards an apoptotic fate. As such employing an anti-oxidant approach at high V_m^{GTHO} and a pro-oxidant approach at low V_m^{GTHO} will provide a better surveillance strategy to eliminate cancer cell progression. We observed only a slight difference in the $nadph/nadp^+$ ratio under present simulation conditions. Regulation of $nadph/nadp^+$ ratio, however, can be employed to facilitate the pro- or anti-oxidant approach by modulating the $nadph/nadp^+$ ratio either by inhibition or activation of NAD kinase, a potent regulator of the $nadph-nadp^+$ pool within the cell (255, 256).

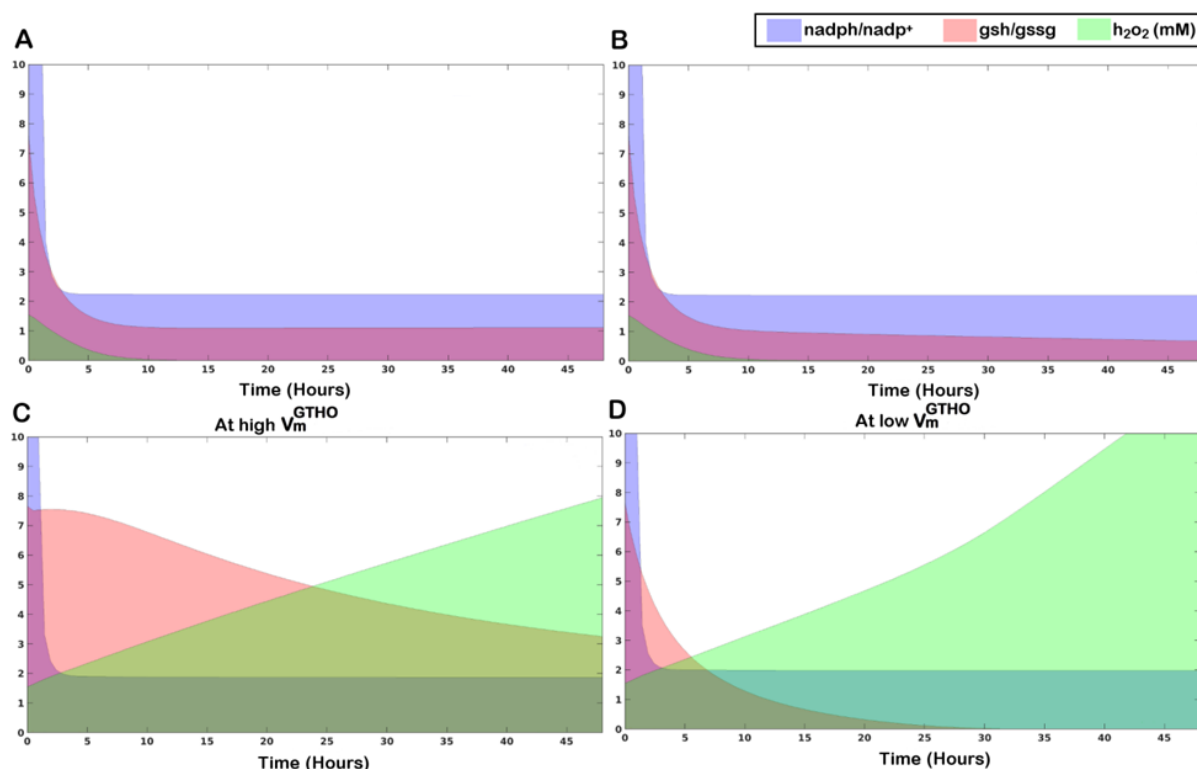


Figure 4.4: Temporal area plots of changing $nadph/nadp^+$ and $gsh/gssg$ ratios along with a change in h_2o_2 concentration. (A) Normal condition, (B) Hypoxia, (C) Glioma at high V_m^{GTHO} (0.19 mM hr^{-1}), (D) Glioma at low V_m^{GTHO} (0.001 mM hr^{-1}).

In order to identify parameters that influence the cellular properties under these different conditions, sensitivity analyses were performed for the model with high oxygen demand (hypoxia scenario, by changing $k_m^{O_2}$) and for the model with multiple mutations (glioma scenario). A comparison of the sensitive parameters (p-value <0.05) for the variables h_2o_2 , gsh , and $gssg$ for the three conditions: normal, hypoxic, and glioma, showed common and unique sensitive parameters for each scenario (**Figure 4.5 & Table 4.2**). The kinetics of the enzyme GTHP remained crucial in all three scenarios owing to its direct involvement in the production of gsh . Apart from the parameters which directly regulated the variables, a few non-intuitive parameters were found to be sensitive for the different scenarios. Analyses of these parameters show that the influence exerted by them on the variables resulted in micromolar and nanomolar concentrations changes for the present simulation conditions. The set of parameters that were unique and common to the three different simulation scenarios are shown in **Figure 4.5**. We suggested that regulation of these parameters might help in facilitating pro- or anti-oxidant therapeutic strategies.

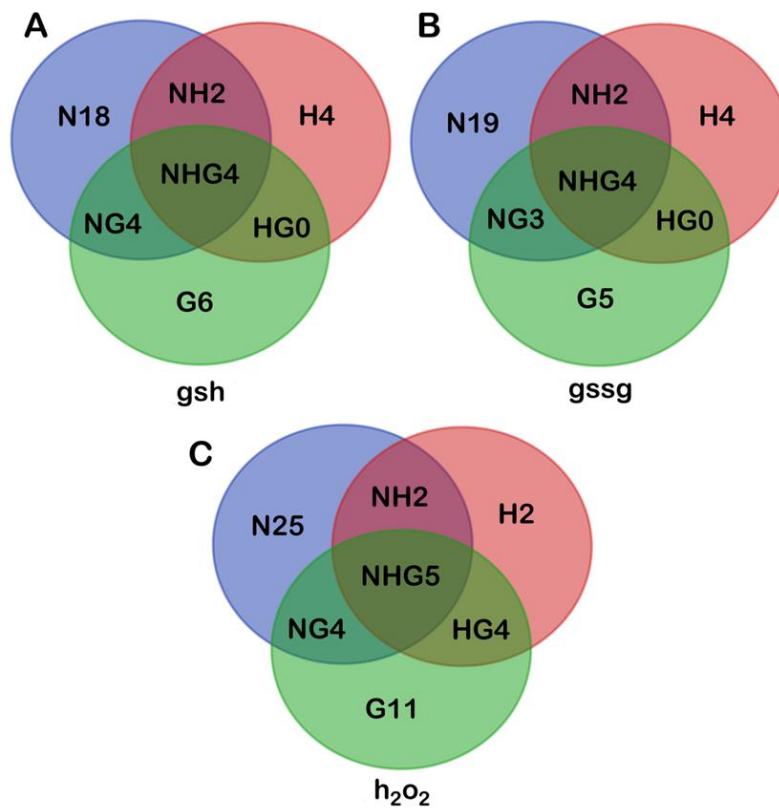


Figure 4.5: Comparison of sensitive parameters in Normal, Hypoxia, and Gliomas for the variables gsh , $gssg$, and h_2o_2 . The abbreviations used here are **N**: Normal, **H**: Hypoxia, **G**: Gliomas, **NH**: Normal and Hypoxia, **NG**: Normal and Gliomas, **HG**: Hypoxia and Gliomas, and **NHG**: Normal, Hypoxia and Gliomas. The sensitive parameters for each variable under each condition have been tabulated in **Table 4.1**.

Table 4.1: List of sensitive parameters for gsh , $gssg$, and h_2o_2 under normal, hypoxic, and glioma scenarios.

<i>gsh</i>	
N18	$V_m^{PGI}, k_{3php}^{PST}, k_{atp}^{GS}, k_m^{O_2}, k_{i(3pg)}^{PGCDH}, k_{atp}^{GCL}, k_{i(cys)}^{CR}, V_m^{GHMT}, k_{cys}^{CR}, k_{f6p}^{PFK}, d_{oxy}, k_{i(glut)}^{PST}, V_m^{GLUTEX}, V_m^{PSP}, k_{i(gap)}^{GAPDH}, k_{gap}^{GAPDH}, k_{i(gly)}^{GS}, V_m^{PFK}$
H4	$k_{i(atp)}^{HK}, k_{oxrad}^{SOD}, k_{i(atp)}^{PFK}, k_{O_2}^{NOX}$
G6	$k_{i(gssg)}^{GTHO}, V_m^{NOX}, V_m^{GS}, l_{nadp}, l_{nadph}, d_{nadph}$
NH2	k_{adp}^{PGK}, V_m^{GCL}
HG0	-
NG4	$V_m^{GTHO}, k_{gssg}^{GTHO}, k_{i(atp)}^{GS}, k_{nadph}^{GTHO}$

NHG4	$k_{i(h_2O_2)}^{GTHP}, V_m^{GTHP}, k_{h_2O_2}^{GTHP}, k_{gsh}^{GTHP}$
gssg	
N19	$V_m^{PGI}, k_{3php}^{PST}, k_{atp}^{GS}, k_m^{O_2}, k_{i(3pg)}^{PGCDH}, k_{atp}^{GCL}, k_{i(cys)}^{CR}, V_m^{HK}, V_m^{GHMT}, k_{cys}^{CR}, k_{f6p}^{PFK}, d_{oxy},$ $k_{i(glut)}^{PST}, V_m^{GLUTEX}, V_m^{PSP}, k_{i(gap)}^{GAPDH}, k_{gap}^{GAPDH}, k_{i(atp)}^{GS}, V_m^{PFK}$
H4	$k_{i(atp)}^{HK}, k_{oxrad}^{SOD}, k_{i(atp)}^{PFK}, k_{O_2}^{NOX}$
G5	$k_{i(gssg)}^{GTHO}, V_m^{NOX}, l_{nadph}, l_{nadp}, d_{nadph}$
NH2	k_{adp}^{PGK}, V_m^{GCL}
HG0	-
NG3	$V_m^{GTHO}, k_{gssg}^{GTHO}, k_{nadph}^{GTHO}$
NHG4	$k_{i(h_2O_2)}^{GTHP}, V_m^{GTHP}, k_{h_2O_2}^{GTHP}, k_{gsh}^{GTHP}$
h_2O_2	
N25	$V_m^{PGI}, k_{3php}^{PST}, k_{atp}^{GS}, k_m^{O_2}, k_{i(3pg)}^{PGCDH}, d_{nadh}, k_{atp}^{GCL}, k_{i(cys)}^{CR}, V_m^{HK}, d_{glut}, V_m^{GHMT}, k_{cys}^{CR}, k_{f6p}^{PFK},$ $V_m^{PFK}, k_{i(glut)}^{PST}, V_m^{GLUTEX}, V_m^{GTHO}, V_m^{PSP}, k_{i(gap)}^{GAPDH}, k_{gssg}^{GTHO}, k_{gap}^{GAPDH}, d_{h_2O_2}, V_m^{GLYex},$ $k_{i(atp)}^{GS}, k_{i(glut)}^{GLUD}$
H2	$k_{i(atp)}^{HK}, k_{oxrad}^{SOD}$
G11	$d_{mlthf}, k_{3pg}^{PGCDH}, L_{oxy}, d_{php}, k_{glut}^{xCT}, k_{i(nadph)}^{NOX}, k_{nadph}^{NOX}, V_m^{FBA}, k_{glucys}^{GS}, k_{nadph}^{CR}, l_{atp}$
NH2	$V_m^{GCL}, V_m^{O_2}$
HG4	$V_m^{NOX}, l_{nadph}, d_{in}, k_{O_2}^{NOX}$
NG4	$l_{glut}, k_{i(atp)}^{GCL}, l_{nadp}, d_{oxy}$
NHG5	$k_{adp}^{PGK}, k_{i(h_2O_2)}^{GTHP}, V_m^{GTHP}, k_{h_2O_2}^{GTHP}, k_{gsh}^{GTHP}$

4.2.5. Identification of combinatory targets for pro and anti-oxidant therapy

We analyzed the influence of parameters sensitive in regulating h_2O_2 levels under the glioma scenario using the parameters listed in G11 in **Table 4.1**. These parameters did not regulate the ROS levels directly yet showed differences in the ROS levels along with

changes in $gsh/gssg$ and $nadph/nadp^+$ ratios when varied individually or in combination. Enzymes and metabolites associated with a few of these parameters like methyltetrahydrofolate ($mlthf$) (257, 258), NADPH Oxidase (NOX) (250, 259, 260), cystine-glutamate antiporter (xCT) (261), etc., have already been implicated in having a crucial role in regulating ROS levels in the cell. A few parameters associated with enzymes that did not directly regulate the ROS and glutathione production, like Phosphoglycerate Dehydrogenase (PGCDH), Cystine Reductase (CR), and Fructose Bis-phosphate Aldolase (FBA), were also identified. These parameters did not necessarily show a significant difference in the ROS levels when varied individually but showed characteristic difference when varied in combinations. These changes can be utilized for designing pro-oxidant or anti-oxidant approaches for therapeutic targeting. A few of the combinations which brought distinct changes in the h_2o_2 level, $gsh/gssg$, and $nadph/nadp^+$ ratio under the glioma model condition, have been listed in **Table 4.2**. k_{nadph}^{CR} , a parameter that was considered in the model, which catalyzes the conversion of cystine into cysteine subsequently using it for glutathione production, was found to have an effect on the h_2o_2 level, $gsh/gssg$, and $nadph/nadp^+$ ratio when varied in combination with other parameters. Availability of oxygen in the ECM for cellular uptake (L_{oxy}) when modulated in combination with k_{nadph}^{CR} showed significant change in level. Interestingly, a combinatorial variation of L_{oxy} with V_m^{FBA} caused a decline in the h_2o_2 concentration, which can be utilized for antioxidant therapy, and a variation of k_{nadph}^{CR} with k_{glucys}^{GS} induced changes the h_2o_2 concentration which can possibly be used for pro-oxidant therapeutic design. **Table 4.2** provides the value of parameters in combinations and their pro- or anti-oxidant fate depending upon their influence on the h_2o_2 level, $gsh/gssg$, and $nadph/nadp^+$ ratio. The changes in h_2o_2 , $gsh/gssg$, and $nadph/nadp^+$ profiles as a result of these combinatorial variations in the glioma scenario are shown in **APPENDIX B: Figure B. 4** and the regulation for which the profiles are obtained have been listed in **APPENDIX B: Table B. 3**. These combinations could be explored for their possible role in the development of future therapeutic strategies. Altering the kinetic parameters like the V_{max} or k_m of an enzyme is challenging, though possible with the help of enzyme modulators and competitive and non-competitive inhibitors. Non-competitive inhibitors are capable of altering the V_{max} of an enzyme while keeping the k_m unaltered, while

competitive inhibitors can alter the k_m of the enzyme (262). A few of the inhibitors for the aforementioned enzymes are already available in the market, that could be checked for their effectiveness in the present context. For e.g., iodoacetate, N-ethylmaleimide (NEM), and 5,5'-dithiobis-(2-nitrobenzoate) (DTNB) have been reported as potent inhibitors of glutathione synthase (263), and neopterin, magnolol, apocyanin and gliotoxin for NADPH oxidase (264). However, the exact type of inhibition for these inhibitors i.e., competitive or non-competitive is not yet known and has to be understood. A context-based understanding of the involvement of these parameters in ROS production or scavenging mechanism under different conditions has to be made through experiments in order to employ them for therapeutic strategies.

Table 4.2: Values of parameters for which pro- and anti-oxidant effects could be induced in the glioma scenario.

Sr. No.	Parameter 1	Parameter 2	Value of Parameter 1	Value of Parameter 2	Effect
1.	$k_{i(nadph)}^{NOX}$	k_{nadph}^{CR}	1 mM	15 mM	Pro-oxidant
2.	$k_{i(nadph)}^{NOX}$	k_{nadph}^{NOX}	20 mM	10 mM	Anti-oxidant
			1 mM	0.0001 mM	Pro-oxidant
3.	L_{oxy}	k_{nadph}^{CR}	20 mM hr ⁻¹	15 mM	Pro-oxidant
4.	$k_{i(nadph)}^{NOX}$	l_{atp}	0.5 mM	20 mM hr ⁻¹	Pro-oxidant
5.	V_m^{FBA}	L_{oxy}	0.0001 mM hr ⁻¹	5 mM hr ⁻¹	Anti-oxidant
6.	k_{glucys}^{GS}	k_{nadph}^{CR}	0.0001 mM	0.5 mM	Pro-oxidant

4.3. Discussion

ROS, produced as a by-product of cellular metabolism, are often considered toxic to the cells. Nonetheless, in recent years, their functions as second messengers in signal transduction processes have been highly appreciated. In normal cells, any excess production of ROS is scavenged by the antioxidant machinery. ROS, however, exhibit a paradoxical behavior in augmenting or hindering tumor progression. It is described to have a “double-edged sword” property having both tumor-promoting and tumor-suppressing functions. Currently, both pro-oxidant and anti-oxidant approaches are

employed as cancer therapeutics. However, owing to the paradoxical behavior, the employment and effectiveness of which strategy will suit a better therapeutic approach for any particular cancerous situation still remains unclear.

The oxidative status and functioning of anti-oxidant machinery have a crucial role in determining the proliferative fates of the cancer cells. The cellular *nadph/nadp⁺* ratio is a measure of the reducing potential of the cells, which is usually maintained high for proper cellular functioning (244, 245). A decline in the *nadph/nadp⁺* ratio is observed in many cancer types (265, 266), although a high *nadph/nadp⁺* ratio was observed to promote cancer cell growth and proliferation by stimulating anabolism and by protecting cancer cells against oxidative stress during nutrient limitation (267). Thiol ratios are another important determinant of cellular apoptotic or anti-apoptotic fates. A high *gsh/gssg* ratio is maintained under normal conditions, which often changes during cancerous transformations. A decline in the *gsh/gssg* ratio induces initiation of apoptosis, while an increase might help the cells escape apoptosis. The puzzling duality of ROS in exhibiting varying cellular fates is determined by a coordinated response of these factors. Understanding the effect of these factors cumulatively under different cancerous scenarios is a challenge.

Motivated by these findings, we designed a kinetic metabolic framework for glial cells to trace the possible changes that might be occurring within them during their transformation into gliomas. The model took into account the metabolic reactions involved in the production of the components of the tri-peptide complex, glutathione, and ROS-producing machinery. A part of the glycolytic pathway which enters the glycine-serine metabolism was considered along with cysteine and glutamate metabolism, which result in the production of the components of the tri-peptide: glycine, cysteine, and glutamate, respectively. Herein, we considered the effect of these pathways on the anti-oxidant production machinery, simultaneously looking for their effect on ROS production and scavenging and vice versa. To understand the effect of glutathione over ROS metabolism, reactions metabolizing the production of glutathione and ROS, along with the *gsh-gssg* cycle, were considered. Important reactions involving the *nadph-nadp⁺* conversions were considered to take into account the changes in the *nadph/nadp⁺* ratio while manipulating ROS-glutathione profiles. We postulated that the paradoxical

behavior of ROS is governed by changes in the $nadph/nadp^+$ and $gsh/gssg$ when considered together. An increase in h_2o_2 along with a decline in both $gsh/gssg$ and $nadph/nadp^+$ will disrupt the cellular redox status and drive the cell towards apoptosis by inducing toxicity due to the accumulation of ROS.

Numerical simulations of the model provide us with a set of sensitive enzyme parameters, which are affected during a transition from normal glial conditions to hypoxia to the development of gliomas. Upon introducing variations into the parameters, which were sensitive under normal glial conditions, interesting changes in the dynamics of h_2o_2 , $nadph/nadp^+$ and $gsh/gssg$ were observed. The uptake of oxygen by the cells was represented in Michaelis-Menten equation form where $k_m^{O_2}$ determined the affinity of the cell for external oxygen. Decrease in $k_m^{O_2}$ resulted in a decline in the external oxygen concentration as the cellular affinity for external oxygen increases. This represented a condition with high cellular oxygen demand, which is reflected as hypoxia in the external microenvironment.

GTHP is one of the important enzymes involved in the regulation of $gsh/gssg$, along with controlling the cellular content of h_2o_2 and maintaining $nadph/nadp^+$. Through our simulation on the glial cell model, we observed that with an increase in V_m^{GTHP} there was a considerable decline in the h_2o_2 level and $gsh/gssg$ ratio, although the effect on the $nadph/nadp^+$ ratio was only trivial. GTHO is another important enzyme, and the GTHP-GTHO duo completes the $gsh-gssg$ cycle. Not much difference in $gsh/gssg$ and $nadph/nadp^+$ could be observed for a change of GTHO alone, keeping all other parameters fixed. However, simultaneously varying GTHP and GTHO resulted in interesting changes in $nadph/nadp^+$ and $gsh/gssg$ with a decrease in h_2o_2 concentration. We interpreted that at any given time point under the normal condition, there is a decline in the $nadph/nadp^+$ and $gsh/gssg$ until the $gsh-gssg$ cycle neutralizes h_2o_2 concentration to micromolar levels rendering it non-toxic to cellular processes, after which the cell regains a stable $nadph/nadp^+$ and $gsh/gssg$ ratio. The involvement of NADPH Oxidase (NOX) was found to be crucial in the present simulation scenario. The activity of NOX determines the rate of production of free oxygen radicals which act as a substrate for superoxide dismutase (SOD) and is readily converted into h_2o_2 given V_m^{SOD} is sufficiently high. An increase in the

NOX activity rapidly increased the h_2o_2 level, decreasing both the $nadph/nadp^+$ and $gsh/gssg$ ratio.

While analyzing the dynamics of these parameters under changing affinity for oxygen, we observed that under hypoxic conditions increase in V_m^{GTHP} acts as the protective barrier against ROS by readily neutralizing h_2o_2 levels at the cost of reduced $gsh/gssg$, although the change in $nadph/nadp^+$ ratio remains trivial. A decrease in the V_m^{GTHP} can, however, help cancer development by causing h_2o_2 accumulation and inducing oncogenic signal transductions. The changes occurring due to the increase in activity of NOX and GTHO under hypoxia could also be interpreted as a condition initiating cancer development. While increasing NOX activity under hypoxia certainly disrupted cellular redox balance by reducing $gsh/gssg$ and $nadph/nadp^+$, the effect of changes in GTHO activity was minimal at the cost of a sudden decrease in $nadph/nadp^+$ and reduced $gsh/gssg$, with its effect being severe at lower values. When considered together, changes in NOX and GTHO activity under normal and hypoxic conditions showed substantial differences suggesting their involvement in tumor initiation.

A decrease in V_m^{GTHP} and V_m^{GTHO} , and an increase in V_m^{NOX} along with a low $k_m^{O_2}$ were considered to create a situation under hypoxia with multiple mutations representing a glioma-like situation. Comparisons of sensitive parameters under normal, hypoxic, and glioma-like situations provided an insight into the directly and distantly related parameters which affect the production of gsh , $gssg$, and h_2o_2 . Through parameter variation analysis of sensitive parameters under the glioma-like scenario, it was observed that different values of V_m^{GTHO} had a differing effect on the overall redox status of the cell. We interpreted that differing GTHO activity during cancerous transformation can govern the pro-apoptotic or anti-apoptotic fate. This partially accounts for the paradoxical behavior of ROS and helps in the therapeutic determination of pro-oxidant or antioxidant approaches either by augmenting glioma cell death and clearance or by controlling it by using antioxidant therapies. We proposed that under high GTHO activity, an antioxidant approach will be suitable to control glioma progression, whereas, under low GTHO activity, a pro-oxidant approach will be appropriate to induce apoptosis of the glioma cells.

Further analysis of the glioma scenario created *in-silico* in the model showed the involvement of non-trivial parameters in the regulation of *gsh*, *gssg*, and h_2O_2 . It was interesting to note that a combinatorial parameter variation of enzymes belonging to the glycolytic pathway (V_m^{FBA}) and cysteine metabolism (k_{nadph}^{CR}) could induce changes in the h_2O_2 level along with changes in *nadph/nadp⁺* and *gsh/gssg* profiles during glioma. Additionally, a combinatorial variation of a few other parameters like k_{glucys}^{GS} , L_{oxy} , I_{atp} and k_{nadph}^{NOX} which were not directly involved in ROS manipulation also showed changes in the h_2O_2 level. Combinatorial response of these parameters was captured, which suggested the possibility of utilizing these combinations in designing pro- or anti-oxidant therapeutic approaches based on their effect on ROS manipulation.

To summarize, GTHP, GTHO, and NOX were important in determining the transition from normal glial to hypoxia to glioma situation and in regulating ROS levels with the cell. Additionally, changes in the redox and thiol status represented by the *nadph/nadp⁺* and *gsh/gssg* ratios along with changes in the enzymes could determine the pro-apoptotic or anti-apoptotic fate of gliomas. The differing activity of GTHO during glioma development helped in understanding the paradoxical behavior of ROS in gliomas and hence was helpful in determining the selection of therapeutic strategies: pro-oxidant or anti-oxidant against glioma progression. Also, the involvement of enzymes that were not directly involved in the regulation of ROS but affected the process by inducing effect distantly in the metabolic network was important in augmenting the effectiveness of the selected therapeutic approach. The understanding of these mechanisms and identification of important enzymes which affect the ROS manipulation process can potentially build a better prospect of developing effective and efficient therapeutic strategies for the treatment of gliomas.

CHAPTER 5

POST-TRANSCRIPTIONAL REGULATION BY MICRORNAS ON METABOLISM AND CELLULAR PHENOTYPES IN GLIOBLASTOMA

5.1. Rationale of the study

The increase in omics and high-throughput research has enabled the identification of genetic factors regulating the expression of metabolic genes. The mutations, epigenetic modifications, and transcriptional regulations affecting metabolic genes are one of the primary underlying factors responsible for the metabolic alterations in glioblastoma (**Section 1.5.1**). Additional regulatory mechanisms on metabolism are currently being explored. Growing evidence of the microRNAs dependent regulation of metabolism has initiated research interest to explore their role in cancer metabolism (34). In the present chapter, which fulfils the second and the fourth objectives of the thesis, we investigate the effect of post-transcriptional regulation imposed by differentially expressed microRNAs on the metabolic gene and associated phenotypes in glioblastoma. MicroRNAs (miRNAs) are 18-25 nucleotide long small non-coding RNAs produced endogenously within the cell. miRNAs bind to the 3' UTR of the target genes via base complementarity between the seed sequences of the miRNAs and the 3' UTR of the gene and regulate gene expression (35). The role of miRNAs is currently being explored for prospects of miRNA-based therapeutics in glioblastoma (36-38). Computational analysis of omics and high-throughput data on the miRNA and gene expression has been successful in establishing a cause-and-effect relationship between differential expression of miRNAs and target genes (268). Graph network-based approaches are being popularly used for such gene regulatory networks. While such analyses are incremental in the identification of key regulators of gene expression and the highly targeted genes (37), the regulatory effect on metabolic genes often remains abeyant in these studies.

MicroRNAs have been implicated in the regulation of cellular phenotypes as well (269). Multiple oncogenic phenotypes like proliferation (270), cell invasion (271, 272), tumor survival (273), multi-drug resistance (274), and stemness (275) of glioblastoma are influenced by miRNA regulation. The effect of miRNA binding on important regulatory

genes associated with these phenotypes is tested to define a possible mechanism of action. However, despite their role in controlling cancerous phenotypes and regulating phenotype switching, the metabolic aspect of these regulations mostly remains unravelled. Studying the effect of miRNA regulation on the metabolism associated with these phenotypes will be helpful to delineate the role of miRNAs in metabolic plasticity that aid phenotype switching in glioblastoma and will help identify targets for miRNA-based therapeutics. The heterogeneity in patient-derived omics data adds complexity to the identification of unique targetable miRNAs. This heterogeneity necessitates the requirement of personalized treatment strategies. Continuous assessment of these data has helped to identify repeated patterns in expression profiles and correlate them with oncogenic phenotypes to classify patients categorically for suitable treatment strategy. The use of computational pipelines can be instrumental in this context to simplify the formidable data into useful information that can be utilized to decide treatment strategy. Hence, the present work focusses on the miRNA regulation of metabolism and its role in regulating cellular phenotypes in glioblastoma. Graph networks of miRNA - metabolic target gene and miRNA - metabolic pathway created using patient-derived differential expression data of miRNAs and metabolic genes were used for the study (**Section 2.3.1 & 2.3.5**). The effect of 26 upregulated and 46 downregulated miRNAs (**Section 2.3.2**) on the metabolism of glioblastoma were studied. Glioblastoma-specific target metabolic genes of these differentially expressed miRNAs were obtained from the miRDB database (**Section 2.3.3**). Functional annotation using pathway enrichment was performed to identify frequently regulated metabolic pathways (**Section 2.3.7**). Bipartite projection and backbone analysis were performed to identify important miRNAs that regulate central carbon metabolism, fatty acid, lipid, glycan, amino acid, and nucleotide metabolism (**Section 2.3.10**). MiRNA - metabolic gene subnetworks were identified for proliferation and growth, survival, cell migration and invasion, stemness, and drug resistance in glioblastoma using network diffusion (**Section 2.3.11**). The identified subnetworks were further used for miRNA knockout analysis to predict target combinations of miRNAs that regulate these phenotypes maximally. New centrality measures, pairwise disconnectivity index, and Katz centrality are used to predict the influence of miRNA on the subnetworks and the impact of miRNA deletion on target genes (**Section 2.3.12**). MiRNA targets predicted from the analyses can be tested through *in-*

vivo and *in-vitro* studies to test their feasibility as miRNA-based therapeutics in glioblastoma. The strategies employed can be used for the identification of *in-silico* leads for experimental verification in other gene regulatory networks as well.

5.2. Results

5.2.1. Differentially expressed miRNAs and target metabolic genes

To identify differentially expressed miRNAs that potentially regulate the expression of metabolic genes in glioblastoma, patient-derived miRNA dataset GSE90603 was screened. Comparison of miRNA expression profiles from GBM patient-derived tumor tissue samples vs. normal brain tissue sample from healthy volunteers and GBM patient-derived normal tissue samples yielded 26 upregulated and 46 downregulated miRNAs (**Section 2.3.2**). The upregulated set of miRNAs consists of hsa-miR-106b-3p, hsa-miR-10b-5p, hsa-miR-155-5p, hsa-miR-15b-5p, hsa-miR-181a-2-3p, hsa-miR-18a-5p, hsa-miR-21-5p, hsa-miR-23a-3p, hsa-miR-24-2-5p, hsa-miR-25-3p, hsa-miR-28-3p, hsa-miR-320a, hsa-miR-320b, hsa-miR-320c, hsa-miR-320d, hsa-miR-339-5p, hsa-miR-3651, hsa-miR-424-3p, hsa-miR-4429, hsa-miR-455-3p, hsa-miR-500a-5p, hsa-miR-6872-3p, hsa-miR-92a-3p, hsa-mir-92b, hsa-miR-92b-3p and hsa-miR-93-5p. And the downregulated set comprises of hsa-mir-1225, hsa-miR-1236-5p, hsa-mir-124-1, hsa-mir-124-2, hsa-mir-124-3, hsa-miR-124-3p, hsa-miR-124-5p, hsa-miR-128-1-5p, hsa-miR-128-2-5p, hsa-miR-128-3p, hsa-miR-129-1-3p, hsa-miR-137, hsa-miR-138-2-3p, hsa-mir-139, hsa-miR-139-3p, hsa-miR-139-5p, hsa-miR-211-3p, hsa-miR-218-5p, hsa-miR-3188, hsa-miR-3200-3p, hsa-miR-323a-5p, hsa-miR-330-3p, hsa-miR-330-5p, hsa-miR-338-3p, hsa-miR-4257, hsa-miR-4281, hsa-miR-4322, hsa-miR-433-3p, hsa-miR-4433b-3p, hsa-miR-4447, hsa-miR-4463, hsa-miR-4525, hsa-miR-485-5p, hsa-miR-490-5p, hsa-miR-5698, hsa-miR-6782-5p, hsa-miR-6790-5p, hsa-miR-6810-5p, hsa-miR-6861-5p, hsa-miR-758-5p, hsa-miR-7-5p, hsa-miR-769-5p, hsa-mir-770, hsa-miR-770-5p, hsa-miR-873-3p and hsa-miR-874-3p.

A few of the miRNAs in both sets were observed to share the same seed sequence and target similar genes. Such miRNAs belonged to the same family and were considered together as a single entity in further analyses. These miRNAs are hsa-miR-25-3p, hsa-

miR-92a-3p, hsa-miR-92b and hsa-miR-92b-3p of MIR25/92 family and hsa-miR-320a, hsa-miR-320b, hsa-miR-320c and hsa-miR-320d of MIR320 family in the upregulated set and hsa-miR-124-1, hsa-miR-124-2, hsa-miR-124-3 and hsa-miR-124-3p of MIR124 microRNA precursor family, hsa-miR-128-1-5p and hsa-miR-128-2-5p of MIR128 family and hsa-miR-770, hsa-miR-770-5p of MIR770 family in the downregulated set. Further analysis showed that hsa-miR-4429 shared the same target genes as that of the MIR320 family miRNAs and have been predicted to share the same seed sequence with the family. Hence, hsa-miR-4429 was considered a member of the MIR320 family. The identified differentially expressed miRNAs were further validated with additional datasets as described in **Section 2.3.4**. **Figure 5.1A** shows the observed difference in the differential expression of miRNAs across all the datasets considered for validation.

Predicted target genes specific to glioblastoma for each of the differentially expressed miRNAs were obtained from the miRDB database (**Section 2.3.3**). Only metabolic genes were considered for the study. A composite list of 1865 unique metabolic genes was obtained from the Recon3D human genome model (**APPENDIX C: Section C**). The predicted metabolic genes from all the predicted target genes of each miRNA were identified and filtered by mapping over this list. The predicted metabolic target genes were matched with the differentially expressed genes obtained from the TCGA GBM project (**Section 2.3.5**). Only those predicted genes that showed differential expression were considered as the target for the differentially expressed miRNAs. Since miRNA regulated gene expression by gene silencing, the effect of an upregulated miRNA would be mediated by a downregulation of its target genes and vice versa. Hence, the downregulated metabolic genes were considered as targets of upregulated miRNAs and the upregulated metabolic genes as potential targets of downregulated miRNAs. Pathway enrichment of each miRNA-regulated target gene set was performed. A list of all the upregulated and downregulated miRNAs, their target metabolic genes, and the enriched pathways is tabulated in **APPENDIX C: Table C. 1 & Table C. 2**.

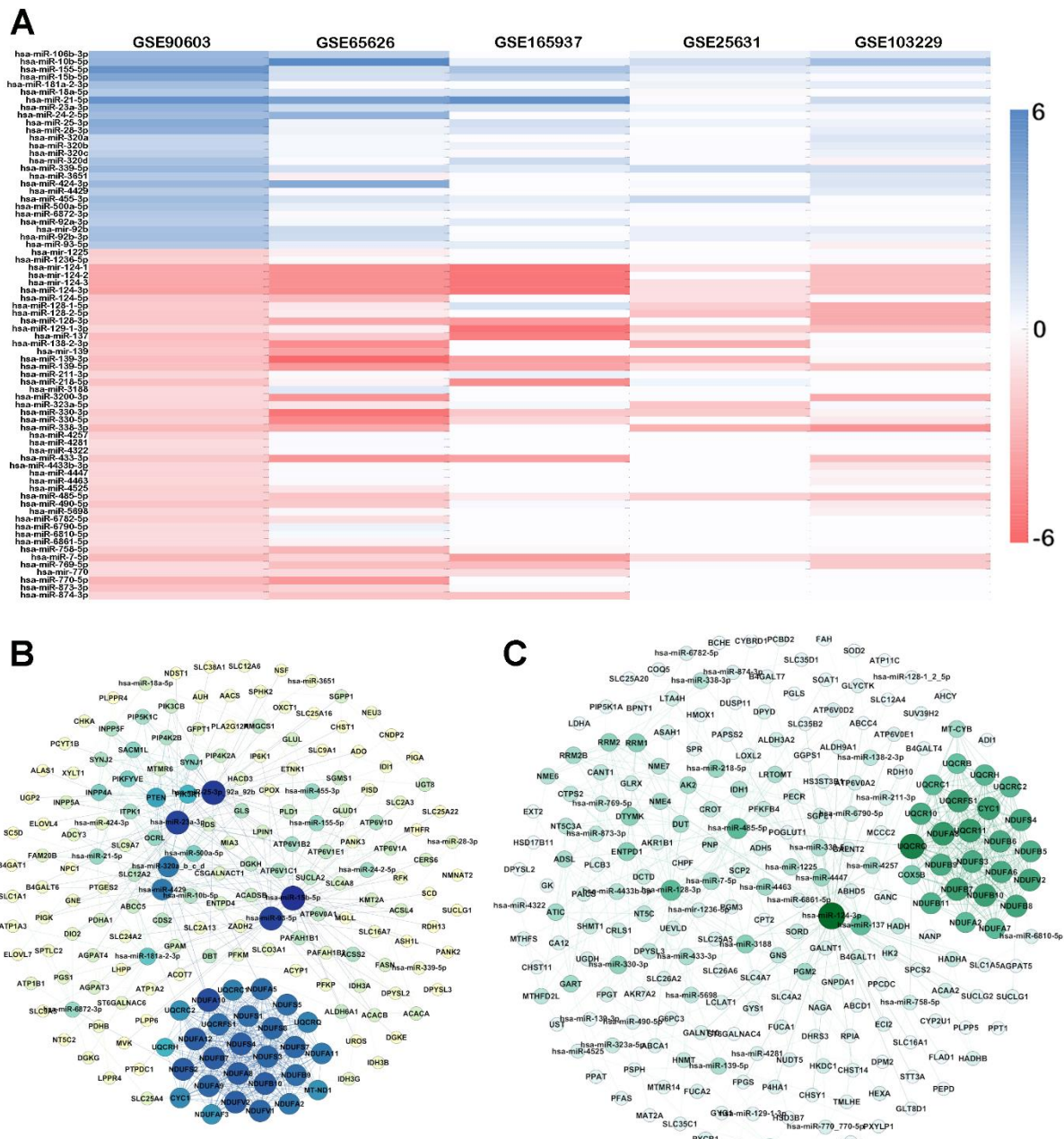


Figure 5.1: Validation of differentially expressed miRNAs and network visualization. (A) Validation of miRNA expression with other GEO datasets; miRNA- target metabolic gene interaction network of (B) Upregulated miRNAs (C) Downregulated miRNAs.

5.2.2. Identification and analysis of hub miRNAs and metabolic genes

With the identification and inclusion of additional genes relevant to the expression of miRNA-regulated targets at the network level, two composite miRNA-target metabolic gene interaction networks were formulated for the upregulated and downregulated sets of miRNAs. **Figure 5.1B** provides a visualization of the upregulated miRNA- target gene

interaction network with 109 nodes and 696 interactions and **Figure 5.1C** of downregulated miRNA-target gene interaction network with 225 nodes and 650 interactions.

The miRNA-target gene network exhibited anti-modularity, a property in which nodes from one functional group tend to have lesser interaction as compared to their interaction with the nodes of the other functional group. This property holds true for bimodal gene-regulatory networks, for, e.g., the flow of regulatory information from the transcriptional regulators is more likely to pass down to the promoters of genes than to other transcription regulators (276). However, the information flow is modular at the gene-reaction level, defined as the high connectivity of nodes within each functional group (277). The gene network was expanded based on the modularity of genes encoding enzymes/proteins that interact at the reaction level, and the effect of each miRNA regulation on the network was checked.

Directed network analyses of miRNA-target gene interaction networks were performed. The degree distribution of indegree and outdegree of these networks followed a power law, indicating the scale-free nature of these networks (**APPENDIX C: Figure C. 2**). Based on the topological properties, important upregulated and downregulated miRNAs were identified.

Upregulated miRNA-target metabolic gene interaction network

Hsa-miR-15b-5p, MIR25/92 family miRNAs, hsa-miR-93-5p, hsa-miR-23a-3p, and MIR320 family miRNAs were the top five upregulated miRNAs regulating metabolic genes, identified based on total degree and topological coefficient. Topological coefficient, by definition, is a relative measure for the extent to which a node shares neighbours with other nodes. High degree and low topological coefficients provide an idea about the exclusiveness of target genes for each miRNA. Hsa-miR-15b-5p combined with hsa-miR-21 forms a diagnostic biomarker for glioma patients with high sensitivity and specificity (278). We observe an overexpression of both hsa-miR-15b-5p and hsa-miR-21-5p from our patient-derived data analysis. Crucial metabolic targets of hsa-miR-15b-5p include GLUD1, IDH3A, MTHFR, FASN, and PTEN (**APPENDIX C: Table C. 1**). Expression of GLUD1 is regulated by mTOR via mTORC1 activity that is often enhanced to allow

switching to glutamine uptake as an alternate energy source. Targeting GLUD1 expression by regulating hsa-miR-15b-5p expression is a possible strategy to regulate this phenotype switching. A similar approach can be used for IDH3A expression, which is often enhanced in IDH mutant glioblastomas with loss-of-function mutation of IDH1 and IDH2. MTHFR c.677C>T variant of MTHFR is an identified risk factor for the survival of glioblastoma patients (279). Also, MTHFD2, an enzyme that metabolizes the product of MTHFR, is often overexpressed in glioblastoma via MYC transcription regulation. miRNA-based therapy is in use for MTHFD2 regulation via hsa-miR-920 (280). Using hsa-miR-15b-5p based therapy can have added advantages as it can regulate MTHFR directly and MTHFD2 by limiting its substrate production. Furthermore, hsa-miR-15b-5p regulates a large number of genes belonging to fatty acid metabolism (ACACB, ACSL4, ACSS2, FASN). FASN overexpression has been reported in some cases of glioblastoma due to SREBP-1 transcription regulation (281). FASN expression can be regulated by hsa-miR-15b-5p based therapy.

Upregulation of MIR25/92 family miRNAs is identified as a biomarker and potential therapeutic target in different types of cancer. From the present study, we identified an upregulation of hsa-miR-25-3p, hsa-miR-92a-3p, hsa-miR-92b and hsa-miR-92b-3p. Important target genes include ELOVL4, ATP6V1B2, ADCY3, PTEN, and PLD1. Fatty acid elongase ELOVL4 supports extracellular vesicle formation and release in glioblastoma and is implicated in controlling tumorigenesis (282). Downregulated expression of ATP6V1B2 is implicated in chemo-resistant protein expression patterns of glioblastoma (283). Downregulation of these genes in glioblastoma patient samples and upregulated expression of MIR25/92 family miRNAs suggest the possibility of correlation, although testing the hypothesis was beyond the scope of this work. The understanding provides an opportunity for miRNA-based targeting of these genes. Besides, hsa-miR-25-3p, hsa-miR-10b, and hsa-miR-21, and the miR-106b~25 cluster are frequently upregulated in glioblastoma, all of which could be captured in the present analysis. The miR-106b~25 cluster comprises hsa-miR-25, hsa-miR-93, and hsa-miR-106b, all of which show cooperated response to decrease PTEN expression in different cancer. In our study, PTEN was a predicted target of hsa-miR-25-3p and was downregulated in patient-derived data.

Hsa-miR-23a-3p is another prognostic marker frequently upregulated in glioblastoma. Sponging hsa-miR-23a-3p results in antiproliferative and antimetastatic response via elevated expression of PTEN. Apart from this, hsa-miR-23a-3p potentially targets a number of important metabolic genes, namely ATP6V1E1, GLS, AGPAT4, NDUFA5, AACSB, ACADSB, OXCT1, PDHA1, and ATP6V1B2, many of which assist metabolic switching in glioblastoma. c-MYC regulation allows GLS overexpression by repressing hsa-miR-23a. The mechanism can be used for miRNA-based therapy to target glioblastoma with high GLS expression. The MIR320 family miRNAs also have a pool of important target metabolic genes consisting of PFKM, ACOT7, ADCY3, PTEN, GLS, NDUFA10, and ATP6V1C1. Downregulation of the MIR320 family is associated with the promotion of growth and invasion and poor prognosis in glioblastoma (284), and their upregulation has anti-tumor effects. PTEN was a common target of many of the upregulated miRNAs suggesting miRNA regulation as one of the primary factors controlling downregulation of PTEN in glioblastoma. Due to the high modularity of genes encoding subunits of ETC complexes, these genes appeared as a highly connected hub. The effect of miRNA regulation is expected to propagate faster within the hub. Several miRNAs have been identified as mitomiRs that regulate mitochondria-related mechanisms, particularly related to the ETC. From our study, we identified hsa-miR-93-5p, hsa-miR-181a-2-3p, hsa-miR-23a-3p, MIR25/92 family miRNAs, MIR320 family miRNAs, and hsa-miR-6872-3p regulate genes belonging to mitochondrial ETC complexes.

Downregulated miRNA-target metabolic gene interaction network

MIR124 family miRNAs, hsa-miR-137, hsa-miR-485-5p, hsa-miR-128-3p, and hsa-miR-3188 were the top five downregulated miRNAs based on the highest degree and lowest topological coefficient. MIR124 family miRNAs, particularly hsa-miR-124-3p, are a crucial mediator of glioblastoma growth and angiogenesis. Studies on the regulation of signalling genes by this family of miRNAs suggest the potential for therapeutic targeting in brain tumors (285). In the present study, we observe that a large number of genes belonging to β -oxidation of fatty acids (ACAA2, ECI2, ALDH9A1, HADHA, PECCR, and HADH) in glioblastoma are targeted by miRNAs of this family. The involvement of these miRNAs in the regulation of fatty acid and triglyceride metabolism indicates their role in cancer proliferation and progression. Apart from the β -oxidation, these miRNAs also regulate

the expression of ATP6V0A2, SUCLG2, ATP6V0E1, and PGM2. The ability of hsa-miR-137 to target multiple genes of central carbon metabolism, including PFKFB4, AGPAT5, PGM2, IDH1, and PEPD, makes it a crucial therapeutic target. Both hsa-miR-124 and hsa-miR-137 are downregulated in glioblastoma, and inducing these miRNAs promote antiproliferative and pro-differentiation effects (270). Their ability to regulate the fatty acid oxidation, glycolysis, and TCA cycle potentially contribute to the antiproliferative effect.

Experimental analysis shows hsa-miR-485-5p in glioblastoma acts as a tumor-suppressive miRNA (286), although it is frequently downregulated in these tumors. The downregulation of the miRNA upregulates a large number of metabolic genes, including ATP6V0D2, CROT, AK2, ADH5, UEVLD, and UQCRCQ, that regulate energy metabolism and drug metabolism. Upregulated expression of these genes is likely to aid tumor proliferation by providing for the excess energy requirement of the tumor cells. hsa-miR-128-3p has a distinct difference in expression patterns in low-grade gliomas and glioblastoma (287, 288). It functions to inhibit proliferation and differentiation in all grades of glioma and enhance TMZ sensitivity in glioblastoma (289). Regulation of metabolic targets like G6PC3, PFKFB4, AK2, GYS1, HMOX1, ADH5, and GLRX possibly confers the miRNA the ability to control energy metabolism in glioblastoma. Both hsa-miR-485-5p and hsa-miR-128-3p are suitable targets of miRNA-based targeted therapy.

Hsa-miR-3188 is one of the less explored miRNAs in glioblastoma. Its metabolic targets ADH5 and PLCB3 confers it the ability to target multiple metabolic functions, including drug and xenobiotic metabolism and signalling responses, owing to the involvement of these genes in multiple cellular processes. Other important metabolic targets are CROT, UQCRCQ, AKR7A2, and GNPDA1. Some of the additional downregulated miRNAs identified from the analysis include hsa-miR-7-5p, hsa-miR-139-5p, hsa-miR-218-5p, hsa-miR-330-3p, and hsa-miR-4463 (**APPENDIX C: Table C. 2**).

5.2.3. Metabolic pathway regulation by differentially expressed miRNA

Functional analysis of the target genes was done using pathway enrichment. The target genes of each miRNA were enriched against the KEGG and Reactome databases (**Section 2.3.7**). A list of the top 30 pathways targeted by the upregulated and downregulated

miRNAs has been shown in **Figure 5.2A and B**, and a list of all enriched pathways for each miRNA target is provided in **APPENDIX C: Table C. 1 & Table C. 2**.

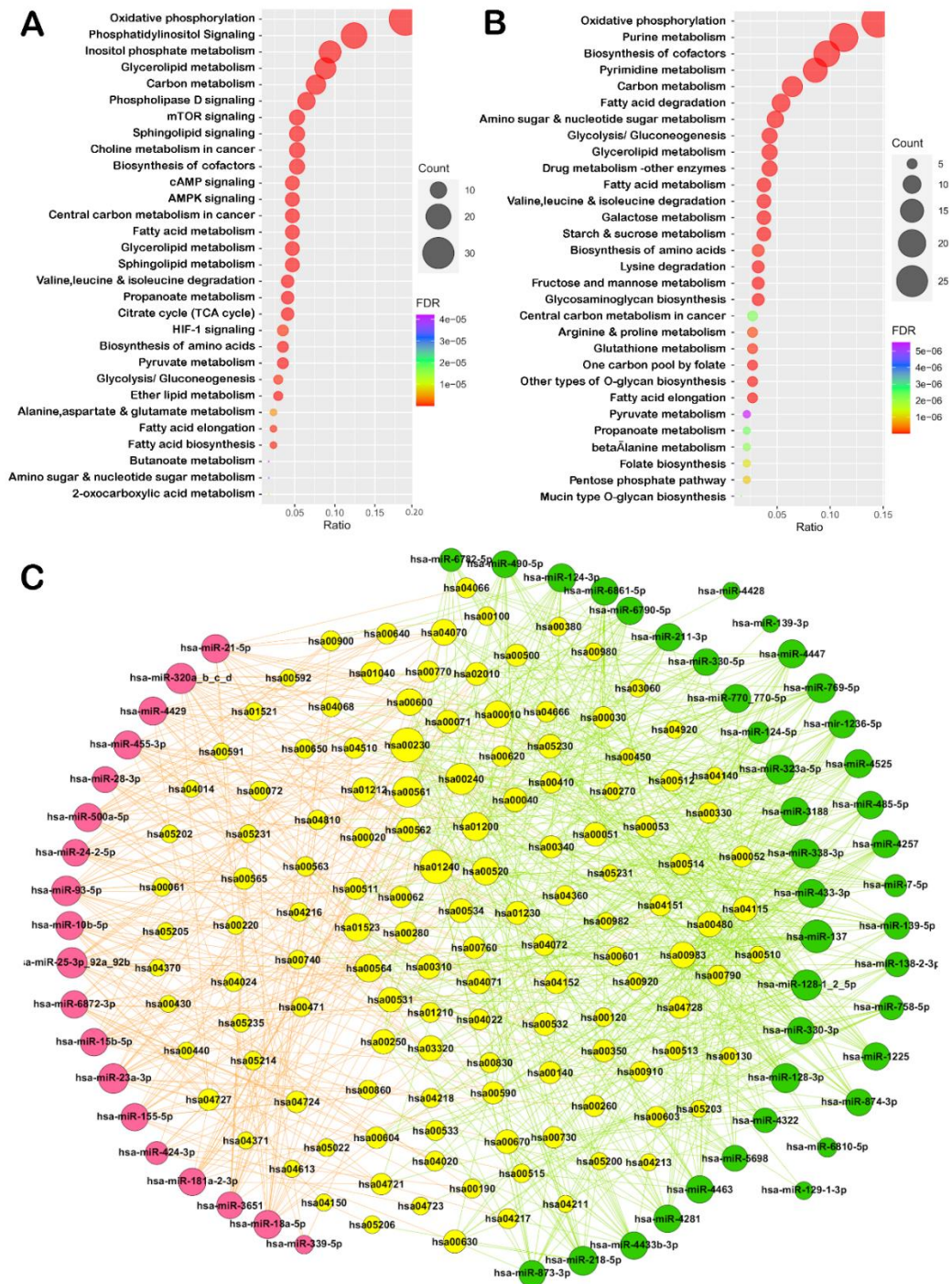


Figure 5.2: Metabolic Pathways regulated by differentially expressed miRNAs. (A) Top 30 enriched pathways of the upregulated miRNA-target metabolic gene network, (B) Top 30 enriched pathways of the downregulated miRNA-target metabolic gene network, (C) Integrated miRNA-metabolic pathway network of the differentially expressed miRNAs.

While pathways belonging to the carbon metabolism, fatty acid metabolism, and central carbon metabolism in cancer were common targets of both upregulated and downregulated miRNAs, lipid metabolism was a major target of the upregulated miRNAs, and purine and pyrimidine metabolism were exclusive targets of the downregulated miRNAs. Lipid and inositol-phosphate metabolism are the most enriched pathways regulated by the upregulated miRNAs (**Figure 5.2A**). Drug and glutathione metabolism are common targets of the downregulated miRNAs (**Figure 5.2B**). The upregulation of drug metabolism results in rapid drug metabolization eliminating effective concentration of drugs in blood and tissues.

With an extensive functional analysis (**Section 2.3.7**), an integrated miRNA-pathway network was formed (**Figure 5.2C**). Hsa-miR-137 and MIR128 family downregulated miRNAs, and MIR25/92 family, MIR320 family, and hsa-miR-23a-3p upregulated miRNAs are the top regulators of various metabolic processes. Differential regulation of lipid metabolism, carbon metabolism, amino sugar, and nucleotide sugar metabolism, glycolysis/gluconeogenesis, inositol phosphate metabolism, one-carbon pool, and fatty acid metabolism by a number of differentially expressed miRNAs make metabolic plasticity and acquiring adaptive phenotypes easier.

Further, we used the miRNA pathway network to identified important miRNAs that regulate central carbon metabolism, fatty acid metabolism, glycan metabolism, lipid metabolism, amino acid metabolism, and nucleotide metabolism with backbone analysis. The bipartite structure of the miRNA-pathway network was transformed to a unipartite weighted graph of miRNAs with network projection (**Section 2.3.10**), and a backbone of crucial miRNAs was obtained. The extracted backbone preserved the most significant miRNAs that could regulate each of the aforementioned metabolism (**Figure 5.3**). A description has been provided below.

Central Carbon Metabolism

A total of 16 pathways regulated by 42 differentially expressed miRNAs were considered as a part of central carbon metabolism from the miRNA pathway network (**APPENDIX C: Table C. 3**). A significant total of 3 miRNAs were obtained from the backbone extraction

consisting of hsa-miR-1225, hsa-miR-211-3p, and MIR770 family miRNAs hsa-miR-770 and hsa-miR-770-5p. All three miRNAs were downregulated in glioblastoma patient-derived data. Together, this set of miRNAs could regulate 7 of the 16 pathways of central carbon metabolism. **Figure 5.3A** shows the whole set of miRNAs consisting of both upregulated and downregulated miRNAs that control central carbon metabolism.

Fatty Acid Metabolism

Eight pathways from the integrated miRNA-pathway network were classified to contribute to the fatty acid metabolism. These pathways were regulated by 23 miRNAs (**Figure 5.3B**). Two groups of miRNAs, first consisting of hsa-miR-24-2-5p and hsa-miR-28-3p, and the second consisting of hsa-miR-124-3p, hsa-miR-181a-2-3p, and hsa-miR-6790-5p, were obtained as the backbone. Each group could target 2 of the 8 pathways belonging to fatty acid metabolism. The fatty acid metabolism was largely controlled by the miRNA regulation of genes belonging to β -oxidation and fatty acid elongation.

Lipid Metabolism

As many as 44 miRNAs regulated 12 pathways of lipid metabolism. Upregulated miRNAs hsa-miR-24-2-5p, hsa-miR-500a-5p, MIR25/92 family and downregulated hsa-miR-137 were extracted as backbone (**Figure 5.3C**). Glycerophospholipid metabolism was the most common miRNA-regulated pathway of lipid metabolism. Glycerophospholipids are reportedly one of the most significantly expressed lipids in glioblastoma, and regulation by these backbone miRNAs provides the opportunity for miRNA-based therapy.

Glycan Metabolism

hsa-miR-4257 and hsa-miR-758-5p were identified as crucial regulators of glycan metabolism. There were 13 pathways of glycan metabolism regulated by 36 miRNAs (**Figure 5.3D**). Aberrant expression of glycan has been implicated in brain cancer and plays a role in cancer development and progression (290). The proper function of glycan metabolism is crucial to carry out glycosylation of proteins and produce glycoproteins. Glycosaminoglycan metabolism was a key pathway targeted by the two miRNAs (and most other miRNAs). As observed from the patient-derived data, the upregulation of the glycosaminoglycan metabolism can prevent proteins (especially growth factors) from

proteolysis, generating prolonged growth signals. Identifying miRNA regulators of this metabolism can be used for therapeutic gain.

Amino Acid Metabolism

Seventeen pathways were classified under the amino acid metabolism, targeted by 48 miRNAs (**Figure 5.3E**). The miRNA regulation of the amino acid metabolism was sparse and widely distributed. Two groups of miRNAs, the first comprising of hsa-miR-10b-5p, hsa-miR-155-5p, and hsa-miR-424-3p, and the second comprising of MIR124 family miRNAs, hsa-miR-455-3p, hsa-miR-6790-5p, and hsa-miR-128-3p, were obtained. Each of these groups could target at least 3 of the 17 amino acid metabolism-related pathways. The ability of these miRNAs to control arginine and glutamate metabolism can be used to modulate the effect of therapeutic strategies like arginine depletion in glioblastoma.

Nucleotide Metabolism

As many as 31 miRNAs regulated the 3 pathways classified under nucleotide metabolism. hsa-miR-1225, hsa-miR-155-5p, MIR320 family miRNAs, hsa-miR-433-3p, hsa-miR-4463 and hsa-miR-490-5p were identified (**Figure 5.3F**). Capable of regulating the purine and pyrimidine metabolism and the formation of nucleotide sugars, these miRNAs can be targeted to restrict nucleotide synthesis restricting rapid cell proliferation during tumorigenesis.

Lipid and amino acid metabolism were regulated by the widest range of miRNAs, followed by the central carbon metabolism. Due to the modular nature of the central carbon metabolism, the effect of miRNA regulation propagates faster in the close-knit network of reactions, thereby affecting the energy metabolism as a whole.

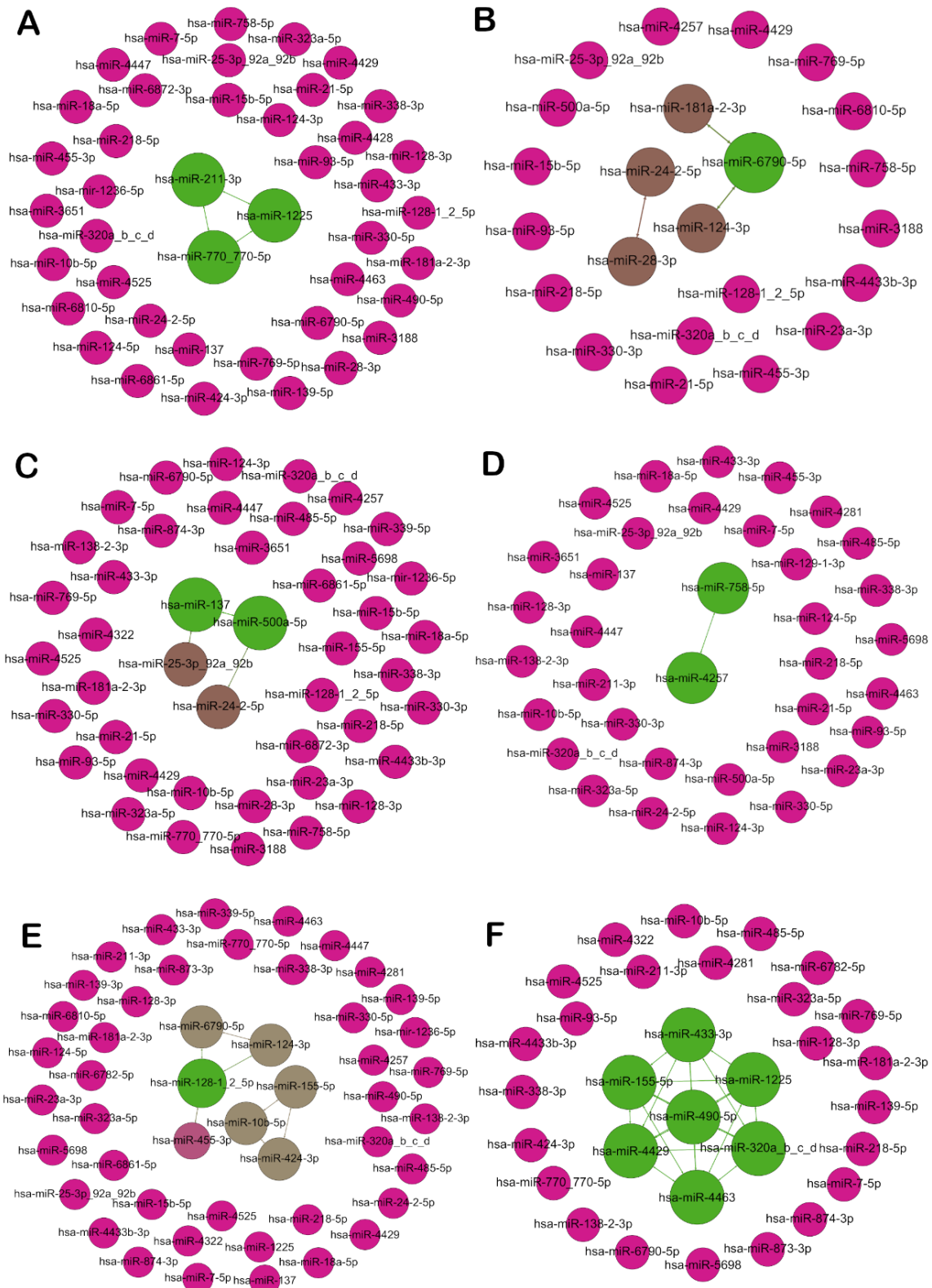


Figure 5.3: MicroRNA backbone of metabolic processes. (A) Central Carbon metabolism, (B) Fatty Acid metabolism, (C) Lipid metabolism, (D) Glycan metabolism, (E) Amino Acid metabolism, (F) Nucleotide metabolism.

5.2.4. Identification of miRNA regulated metabolic gene sub-network of cellular phenotypes

Cellular phenotypes in cancer are often guided by changes in metabolic regulations that facilitate re-wiring of the metabolic network, allowing rapid proliferation, invasion, and stemness, thereby regulating survival. With increasing evidence, the regulatory role of miRNAs on the metabolic genes critical to oncogenic phenotypes is being established and explored further. We attempted to identify a subnetwork of miRNA target genes that regulate proliferation and growth, survival, cell migration and invasion, stemness, and drug resistance in glioblastoma using an integrated network as described in **Section 2.3.11**. With an extensive literature search, we identified key metabolic genes directly associated with each of the phenotypes, determined experimentally. A list of all the key regulatory genes used as seed sequences for each of the phenotypes, along with their literature references, is provided in **APPENDIX C: Table C. 4**. These genes were used as seed nodes in the integrated network of miRNA-predicted target genes to induce network diffusion. A subset of highly connected miRNA-target genes obtained from the top 70th percentile of the diffusion output rank was selected as the subnetwork (**Figure 5.4**). Statistics of these networks, along with the miRNAs identified to be associated with the gene regulation of each of the cellular phenotypes, are provided in **Figure 5.5**.

We identified an additional set of genes that are functionally associated with the key regulators and may have a concomitant effect on the expression of these phenotypes in glioblastoma. Detail list of all the genes and miRNAs of the subnetwork is provided in **APPENDIX C: Table C. 5**. The majority of the genes associated with proliferation and growth were functionally related to the inositol-phosphate metabolism, central carbon metabolism, and amino acid metabolism (**APPENDIX C: Table C. 6**). This trend differed from phenotype to phenotype. Similar to proliferation and growth, the functional responses of cell migration and invasion were primarily associated with the central carbon metabolism and partly with the amino acid metabolism. Interestingly, survival was mostly determined by the lipid, fatty acid, and glycan metabolism. The role of fatty acids as alternate energy sources under nutrient deprivation, lipids as an integral part of the cell membrane formation, and glycan metabolism in glycosylation and proteolytic mechanisms make them crucial regulators of survival. Amino acid metabolism

contributed significantly to the generation of stemness in glioblastoma, followed by fatty acid metabolism. The ABC/MDR transporters and the Glutathione S-Transferase genes GSTM1 and GSTM2 are important regulators of drug resistance as they are involved in the exocytosis of xenobiotics and drugs from the cell. Genes belonging to the carbon and fatty acid metabolism are associated with the sensitization of cells to drugs and therapeutics by targeting resistance mechanisms.

The reliability of the subnetworks was strengthened by the identification of additional genes that are implicated to be involved in the regulation of corresponding phenotypes. For example, the ALDHs, ACLY, COX, ME2, and MTHFD2 contribute to glioblastoma growth and proliferation (291-294). Concurrent evidence of the role of MTHFR in influencing survival of glioblastoma patients (279) and ME2 in inducing cell migration and invasion (293) validate that the additionally identified genes potentially participate in the regulation of these phenotypes.

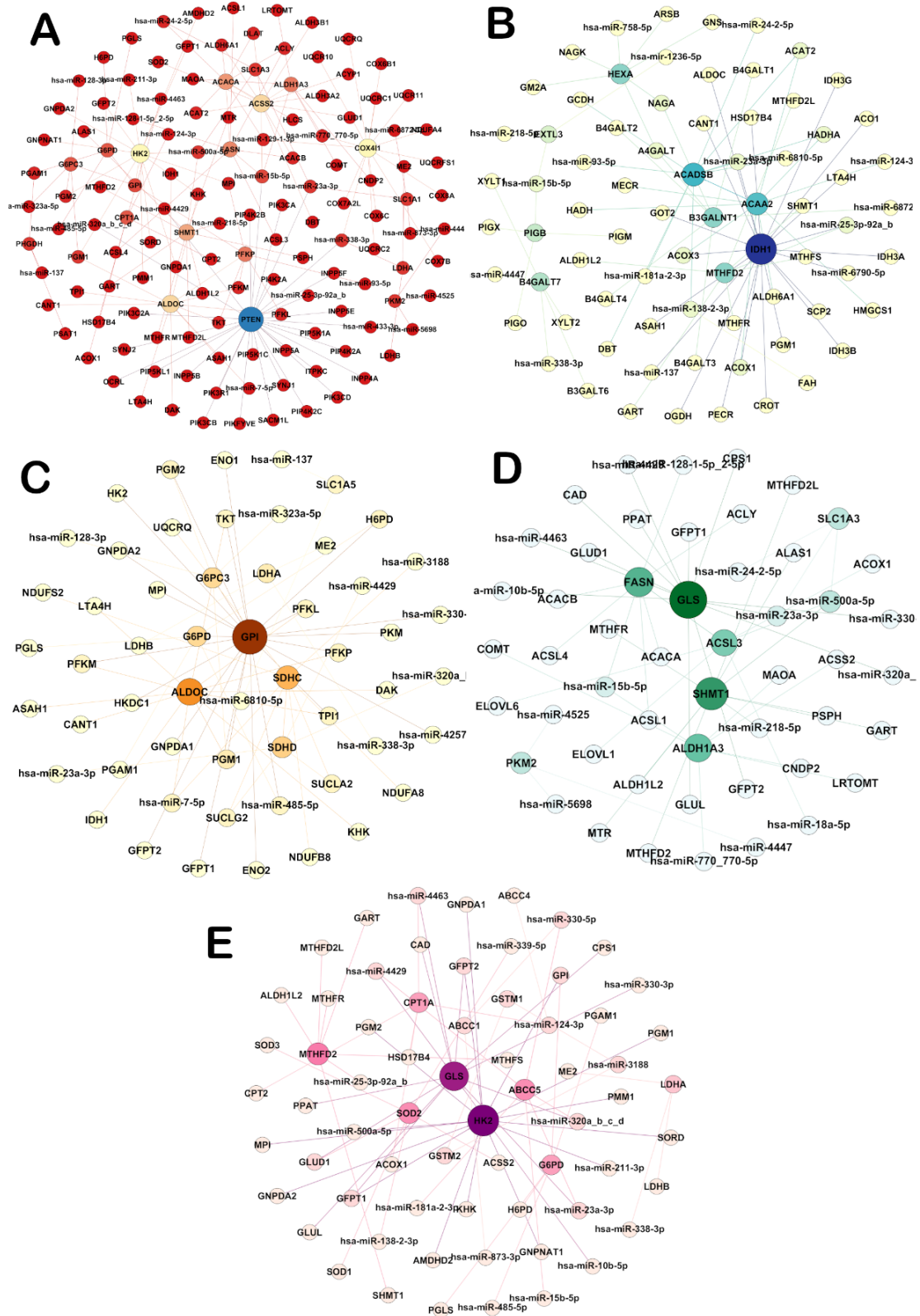


Figure 5.4: MiRNA-metabolic gene subnetwork of cellular phenotypes in glioblastoma. (A) Proliferation and growth, **(B)** Survival, **(C)** Cell migration and invasion, **(D)** Stemness, and **(E)** Drug resistance

5.2.5. Prediction of miRNA targets for miRNA-based therapeutic approaches

Pairwise disconnectivity index was used to quantify the regulatory effect of miRNAs in the subnetworks (**Section 2.3.12**). The values of PDI ranged between 0.001 to 0.08. We considered miRNAs with PDI > 0.02 for the knockout analysis. All the miRNAs associated with the gene regulation of each of the cellular phenotypes ranked based on their PDI values are shown in **Figure 5.5**. It was observed that most of the miRNAs with high PDI also had a higher stress centrality than the rest of the miRNAs, further strengthening our inference that these miRNAs were heavily involved in the regulation of target genes in the subnetworks.

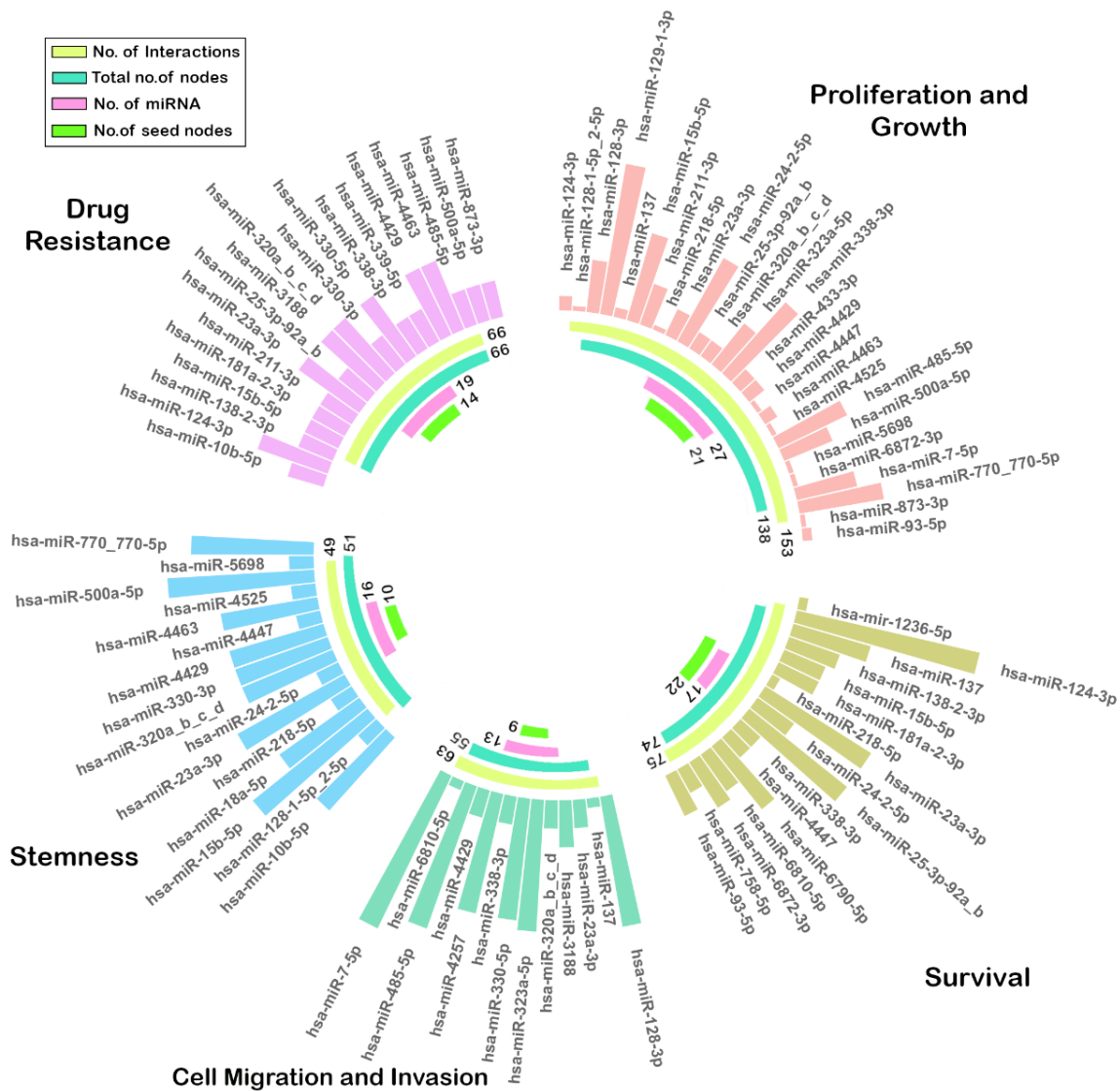


Figure 5.5: MiRNAs involved in the regulation of genes associated with cellular phenotypes in glioblastoma.

The effect of miRNA knockout on the key regulatory genes controlling each cellular phenotype in glioblastoma was measured by comparing the change in Katz centrality of the gene nodes before and after a miRNA deletion. **Figure 5.6** shows the percentage change in Katz centrality of the important nodes upon deletion of individual and combination of miRNAs, the initial values without knockout being 100% forming the periphery of the radar. All possible double and triple knockout combinations of miRNA were checked. Combinations of miRNAs that could impact the maximum number of key regulatory genes were proposed as a suitable target combination for miRNA-based therapy and have been shown in **Figure 5.6**. A combination of hsa-miR-15b-5p + hsa-miR-500a-5p + hsa-miR-129-1-3p was proposed suitable for targeting proliferation of glioblastoma (**Figure 5.6A**). Important genes whose activity in the network was influenced by the deletion of this combination were ACSS2, ALDH1A3, ACACA, COX4|1, SLC1A3, FASN, HK2, SHMT1, PTEN, CPT1A, PFKP, and PHGDH. The involvement of these genes in regulating the carbon and fatty acid metabolism is crucial in sustaining the proliferative requirement of the tumors. Similarly, a combination of hsa-miR-15b-5p + hsa-miR-124-3p + hsa-miR-138-2-3p was observed suitable for targeting survival (**Figure 5.6B**), hsa-miR-7-5p + hsa-miR-128-3p + hsa-miR-485-5p for cell migration and invasion (**Figure 5.6C**), hsa-miR-15b-5p + hsa-miR-23a-3p for stemness (**Figure 5.6D**) and hsa-miR-124-3p + hsa-miR-300-5p + hsa-miR-23a-3p was found suitable for managing genes associated with drug resistance in glioblastoma (**Figure 5.6E**).

It is worth mentioning here that the role of hsa-miR-7-5p is vital in the regulation of cell migration and invasion that has been established experimentally (271). This finding corroborates with the observations of the present study where hsa-miR-7-5p has been identified as the most important miRNA in the cell migration and invasion subnetwork with the highest PDI (0.069230769) and also the most stress central miRNA in the subnetwork. hsa-miR-15b-5p showed efficiency as a component of multiple combinations targeting proliferation and growth, survival, and stemness in glioblastoma. hsa-miR-15b-5p has been identified as a diagnostic marker for glioblastoma (295) and is associated with the regulation of a number of target genes (**APPENDIX C: Table C. 1**). It was observed that genes with isoforms like PFKP, B3GALNT1, B3GALNT7, GSTM1, and GSTM2, were difficult to be targeted due to the compensatory connections formed by the other isoforms in the network. A combinatory elimination of multiple miRNAs regulating

multiple isoforms were deemed fit for targeting such genes. The identified miRNA targets were verified with existing literature and experimental evidence that are discussed in the next subsection.

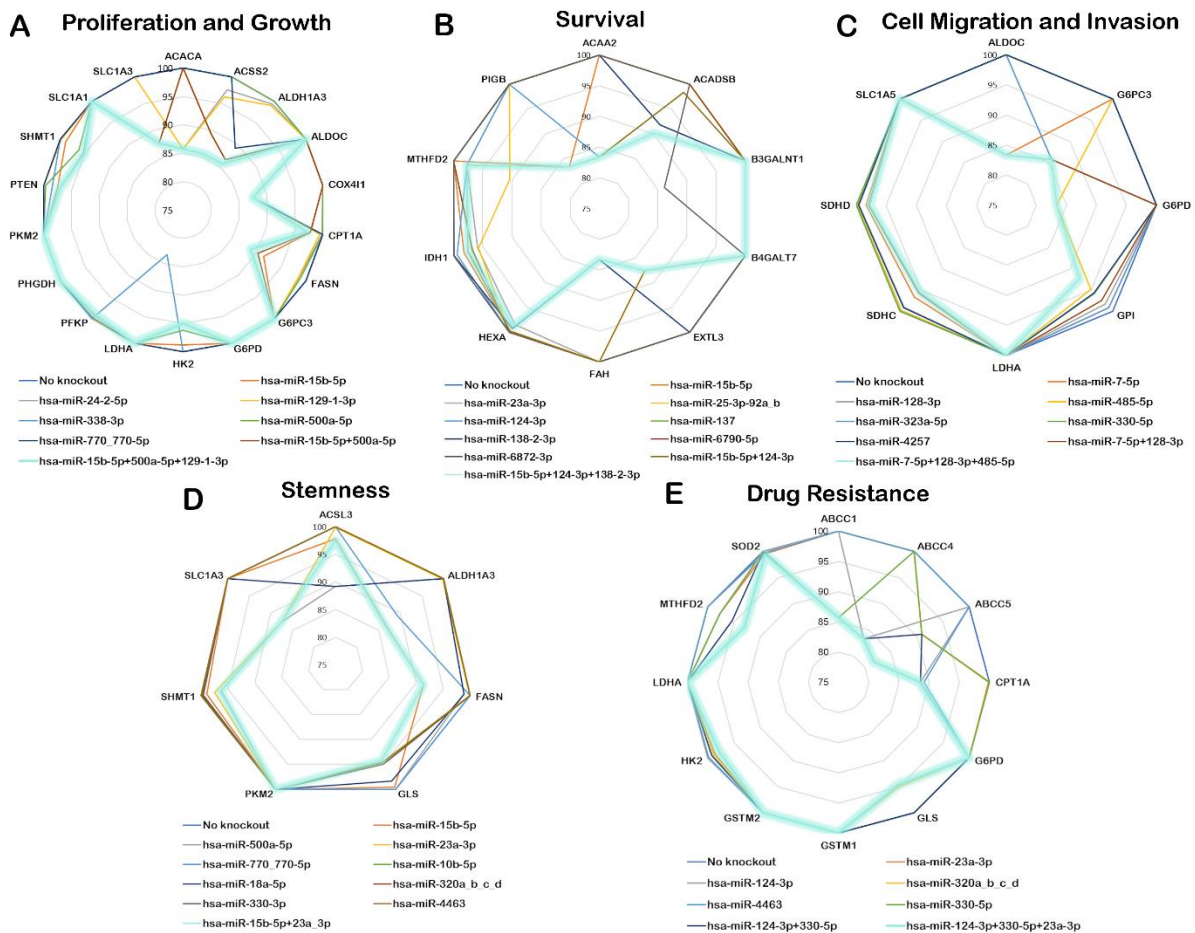


Figure 5.6: Radar plot representing percentage change in Katz centrality of key regulatory target genes upon miRNA knockout. (A) Proliferation and Growth, (B) Survival, (C) Cell Migration and Invasion, (D) Stemness, and (E) Drug Resistance in glioblastoma.

5.2.6. Verification of miRNA targets using prior literature and experimental evidence

Identified miRNA targets were further reviewed for any prior literary evidence of their involvement in the regulation of the respective cellular phenotypes to substantiate the credibility of the study. Restoration of downregulated miRNA hsa-miR-129-1-3p was previously observed to reduce cell proliferation (296), and hsa-miR-24-2-5p was observed to promote it (297). The impact of hsa-miR-15b-5p upregulation on proliferation, invasion, and migration is verified in other types of cancer (298) but not in

glioblastoma, although a definite upregulation of the miRNA is frequently observed. Hsa-miR-770, hsa-miR-485-5p, hsa-miR-500a-5p, and hsa-miR-128-3p were also verified for their involvement in the regulation of proliferation and growth of glioblastoma (299-302).

Hsa-miR-124-3p, which was observed to be important in regulating survival scenarios of glioblastoma, is associated with the inhibition of viability of the glioblastoma (303). Hsa-miR-137 overexpression inversely correlates with glioblastoma proliferation, migration, and survival (304). The miRNA was identified in all the three subnetworks associated with these phenotypes, the influence being maximum on the genes associated with survival. Downregulated expression of hsa-miR-138 is associated with progression-related poor survival of glioblastoma patients (305). Hsa-miR-128-3p has been implicated in the clinical prognosis of glioblastoma and has the potential to inhibit proliferation, migration, and invasion in these tumors (289). Hsa-miR-330-5p is associated with the suppression of invasiveness of glioblastoma (306). Hsa-miR-10b and hsa-miR-18a are associated with the generation of stemness in glioblastoma cells (307). Increased expression of hsa-miR-124 target genes due to its downregulation is observed to regulate epigenetic changes that promote tumor survival and resistance against chemotherapeutic drugs (308). Evidence also suggests the role of hsa-miR-23a in chemoresistance in different types of cancer, although its effect in the development of resistance in glioblastoma is yet not confirmed (309).

5.3. Discussion

Graph theoretical analyses of differentially expressed miRNAs and metabolic genes deduced meaningful inferences on miRNA regulated metabolism and cellular phenotypes in glioblastoma. Patient-derived data were used, and systematic verification with available literature evidence was done to ensure the reliability of the results obtained. Hsa-miR-15b-5p, MIR25/92 family miRNAs, hsa-miR-93-5p, hsa-miR-23a-3p, and MIR320, were the top upregulated miRNAs, and MIR124 family miRNAs, hsa-miR-137, hsa-miR-485-5p, hsa-miR-128-3p, and hsa-miR-3188 were the top downregulated miRNAs. Functional annotation of the target genes of these miRNAs showed their effect on metabolic pathways. Genes encoding the subunits of the ubiquinol-cytochrome

complex, NADH: ubiquinone complexes and the F_0F_1 complex were the most frequent targets of both upregulated and downregulated miRNAs, thus affecting the oxidative phosphorylation. The carbon metabolism was another common target. The inositol phosphate metabolism and glycerophospholipid metabolism were frequently targeted by the upregulated miRNAs, whereas purine and pyrimidine metabolism were frequent targets of the downregulated miRNAs.

Bipartite projection of pathways onto the regulatory miRNAs showed that the miRNAs highly regulated the central carbon metabolism, lipid, and amino acid metabolism. MiRNA regulation of crucial genes associated with energy metabolism can be exploited for miRNA-based therapeutic designs. The key miRNAs identified for the central carbon metabolism were hsa-miR-1225, hsa-miR-211-3p, and MIR770 family miRNAs. The backbone of miRNAs identified for fatty acid, lipid, glycan, amino acid, and nucleotide metabolism could be subjugated for regulating these metabolisms in glioblastoma.

Subnetworks obtained using network diffusion algorithm ensured identification of key regulatory genes, additional functionally related genes, and miRNAs associated with each of the cellular phenotypes. Subnetworks were obtained for proliferation and growth, survival, cell migration and invasion, stemness, and drug resistance in glioblastoma. The additional related genes like ACLY, COX, ME2, MTHFD2, GLS, GOT2, LDHA, and GLUD1, identified from the subnetwork, were able to regulate the functional response of the key regulatory genes at the reaction level. Hence, these genes can be considered important determinants of metabolic rerouting that allow phenotype switching. All the genes were controlled by miRNAs, and hence, could be controlled via the differential regulation of the miRNAs.

Due to the partial connectivity of the subnetworks, the commonly used centrality measures were inadequate to identify the important miRNAs and their impact on the key regulatory genes. Hence, the pairwise disconnectivity index was used to quantify the impact of a miRNA on the genes, and Katz centrality was used to determine the effect on the key regulatory genes of a subnetwork. The PDI was developed and discussed previously in context to gene regulatory networks, while Katz centrality was discussed in context to partially connected networks. The miRNA combination hsa-miR-15b-5p + hsa-miR-500a-5p + hsa-miR-129-1-3p was found to affect most of the regulatory genes

associated with proliferation and growth. Similarly, miRNA combinations hsa-miR-15b-5p + hsa-miR-124-3p + hsa-miR-138-2-3p, hsa-miR-7-5p + hsa-miR-128-3p + hsa-miR-485-5p, hsa-miR-15b-5p + hsa-miR-23a-3p and hsa-miR-124-3p + hsa-miR-300-5p + hsa-miR-23a-3p were identified as respective miRNA target combinations for survival, cell migration and invasion, stemness and drug resistance in glioblastoma.

The present study provides a strategy for a miRNA-based therapeutic design using graph-theoretical approaches. The combinations can be decided and altered as per the target genes of interest, allowing flexibility in the usage of the strategy. However, a major drawback of the present work is the acquisition of data from different sources. Since the data for differentially expressed miRNA and target genes have been obtained from different sources, it remains beyond the scope of this work to correlate the cause of differential gene expression with the miRNA expression. The miRNA targets obtained solely from the graph-theoretical analyses should be corroborated with experimental analysis. Despite the limitations, inferences drawn from the graph-theoretical analyses are useful for generating testable hypotheses and designing context-specific miRNA-based therapeutic approaches for personalized treatment using patient-specific expression data.

CHAPTER 6

CONCLUSION AND FUTURE PERSPECTIVES

“As for the future, your task is not to foresee it, but to enable it.”

- Antoine de Saint Exupery

6.1. Conclusion

The management of cellular metabolism in cancer is a complex process governed by multiple intracellular and extracellular factors. The characteristic changes in the metabolism of glioblastoma are of particular interest. Originating from the astrocyte glial cells, the disruption of metabolic homeostasis between these cells and the neurons severely affects the brain function. The stress generated in these tumors due to the insults incurred within the genome and the highly oxidative extracellular tumor microenvironment is manifested as altered metabolic phenotypes. Within the glioblastoma cell, the metabolic network reprogrammes itself as per the growth conditions, giving rise to complex adaptive phenotypes. With rationalized evaluation and computational analyses of the deregulated metabolic network, the present thesis has provided explanations to some of the commonly observed but less understood phenomena in glioblastoma and generated testable hypotheses for potential therapeutic targets against cancer.

With the aim to understand the pathway-level changes in metabolic flux distribution, the constraint-based metabolic model in **Chapter 3** showed the condition-specific differences in the preferred metabolic route to meet the energy and growth requirement of glioblastoma. The model showed a distinct increase in flux through the glycolytic and pentose phosphate pathway while optimizing the energy requirement of glioblastoma. The distribution of flux differed while optimizing the growth requirement of the cancer cell, where the flux flow was redistributed to ensure optimal production of ribose-5-phosphate. An assessment of the excess glutamate generated as a result of glutaminolysis in glioblastoma showed that the flux of glutamate could have three different fates: (i) consumption of glutamate in anaplerotic TCA cycle via glutamate dehydrogenase catalyzed formation of *akg*, (ii) formation of glutathione, and (iii) release to the

extracellular matrix via the cystine-glutamate antiporter (xCT) with a simultaneous uptake of cystine from the extracellular matrix. It was observed that the consumption of glutamate in the anaplerotic cycle was preferred in glioblastoma. However, as the metabolic demand shifted to enhance the glutathione production with the optimization of glioblastoma growth, the flux through xCT increased, releasing glutamate to the extracellular space. The cystine that was uptaken by the cell was converted to its monosulfide form, cysteine. Subsequently, cysteine and a considerable amount of the remaining glutamate formed the complex glutamyl-cysteine by the activity of γ -glutamyl-cysteine ligase that was converted to glutathione with the addition of glycine into the complex. The dependence of glioblastoma on the exogenous glycine and the overexpression of glycine transporters could also be explained in context to the increased growth demands of glioblastoma. A major flux re-routing was observed to be associated with the production of glutathione, which was an important component of the growth requirement of glioblastoma.

Evaluation of the minimal nutrient requirement of glioblastoma to sustain growth under nutrient-stressed conditions revealed the essentiality of cystine and glucose. Together, the two uptake metabolites were capable of driving considerable flux through the growth objective as compared to any other input metabolite considered in the model. The understanding of flux re-routing through metabolic pathways and essentiality of reactions and metabolites in context to maximization of growth in glioblastoma enabled the identification of blind spots within the network that could be exploited for therapeutic gain. The faulty endogenous glycine-serine biosynthesis and dependence of glioblastoma on exogenous glycine supplies created the opportunity for therapeutic targeting to reduce glioblastoma growth. It was observed under model conditions that the knockout of glycine transporter in combination with the serine biosynthesis enzymes phosphoglycerate dehydrogenase, or phosphoserine phosphatase, or phosphoserine transaminase effectively reduced glioblastoma growth. Analyses yielded additional non-intuitive target options that work effectively in combination as opposed to individual knockouts (185).

Exploring further, the additional challenges in glioblastoma were taken into account. Microenvironmental stress generated due to limited nutrient availability and oxidative

stress further shape the metabolic changes within the tumor cells (**Section 1.5.2**). In addition to the identification of essential nutrients for growth under limited nutrient availability, the constraint-based model for glioblastoma also showed shifting dependence on glutamine and fatty acids as alternate energy substrates under certain model conditions. Furthermore, to understand the metabolic responses generated within these tumors against oxidative stress, in **Chapter 4**, the dynamics between oxidant and antioxidant machinery were studied in depth using a dynamic model of reaction kinetics. The observed metabolic re-routing towards the glutathione metabolism was a preliminary motivation to proceed with the in-depth study of the reprogrammed metabolism. With initial analyses, the reactions glutathione peroxidase (GTHP), glutathione oxidoreductase (GTHO), NADPH oxidase (NOX), and superoxide dismutase (SOD) were identified as keepers of the antioxidant and oxidant producing machinery. Sensitivity analysis of the model parameters showed the involvement of GTHP, GTHO, and NOX in gliomagenesis. As we delved deeper into the dynamics of these machineries, their effect on the redox and thiol status of the cell was realized (310).

Assessment of the three model conditions: normal glial, hypoxic, and glioma showed that GTHP could primarily drive the proper functioning of antioxidant machinery, effectively scavenging reactive oxygen species produced under normal glial conditions. However, the activity of GTHO was more crucial in ROS scavenging in hypoxic and glioma model conditions. The dynamics of NOX was important in determining ROS levels. The changes in both GTHO and NOX determined the changes in the ROS levels and the redox and thiol status of the cell under hypoxic and glioma model conditions. Evaluation of unique sensitive parameters for hydrogen peroxide under glioma condition helped identification of parameters that would augment pro-oxidant and/or antioxidant therapeutic approaches against gliomas. All reactions and parameters in the re-routed metabolism towards glutathione production obtained from the previous study were considered for the analysis. Parameters of non-intuitive reactions in the network like cystine reductase, glutathione synthase, and fructose-bisphosphate aldolase were observed to influence the ROS level and thiol ratio of the cells and were proposed to alter the ROS manipulative strategies in glioma treatment.

In **Chapter 5**, we investigated the gene regulatory effect of microRNA on the metabolic genes that are associated with oncogenic phenotypes in glioblastoma. Our aim was to identify microRNA targets that could regulate metabolic processes and control cancerous phenotypes in glioblastoma and could be used for microRNA-based therapeutic designs. Graph theoretical analyses of microRNA-controlled metabolic networks helped identify microRNAs that controlled a large number of metabolic genes. Upregulated microRNAs hsa-miR-15b-5p, MIR25/92 family, and hsa-miR-23a-3p, and downregulated microRNAs MIR124 family, hsa-miR-137, and hsa-miR-485-5p were associated with the regulation of the maximum number of differentially expressed metabolic genes. Using bipartite projection and backbone extraction techniques, the key regulatory microRNAs controlling central carbon, fatty acid, lipid, glycan, amino acid, and nucleotide metabolism were identified. It was evident from the backbone analysis that the central carbon metabolism, lipid, and amino acid metabolism were highly regulated by the microRNAs.

The microRNA regulated metabolic gene networks associated with oncogenic phenotypes were traced back using network diffusion method. Pairwise disconnectivity indices of microRNAs and Katz centrality of target metabolic genes were used to identify knockout combination of miRNAs that could regulate the oncogenic phenotypes. The microRNA combinations hsa-miR-15b-5p + hsa-miR-500a-5p + hsa-miR-129-1-3p, hsa-miR-15b-5p + hsa-miR-124-3p + hsa-miR-138-2-3p, hsa-miR-7-5p + hsa-miR-128-3p + hsa-miR-485-5p, hsa-miR-15b-5p + hsa-miR-23a-3p and hsa-miR-124-3p + hsa-miR-300-5p + hsa-miR-23a-3p were identified as respective target combinations for proliferation and growth, survival, cell migration and invasion, stemness and drug resistance in glioblastoma.

The graph-theoretical approaches of network diffusion, backbone extraction, and measures like the pairwise disconnectivity index and Katz centrality and the strategies used in the study provide the opportunity to identify miRNA targets. The strategy can be implemented for other gene regulatory networks as well. However, a major drawback of the present work is the acquisition of data from different sources. Since the data for differentially expressed miRNA and target genes have been obtained from different sources, it remained beyond the scope of the work to correlate the cause of differential gene expression to miRNA expression. The miRNA targets obtained solely from the

graph-theoretical analyses need to be corroborated with experimental analysis. Despite the limitations, inferences drawn from the graph-theoretical analyses generate testable hypotheses for miRNA-based therapeutic design and reduce down the wide range of possibilities generated by the high throughput data to a feasible number.

6.2. Future perspectives

The present thesis provides answers to many of the observable but less understood phenomena of glioblastoma metabolism by performing thorough computational analyses of events occurring across different biological scales. While the computational models have generated plausible testable hypotheses, further validation of these testable hypotheses with experimental verification will provide the opportunity for their proper bench to bedside application.

The very essence of systems biology models is to provide a comprehensive understanding of the biological processes as integrated system, that can be served better with the incorporation of real-time omics data. The correlational pattern between genes under a pathophysiological condition can be deciphered using gene correlated network analysis. The use of weighted gene correlation network analysis (WGCNA) has gained popularity over the years. The integration of metabolomic and metabonomic data in the computational models of metabolism can provide insightful inference on the extent of change in the transcriptome, proteome and other regulatory interactions influencing metabolic profile in response to changing stimulus under pathological condition. Metabonomics is an emerging field of metabolomic study that considers the dynamic changes in the metabolomic profile of a cell under environmental, pathological or genetic perturbation (311). The incorporation of real time metabolomic data from single-cell analysis into multi-scale model of multicellular tissues might be a challenging thought-experiment, but with extremely beneficial results, if realized, in determining personalized approach of therapeutic design for heterogenous tumor population.

In line with the thesis outcomes, an important area that can be included as the future endeavour of the study is the crosstalk between signalling and metabolism in cancer. Dynamic crosstalk between signalling and metabolism supports phenotypic plasticity. The consequence of these mutual crosstalk is reflected during the therapeutic

intervention and create challenges in designing effective treatment protocols. These assist metabolic rewiring during the administration of drugs or therapies and make the prognosis difficult. In continuation to our thesis outcomes, we have thoroughly reviewed the crosstalking molecular interactions between signalling and metabolism. The understanding has been insightful in identifying suitable drug targets, developing therapeutics, and repurposing existing drugs for better efficacy. In an ongoing work, we are trying to integrate these understandings into a computational model with the addition of interaction with the immune cell as well, that can be used to infer important immunomodulatory responses generated by cancer cells.

Another important aspect of studying metabolism in cancer is to understand the changes in immune cell metabolism or immunometabolism. Immunometabolism is a flourishing area in the study, and its understanding in context to cancer cells can help in the development of strategies for immunotherapy following the standard treatment protocol to ensure a better prognosis. We have been able to gain an understanding of the metabolism of T-cells by reviewing through the signalling and metabolic pathways and their mutual crosstalk in guiding the activation and differentiation of naïve T-cells into the different subtypes (70). Further studies on the changing immunometabolism under the tumor microenvironment by considering different types of immune cells will be insightful in delineating the tumor-immune responses that will be of great prognostic value.

To overcome the limitations of existing therapies and drugs, drug repurposing and combinatorial approaches are increasingly gaining attention. Repurposing of metformin and disulfiram, two popular drugs used to treat type 2 diabetes and alcohol dependence, respectively, have been successful in glioblastoma treatment. Although, in a very recent update, the use of metformin has been revoked by FDA due to the presence of N-nitrosodimethylamine (NDMA) above the acceptable intake limit and associated side-effects. Popular drugs like bevacizumab, enzastuarin, rapamycin, etc., that target key regulatory proteins often associate severe off-target responses. Yet, the treatment protocols continue to largely rely on them, as the discovery of suitable drugs to replace them is still on the way. Understanding the crosstalk mechanism will help anticipate such off-target responses and identify the side effects. Furthermore, prospects created by the

crosstalk at the intercellular level will pave the way to design immune-modulatory therapeutic strategies against cancer. Association of arginine depletion strategy in gliomas having auxotrophic dependence on arginine with the immune effector cells is one such example. Undoubtedly, the future of drug and therapeutic discovery and development that aims to automate the whole process using cutting-edge technology must consider building a holistic platform that includes the understanding of crosstalking molecular interactions, with the option to continuously update the platform with new findings.

APPENDIX

APPENDIX A**Table A. 1: Details of reactions and pathways considered in the constraint-based metabolic model**

Abbrv.	Reaction Name	Reaction	Subcel Loc.	EC No.	NCBI Gene ID	Pathway
ASPTAm	Aspartate Transaminase	akg[m] + asp-L[m] <=> oaa[m] + glut[m]	m	2.6.1.1	2805	Alanine and Aspartate Metabolism
ASPTc	Aspartate Transaminase Cyt	akg[c] + asp-L[c] <=> oaa[c] + glut[c]	c	2.6.1.1	2806	Alanine and Aspartate Metabolism
2OADOX	2-Oxoacid: Lipoamide 2-Oxidoreductase	2oxoadp[m] + co-A-SH[m] + nad+[m] -> nadh[m] + co2[m] + glutcoa[m]	m	1.2.4.2	4967	Beta Oxidation of Fatty acid
AAAT	Acetyl-Coa:Acetyl-Coa C-Acetyltransferase	co-A-SH[m] + acacoa[m] <=> 2 accoa[m]	m	2.3.1.9	38	Beta Oxidation of Fatty acid
AMT	Acetylcoa C-Myristoyltransferase	co-A-SH[m] + opacoa[m] <=> accoa[m] + tdcoa[m]	m	2.3.1.16	10449; 30; 3032	Beta Oxidation of Fatty acid
BAT	Butanoyl-Coa:Acetyl-Coa C-Butanoyltransferase	co-A-SH[m] + 3ohcoa[m] <=> accoa[m] + bcoa[m]	m	2.3.1.16	10449; 30; 3032	Beta Oxidation of Fatty acid
BTCR	Butanoyl-Coa:FAD Oxidoreductase	bcoa[m] + fad[m] <=> fadh2[m] + b2coa[m]	m	1.3.8.7	34	Beta Oxidation of Fatty acid
DAT	Decanoyl-Coa:Acetyl-Coa C-Acyltransferase	co-A-SH[m] + 3oddcoa[m] <=> accoa[m] + dcoa[m]	m	2.3.1.16	10449; 30; 3032	Beta Oxidation of Fatty acid
DCFR	Decanoyl-Coa:FAD Oxidoreductase	fad[m] + dcoa[m] <=> fadh2[m] + td2coa[m]	m	1.3.8.7	34	Beta Oxidation of Fatty acid
ECOAH	3-Hydroxybutanoyl-Coa Hydro-Lyase	h2o[m] + b2coa[m] <=> 3hbcoa[m]	m	4.2.1.17	1892; 1962; 3030	Beta Oxidation of Fatty acid

GLUTCO ADH	Glutaryl-Coa Dehydrogenase	glutcoa[m] + h+[m] + fad[m] <=> co2[m] + fadh2[m] + b2coa[m]	m	1.3.8.6	2639	Beta Oxidation of Fatty acid
HBR	3- Hydroxybutanoy l-Coa: NAD+ Oxidoreductase	nad+[m] + 3hbcoa[m] <=> nadh[m] + acacoa[m] + h+[m]	m	1.1.1.35	1962; 3028; 3033; 3295	Beta Oxidation of Fatty acid
HCFR	Hexanoyl- Coa:FAD Oxidoreductase	fad[m] + hcoa[m] <=> fadh2[m] + th2coa[m]	m	1.3.8.7	34	Beta Oxidation of Fatty acid
HCT	Hexanoyl- Coa:Acetyl-Coa C- Acyltransferase	co-A-SH[m] + 3oocoa[m] <=> accoa[m] + hcoa[m]	m	2.3.1.16	10449; 30; 3032	Beta Oxidation of Fatty acid
HDDL	3- Hydroxydodecan oyl-Coa Hydro- Lyase	h2o[m] + tdecoa[m] <=> 3hddcoa[m]	m	4.2.1.17	1892	Beta Oxidation of Fatty acid
HDDR	3- Hydroxydodecan oyl-Coa: NAD+ Oxidoreductase	nad+[m] + 3hddcoa[m] <=> nadh[m] + h+[m] + 3oddcoa[m]	m	1.1.1.35	2194	Beta Oxidation of Fatty acid
HDL	Hydroxydecanoy l-Coa Hydro- Lyase	h2o[m] + td2coa[m] <=> 2hdcoa[m]	m	4.2.1.17	1892	Beta Oxidation of Fatty acid
HDR	Hydroxydecanoy l-Coa: NAD+ Oxidoreductase	nad+[m] + 2hdcoa[m] <=> nadh[m] + h+[m] + 3odcoa[m]	m	1.1.1.35	1962	Beta Oxidation of Fatty acid
HHDY	Hydroxyhexadec anoyl-Coa Hydro-Lyase	h2o[m] + hdd2coa[m] <=> 3hhdcoa[m]	m	4.2.1.17	1892	Beta Oxidation of Fatty acid
HHHL	Hydroxyhexanoy l-Coa Hydro- Lyase	h2o[m] + th2coa[m] <=> hhcoa[m]	m	4.2.1.17	1892	Beta Oxidation of Fatty acid
HHL	Hydroxyoctanoyl -Coa Hydro- Lyase	h2o[m] + to2coa[m] <=> 3hocoa[m]	m	4.2.1.17	1892	Beta Oxidation of Fatty acid
HHNO	3- Hydroxyhexadec anoyl-Coa: NAD+ Oxidoreductase	nad+[m] + 3hhdcoa[m] <=> nadh[m] + opacoa[m] + h+[m]	m	1.1.1.211	3030	Beta Oxidation of Fatty acid

HHOR	Hydroxyhexanoyl-Coa: NAD+ Oxidoreductase	nad+[m] + hhcoa[m] <=> nadh[m] + h+[m] + 3ohcoa[m]	m	1.1.1.35	1962	Beta Oxidation of Fatty acid
HOR	Hydroxyoctanoyl-Coa: NAD+ Oxidoreductase	nad+[m] + 3hocoa[m] <=> nadh[m] + h+[m] + 3oocoa[m]	m	1.1.1.35	1962	Beta Oxidation of Fatty acid
HTDCL	3-Hydroxytetradecanoyl-Coa Hydro-Lyase	h2o[m] + tt2coa[m] <=> 3htdcoa[m]	m	4.2.1.17	1892	Beta Oxidation of Fatty acid
HTDR	3-Hydroxytetradecanoyl-Coa: NAD+ Oxidoreductase	nad+[m] + 3htdcoa[m] <=> nadh[m] + h+[m] + 3otdcoa[m]	m	1.1.1.211	3030	Beta Oxidation of Fatty acid
LAT	Lauroyl-Coa:Acetyl-Coa C-Acyltransferase	co-A-SH[m] + 3otdcoa[m] <=> accoa[m] + lcoa[m]	m	2.3.1.16	10449; 30; 3032	Beta Oxidation of Fatty acid
LCFR	Lauroyl-Coa:FAD Oxidoreductase	fad[m] + lcoa[m] <=> fadh2[m] + tdecoa[m]	m	1.3.8.7	34	Beta Oxidation of Fatty acid
LCPT	L-Carnitine O-Palmitoyltransferase	pacoa[c] + crn[c] <=> co-A-SH[c] + pacrn[c]	c	2.3.1.21	126129; 1374; 1375; 1376	Beta Oxidation of Fatty acid
LCPT2	L-Carnitine O-Palmitoyltransferase 2	co-A-SH[m] + pacrn[m] <=> pacoa[m] + crn[m]	m	2.3.1.21	126129; 1374; 1375; 1376	Beta Oxidation of Fatty acid
OACT	Octanoyl-Coa:Acetyl-Coa C-Acyltransferase	co-A-SH[m] + 3odcoa[m] <=> accoa[m] + ocoa[m]	m	2.3.1.16	10449; 30; 3032	Beta Oxidation of Fatty acid
OCFR	Octanoyl-Coa:FAD Oxidoreductase	fad[m] + ocoa[m] <=> fadh2[m] + to2coa[m]	m	1.3.8.7	34	Beta Oxidation of Fatty acid
PCFR	Palmitoyl-Coa:FAD Oxidoreductase	fad[m] + pacoa[m] <=> fadh2[m] + hdd2coa[m]	m	1.3.8.7	34	Beta Oxidation of Fatty acid
PCH	Palmitoyl-Coa Hydrolase	co-A-SH[c] + pa[c] <=> h2o[c] + pacoa[c]	c	3.1.2.2	122970; 10965; 11332;	Beta Oxidation of Fatty acid

					570; 641371	
TCFR	Tetradecanoylco a:FAD Oxidoreductase	tdcoa[m] + fad[m] <=> fadh2[m] + tt2coa[m]	m	1.3.8.7	34	Beta Oxidation of Fatty acid
CD	Cysteine Dioxygenase	cys-L[c] + o2[c] -> 2 h+[c] + 3sala[c]	c	1.13.11.2 0	1036	Cysteine Metabolism
CGL	Cystathionine Gamma-Lyase	h2o[c] + cyst- L[c] -> cys-L[c] + nh4+[c] + 2obut[c]	c	4.4.1.1	1491	Cysteine Metabolism
CST	Cysteine Sulfinat Transaminase	akg[c] + 3sala[c] <=> glut[c] + 3snpyr[c]	c	2.6.1.1	2805	Cysteine Metabolism
CystRed	Cystine Reductase	h+[c] + nadh[c] + cystine[c] <=> nad+[c] + 2 cys-L[c]	c	1.8.1.6	1109	Cysteine Metabolism
SPON1	Spontaneous 3snpyr	h2o[c] + 3snpyr[c] -> h+[c] + pyr[c] + so3[c]	c	3.13.1.-		Cysteine Metabolism
Ex_adn	Adenosine Exchange	adn[e] <=>	e			Exchange Reaction
Ex_akg	Ketoglutarate Exchange	akg[e] <=>	e			Exchange Reaction
Ex_ala	Alanine Exchange	ala-L[e] <=>	e			Exchange Reaction
Ex_asp-L	Aspartate Exchange	asp-L[e] <=>	e			Exchange Reaction
Ex_cit	Citrate Exchange	cit[e] <=>	e			Exchange Reaction
Ex_co2	Carbon Dioxide Exchange	co2[e] <=>	e			Exchange Reaction
Ex_co-A- SH	Coenzyme A Exchange	co-A-SH[e] <=>	e			Exchange Reaction
Ex_crn	L-Carnitine Exchange	crn[e] <=>	e			Exchange Reaction
Ex_cystin e	Cystine Exchange	cystine[e] <=>	e			Exchange Reaction
Ex_for	Formate Exchange	for[e] <=>	e			Exchange Reaction
Ex_gdp	Gdp Exchange	gdp[e] <=>	e			Exchange Reaction

Ex_gln(c)	Glutamine Exchange	gln[e] <=>	e			Exchange Reaction
Ex_glt	Glutathione Exchange	glt[e] <=>	e			Exchange Reaction
Ex_glu	Glucose Exchange	b-D-glu[e] <=>	e			Exchange Reaction
Ex_glut	L-Glutamate Exchange	glut[e] <=>	e			Exchange Reaction
Ex_glycine	Glycine Exchange	gly[e] <=>	e			Exchange Reaction
Ex_gtp	Gtp Exchange	gtp[e] <=>	e			Exchange Reaction
Ex_h+	Proton Exchange	h+[e] <=>	e			Exchange Reaction
Ex_h2o	Water Exchange	h2o[e] <=>	e			Exchange Reaction
Ex_hco3	Bicarbonate Exchange	hco3[e] <=>	e			Exchange Reaction
Ex_K+	Potassium Ion Exchange	K+[e] <=>	e			Exchange Reaction
Ex_lac	Lactate Exchange	lac[e] <=>	e			Exchange Reaction
Ex_mlthf	5,10-Methylenetetrahydrofolate Exchange	mlthf[e] <=>	e			Exchange Reaction
Ex_Na+	Sodium Ion Exchange	Na+[e] <=>	e			Exchange Reaction
Ex_nh4+	Ammonium Exchange	nh4+[e] <=>	e			Exchange Reaction
Ex_nmg	N-Methyl-Glycine Exchange	Nmg[e] <=>	e			Exchange Reaction
Ex_o2	Oxygen Exchange	o2[e] <=>	e			Exchange Reaction
Ex_oaa	Oxaloacetate Exchange	oaa[e] <=>	e			Exchange Reaction
Ex_obut	2-Oxobutanoate Exchange	2obut[e] <=>	e			Exchange Reaction
Ex_pa	Palmitic Acid Exchange	pa[e] <=>	e			Exchange Reaction
Ex_pi	Phosphate Exchange	pi[e] <=>	e			Exchange Reaction
Ex_po	Orthophosphate Exchange	po[e] <=>	e			Exchange Reaction

Ex_ppi	Pyrophosphate Exchange	ppi[e] <=>	e			Exchange Reaction
Ex_quln	Quinolate Exchange	quln[e] <=>	e			Exchange Reaction
Ex_succ	Succinate Exchange	succ[e] <=>	e			Exchange Reaction
Ex_sulfite	Sulfite Exchange	so3[e] <=>	e			Exchange Reaction
Ex_thf	Tetrahydrofolate Exchange	thf[e] <=>	e			Exchange Reaction
Ex_try	Tryptophan Exchange	try[e] <=>	e			Exchange Reaction
Ex-met	L-Methionine Exchange	met-L[e] <=>	e			Exchange Reaction
ATA	Alanine Transaminase	glut[c] + pyr[c] <=> akg[c] + ala-L[c]	c	2.6.1.2	2875	Glutamate Metabolism
Glnase	Glutaminase	glut[m] + nh4+[m] -> h2o[m] + gln[m]	m	3.5.1.2	2744	Glutamate Metabolism
GlnSyn	Glutamine Synthetase	atp[c] + glut[c] + nh4+[c] <=> h+[c] + adp[c] + pi[c] + gln[c]	c	6.3.1.2	2752	Glutamate Metabolism
GlutDH	Glutamate Dehydrogenase	akg[m] + h+[m] + nh4+[m] + nadph[m] <=> h2o[m] + glut[m] + nadp[m]	m	1.4.1.4	2747	Glutamate Metabolism
GCL	Glutamate-Cysteine Ligase	atp[c] + glut[c] + cys-L[c] -> h+[c] + adp[c] + pi[c] + glucys[c]	c	6.3.2.2	2730; 2729	Glutathione Metabolism
GS	Glutathione Synthase	atp[c] + gly[c] + glucys[c] -> h+[c] + adp[c] + pi[c] + glt[c]	c	6.3.2.3	2937	Glutathione Metabolism
GHMT	Glycine Hydroxymethyltransferase	ser-L[c] + thf[c] <=> h2o[c] + gly[c] + mlthf[c]	c	2.1.2.1	6470	Glycine-Serine Metabolism
PGDH	Phosphoglycerate Dehydrogenase	nad+[c] + 3-pg[c] <=> h+[c] + nadh[c] + 3php[c]	c	1.1.1.95	26227	Glycine-Serine Metabolism

PSP	Phosphoserine Phosphatase	$\text{h2o}[c] + \text{pser-L}[c] \rightleftharpoons \text{pi}[c] + \text{ser-L}[c]$	c	3.1.3.3	5723	Glycine-Serine Metabolism
PST	Phosphoserine Transaminase	$\text{glut}[c] + 3\text{php}[c] \rightleftharpoons \text{akg}[c] + \text{pser-L}[c]$	c	2.6.1.52	29968	Glycine-Serine Metabolism
ENO	Enolase	$2\text{-pg}[c] \rightleftharpoons \text{h2o}[c] + \text{pep}[c]$	c	4.2.1.11	2026	Glycolysis
FBA	Fructose-1,6-Bisphosphate Aldolase	$\text{f16bp}[c] \rightleftharpoons \text{dhap}[c] + \text{gap}[c]$	c	4.1.2.13	226; 229	Glycolysis
GAPDH	Glyceraldehyde-3-Phosphate Dehydrogenase	$\text{nad}^+[c] + \text{pi}[c] + \text{dhap}[c] \rightleftharpoons \text{h}^+[c] + \text{nadh}[c] + 13\text{dpg}[c]$	c	1.2.1.12	2597	Glycolysis
HEX	Hexokinase	$\text{atp}[c] + \text{b-D-glu}[c] \rightleftharpoons \text{h}^+[c] + \text{adp}[c] + \text{g6p-B}[c]$	c	2.7.1.1	3098; 3099; 3101	Glycolysis
Lac_dehyd	L-Lactate Dehydrogenase	$\text{h}^+[c] + \text{nadh}[c] + \text{pyr}[c] \rightleftharpoons \text{nad}^+[c] + \text{lac}[c]$	c	1.1.1.27	3939; 3945; 3948	Glycolysis
PFK	Phosphofructokinase	$\text{atp}[c] + \text{f6p}[c] \rightleftharpoons \text{h}^+[c] + \text{adp}[c] + \text{f16bp}[c]$	c	2.7.1.11	5211; 5213; 5214	Glycolysis
PGI	Phosphoglucose Isomerase	$\text{g6p-B}[c] \rightleftharpoons \text{f6p}[c]$	c	5.3.1.9	2821	Glycolysis
PGK	Phosphoglycerate Kinase	$\text{adp}[c] + 13\text{dpg}[c] \rightleftharpoons \text{atp}[c] + 3\text{-pg}[c]$	c	2.7.2.3	5230; 5232	Glycolysis
PGM	Phosphoglycerate Mutase	$3\text{-pg}[c] \rightleftharpoons 2\text{-pg}[c]$	c	5.4.2.11	441531; 5223; 5224; 669	Glycolysis
PYK	Pyruvate Kinase	$\text{h}^+[c] + \text{adp}[c] + \text{pep}[c] \rightleftharpoons \text{atp}[c] + \text{pyr}[c]$	c	2.7.1.40	5315	Glycolysis
TPI	Triose Phosphate Isomerase	$\text{gap}[c] \rightleftharpoons \text{dhap}[c]$	c	5.3.1.1	7167	Glycolysis
AHC	Adenosylhomocysteinase	$\text{h2o}[c] + \text{ahcys}[c] \rightarrow \text{adn}[c] + \text{hcys-L}[c]$	c	3.3.1.1	191	Methionine Metabolism
CBS	Cystathionine Beta-Synthase	$\text{hcys-L}[c] + \text{ser-L}[c] \rightarrow \text{h2o}[c] + \text{cyst-L}[c]$	c	4.2.1.22	875	Methionine Metabolism

HCMT	Homocysteine S-Methyltransferase	amet[n] + gly[n] -> Nmg[n] + ahcys[n]	n	2.1.1.10	23743	Methionine Metabolism
MAT	Methionine Adenosyltransferase	h2o[c] + atp[c] + met-L[c] -> h+[c] + pi[c] + amet[c] + ppi[c]	c	2.5.1.6	27430; 4143; 4144	Methionine Metabolism
GBM_BM	Metabolic Demand Reaction	oaa[m] + glt[c] + r5p[c] + succ[m] ->				Objective Function
ATPS_1	Cytosolic Atpase	h2o[c] + atp[c] -> h+[c] + adp[c] + pi[c]	c	3.6.1.3	954	Others
MDH (Cyto)	Cytoplasmic Malate Dehydrogenase	nad+[c] + mal[c] <=> nadh[c] + co2[c] + pyr[c]	c	1.1.1.38	4190	Others
PEP_Carb K_1	Phosphoenolpyruvate Carboxykinase (GTP)	oaa[c] + gtp[c] <=> co2[c] + pi[c] + pep[c] + gdp[c]	c	4.1.1.32	5105; 5106	Others
Pyr_Carb m	Mitochondrial Pyruvate Carboxylase	atp[m] + pyr[m] + hco3[m] <=> oaa[m] + adp[m] + pi[m] + h+[m]	m	1.2.4.1	5160; 5161; 5162	Others
ATPSyn	ATP Synthase	adp[m] + pi[m] + 4 h+[i] <=> h2o[m] + atp[m] + 3 h+[m]	i	3.6.3.14	514; 506; 91647	Oxidative Phosphorylation
Cytox(Co mplex IV)	Cytochrome Oxidase (Complex IV)	8 h+[m] + 4 focytc[m] + o2[m] <=> 2 h2o[m] + 4 h+[i] + 4 ficytc[m]	i	1.9.3.1	9997; 6341	Oxidative Phosphorylation
NADH:Ubioxred(Co mplex I)	NADH:Ubiquinone Oxidoreductase (Complex I)	nadh[m] + 5 h+[m] + Q[m] <=> nad+[m] + 4 h+[i] + QH2[m]	i	1.6.5.3	4537	Oxidative Phosphorylation
Ubi:Cytoxred(Co mplex III)	Ubiquinone: Cytochrome C Oxidoreductase (Complex III)	2 h+[m] + 2 ficytc[m] + QH2[m] <=> 4 h+[i] + 2 focytc[m] + Q[m]	i	1.10.2.2	7386	Oxidative Phosphorylation

ACOC	Acetyl-Coa Carboxylase	atp[c] + accoa[c] + hco3[c] -> adp[c] + malo-CoA[c] + po[c]	c	6.4.1.2	31	Palmitic Acid Biosynthesis
AMAT	Acyl-Malonyl-Acyltransferase	aACP[c] + malACP[c] -> hs-acp[c] + aacACP[c] + co2[c]	c	2.3.1.39	2194	Palmitic Acid Biosynthesis
ATF	S-Acetyltransferase	accoa[c] + hs-acp[c] -> aACP[c] + co-A-SH[c]	c	2.3.1.38	1737	Palmitic Acid Biosynthesis
BAAT	Butyryl-[Acyl-Carrier Protein]:Malonyl-ACP C-Acyltransferase	malACP[c] + butACP[c] -> hs-acp[c] + co2[c] + 3ohACP[c]	c	2.3.1.85	2194	Palmitic Acid Biosynthesis
BNTO	Butyryl-[Acp]:NADP+ Trans-2-Oxidoreductase	butACP[c] + nadp[c] <=> h+[c] + nadph[c] + tbut2eACP[c]	c	1.3.1.39	2194	Palmitic Acid Biosynthesis
DDMT	Dodecanoyl-[Acyl-Carrier Protein]:Malonyl-ACP- C-Acyltransferase	malACP[c] + ddcaACP[c] -> hs-acp[c] + co2[c] + 3ottdcACP[c]	c	2.3.1.85	2194	Palmitic Acid Biosynthesis
DENTO	Decanoyl-[Acp]:NAP+ Trans-2-Oxidoreductase	nadp[c] + dcaACP[c] <=> h+[c] + nadph[c] + tdc2eACP[c]	c	1.3.1.39	2194	Palmitic Acid Biosynthesis
DMACT	Decanoyl-[Acyl-Carrier Protein]:Malonyl-ACP C-Acyltransferase	malACP[c] + dcaACP[c] -> hs-acp[c] + co2[c] + 3oddcACP[c]	c	2.3.1.85	2194	Palmitic Acid Biosynthesis
DNTO	Dodecanoyl-[Acp]:NADP+ Trans-2-Oxidoreductase	nadp[c] + ddcaACP[c] <=> h+[c] + nadph[c] + tddcACP[c]	c	1.3.1.39	2194	Palmitic Acid Biosynthesis
HAMAT	Hexanoyl-[Acyl-Carrier Protein]:Malonyl-ACP- C-Acyltransferase	malACP[c] + hexACP[c] -> hs-acp[c] + co2[c] + 3ooctACP[c]	c	2.3.1.85	2194	Palmitic Acid Biosynthesis

HAOR	3-Hydroxyoctanoyl-[Acyl-Carrier-Protein]: NADP+ Oxidoreductase	$h+[c] + nadph[c] + 3oactACP[c] \rightarrow nadp[c] + 3hoactACP[c]$	c	1.1.1.100	2194	Palmitic Acid Biosynthesis
HBACL	3-Hydroxybutanoyl-[Acyl-Carrier-Protein] Hydro-Lyase	$3hoactACP[c] \rightarrow h_2o[c] + toct2eACP[c]$	c	4.2.1.59	2194	Palmitic Acid Biosynthesis
HBAL	3-Hydroxybutanoyl-[Acyl-Carrier-Protein] Hydro-Lyase	$3hbutACP[c] \rightarrow h_2o[c] + tbut2eACP[c]$	c	4.2.1.59	2194	Palmitic Acid Biosynthesis
HBAR	3-Hydroxybutanoyl-[Acyl-Carrier Protein]:NADP+ Oxidoreductase	$h+[c] + aacACP[c] + nadph[c] \rightarrow nadp[c] + 3hbutACP[c]$	c	1.1.1.100	2194	Palmitic Acid Biosynthesis
HDDHL	3-Hydroxydodecanoyl-ACP Hydro-Lyase	$3hddecACP[c] \rightarrow h_2o[c] + tddcACP[c]$	c	4.2.1.59	2194	Palmitic Acid Biosynthesis
HDDOR	3-Hydroxydodecanoyl-[Acyl-Carrier-Protein]: NADP+ Oxidoreductase	$h+[c] + nadph[c] + 3oddcACP[c] \rightarrow nadp[c] + 3hddecACP[c]$	c	1.1.1.100	2194	Palmitic Acid Biosynthesis
HDHL	3-Hydroxydecanoyl-[Acyl-Carrier-Protein] Hydro-Lyase	$3hdeACP[c] \rightarrow h_2o[c] + tdc2eACP[c]$	c	4.2.1.59	2194	Palmitic Acid Biosynthesis
HDMT	Hexadecanoyl-[Acyl-Carrier Protein]:Malonyl-Coa C-Acyltransferase	$h+[c] + nadph[c] + th_2eACP[c] \rightarrow nadp[c] + hdecACP[c]$	c	1.1.1.100	2194	Palmitic Acid Biosynthesis
HDOR	3-Hydroxydecanoyl-[Acyl-Carrier-Protein]: NADP+ Oxidoreductase	$h+[c] + nadph[c] + 3odcaACP[c] \rightarrow nadp[c] + 3hdeACP[c]$	c	1.1.1.100	2194	Palmitic Acid Biosynthesis
HHAL	3-Hydroxyhexanoyl-[Acyl-Carrier-Protein] Hydro-Lyase	$3hhexACP[c] \rightarrow h_2o[c] + thex_2eACP[c]$	c	4.2.1.59	2194	Palmitic Acid Biosynthesis

HHAR	3-Hydroxyhexanoyl-ACP: NADP+ Oxidoreductase	$h+[c] + 3ohACP[c] + nadph[c] \rightarrow nadp[c] + 3hhexACP[c]$	c	1.1.1.100	2194	Palmitic Acid Biosynthesis
HNTD	Hexanoyl-[Acp]: NADP+ Trans-2-Oxidoreductase	$nadp[c] + hexACP[c] \rightleftharpoons h+[c] + nadph[c] + thex2eACP[c]$	c	1.3.1.39	2194	Palmitic Acid Biosynthesis
HPHL	3-Hydroxypalmitoyl-[Acyl-Carrier-Protein] Hydro-Lyase	$2hpaACP[c] \rightarrow h2o[c] + th2eACP[c]$	c	4.2.1.17	1892	Palmitic Acid Biosynthesis
HPOR	3-Hydroxypalmitoyl-[Acyl-Carrier-Protein]: NADP+ Oxidoreductase	$h+[c] + nadph[c] + 3ohdcACP[c] \rightarrow nadp[c] + 2hpaACP[c]$	c	1.1.1.100	2194	Palmitic Acid Biosynthesis
HTDHL	3-Hydroxytetradecanoyl-[Acyl-Carrier-Protein] Hydro-Lyase	$3httdcACP[c] \rightarrow h2o[c] + ttttdc2eACP[c]$	c	4.2.1.17	1892	Palmitic Acid Biosynthesis
HTDOR	3-Hydroxytetradecanoyl-[Acyl-Carrier-Protein]: NADP+ Oxidoreductase	$h+[c] + nadph[c] + 3ottdcACP[c] \rightarrow nadp[c] + 3httdcACP[c]$	c	1.1.1.100	2194	Palmitic Acid Biosynthesis
MT	S-Malonyltransferase	$h+[c] + mal-CoA[c] + hs-acp[c] \rightarrow malACP[c] + co-A-SH[c]$	c	2.3.1.39	27349	Palmitic Acid Biosynthesis
OH	Oleoyl-[Acyl-Carrier Protein] Hydrolase	$h2o[c] + hdecACP[c] \rightleftharpoons hs-acp[c] + pa[c]$	c	3.1.2.14	2194	Palmitic Acid Biosynthesis
OMACT	Octanoyl-[Acyl-Carrier Protein]:Malonyl-ACP C-Acyltransferase	$malACP[c] + ocACP[c] \rightarrow hs-acp[c] + co2[c] + 3odcaACP[c]$	c	2.3.1.85	2194	Palmitic Acid Biosynthesis
ONTO	Octanoyl-[Acp]: NADP+ Trans-2-Oxidoreductase	$nadp[c] + ocACP[c] \rightleftharpoons h+[c] + nadph[c] + toct2eACP[c]$	c	1.3.1.39	2194	Palmitic Acid Biosynthesis

TDTNO	Tetradecanoyl-[Acp]:NADP+ Trans-2-Oxidoreductase	nadp[c] + ttdcACP[c] <=> h+[c] + nadph[c] + ttdc2eACP[c]	c	1.3.1.39	2194	Palmitic Acid Biosynthesis
TTDT	Tetradecanoyl-[Acyl-Carrier Protein]:Malonyl-ACP C-Acyltransferase	malACP[c] + ttdcACP[c] -> hs-acp[c] + co2[c] + 3ohdcACP[c]	c	2.3.1.85	2194	Palmitic Acid Biosynthesis
6PGLase	6-Phosphogluconolactonase	h2o[c] + 6pgl[c] <=> h+[c] + 6-pgc[c]	c	3.1.1.31	25796	PPP
G6PDH	Beta-D-Glucose-6-Phosphate Dehydrogenase	nadp[c] + g6p-B[c] <=> 6pgl[c] + h+[c] + nadph[c]	c	1.1.1.49	2539	PPP
PGCDH	6-Phosphogluconolactone Dehydrogenase	6-pgc[c] + nadp[c] <=> co2[c] + nadph[c] + ru5p-D[c]	c	1.1.1.44	5226	PPP
RPE	Ribulose Phosphate-3 Epimerase	ru5p-D[c] <=> xu5p-D[c]	c	5.1.3.1	6120; 729020	PPP
RPI	Ribulose Phosphate Isomerase	ru5p-D[c] <=> r5p[c]	c	5.3.1.6	22934	PPP
TA	Transaldolase	gap[c] + s7p[c] <=> f6p[c] + e4p[c]	c	2.2.1.2	6888	PPP
TK1	Transketolase 1	r5p[c] + xu5p-D[c] <=> gap[c] + s7p[c]	c	2.2.1.1	7086; 8277; 84076	PPP
TK2	Transketolase 2	xu5p-D[c] + e4p[c] <=> gap[c] + f6p[c]	c	2.2.1.1	7086; 8277; 84076	PPP
2OXOAD PTm	2-Oxoadipate Shuttle	2oxoadp[m] + akg[c] <=> 2oxoadp[c] + akg[m]	mms		89874	Shuttle
Sh_cit-mal	Citrate-Malate Shuttle	cit[m] + mal[c] <=> mal[m] + cit[c]	mms			Shuttle
Sh_glut-asp	Glutamate-Aspartate Shuttle	asp-L[m] + glut[c] <=> glut[m] + asp-L[c]	mms		6507	Shuttle
Sh_mal-asp1	Malate-Aspartate Shuttle	akg[m] + mal[c] <=>	mms			Shuttle

		akg[c] + mal[m]				
AH_1	Aconitate Hydratase	cit[m] <=> cis-acon[m] + h2o[m]	m	4.2.1.3	48	TCA Cycle
AH_2	Aconitate Hydratase	cis-acon[m] + h2o[m] <=> isocit[m]	m	4.2.1.3	50	TCA Cycle
AKGDH	Alpha Ketoglutarate Dehydrogenase	co-A-SH[m] + nad+[m] + akg[m] <=> nadh[m] + co2[m] + succoa[m]	m	1.2.4.2	4967	TCA Cycle
CS	Citrate Synthase	accoa[m] + h2o[m] + oaa[m] <=> co-A-SH[m] + cit[m] + h+[m]	m	2.3.3.1	1431	TCA Cycle
FUMH	Fumarate Hydratase	h2o[m] + fum[m] <=> mal[m]	m	4.2.1.2	2271	TCA Cycle
IDH	Isocitrate Dehydrogenase	nad+[m] + isocit[m] <=> nadh[m] + co2[m] + akg[m]	m	1.1.1.41	3419	TCA Cycle
IDH (nadp)	Isocitrate Dehydrogenase(nadp)	isocit[m] + nadp[m] <=> co2[m] + akg[m] + nadph[m]	m	1.1.1.42	3418	TCA Cycle
MDH	Malate Dehydrogenase	nad+[m] + mal[m] <=> nadh[m] + oaa[m] + h+[m]	m	1.1.1.37	4191	TCA Cycle
PYDH	Pyruvate Dehydrogenase	co-A-SH[m] + nad+[m] + pyr[m] <=> nadh[m] + co2[m] + accoa[m]	m	1.2.4.1	5160; 5161; 5162	TCA Cycle
SCS	Succinyl-Coa Synthetase	succoa[m] + adp[m] + pi[m] <=> co-A-SH[m] + atp[m] + succ[m]	m	6.2.1.5	8801; 8802; 8803	TCA Cycle
SDH	Succinate Dehydrogenase	succ[m] + fad[m] <=> fadh2[m] + fum[m]	m	1.3.5.1	6389; 6390	TCA Cycle

SDH (Complex II)	Succinate Dehydrogenase (Complex II)	succ[m] + Q[m] => fum[m] + QH2[m]	m	1.3.5.1	6389; 6390	TCA Cycle
Anti_cyst ine_glut	Cystine Glutamate Antiporter	glut[c] + cystine[e] => cystine[c] + glut[e]	pms		23657	Transport Reaction
Na+/K+_ glut_up	Na+/K+ Dependent Glutamate Uptake	h+[c] + atp[c] + glut[c] + K+[e] + hco3[e] + 2 Na+[c] => hco3[c] + adp[c] + pi[c] + glut[e] + 2 Na+[e] + h+[e] + K+[c]	pms		6506	Transport Reaction
Trans_ac coa	Acetyl-Coa Transport	accoa[m] => accoa[c]	mms		9197	Transport Reaction
Trans_ad n	Adenosine Transport	adn[c] => adn[e]	pms			Transport Reaction
Trans_ad p	Adp Transport	adp[m] -> adp[c]	mms			Transport Reaction
Trans_adp (m)	Adp Transport	adp[c] => adp[m]	mms			Transport Reaction
trans_ahc ys	S-Adenosyl-L- Homocysteine	ahcys[n] -> ahcys[c]	nms			Transport Reaction
Trans_ak g	Ketoglutarate Transport	akg[c] => akg[e]	pms			Transport Reaction
Trans_ala	Alanine Transport	ala-L[c] => ala-L[e]	pms		6509	Transport Reaction
Trans_a met	S-Adenosyl-L- Methionine	amet[c] -> amet[n]	nms		115286	Transport Reaction
Trans_as p-L	Aspartate Transport	asp-L[c] => asp-L[e]	pms			Transport Reaction
Trans_as p-L(m)	Mitochondrial Aspartate Transport	asp-L[c] => asp-L[m]	mms			Transport Reaction
Trans_at p	Atp Transport	atp[m] -> atp[c]	mms			Transport Reaction
Trans_at p (m)	Atp Transport	atp[m] => atp[c]	mms			Transport Reaction
Trans_cit (c)	Cytoplasmic Citrate Transport	cit[c] => cit[e]	pms			Transport Reaction
Trans_co 2 (c)	Cytoplasmic Carbon Dioxide Transport	co2[c] => co2[e]	pms			Transport Reaction

Trans_co 2 (m)	Mitochondrial Carbon Dioxide Transport	co2[m] <=> co2[c]	mms			Transport Reaction
Trans_co -A-SH(c)	Cytoplasmic Coenzyme A Transport	co-A-SH[c] <=> co-A-SH[e]	pms			Transport Reaction
Trans_co -A-SH(m)	Mitochondrial Coenzyme A Transport	co-A-SH[m] <=> co-A-SH[c]	mms		284439	Transport Reaction
Trans_cr n	L-Carnitine Transport	crn[c] <=> crn[e]	pms			Transport Reaction
Trans_cr n (m)	L-Carnitine Transport (m)	crn[m] <=> crn[c]	mms			Transport Reaction
Trans_for	Formate Transport	for[c] <=> for[e]	pms		65010	Transport Reaction
Trans_gd p	Gdp Transport	gdp[c] <=> gdp[e]	pms			Transport Reaction
Trans_gl n (c)	Cytoplasmic Glutamine Transport	gln[c] <=> gln[e]	pms			Transport Reaction
Trans_gl n (m)	Mitochondrial Glutamine Transport	gln[m] <=> gln[c]	mms			Transport Reaction
Trans_glt	Glutathione Transport	glt[c] <=> glt[e]	pms			Transport Reaction
Trans_gl u	Glucose Transport	h+[c] + b-D- glu[c] <=> b-D- glu[e] + h+[e]	pms		6513	Transport Reaction
Trans_Gl ut(ATP)	ATP Dependent Glutamate Uptake	adp[c] + glut[c] + pi[c] <=> atp[c] + glut[e]	pms		6506	Transport Reaction
Trans_gl ut(c)	L-Glutamate Transport	glut[c] <=> glut[e]	pms			Transport Reaction
Trans_gly	Glycine Transport	gly[c] <=> gly[n]	nms			Transport Reaction
Trans_gly cine	Glycine Transport	gly[c] <=> gly[e]	pms		6536	Transport Reaction
Trans_gt p	Gtp Transport	gtp[c] <=> gtp[e]	pms			Transport Reaction
Trans_h+ (c)	Cytoplasmic Proton Transport	h+[c] <=> h+[e]	pms			Transport Reaction
Trans_h+ (m)	Mitochondrial Proton Transport	h+[c] <=> h+[m]	mms			Transport Reaction
Trans_h2 o (c)	Cytoplasmic Water Transport	h2o[c] <=> h2o[e]	pms			Transport Reaction

Trans_h2o (m)	Mitochondrial Water Transport	$\text{h2o}[m] \rightleftharpoons \text{h2o}[c]$	mms			Transport Reaction
Trans_hco3	Bicarbonate Transport	$\text{hco3}[c] \rightleftharpoons \text{hco3}[e]$	pms		8671	Transport Reaction
Trans_hco3(m)	Mitochondrial Bicarbonate Ion Transport	$\text{hco3}[m] \rightleftharpoons \text{hco3}[c]$	mms		8671	Transport Reaction
Trans_K+	Potassium Ion Transport	$\text{K}+[c] \rightleftharpoons \text{K}+[e]$	pms			Transport Reaction
Trans_lac	Lactate Transport	$\text{lac}[c] \rightleftharpoons \text{lac}[e]$	pms			Transport Reaction
Trans_mlthf	5,10-Methylenetetrahydrofolate Transport	$\text{mlthf}[c] \rightleftharpoons \text{mlthf}[e]$	pms			Transport Reaction
Trans_Na+	Sodium Ion Transport	$\text{Na}+[c] \rightleftharpoons \text{Na}+[e]$	pms		6558	Transport Reaction
Trans_nad+(m)	Mitochondrial Nad+ Transpory	$\text{nad}+[m] \rightleftharpoons \text{nad}+[c]$	mms			Transport Reaction
Trans_nadh(m)	Mitochondrial Nadh Transpory	$\text{nadh}[m] \rightleftharpoons \text{nadh}[c]$	mms			Transport Reaction
Trans_nadp(m)	Mitochondrial Nadp Transport	$\text{nadp}[c] \rightleftharpoons \text{nadp}[m]$	mms			Transport Reaction
trans_nadph(m)	Mitochondrial Nadph Transport	$\text{nadph}[c] \rightleftharpoons \text{nadph}[m]$	mms			Transport Reaction
Trans_nh4+	Ammonium Ion Transport	$\text{nh4}+[m] \rightleftharpoons \text{nh4}+[c]$	mms			Transport Reaction
Trans_nh4+(c)	Cytoplasmic Ammonium Ion Transport	$\text{nh4}+[c] \rightleftharpoons \text{nh4}+[e]$	pms			Transport Reaction
Trans_Nmg	N-Methyl-Glycine Transport	$\text{Nmg}[c] \rightleftharpoons \text{Nmg}[n]$	nms			Transport Reaction
Trans_nmg	N-Methyl-Glycine Transport	$\text{Nmg}[c] \rightleftharpoons \text{Nmg}[e]$	pms			Transport Reaction
Trans_o2	Oxygen Transport	$\text{o2}[c] \rightleftharpoons \text{o2}[e]$	pms			Transport Reaction
Trans_o2(m)	Mitochondrial Oxygen Transport	$\text{o2}[m] \rightarrow \text{o2}[c]$	mms			Transport Reaction
Trans_oaa(c)	Cytoplasmic Oxaloacetate Transport	$\text{h}+[c] + \text{oaa}[c] \rightleftharpoons \text{h}+[e] + \text{oaa}[e]$	pms			Transport Reaction
Trans_oaa(m)	Mitochondrial Oxaloacetate Transport	$\text{oaa}[m] + \text{h}+[m] \rightleftharpoons \text{h}+[c] + \text{oaa}[c]$	mms			Transport Reaction

Trans_obut	2-Oxobutanoate Transport	2obut[c] <=> 2obut[e]	pms			Transport Reaction
Trans_pa	Palmitic Acid Transport	pa[c] <=> pa[e]	pms			Transport Reaction
Trans_pacrn(m)	L-Palmitoylcarnitine Transport	pacrn[c] <=> pacrn[m]	mms			Transport Reaction
Trans_pi(c)	Cytoplasmic Phosphate Transport	pi[c] <=> pi[e]	pms			Transport Reaction
Trans_pi(m)	Phosphate Transport	pi[c] <=> pi[m]	mms			Transport Reaction
Trans_po	Orthophosphate Transport	po[c] <=> po[e]	pms			Transport Reaction
Trans_ppi	Pyrophosphate Transport	ppi[c] <=> ppi[e]	pms			Transport Reaction
Trans_pyr(m)	Mitochondrial Pyruvate Transport	h+[m] + pyr[m] <=> h+[c] + pyr[c]	mms		51660	Transport Reaction
Trans_quln	Quinolate Transport	quln[c] <=> quln[e]	pms			Transport Reaction
Trans_succ(c)	Cytoplasmic Succinate Transport	h+[c] + succ[c] <=> h+[e] + succ[e]	pms			Transport Reaction
Trans_succ(m)	Mitochondrial Succinate Transport	h+[m] + succ[m] <=> h+[c] + succ[c]	mms			Transport Reaction
Trans_sulfite	Sulfite Transport	so3[c] <=> so3[e]	pms			Transport Reaction
Trans_thf	Tetrahydrofolate Transport	thf[c] <=> thf[e]	pms			Transport Reaction
Trans_try	Tryptophan Transport	try[c] <=> try[e]	pms			Transport Reaction
Trans-met	L-Methionine Transport	met-L[c] <=> met-L[e]	pms			Transport Reaction
AM6SAD	Aminomuconate-Semialdehyde Dehydrogenase	h2o[c] + nad+[c] + am6sa[c] -> 2 h+[c] + amuco[c] + nadh[c]	c	1.2.1.32		Tryptophan Metabolism
AMCOXO	Aminomuconate Reductase_1	h2o[c] + h+[c] + amuco[c] + nadh[c] -> 2oxoadp[c] + nad+[c] + nh4+[c]	c	1.5.1.-		Tryptophan Metabolism

HADO	3-Hydroxyanthranilate 3,4-Dioxygenase	$\text{o}_2[\text{c}] + 3\text{hanthrn}[\text{c}] \rightarrow \text{h}[\text{c}] + \text{cmusa}[\text{c}]$	c	1.13.11.6	23498	Tryptophan Metabolism
KF	Arylformamidase	$\text{h}_2\text{o}[\text{c}] + \text{Lfmkynr}[\text{c}] \rightarrow \text{h}[\text{c}] + \text{for}[\text{c}] + \text{Lkynr}[\text{c}]$	c	3.5.1.9	125061	Tryptophan Metabolism
KMO	Kynurenine 3-Monooxygenase	$\text{h}[\text{c}] + \text{nadh}[\text{c}] + \text{o}_2[\text{c}] + \text{Lkynr}[\text{c}] \rightarrow \text{h}_2\text{o}[\text{c}] + \text{nadp}[\text{c}] + \text{hLkynr}[\text{c}]$	c	1.14.13.9	8564	Tryptophan Metabolism
KY	Kynureninase	$\text{h}_2\text{o}[\text{c}] + \text{hLkynr}[\text{c}] \rightarrow \text{ala-L}[\text{c}] + 3\text{hanthrn}[\text{c}]$	c	3.7.1.3	8942	Tryptophan Metabolism
PCLAD	Picolinic Acid Decarboxylase	$\text{h}[\text{c}] + \text{cmusa}[\text{c}] \rightarrow \text{am6sa}[\text{c}] + \text{co}_2[\text{c}]$	c	4.1.1.45	130013	Tryptophan Metabolism
SPON2	Spontaneous Quln	$\text{cmusa}[\text{c}] \rightarrow \text{h}_2\text{o}[\text{c}] + \text{h}[\text{c}] + \text{quln}[\text{c}]$	c	4.1.1.45	130013	Tryptophan Metabolism
TDO	Tryptophan 2,3-Dioxygenase	$\text{o}_2[\text{c}] + \text{try}[\text{c}] \rightarrow \text{Lfmkynr}[\text{c}]$	c	1.13.11.1 1	6999	Tryptophan Metabolism

c: cytoplasm; e: extracellular space; i: intermembrane space; m: mitochondria; n: nucleus; mms: mitochondrial membrane spanning; nms: nuclear membrane spanning; pms: plasma membrane spanning

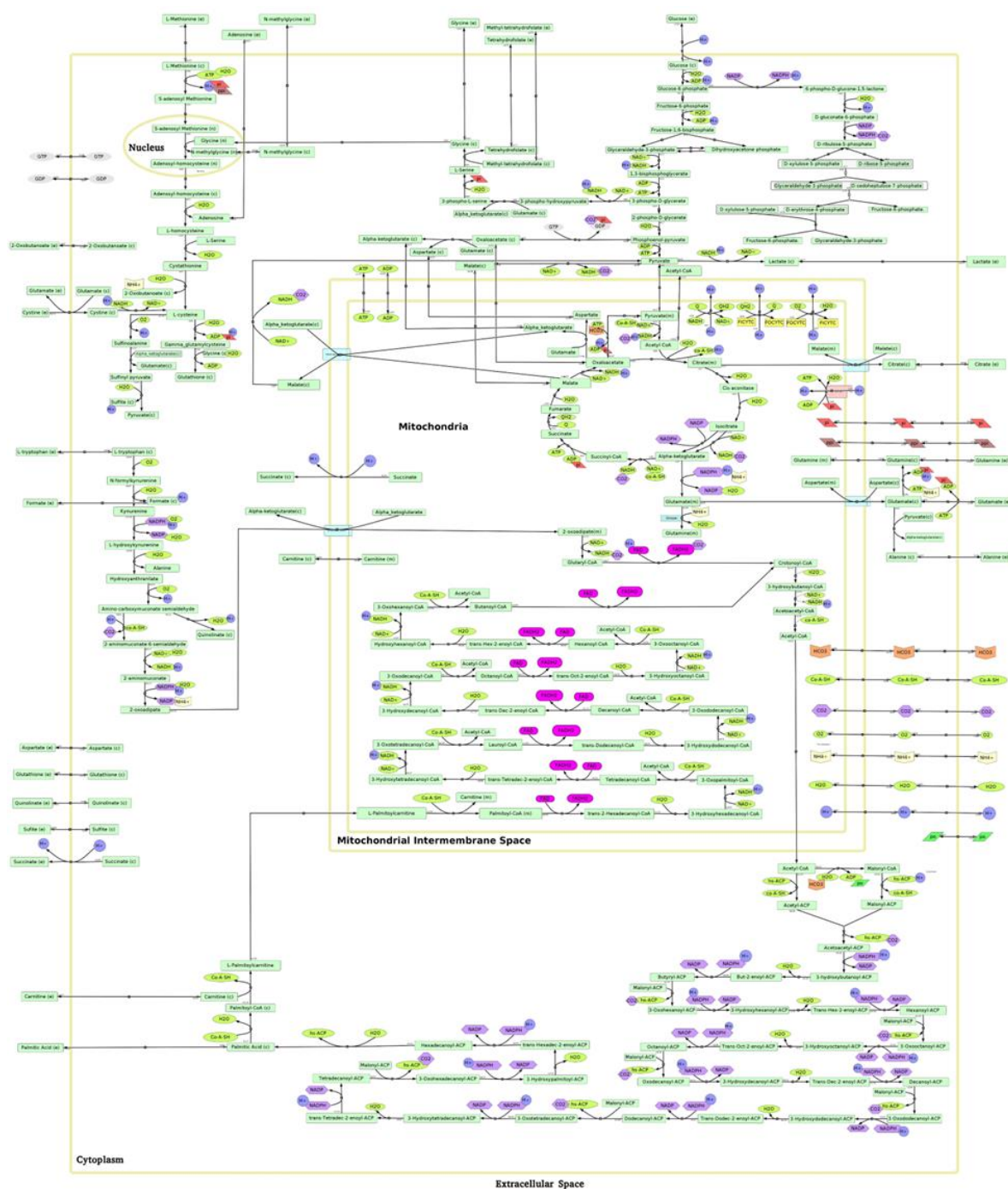


Figure A. 1: Pathway Diagram of the reconstructed constraint-based metabolic network for Glioblastoma

Table A. 2: Lethal Single Knockout Reactions

Reaction Name	% Growth
RPI	0.000
GBM_BM	0.000
GCL	0.000
GS	0.000
Anti_cystine_glut	0.000
CystRed	0.000

Table A. 3: Lethal Non-trivial Double Knockouts Reaction Combinations

Reaction combination		% Growth
AKGDH	FUMH	0
FBA	HEX	0
GAPDH	HEX	0
HEX	PFK	0
HEX	PGK	0
6PGLase	RPE	0
G6PDH	RPE	0
HEX	RPE	0
PGCDH	RPE	0
FUMH	SCS	0
6PGLase	TA	0
G6PDH	TA	0
HEX	TA	0
PGCDH	TA	0
6PGLase	TK1	0
G6PDH	TK1	0
HEX	TK1	0
PGCDH	TK1	0
6PGLase	TK2	0
G6PDH	TK2	0
HEX	TK2	0
PGCDH	TK2	0
HEX	TPI	0
FBA	Trans_glu	0
GAPDH	Trans_glu	0
PFK	Trans_glu	0
PGK	Trans_glu	0
RPE	Trans_glu	0
TA	Trans_glu	0
TK1	Trans_glu	0

TK2	Trans_glu	0
TPI	Trans_glu	0
GHMT	Trans_glycine	0
PGDH	Trans_glycine	0
PSP	Trans_glycine	0
PST	Trans_glycine	0
Trans_glycine	Trans_mlthf	0
PEP_CarbK_1	Trans_pi (c)	0
Trans_gdp	Trans_pi (c)	0
Trans_gtp	Trans_pi (c)	0
Trans_glycine	Trans_thf	0

Table A. 4: Identified combinations of therapeutic targets

Reaction combination		% Growth
6PGLase	RPE	0.00
6PGLase	TA	0.00
6PGLase	TK1	0.00
6PGLase	TK2	0.00
AKGDH	FUMH	0.00
FBA	HEX	0.00
FBA	Trans_glu	0.00
FUMH	SCS	0.00
G6PDH	RPE	0.00
G6PDH	TA	0.00
G6PDH	TK1	0.00
G6PDH	TK2	0.00
GAPDH	HEX	0.00
GAPDH	Trans_glu	0.00
GHMT	Trans_glycine	0.00
HEX	PFK	0.00
HEX	PGK	0.00
HEX	RPE	0.00
HEX	TA	0.00
HEX	TK1	0.00
HEX	TK2	0.00
HEX	TPI	0.00
PFK	Trans_glu	0.00
PGCDH	RPE	0.00
PGCDH	TA	0.00
PGCDH	TK1	0.00
PGCDH	TK2	0.00
PGDH	Trans_glycine	0.00

PGK	Trans_glu	0.00
PSP	Trans_glycine	0.00
PST	Trans_glycine	0.00
RPE	Trans_glu	0.00
TA	Trans_glu	0.00
TK1	Trans_glu	0.00
TK2	Trans_glu	0.00
TPI	Trans_glu	0.00

Table A. 5: Percentage reduction of flux through combinatorial reaction targets

Reaction Combination	Percentage reduction of flux for complete reduction of growth		Percentage reduction of flux for Normal growth	
HEX + FBA	HEX 85-100%	FBA 95-100%	HEX 10-40%	FBA 15-60%
RPE + 6PGLase	RPE 80-100%	6PGLase 50-100%	RPE 15-35%	6PGLase 10-100%
FUMH + AKGDH	FUMH 60-100%	AKGDH 70-100%	FUMH 25-65%	AKGDH 5-55%
Trans_Glycine + PGDH	Trans_Glycine 80-100%	PGDH 80-100%	Trans_Glycine 10-55%	PGDH 10-100%
TPI + HEX	TPI 80-100%	HEX 85-100%	TPI 10-60%	HEX 15-40%
Trans_Glucose + GAPDH	Trans_Glucose 85-100%	GAPDH 85-100%	Trans_Glucose 10-40%	GAPDH 15-55%
PFK + HEX	PFK 80-100%	HEX 85-100%	PFK 15-55%	HEX 15-45%
SCS + FUMH	SCS 70-100%	FUMH 65-100%	SCS 25-55%	FUMH 10-60%
RPE + G6PDH	RPE 80-100%	G6PDH 50-100%	RPE 15-35%	G6PDH 10-100%
Trans_Glucose + PGK	Trans_Glucose 85-100%	PGK 85-100%	Trans_Glucose 10-30%	PGK 45-55%

Table A. 6: List of available inhibitors for the predicted reaction targets.

Sr. No.	Protein Name	Inhibitor Name	Reference
1	Alpha-ketoglutarate dehydrogenase (AKGDH)	a. CPI-613	(312, 313)
2	Hexokinase (HEX)	a. Lonidamine b. 3-Bromopyruvate c. Imatinib (Gleevec)	(314, 315)
3	Glucose transporter (Trans_Glucose)	a. UDP-glucose b. <i>N</i> -(4-Azidosalicyl)-6-amido-6-deoxyglucopyranose	(316, 317)
4	Glycine transporter (Trans_Glycine)	a. SSR 504734 b. SSR 103800 c. ORG 25935 d. 2-methoxy-N-{1-[4-phenyl-1-(propylsulfonyl) piperidin-4-yl]-methyl} benzamide	(237)
5	6-phosphogluconolactone dehydrogenase (PGCDH)	a. 6-Aminonicotinamide	(318)
6	Glucose-6-phosphate dehydrogenase (G6PDH)	a. Imatinib (Gleevec) b. 6-aminonicotinamide	(319) (319)
7	Transketolase 1 (TK1)	a. Oxythiamine	(319)

APPENDIX B**Table B. 1: Parameter values and their units used for the dynamic model simulation and their references**

Sr. No.	Parameter	Description	Value	Unit	Reference
1.	V_m^{GLCT}	V_{max} of Glucose transporter	7.67	mM hr ⁻¹	(186)
2.	$k_{glc_e}^{GLCT}$	Rate constant for association of cytosolic glucose with Glucose transporter	2.1	mM	(186)
3.	l_g	Rate of glucose influx from other extracellular sources in the ECM	5.6	mM hr ⁻¹	Expected*
4.	d_g	Depletion of extracellular glucose for utilization by other cell types	0.2	hr ⁻¹	
5.	V_m^{HK}	V_{max} of Hexokinase	$9.59 \cdot 10^2$	mM hr ⁻¹	(186)
6.	$k_{i(atp)}^{HK}$	Rate constant for dissociation of ATP with Hexokinase	1	mM	(186)
7.	$k_{glc_c}^{HK}$	Rate constant for association of cytosolic glucose with Hexokinase	0.47	mM	**
8.	k_{atp}^{HK}	Rate constant for association of ATP with Hexokinase	1	mM	(186)
9.	V_m^{PGI}	V_{max} of Phosphoglucose Isomerase	$2.4 \cdot 10^3$	mM hr ⁻¹	(186)
10.	k_{g6p}^{PGI}	Rate constant for association of G6P with Phosphoglucose Isomerase	$9.6 \cdot 10^{-1}$	mM	(186)
11.	V_m^{PFK}	V_{max} of Phosphofructokinase	$2.63 \cdot 10^2$	mM hr ⁻¹	(186)
12.	k_{f6p}^{PFK}	Rate constant for association of F6P with Phosphofructokinase	$6 \cdot 10^{-2}$	mM	(186)
13.	k_{atp}^{PFK}	Rate constant for association of ATP with Phosphofructokinase	$6.8 \cdot 10^{-2}$	mM	(186)
14.	$k_{i(atp)}^{PFK}$	Rate constant for dissociation of ATP from Phosphofructokinase	10.204	mM	Estimated
15.	V_m^{FBA}	V_{max} of Fructose Bisphosphate Aldolase	$1.33 \cdot 10^2$	mM hr ⁻¹	(186)

16.	k_{f16bp}^{FBA}	Rate constant for association of F16BP with Fructose Bisphosphate Aldolase	$5 \cdot 10^{-2}$	mM	(186)
17.	V_m^{TPI}	V_{max} of Triosephosphate Isomerase	$5.10 \cdot 10^2$	mM hr ⁻¹	(186)
18.	k_{dhap}^{TPI}	Rate constant for association of Triosephosphate Isomerase	$1.62 \cdot 10^{-1}$	mM	(186)
19.	V_m^{GAPDH}	V_{max} of Glyceraldehyde phosphate dehydrogenase	781	mM hr ⁻¹	(320)
20.	k_{gap}^{GAPDH}	Rate constant for association of GAP with Glyceraldehyde phosphate dehydrogenase	1.4	mM	(321)
21.	$k_{i(gap)}^{GAPDH}$	Rate constant for dissociation of GAP from Glyceraldehyde phosphate dehydrogenase	$1.59 \cdot 10^{-16}$	mM	(186)
22.	$k_{ii(h_2o_2)}^{GAPDH}$	Inhibition constant of H ₂ O ₂ for Glyceraldehyde phosphate dehydrogenase	21.044	mM	Estimated
23.	k_{nad}^{GAPDH}	Rate constant for association of NAD with Glyceraldehyde phosphate dehydrogenase	1.3	mM	(321)
24.	l_{nad}	Rate of formation of intracellular NAD ⁺ from other internal sources	12.5	mM hr ⁻¹	Expected
25.	d_{nad}	Depletion of NAD ⁺ in other intracellular reactions	0.5	hr ⁻¹	
26.	V_m^{PGK}	V_{max} of Phosphoglycerate kinase	$2.21 \cdot 10^2$	mM hr ⁻¹	(320)
27.	$k_{i(1,3bpg)}^{PGK}$	Rate constant for dissociation of BPG from Phosphoglycerate kinase	1.6	mM	(186)
28.	k_{adp}^{PGK}	Rate constant for association of ADP with Phosphoglycerate kinase	0.1	mM	(186)
29.	d_{pg}	Natural decay of intracellular 3-phosphoglycerate	1.8	hr ⁻¹	Expected
30.	V_m^{PGCDH}	V_{max} of Phosphoglycerate dehydrogenase	0.0021	mM hr ⁻¹	(322)
31.	k_{nad}^{PGCDH}	Rate constant for association of NAD with Phosphoglycerate kinase	0.022	mM	(323)
32.	k_{3pg}^{PGCDH}	Rate constant for association of PG with Phosphoglycerate kinase	0.26	mM	(323)

33.	$k_{i(3pg)}^{PGCDH}$	Rate constant for dissociation of PG from Phosphoglycerate kinase	20	mM	Estimated
34.	d_{php}	Natural decay of intracellular phosphohydroxy phosphate	0.005	hr ⁻¹	Expected
35.	V_m^{PST}	V_{max} of Phosphoserine transaminase	0.081	mM hr ⁻¹	(324)
36.	$k_{i(glut)}^{PST}$	Rate constant for dissociation of Glutamate from Phosphoserine transaminase	7.42	mM	(324)
37.	k_{3php}^{PST}	Rate constant for association of PHP from Phosphoserine transaminase	0.005	mM	(324)
38.	k_{glut}^{PST}	Rate constant for association of Glutamate with Phosphoserine transaminase	1.2	mM	(324)
39.	d_{akg}	Utilization of α -ketoglutarate into intracellular reactions	0.8	hr ⁻¹	Expected
40.	V_m^{PST}	V_{max} of Phosphoserine Phosphatase	0.162	mM hr ⁻¹	(325)
41.	k_m^{PST}	K_m of Phosphoserine transaminase	0.1	mM	(326)
42.	V_m^{GHMT}	V_{max} of Glycine hydroxymethyltransferase	40	mM hr ⁻¹	(327)
43.	k_{thf}^{GHMT}	Rate constant for association of THF with Glycine hydroxymethyltransferase	0.05	mM	(327, 328)
44.	k_{ser}^{GHMT}	Rate constant for association of Serine with Glycine hydroxymethyltransferase	0.6	mM	(327, 328)
45.	$K_{i(ser)}^{GHMT}$	Rate constant for dissociation of Serine from Glycine hydroxymethyltransferase	14	mM	Estimated
46.	V_m^{GLUTEX}	V_{max} of Glutamate exchanger	38.691	mM hr ⁻¹	Estimated
47.	k_m^{GLUTEX}	K_m of Glutamate exchanger	0.097371	mM	Estimated
48.	l_{thf}	Rate of formation of tetrahydrofolate from internal reactions	4	mM hr ⁻¹	Expected***
49.	d_{thf}	Depletion of tetrahydrofolate in other intracellular reactions	0.5	hr ⁻¹	Expected
50.	l_{mlthf}	Rate of formation of methyl-tetrahydrofolate from other internal reactions	6	mM hr ⁻¹	Expected***

51.	d_{mlthf}	Depletion of methyl-tetrahydrofolate in intracellular reactions	0.5	hr ⁻¹	Expected
52.	V_m^{GLUD}	V_{max} of Glutamate dehydrogenase	$5.55 \cdot 10^3$	mM hr ⁻¹	(186)
53.	$k_{i(glut)}^{GLUD}$	Rate constant for dissociation of Glutamate from Glutamate dehydrogenase	3.5	mM	(186)
54.	k_{glut}^{GLUD}	Rate constant for association of Glutamate with Glutamate dehydrogenase	3.5	mM	(186)
55.	k_{nadp}^{GLUD}	Rate constant for association of NADP with Glutamate dehydrogenase	5.6	mM	Estimated
56.	l_{glut}	Rate of glutamate influx into the ECM from other cellular processes	3	mM hr ⁻¹	Expected
57.	d_{glut}	Depletion of extracellular glutamate from other cellular processes	0.3	hr ⁻¹	
58.	V_m^{GCL}	V_{max} of Glutamyl-cysteine Ligase	14	mM hr ⁻¹	Estimated
59.	k_{cysl}^{GCL}	Rate constant for association of Cysteine with Glutamyl-cysteine Ligase	0.07	mM	(329)
60.	k_{glut}^{GCL}	Rate constant for association of Glutamate with Glutamyl-cysteine Ligase	0.46	mM	(329)
61.	k_{atp}^{GCL}	Rate constant for association of ATP with Glutamyl-cysteine Ligase	0.44	mM	(329)
62.	$k_{i(atp)}^{GCL}$	Rate constant for dissociation of ATP from Glutamyl-cysteine Ligase	9.73	mM	Estimated
63.	$k_{i(glut)}^{GCL}$	Rate constant for dissociation of Glutamate from Glutamyl-cysteine Ligase	9.72	mM	Estimated
64.	d_{glucys}	Natural decay of intracellular gamma- glutamyl cysteine	0.08	hr ⁻¹	Expected
65.	V_m^{GS}	V_{max} of Glutathione synthase	0.1174	mM hr ⁻¹	(330)#
66.	k_{glucys}^{GS}	Rate constant for association of Glutamyl-cysteine with Glutathione synthase	0.99	mM	(331)

67.	k_{gly}^{GS}	Rate constant for association of Glycine with Glutathione synthase	1.37	mM	(331)
68.	k_{atp}^{GS}	Rate constant for association of ATP with Glutathione synthase	0.23	mM	(331)
69.	$k_{i(atp)}^{GS}$	Rate constant for dissociation of ATP from Glutathione Synthase	11.8	mM	Estimated
70.	$k_{i(gly)}^{GS}$	Rate constant for dissociation of Glycine from Glutathione Synthase	6.0699	mM	Estimated
71.	V_m^{NOX}	V_{max} of NADPH Oxidase	0.0468	mM hr ⁻¹	(332)
72.	$k_{O_2}^{NOX}$	Rate constant for association of Oxygen with NADPH Oxidase	0.22	mM	(333)
73.	k_{nadph}^{NOX}	Rate constant for association of NADPH with NADPH Oxidase	0.055	mM	(333)
74.	$k_{i(nadph)}^{NOX}$	Rate constant for dissociation of NADPH from NADPH Oxidase	11.624	mM	Estimated
75.	l_{nadph}	Rate of formation of intracellular NADPH from other internal sources	8	mM hr ⁻¹	Expected
76.	d_{nadph}	Depletion of NADPH in other intracellular reactions	0.8	hr ⁻¹	Expected
77.	V_m^{SOD}	V_{max} of Superoxide Dismutase	11.4*10 ³	mM hr ⁻¹	(334)
78.	k_{oxrad}^{SOD}	Rate constant for association of free oxygen radical with Superoxide Dismutase	0.054	mM	(334)
79.	V_m^{GTHP}	V_{max} of Glutathione Peroxidase	0.438	mM hr ⁻¹	(335, 336) (Ranges: 0.2874 to 2.697 mM/hr)
80.	k_{gsh}^{GTHP}	Rate constant for association of GSH with Glutathione Peroxidase	0.2	mM	(337)
81.	d_{gsh}	Natural decay of intracellular reduced glutathione	0.00016	hr ⁻¹	Expected
82.	$k_{h_2o_2}^{GTHP}$	Rate constant for association of H ₂ O ₂ with Glutathione Peroxidase	0.45	mM	(337)
83.	$K_{i(h_2o_2)}^{GTHP}$	Rate constant for dissociation of H ₂ O ₂ from Glutathione Peroxidase	5.3677	mM	Estimated

84.	$d_{h_2O_2}$	Natural decay of intracellular hydrogen peroxide	0.001	hr ⁻¹	Expected
85.	V_m^{GTHO}	V_{max} of Glutathione Oxidoreductase	0.00216	mM hr ⁻¹	(338)
86.	k_{nadph}^{GTHO}	Rate constant for association of NADPH with Glutathione Oxidoreductase	0.063	mM	(339)
87.	k_{gssg}^{GTHO}	Rate constant for association of GSSG with Glutathione Oxidoreductase	0.154	mM	(339)
88.	$k_{i(gssg)}^{GTHO}$	Rate constant for dissociation of GSSG from Glutathione Oxidoreductase	5.05	mM	Estimated
89.	d_{gssg}	Natural decay of intracellular oxidized glutathione	0.00020	hr ⁻¹	Expected
90.	V_m^{xCT}	V_{max} of Cystine-glutamate antiporter	0.001272	mM hr ⁻¹	(340)
91.	$k_{i(cyse)}^{xCT}$	Rate constant for dissociation of Cystine from Cystine-glutamate antiporter	0.0249	mM	(341)
92.	k_{glut}^{xCT}	Rate constant for association of Glutamate with Cystine-glutamate antiporter	0.084	mM	(342)
93.	$k_{cys_e}^{xCT}$	Rate constant for association of Cystine with Cystine-glutamate antiporter	0.084	mM	(342)
94.	l_{cys_e}	Rate of cystine influx into the ECM via other cellular processes	3	mM hr ⁻¹	Expected
95.	d_{cys_e}	Depletion of extracellular cystine into other cellular processes	0.6	hr ⁻¹	Expected
96.	L_{oxy}	Rate of Oxygen diffusing into the ECM and available for cellular uptake	10	mM hr ⁻¹	Expected
97.	d_{oxy}	Utilization of Oxygen by other cell types	0.7	hr ⁻¹	Expected
98.	$V_m^{O_2}$	V_{max} of external Oxygen uptake	15.278	mM hr ⁻¹	(343)
99.	$k_m^{O_2}$	K_m of external Oxygen uptake	164	mM	(320)
100.	d_{in}	Utilization of Oxygen in other intracellular reactions	50.313	hr ⁻¹	Estimated
101.	l_{gly_e}	Rate of glycine influx into the ECM via other cellular processes	4	mM hr ⁻¹	Expected

102.	d_{gly_e}	Depletion of extracellular glycine into other cellular processes	0.5	hr ⁻¹	Expected
103.	V_m^{GLYex}	V_{max} of Glycine Exchanger	0.0287	mM hr ⁻¹	(344)
104.	k_m^{GLYex}	K_m of Glycine Exchanger	0.029	mM	(344, 345)
105.	d_{gly}	Natural decay of intracellular glycine	0.0586	hr ⁻¹	Expected
106.	V_m^{G6PDH}	V_{max} of Glucose-6-phosphate dehydrogenase	5.337	mM hr ⁻¹	Estimated
107.	$k_{i(g6p)}^{G6PDH}$	Rate constant for dissociation of G6P from Glucose-6-phosphate dehydrogenase	6.904	mM	Estimated
108.	k_{nadp}^{G6PDH}	Rate constant for association of NADP with Glucose-6-phosphate dehydrogenase	4.9725	mM	Estimated
109.	k_{g6p}^{G6PDH}	Rate constant for association of G6P with Glucose-6-phosphate dehydrogenase	6.627	mM	Estimated
110.	$k_{ii(atp)}^{G6PDH}$	Inhibition constant of ATP for Glucose-6-phosphate dehydrogenase	6.0885	mM	Estimated
111.	l_{nadp}	Rate of formation of intracellular NADP ⁺ from other internal sources	6	mM hr ⁻¹	Expected
112.	d_{nadp}	Depletion of NADP ⁺ in other intracellular reactions	0.5	hr ⁻¹	Expected
113.	V_m^{CR}	V_{max} of Cystine Reductase	12	mM hr ⁻¹	Estimated
114.	$k_{i(cys)}^{CR}$	Rate constant for dissociation of Cystine from Cystine Reductase	10	mM	Estimated
115.	k_{nadph}^{CR}	Rate constant for association of NADPH with Cystine Reductase	5.536	mM	Estimated
116.	k_{cys}^{CR}	Rate constant for association of Cystine with Cystine Reductase	5.1175	mM	Estimated
117.	d_{cysL}	Natural decay of intracellular cysteine	0.0517	hr ⁻¹	Expected
118.	l_{atp}	Rate of formation of intracellular ATP from other internal reactions	8	mM hr ⁻¹	(346)
119.	d_{atp}	Depletion of ATP in other intracellular reactions	0.5	hr ⁻¹	Expected

120.	l_{adp}	Rate of formation of intracellular ADP from other internal reactions	0.8	mM hr ⁻¹	(347)
121.	d_{atp}	Depletion of ADP in other intracellular reactions	0.4	hr ⁻¹	Expected
122.	l_{nadh}	Rate of formation of intracellular NADH from other internal sources	5	mM hr ⁻¹	Expected
123.	d_{nadh}	Depletion of NADH in other intracellular reactions	0.7	hr ⁻¹	Expected

* Assumptions to the values of rate of influx of glucose and depletion from extracellular matrix are assumed such that they yielded an extracellular concentration of around 3.9 to 5.4 mM.

** The value has been taken from Brenda and it ranges between 0.37 mM to 0.76 mM (348, 349)

*** The values are assumed based on the reported value of V_m^{DHFR} and V_m^{MTHFR} to be 5000 μ M/hr (or 5 mM/hr) (350).

The value ranges around the reported value.

Table B. 2: Initial values to all the variables considered in the model and their reported range in the biological systems

Variable	Description	Reported Range	Initial Value	Reference
glc_e	Extracellular Glucose	2.0 – 4.0 mM	4 mM	(351)
glc_c	Cytoplasmic Glucose	1.0 – 7.0 mM	4 mM	(352)
$g6p$	Glucose-6-phosphate	~ 0.12 mM	0.38 mM	(353)
$f6p$	Fructose-6-phosphate	~ 0.016 mM	0.016 mM	(354)
$f16bp$	Fructose-1,6-bisphosphate	~ 0.0076 mM	0.0076 mM	(354)
gap	Glyceraldehyde Phosphate	~ 0.0076 mM	0.0076 mM	(354)
$dhap$	Dihydroacetone phosphate	~ 0.14 mM	0.14 mM	(354)
$1,3bpg$	1,3-bisphosphoglycerate	~ 0.0004 mM	0.0004 mM	(354)
$3pg$	3-phosphoglycerate	~ 0.045 mM	0.045 mM	(354)
$3php$	3-Phosphohydroxypyruvate	0.01 to 0.4 mM	0.45 mM	(355)
$pser$	Phosphoserine	~ 0.446 mM	0.446 mM	(356)
ser	Serine	0.5 – 1.0 mM	0.7 mM	(352)
gly	Cytoplasmic Glycine	4.4 – 8.4 mM	5 mM	(352)
thf	Tetrahydrofolate		2.5 mM	Expected
$mlthf$	Methyl-tetrahydrofolate		2.5 mM	Expected
$glut_e$	Extracellular Glutamate	0.00002 - 0.02 mM	0.02 mM	(357)
$glut$	Cytoplasmic Glutamate	2.6 – 4.6 mM	2.5 mM	(352)
cys_e	Extracellular Cystine	~1.6 mM	1.5 mM	(358)
cys	Cytoplasmic Cystine		3.6 mM	Expected
$cysL$	Cysteine	0.5 – 5 mM	1.6 mM	(352)

<i>glucys</i>	γ -glutamyl cysteine		2.5 mM	Expected
<i>gsh</i>	Reduced Glutathione	2.0 – 3.0 mM	3.83 mM	(247)
<i>gssg</i>	Oxidised Glutathione	0.024 – 3.0 mM	0.5 mM	(156)
<i>h₂o₂</i>	Hydrogen peroxide	0.01 – 2 mM	1.55 mM	(359, 360)
<i>oxrad</i>	Oxygen free radicals		0.05 mM	Expected
<i>atp</i>	Adenosine tri-phosphate	1.5 – 6.0 mM	1.54 mM	(353)
<i>adp</i>	Adenosine di-phosphate	~ 0.27 mM	2.7 mM	(354)
<i>nad</i>	Nicotinamide adenine Dinucleotide (oxidized)	~ 0.05840 mM	0.0584 mM	(354)
<i>nadh</i>	Nicotinamide adenine Dinucleotide (reduced)	~ 0.03060 mM	0.03060 mM	(354)
<i>nadp⁺</i>	Nicotinamide adenine dinucleotide phosphate (oxidized)	~ 0.0002 mM	0.0002 mM	(354)
<i>nadph</i>	Nicotinamide adenine dinucleotide phosphate (reduced)	~ 0.0658 mM	0.0658 mM	(354)
<i>akg</i>	α -ketoglutarate	~ 0.157 mM	1.4 mM	(356)
<i>O₂(ex)</i>	Extracellular oxygen	12 - 22mM	15 mM	(343)
<i>O₂</i>	Intracellular oxygen		5 mM	Expected
<i>gly_e</i>	Extracellular glycine	0.2-2 mM	0.2 mM	(344)

A. Parameter Estimation of glutamate exchange reaction

The values of parameters V_m^{GLUTEX} and k_m^{GLUTEX} were evaluated with an available data for glutamate exchange in astrocytes [45] in the ODE model presented in **Chapter 4**. The predictive plot for the same has been provided in **Figure B. 1A** and the distribution plot and trace plot of estimated parameters have been shown in **Figure B. 1B** and **Figure B. 1C** respectively.

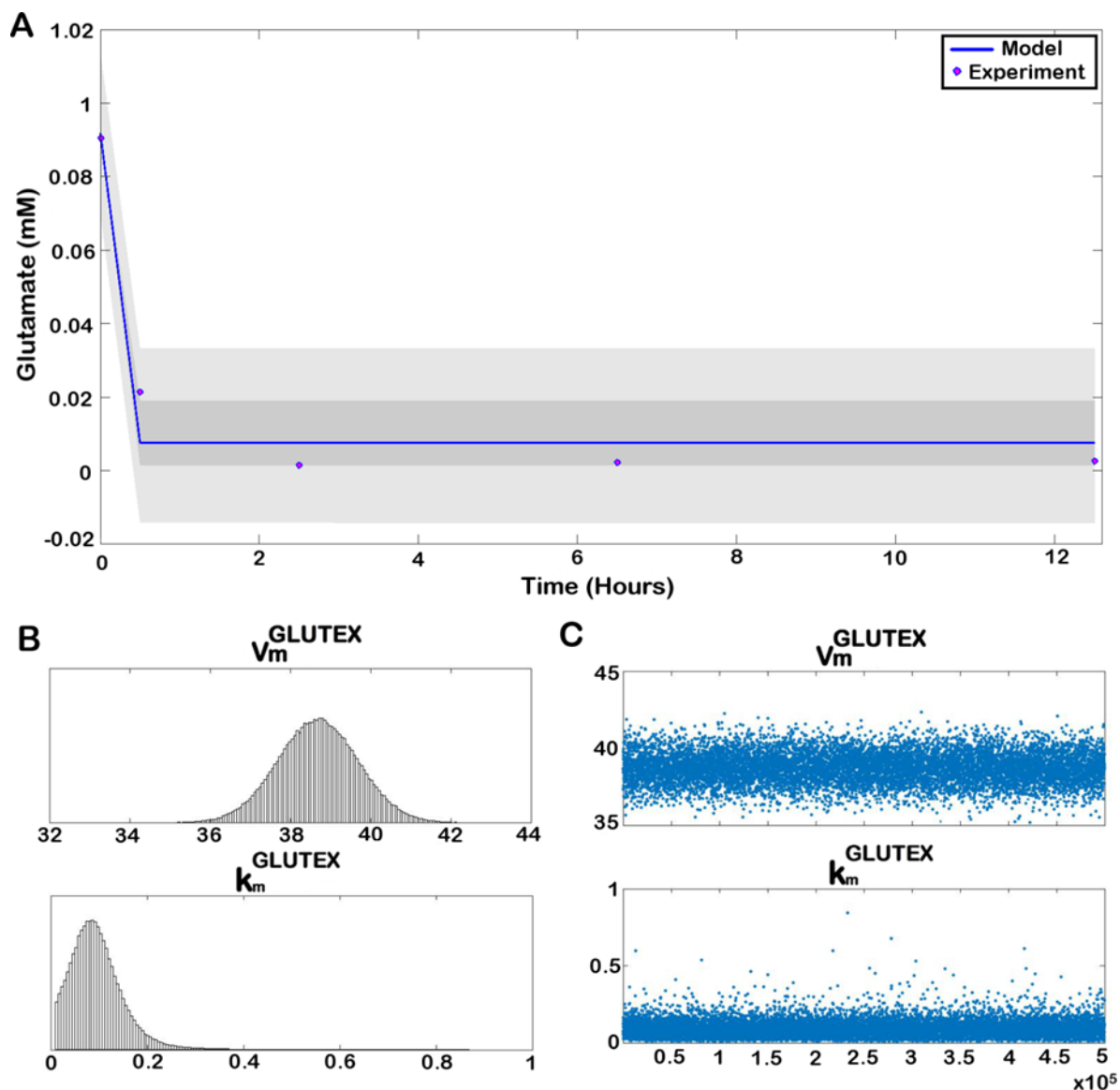


Figure B. 1: Parameter estimation of glutamate exchange reaction. A. Predictive plot demonstrating the fitted model for glutamate exchange and uncertainty regions; B. Parameter distribution curve of the estimated parameters; C. Trace plots of the estimated parameters generated after 5 lakh chains of MCMC DRAM.

B. Effect of changing $k_m^{O_2}$ on uptake of Oxygen

The $k_m^{O_2}$ represented the cellular affinity for external oxygen in the dynamic ODE model. The model was simulated for different values of $k_m^{O_2}$. A lowering in the value of $k_m^{O_2}$ showed a reduction in the concentration of external oxygen representing increasing affinity for external oxygen. The changing concentration of external oxygen with changing values of $k_m^{O_2}$ is shown in **Figure B. 2**.

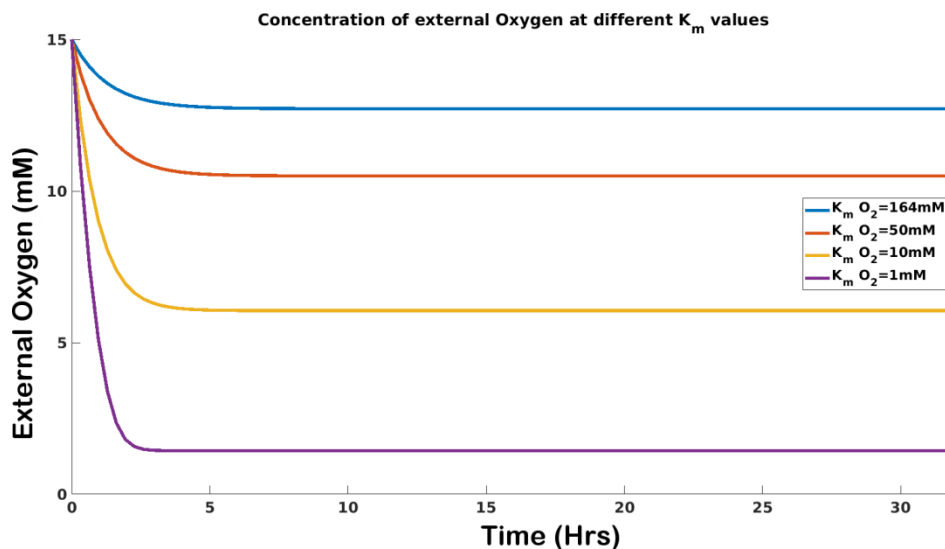


Figure B. 2: Change in external oxygen concentration with respect to changing $k_m^{O_2}$

C. Effect of changing V_m^{GTHO} on $nadph/nadp^+$ ratio

A change in the $nadph/nadp^+$ ratio was observed depending on the changing value of V_m^{GTHO} . This change is captured in **Figure B. 3**. A dip in $nadph/nadp^+$ ratio is observed for all the values of V_m^{GTHO} . However, with increasing value of V_m^{GTHO} , the decline in the $nadph/nadp^+$ ratio increases which is regained back to normal and the dynamics depend on the value of V_m^{GTHO} and the persisting amount of oxidant (h_2o_2) concentration at any point of time.

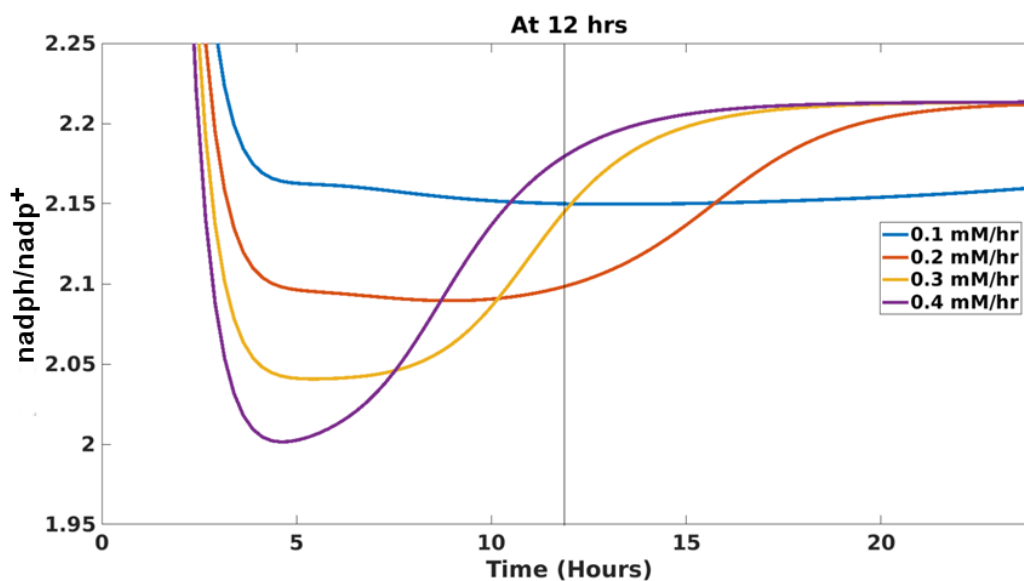


Figure B. 3: Temporal plot of changes in $nadph/nadp^+$ ratio with varying V_m^{GTHO} at $k_m^{O_2} = 1 \text{ mM}$

D. Evaluation of parameter combinations for pro- and anti- oxidant therapy

Glioma scenario was created in the model by incorporating changes in the parameter values V_m^{NOX} , V_m^{GTHO} , V_m^{GTHP} and $k_m^{O_2}$ which were changed to 1mM hr⁻¹, 0.2 mM hr⁻¹, 0.19 mM hr⁻¹ and 1mM from 0.0468 mM hr⁻¹, 0.5 mM hr⁻¹, 0.00216 mM hr⁻¹ and 164mM respectively. Combinatorial variations of sensitive parameters reported in the glioma scenario G11 specified in Table 1 of main text were made. The values of the parameters were varied between a wide range (0.0001 to 100 units) and changes were observed. Here we have reported the temporal variation in the h_2o_2 , $gsh/gssg$ and $nadph/nadp^+$ profiles for a particular value of the parameters. The changes in parameter values for which the pro-oxidant or anti-oxidant properties were observable have been specified in **Table B. 3** and the temporal plots have been shown in the **Figure B. 4**.

Table B. 3: Combinatorial effect of sensitive parameters on gliomas

Sr. No.	Parameter 1	Parameter 2	Variation of Parameter 1*	Variation of Parameter 2*	Effect
1.	$k_{i(nadph)}^{NOX}$	k_{nadph}^{CR}	Decrease	Increase	Pro-oxidant
2.	$k_{i(nadph)}^{NOX}$	k_{nadph}^{NOX}	Increase	Increase	Anti-oxidant
			Decrease	Decrease	Pro-oxidant
3.	L_{oxy}	k_{nadph}^{CR}	Increase	Increase	Pro-oxidant
4.	$k_{i(nadph)}^{NOX}$	l_{atp}	Decrease	Increase	Pro-oxidant
5.	V_m^{FBA}	L_{oxy}	Decrease	Decrease	Anti-oxidant
6.	k_{glucys}^{GS}	k_{nadph}^{CR}	Decrease	Decrease	Pro-oxidant

*Increase or decrease in the parameter value with respect to normal value

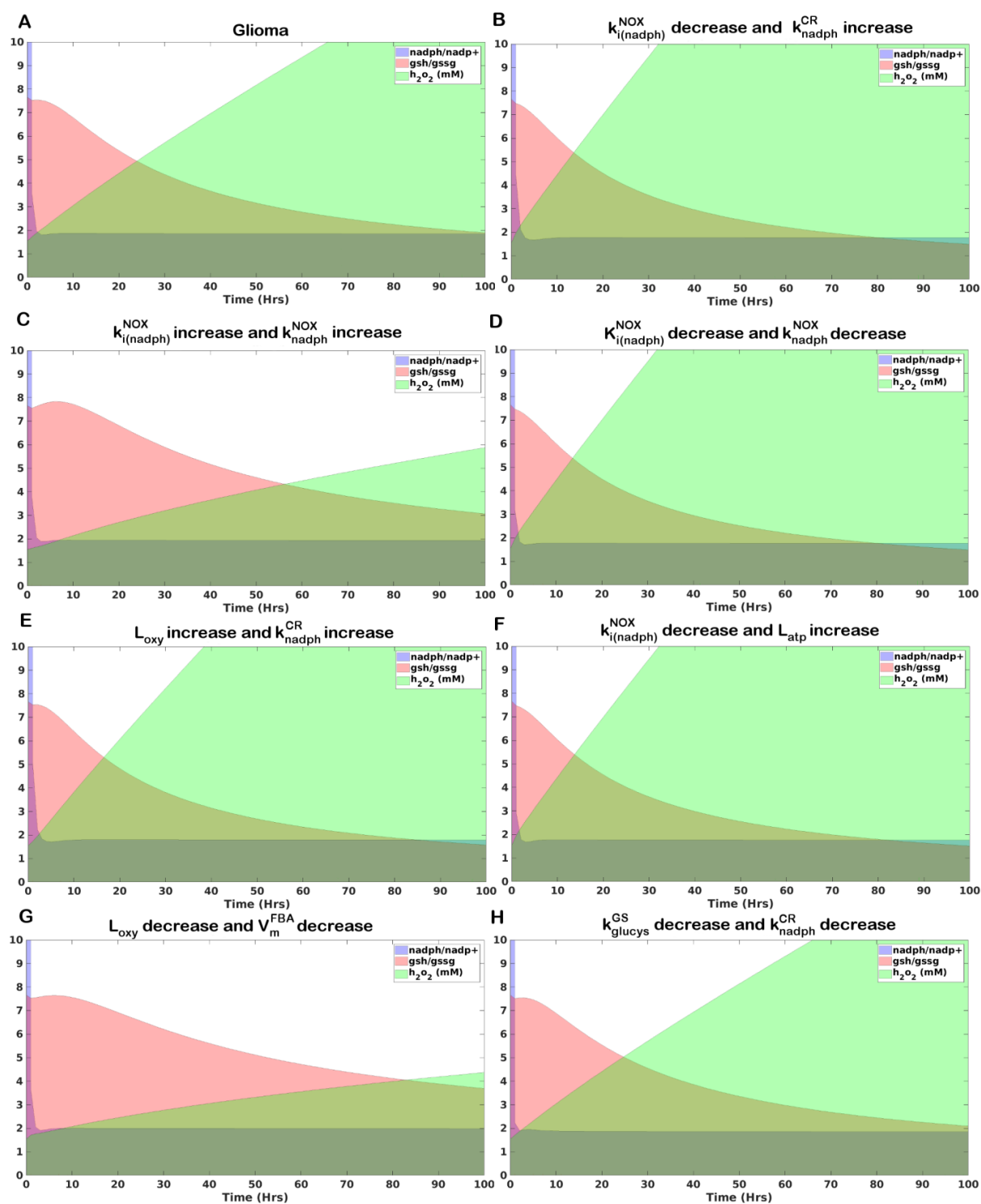


Figure B. 4: Temporal area plots of changing $nadph/nadp^+$ and $gsh/gssg$ ratios along with change in h_2o_2 concentration with combinatorial variation of parameters made in glioma scenario.

APPENDIX C

A. Data distribution of patient-derived differentially expressed miRNA

Patient-derived datasets from GEO database were used to obtain differentially expressed miRNAs in glioblastoma. GSE90603, GSE165937, GSE25631, GSE65626, and GSE103229 were used for the study. The distribution of the data was checked for each dataset. This ensures selection of proper dataset with significant amount of relevant data that can be used to infer meaningful understanding of the biological system in concern. The data distribution of all the five datasets were checked. The volcano plots of data distribution are provided in **Figure C. 1**. Based on the distribution, GSE90603 was selected as the primary dataset to obtain differentially expressed miRNAs. All other datasets were used to validate the differential upregulation or downregulation of miRNAs obtained from the dataset GSE90603.

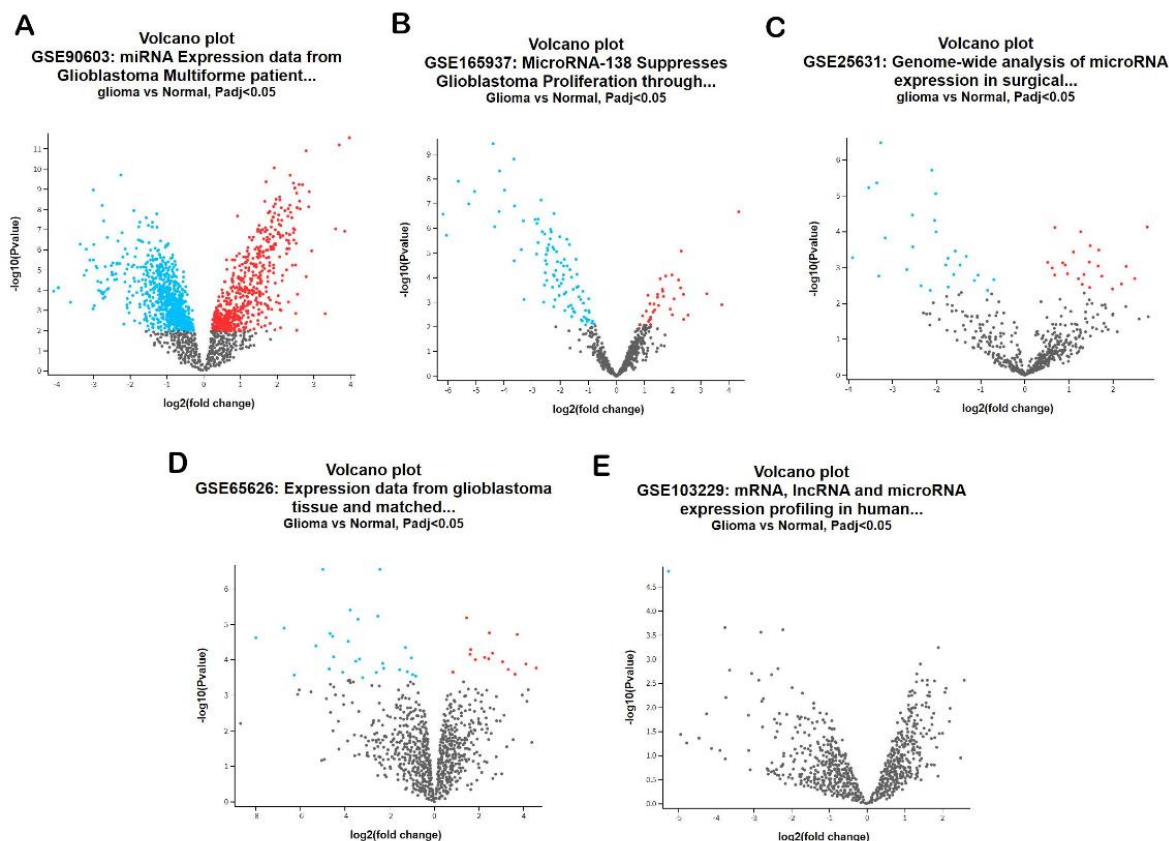


Figure C. 1: Volcano plot of data distribution for differentially expressed miRNA obtained from GEO datasets. Data distribution for (A) GSE90603, (B) GSE165937, (C) GSE25631, (D) GSE65626 and (E) GSE103229. The blue dots represent significantly downregulated miRNAs and the red dots represent significantly upregulated miRNAs.

B. Structural properties of the network

The topological properties of miRNA- target metabolic gene networks for upregulated and downregulated miRNA sets were computed as directed networks. Degree distribution of the networks were observed to follow the power law determining their scale-free nature. This holds true for the biological networks, where it implies that a few nodes have a higher degree of connectivity in the network as compared to others nodes. Analysis of such nodes help determine targetable components of the biological systems that can affect the whole network maximally.

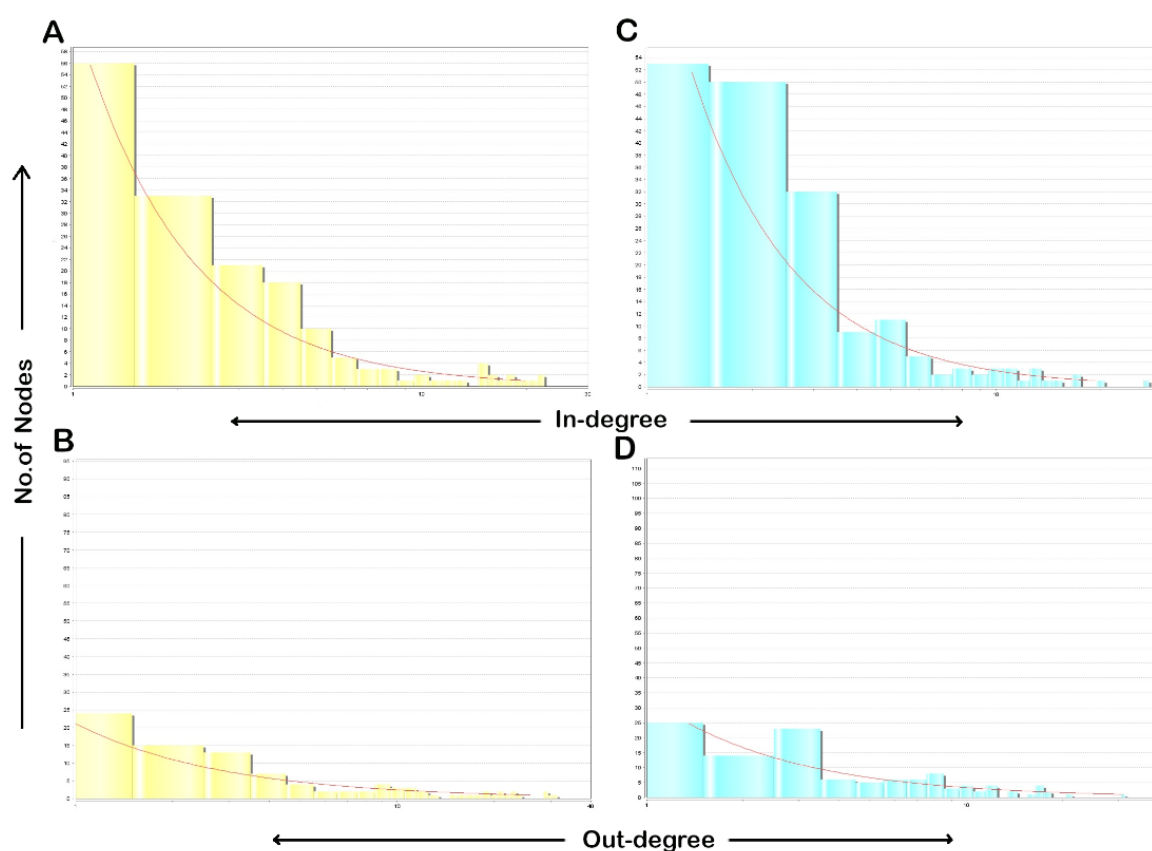


Figure C. 2: Degree distribution in the directed graphs of upregulated and downregulated miRNA- target gene network with power law fit. (A) In-degree, (B) Out-degree of upregulated miRNA-target gene network, (C) In-degree and (D) Out-degree of downregulated miRNA-target gene network. The red line represents the power law fit.

C. List of 1865 unique metabolic genes obtained from Recon3D

A4GALT	ACOT2	AGA	ALOX5	ATP2B2	B3GNT4	CD38	COMTD1
A4GNT	ACOT4	AGK	ALPI	ATP2B3	B3GNT5	CDA	COQ2
AACS	ACOT6	AGL	ALPL	ATP2B4	B3GNT6	CDIPT	COQ3
AADAC	ACOT7	AGMAT	ALPP	ATP4A	B3GNT7	CDO1	COQ5
AADAT	ACOT8	AGPAT1	ALPPL2	ATP4B	B3GNT8	CDS1	COQ6
AANAT	ACOX1	AGPAT2	AMACR	ATP5A1	B3GNT9	CDS2	COQ7
AASS	ACOX2	AGPAT3	AMD1	ATP5B	B3GNTL1	CEL	COX1
ABAT	ACOX3	AGPAT4	AMDHD1	ATP5C1	B4GALNT1	CEPT1	COX2
ABCA1	ACP1	AGPAT5	AMDHD2	ATP5D	B4GALNT2	CERK	COX3
ABCA3	ACP2	AGXT	AMPD1	ATP5E	B4GALNT3	CERS1	COX4I1
ABCA4	ACP5	AGXT2	AMPD2	ATP5F1	B4GALNT4	CERS2	COX4I2
ABCA8	ACP6	AHCY	AMPD3	ATP5G1	B4GALT1	CERS3	COX5A
ABCB1	ACP7	AHCYL1	AMT	ATP5G2	B4GALT2	CERS4	COX5B
ABCB11	ACPP	AICDA	AMY1A	ATP5G3	B4GALT3	CERS5	COX6A1
ABCB4	ACPT	AK1	AMY1B	ATP5H	B4GALT4	CERS6	COX6A2
ABCB6	ACSBG1	AK2	AMY1C	ATP5I	B4GALT5	CES1	COX6B1
ABCC1	ACSBG2	AK3	AMY2A	ATP5J	B4GALT6	CES2	COX6B2
ABCC11	ACSL1	AK4	AMY2B	ATP5J2	B4GALT7	CES3	COX6C
ABCC2	ACSL3	AK5	ANPEP	ATP5L	B4GAT1	CESSA	COX7A1
ABCC3	ACSL4	AK7	AOC1	ATP5L2	BAAT	CFTR	COX7A2
ABCC4	ACSL5	AKR1A1	AOC2	ATP5O	BBOX1	CH25H	COX7A2L
ABCC5	ACSL6	AKR1B1	AOC3	ATP5S	BCAT1	CHAT	COX7B
ABCC8	ACSM1	AKR1B10	AOX1	ATP6V0A1	BCAT2	CHDH	COX7B2
ABCC9	ACSM2A	AKR1B15	APRT	ATP6V0A2	BCHE	CHIA	COX7C
ABCD1	ACSM2B	AKR1C1	AQP1	ATP6V0A4	BCKDHA	CHIT1	COX8A
ABCD2	ACSM3	AKR1C2	AQP10	ATP6V0B	BCKDHB	CHKA	COX8C
ABCD3	ACSM4	AKR1C3	AQP2	ATP6V0C	BCO1	CHKB	CP
ABCG2	ACSM5	AKR1C4	AQP3	ATP6V0D1	BDH1	CHPF	CPA1
ABCG5	ACSS1	AKR1D1	AQP4	ATP6V0D2	BDH2	CHPF2	CPA2
ABCG8	ACSS2	AKR7A2	AQP5	ATP6V0E1	BHMT	CHPT1	CPA5
ABHD5	ACSS3	ALAD	AQP7	ATP6V1A	BHMT2	CHST1	CPA6
ABO	ACY1	ALAS1	AQP8	ATP6V1B1	BLVRA	CHST11	CPOX
ACAA1	ACY3	ALAS2	AQP9	ATP6V1B2	BLVRB	CHST12	CPS1
ACAA2	ACYP1	ALDH18A1	ARG1	ATP6V1C1	BPGM	CHST13	CPT1A
ACACA	ACYP2	ALDH1A1	ARG2	ATP6V1C2	BPNT1	CHST14	CPT1B
ACACB	ADA	ALDH1A2	ARSA	ATP6V1D	BSG	CHST2	CPT1C
ACAD10	ADCY1	ALDH1A3	ARSB	ATP6V1E1	BTD	CHST3	CPT2
ACAD11	ADCY10	ALDH1B1	ASAH1	ATP6V1E2	C1GALT1	CHST4	CRAT
ACAD8	ADCY2	ALDH1L1	ASAH2	ATP6V1F	CA1	CHST5	CRLS1
ACAD9	ADCY3	ALDH1L2	ASH1L	ATP6V1G1	CA12	CHST6	CROT
ACADL	ADCY4	ALDH2	ASL	ATP6V1G2	CA13	CHST7	CS
ACADM	ADCY5	ALDH3A1	ASMT	ATP6V1G3	CA14	CHSY1	CSAD
ACADS	ADCY6	ALDH3A2	ASNS	ATP6V1H	CA2	CHSY3	CSGALNACT1
ACADSB	ADCY7	ALDH3B1	ASPA	ATP8A1	CA3	CKB	CSGALNACT2
ACADVL	ADCY8	ALDH3B2	ASPG	ATP8B1	CA4	CKM	CTBP1
ACAT1	ADCY9	ALDH4A1	ASRGL1	ATP8B2	CA5A	CKMT1A	CTDSPL2
ACAT2	ADH1A	ALDH5A1	ASS1	AUH	CA5B	CKMT1B	CTH
ACE	ADH1B	ALDH6A1	ATHL1	AZIN2	CA6	CKMT2	CTPS1
ACE2	ADH1C	ALDH7A1	ATIC	B3GALNT1	CA7	CLC	CTPS2
ACER1	ADH4	ALDH9A1	ATP10A	B3GALNT2	CA8	CLPS	CTSA
ACER2	ADH5	ALDOA	ATP11A	B3GALT1	CA9	CLYBL	CYB5D1
ACER3	ADH6	ALDOB	ATP11C	B3GALT2	CAD	CMA1	CYB5R1
ACHE	ADH7	ALDOC	ATP1A1	B3GALT4	CANT1	CMAS	CYB5R2
ACLY	ADHFE1	ALG10	ATP1A2	B3GALT5	CARNS1	CMPK1	CYB5R3
ACMSD	ADI1	ALG12	ATP1A3	B3GALT6	CAT	CMPK2	CYBRD1
ACO1	ADK	ALG1L	ATP1A4	B3GAT1	CBR1	CNDP1	CYC1
ACO2	ADO	ALG1L2	ATP1B1	B3GAT2	CBR3	CNDP2	CYP11A1
ACOT1	ADSL	ALG5	ATP1B2	B3GAT3	CBR4	CNP	CYP11B1
ACOT11	ADSS	ALOX12	ATP1B3	B3GLCT	CBS	COASY	CYP11B2
ACOT12	ADSSL1	ALOX15	ATP1B4	B3GNT2	CBSL	COL4A3BP	CYP17A1
ACOT13	AFMID	ALOX15B	ATP2B1	B3GNT3	CD36	COMT	CYP19A1

CYP1A1	DGKB	ENTPD1	FUT1	GFPT2	GRHPR	HPGDS	ITPA
CYP1A2	DGKD	ENTPD2	FUT10	GGCT	GSR	HPRT1	ITPK1
CYP1B1	DGKE	ENTPD3	FUT11	GGH	GSS	HS2ST1	ITPKA
CYP21A2	DGKG	ENTPD4	FUT2	GGPS1	GSTM1	HS3ST1	ITPKB
CYP24A1	DGKH	ENTPD5	FUT3	GGT1	GSTM2	HS3ST2	ITPKC
CYP27A1	DGKI	ENTPD6	FUT4	GGT2	GSTZ1	HS3ST3A1	IVD
CYP27B1	DGKQ	ENTPD8	FUT5	GGT5	GUCA1A	HS3ST3B1	KCNJ11
CYP2A13	DGKZ	EPHX2	FUT6	GGT6	GUCY1A2	HS3ST4	KCNJ8
CYP2A6	DGUOK	EPT1	FUT7	GGT7	GUCY1A3	HS3ST5	KDSR
CYP2A7	DHCR24	EPX	FUT9	GGTLC1	GUCY1B3	HS3ST6	KHK
CYP2B6	DHCR7	ESD	G6PC	GGTLC2	GUCY2C	HS6ST1	KL
CYP2C18	DHFR	ETFA	G6PC2	GK	GUCY2D	HS6ST2	KMO
CYP2C19	DHODH	ETFB	G6PC3	GK2	GUCY2F	HS6ST3	KMT2A
CYP2C8	DHRS2	ETFDH	G6PD	GLA	GUK1	HSD11B1	KMT2B
CYP2C9	DHRS3	ETNK1	GAA	GLB1	GUSB	HSD11B1L	KMT2C
CYP2D6	DHRS4	ETNK2	GAD1	GLB1L	GYG1	HSD11B2	KMT2D
CYP2E1	DHRS9	ETNPPL	GAD2	GLCE	GYG2	HSD17B1	KMT2E
CYP2F1	DIO1	EXT1	GAL3ST1	GLDC	GYS1	HSD17B10	KMT5A
CYP2J2	DIO2	EXT2	GALC	GLO1	GYS2	HSD17B11	KMT5B
CYP2S1	DIO3	EXTL1	GALE	GLRX	H6PD	HSD17B12	KMT5C
CYP2U1	DLAT	EXTL2	GALK1	GLRX2	HAAO	HSD17B14	KYAT1
CYP39A1	DLD	EXTL3	GALK2	GLS	HACD1	HSD17B2	KYNU
CYP3A4	DLST	FAAH2	GALNS	GLS2	HACD2	HSD17B3	LALBA
CYP3A43	DMGDH	FABP1	GALNT1	GLT6D1	HACD3	HSD17B4	LAP3
CYP3A5	DOLPP1	FABP12	GALNT10	GLT8D1	HACD4	HSD17B6	LBR
CYP3A7	DOT1L	FABP2	GALNT11	GLT8D2	HACL1	HSD17B7	LCAT
CYP46A1	DPEP1	FABP3	GALNT12	GLTP	HADH	HSD17B8	LCLAT1
CYP4A11	DPEP2	FABP4	GALNT13	GLUD1	HADHA	HSD3B1	LCT
CYP4B1	DPEP3	FABP5	GALNT14	GLUD2	HADHB	HSD3B2	LDHA
CYP4F11	DPM2	FABP6	GALNT15	GLUL	HAGH	HSD3B7	LDHAL6A
CYP4F12	DPYD	FABP7	GALNT2	GLYAT	HAGHL	HTATIP2	LDHAL6B
CYP4F2	DPYS	FABP9	GALNT3	GLYCTK	HAL	HYAL3	LDHB
CYP4F22	DPYSL2	FADS1	GALNT4	GM2A	HAO1	HYKK	LDHC
CYP4F3	DPYSL3	FADS2	GALNT5	GMDS	HAO2	IDH1	LDHD
CYP4F8	DTYMK	FADS3	GALNT6	GMPPA	HAS1	IDH2	LGALS13
CYP4V2	DUOX1	FADS6	GALNT7	GMPPB	HAS2	IDH3A	LGSN
CYP4X1	DUOX2	FAH	GALNT8	GMPR	HAS3	IDH3B	LHPP
CYP4Z1	DUSP11	FAM20B	GALNT9	GMPR2	HCST	IDH3G	LIPA
CYP51A1	DUT	FASN	GALNTL5	GMPS	HDC	IDI1	LIPC
CYP7A1	EBP	FAXDC2	GALT	GNE	HDLBP	IDI2	LIPE
CYP7B1	ECH1	FBP1	GAMT	GNMT	HEPH	IDO1	LIPF
CYP8B1	ECHDC2	FBP2	GANC	GNPDA1	HEXA	IDO2	LIPG
CYTB	ECHS1	FDFT1	GAPDH	GNPDA2	HEXB	IDS	LOXL2
DAGLA	ECI1	FDPS	GAPDHS	GNPNAT1	HEXDC	IDUA	LPIN1
DAGLB	ECI2	FECH	GART	GNS	HGD	IL4I1	LPIN2
DAO	EHHADH	FGGY	GATM	GOT1	HIBADH	IMPA1	LPIN3
DBH	EHMT1	FH	GBA	GOT2	HIBCH	IMPA2	LPL
DBI	EHMT2	FIG4	GBA2	GPAA1	HIGD2A	IMPDH1	LPO
DBT	ELOVL1	FLAD1	GBE1	GPAM	HK1	IMPDH2	LRAT
DCK	ELOVL2	FLVCR1	GBGT1	GPAT4	HK2	INPP1	LRTOMT
DCT	ELOVL3	FN3K	GCAT	GPCPD1	HK3	INPP4A	LSS
DCTD	ELOVL4	FN3KRP	GCDH	GPD1	HKDC1	INPP4B	LTA4H
DCTPP1	ELOVL5	FOLR1	GCH1	GPD2	HLCS	INPP5A	LTC4S
DCXR	ELOVL6	FOLR2	GCK	GPI	HMBS	INPP5B	LYZL1
DDC	ELOVL7	FOLR3	GCLC	GPT	HMGCL	INPP5D	MAGEA2B
DDO	ENO1	FPGS	GCLM	GPT2	HMGCLL1	INPP5E	MAN2B1
DECR1	ENO2	FPGT	GCNT1	GPX1	HMGCR	INPP5F	MANBA
DECR2	ENO3	FTCD	GCNT2	GPX2	HMGCS1	INPP5J	MANSC1
DEGS1	ENOPH1	FTH1	GCNT3	GPX3	HMGCS2	INPPL1	MAOA
DEGS2	ENPP1	FTL	GCNT4	GPX4	HMOX1	IP6K1	MAOB
DERA	ENPP2	FTMT	GCNT7	GPX5	HMOX2	IP6K2	MAT1A
DGAT1	ENPP3	FUCA1	GCSH	GPX6	HNMT	IP6K3	MAT2A
DGAT2	ENPP6	FUCA2	GDA	GPX7	HPD	IREB2	MAT2B
DGKA	ENPP7	FUK	GFPT1	GPX8	HPGD	ISYNA1	MBOAT1

MBOAT2	NAPRT	NMRK1	PDE1C	PIGH	PLCH2	PTGES	SDR9C7
MCCC1	ND1	NNMT	PDE2A	PIGK	PLCL1	PTGES2	SDS
MCCC2	ND2	NNT	PDE3A	PIGL	PLCXD2	PTGES3	SDSL
MCEE	ND3	NOL9	PDE3B	PIGM	PLCZ1	PTGIS	SEC11A
MDH1	ND4	NOS1	PDE4A	PIGN	PLD1	PTGS1	SEC11C
MDH1B	ND4L	NOS2	PDE4B	PIGO	PLD2	PTGS2	SETD1A
MDH2	ND5	NOS3	PDE4C	PIGP	PLD3	PTPDC1	SETD1B
MDP1	ND6	NPC1	PDE4D	PIGQ	PLD4	PTPMT1	SETD2
ME1	NDST1	NPC1L1	PDE5A	PIGS	PLD6	PTPRQ	SETD7
ME2	NDST2	NPR1	PDE6A	PIGT	PLPP1	PTS	SETDB1
ME3	NDST3	NPR2	PDE6B	PIGU	PLPP2	PXDN	SETDB2
MECR	NDST4	NQO1	PDE6C	PIGV	PLPP3	PXDNL	SETMAR
MGAM	NDUFA1	NSD1	PDE6D	PIGW	PLPP4	PXYLP1	SGMS1
MGAT4C	NDUFA10	NSDHL	PDE6G	PIGX	PLPP5	PYCR1	SGMS2
MGAT4D	NDUFA11	NSF	PDE6H	PIGZ	PLPP6	PYCR2	SGPL1
MGAT5	NDUFA12	NT5C	PDE7A	PIK3C2A	PLPP7	PYCR1	SGPP1
MGAT5B	NDUFA13	NT5C1A	PDE7B	PIK3C2B	PLPPR2	PYGB	SGPP2
MGEA5	NDUFA2	NT5C1B	PDE8A	PIK3C2G	PLPPR3	PYGL	SGSH
MGLL	NDUFA3	NT5C1B-	PDE8B	PIK3C3	PLPPR4	PYGM	SHMT1
MGST2	NDUFA4	RDH14	PDE9A	PIK3CA	PLPPR5	QDPR	SHMT2
MGST3	NDUFA5	NT5C2	PDHA1	PIK3CB	PMM1	QPRT	SI
MIA3	NDUFA6	NT5C3A	PDHA2	PIK3CD	PMM2	RALBP1	SLC10A1
MINPP1	NDUFA7	NT5DC3	PDHB	PIK3CG	PMPCA	RBKS	SLC10A2
MIOX	NDUFA8	NT5E	PDHX	PIK3R1	PMVK	RBP1	SLC10A6
MIP	NDUFA9	NT5M	P DPR	PIK3R2	PNLIP	RBP2	SLC11A1
MLYCD	NDUFAB1	NUDT12	PDXK	PIK3R3	PNLIPRP1	RBP4	SLC11A2
MMAA	NDUFB1	NUDT5	PDXP	PIK3R5	PNLIPRP2	RDH10	SLC12A1
MOGAT1	NDUFB10	OAT	PECR	PIKFYVE	PNLIPRP3	RDH11	SLC12A2
MOGAT2	NDUFB11	OCRL	PEMT	PIP4K2A	PNMT	RDH12	SLC12A3
MOXD1	NDUFB2	ODC1	PEPD	PIP4K2B	PNP	RDH13	SLC12A4
MPC1	NDUFB3	OGDH	PFAS	PIP4K2C	PNPLA2	RDH14	SLC12A5
MPC2	NDUFB4	OGT	PFKFB1	PIP5K1A	PNPLA3	RDH16	SLC12A6
MPI	NDUFB5	OPLAH	PFKFB2	PIP5K1B	PNPLA4	RDH5	SLC12A7
MPO	NDUFB6	OTC	PFKFB3	PIP5K1C	PNPO	RDH8	SLC13A1
MPST	NDUFB7	OXCT1	PFKFB4	PIP5KL1	POGLUT1	RENBP	SLC13A2
MSMO1	NDUFB8	OXCT2	PFKL	PIPOX	POMGNT1	RFK	SLC13A3
MTAP	NDUFB9	OXSM	PFKM	PISD	PON3	RHAG	SLC13A4
MTHFD1	NDUFC1	P4HA1	PFKP	PKLR	PPA1	RHBG	SLC13A5
MTHFD1L	NDUFC2	P4HA2	PGAM1	PKM	PPA2	RHCG	SLC14A1
MTHFD2	NDUFS1	P4HA3	PGAM2	PLA2G10	PPAT	RPE	SLC14A2
MTHFD2L	NDUFS2	PAFAH1B1	PGAP1	PLA2G12A	PPCDC	RPIA	SLC15A1
MTHFR	NDUFS3	PAFAH1B2	PGD	PLA2G1B	PPCS	RPL14	SLC15A2
MTHFS	NDUFS4	PAFAH1B3	PGK1	PLA2G2A	PPIP5K1	RPP14	SLC16A1
MTMR1	NDUFS5	PAFAH2	PGK2	PLA2G2D	PPIP5K2	RRM1	SLC16A10
MTMR14	NDUFS6	PAH	PGLS	PLA2G2E	PPOX	RRM2	SLC16A2
MTMR2	NDUFS7	PAICS	PGM1	PLA2G2F	PPT1	RRM2B	SLC16A3
MTMR3	NDUFS8	PANK1	PGM2	PLA2G3	PPT2	RWDD2A	SLC16A7
MTMR6	NDUFV1	PANK2	PGM2L1	PLA2G4A	PRDX1	SACM1L	SLC16A8
MTMR7	NDUFV2	PANK3	PGM3	PLA2G4B	PRDX2	SARDH	SLC17A1
MTMR8	NDUFV3	PANK4	PGS1	PLA2G4E	PRDX3	SAT1	SLC17A2
MTR	NEU1	PAPSS1	PHFX	PLA2G5	PRDX6	SAT2	SLC17A3
MUT	NEU2	PAPSS2	PHGDH	PLA2G6	PRODH	SC5D	SLC17A4
MVD	NEU3	PC	PHOSPHO1	PLA2G7	PRODH2	SCARB1	SLC17A5
MVK	NEU4	PCBD1	PHPT1	PLCB1	PROSC	SCARF2	SLC17A6
MYO5B	NIT2	PCBD2	PHYH	PLCB2	PRPS1	SCD	SLC17A7
NADK	NME1	PCK1	PHYKPL	PLCB3	PRPS1L1	SCD5	SLC17A8
NADSYN1	NME2	PCK2	PI4K2A	PLCB4	PRPS2	SCP2	SLC18A1
NAGA	NME3	PCYT1A	PI4KA	PLCD1	PSAP	SDHA	SLC18A2
NAGK	NME4	PCYT1B	PI4KB	PLCD3	PSAT1	SDHB	SLC18A3
NAGLU	NME6	PCYT2	PIGA	PLCD4	PSPH	SDHC	SLC19A1
NAGS	NME7	PDE10A	PIGB	PLCE1	PTDSS1	SDHD	SLC19A2
NAMPT	NMNAT1	PDE11A	PIGC	PLCG1	PTDSS2	SDR16C5	SLC19A3
NANP	NMNAT2	PDE1A	PIGF	PLCG2	PTEN	SDR42E1	SLC1A1
NANS	NMNAT3	PDE1B	PIGG	PLCH1	PTGDS	SDR42E2	SLC1A2

SLC1A3	SLC25A37	SLC34A3	SLC5A2	SLC01B3	ST8SIA4	TNNI3K	UGT2A1
SLC1A4	SLC25A4	SLC35A1	SLC5A3	SLC01C1	ST8SIA5	TNS2	UGT2A3
SLC1A5	SLC25A5	SLC35A2	SLC5A5	SLC02A1	STARD3	TPH1	UGT2B10
SLC1A6	SLC25A6	SLC35A3	SLC5A6	SLC02B1	STRA6	TPH2	UGT2B11
SLC1A7	SLC26A1	SLC35B2	SLC5A7	SLC03A1	STS	TPI1	UGT2B15
SLC20A1	SLC26A11	SLC35B4	SLC5A8	SLC04A1	STT3A	TPK1	UGT2B17
SLC20A2	SLC26A2	SLC35C1	SLC5A9	SMPD1	STT3B	TPO	UGT2B28
SLC22A1	SLC26A3	SLC35D1	SLC6A1	SMPD2	SUCLA2	TPP1	UGT2B4
SLC22A10	SLC26A4	SLC35D2	SLC6A11	SMPD3	SUCLG1	TPSAB1	UGT2B7
SLC22A11	SLC26A6	SLC36A1	SLC6A12	SMPD4	SUCLG2	TPSB2	UGT8
SLC22A12	SLC26A7	SLC36A2	SLC6A13	SMS	SULT1A1	TPSD1	UMPS
SLC22A13	SLC26A8	SLC36A4	SLC6A14	SMYD3	SULT1A2	TPTE2	UPB1
SLC22A2	SLC26A9	SLC37A1	SLC6A18	SOAT1	SULT1A3	TREH	UPP1
SLC22A3	SLC27A1	SLC37A4	SLC6A19	SOAT2	SULT1B1	TST	UPP2
SLC22A4	SLC27A2	SLC38A1	SLC6A2	SOD1	SULT1C2	TSTA3	UPRT
SLC22A5	SLC27A3	SLC38A2	SLC6A20	SOD2	SULT1E1	TUSC3	UQCR10
SLC22A6	SLC27A4	SLC38A3	SLC6A3	SOD3	SULT2A1	TXNRD1	UQCR11
SLC22A7	SLC27A5	SLC38A4	SLC6A4	SORD	SULT2B1	TXNRD2	UQCRB
SLC22A8	SLC27A6	SLC38A5	SLC6A5	SPCS1	SULT4A1	TYMP	UQCRC1
SLC22A9	SLC28A1	SLC3A1	SLC6A6	SPCS2	SUOX	TYMS	UQCRC2
SLC23A1	SLC28A2	SLC3A2	SLC6A7	SPCS3	SUV39H1	TYR	UQCRFS1
SLC23A2	SLC28A3	SLC40A1	SLC6A8	SPHK1	SUV39H2	TYRP1	UQCRH
SLC24A1	SLC29A1	SLC43A1	SLC6A9	SPHK2	SYNJ1	UAP1	UQCRQ
SLC24A2	SLC29A2	SLC43A2	SLC7A1	SPR	SYNJ2	UAP1L1	UROC1
SLC24A3	SLC29A3	SLC46A1	SLC7A10	SPTLC1	TALDO1	UCK1	UROD
SLC24A4	SLC29A4	SLC47A1	SLC7A11	SPTLC2	TAT	UCK2	UROS
SLC25A1	SLC2A1	SLC47A2	SLC7A2	SPTLC3	TBCB	UCKL1	UST
SLC25A10	SLC2A10	SLC4A1	SLC7A3	SQLE	TBXAS1	UCP1	UXS1
SLC25A11	SLC2A11	SLC4A10	SLC7A5	SRD5A1	TCIRG1	UCP2	VNN1
SLC25A12	SLC2A12	SLC4A2	SLC7A6	SRD5A2	TDO2	UCP3	VNN2
SLC25A13	SLC2A13	SLC4A3	SLC7A7	SRD5A3	TECR	UEVLD	VNN3
SLC25A14	SLC2A14	SLC4A4	SLC7A8	SRM	TECRL	UGCG	WHSC1
SLC25A15	SLC2A2	SLC4A5	SLC7A9	ST3GAL1	TH	UGDH	WHSC1L1
SLC25A16	SLC2A3	SLC4A7	SLC8A1	ST3GAL2	THNSL1	UGGT1	WVVOX
SLC25A17	SLC2A4	SLC4A8	SLC8A2	ST3GAL3	THTPA	UGGT2	XDH
SLC25A18	SLC2A5	SLC4A9	SLC8A3	ST3GAL4	TK1	UGP2	XYLB
SLC25A19	SLC2A6	SLC51A	SLC9A1	ST3GAL5	TK2	UGT1A1	XYLT1
SLC25A2	SLC2A7	SLC51B	SLC9A2	ST3GAL6	TKFC	UGT1A10	XYLT2
SLC25A20	SLC2A8	SLC52A1	SLC9A3	ST6GALNAC1	TKT	UGT1A3	ZADH2
SLC25A21	SLC2A9	SLC52A2	SLC9A4	ST6GALNAC2	TKTL1	UGT1A4	
SLC25A22	SLC30A1	SLC52A3	SLC9A5	ST6GALNAC3	TKTL2	UGT1A5	
SLC25A26	SLC32A1	SLC5A1	SLC9A7	ST6GALNAC4	TM7SF2	UGT1A6	
SLC25A27	SLC33A1	SLC5A10	SLC9A8	ST6GALNAC5	TMEM27	UGT1A7	
SLC25A28	SLC34A1	SLC5A11	SLC01A2	ST6GALNAC6	TMEM91	UGT1A8	
SLC25A29	SLC34A2	SLC5A12	SLC01B1	ST8SIA1	TMLHE	UGT1A9	

Table C. 1: Upregulated miRNAs with downregulated target metabolic genes and enriched pathways

Sr. No.	miRNA (Upregulated)	Target Metabolic Genes (Downregulated)	Enriched Metabolic Pathways (p value < 0.05)
1.	hsa-miR-10b-5p	GLS, ATP6V1B2, CSGALNACT1, PAFAH1B1, AGPAT3, ST6GALNAC6, XYLT1	D-Glutamine and D-glutamate metabolism, Glycosaminoglycan biosynthesis
2.	hsa-miR-18a-5p	HMGCS1, XYLT1, SLC12A6, INPP5F	Glycosaminoglycan biosynthesis, Terpenoid backbone biosynthesis, Butanoate metabolism, Valine,

			leucine and isoleucine degradation, Inositol phosphate metabolism
3.	hsa-miR-93-5p	SGMS1, SLC24A2, PFKP, KMT2A, OCRL, ACSL4, DPYSL2, SLC4A8, ST6GALNAC6, PIK3R1, ENTPD4, PTPDC1, PAFAH1B1, ATP1A2, PAFAH1B2, SLC16A7, ZADH2, CSGALNACT1, MVK, GPAM, DGKH, PANK3, CERS6, DGKE, LPIN1, PIP4K2A, CPOX, ACADSB, SCD	Glycerolipid metabolism, Glycerophospholipid metabolism, Fatty acid metabolism, Choline metabolism in cancer, Sphingolipid signalling pathway, AMPK signalling pathway, Fatty acid degradation, Inositol phosphate metabolism, Central carbon metabolism in cancer, Biosynthesis of cofactors, mTOR signalling pathway, HIF-1 signalling pathway, Glycosaminoglycan biosynthesis - chondroitin sulfate / dermatan sulfate
4.	hsa-miR-106b-3p	-	-
5.	hsa-miR-155-5p	GLUL, ENTPD4, ZADH2, SLC4A8, DGKH, RFK, LPIN1, SLC16A7, SLC12A6	Glycerolipid metabolism, Arginine biosynthesis, Glycerophospholipid metabolism, Riboflavin metabolism, Nitrogen metabolism, SLC-mediated transmembrane transport, Pyrimidine metabolism, Alanine, aspartate and glutamate metabolism
6.	hsa-miR-15b-5p	ABCC5, ACACB, ACSL4, ACSS2, ALDH6A1, ASH1L, CDS2, ETNK1, FASN, GLUD1, IDH3A, IP6K1, KMT2A, LHPP, MTHFR, OCRL, PAFAH1B1, PAFAH1B2, PANK2, PIK3R1, PISD, PLPP6, PTEN, RDH13, RFK, SLC12A2, SLC25A22, SLC2A3, SLC4A8, SYNJ1, UROS	Phosphatidylinositol signalling system, Carbon metabolism, Fatty acid biosynthesis, Inositol phosphate metabolism, Propanoate metabolism, SLC-mediated transmembrane transport
7.	hsa-miR-181a-2-3p	DGKG, SLC9A5, PTGES2, ATP6V0A1, NT5C2, SLC2A13, ABCC5, ACYP1, ATP1A3, SLC12A2, ACADSB, PGS1, SLC24A2	Arachidonic acid metabolism, Glycerophospholipid Biosynthetic Pathway, SLC-mediated transmembrane transport
8.	hsa-miR-21-5p	MIA3, INPP4A, SC5D, PIK3R1, PIKFYVE, FAM20B, ELOVL7, PDHA1, SACM1L	Inositol phosphate metabolism, Central carbon metabolism in cancer, Fatty acyl-CoA biosynthesis
9.	hsa-miR-23a-3p	AUH, ETNK1, PTEN, SLC1A1, ATP6V1E1, SLC12A2, PIP4K2B, GLS, SYNJ1, SLC38A1, INPP5A,	Inositol phosphate metabolism, Valine, leucine and isoleucine degradation, Glycerophospholipid metabolism, Glycerolipid

		AGPAT4, NDUFA5, CDS2, B4GAT1, AACS, NDST1, PIKFYVE, ABCC5, CPOX, DGKH, ACADSB, OXCT1, ALAS1, IDS, PDHA1, ATP6V1B2, SLC9A7, LPIN1	metabolism, Central carbon metabolism in cancer, Butanoate metabolism, Glutamatergic synapse, Astrocytic Glutamate-Glutamine Uptake and Metabolism, SLC-mediated transmembrane transport
10.	hsa-miR-24-2-5p	CERS6, ACADSB, SGMS1, UGT8, DGKH, IDI1, SLCO3A1, ACACA	Sphingolipid metabolism, Fatty acid metabolism, Glycerophospholipid metabolism, Fatty acid biosynthesis, Ether lipid metabolism
11.	hsa-miR-25-3p, 92a-3p, 92b, 92b-3p	PIKFYVE, UGP2, NSF, PTEN, MIA3, SYNJ1, NPC1, PIK3CB, SGPP1, ADCY3, SLC9A7, SLC25A16, SLC4A8, PCYT1B, ELOVL4, ATP6V1B2, SLC9A1, PIP5K1C, DBT, PTGES2, CHKA, CHST1, PANK3, SLC12A2, ADO, LPIN1, PIK3R1, PLD1, SPHK2, MGLL	Inositol phosphate metabolism, Glycerophospholipid metabolism, Central carbon metabolism in cancer, Coenzyme A biosynthesis, Metabolism of carbohydrates, Degradation of cysteine and homocysteine, Fatty acid metabolism, SLC-mediated transmembrane transport
12.	hsa-miR-28-3p	NMNAT2, ACSL4, CERS6	Fatty acid metabolism, Sphingolipid metabolism
13.	hsa-miR-320a, 320b, 320c, 320d	ENTPD4, IDS, PFKM, ABCC5, PIGK, ACOT7, ADCY3, ITPK1, PTEN, GNE, MTMR6, SLC12A2, SUCLA2, GLS, B4GALT6, DGKH, FAM20B, HACD3, NDUFA10, DIO2, ATP6V1C1, PIK3R1, SLCO3A1	Central carbon metabolism in cancer, Inositol phosphate metabolism, Fatty acid elongation, MicroRNAs in cancer, Oxidative phosphorylation, Purine metabolism, D-Glutamine and D-glutamate metabolism
14.	hsa-miR-339-5p	KMT2A, PFAH1B1	Lysine degradation
15.	hsa-miR-3651	NEU3, SYNJ1	Inositol phosphate metabolism, Sphingolipid metabolism
16.	hsa-miR-424-3p	GFPT1, UQCRC2, PLPPR4	Alanine, aspartate and glutamate metabolism, Respiratory electron transport, ATP synthesis by chemiosmotic coupling, Lysosphingolipid and LPA receptors
17.	hsa-miR-4429	ENTPD4, IDS, PFKM, ABCC5, PIGK, ACOT7, ITPK1, ADCY3, PTEN, GNE, MTMR6, SLC12A2, SUCLA2, B4GALT6, GLS, DGKH, HACD3, FAM20B, NDUFA10, DIO2,	Central carbon metabolism in cancer, Inositol phosphate metabolism, Fatty acid elongation, MicroRNAs in cancer, Oxidative phosphorylation, Purine metabolism, D-Glutamine and D-glutamate metabolism

		ATP6V1C1, PIK3R1, SLC03A1	
18.	hsa-miR-455-3p	PIK3R1, KMT2A, IDS, HACD3, PIGA, CNDP2, CSGALNACT1, MIA3, SUCLA2	Pyruvate metabolism and Citric Acid (TCA) cycle, respiratory electron transport, Central carbon metabolism in cancer, Arginine and proline metabolism, Lysine degradation
19.	hsa-miR-500a-5p	SPTLC2, HMGCS1, PLA2G12A, MTMR6, SYNJ2, GPAM, PAFAH1B1, OCRL, SUCLA2, SLC2A13, SLC9A7	Inositol phosphate metabolism, Lipid metabolism, Glycerophospholipid metabolism, Synthesis and degradation of ketone bodies, SLC-mediated transmembrane transport
20.	hsa-miR-6872-3p	ATP1B1, ST6GALNAC6, DIO2, SLC1A1, NDUFS2, SPTLC2, SLC25A4, PGS1, DGKG	Electron Transport Chain (OXPHOS system in mitochondria), Synthesis of Prostaglandin

Table C. 2: Downregulated miRNAs with upregulated target metabolic genes and enriched pathways

Sr. No.	miRNA (Downregulated)	Target Metabolic Genes (Upregulated)	Enriched Metabolic Pathways (p value < 0.05)
1.	hsa-miR-1225	NDUFB11, PNP, ATP6V0A2, AK2, ST6GALNAC4, PGLS, GNPDA1, GANC	Purine metabolism, Sphingolipid Metabolism, Pentose Phosphate Metabolism, Mitochondrial complex I assembly model OXPHOS system
2.	hsa-miR-1236-5p	ALDH3A2, HNMT, AKR1B1, SLC25A5	Histidine metabolism, Glycerolipid metabolism, Arginine and proline metabolism, Fructose metabolism, Metabolism of lipids
3.	hsa-miR-124-1/ 124-2/124-3/ 124-3p	B4GALT1, P4HA1, ACAA2, ECI2, FPGS, CHSY1, SLC16A1, ATP6V0A2, STT3A, CHST14, ABCC4, GALNT10, SUCLG2, PAPSS2, ALDH9A1, SLC35B2, SGPL1, GGPS1, ATP6V0E1, HADHA, POGLUT1, LCLAT1, PECR, GLT8D1, NME4, HADH, PGM2, ABHD5, RDH10, SPCS2, SORD	Fatty acid degradation, Valine, leucine and isoleucine degradation, Tryptophan metabolism, Lysine degradation, Glycosaminoglycan biosynthesis, Galactose metabolism, beta-Alanine metabolism, Arginine and proline metabolism, Purine metabolism.
4.	hsa-miR-124-5p	HNMT, CHSY1, GYG1, SLC35C1, NADK	Glycogen metabolism,

			Histidine metabolism, Nicotinate and nicotinamide metabolism, Glycosaminoglycan biosynthesis
5.	hsa-miR-128-1-5p/ hsa-miR-128-2-5p	LRTOMT	Steroid hormone biosynthesis, Dopamine clearance from the synaptic cleft
6.	hsa-miR-128-3p	POGLUT1, AK2, AKR7A2, GNS, G6PC3, CA12, PFKFB4, ASAH1, NME4, GYS1, CTPS2, CHST11, HMOX1, ADH5, ABCA1, GLRX, SLC26A2	Glycogen metabolism, Pyrimidine metabolism, Purine metabolism, Glycolysis / Gluconeogenesis, Glycosaminoglycan metabolism, Metabolism of xenobiotics by cytochrome P450, Tyrosine metabolism
7.	hsa-miR-129-1-3p	CHST14, DPYSL3	Glycosaminoglycan biosynthesis
8.	hsa-miR-137	SLC1A5, TMLHE, SLC4A7, SGPL1, GALNT1, SLC25A5, PLPP5, PFKFB4, ABHD5, DUT, AGPAT5, PGM2, HS3ST3B1, IDH1, PEPD, B4GALT4, FLAD1	Glycerophospholipid metabolism, Glycerolipid metabolism, Central carbon metabolism in cancer, Glycolysis / Gluconeogenesis, TCA cycle, NADPH regeneration, Lipid metabolism, Drug metabolism - other enzymes
9.	hsa-miR-138-2-3p	NANP, ATP11C, SUV39H2, SOD2, FAH, GNS	Glycosaminoglycan degradation, Amino sugar and nucleotide sugar metabolism, Lysine degradation
10.	hsa-miR-139-3p	HNMT, UEVLD	Histidine metabolism, Selenoamino acid metabolism
11.	hsa-miR-139-5p	HNMT, UEVLD, ABCA1, PSPH, DHRS3, FPGT, TMLHE, PXYLP1	Glycine, serine and threonine metabolism, Lysine degradation, Cholesterol metabolism, Fructose and mannose metabolism, Retinol metabolism, Biosynthesis of amino acids, Biosynthesis of cofactors, Amino sugar and nucleotide sugar metabolism, Carbon metabolism, Histidine metabolism
12.	hsa-miR-211-3p	AHCY, SLC35D1, HK2, GANC	Galactose metabolism, Starch and sucrose metabolism, Fructose and mannose metabolism, Amino sugar and nucleotide sugar metabolism, Cysteine and methionine metabolism, Glycolysis / Gluconeogenesis, Central carbon metabolism in cancer, HIF-1 signalling pathway, Carbon metabolism

13.	hsa-miR-218-5p	SHMT1, UEVLD, HS3ST3B1, CYBRD1, SGPL1, LTA4H, LOXL2, SLC35B2, HMOX1, BCHE	Glycosaminoglycan biosynthesis - heparan sulfate / heparin, Sphingolipid metabolism, Arachidonic acid metabolism, Glycine, serine and threonine metabolism, One carbon pool by folate, Antifolate resistance, Glyoxylate and dicarboxylate metabolism, Biosynthesis of amino acids, Biosynthesis of cofactors, HIF-1 signalling pathway, Carbon metabolism
14.	hsa-miR-3188	DPYSL3, CROT, ADH5, DCTD, HSD3B7, UQCRQ, PLCB3, SLC26A6, AKR7A2, GNPDA1, ABCD1, SLC4A7	Metabolism of xenobiotics by cytochrome P450, Phosphatidylinositol signalling system, Glycolysis / Gluconeogenesis, Inositol phosphate metabolism, Carbon metabolism, Fatty acid degradation, Tyrosine metabolism, Oxidative phosphorylation, Pyrimidine metabolism, Pyruvate metabolism, Phospholipase D signalling pathway, Sphingolipid signalling pathway, Drug metabolism - cytochrome P450, Amino sugar and nucleotide sugar metabolism
15.	hsa-miR-3200-3p	-	-
16.	hsa-miR-323a-5p	GK, G6PC3, PYCR1, GALNT10, MTMR14	Glycolysis / Gluconeogenesis, Inositol phosphate metabolism, Glycerolipid metabolism, Biosynthesis of amino acids, Galactose metabolism
17.	hsa-miR-330-3p	SCP2, DPYSL3, FPGT, CA12, MAT2A, CRLS1, GALNT10, ABCA1, UST, PLCB3, EXT2	Metabolism of carbohydrates, Methylation, alpha-linolenic acid (ALA) metabolism, Beta-oxidation of pristanoyl-CoA, Dermatan sulfate biosynthesis
18.	hsa-miR-330-5p	B4GALT1, FUCA1, PFKFB4, GLYCTK, SGPL1, SORD, DPYD, PPCDC	Pantothenate and CoA biosynthesis, Fructose and mannose metabolism, Galactose metabolism, Glyoxylate and dicarboxylate metabolism, beta-Alanine metabolism, Pentose phosphate pathway, Glycosaminoglycan biosynthesis, Glycerolipid metabolism
19.	hsa-miR-338-3p	SLC25A20, B4GALT7, PIP5K1A, LDHA, SLC35D1, LRTOMT, RRM1	Dopamine clearance from the synaptic cleft, Carnitine metabolism, Pyruvate metabolism, The citric acid (TCA) cycle and respiratory electron transport, Metabolism of lipids
20.	hsa-miR-4257	B4GALT4, RDH10, AK2, ECI2, LRTOMT, CYP2U1, SUV39H2, NAGA	Glycosaminoglycan biosynthesis, Glycosphingolipid biosynthesis, Arachidonic acid metabolism, Steroid

			hormone biosynthesis, Fatty acid degradation, Lysine degradation
21.	hsa-miR-4281	NT5C, ODC1, DPM2	Glutathione metabolism, Pyrimidine metabolism, Arginine and proline metabolism, Nicotinate and nicotinamide metabolism, N-Glycan biosynthesis, Purine metabolism
22.	hsa-miR-4322	NME6, CRLS1, MTHFD2L	One carbon pool by folate, Pyrimidine metabolism, Glycerophospholipid metabolism, Purine metabolism
23.	hsa-miR-433-3p	HNMT, NAGA, GLRX, GALNT1, HSD17B11, UGDH, CPT2, MTMR14	Formation of the active cofactor, UDP-glucuronate, Metabolism of lipids, Carnitine metabolism, Amino sugar and nucleotide sugar metabolism
24.	hsa-miR-4433b-3p	NT5C3A, LRTOMT, MTHFS, SLC25A5, CANT1, FPGT, ENTPD1	Pyrimidine metabolism, Purine metabolism, Dopamine clearance from the synaptic cleft, Metabolism of folate and pterines
25.	hsa-miR-4447	ABCD1, GALNT2, GYS1, SLC4A2, SLC12A4, SPR, LRTOMT, DHRS3, B4GALT7, SPCS2	Glycogen storage, alpha-linolenic acid (ALA) metabolism, Metabolism of cofactors, Class I peroxisomal membrane protein import
26.	hsa-miR-4463	RPIA, MCCC2, LOXL2, NME7, PGM3, ENTPD1, DUSP11, NUDT5, B4GALT1	Purine metabolism, Pyrimidine metabolism, Glycosaminoglycan biosynthesis, Pentose phosphate pathway, Lactose synthesis, Asparagine N-linked glycosylation
27.	hsa-miR-4525	MTHFD2L, FUCA2, SLC26A2	One carbon pool by folate, Multifunctional anion exchangers
28.	hsa-miR-485-5p	SGPL1, DPYSL3, ENTPD1, HS3ST3B1, SLC26A2, LRTOMT, ATP6V0D2, CROT, AK2, PCBD2, SLC26A6, SOAT1, ADH5, PAICS, GNS, UEVLD, UQCRQ	Purine metabolism, Oxidative phosphorylation, Glycosaminoglycan metabolism, Beta-oxidation of pristanoyl-CoA, Respiratory electron transport, Dopamine clearance from the synaptic cleft
29.	hsa-miR-490-5p	P4HA1, UGDH, ENTPD1	Pyrimidine metabolism, Pentose and glucuronate interconversions, Arginine and proline metabolism, Purine metabolism
30.	hsa-miR-5698	CHPF, FPGS, LCLAT1, SLC4A2, SLC35C1, ENTPD1	Glycosaminoglycan biosynthesis, Pyrimidine metabolism, Glycerolipid metabolism, Folate biosynthesis, Glycerophospholipid metabolism, Purine metabolism

31.	hsa-miR-6782-5p	AK2, COQ5, RRM1	Purine metabolism, Ubiquinone and other terpenoid-quinone biosynthesis, Glutathione metabolism, Pyrimidine metabolism
32.	hsa-miR-6790-5p	IDH1, HADH, SOAT1, PGM2, ALDH3A2	Valine, leucine and isoleucine degradation, Tryptophan metabolism, Glycolysis / Gluconeogenesis, Fatty acid degradation, Pentose phosphate pathway, Citrate cycle (TCA cycle), Glutathione metabolism, Galactose metabolism, Central carbon metabolism in cancer, Arginine and proline metabolism
33.	hsa-miR-6810-5p	SLC1A5, ADI1, PPT1	Central carbon metabolism in cancer, Fatty acid elongation, Cysteine and methionine metabolism, Methionine salvage pathway, SLC-mediated transmembrane transport
34.	hsa-miR-6861-5p	PPCDC, PFKFB4, LRTOMT	Fructose and mannose metabolism, Steroid hormone biosynthesis, Dopamine clearance from the synaptic cleft, Glycolysis, Coenzyme A biosynthesis
35.	hsa-miR-758-5p	UQCRQ, CYP2U1, HEXA, B4GALT1	Glycosaminoglycan biosynthesis, Glycosphingolipid biosynthesis, Amino sugar and nucleotide sugar metabolism, Oxidative phosphorylation, Galactose metabolism, Respiratory electron transport, Arachidonic acid metabolism, The citric acid (TCA) cycle, Fatty acid metabolism
36.	hsa-miR-7-5p	SLC4A7, LOXL2, DTYMK, FPGT, DPYSL3, CRLS1, PGM3, ABHD5, GALNT2	Amino sugar and nucleotide sugar metabolism, Fructose and mannose metabolism, Mucin type O-glycan biosynthesis, Pyrimidine metabolism, Glycerophospholipid metabolism,
37.	hsa-miR-769-5p	BPNT1, PAPSS2, CROT, UGDH, CRLS1	Sulfur metabolism, Amino sugar and nucleotide sugar metabolism, Ascorbate and aldarate metabolism, Glycerophospholipid metabolism, Purine metabolism, Glycerophospholipid biosynthesis
38.	hsa-miR-770/ 770-5p	HKDC1, LBR, ECI2	Galactose metabolism, Fructose and mannose metabolism, Fatty acid degradation, Glycolysis / Gluconeogenesis, Central carbon metabolism in cancer, Amino sugar and nucleotide sugar metabolism

39.	hsa-miR-873-3p	PGM3, CA12, COQ5, RRM2, ADSL, GART	Purine metabolism, Nitrogen metabolism, Ubiquinone and other terpenoid-quinone biosynthesis, Pyrimidine metabolism, Glutathione metabolism, Alanine, aspartate and glutamate metabolism, One carbon pool by folate
40.	hsa-miR-874-3p	RRM2, PFKFB4, DPYD	Pyrimidine metabolism, Pantothenate and CoA biosynthesis, Glutathione metabolism, Fructose and mannose metabolism, beta-Alanine metabolism, Glycolysis, Nucleobase catabolism

Table C. 3: Details and statistics of the backbone analysis

Metabolism	Pathways	Total No. of miRNA	Backbone miRNAs	Max. no. of pathways targeted by backbone
Central Carbon Metabolism	Glycolysis / Gluconeogenesis (hsa00010), Citrate cycle (TCA cycle) (hsa00020), Pentose phosphate pathway (hsa00030), Pentose and glucuronate interconversions (hsa00040), Fructose and mannose metabolism (hsa00051), Galactose metabolism (hsa00052), Oxidative phosphorylation (hsa00190), Starch and sucrose metabolism (hsa00500), Pyruvate metabolism (hsa0062), Carbon metabolism (hsa01200), 2-Oxocarboxylic acid metabolism (hsa01210), HIF-1 signalling pathway (hsa04066), mTOR signalling pathway (hsa04150), PI3K-Akt signalling pathway (hsa04151), AMPK signalling pathway (hsa04152), Central carbon metabolism in cancer (hsa05230)	42	hsa-miR-1225, hsa-miR-211-3p and MIR770 family miRNAs	7
Fatty Acid Metabolism	Fatty acid biosynthesis (hsa00061), Fatty acid elongation (hsa00062), Fatty acid degradation (hsa00071), Arachidonic acid metabolism (hsa00590), Linoleic acid metabolism (hsa00591), alpha-	23	hsa-miR-24-2-5p, hsa-miR-28-3p and hsa-miR-124-3p, hsa-miR-	2

	Linolenic acid metabolism (hsa00592), Biosynthesis of unsaturated fatty acids (hsa01040), Fatty acid metabolism (hsa01212)		181a-2-3p and hsa-miR-6790-5p	
Lipid Metabolism	Synthesis and degradation of ketone bodies (hsa00072), Steroid biosynthesis (hsa00100), Steroid hormone biosynthesis (hsa00140), Glycerolipid metabolism (hsa00561), Glycerophospholipid metabolism (hsa00564), Ether lipid metabolism (hsa00565), Sphingolipid metabolism (hsa00600), Glycosphingolipid biosynthesis - lacto and neolacto series (hsa00601), Glycosphingolipid biosynthesis - globo and isoglobo series (hsa00603), Glycosphingolipid biosynthesis - ganglio series (hsa00604), Sphingolipid signalling pathway (hsa04071), Phospholipase D signalling pathway (hsa04072)	44	hsa-miR-24-2-5p, hsa-miR-500a-5p, hsa-miR-137 and MIR25/92 family miRNAs	3
Glycan Metabolism	N-Glycan biosynthesis (hsa00510), Other glycan degradation (hsa00511), Mucin type O-glycan biosynthesis (hsa00512), Various types of N-glycan biosynthesis (hsa00513), Other types of O-glycan biosynthesis (hsa00514), Mannose type O-glycan biosynthesis (hsa00515), Glycosaminoglycan degradation (hsa00531), Glycosaminoglycan biosynthesis - chondroitin sulfate / dermatan sulfate (hsa00532), Glycosaminoglycan biosynthesis - keratan sulfate (hsa00533), Glycosaminoglycan biosynthesis - heparan sulfate / heparin (hsa00534), Glycerolipid metabolism (hsa00561), Inositol phosphate metabolism (hsa00562), Glycosylphosphatidylinositol (GPI)-anchor biosynthesis (hsa00563)	36	hsa-miR-4257 and hsa-miR-758-5p	3
Amino Acid Metabolism	Arginine biosynthesis (hsa00220), Alanine, aspartate and glutamate metabolism (hsa00250), Glycine, serine and threonine metabolism (hsa00260), Cysteine and	48	hsa-miR-10b-5p, hsa-miR-155-5p hsa-miR-424-3p, and	3

	methionine metabolism (hsa00270), Valine, leucine and isoleucine degradation (hsa00280), Lysine degradation (hsa00310), Arginine and proline metabolism (hsa00330), Histidine metabolism (hsa00340), Tyrosine metabolism (hsa00350), Tryptophan metabolism (hsa00380), beta-Alanine metabolism (hsa00410), Taurine and hypotaurine metabolism (hsa00430), Phosphonate and phosphinate metabolism (hsa00440), Selenocompound metabolism (hsa00450), D-Glutamine and D-glutamate metabolism (hsa00471), Glutathione metabolism (hsa00480), Amino sugar and nucleotide sugar metabolism (hsa00520)		MIR124 family miRNAs, hsa-miR-455-3p, hsa-miR-6790-5p, and hsa-miR-128-3p	
Nucleotide Metabolism	Purine metabolism (hsa00230), Pyrimidine metabolism (hsa00240), Amino sugar and nucleotide sugar metabolism (hsa00520)	31	hsa-miR-1225, hsa-miR-155-5p, MIR320 family miRNAs, hsa-miR-433-3p, hsa-miR-4463 and hsa-miR-490-5p	2

Table C. 4: Key regulatory metabolic genes selected as seed sequence for network diffusion and identification of cellular phenotype subnetworks.

Cellular Phenotype	Regulatory genes	Reference
Proliferation and growth	HK2	(361)
	PFKP	(361)
	G6PD	(361)
	LDHA	(361)
	COX4 1	(361)
	CPT1A	(361)
	FASN	(361)
	G6PC3	(361)
	ALDOC	(361)
	SLC1A1	(361)
	SLC1A3	(361)
	PDK1	(361)

	PTEN	(361)
	ALDH1A3	(361)
	PKM2	(361)
	ELOVL2	(361)
	LPCAT1	(361)
	PHGDH	(361)
	ACACA	(361)
	ACSS2	(361)
	SHMT1	(361)
Survival	ALOX5AP	(362)
	ACAA2	(362)
	PYGL	(362)
	OAS1	(362)
	NNMT	(362)
	FAH	(362)
	EXTL3	(362)
	B3GALNT1	(362)
	UPP1	(362)
	NQO2	(362)
	MAN1B1	(362)
	CNGA3	(362)
	PIGB	(362)
	HEXA	(362)
	CYB561	(362)
	ACADSB	(362)
	NPC2	(362)
	SLC12A7	(362)
	ACOX2	(362)
	B4GALT7	(362)
IDH1	(363)	
MTHFD2	(294)	
Cell Migration and Invasion	ALDOC	(364)
	G6PC3	(365)
	G6PD	(364)
	GPI	(366)
	FH	(367)
	LDHA	(367)
	SDHC	(367)
	SDHD	(367)
SLC1A5	(367)	
Stemness	ACSL3	(368)
	ALOX5	(368)
	ALDH1A3	(369)
	CPE	(368)
	FASN	(368)
	GLS	(368)
	PKM2	(368)
	SHMT1	(368)
SLC1A3	(368)	

	SDHB	(368)
	CPT1A	(370)
	G6PD	(41)
	IDO	(371)
	GLS	(372)
	HK2	(373)
	LDHA	(374)
	MTHFD2	(375)
	GSTM1	(376)
	GSTM2	(376)
	ABCC1	(377)
	SOD2	(378)
	ABCC2	(379)
	ABCC4	(379)
	ABCC5	(379)

Table C. 5: List of metabolic genes and miRNAs in the subnetworks of cellular phenotypes

Proliferation and growth	ACACA, ACACB, ACAT2, ACLY, ACOX1, ACSL1, ACSL3, ACSL4, ACSS2, ACYP1, ALAS1, ALDH1A3, ALDH1L2, ALDH3A2, ALDH3B1, ALDH6A1, ALDOC, AMDHD2, ASAH1, CANT1, CNDP2, COMT, COX4I1, COX6B1, COX6C, COX7A2L, COX7B, COX8A, CPT1A, CPT2, DAK, DBT, DLAT, FASN, G6PC3, G6PD, GART, GFPT1, GFPT2, GLUD1, GNPDA1, GNPDA2, GNPAT1, GPI, H6PD, HK2, HLCS, HSD17B4, IDH1, INPP4A, INPP5A, INPP5B, INPP5E, INPP5F, ITPKC, KHK, LDHA, LDHB, LRTOMT, LTA4H, MAOA, ME2, MPI, MTHFD2, MTHFD2L, MTHFR, MTR, NDUFA4, OCRL, PFKL, PFKM, PFKP, PGAM1, PGLS, PGM1, PGM2, PHGDH, PI4K2A, PIK3C2A, PIK3CA, PIK3CB, PIK3CD, PIK3R1, PIKFYVE, PIP4K2A, PIP4K2B, PIP4K2C, PIP5K1A, PIP5K1C, PIP5KL1, PKM2, PMM1, PSAT1, PSPH, PTEN, SACM1L, SHMT1, SLC1A1, SLC1A3, SOD2, SORD, SYNJ1, SYNJ2, TKT, TPI1, UQCR10, UQCR11, UQCRC1, UQCRC2, UQCRFS1, UQCRQ, hsa-miR-500a-5p, hsa-miR-23a-3p, hsa-miR-24-2-5p, hsa-miR-338-3p, hsa-miR-15b-5p, hsa-miR-129-1-3p, hsa-miR-770_770-5p, hsa-miR-128-1-5p_2-5p, hsa-miR-4525, hsa-miR-873-3p, hsa-miR-6872-3p, hsa-miR-5698, hsa-miR-4463, hsa-miR-4447, hsa-miR-485-5p, hsa-miR-124-3p, hsa-miR-218-5p, hsa-miR-137, hsa-miR-93-5p, hsa-miR-211-3p, hsa-miR-7-5p, hsa-miR-25-3p-92a_b, hsa-miR-320a_b_c_d, hsa-miR-4429, hsa-miR-433-3p, hsa-miR-128-3p, hsa-miR-323a-5p
Survival	A4GALT, ACAA2, ACADSB, ACAT2, ACO1, ACOX1, ACOX3, ALDH1L2, ALDH6A1, ALDOC, ARSB, ASAH1, B3GALNT1, B3GALT6, B4GALT1, B4GALT2, B4GALT3, B4GALT4, B4GALT7, CANT1, CROT, DBT, EXTL3, FAH, GART, GCDH, GM2A, GNS, GOT2, HADH, HADHA, HEXA, HMGCS1, HSD17B4, IDH1, IDH3A, IDH3B, IDH3G, LTA4H, MECR, MTHFD2, MTHFD2L, MTHFR, MTHFS, NAGA, NAGK, OGDH, PECR, PGM1, PIGB, PIGM, PIGO, PIGX, SCP2, SHMT1, XYLT1, XYLT2, hsa-miR-758-5p, hsa-miR-138-2-3p, hsa-miR-1236-5p, hsa-miR-24-2-5p, hsa-miR-6872-3p, hsa-miR-338-3p, hsa-miR-15b-5p, hsa-miR-6790-5p, hsa-miR-6810-5p, hsa-miR-25-3p-92a_b, hsa-miR-181a-

	2-3p, hsa-miR-218-5p, hsa-miR-4447, hsa-miR-124-3p, hsa-miR-23a-3p, hsa-miR-93-5p, hsa-miR-137
Cell migration and invasion	ALDOC, ASAH1, CANT1, DAK, ENO1, ENO2, G6PC3, G6PD, GFPT1, GFPT2, GNPDA1, GNPDA2, GPI, H6PD, HK2, HKDC1, IDH1, KHK, LDHA, LDHB, LTA4H, ME2, MPI, NDUFA8, NDUFB8, NDUFS2, PFKL, PFKM, PFKP, PGAM1, PGLS, PGM1, PGM2, PKM, SDHC, SDHD, SLC1A5, SUCLA2, SUCLG2, TKT, TPI1, UQCRQ, hsa-miR-323a-5p, hsa-miR-6810-5p, hsa-miR-338-3p, hsa-miR-3188, hsa-miR-7-5p, hsa-miR-485-5p, hsa-miR-4429, hsa-miR-320a_b_c_d, hsa-miR-137, hsa-miR-128-3p, hsa-miR-23a-3p, hsa-miR-4257, hsa-miR-330-5p
Stemness	ACACA, ACACB, ACLY, ACOX1, ACSL1, ACSL3, ACSL4, ACSS2, ALAS1, ALDH1A3, ALDH1L2, CAD, CNDP2, COMT, CPS1, ELOVL1, ELOVL6, FASN, GART, GFPT1, GFPT2, GLS, GLUD1, GLUL, LRTOMT, MAOA, MTHFD2, MTHFD2L, MTHFR, MTR, PKM2, PPAT, PSPH, SHMT1, SLC1A3, hsa-miR-500a-5p, hsa-miR-128-1-5p_2-5p, hsa-miR-4525, hsa-miR-24-2-5p, hsa-miR-18a-5p, hsa-miR-770_770-5p, hsa-miR-10b-5p, hsa-miR-5698, hsa-miR-15b-5p, hsa-miR-4447, hsa-miR-23a-3p, hsa-miR-218-5p, hsa-miR-4463, hsa-miR-330-3p, hsa-miR-4429, hsa-miR-320a_b_c_d
Drug resistance	ABCC1, ABCC4, ABCC5, ACOX1, ACSS2, ALDH1L2, AMDHD2, CAD, CPS1, CPT1A, CPT2, G6PD, GART, GFPT1, GFPT2, GLS, GLUD1, GLUL, GNPDA1, GNPDA2, GNPAT1, GPI, GSTM1, GSTM2, H6PD, HK2, HSD17B4, KHK, LDHA, LDHB, ME2, MPI, MTHFD2, MTHFD2L, MTHFR, MTHFS, PGAM1, PGLS, PGM1, PGM2, PMM1, PPAT, SHMT1, SOD1, SOD2, SOD3, SORD, hsa-miR-3188, hsa-miR-339-5p, hsa-miR-873-3p, hsa-miR-330-5p, hsa-miR-4463, hsa-miR-124-3p, hsa-miR-338-3p, hsa-miR-10b-5p, hsa-miR-181a-2-3p, hsa-miR-320a_b_c_d, hsa-miR-4429, hsa-miR-138-2-3p, hsa-miR-23a-3p, hsa-miR-485-5p, hsa-miR-15b-5p, hsa-miR-25-3p_92a_b, hsa-miR-500a-5p, hsa-miR-211-3p, hsa-miR-330-3p

Table C. 6: Significantly enriched metabolic pathways for the subnetworks of cellular phenotypes

Phenotype	Significantly Enriched Pathways
Proliferation and growth	hsa00562: Inositol phosphate metabolism, hsa01200: Carbon metabolism, hsa04070: Phosphatidylinositol signalling system, hsa00010: Glycolysis / Gluconeogenesis, hsa05230: Central carbon metabolism in cancer, hsa00190: Oxidative phosphorylation, hsa01230: Biosynthesis of amino acids, hsa00520: Amino sugar and nucleotide sugar metabolism, hsa00030: Pentose phosphate pathway, hsa00051: Fructose and mannose metabolism, hsa00620: Pyruvate metabolism, hsa04152: AMPK signalling pathway, hsa04922: Glucagon signalling pathway, hsa01212: Fatty acid metabolism, hsa00640: Propanoate metabolism, hsa04066: HIF-1 signalling pathway, hsa04931: Insulin resistance, hsa00670: One carbon pool by folate, hsa00071: Fatty acid degradation, hsa01240: Biosynthesis of cofactors, hsa00052: Galactose metabolism, hsa00260: Glycine, serine and threonine metabolism, hsa00061: Fatty acid biosynthesis, hsa04810: Regulation of actin cytoskeleton, hsa04973: Carbohydrate digestion and absorption, hsa00500: Starch and sucrose metabolism, hsa00410: beta-

	<p>Alanine metabolism, hsa03320: PPAR signalling pathway, hsa04068: FoxO signalling pathway, hsa04920: Adipocytokine signalling pathway, hsa05231: Choline metabolism in cancer, hsa00270: Cysteine and methionine metabolism, hsa04666: Fc gamma R-mediated phagocytosis, hsa04071: Sphingolipid signalling pathway, hsa04510: Focal adhesion, hsa00340: Histidine metabolism, hsa04213: Longevity regulating pathway - multiple species, hsa05213: Endometrial cancer, hsa05218: Melanoma, hsa04072: Phospholipase D signalling pathway, hsa05214: Glioma, hsa00350: Tyrosine metabolism, hsa00230: Purine metabolism, hsa04960: Aldosterone-regulated sodium reabsorption, hsa01521: EGFR tyrosine kinase inhibitor resistance, hsa04211: Longevity regulating pathway, hsa05222: Small cell lung cancer, hsa05235: PD-L1 expression and PD-1 checkpoint pathway in cancer, hsa04150: mTOR signalling pathway, hsa00280: Valine, leucine and isoleucine degradation, hsa03018: RNA degradation, hsa04370: VEGF signalling pathway, hsa01524: Platinum drug resistance, hsa04218: Cellular senescence, hsa04664: Fc epsilon RI signalling pathway, hsa05206: MicroRNAs in cancer, hsa05203: Viral carcinogenesis, hsa04662: B cell receptor signalling pathway, hsa04151: PI3K-Akt signalling pathway, hsa00020: Citrate cycle (TCA cycle), hsa04750: Inflammatory mediator regulation of TRP channels, hsa04550: Signalling pathways regulating pluripotency of stem cells, hsa04024: cAMP signalling pathway, hsa04012: ErbB signalling pathway, hsa00630: Glyoxylate and dicarboxylate metabolism, hsa04650: Natural killer cell mediated cytotoxicity, hsa04620: Toll-like receptor signalling pathway, hsa01523: Antifolate resistance, hsa04935: Growth hormone synthesis, secretion and action, hsa00330: Arginine and proline metabolism, hsa00250: Alanine, aspartate and glutamate metabolism, hsa00380: Tryptophan metabolism, hsa04668: TNF signalling pathway, hsa04210: Apoptosis, hsa04630: JAK-STAT signalling pathway, hsa04062: Chemokine signalling pathway, hsa05205: Proteoglycans in cancer, hsa04015: Rap1 signalling pathway, hsa04014: Ras signalling pathway, hsa01040: Biosynthesis of unsaturated fatty acids, hsa00360: Phenylalanine metabolism, hsa05200: Pathways in cancer, hsa00480: Glutathione metabolism, hsa00982: Drug metabolism - cytochrome P450, hsa00310: Lysine degradation, hsa00561: Glycerolipid metabolism, hsa00471: D-Glutamine and D-glutamate metabolism, hsa00072: Synthesis and degradation of ketone bodies, hsa00910: Nitrogen metabolism, hsa00770: Pantothenate and CoA biosynthesis, hsa00900: Terpenoid backbone biosynthesis, hsa00592: alpha-Linolenic acid metabolism, hsa00450: Selenocompound metabolism, hsa01210: 2-Oxocarboxylic acid metabolism, hsa00053: Ascorbate and aldarate metabolism, hsa00040: Pentose and glucuronate interconversions, hsa00600: Sphingolipid metabolism, hsa00650: Butanoate metabolism, hsa00220: Arginine biosynthesis, hsa00240: Pyrimidine metabolism</p>
Survival	<p>hsa01200: Carbon metabolism, hsa01212: Fatty acid metabolism, hsa00071: Fatty acid degradation, hsa00280: Valine, leucine and isoleucine degradation, hsa00670: One carbon pool by folate, hsa01230: Biosynthesis of amino acids, hsa00601: Glycosphingolipid biosynthesis - lacto and neolacto series, hsa01210: 2-Oxocarboxylic acid metabolism, hsa00020: Citrate cycle (TCA cycle), hsa00534: Glycosaminoglycan biosynthesis - heparan sulfate / heparin, hsa00640: Propanoate</p>

	<p>metabolism, hsa00563: Glycosylphosphatidylinositol (GPI)-anchor biosynthesis, hsa00532: Glycosaminoglycan biosynthesis - chondroitin sulfate / dermatan sulfate, hsa00533: Glycosaminoglycan biosynthesis - keratan sulfate, hsa00603: Glycosphingolipid biosynthesis - globo and isoglobo series, hsa00513: Various types of N-glycan biosynthesis, hsa00062: Fatty acid elongation, hsa01040: Biosynthesis of unsaturated fatty acids, hsa00650: Butanoate metabolism, hsa00410: beta-Alanine metabolism, hsa00310: Lysine degradation, hsa00380: Tryptophan metabolism, hsa00531: Glycosaminoglycan degradation, hsa00515: Mannose type O-glycan biosynthesis, hsa00514: Other types of O-glycan biosynthesis, hsa03320: PPAR signalling pathway, hsa00510: N-Glycan biosynthesis, hsa00520: Amino sugar and nucleotide sugar metabolism, hsa00052: Galactose metabolism, hsa00630: Glyoxylate and dicarboxylate metabolism, hsa01523: Antifolate resistance, hsa00230: Purine metabolism, hsa01240: Biosynthesis of cofactors, hsa00592: alpha-Linolenic acid metabolism, hsa00030: Pentose phosphate pathway, hsa00350: Tyrosine metabolism, hsa04975: Fat digestion and absorption, hsa00010: Glycolysis / Gluconeogenesis, hsa00400: Phenylalanine, tyrosine and tryptophan biosynthesis, hsa00604: Glycosphingolipid biosynthesis - ganglio series, hsa04024: cAMP signalling pathway, hsa00511: Other glycan degradation, hsa00061: Fatty acid biosynthesis, hsa00360: Phenylalanine metabolism, hsa00600: Sphingolipid metabolism, hsa00220: Arginine biosynthesis, hsa00500: Starch and sucrose metabolism, hsa00051: Fructose and mannose metabolism, hsa00240: Pyrimidine metabolism, hsa00480: Glutathione metabolism, hsa00330: Arginine and proline metabolism, hsa00270: Cysteine and methionine metabolism, hsa00250: Alanine, aspartate and glutamate metabolism, hsa00260: Glycine, serine and threonine metabolism, hsa00620: Pyruvate metabolism, hsa00590: Arachidonic acid metabolism, hsa00562: Inositol phosphate metabolism, hsa05230: Central carbon metabolism in cancer</p>
<p>Cell migration and invasion</p>	<p>hsa01200: Carbon metabolism, hsa00010: Glycolysis / Gluconeogenesis, hsa00030: Pentose phosphate pathway, hsa05230: Central carbon metabolism in cancer, hsa00520: Amino sugar and nucleotide sugar metabolism, hsa00051: Fructose and mannose metabolism, hsa01230: Biosynthesis of amino acids, hsa04066: HIF-1 signalling pathway, hsa00052: Galactose metabolism, hsa04922: Glucagon signalling pathway, hsa00500: Starch and sucrose metabolism, hsa00190: Oxidative phosphorylation, hsa03018: RNA degradation, hsa00020: Citrate cycle (TCA cycle), hsa00640: Propanoate metabolism, hsa00620: Pyruvate metabolism, hsa05022: Pathways of neurodegeneration - multiple diseases, hsa00230: Purine metabolism, hsa04152: AMPK signalling pathway, hsa04910: Insulin signalling pathway, hsa00480: Glutathione metabolism, hsa00250: Alanine, aspartate and glutamate metabolism, hsa00270: Cysteine and methionine metabolism, hsa01240: Biosynthesis of cofactors, hsa01210: 2-Oxocarboxylic acid metabolism, hsa00600: Sphingolipid metabolism, hsa00240: Pyrimidine metabolism, hsa00260: Glycine, serine and threonine metabolism, hsa00562: Inositol phosphate metabolism, hsa00590: Arachidonic acid metabolism, hsa00561: Glycerolipid metabolism, hsa04071: Sphingolipid signalling pathway</p>

Stemness	<p>hsa00250: Alanine, aspartate and glutamate metabolism, hsa01212: Fatty acid metabolism, hsa00670: One carbon pool by folate, hsa01200: Carbon metabolism, hsa00061: Fatty acid biosynthesis, hsa01230: Biosynthesis of amino acids, hsa01240: Biosynthesis of cofactors, hsa00220: Arginine biosynthesis, hsa00640: Propanoate metabolism, hsa00620: Pyruvate metabolism, hsa00260: Glycine, serine and threonine metabolism, hsa00071: Fatty acid degradation, hsa00910: Nitrogen metabolism, hsa03320: PPAR signalling pathway, hsa01040: Biosynthesis of unsaturated fatty acids, hsa00350: Tyrosine metabolism, hsa00630: Glyoxylate and dicarboxylate metabolism, hsa01523: Antifolate resistance, hsa04922: Glucagon signalling pathway, hsa00471: D-Glutamine and D-glutamate metabolism, hsa00230: Purine metabolism, hsa04931: Insulin resistance, hsa04724: Glutamatergic synapse, hsa04152: AMPK signalling pathway, hsa04910: Insulin signalling pathway, hsa00340: Histidine metabolism, hsa00062: Fatty acid elongation, hsa00520: Amino sugar and nucleotide sugar metabolism, hsa00410: beta-Alanine metabolism, hsa00330: Arginine and proline metabolism, hsa00010: Glycolysis / Gluconeogenesis, hsa05230: Central carbon metabolism in cancer, hsa00360: Phenylalanine metabolism, hsa00020: Citrate cycle (TCA cycle), hsa00240: Pyrimidine metabolism, hsa00982: Drug metabolism - cytochrome P450, hsa00830: Retinol metabolism, hsa00270: Cysteine and methionine metabolism, hsa00380: Tryptophan metabolism</p>
Drug resistance	<p>hsa00520: Amino sugar and nucleotide sugar metabolism, hsa01200: Carbon metabolism, hsa00250: Alanine, aspartate and glutamate metabolism, hsa00670: One carbon pool by folate, hsa00010: Glycolysis / Gluconeogenesis, hsa00030: Pentose phosphate pathway, hsa01523: Antifolate resistance, hsa05230: Central carbon metabolism in cancer, hsa00051: Fructose and mannose metabolism, hsa01240: Biosynthesis of cofactors, hsa00500: Starch and sucrose metabolism, hsa00220: Arginine biosynthesis, hsa00640: Propanoate metabolism, hsa00620: Pyruvate metabolism, hsa01212: Fatty acid metabolism, hsa00910: Nitrogen metabolism, hsa01230: Biosynthesis of amino acids, hsa04922: Glucagon signalling pathway, hsa00230: Purine metabolism, hsa00052: Galactose metabolism, hsa00480: Glutathione metabolism, hsa00630: Glyoxylate and dicarboxylate metabolism, hsa00071: Fatty acid degradation, hsa00471: D-Glutamine and D-glutamate metabolism, hsa03320: PPAR signalling pathway, hsa04931: Insulin resistance, hsa04066: HIF-1 signalling pathway, hsa01040: Biosynthesis of unsaturated fatty acids, hsa00983: Drug metabolism - other enzymes, hsa00982: Drug metabolism - cytochrome P450, hsa00260: Glycine, serine and threonine metabolism, hsa00270: Cysteine and methionine metabolism, hsa00980: Metabolism of xenobiotics by cytochrome P450, hsa01524: Platinum drug resistance, hsa05206: MicroRNAs in cancer, hsa04024: cAMP signalling pathway, hsa00592: alpha-Linolenic acid metabolism, hsa00040: Pentose and glucuronate interconversions, hsa00240: Pyrimidine metabolism, hsa04973: Carbohydrate digestion and absorption, hsa00410: beta-Alanine metabolism</p>

BIBLIOGRAPHY

1. Warburg O. On the origin of cancer cells. *Science*. 1956;123(3191):309-14. DOI:10.1126/science.123.3191.309.
2. Wise DR, DeBerardinis RJ, Mancuso A, Sayed N, Zhang XY, Pfeiffer HK, et al. Myc regulates a transcriptional program that stimulates mitochondrial glutaminolysis and leads to glutamine addiction. *Proc. Natl. Acad. Sci. U S A*. 2008;105(48):18782-7. DOI:10.1073/pnas.0810199105.
3. Hanahan D, Weinberg RA. Hallmarks of cancer: the next generation. *Cell*. 2011;144(5):646-74. DOI:10.1016/j.cell.2011.02.013.
4. Seyfried TN, Shelton LM. Cancer as a metabolic disease. *Nutr. Metab.* 2010;7(1):7. DOI:10.1186/1743-7075-7-7.
5. Vander Heiden MG, Cantley LC, Thompson CB. Understanding the Warburg effect: the metabolic requirements of cell proliferation. *Science*. 2009;324(5930):1029-33. DOI:10.1126/science.1160809.
6. Ng HK, Lam PY. The molecular genetics of central nervous system tumors. *Pathology*. 1998;30(2):196-202. DOI:10.1080/00313029800169236.
7. Rajesh Y, Pal I, Banik P, Chakraborty S, Borkar SA, Dey G, et al. Insights into molecular therapy of glioma: current challenges and next generation blueprint. *Acta Pharmacol. Sin.* 2017;38(5):591-613. DOI:10.1038/aps.2016.167.
8. Zhou B, Zuo Y-X, Jiang R-T. Astrocyte morphology: Diversity, plasticity, and role in neurological diseases. *CNS Neurosci. Ther.* 2019;25(6):665-73. DOI:10.1111/cns.13123.
9. Şovrea AS, Boşca AB. Astrocytes reassessment - an evolving concept part one: embryology, biology, morphology and reactivity. *J. Mol. Psychiatry*. 2013;1(1):18-. DOI:10.1186/2049-9256-1-18.
10. Jäkel S, Dimou L. Glial Cells and Their Function in the Adult Brain: A Journey through the History of Their Ablation. *Front. Cell. Neurosci.* 2017;11(24):24. DOI:10.3389/fncel.2017.00024.
11. Pellerin L, Magistretti PJ. Glutamate uptake into astrocytes stimulates aerobic glycolysis: a mechanism coupling neuronal activity to glucose utilization. *Proc. Natl. Acad. Sci. U S A*. 1994;91(22):10625-9. DOI:10.1073/pnas.91.22.10625.
12. Schousboe A, Scafidi S, Bak LK, Waagepetersen HS, McKenna MC. Glutamate metabolism in the brain focusing on astrocytes. *Adv. Neurobiol.* 2014;11:13-30. DOI:10.1007/978-3-319-08894-5_2.
13. Malarkey EB, Parpura V. Mechanisms of glutamate release from astrocytes. *Neurochem. Int.* 2008;52(1-2):142-54. DOI:10.1016/j.neuint.2007.06.005.
14. Chinnaiyan P, Kensicki E, Bloom G, Prabhu A, Sarcar B, Kahali S, et al. The metabolomic signature of malignant glioma reflects accelerated anabolic metabolism. *Cancer Res.* 2012;72(22):5878-88. DOI:10.1158/0008-5472.CAN-12-1572-T.

15. Zhou Y, Zhou Y, Shingu T, Feng L, Chen Z, Ogasawara M, et al. Metabolic alterations in highly tumorigenic glioblastoma cells: preference for hypoxia and high dependency on glycolysis. *J. Biol. Chem.* 2011;286(37):32843-53. DOI:10.1074/jbc.M111.260935.
16. Sahm F, Oezen I, Opitz CA, Radlwimmer B, von Deimling A, Ahrendt T, et al. The endogenous tryptophan metabolite and NAD⁺ precursor quinolinic acid confers resistance of gliomas to oxidative stress. *Cancer Res.* 2013;73(11):3225-34. DOI:10.1158/0008-5472.CAN-12-3831.
17. Ye Z-C, Rothstein JD, Sontheimer H. Compromised glutamate transport in human glioma cells: reduction-mislocalization of sodium-dependent glutamate transporters and enhanced activity of cystine-glutamate exchange. *J. Neurosci.* 1999;19(24):10767-77. DOI:10.1523/JNEUROSCI.19-24-10767.1999.
18. Hattingen E, Lanfermann H, Quick J, Franz K, Zanella FE, Pilatus U. 1H MR spectroscopic imaging with short and long echo time to discriminate glycine in glial tumours. *MAGMA.* 2009;22(1):33-41. DOI:10.1007/s10334-008-0145-z.
19. Chung WJ, Lyons SA, Nelson GM, Hamza H, Gladson CL, Gillespie GY, et al. Inhibition of cystine uptake disrupts the growth of primary brain tumors. *J. Neurosci.* 2005;25(31):7101-10. DOI:10.1523/JNEUROSCI.5258-04.2005.
20. Kant S, Kesarwani P, Prabhu A, Graham SF, Buelow KL, Nakano I, et al. Enhanced fatty acid oxidation provides glioblastoma cells metabolic plasticity to accommodate to its dynamic nutrient microenvironment. *Cell Death Dis.* 2020;11(4):253. DOI:10.1038/s41419-020-2449-5.
21. Dong Z, Cui H. Epigenetic modulation of metabolism in glioblastoma. *Semin. Cancer Biol.* 2019;57:45-51. DOI:10.1016/j.semcancer.2018.09.002.
22. Zhou W, Wahl DR. Metabolic Abnormalities in Glioblastoma and Metabolic Strategies to Overcome Treatment Resistance. *Cancers.* 2019;11(9). DOI:10.3390/cancers11091231.
23. Quinones A, Le A. The Multifaceted Glioblastoma: From Genomic Alterations to Metabolic Adaptations. In: Le A, editor. *The Heterogeneity of Cancer Metabolism.* Cham: Springer International Publishing; 2021. p. 59-76. DOI:10.1007/978-3-030-65768-0_4
24. Gupta MK, Polisetty RV, Sharma R, Ganesh RA, Gowda H, Purohit AK, et al. Altered transcriptional regulatory proteins in glioblastoma and YBX1 as a potential regulator of tumor invasion. *Sci. Rep.* 2019;9(1):10986. DOI:10.1038/s41598-019-47360-9.
25. Bonnet C, Thomas L, Psimaras D, Bielle F, Vauléon E, Loiseau H, et al. Characteristics of gliomas in patients with somatic IDH mosaicism. *Acta Neuropathol. Commun.* 2016;4(1):31. DOI:10.1186/s40478-016-0302-y.
26. Christensen BC, Smith AA, Zheng S, Koestler DC, Houseman EA, Marsit CJ, et al. DNA Methylation, Isocitrate Dehydrogenase Mutation, and Survival in Glioma. *J. Natl. Cancer Inst.* 2011;103(2):143-53. DOI:10.1093/jnci/djq497.

27. Romani M, Pistillo MP, Banelli B. Epigenetic Targeting of Glioblastoma. *Front. Oncol.* 2018;8(448):448. DOI:10.3389/fonc.2018.00448.
28. Syed N, Langer J, Janczar K, Singh P, Nigro CL, Lattanzio L, et al. Epigenetic status of argininosuccinate synthetase and argininosuccinate lyase modulates autophagy and cell death in glioblastoma. *Cell Death Dis.* 2013;4(1):e458-e. DOI:10.1038/cddis.2012.197.
29. Xiong M, Dong H, Siu H, Peng G, Wang Y, Jin L, editors. Genome-Wide Association Studies of Copy Number Variation in Glioblastoma. 2010 4th International Conference on Bioinformatics and Biomedical Engineering; 2010 18-20 June 2010. DOI:10.1109/ICBBE.2010.5516437
30. Graham NA, Minasyan A, Lomova A, Cass A, Balanis NG, Friedman M, et al. Recurrent patterns of DNA copy number alterations in tumors reflect metabolic selection pressures. *Mol. Syst. Biol.* 2017;13(2):914. DOI:10.15252/msb.20167159.
31. Beckner ME, Pollack IF, Nordberg ML, Hamilton RL. Glioblastomas with copy number gains in EGFR and RNF139 show increased expressions of carbonic anhydrase genes transformed by ENO1. *BBA Clinical.* 2016;5:1-15. DOI: 10.1016/j.bbacli.2015.11.001.
32. Pesenti C, Navone SE, Guarnaccia L, Terrasi A, Costanza J, Silipigni R, et al. The Genetic Landscape of Human Glioblastoma and Matched Primary Cancer Stem Cells Reveals Intratumour Similarity and Intertumour Heterogeneity. *Stem Cells Int.* 2019;2019:2617030. DOI:10.1155/2019/2617030.
33. Rodríguez-Enríquez S, Marín-Hernández Á, Gallardo-Pérez JC, Pacheco-Velázquez SC, Belmont-Díaz JA, Robledo-Cadena DX, et al. Transcriptional Regulation of Energy Metabolism in Cancer Cells. *Cells.* 2019;8(10). DOI:10.3390/cells8101225.
34. Pedroza-Torres A, Romero-Córdoba SL, Justo-Garrido M, Salido-Guadarrama I, Rodríguez-Bautista R, Montañó S, et al. MicroRNAs in Tumor Cell Metabolism: Roles and Therapeutic Opportunities. *Front. Oncol.* 2019;9(1404):1404. DOI:10.3389/fonc.2019.01404.
35. Macfarlane LA, Murphy PR. MicroRNA: Biogenesis, Function and Role in Cancer. *Curr. Genomics.* 2010;11(7):537-61. DOI:10.2174/138920210793175895.
36. Yan C, Kong X, Gong S, Liu F, Zhao Y. Recent advances of the regulation roles of MicroRNA in glioblastoma. *Int. J. Clin. Oncol.* 2020;25(7):1215-22. DOI:10.1007/s10147-020-01685-y.
37. Lou W, Ding B, Xu L, Fan W. Construction of Potential Glioblastoma Multiforme-Related miRNA-mRNA Regulatory Network. *Front. Mol. Neurosci.* 2019;12(66):66. DOI:10.3389/fnmol.2019.00066.
38. Banelli B, Forlani A, Allemanni G, Morabito A, Pistillo MP, Romani M. MicroRNA in Glioblastoma: An Overview. *Int. J. Genomics.* 2017;2017:7639084. DOI:10.1155/2017/7639084.
39. Yuan Y, Jiang YC, Sun CK, Chen QM. Role of the tumor microenvironment in tumor progression and the clinical applications (Review). *Oncol. Rep.* 2016;35(5):2499-515. DOI:10.3892/or.2016.4660.

40. Schuler R, Seebeck N, Osterhoff MA, Witte V, Floel A, Busjahn A, et al. VEGF and GLUT1 are highly heritable, inversely correlated and affected by dietary fat intake: Consequences for cognitive function in humans. *Mol. Metab.* 2018;11:129-36. DOI:10.1016/j.molmet.2018.02.004.
41. Yang CA, Huang HY, Lin CL, Chang JG. G6PD as a predictive marker for glioma risk, prognosis and chemosensitivity. *J. Neurooncol.* 2018;139(3):661-70. DOI:10.1007/s11060-018-2911-8.
42. Jin L, Zhou Y. Crucial role of the pentose phosphate pathway in malignant tumors. *Oncol Lett.* 2019;17(5):4213-21. DOI:10.3892/ol.2019.10112.
43. Duvel K, Yecies JL, Menon S, Raman P, Lipovsky AI, Souza AL, et al. Activation of a metabolic gene regulatory network downstream of mTOR complex 1. *Mol. Cell.* 2010;39(2):171-83. DOI:10.1016/j.molcel.2010.06.022.
44. Ye H, Huang H, Cao F, Chen M, Zheng X, Zhan RJ. HSPB1 enhances SIRT2-mediated G6PD activation and promotes glioma cell proliferation. *PLoS ONE.* 2016;11(10):e0164285. DOI:10.1371/journal.pone.0164285.
45. Ding J, Li T, Wang X, Zhao E, Choi JH, Yang L, et al. The histone H3 methyltransferase G9A epigenetically activates the serine-glycine synthesis pathway to sustain cancer cell survival and proliferation. *Cell Metab.* 2013;18(6):896-907. DOI:10.1016/j.cmet.2013.11.004.
46. Tarrado-Castellarnau M, de Atauri P, Cascante M. Oncogenic regulation of tumor metabolic reprogramming. *Oncotarget.* 2016;7(38):62726-53. DOI:10.18632/oncotarget.10911.
47. Maher M, Diesch J, Casquero R, Buschbeck MJ. Epigenetic-transcriptional regulation of fatty acid metabolism and its alterations in leukaemia. *Front. Genet.* 2018;9:405. DOI:10.3389/fgene.2018.00405.
48. Andrisse S, Patel GD, Chen JE, Webber AM, Spears LD, Koehler RM, et al. ATM and GLUT1-S490 phosphorylation regulate GLUT1 mediated transport in skeletal muscle. *PLoS ONE.* 2013;8(6):e66027. DOI:10.1371/journal.pone.0066027.
49. McFate T, Mohyeldin A, Lu H, Thakar J, Henriques J, Halim ND, et al. Pyruvate dehydrogenase complex activity controls metabolic and malignant phenotype in cancer cells. *J. Biol. Chem.* 2008;283(33):22700-8. DOI:10.1074/jbc.M801765200.
50. Li Z, Bao S, Wu Q, Wang H, Eyler C, Sathornsumetee S, et al. Hypoxia-inducible factors regulate tumorigenic capacity of glioma stem cells. *Cancer Cell.* 2009;15(6):501-13. DOI:10.1016/j.ccr.2009.03.018.
51. Gabriely G, Wheeler MA, Takenaka MC, Quintana FJ. Role of AHR and HIF-1 α in Glioblastoma Metabolism. *Trends Endocrin. Met.* 2017;28(6):428-36. DOI:10.1016/j.tem.2017.02.009.
52. Miska J, Lee-Chang C, Rashidi A, Muroski ME, Chang AL, Lopez-Rosas A, et al. HIF-1 α Is a Metabolic Switch between Glycolytic-Driven Migration and Oxidative Phosphorylation-Driven Immunosuppression of Tregs in Glioblastoma. *Cell Rep.* 2019;27(1):226-37.e4. DOI:10.1016/j.celrep.2019.03.029.

-
-
53. Valvona CJ, Fillmore HL, Nunn PB, Pilkington GJ. The Regulation and Function of Lactate Dehydrogenase A: Therapeutic Potential in Brain Tumor. *Brain Pathol.* 2016;26(1):3-17. DOI:10.1111/bpa.12299.
 54. Wu S, Wang H, Li Y, Xie Y, Huang C, Zhao H, et al. Transcription Factor YY1 Promotes Cell Proliferation by Directly Activating the Pentose Phosphate Pathway. *Cancer Res.* 2018;78(16):4549-62. DOI:10.1158/0008-5472.CAN-17-4047.
 55. Pikman Y, Puissant A, Alexe G, Furman A, Chen LM, Frumm SM, et al. Targeting MTHFD2 in acute myeloid leukemia. *J. Exp. Med.* 2016;213(7):1285-306. DOI:10.1084/jem.20151574.
 56. DeNicola GM, Chen P-H, Mullarky E, Sudderth JA, Hu Z, Wu D, et al. NRF2 regulates serine biosynthesis in non-small cell lung cancer. *Nat. Genet.* 2015;47(12):1475-81. DOI:10.1038/ng.3421.
 57. Hao S, Yu J, He W, Huang Q, Zhao Y, Liang B, et al. Cysteine Dioxygenase 1 Mediates Erastin-Induced Ferroptosis in Human Gastric Cancer Cells. *Neoplasia.* 2017;19(12):1022-32. DOI:10.1016/j.neo.2017.10.005.
 58. Harami-Papp H, Pongor LS, Munkácsy G, Horváth G, Nagy ÁM, Ambrus A, et al. TP53 mutation hits energy metabolism and increases glycolysis in breast cancer. *Oncotarget.* 2016;7(41):67183. DOI:10.18632/oncotarget.11594.
 59. Csibi A, Fendt S-M, Li C, Pouligiannis G, Choo AY, Chapski DJ, et al. The mTORC1 pathway stimulates glutamine metabolism and cell proliferation by repressing SIRT4. *Cell.* 2013;153(4):840-54. DOI:10.1016/j.cell.2013.04.023.
 60. Minchenko O, Garmash I, Minchenko D, Kuznetsova A, Ratushna OJTUBJ. Inhibition of IRE1 modifies hypoxic regulation of G6PD, GPI, TKT, TALDO1, PGLS and RPIA genes expression in U87 glioma cells. *Ukr. Biochem. J.* 2017;89(89,Nº 1):38-49. DOI:10.15407/ubj89.01.038.
 61. Zhu Z, Du S, Du Y, Ren J, Ying G, Yan Z. Glutathione reductase mediates drug resistance in glioblastoma cells by regulating redox homeostasis. *J. Neurochem.* 2018;144(1):93-104. DOI:10.1111/jnc.14250.
 62. Yang HC, Wu YH, Yen WC, Liu HY, Hwang TL, Stern A, et al. The Redox Role of G6PD in Cell Growth, Cell Death, and Cancer. *Cells.* 2019;8(9). DOI:10.3390/cells8091055.
 63. Hansen LJ, Sun R, Yang R, Singh SX, Chen LH, Pirozzi CJ, et al. MTAP Loss Promotes Stemness in Glioblastoma and Confers Unique Susceptibility to Purine Starvation. *Cancer Res.* 2019;79(13):3383-94. DOI:10.1158/0008-5472.CAN-18-1010.
 64. Yan H, Parsons DW, Jin G, McLendon R, Rasheed BA, Yuan W, et al. IDH1 and IDH2 mutations in gliomas. *N. Engl. J. Med.* 2009;360(8):765-73. DOI:10.1056/NEJMoa0808710.
 65. Reitman ZJ, Yan H. Isocitrate Dehydrogenase 1 and 2 Mutations in Cancer: Alterations at a Crossroads of Cellular Metabolism. *J. Natl. Cancer Inst.* 2010;102(13):932-41. DOI:10.1093/jnci/djq187.
 66. Lloyd RE, Keatley K, Littlewood DTJ, Meunier B, Holt WV, An Q, et al. Identification and functional prediction of mitochondrial complex III and IV mutations associated

-
-
- with glioblastoma. *Neuro. Oncol.* 2015;17(7):942-52. DOI:10.1093/neuonc/nov020.
67. DeHaan C, Habibi-Nazhad B, Yan E, Salloum N, Parliament M, Allalunis-Turner J. Mutation in mitochondrial complex I ND6 subunit is associated with defective response to hypoxia in human glioma cells. *Mol. Cancer.* 2004;3:19. DOI:10.1186/1476-4598-3-19.
68. Locasale JW, Grassian AR, Melman T, Lyssiotis CA, Mattaini KR, Bass AJ, et al. Phosphoglycerate dehydrogenase diverts glycolytic flux and contributes to oncogenesis. *Nat. Genet.* 2011;43(9):869-74. DOI:10.1038/ng.890.
69. Agarwal P, Pajor MJ, Anson DM, Guda MR, Labak CM, Tsung AJ, et al. Elucidating immunometabolic targets in glioblastoma. *Am. J. Cancer Res.* 2017;7(10):1990. Available at: <http://ajcr.us/files/ajcr0065146.pdf>.
70. Bhowmick R, Ganguli P, Sarkar RR. T-Cell Activation and Differentiation: Role of Signaling and Metabolic Cross-Talk. *Syst. Synth. Immunol.*: Springer; 2020. p. 153-82. DOI:10.1007/978-981-15-3350-1_6.
71. Geiger R, Rieckmann JC, Wolf T, Basso C, Feng Y, Fuhrer T, et al. L-arginine modulates T cell metabolism and enhances survival and anti-tumor activity. *Cell.* 2016;167(3):829-42. e13. DOI:10.1016/j.cell.2016.09.031.
72. Kesarwani P, Kant S, Prabhu A, Chinnaiyan P. The interplay between metabolic remodeling and immune regulation in glioblastoma. *J. Neurooncol.* 2017;19(10):1308-15. DOI:10.1093/neuonc/nox079.
73. Zhang J, Stevens MF, Bradshaw TD. Temozolomide: mechanisms of action, repair and resistance. *Curr. Mol. Pharmacol.* 2012;5(1):102-14. DOI:10.2174/1874467211205010102.
74. Piao Y, Liang J, Holmes L, Henry V, Sulman E, de Groot JF. Acquired resistance to anti-VEGF therapy in glioblastoma is associated with a mesenchymal transition. *J. Clin. Can. Res.* 2013;19(16):4392-403. DOI:10.1158/1078-0432.CCR-12-1557.
75. Miranda-Gonçalves V, Cardoso-Carneiro D, Valbom I, Cury FP, Silva VA, Granja S, et al. Metabolic alterations underlying Bevacizumab therapy in glioblastoma cells. *J. Oncotarget.* 2017;8(61):103657. DOI:10.18632/oncotarget.21761.
76. Gunther J, Dabritz J, Wirthgen E. Limitations and Off-Target Effects of Tryptophan-Related IDO Inhibitors in Cancer Treatment. *Front. Immunol.* 2019;10:1801. DOI:10.3389/fimmu.2019.01801.
77. Tanaka K, Sasayama T, Kohmura EJO. Targeting glutaminase and mTOR. *Oncotarget.* 2015;6(29):26544. DOI:10.18632/oncotarget.5263.
78. St-Coeur PD, Poitras JJ, Cuperlovic-Culf M, Touaibia M, Morin P, Jr. Investigating a signature of temozolomide resistance in GBM cell lines using metabolomics. *J. Neurooncol.* 2015;125(1):91-102. DOI:10.1007/s11060-015-1899-6.
79. Grombacher T, Mitra S, Kaina BJC. Induction of the alkyltransferase (MGMT) gene by DNA damaging agents and the glucocorticoid dexamethasone and comparison with the response of base excision repair genes. *Carcinogenesis.* 1996;17(11):2329-36. DOI:10.1093/carcin/17.11.2329.
-
-

-
-
80. Dolan ME, Pegg AE. O6-benzylguanine and its role in chemotherapy. *Clin. Cancer Res.* 1997;3(6):837-47. Available at: <https://clincancerres.aacrjournals.org/content/clincanres/3/6/837.full.pdf>.
 81. Dolan ME, Moschel RC, Pegg AE. Depletion of mammalian O6-alkylguanine-DNA alkyltransferase activity by O6-benzylguanine provides a means to evaluate the role of this protein in protection against carcinogenic and therapeutic alkylating agents. *Proc. Natl. Acad. Sci. U S A.* 1990;87(14):5368-72. DOI:10.1073/pnas.87.14.5368.
 82. Silber JR, Bobola MS, Blank A, Schoeler KD, Haroldson PD, Huynh MB, et al. The apurinic/apyrimidinic endonuclease activity of Ape1/Ref-1 contributes to human glioma cell resistance to alkylating agents and is elevated by oxidative stress. *J. Clin. Can. Res.* 2002;8(9):3008-18. Available at: http://depts.washington.edu/loeblabs/pdf/2002_Silber.pdf.
 83. Bobola MS, Emond MJ, Blank A, Meade EH, Kolstoe DD, Berger MS, et al. Apurinic endonuclease activity in adult gliomas and time to tumor progression after alkylating agent-based chemotherapy and after radiotherapy. *Clin. Cancer Res.* 2004;10(23):7875-83. DOI:10.1158/1078-0432.CCR-04-1161.
 84. Gamcsik MP, Kasibhatla MS, Teeter SD, Colvin OMJB. Glutathione levels in human tumors. *Biomarkers.* 2012;17(8):671-91. DOI:10.3109/1354750X.2012.715672.
 85. Bansal A, Simon MC. Glutathione metabolism in cancer progression and treatment resistance. *J. Cell Biol.* 2018;217(7):2291-8. DOI:10.1083/jcb.201804161.
 86. Westerhoff HV, Palsson BO. The evolution of molecular biology into systems biology. *Nat. Biotechnol.* 2004;22(10):1249-52. DOI:10.1038/nbt1020.
 87. Price ND, Reed JL, Palsson BØJNRM. Genome-scale models of microbial cells: evaluating the consequences of constraints. *Nat. Rev. Microbiol.* 2004;2(11):886. DOI:10.1038/nrmicro1023.
 88. Blazier AS, Papin JAJFip. Integration of expression data in genome-scale metabolic network reconstructions. *Front. Physiol.* 2012;3:299. DOI:10.3389/fphys.2012.00299.
 89. Orth JD, Palsson BØJB, bioengineering. Systematizing the generation of missing metabolic knowledge. *Biotechnol. Bioeng.* 2010;107(3):403-12. DOI:10.1002/bit.22844.
 90. O'Brien EJ, Monk JM, Palsson BO. Using genome-scale models to predict biological capabilities. *Cell.* 2015;161(5):971-87. DOI:10.1016/j.cell.2015.05.019.
 91. Bordbar A, Monk JM, King ZA, Palsson BOJNRG. Constraint-based models predict metabolic and associated cellular functions. *Nat. Rev. Genet.* 2014;15(2):107-20. DOI:10.1038/nrg3643.
 92. Patil KR, Nielsen J. Uncovering transcriptional regulation of metabolism by using metabolic network topology. *Proc. Natl. Acad. Sci. U S A.* 2005;102(8):2685-9. DOI:10.1073/pnas.0406811102.
 93. AbuOun M, Suthers PF, Jones GI, Carter BR, Saunders MP, Maranas CD, et al. Genome scale reconstruction of a salmonella metabolic model comparison of similarity and

- differences with a commensal *Escherichia coli* strain. *J. Biol. Chem.* 2009;284(43):29480-8. DOI:10.1074/jbc.M109.005868.
94. Pharkya P, Burgard AP, Maranas CDJGr. OptStrain: a computational framework for redesign of microbial production systems. *Genome Res.* 2004;14(11):2367-76. DOI:10.1101/gr.2872004.
 95. Pharkya P, Maranas CDJMe. An optimization framework for identifying reaction activation/inhibition or elimination candidates for overproduction in microbial systems. *Metab. Eng.* 2006;8(1):1-13. DOI:10.1016/j.ymben.2005.08.003.
 96. Förster J, Famili I, Fu P, Palsson BØ, Nielsen J. Genome-scale reconstruction of the *Saccharomyces cerevisiae* metabolic network. *Genome Res.* 2003;13(2):244-53. DOI:10.1101/gr.234503.
 97. Becker SA, Palsson BO. Context-specific metabolic networks are consistent with experiments. *PLoS Comput. Biol.* 2008;4(5):e1000082. DOI:10.1371/journal.pcbi.1000082.
 98. Orth JD, Thiele I, Palsson BØ. What is flux balance analysis? *Nat. Biotechnol.* 2010;28(3):245. DOI:10.1038/nbt.1614.
 99. Papoutsakis ET. Equations and calculations for fermentations of butyric acid bacteria. *Biotechnol. Bioeng.* 1984;26(2):174-87. DOI:10.1002/bit.260260210.
 100. Fell DA, Small JR. Fat synthesis in adipose tissue. An examination of stoichiometric constraints. *Biochem. J.* 1986;238(3):781-6. DOI:10.1042/bj2380781.
 101. Majewski R, Domach M. Simple constrained-optimization view of acetate overflow in *E. coli*. *Biotechnol. Bioeng.* 1990;35(7):732-8. DOI:10.1002/bit.260350711.
 102. Savinell JM, Palsson BO. Network analysis of intermediary metabolism using linear optimization. I. Development of mathematical formalism. *J. Theor. Biol.* 1992;154(4):421-54. DOI:10.1016/s0022-5193(05)80161-4.
 103. Varma A, Palsson BO. Stoichiometric flux balance models quantitatively predict growth and metabolic by-product secretion in wild-type *Escherichia coli* W3110. *Appl. Environ. Microbiol.* 1994;60(10):3724-31. DOI:10.1128/aem.60.10.3724-3731.1994.
 104. Pramanik J, Keasling J. Stoichiometric model of *Escherichia coli* metabolism: incorporation of growth-rate dependent biomass composition and mechanistic energy requirements. *Biotechnol. Bioeng.* 1997;56(4):398-421. DOI:10.1002/(SICI)1097-0290(19971120)56:4<398::AID-BIT6>3.0.CO;2-J.
 105. Pfeiffer T, Sánchez-Valdenebro I, Nuñez J, Montero F, Schuster S. METATOOL: for studying metabolic networks. *Bioinformatics.* 1999;15(3):251-7. DOI:10.1093/bioinformatics/15.3.251.
 106. Covert MW, Schilling CH, Palsson B. Regulation of gene expression in flux balance models of metabolism. *J. Theor. Biol.* 2001;213(1):73-88. DOI:10.1006/jtbi.2001.2405.
 107. Segre D, Vitkup D, Church GM. Analysis of optimality in natural and perturbed metabolic networks. *Proc. Natl. Acad. Sci. U S A.* 2002;99(23):15112-7. DOI:10.1073/pnas.232349399.

-
-
108. Shlomi T, Berkman O, Ruppin E. Regulatory on/off minimization of metabolic flux changes after genetic perturbations. *Proc. Natl. Acad. Sci. U S A.* 2005;102(21):7695-700. DOI:10.1073/pnas.0406346102.
 109. Sauer U. Metabolic networks in motion: 13 C-based flux analysis. *Mol. Syst. Biol.* 2006;2(1):62. DOI:10.1038/msb4100109.
 110. Shlomi T, Eisenberg Y, Sharan R, Ruppin E. A genome-scale computational study of the interplay between transcriptional regulation and metabolism. *Mol. Syst. Biol.* 2007;3(1):101. DOI:10.1038/msb4100141.
 111. Folger O, Jerby L, Frezza C, Gottlieb E, Ruppin E, Shlomi T. Predicting selective drug targets in cancer through metabolic networks. *Mol. Syst. Biol.* 2011;7(1):501. DOI:10.1038/msb.2011.35.
 112. Schuetz R, Zamboni N, Zampieri M, Heinemann M, Sauer U. Multidimensional optimality of microbial metabolism. *Science.* 2012;336(6081):601-4. DOI:10.1126/science.1216882.
 113. Uhlen M, Zhang C, Lee S, Sjöstedt E, Fagerberg L, Bidkhori G, et al. A pathology atlas of the human cancer transcriptome. *Science.* 2017;357(6352):eaan2507. DOI:10.1126/science.aan2507.
 114. Mahadevan R, Edwards JS, Doyle FJ, 3rd. Dynamic flux balance analysis of diauxic growth in *Escherichia coli*. *Biophys. J.* 2002;83(3):1331-40. DOI:10.1016/s0006-3495(02)73903-9.
 115. Covert MW, Xiao N, Chen TJ, Karr JR. Integrating metabolic, transcriptional regulatory and signal transduction models in *Escherichia coli*. *Bioinformatics.* 2008;24(18):2044-50. DOI:10.1093/bioinformatics/btn352.
 116. Becker SA, Feist AM, Mo ML, Hannum G, Palsson BO, Herrgard MJ. Quantitative prediction of cellular metabolism with constraint-based models: the COBRA Toolbox. *Nat. Protoc.* 2007;2(3):727-38. DOI:10.1038/nprot.2007.99.
 117. Ebrahim A, Lerman JA, Palsson BO, Hyduke DRJBSb. COBRApy: constraints-based reconstruction and analysis for python. *BMC Syst. Biol.* 2013;7(1):74. DOI:10.1186/1752-0509-7-74.
 118. Steffensen JL, Dufault-Thompson K, Zhang YJPcb. PSAMM: a portable system for the analysis of metabolic models. *PLoS Comput. Biol.* 2016;12(2):e1004732. DOI:10.1371/journal.pcbi.1004732.
 119. Rocha I, Maia P, Evangelista P, Vilaça P, Soares S, Pinto JP, et al. OptFlux: an open-source software platform for in silico metabolic engineering. *BMC Syst. Biol.* 2010;4(1):45. DOI:10.1186/1752-0509-4-45.
 120. Grafahrend-Belau E, Klukas C, Junker BH, Schreiber FJB. FBA-SimVis: interactive visualization of constraint-based metabolic models. *Bioinformatics.* 2009;25(20):2755-7. DOI:10.1093/bioinformatics/btp408.
 121. König M, Holzhütter H-G. Fluxviz—Cytoscape plug-in for visualization of flux distributions in networks. *Genome Informatics 2010: Genome Informatics Series Vol 24: World Scientific; 2010.* p. 96-103. DOI:10.1142/9781848166585_0008.

-
-
122. Marmiesse L, Peyraud R, Cottret LJBsb. FlexFlux: combining metabolic flux and regulatory network analyses. *BMC Syst. Biol.* 2015;9(1):93. DOI:10.1186/s12918-015-0238-z.
 123. Kirchmair J, Williamson MJ, Afzal AM, Tyzack JD, Choy AP, Howlett A, et al. FAST METabolizer (FAME): A rapid and accurate predictor of sites of metabolism in multiple species by endogenous enzymes. *J. Chem. Inf. Model.* 2013;53(11):2896-907. DOI:10.1021/ci400503s.
 124. Greenspan H. On the growth and stability of cell cultures and solid tumors. *J. Theor. Biol.* 1976;56(1):229-42. DOI:10.1016/s0022-5193(76)80054-9.
 125. Vaidya VG, Alexandro FJ. Evaluation of some mathematical models for tumor growth. *Int. J. Biomed. Comp.* 1982;13(1):19-35. DOI:10.1016/0020-7101(82)90048-4.
 126. Fowler JF. The linear-quadratic formula and progress in fractionated radiotherapy. *Br. J. Radiol.* 1989;62(740):679-94. DOI:10.1259/0007-1285-62-740-679.
 127. Chaplain M, Sleeman B. Modelling the growth of solid tumours and incorporating a method for their classification using nonlinear elasticity theory. *J. Math. Biol.* 1993;31(5):431-73. DOI:10.1007/BF00173886.
 128. Marušić M, Vuk-Pavlovic S, Freyer JP. Tumor growth in vivo and as multicellular spheroids compared by mathematical models. *Bull. Math. Biol.* 1994;56(4):617-31. DOI:10.1007/BF02460714.
 129. Tracqui P, Cruywagen G, Woodward D, Bartoo G, Murray J, Alvord E. A mathematical model of glioma growth: the effect of chemotherapy on spatio-temporal growth. *Cell Prolif.* 1995;28(1):17-31. DOI:10.1111/j.1365-2184.1995.tb00036.x.
 130. Woodward Diw, Cook J, Tracqui P, Cruywagen G, Murray J, Alvord E. A mathematical model of glioma growth: the effect of extent of surgical resection. *Cell Prolif.* 1996;29(6):269-88. DOI:10.1111/j.1365-2184.1996.tb01580.x.
 131. Burgess PK, Kulesa PM, Murray JD, Alvord Jr EC. The interaction of growth rates and diffusion coefficients in a three-dimensional mathematical model of gliomas. *Journal of Neuropathology & Experimental Neurology.* 1997;56(6):704-13. DOI:10.1097/00005072-199756060-00008.
 132. Orme M, Chaplain MA. Two-dimensional models of tumour angiogenesis and anti-angiogenesis strategies. *Math. Med. Biol.* 1997;14(3):189-205. DOI:10.1093/IMAMMB/14.3.189.
 133. Swanson KR, Alvord E, Murray J. A quantitative model for differential motility of gliomas in grey and white matter. *Cell Prolif.* 2000;33(5):317-29. DOI:10.1046/j.1365-2184.2000.00177.x.
 134. Swanson KR, Bridge C, Murray J, Alvord EC. Virtual and real brain tumors: using mathematical modeling to quantify glioma growth and invasion. *J. Neurol. Sci.* 2003;216(1):1-10. DOI:10.1016/j.jns.2003.06.001.
 135. Mansury Y, Kimura M, Lobo J, Deisboeck TS. Emerging patterns in tumor systems: simulating the dynamics of multicellular clusters with an agent-based spatial

-
-
- agglomeration model. *J. Theor. Biol.* 2002;219(3):343-70. DOI:10.1006/jtbi.2002.3131.
136. Gatenby RA, Vincent TL. An evolutionary model of carcinogenesis. *Cancer Res.* 2003;63(19):6212-20. Available at: <https://cancerres.aacrjournals.org/content/63/19/6212.long>.
137. Alarcón T, Byrne HM, Maini PK. A cellular automaton model for tumour growth in inhomogeneous environment. *J. Theor. Biol.* 2003;225(2):257-74. DOI:10.1016/S0022-5193(03)00244-3.
138. Plank M, Sleeman B. Lattice and non-lattice models of tumour angiogenesis. *Bull. Math. Biol.* 2004;66(6):1785-819. DOI:10.1016/j.bulm.2004.04.001.
139. Wu JT, Kirn DH, Wein LM. Analysis of a three-way race between tumor growth, a replication-competent virus and an immune response. *Bull. Math. Biol.* 2004;66(4):605-25. DOI:10.1016/J.BULM.2003.08.016.
140. Norton L. Conceptual and practical implications of breast tissue geometry: toward a more effective, less toxic therapy. *Oncologist.* 2005;10(6):370-81. DOI:10.1634/theoncologist.10-6-370.
141. Castiglione F, Toschi F, Bernaschi M, Succi S, Benedetti R, Falini B, et al. Computational modeling of the immune response to tumor antigens. *J. Theor. Biol.* 2005;237(4):390-400. DOI:10.1016/j.jtbi.2005.04.024.
142. Zheng X, Wise S, Cristini V. Nonlinear simulation of tumor necrosis, neo-vascularization and tissue invasion via an adaptive finite-element/level-set method. *Bull. Math. Biol.* 2005;67(2):211-59. DOI:10.1016/j.bulm.2004.08.001.
143. Clatz O, Sermesant M, Bondiau P-Y, Delingette H, Warfield SK, Malandain G, et al. Realistic simulation of the 3-D growth of brain tumors in MR images coupling diffusion with biomechanical deformation. *IEEE Trans. Med. Imaging.* 2005;24(10):1334-46. DOI:10.1109/TMI.2005.857217.
144. Athale C, Mansury Y, Deisboeck TS. Simulating the impact of a molecular 'decision-process' on cellular phenotype and multicellular patterns in brain tumors. *J. Theor. Biol.* 2005;233(4):469-81. DOI:10.1016/j.jtbi.2004.10.019.
145. Lowengrub JS, Frieboes HB, Jin F, Chuang Y-L, Li X, Macklin P, et al. Nonlinear modelling of cancer: bridging the gap between cells and tumours. *Nonlinearity.* 2009;23(1):R1-R9. DOI:10.1088/0951-7715/23/1/R01.
146. Marín-Hernández A, Gallardo-Pérez JC, Rodríguez-Enríquez S, Encalada R, Moreno-Sánchez R, Saavedra E. Modeling cancer glycolysis. *BBA-Bioenergetics.* 2011;1807(6):755-67. DOI:10.1016/j.bbabi.2010.11.006.
147. Molina-Peña R, Álvarez MM. A simple mathematical model based on the cancer stem cell hypothesis suggests kinetic commonalities in solid tumor growth. *PLoS ONE.* 2012;7(2):e26233. DOI:10.1371/journal.pone.0026233.
148. Palsson BØ. *Systems biology: properties of reconstructed networks*: Cambridge university press; 2006. DOI:10.1017/cbo9780511790515.
-
-

-
-
149. Beguerisse-Díaz M, Bosque G, Oyarzún D, Picó J, Barahona M. Flux-dependent graphs for metabolic networks. *NPJ Syst. Biol. Appl.* 2018;4(1):32. DOI:10.1038/s41540-018-0067-y.
 150. Winterbach W, Mieghem PV, Reinders M, Wang H, Ridder Dd. Topology of molecular interaction networks. *BMC Syst. Biol.* 2013;7(1):90. DOI:10.1186/1752-0509-7-90.
 151. Wagner A, Fell DA. The small world inside large metabolic networks. *Proc. Royal Soc. B: Biol. Sci.* 2001;268(1478):1803-10. DOI:10.1098/rspb.2001.1711.
 152. Sauer U, Lasko DR, Fiaux J, Hochuli M, Glaser R, Szyperski T, et al. Metabolic flux ratio analysis of genetic and environmental modulations of *Escherichia coli* central carbon metabolism. *J. Bacteriol.* 1999;181(21):6679-88. DOI:10.1128/jb.181.21.6679-6688.1999.
 153. Raman K, Damaraju N, Joshi GK. The organisational structure of protein networks: revisiting the centrality-lethality hypothesis. *Syst. Synth. Biol.* 2014;8(1):73-81. DOI:10.1007/s11693-013-9123-5.
 154. Koschützki D, Junker BH, Schwender J, Schreiber F. Structural analysis of metabolic networks based on flux centrality. *J. Theor. Biol.* 2010;265(3):261-9. DOI: 10.1016/j.jtbi.2010.05.009.
 155. Galadari S, Rahman A, Pallichankandy S, Thayyullathil F. Reactive oxygen species and cancer paradox: to promote or to suppress? *Free Rad. Biol. Med.* 2017;104:144-64. DOI:10.1016/j.freeradbiomed.2017.01.004.
 156. Zitka O, Skalickova S, Gumulec J, Masarik M, Adam V, Hubalek J, et al. Redox status expressed as GSH: GSSG ratio as a marker for oxidative stress in paediatric tumour patients. *Oncol. Lett.* 2012;4(6):1247-53. DOI:10.3892/OL.2012.931.
 157. Hosios AM, Vander Heiden MG. The redox requirements of proliferating mammalian cells. *J. Biol. Chem.* 2018;293(20):7490-8. DOI:10.1074/jbc.TM117.000239.
 158. Halliwell B. The antioxidant paradox. *Lancet.* 2000;355(9210):1179-80. DOI:10.1016/S0140-6736(00)02075-4.
 159. Park JH, Pyun WY, Park HW. Cancer Metabolism: Phenotype, Signaling and Therapeutic Targets. *Cells.* 2020;9(10). DOI:10.3390/cells9102308.
 160. Ahir BK, Engelhard HH, Lakka SS. Tumor Development and Angiogenesis in Adult Brain Tumor: Glioblastoma. *Mol. Neurobiol.* 2020;57(5):2461-78. DOI:10.1007/s12035-020-01892-8.
 161. Wang X, Lu J, Guo G, Yu J. Immunotherapy for recurrent glioblastoma: practical insights and challenging prospects. *Cell Death Dis.* 2021;12(4):299. DOI:10.1038/s41419-021-03568-0.
 162. Bairoch A. The ENZYME database in 2000. *Nucleic Acids Res.* 2000;28(1):304-5. DOI:10.1093/nar/28.1.304.
 163. Kanehisa M, Goto S, Sato Y, Kawashima M, Furumichi M, Tanabe M. Data, information, knowledge and principle: back to metabolism in KEGG. *Nucleic Acids Res.* 2014;42(D1):D199-D205. DOI:10.1093/nar/gkt1076.

-
-
164. Brown G, Wallin C, Tatusova T, Pruitt K, Maglott D. Gene Help: Integrated Access to Genes of Genomes in the Reference Sequence Collection. 2014.
 165. Consortium U. Activities at the universal protein resource (UniProt). *Nucleic Acids Res.* 2014;42(D1):D191-D8. DOI:10.1093/nar/gkt1140.
 166. Schellenberger J, Que R, Fleming RM, Thiele I, Orth JD, Feist AM, et al. Quantitative prediction of cellular metabolism with constraint-based models: the COBRA Toolbox v2.0. *Nat. Protoc.* 2011;6(9):1290-307. DOI:10.1038/nprot.2011.308.
 167. van Veelen CW, Verbiest H, Zülch KJ, van Ketel BA, van der Vlist MJ, Vlug AM, et al. l- α -Alanine inhibition of pyruvate kinase from tumors of the human central nervous system. *Cancer Res.* 1979;39(10):4263-9. DOI:10.1007/978-3-662-08801-2_14.
 168. Berge K. Impact of mitochondrial beta-oxidation in fatty acid-mediated inhibition of glioma cell proliferation. *J. Lipid Res.* 2002;44(1):118-27. DOI:10.1194/jlr.M200312-JLR200.
 169. Wise DR, Thompson CB. Glutamine addiction: a new therapeutic target in cancer. *Trends Biochem. Sci.* 2010;35(8):427-33. DOI:10.1016/j.tibs.2010.05.003.
 170. Ogunrinu TA, Sontheimer H. Hypoxia increases the dependence of glioma cells on glutathione. *J. Biol. Chem.* 2010;285(48):37716-24. DOI:10.1074/jbc.M110.161190.
 171. Hayashi F, Takahashi K, Nishikawa T. Uptake of D- and L-serine in C6 glioma cells. *Neurosci. Lett.* 1997;239(2):85-8. DOI:10.1016/S0304-3940(97)00892-6.
 172. Wolf A, Agnihotri S, Guha A. Targeting metabolic remodeling in glioblastoma multiforme. *Oncotarget.* 2010;1(7):567. DOI:10.18632/oncotarget.190.
 173. Fiskerstrand T, Christensen B, Tysnes OB, Ueland PM, Refsum H. Development and reversion of methionine dependence in a human glioma cell line: relation to homocysteine remethylation and cobalamin status. *Cancer Res.* 1994;54(18):4899-906. Available at: <https://cancerres.aacrjournals.org/content/54/18/4899.long>.
 174. Feichtinger RG, Weis S, Mayr JA, Zimmermann F, Geilberger R, Sperl W, et al. Alterations of oxidative phosphorylation complexes in astrocytomas. *Glia.* 2014;62(4):514-25. DOI:10.1002/glia.22621.
 175. Kathagen A, Schulte A, Balcke G, Phillips HS, Martens T, Matschke J, et al. Hypoxia and oxygenation induce a metabolic switch between pentose phosphate pathway and glycolysis in glioma stem-like cells. *Acta neuropathol.* 2013;126(5):763-80. DOI:10.1007/s00401-013-1173-y.
 176. Jurchott K, Guo KT, Catchpole G, Feher K, Willmitzer L, Schichor C, et al. Comparison of metabolite profiles in U87 glioma cells and mesenchymal stem cells. *BioSystems.* 2011;105(2):130-9. DOI:10.1016/j.biosystems.2011.05.005.
 177. Lee JM, Gianchandani EP, Papin JA. Flux balance analysis in the era of metabolomics. *Brief. Bioinformatics.* 2006;7(2):140-50. DOI:10.1093/bib/bbl007.
 178. Pistollato F, Abbadi S, Rampazzo E, Viola G, Della Puppa A, Cavallini L, et al. Hypoxia and succinate antagonize 2-deoxyglucose effects on glioblastoma. *Biochem. Pharmacol.* 2010;80(10):1517-27. DOI:10.1016/j.bcp.2010.08.003.

-
-
179. Mangia S, Simpson IA, Vannucci SJ, Carruthers A. The in vivo neuron-to-astrocyte lactate shuttle in human brain: evidence from modeling of measured lactate levels during visual stimulation. *J. Neurochem.* 2009;109 Suppl 1:55-62. DOI:10.1111/j.1471-4159.2009.06003.x.
 180. Marrif H, Juurlink BH. Astrocytes respond to hypoxia by increasing glycolytic capacity. *J. Neurosci. Res.* 1999;57(2):255-60. DOI:10.1002/(SICI)1097-4547(19990715)57:2<255::AID-JNR11>3.0.CO;2-6.
 181. Pellerin L, Magistretti PJ. Glutamate uptake into astrocytes stimulates aerobic glycolysis: a mechanism coupling neuronal activity to glucose utilization. *Proc. Natl. Acad. Sci. U S A.* 1994;91(22):10625-9. DOI:10.1073/PNAS.91.22.10625.
 182. Hertz L, Zielke HR. Astrocytic control of glutamatergic activity: astrocytes as stars of the show. *Trends Neurosci.* 2004;27(12):735-43. DOI:10.1016/j.tins.2004.10.008.
 183. Anton K, Glod J. An Orchestrated Response To Tumor Signals By Macrophages and Mesenchymal Stem Cells Potentiates Interleukin-6 Secretion In Glioblastoma. *Cell Death Dis.* 2014;1(1). DOI:10.2478/CDTH-2014-0001.
 184. Guessous F, Alvarado-Velez M, Marcinkiewicz L, Zhang Y, Kim J, Heister S, et al. Oncogenic effects of miR-10b in glioblastoma stem cells. *J. Neurooncol.* 2013;112(2):153-63. DOI:10.1007/s11060-013-1047-0.
 185. Bhowmick R, Subramanian A, Sarkar RR. Exploring the differences in metabolic behavior of astrocyte and glioblastoma: a flux balance analysis approach. *Syst. Synth. Biol.* 2015;9(4):159-77. DOI:10.1007/s11693-015-9183-9.
 186. Mulukutla BC, Yongky A, Grimm S, Daoutidis P, Hu W-S. Multiplicity of steady states in glycolysis and shift of metabolic state in cultured mammalian cells. *PLoS ONE.* 2015;10(3):e0121561. DOI:10.1371/journal.pone.0121561.
 187. Huster D, Reichenbach A, Reichelt W. The glutathione content of retinal Müller (glial) cells: effect of pathological conditions. *Neurochem. Int.* 2000;36(4-5):461-9. DOI:10.1016/S0197-0186(99)00149-7.
 188. Haario H, Laine M, Mira A, Saksman E. DRAM: Efficient adaptive MCMC. *Stat. Comp.* 2006;16(4):339-54. DOI:10.1007/s11222-006-9438-0.
 189. Ye ZC, Sontheimer H. Glioma cells release excitotoxic concentrations of glutamate. *Cancer Res.* 1999;59(17):4383-91. Available at: <https://cancerres.aacrjournals.org/content/canres/59/17/4383.full.pdf>.
 190. Marino S, Hogue IB, Ray CJ, Kirschner DE. A methodology for performing global uncertainty and sensitivity analysis in systems biology. *J. Theor. Biol.* 2008;254(1):178-96. DOI:10.1016/j.jtbi.2008.04.011.
 191. Shono T, Yokoyama N, Uesaka T, Kuroda J, Takeya R, Yamasaki T, et al. Enhanced expression of NADPH oxidase Nox4 in human gliomas and its roles in cell proliferation and survival. *Int. J. Cancer.* 2008;123(4):787-92. DOI:10.1002/ijc.23569.

-
-
192. Rinaldi M, Caffo M, Minutoli L, Marini H, Abbritti R, Squadrito F, et al. ROS and brain gliomas: an overview of potential and innovative therapeutic strategies. *Int. J. Mol. Sci.* 2016;17(6):984. DOI:10.3390/ijms17060984.
 193. Zhong W, Yan T, Lim R, Oberley LW. Expression of superoxide dismutases, catalase, and glutathione peroxidase in glioma cells. *Free Rad. Biol. Med.* 1999;27(11-12):1334-45. DOI:10.1016/s0891-5849(99)00181-1.
 194. Dokic I, Hartmann C, Herold-Mende C, Régnier-Vigouroux A. Glutathione peroxidase 1 activity dictates the sensitivity of glioblastoma cells to oxidative stress. *Glia.* 2012;60(11):1785-800. DOI:10.1002/glia.22397.
 195. Zhu Z, Du S, Du Y, Ren J, Ying G, Yan Z. Glutathione reductase mediates drug resistance in glioblastoma cells by regulating redox homeostasis. *J. Neurochem.* 2018;144(1):93-104. DOI:10.1111/jnc.14250.
 196. Szatrowski TP, Nathan CF. Production of large amounts of hydrogen peroxide by human tumor cells. *Cancer Res.* 1991;51(3):794-8. Available at: <https://cancerres.aacrjournals.org/content/canres/51/3/794.full.pdf>.
 197. Zhang H, Kong X, Kang J, Su J, Li Y, Zhong J, et al. Oxidative stress induces parallel autophagy and mitochondria dysfunction in human glioma U251 cells. *Toxicol. Sci.* 2009;110(2):376-88. DOI:10.1093/toxsci/kfp101.
 198. Gulluoglu S, Tuysuz EC, Sahin M, Kuskucu A, Kaan Yaltirik C, Ture U, et al. Simultaneous miRNA and mRNA transcriptome profiling of glioblastoma samples reveals a novel set of OncomiR candidates and their target genes. *Brain Res.* 2018;1700:199-210. DOI:10.1016/j.brainres.2018.08.035.
 199. Barrett T, Wilhite SE, Ledoux P, Evangelista C, Kim IF, Tomashevsky M, et al. NCBI GEO: archive for functional genomics data sets—update. *Nucleic Acids Res.* 2012;41(D1):D991-D5. DOI:10.1093/nar/gks1193.
 200. Chen Y, Wang X. miRDB: an online database for prediction of functional microRNA targets. *Nucleic Acids Res.* 2019;48(D1):D127-D31. DOI:10.1093/nar/gkz757.
 201. Ritchie ME, Phipson B, Wu D, Hu Y, Law CW, Shi W, et al. Limma powers differential expression analyses for RNA-sequencing and microarray studies. *Nucleic Acids Res.* 2015;43(7):e47-e. DOI:10.1093/nar/gkv007.
 202. McCarthy DJ, Chen Y, Smyth GK. Differential expression analysis of multifactor RNA-Seq experiments with respect to biological variation. *Nucleic Acids Res.* 2012;40(10):4288-97. DOI:10.1093/nar/gks042.
 203. Szklarczyk D, Gable AL, Nastou KC, Lyon D, Kirsch R, Pyysalo S, et al. The STRING database in 2021: customizable protein–protein networks, and functional characterization of user-uploaded gene/measurement sets. *Nucleic Acids Res.* 2020;49(D1):D605-D12. DOI:10.1093/nar/gkaa1074.
 204. García-Moreno A, López-Domínguez R, Ramirez-Mena A, Pascual-Montano A, Aparicio-Puerta E, Hackenberg M, et al. GeneCodis 4: Expanding the modular enrichment analysis to regulatory elements. *bioRxiv.* 2021:2021.04.15.439962. DOI:10.1101/2021.04.15.439962.

-
-
205. Kanehisa M, Sato Y. KEGG Mapper for inferring cellular functions from protein sequences. *Protein Sci.* 2020;29(1):28-35. DOI:10.1002/pro.3711.
 206. Shannon P, Markiel A, Ozier O, Baliga NS, Wang JT, Ramage D, et al. Cytoscape: a software environment for integrated models of biomolecular interaction networks. *Genome Res.* 2003;13(11):2498-504. DOI:10.1101/gr.1239303.
 207. Carlin DE, Demchak B, Pratt D, Sage E, Ideker T. Network propagation in the cytoscape cyberinfrastructure. *PLoS Comput. Biol.* 2017;13(10):e1005598. DOI:10.1371/journal.pcbi.1005598.
 208. Bastian M, Heymann S, Jacomy M, editors. Gephi: an open source software for exploring and manipulating networks. *Proceedings of the International AAAI Conference on Web and Social Media*; 2009
 209. Csardi G, Nepusz T. The igraph software package for complex network research. *Int. J. Complex Syst.* 2006;1695(5):1-9. Available at: <https://www.semanticscholar.org>
 210. Gustavsen JA, Pai S, Isserlin R, Demchak B, Pico AR. RCy3: Network biology using Cytoscape from within R. *F1000Research.* 2019;8:1774. DOI:10.12688/f1000research.20887.2.
 211. Pavlopoulos GA, Kontou PI, Pavlopoulou A, Bouyioukos C, Markou E, Bagos PG. Bipartite graphs in systems biology and medicine: a survey of methods and applications. *GigaScience.* 2018;7(4):1-31. DOI:10.1093/gigascience/giy014.
 212. Domagalski R, Neal ZP, Sagan B. Backbone: An R package for extracting the backbone of bipartite projections. *PLoS ONE.* 2021;16(1):e0244363. DOI:10.1371/journal.pone.0244363.
 213. Wickham H, Averick M, Bryan J, Chang W, McGowan LDA, François R, et al. Welcome to the Tidyverse. *J. Open Source Softw.* 2019;4(43):1686. DOI:10.21105/joss.01686.
 214. Potapov AP, Goemann B, Wingender E. The pairwise disconnectivity index as a new metric for the topological analysis of regulatory networks. *BMC Bioinformatics.* 2008;9:227. DOI:10.1186/1471-2105-9-227.
 215. Katz L. A new status index derived from sociometric analysis. *Psychometrika.* 1953;18(1):39-43. DOI:10.1007/BF02289026.
 216. Sharkey KJ. A control analysis perspective on Katz centrality. *Sci Rep.* 2017;7(1):17247. DOI:10.1038/s41598-017-15426-1.
 217. Zhan J, Gurung S, Parsa SPK. Identification of top-K nodes in large networks using Katz centrality. *J. Big Data.* 2017;4(1):16. DOI:10.1186/s40537-017-0076-5.
 218. Jalili M, Salehzadeh-Yazdi A, Asgari Y, Arab SS, Yaghmaie M, Ghavamzadeh A, et al. CentiServer: A Comprehensive Resource, Web-Based Application and R Package for Centrality Analysis. *PLoS ONE.* 2015;10(11):e0143111. DOI:10.1371/journal.pone.0143111.
 219. Adams S, Teo C, McDonald KL, Zinger A, Bustamante S, Lim CK, et al. Involvement of the kynurenine pathway in human glioma pathophysiology. *PLoS ONE.* 2014;9(11):e112945. DOI:10.1371/journal.pone.0112945.

-
-
220. Mandonnet E, Pallud J, Clatz O, Taillandier L, Konukoglu E, Duffau H, et al. Computational modeling of the WHO grade II glioma dynamics: principles and applications to management paradigm. *Neurosurg. Rev.* 2008;31(3):263-9. DOI:10.1007/s10143-008-0128-6.
 221. Acker H, Carlsson J, Holtermann G, Nederman T, Nylen T. Influence of glucose and buffer capacity in the culture medium on growth and pH in spheroids of human thyroid carcinoma and human glioma origin. *Cancer Res.* 1987;47(13):3504-8.
 222. Sonnewald U, Westergaard N, Jones P, Taylor A, Bachelard H, Schousboe A. Metabolism of [U-13C5] glutamine in cultured astrocytes studied by NMR spectroscopy: First evidence of astrocytic pyruvate recycling. *J. Neurochem.* 1996;67(6):2566-72. DOI:10.1046/j.1471-4159.1996.67062566.x.
 223. Deighton RF, Le Bihan T, Martin SF, Barrios-Llerena ME, Gerth AM, Kerr LE, et al. The proteomic response in glioblastoma in young patients. *J. Neurooncol.* 2014;119(1):79-89. DOI:10.1007/s11060-014-1474-6.
 224. Roux MJ, Supplisson S. Neuronal and glial glycine transporters have different stoichiometries. *Neuron.* 2000;25(2):373-83. DOI:10.1016/S0896-6273(00)80901-0.
 225. Nicklas WJ, Browning ET. AMINO ACID METABOLISM IN GLIAL CELLS: HOMEOSTATIC REGULATION OF INTRA-and EXTRACELLULAR MILIEU BY C-6 GLIOMA CELLS. *J. Neurochem.* 1978;30(5):955-63. DOI:10.1111/j.1471-4159.1978.tb12387.x.
 226. Dringen R, Verleysdonk S, Hamprecht B, Willker W, Leibfritz D, Brand A. Metabolism of glycine in primary astroglial cells: synthesis of creatine, serine, and glutathione. *J. Neurochem.* 1998;70(2):835-40. DOI:10.1046/j.1471-4159.1998.70020835.x.
 227. Zafra F, Gimenez C. Characterization of glycine uptake in plasma membrane vesicles isolated from cultured glioblastoma cells. *Brain Res.* 1986;397(1):108-16. DOI:10.1016/0006-8993(86)91374-0.
 228. Chatterjee A, Mambo E, Sidransky D. Mitochondrial DNA mutations in human cancer. *Oncogene.* 2006;25(34):4663-74. DOI:10.1038/sj.onc.1209604.
 229. Oudard S, Arvelo F, Miccoli L, Apiou F, Dutrillaux A, Poisson M, et al. High glycolysis in gliomas despite low hexokinase transcription and activity correlated to chromosome 10 loss. *Br. J. Cancer.* 1996;74(6):839. DOI:10.1038/bjc.1996.446.
 230. Brekke E, Walls AB, Norfeldt L, Schousboe A, Waagepetersen HS, Sonnewald U. Direct measurement of backflux between oxaloacetate and fumarate following pyruvate carboxylation. *Glia.* 2012;60(1):147-58. DOI:10.1002/glia.21265.
 231. Griguer CE, Oliva CR, Gillespie GY. Glucose metabolism heterogeneity in human and mouse malignant glioma cell lines. *J. Neurooncol.* 2005;74(2):123-33. DOI:10.1007/s11060-004-6404-6.
 232. Boada J, Roig T, Perez X, Gamez A, Bartrons R, Cascante M, et al. Cells overexpressing fructose-2, 6-bisphosphatase showed enhanced pentose phosphate pathway flux and resistance to oxidative stress. *FEBS Lett.* 2000;480(2):261-4. DOI:10.1016/S0014-5793(00)01950-5.
-
-

-
-
233. Resendis-Antonio O, Checa A, Encarnación S. Modeling core metabolism in cancer cells: surveying the topology underlying the Warburg effect. *PLoS ONE*. 2010;5(8):e12383. DOI:10.1371/journal.pone.0012383.
234. Wang D-S, Mangin J-M, Moonen G, Rigo J-M, Legendre P. Mechanisms for picrotoxin block of $\alpha 2$ homomeric glycine receptors. *J. Biol. Chem.* 2006;281(7):3841-55. DOI:10.1074/jbc.M511022200.
235. García-Colunga J, Miledi R. Modulation of nicotinic acetylcholine receptors by strychnine. *Proc. Natl. Acad. Sci. U S A.* 1999;96(7):4113-8. DOI:10.1073/PNAS.96.7.4113.
236. Jursky F, Nelson N. Localization of glycine neurotransmitter transporter (GLYT2) reveals correlation with the distribution of glycine receptor. *J. Neurochem.* 1995;64(3):1026-33. DOI:10.1046/j.1471-4159.1995.64031026.x.
237. Hashimoto K. Glycine transport inhibitors for the treatment of schizophrenia. *Med. Chem. J.* 2010;4:10. DOI:10.2174/1874104501004010010.
238. Banerji A. An attempt to construct a (general) mathematical framework to model biological “context-dependence”. *Syst. Synth. Biol.* 2013;7(4):221-7. DOI:10.1007/s11693-013-9122-6.
239. Jeong H, Mason SP, Barabási A-L, Oltvai ZN. Lethality and centrality in protein networks. *Nature*. 2001;411(6833):41-2. DOI:10.1038/35075138.
240. Wang J, Yi J. Cancer cell killing via ROS: to increase or decrease, that is the question. *Cancer Biol. Ther.* 2008;7(12):1875-84. DOI:10.4161/cbt.7.12.7067.
241. Ramsey MR, Sharpless NE. ROS as a tumour suppressor? *Nat. Cell Biol.* 2006;8(11):1213-5. DOI:10.1038/ncb1106-1213.
242. Kramer RA, Zakher J, Kim G. Role of the glutathione redox cycle in acquired and de novo multidrug resistance. *Science*. 1988;241(4866):694-7. DOI:10.1126/science.3399900.
243. Kong Q, Beel J, Lillehei K. A threshold concept for cancer therapy. *Med. Hypotheses*. 2000;55(1):29-35. DOI:10.1054/mehy.1999.0982.
244. Blacker TS, Duchon MR. Investigating mitochondrial redox state using NADH and NADPH autofluorescence. *Free Rad. Biol. Med.* 2016;100:53-65. DOI:10.1016/j.freeradbiomed.2016.08.010.
245. Agledal L, Niere M, Ziegler M. The phosphate makes a difference: cellular functions of NADP. *Redox Rep.* 2010;15(1):2-10. DOI:10.1179/174329210X12650506623122.
246. Aquilano K, Baldelli S, Ciriolo MR. Glutathione: new roles in redox signaling for an old antioxidant. *Front. Pharmacol.* 2014;5:196. DOI:10.3389/fphar.2014.00196.
247. Aoyama K, Nakaki T. Impaired glutathione synthesis in neurodegeneration. *Int. J. Mol. Sci.* 2013;14(10):21021-44. DOI:10.3390/ijms141021021.
248. Amelio I, Cutruzzolá F, Antonov A, Agostini M, Melino G. Serine and glycine metabolism in cancer. *Trends Biochem. Sci.* 2014;39(4):191-8. DOI:10.1016/j.tibs.2014.02.004.
-
-

-
-
249. Ye Z-C, Rothstein JD, Sontheimer H. Compromised glutamate transport in human glioma cells: reduction-mislocalization of sodium-dependent glutamate transporters and enhanced activity of cystine-glutamate exchange. *J. Neurosci.* 1999;19(24):10767-77.
 250. Skonieczna M, Hejmo T, Poterala-Hejmo A, Cieslar-Pobuda A, Buldak RJ. NADPH oxidases: insights into selected functions and mechanisms of action in cancer and stem cells. *Oxid. Med. Cell Longev.* 2017;2017. DOI:10.1155/2017/9420539.
 251. Sheeran FL, Rydström J, Shakhparonov MI, Pestov NB, Pepe S. Diminished NADPH transhydrogenase activity and mitochondrial redox regulation in human failing myocardium. *BBA-Bioenergetics.* 2010;1797(6-7):1138-48. DOI:10.1016/j.bbabi.2010.04.002.
 252. Tantama M, Martínez-François JR, Mongeon R, Yellen G. Imaging energy status in live cells with a fluorescent biosensor of the intracellular ATP-to-ADP ratio. *Nat. Comm.* 2013;4:2550. DOI:10.1038/ncomms3550.
 253. Mörikofer-Zwez S, Walter P. Binding of ADP to rat liver cytosolic proteins and its influence on the ratio of free ATP/free ADP. *Biochem. J.* 1989;259(1):117-24. DOI:10.1042/BJ2590117.
 254. Rao GM, Rao AV, Raja A, Rao S, Rao A. Role of antioxidant enzymes in brain tumours. *Clin. Chim. Acta.* 2000;296(1-2):203-12. DOI:10.1016/s0009-8981(00)00219-9.
 255. Tedeschi PM, Bansal N, Kerrigan JE, Abali EE, Scotto KW, Bertino JR. NAD⁺ kinase as a therapeutic target in cancer. *Clin. Can. Res.* 2016;22(21):5189-95. DOI: 10.1158/1078-0432.CCR-16-1129.
 256. Liao B, Gawienowski MC, Zielinski RE. Differential stimulation of NAD kinase and binding of peptide substrates by wild-type and mutant plant calmodulin isoforms. *Arch. Biochem. Biophys.* 1996;327(1):53-60. DOI:10.1006/ABBI.1996.0092
 257. Aylett S-B, Neergheen V, Hargreaves IP, Eaton S, Land JM, Rahman S, et al. Levels of 5-methyltetrahydrofolate and ascorbic acid in cerebrospinal fluid are correlated: implications for the accelerated degradation of folate by reactive oxygen species. *Neurochem. Int.* 2013;63(8):750-5. DOI:10.1016/j.neuint.2013.10.002.
 258. Stankova J, Lawrence A, Rozen R. Methylene tetrahydrofolate reductase (MTHFR): a novel target for cancer therapy. *Curr. Pharm. Des.* 2008;14(11):1143-50. DOI:10.2174/138161208784246171.
 259. Blanchetot C, Boonstra J. The ROS-NOX connection in cancer and angiogenesis. *Crit. Rev. Eukaryot. Gene Expr.* 2008;18(1):35-45. DOI:10.1615/critreveukargeneexpr.v18.i1.30.
 260. Hole PS, Zabkiewicz J, Munje C, Newton Z, Pearn L, White P, et al. Overproduction of NOX-derived ROS in AML promotes proliferation and is associated with defective oxidative stress signaling. *Blood.* 2013;122(19):3322-30. DOI:10.1182/blood-2013-04-491944
 261. Lim JK, Delaidelli A, Minaker SW, Zhang H-F, Colovic M, Yang H, et al. Cystine/glutamate antiporter xCT (SLC7A11) facilitates oncogenic RAS

- transformation by preserving intracellular redox balance. *Proc Natl Acad Sci U S A*. 2019;116(19):9433-42. DOI:10.1073/pnas.1821323116.
262. Blanco G, Blanco A. *Medical biochemistry*: Academic Press; 2017.
263. Philip G. Identification of an essential cysteine residue in human glutathione synthase. *Biochem. J*. 1997;321(1):207-10. DOI:10.1042/BJ3210207.
264. Borbély G, Szabadkai I, Horváth Z, Markó P, Varga Z, Breza N, et al. Small-molecule inhibitors of NADPH oxidase 4. *J. Med. Chem.* 2010;53(18):6758-62. DOI:10.1021/jm1004368
265. Wang Y-P, Zhou W, Wang J, Huang X, Zuo Y, Wang T-S, et al. Arginine methylation of MDH1 by CARM1 inhibits glutamine metabolism and suppresses pancreatic cancer. *Mol. Cell*. 2016;64(4):673-87. DOI:10.1016/j.molcel.2016.09.028.
266. Ren J-G, Seth P, Clish CB, Lorkiewicz PK, Higashi RM, Lane AN, et al. Knockdown of malic enzyme 2 suppresses lung tumor growth, induces differentiation and impacts PI3K/AKT signaling. *Sci. Rep.* 2014;4:5414. DOI:10.1038/srep05414.
267. Jeon S-M, Chandel NS, Hay N. AMPK regulates NADPH homeostasis to promote tumour cell survival during energy stress. *Nature*. 2012;485(7400):661. DOI:10.1038/nature11066.
268. Menyhárt O, Gyórfy B. Multi-omics approaches in cancer research with applications in tumor subtyping, prognosis, and diagnosis. *Comp. Struc. Biotechnol. J*. 2021;19:949-60. DOI: 10.1016/j.csbj.2021.01.009.
269. Bradley BS, Loftus JC, Mielke CJ, Dinu V. Differential expression of microRNAs as predictors of glioblastoma phenotypes. *BMC bioinformatics*. 2014;15(1):21. DOI:10.1186/1471-2105-15-21.
270. Silber J, Lim DA, Petritsch C, Persson AI, Maunakea AK, Yu M, et al. miR-124 and miR-137 inhibit proliferation of glioblastoma multiforme cells and induce differentiation of brain tumor stem cells. *BMC Med*. 2008;6(1):14. DOI:10.1186/1741-7015-6-14.
271. Yin CY, Kong W, Jiang J, Xu H, Zhao W. miR-7-5p inhibits cell migration and invasion in glioblastoma through targeting SATB1. *Oncol. Lett.* 2019;17(2):1819-25. DOI:10.3892/ol.2018.9777.
272. Xiong W, Ran J, Jiang R, Guo P, Shi X, Li H, et al. miRNA-320a inhibits glioma cell invasion and migration by directly targeting aquaporin 4. *Oncol. Rep.* 2018;39(4):1939-47. DOI:10.3892/or.2018.6274.
273. Aloizou A-M, Pateraki G, Siokas V, Mentis A-FA, Liampas I, Lazopoulos G, et al. The role of MiRNA-21 in gliomas: Hope for a novel therapeutic intervention? *Toxicol. Rep.* 2020;7:1514-30. DOI: 10.1016/j.toxrep.2020.11.001.
274. Medarova Z, Pantazopoulos P, Yoo B. Screening of potential miRNA therapeutics for the prevention of multi-drug resistance in cancer cells. *Sci. Rep.* 2020;10(1):1970. DOI:10.1038/s41598-020-58919-2.
275. Sana J, Busek P, Fadrus P, Besse A, Radova L, Vecera M, et al. Identification of microRNAs differentially expressed in glioblastoma stem-like cells and their association with patient survival. *Sci. Rep.* 2018;8(1):2836. DOI:10.1038/s41598-018-20929-6.

-
-
276. Hintze A, Adami C. Modularity and anti-modularity in networks with arbitrary degree distribution. *Biol. Direct.* 2010;5:32. DOI:10.1186/1745-6150-5-32.
277. Wang X, Dalkic E, Wu M, Chan C. Gene module level analysis: identification to networks and dynamics. *Curr. Opin. Biotechnol.* 2008;19(5):482-91. DOI:10.1016/j.copbio.2008.07.011.
278. Sasayama T, Tanaka K, Kohmura E. The roles of microRNAs in glioblastoma biology and biomarker. *Neurooncology*, 1st ed; Newer Developments; Agrawal, A, Ed. 2016:27-66.
279. Linnebank M, Semmler A, Moskau S, Smulders Y, Blom H, Simon M. The methylenetetrahydrofolate reductase (MTHFR) variant c.677C>T (A222V) influences overall survival of patients with glioblastoma multiforme. *Neurooncol.* 2008;10(4):548-52. DOI:10.1215/15228517-2008-020.
280. Li H, Li Y, Tian D, Zhang J, Duan S. miR-940 is a new biomarker with tumor diagnostic and prognostic value. *Mol. Ther. Nucleic Acids.* 2021;25:53-66. DOI: 10.1016/j.omtn.2021.05.003.
281. Wang WY, Lu WC. Reduced Expression of hsa-miR-338-3p Contributes to the Development of Glioma Cells by Targeting Mitochondrial 3-Oxoacyl-ACP Synthase (OXSM) in Glioblastoma (GBM). *Onco Targets Ther.* 2020;13:9513-23. DOI:10.2147/ott.S262873.
282. Saurty-Seerunghen MS, Bellenger L, El-Habr EA, Delaunay V, Garnier D, Chneiweiss H, et al. Capture at the single cell level of metabolic modules distinguishing aggressive and indolent glioblastoma cells. *Acta Neuropathol. Commun.* 2019;7(1):155. DOI:10.1186/s40478-019-0819-y.
283. de Saldanha da Gama Fischer J, Costa Carvalho P, da Fonseca CO, Liao L, Degraeve WM, da Gloria da Costa Carvalho M, et al. Chemo-resistant protein expression pattern of glioblastoma cells (A172) to perillyl alcohol. *J. Proteome Res.* 2011;10(1):153-60. DOI:10.1021/pr100677g.
284. Qin CZ, Lv QL, Yang YT, Zhang JM, Zhang XJ, Zhou HH. Downregulation of MicroRNA-320d predicts poor overall survival and promotes the growth and invasive abilities in glioma. *Chem. Biol. Drug Des.* 2017;89(5):806-14. DOI:10.1111/cbdd.12906.
285. Jia X, Wang X, Guo X, Ji J, Lou G, Zhao J, et al. MicroRNA-124: An emerging therapeutic target in cancer. *Cancer Med.* 2019;8(12):5638-50. DOI:10.1002/cam4.2489.
286. Yu J, Wu SW, Wu WP. A tumor-suppressive microRNA, miRNA-485-5p, inhibits glioma cell proliferation and invasion by down-regulating TPD52L2. *Am. J. Trans. Res.* 2017;9(7):3336-44.
287. Bendahou MA, Ibrahim A, Boutarbouch M. Bioinformatics Analysis of Differentially Expressed Genes and miRNAs in Low-Grade Gliomas. *Cancer Inform.* 2020;19:1176935120969692. DOI:10.1177/1176935120969692.
288. Karsy M, Arslan E, Moy F. Current Progress on Understanding MicroRNAs in Glioblastoma Multiforme. *Genes Cells.* 2012;3(1):3-15. DOI:10.1177/1947601912448068.
-
-

-
-
289. Zhao C, Guo R, Guan F, Ma S, Li M, Wu J, et al. MicroRNA-128-3p Enhances the Chemosensitivity of Temozolomide in Glioblastoma by Targeting c-Met and EMT. *Sci. Rep.* 2020;10(1):9471. DOI:10.1038/s41598-020-65331-3.
290. Veillon L, Fakih C, Abou-El-Hassan H, Kobeissy F, Mechref Y. Glycosylation Changes in Brain Cancer. *ACS Chem. Neurosci.* 2018;9(1):51-72. DOI:10.1021/acchemneuro.7b00271.
291. Rasper M, Schäfer A, Piontek G, Teufel J, Brockhoff G, Ringel F, et al. Aldehyde dehydrogenase 1 positive glioblastoma cells show brain tumor stem cell capacity. *Neuro Oncol.* 2010;12(10):1024-33. DOI:10.1093/neuonc/noq070.
292. Khwairakpam AD, Shyamananda MS, Sailo BL, Rathnakaram SR, Padmavathi G, Kotoky J, et al. ATP citrate lyase (ACLY): a promising target for cancer prevention and treatment. *Curr. Drug Targets.* 2015;16(2):156-63. DOI:10.2174/1389450115666141224125117.
293. Cheng CP, Huang LC, Chang YL, Hsieh CH, Huang SM, Hueng DY. The mechanisms of malic enzyme 2 in the tumorigenesis of human gliomas. *Oncotarget.* 2016;7(27):41460-72. DOI:10.18632/oncotarget.9190.
294. Zhu Z, Leung GKK. More Than a Metabolic Enzyme: MTHFD2 as a Novel Target for Anticancer Therapy? *Front. Oncol.* 2020;10:658. DOI:10.3389/fonc.2020.00658.
295. Ivo D'Urso P, Fernando D'Urso O, Damiano Gianfreda C, Mezzolla V, Storelli C, Marsigliante S. miR-15b and miR-21 as Circulating Biomarkers for Diagnosis of Glioma. *Curr. Genomics.* 2015;16(5):304-11. DOI:10.2174/1389202916666150707155610.
296. Kouhkan F, Mobarra N, Soufi-Zomorrod M, Keramati F, Hosseini Rad SM, Fathi-Roudsari M, et al. MicroRNA-129-1 acts as tumour suppressor and induces cell cycle arrest of GBM cancer cells through targeting IGF2BP3 and MAPK1. *J. Med. Genet.* 2016;53(1):24-33. DOI:10.1136/jmedgenet-2015-103225.
297. Xu W, Liu M, Peng X, Zhou P, Zhou J, Xu K, et al. miR-24-3p and miR-27a-3p promote cell proliferation in glioma cells via cooperative regulation of MXI1. *Int. J. Oncol.* 2013;42(2):757-66. DOI:10.3892/ijo.2012.1742.
298. Piwecka M, Rolle K, Belter A, Barciszewska AM, Żywicki M, Michalak M, et al. Comprehensive analysis of microRNA expression profile in malignant glioma tissues. *Mol. Oncol.* 2015;9(7):1324-40. DOI:10.1016/j.molonc.2015.03.007.
299. Zhang JF, Zhang JS, Zhao ZH, Yang PB, Ji SF, Li N, et al. MicroRNA-770 affects proliferation and cell cycle transition by directly targeting CDK8 in glioma. *Cancer Cell Int.* 2018;18:195. DOI:10.1186/s12935-018-0694-9.
300. Wang R, Zuo X, Wang K, Han Q, Zuo J, Ni H, et al. MicroRNA-485-5p attenuates cell proliferation in glioma by directly targeting paired box 3. *Am. J. Cancer Res.* 2018;8(12):2507-17.
301. Liu Z, Su D, Qi X, Ma J. MiR-500a-5p promotes glioblastoma cell proliferation, migration and invasion by targeting chromodomain helicase DNA binding protein 5. *Mol. Med. Rep.* 2018;18(3):2689-96. DOI:10.3892/mmr.2018.9259.
-
-

-
-
302. Huo L, Wang B, Zheng M, Zhang Y, Xu J, Yang G, et al. miR-128-3p inhibits glioma cell proliferation and differentiation by targeting NPTX1 through IRS-1/PI3K/AKT signaling pathway. *Exp. Ther. Med.* 2019;17(4):2921-30. DOI:10.3892/etm.2019.7284.
 303. Cai S, Shi CJ, Lu JX, Wang YP, Yuan T, Wang XP. miR-124-3p inhibits the viability and motility of glioblastoma multiforme by targeting RhoG. *Int. J. Mol. Med.* 2021;47(5). DOI:10.3892/ijmm.2021.4902.
 304. Wang Y, Chen R, Zhou X, Guo R, Yin J, Li Y, et al. miR-137: A Novel Therapeutic Target for Human Glioma. *Mol. Ther. Nucleic Acids.* 2020;21:614-22. DOI:10.1016/j.omtn.2020.06.028.
 305. Qiu S, Huang D, Yin D, Li F, Li X, Kung HF, et al. Suppression of tumorigenicity by microRNA-138 through inhibition of EZH2-CDK4/6-pRb-E2F1 signal loop in glioblastoma multiforme. *Biochim. Biophys. Acta.* 2013;1832(10):1697-707. DOI:10.1016/j.bbadis.2013.05.015.
 306. Feng L, Ma J, Ji H, Liu Y, Hu W. miR-330-5p suppresses glioblastoma cell proliferation and invasiveness through targeting ITGA5. *Biosci. Rep.* 2017;37(3). DOI:10.1042/bsr20170019.
 307. Shea A, Harish V, Afzal Z, Chijioko J, Kedir H, Dusmatova S, et al. MicroRNAs in glioblastoma multiforme pathogenesis and therapeutics. *Cancer Med.* 2016;5(8):1917-46. DOI:10.1002/cam4.775.
 308. Semonche A, Shah AH, Ivan ME, Komotar RJ. Towards a microRNA-based Gene Therapy for Glioblastoma. *Neurosurgery.* 2019;85(2):E210-e1. DOI:10.1093/neuros/nyz166.
 309. Wang N, Tan HY, Feng YG, Zhang C, Chen F, Feng Y. microRNA-23a in Human Cancer: Its Roles, Mechanisms and Therapeutic Relevance. *Cancers.* 2018;11(1). DOI:10.3390/cancers11010007.
 310. Bhowmick R, Sarkar RR. Differential suitability of reactive oxygen species and the role of glutathione in regulating paradoxical behavior in gliomas: A mathematical perspective. *PLoS ONE.* 2020;15(6):e0235204. DOI:10.1371/journal.pone.0235204.
 311. Nicholson JK, Wilson ID. Understanding 'Global' Systems Biology: Metabonomics and the Continuum of Metabolism. *Nat. Rev. Drug Discov.* 2003;2(8):668-76. DOI:10.1038/nrd1157.
 312. Stuart SD, Schauble A, Gupta S, Kennedy AD, Keppler BR, Bingham PM, et al. A strategically designed small molecule attacks alpha-ketoglutarate dehydrogenase in tumor cells through a redox process. *Cancer Metab.* 2014;2(4). DOI:10.1186/2049-3002-2-4
 313. Bingham PM, Zachar Z. The pyruvate dehydrogenase complex in cancer: implications for the transformed state and cancer chemotherapy. INTECH Open Access Publisher; 2012. DOI:10.5772/48582

-
-
314. Traina ME, Guarino M, Urbani E, Saso L, Eleuteri P, Cordelli E, et al. Lonidamine transiently affects spermatogenesis in pubertal CD1 mice. *Contraception*. 2005;72(4):262-7. DOI:10.1016/j.contraception.2005.04.008.
 315. Gong X, Burbridge SM, Lewis AC, Wong PY, Linsdell P. Mechanism of lonidamine inhibition of the CFTR chloride channel. *Br. J. Pharmacol.* 2002;137(6):928-36. DOI:10.1038/sj.bjp.0704932.
 316. Fricks IP, Carter RL, Lazarowski ER, Harden TK. Gi-dependent cell signaling responses of the human P2Y₁₄ receptor in model cell systems. *J. Pharmacol. Exp. Ther.* 2009;330(1):162-8. DOI:10.1124/jpet.109.150730.
 317. Abbracchio MP, Boeynaems J-M, Barnard EA, Boyer JL, Kennedy C, Miras-Portugal MT, et al. Characterization of the UDP-glucose receptor (re-named here the P2Y₁₄ receptor) adds diversity to the P2Y receptor family. *Trends Pharmacol. Sci.* 2003;24(2):52-5. DOI:10.1016/S0165-6147(02)00038-X.
 318. Balteau M, Tajeddine N, de Meester C, Ginion A, Des Rosiers C, Brady NR, et al. NADPH oxidase activation by hyperglycaemia in cardiomyocytes is independent of glucose metabolism but requires SGLT1. *Cardiovasc. Res.* 2011;92(2):237-46. DOI:10.1093/cvr/cvr230.
 319. Pelicano H, Martin D, Xu R, and, Huang P. Glycolysis inhibition for anticancer treatment. *Oncogene*. 2006;25(34):4633-46. DOI:10.1038/sj.onc.1209597.
 320. Shestov AA, Liu X, Ser Z, Cluntun AA, Hung YP, Huang L, et al. Quantitative determinants of aerobic glycolysis identify flux through the enzyme GAPDH as a limiting step. *Elife*. 2014;3. DOI:10.7554/eLife.03342.
 321. Bell RA, Smith JC, Storey KB. Purification and properties of glyceraldehyde-3-phosphate dehydrogenase from the skeletal muscle of the hibernating ground squirrel, *Ictidomys tridecemlineatus*. *PeerJ*. 2014;2:e634. DOI:10.7717/peerj.634.
 322. Tabatabaie L, De Koning T, Geboers A, van den Berg I, Berger R, Klomp L. Novel mutations in 3-phosphoglycerate dehydrogenase (PHGDH) are distributed throughout the protein and result in altered enzyme kinetics. *Hum. Mutat.* 2009;30(5):749-56. DOI:10.1002/humu.20934.
 323. Fan J, Teng X, Liu L, Mattaini KR, Looper RE, Vander Heiden MG, et al. Human phosphoglycerate dehydrogenase produces the oncometabolite D-2-hydroxyglutarate. *ACS Chem. Biol.* 2014;10(2):510-6. DOI:10.1021/cb500683c.
 324. Hart CE, Race V, Achouri Y, Wiame E, Sharrard M, Olpin SE, et al. Phosphoserine aminotransferase deficiency: a novel disorder of the serine biosynthesis pathway. *Am. J. Hum. Genet.* 2007;80(5):931-7. DOI:10.1086/517888.
 325. Collet J-F, Stroobant V, Van Schaftingen E. Mechanistic studies of phosphoserine phosphatase, an enzyme related to P-type ATPases. *J. Biol. Chem.* 1999;274(48):33985-90. DOI:10.1074/jbc.274.48.33985.
 326. Shetty KT. Phosphoserine phosphatase of human brain: partial purification, characterization, regional distribution, and effect of certain modulators including psychoactive drugs. *Neurochem. Res.* 1990;15(12):1203-10. DOI:10.1007/BF01208581
-
-

-
-
327. Vazquez A, Markert EK, Oltvai ZN. Serine biosynthesis with one carbon catabolism and the glycine cleavage system represents a novel pathway for ATP generation. *PLoS ONE*. 2011;6(11):e25881. DOI:10.1371/journal.pone.0025881.
 328. Nijhout HF, Reed MC, Budu P, Ulrich CM. A mathematical model of the folate cycle new insights into folate homeostasis. *J. Biol. Chem.* 2004;279(53):55008-16. DOI: 10.1074/jbc.M410818200.
 329. Willis MN, Liu Y, Biterova EI, Simpson MA, Kim H, Lee J, et al. Enzymatic defects underlying hereditary glutamate cysteine ligase deficiency are mitigated by association of the catalytic and regulatory subunits. *Biochemistry*. 2011;50(29):6508-17. DOI:10.1021/bi200708w.
 330. York M, Kuchel PW, Chapman BE, Jones A. Incorporation of labelled glycine into reduced glutathione of intact human erythrocytes by enzyme-catalysed exchange. A nuclear-magnetic-resonance study. *Biochem. J.* 1982;207(1):65-72. DOI:10.1042/BJ2070065.
 331. Njålsson R, Carlsson K, Olin B, Carlsson B, Whitbread L, Polekhina G, et al. Kinetic properties of missense mutations in patients with glutathione synthetase deficiency. *Biochem. J.* 2000;349(Pt 1):275. DOI:10.1042/0264-6021:3490275.
 332. Gatto Jr GJ, Ao Z, Kearse MG, Zhou M, Morales CR, Daniels E, et al. NADPH oxidase-dependent and-independent mechanisms of reported inhibitors of reactive oxygen generation. *J. Enzyme Inhib. Med. Chem.* 2013;28(1):95-104. DOI:10.3109/14756366.2011.636360.
 333. Brandes RP, Weissmann N, Schröder K. Nox family NADPH oxidases: molecular mechanisms of activation. *Free Rad. Biol. Med.* 2014;76:208-26. DOI:10.1016/j.freeradbiomed.2014.07.046.
 334. Searcy DG. HS⁻: O₂oxidoreductase activity of Cu, Zn superoxide dismutase. *Arch. Biochem. Biophys.* 1996;334(1):50-8. DOI:10.1006/ABBI.1996.0428.
 335. Suravajjala S, Cohenford M, Frost LR, Pampati PK, Dain JA. Glycation of human erythrocyte glutathione peroxidase: effect on the physical and kinetic properties. *Clin. Chim. Acta.* 2013;421:170-6. DOI:10.1016/j.cca.2013.02.032.
 336. Lankin VZ, Konovalova GG, Tikhaze AK, Shumaev KB, Belova EM, Grechnikova MA, et al. Aldehyde inhibition of antioxidant enzymes in the blood of diabetic patients. *J. Diabetes.* 2016;8(3):398-404. DOI:10.1111/1753-0407.12309.
 337. Liu L, Mao S-z, Liu X-m, Huang X, Xu J-y, Liu J-q, et al. Functional mimicry of the active site of glutathione peroxidase by glutathione imprinted selenium-containing protein. *Biomacromolecules.* 2007;9(1):363-8. DOI:10.1021/bm7008312.
 338. Storey BT, Alvarez JG, Thompson KA. Human sperm glutathione reductase activity in situ reveals limitation in the glutathione antioxidant defense system due to supply of NADPH. *Mol. Reprod. Dev.* 1998;49(4):400-7. DOI:10.1002/(SICI)1098-2795(199804)49:4<400::AID-MRD7>3.0.CO;2-R.
 339. Ulusu NN, Tandoğan B. Purification and kinetic properties of glutathione reductase from bovine liver. *Mol. Cell. Biochem.* 2007;303(1-2):45-51. DOI:10.1007/s11010-007-9454-1.
-
-

-
-
340. Bender A, Reichelt W, Norenberg M. Characterization of cystine uptake in cultured astrocytes. *Neurochem. Int.* 2000;37(2-3):269-76. DOI:10.1016/s0197-0186(00)00035-8.
 341. Hosoya K-i, Tomi M, Ohtsuki S, Takanaga H, Saeki S, Kanai Y, et al. Enhancement of L-cystine transport activity and its relation to xCT gene induction at the blood-brain barrier by diethyl maleate treatment. *J. Pharmacol. Exp. Ther.* 2002;302(1):225-31. DOI:10.1124/JPET.302.1.225.
 342. Thomas AG, Sattler R, Tendyke K, Loiacono KA, Hansen H, Sahni V, et al. High-throughput assay development for cystine-glutamate antiporter (xc-) highlights faster cystine uptake than glutamate release in glioma cells. *PLoS ONE.* 2015;10(8):e0127785. DOI:10.1371/journal.pone.0127785.
 343. Shipley R, Davidson AJ, Chan K, Chaudhuri JB, Waters S, Ellis MJ. A strategy to determine operating parameters in tissue engineering hollow fiber bioreactors. *Biotechnol. Bioeng.* 2011;108(6):1450-61. DOI:10.1002/bit.23062.
 344. Ellory J, Jones S, Young J. Glycine transport in human erythrocytes. *J. Physiol.* 1981;320(1):403-22. DOI:10.1113/jphysiol.1981.sp013958.
 345. Aroeira RI, Sebastião AM, Valente CA. BDNF, via truncated TrkB receptor, modulates GlyT1 and GlyT2 in astrocytes. *Glia.* 2015;63(12):2181-97. DOI:10.1002/glia.22884.
 346. Zimmerman JJ, von Saint André-von Arnim A, McLaughlin J. *Cellular Respiration. Pediatric Critical Care: Elsevier;* 2011. p. 1058-72
 347. Desmoulin F, Cozzzone PJ, Canioni P. Phosphorus-31 nuclear-magnetic-resonance study of phosphorylated metabolites compartmentation, intracellular pH and phosphorylation state during normoxia, hypoxia and ethanol perfusion, in the perfused rat liver. *Eur. J. Biochem.* 1987;162(1):151-9. DOI:10.1111/j.1432-1033.1987.tb10555.x.
 348. Ahn K-J, Kim J-S, Yun M-J, Park J-H, Lee J-D. Enzymatic properties of the N- and C-terminal halves of human hexokinase II. *BMB Rep.* 2009;42(6):350-5. DOI:10.5483/bmbrep.2009.42.6.350.
 349. Antoine M, Boutin JA, Ferry G. Binding kinetics of glucose and allosteric activators to human glucokinase reveal multiple conformational states. *Biochemistry.* 2009;48(23):5466-82. DOI:10.1021/bi900374c.
 350. Reed MC, Nijhout HF, Neuhaus ML, Gregory III JF, Shane B, James SJ, et al. A mathematical model gives insights into nutritional and genetic aspects of folate-mediated one-carbon metabolism. *J. Nutr.* 2006;136(10):2653-61. DOI:10.1093/JN/136.10.2653
 351. Silver IA, Erecinska M. Extracellular glucose concentration in mammalian brain: continuous monitoring of changes during increased neuronal activity and upon limitation in oxygen supply in normo-, hypo-, and hyperglycemic animals. *J. Neurosci.* 1994;14(8):5068-76. DOI:10.1523/JNEUROSCI.14-08-05068.1994.

-
-
352. Behjousiar A, Kontoravdi C, Polizzi KM. In situ monitoring of intracellular glucose and glutamine in CHO cell culture. *PLoS ONE*. 2012;7(4):e34512. DOI:10.1371/journal.pone.0034512.
 353. Rose I A, O'Connell D. The Role of Glucose 6-Phosphate in the Regulation Glucose Metabolism in Human Erythrocytes. *J. Biol. Chem.* 1964;239:12-7. DOI:10.1016/s0021-9258(18)51739-7.
 354. Jamshidi N, Palsson BØ. Mass action stoichiometric simulation models: incorporating kinetics and regulation into stoichiometric models. *Biophys. J.* 2010;98(2):175-85. DOI:10.1016/j.bpj.2009.09.064.
 355. Klomp LW, de Koning TJ, Malingré HE, van Beurden EA, Brink M, Opdam FL, et al. Molecular characterization of 3-phosphoglycerate dehydrogenase deficiency—a neurometabolic disorder associated with reduced L-serine biosynthesis. *Am. J. Human Genet.* 2000;67(6):1389-99. DOI:10.1086/316886.
 356. Snell K, Fell DA. Metabolic control analysis of mammalian serine metabolism. *Adv. Enzym. Regul.* 1990;30:13-32. DOI:10.1016/0065-2571(90)90006-n.
 357. Kalivas P. Extracellular glutamate: functional compartments operate in different concentration ranges. *Front. Syst. Neurosci.* 2011;5:94. DOI:10.3389/fnsys.2011.00094.
 358. Bannai S. Transport of cystine and cysteine in mammalian cells. *Biochim. Biophys. Acta Rev. Biomembr.* 1984;779(3):289-306. DOI:10.1016/0304-4157(84)90014-5.
 359. Nakamura J, Purvis ER, Swenberg JA. Micromolar concentrations of hydrogen peroxide induce oxidative DNA lesions more efficiently than millimolar concentrations in mammalian cells. *Nucleic Acids Res.* 2003;31(6):1790-5. DOI:10.1093/NAR/GKG263.
 360. Clément M-V, Pervaiz S. Intracellular superoxide and hydrogen peroxide concentrations: a critical balance that determines survival or death. *Redox Rep.* 2001;6(4):211-4. DOI:10.1179/135100001101536346.
 361. Libby CJ, Tran AN, Scott SE, Griguer C, Hjelmeland AB. The pro-tumorigenic effects of metabolic alterations in glioblastoma including brain tumor initiating cells. *Biochim. Biophys. Acta Rev. Cancer.* 2018;1869(2):175-88. DOI:10.1016/j.bbcan.2018.01.004.
 362. Xu W, Liu Z, Ren H, Peng X, Wu A, Ma D, et al. Twenty Metabolic Genes Based Signature Predicts Survival of Glioma Patients. *J. Cancer.* 2020;11(2):441-9. DOI:10.7150/jca.30923.
 363. Tabei Y, Kobayashi K, Saito K, Shimizu S, Suzuki K, Sasaki N, et al. Survival in patients with glioblastoma at a first progression does not correlate with isocitrate dehydrogenase (IDH)1 gene mutation status. *Jpn. J. Clin. Oncol.* 2021;51(1):45-53. DOI:10.1093/jjco/hyaa162.
 364. Kathagen-Buhmann A, Schulte A, Weller J, Holz M, Herold-Mende C, Glass R, et al. Glycolysis and the pentose phosphate pathway are differentially associated with the dichotomous regulation of glioblastoma cell migration versus proliferation. *Neuro Oncol.* 2016;18(9):1219-29. DOI:10.1093/neuonc/now024.
-
-

-
-
365. Abbadi S, Rodarte JJ, Abutaleb A, Lavell E, Smith CL, Ruff W, et al. Glucose-6-phosphatase is a key metabolic regulator of glioblastoma invasion. *Mol. Cancer Res.* 2014;12(11):1547-59. DOI:10.1158/1541-7786.MCR-14-0106-T.
 366. Kathagen-Buhmann A, Maire CL, Weller J, Schulte A, Matschke J, Holz M, et al. The secreted glycolytic enzyme GPI/AMF stimulates glioblastoma cell migration and invasion in an autocrine fashion but can have anti-proliferative effects. *Neuro Oncol.* 2018;20(12):1594-605. DOI:10.1093/neuonc/noy117.
 367. Han T, Kang D, Ji D, Wang X, Zhan W, Fu M, et al. How does cancer cell metabolism affect tumor migration and invasion? *Cell Adhes. Migr.* 2013;7(5):395-403. DOI:10.4161/cam.26345.
 368. Kahlert UD, Mooney SM, Natsumeda M, Steiger HJ, Maciaczyk J. Targeting cancer stem-like cells in glioblastoma and colorectal cancer through metabolic pathways. *Int. J. Cancer.* 2017;140(1):10-22. DOI:10.1002/ijc.30259.
 369. Li G, Li Y, Liu X, Wang Z, Zhang C, Wu F, et al. ALDH1A3 induces mesenchymal differentiation and serves as a predictor for survival in glioblastoma. *Cell Death Dis.* 2018;9(12):1190-. DOI:10.1038/s41419-018-1232-3.
 370. Tan Z, Xiao L, Tang M, Bai F, Li J, Li L, et al. Targeting CPT1A-mediated fatty acid oxidation sensitizes nasopharyngeal carcinoma to radiation therapy. *Theranostics.* 2018;8(9):2329-47. DOI:10.7150/thno.21451.
 371. Miyazaki T, Moritake K, Yamada K, Hara N, Osago H, Shibata T, et al. Indoleamine 2,3-dioxygenase as a new target for malignant glioma therapy: Laboratory investigation. *J. Neurosurg.* 2009;111(2):230-7. DOI:10.3171/2008.10.JNS081141.
 372. Tanaka K, Sasayama T, Irino Y, Takata K, Nagashima H, Satoh N, et al. Compensatory glutamine metabolism promotes glioblastoma resistance to mTOR inhibitor treatment. *J. Clin. Invest.* 2015;125(4):1591-602. DOI:10.1172/jci78239.
 373. Vartanian A, Agnihotri S, Wilson MR, Burrell KE, Tonge PD, Alamsahebpour A, et al. Targeting hexokinase 2 enhances response to radio-chemotherapy in glioblastoma. *Oncotarget.* 2016;7(43):69518-35. DOI:10.18632/oncotarget.11680.
 374. Koukourakis M, Tsolou A, Pouliliou S, Lamprou I, Papadopoulou M, Ilemosoglou M, et al. Blocking LDHA glycolytic pathway sensitizes glioblastoma cells to radiation and temozolomide. *Biochem. Biophys. Res. Comm.* 2017;491(4):932-8. DOI:10.1016/j.bbrc.2017.07.138.
 375. Nishimura T, Nakata A, Chen X, Nishi K, Meguro-Horike M, Sasaki S, et al. Cancer stem-like properties and gefitinib resistance are dependent on purine synthetic metabolism mediated by the mitochondrial enzyme MTHFD2. *Oncogene.* 2019;38(14):2464-81. DOI:10.1038/s41388-018-0589-1.
 376. Hayes JD, Pulford DJ. The Glutathione S-Transferase Supergene Family: Regulation of GST and the Contribution of the Isoenzymes to Cancer Chemoprotection and Drug Resistance Part I. *Crit. Rev. Biochem. Mol. Biol.* 1995;30(6):445-520. DOI:10.3109/10409239509083491.

377. Cole SPC. Multidrug resistance protein 1 (MRP1, ABCC1), a "multitasking" ATP-binding cassette (ABC) transporter. *J. Biol. Chem.* 2014;289(45):30880-8. DOI:10.1074/jbc.R114.609248.
378. Olivier C, Oliver L, Lalier L, Vallette FM. Drug Resistance in Glioblastoma: The Two Faces of Oxidative Stress. *Front. Mol. Biosci.* 2021;7(468):620677. DOI:10.3389/fmolb.2020.620677.
379. Stavrovskaya AA, Shushanov SS, Rybalkina EY. Problems of Glioblastoma Multifforme Drug Resistance. *Biochemistry Biokhimiia.* 2016;81(2):91-100. DOI:10.1134/s0006297916020036.

ABSTRACT

Name of the Student: Rupa Bhowmick
Faculty of Study: Biological Sciences (BS)
CSIR Lab: CSIR-NCL, Pune

Registration No.: 10BB17J26062
Year of Submission: 2021
Name of the Supervisor: Dr. Ram Rup Sarkar

Title of the thesis: Deciphering the complexities in oncogenesis: An integrative approach to understand its adaptive phenotypes

Metabolic reprogramming is a hallmark of cancer. Changes in metabolism have been verified for their role in the progression of glioblastomas. Metabolic reprogramming allows the tumor cells to switch between phenotypes under changing growth condition that help these tumors to evolve and develop resistance against the therapeutic regimens. In the present thesis, the alternate routes of therapeutic escape, opportunistic mode of nutrient acquisition, and evolving metabolic routes to sustain oncogenic phenotypes under various growth conditions have been studied by formulating and analyzing computational and mathematical models.

In order to gain a holistic perspective of the pathway behavior and condition specific changes in the metabolic network of glioblastoma, a constraint-based metabolic model was formulated and analyzed. Model simulations showed a major flux re-routing towards glutathione production. Cystine and glucose were observed to be the minimal essential nutrients that could sustain glioblastoma growth under limited nutrient availability. Glycine transporter in combination with the serine biosynthesis enzymes were proposed as potential therapeutic targets, as their knockout was observed to effectively reduce glioblastoma growth.

To understand the changes in the redox and thiol status of the cells and the changes occurring in the oxidant-antioxidant balance during gliomagenesis, a dynamic ordinary differential equation model was formulated. Model analyses established that the changing dynamics of glutathione peroxidase, glutathione oxidoreductase and NADPH oxidase determines the oxidant-antioxidant balance during gliomagenesis. Parameters of non-intuitive reactions in the network like cystine reductase, glutathione synthase, and fructose-bisphosphate aldolase were observed to influence the ROS level and thiol ratio of the cells and were proposed to alter the ROS manipulative strategies in glioma treatment.

The post-transcriptional regulation imposed by microRNAs on the metabolic genes was studied using graph theoretical approach. Using bipartite projection and backbone extraction techniques, the key regulatory microRNAs controlling central carbon, fatty acid, lipid, glycan, amino acid, and nucleotide metabolism were identified. Analysis showed that the central carbon metabolism, lipid, and amino acid metabolism were highly regulated by the microRNAs. The microRNA combinations (hsa-miR-15b-5p + hsa-miR-500a-5p + hsa-miR-129-1-3p), (hsa-miR-15b-5p + hsa-miR-124-3p + hsa-miR-138-2-3p), (hsa-miR-7-5p + hsa-miR-128-3p + hsa-miR-485-5p), (hsa-miR-15b-5p + hsa-miR-23a-3p) and (hsa-miR-124-3p + hsa-miR-300-5p + hsa-miR-23a-3p) were proposed as target combinations regulating proliferation and growth, survival, cell migration and invasion, stemness and drug resistance in glioblastoma respectively, that could be used for miRNA-based therapeutic design.

LIST OF PUBLICATIONS

Publications emanating from Thesis work

1. **Bhowmick R**, Subramanian A and Sarkar RR (2015). Exploring the differences in metabolic behavior of astrocyte and glioblastoma: A flux balance analysis approach. *Systems and Synthetic Biology*. 9, pp 159 – 177. DOI:10.1007/s11693-015-9183-9
2. **Bhowmick R** and Sarkar RR (2020). Differential suitability of Reactive Oxygen Species and the role of Glutathione in regulating their paradoxical behavior in Gliomas, *PLoS ONE*. 15(6): e0235204. DOI: 10.1371/journal.pone.0235204
3. **Bhowmick R**, Ganguli P and Sarkar RR (2020) T-Cell Activation and Differentiation: Role of Signalling and Metabolic Cross-Talk. (Chapter 6) In: Singh S. (eds) *Systems and Synthetic Immunology*. Springer, Singapore. pp 153-182, Online ISBN: 978-981-15-3350-1. DOI: 10.1007/978-981-15-3350-1_6
4. **Bhowmick R** and Sarkar RR (2021). Revisiting the limitations of drugs and therapeutic strategies in Gliomas. (Submitted)
5. **Bhowmick R** and Sarkar RR (2021). Identification of potential microRNAs regulating metabolic plasticity and cellular phenotypes in glioblastoma. (Submitted)

Other Publications

6. Ganguli P, Chowdhury S, **Bhowmick R** and Sarkar RR (2015). Temporal protein expression pattern in intracellular signalling cascade during T-cell activation: A computational study. *Journal of Biosciences*. 40(4), pp769-789. DOI: 10.1007/s12038-015-9561-1
7. **Bhowmick R**, Sinha N and Sarkar RR (2017). An in-silico perspective towards targetability of available drugs in infectious disease treatment: a possible strategy. *Journal of Bioinformatics and Genomics*. 2 (2017): 4. DOI:10.18454/jbg.2017.2.4.1

-
-
8. Chowdhury S, Sinha N, Ganguli P, **Bhowmick R**, Singh V, Nandi S and Sarkar RR (2018). BIOPYDB: A Dynamic Human Cell Specific Biochemical Pathway Database with Advanced Computational Analyses Platform. *Journal of Integrative Bioinformatics*. 15(3), 20170072. DOI: 10.1515/jib-2017-0072

Patent

9. Sarkar RR, **Bhowmick R**, Subramanian A (2015). Identification of combinatorial enzymatic reaction targets in glioblastoma specific metabolic network to suppress human glioblastoma. PCT/IN2016/050425, filed on 30-11-2015. WO2017094025A1 (US)

***THESIS RELATED
PUBLICATIONS***

Exploring the differences in metabolic behavior of astrocyte and glioblastoma: a flux balance analysis approach

Rupa Bhowmick¹ · Abhishek Subramanian^{1,2} · Ram Rup Sarkar^{1,2}

Received: 8 July 2015 / Revised: 8 September 2015 / Accepted: 5 October 2015
© Springer Science+Business Media Dordrecht 2015

Abstract Brain cancers demonstrate a complex metabolic behavior so as to adapt the external hypoxic environment and internal stress generated by reactive oxygen species. To survive in these stringent conditions, glioblastoma cells develop an antagonistic metabolic phenotype as compared to their predecessors, the astrocytes, thereby quenching the resources expected for nourishing the neurons. The complexity and cumulative effect of the large scale metabolic functioning of glioblastoma is mostly unexplored. In this study, we reconstruct a metabolic network comprising of pathways that are known to be deregulated in glioblastoma cells as compared to the astrocytes. The network, consisted of 147 genes encoding for enzymes performing 247 reactions distributed across five distinct model compartments, was then studied using constrained-based modeling approach by recreating the scenarios for astrocytes and glioblastoma, and validated with available experimental evidences. From our analysis, we predict that glycine requirement of the astrocytes are mostly fulfilled by the internal glycine–serine metabolism, whereas glioblastoma cells demand an external uptake of glycine to utilize it for glutathione production. Also, cystine and glucose were identified to be the major

contributors to glioblastoma growth. We also proposed an extensive set of single and double lethal reaction knock-outs, which were further perturbed to ascertain their role as probable chemotherapeutic targets. These simulation results suggested that, apart from targeting the reactions of central carbon metabolism, knockout of reactions belonging to the glycine–serine metabolism effectively reduce glioblastoma growth. The combinatorial targeting of glycine transporter with any other reaction belonging to glycine–serine metabolism proved lethal to glioblastoma growth.

Keywords Astrocyte · Glioblastoma · Metabolic demand reaction · Mitochondrial ATP synthesis · Glycine · Cystine

Introduction

Human brain, in order to ensure its proper functioning, has to account for a highly perplexing conduct which is maintained by the interplay between its distinctive cell sorts. An emerging area of interest in the last decade, pertaining to brain metabolism, has been the study of behavioral aspects of astrocytes (Bouzier-Sore and Pellerin 2013) and their cancerous counterpart, glioblastoma (Wolf et al. 2010). Several studies have been performed to understand the metabolic alterations incurred within the astrocytes, which lead to their phenotypic manifestation as glioblastoma (Chinnaiyan et al. 2012). However, the cumulative effect of a large scale metabolism on the metabolic functioning of glioblastoma still remains unaddressed. The effect of the mutual connectivity of the individual pathways within its metabolic network and the difference in response they show in the astrocytic and glioblastoma scenarios is also largely unknown. Glioblastoma cells can exhibit diversified

Electronic supplementary material The online version of this article (doi:10.1007/s11693-015-9183-9) contains supplementary material, which is available to authorized users.

✉ Ram Rup Sarkar
rr.sarkar@ncl.res.in

¹ Chemical Engineering and Process Development, CSIR-National Chemical Laboratory, Pune, Maharashtra 411008, India

² Academy of Scientific and Innovative Research (AcSIR), CSIR-NCL Campus, Pune 411008, India

response to same stimulus and show a great metabolic heterogeneity, which enable them to thrive even in a glucose starved condition (Griguer et al. 2005). A few of the metabolic phenomena, such as a higher accumulation of glycine in the glioblastoma cells (Hattingen et al. 2009) and the disruption of primary brain tumor growth with the inhibition of cystine (Chung et al. 2005), are known, but the reason to such behavior is still not understood properly. Knowledge about the alternative metabolites, which help the glioblastoma cells to thrive with altered metabolism, also remains largely unexplored.

One of the pioneering work in cancer biology was the discovery of Warburg effect in 1924 (Warburg 1956), which suggested that cancer cells might adapt to a primitive glycolytic pattern of embryonic cells and mitochondrial injury as well as metabolic switching of glycolysis to aerobic glycolysis might be essential for cancer development. Several studies have been carried out to delineate the advantage of such a modification in the tumorous cells. These phenomena are also observable in glioblastoma, enabling them to suffice their rapacious requirements (Zhou et al. 2011). In addition to this remarkable discovery, several other experimental and statistical analyses have been conducted to delineate the phenomenal changes in the properties of glioblastoma as an effect of metabolic alterations in different enzymes belonging to different pathways like tryptophan metabolism (Sahm et al. 2013), cysteine metabolism (Ye et al. 1999), glutamine and glutamate metabolism (Wise et al. 2008). Properties of these individual metabolic pathways have been studied in both astrocytes and glioblastoma, but the difference in their response as a part of a large metabolic network, in the two scenarios, is yet to be studied. A new arena of *in silico* studies have also been employed in the past decade to obtain a large-scale network understanding of glioblastoma. Different types of dynamic modeling approaches, such as spatiotemporal modeling (Burgess et al. 1997; Tracqui et al. 1995), partial differential equation modeling (Swanson et al. 2003), ordinary differential equations, have been used to detect the growth and invasion of glioblastoma cells (Mandonnet et al. 2008). These studies, however, are only a partial picture to the unaddressed questions, and hence, further studies are required to address the same. Further, the aforementioned studies have been largely limited to understand the metabolism of glioblastoma in parts, and have not been focused to identify or predict feasible drug targets on a network scale. Moreover, these studies have also overlooked the context-dependent understanding of glioblastoma metabolism and its role in achieving specific biological goals (Banerji 2013).

Varieties of chemotherapeutic agents are available commercially to treat cancer, possessing a high degree of target specificity and better clinical manifestation. Gleevec

(imatinib), Iressa (gefitinib), Herceptin (trastuzumab), rituximab are a few examples of presently available therapeutics. However, due to multiple genetic and epigenetic alterations, the progression and disease manifestation of cancer turns out to be a complex phenomenon to understand. The malignant cancer cell populations become heterogeneous even within a specific cancer type containing diverse genetic changes, which further alters over time due to genetic instability (Pelicano et al. 2006). A multiple targeting approach in this scenario is favored over single targets to effectively deal with the random mutations generated in a cancer population. The effectiveness of the available therapeutics also has to be monitored, as many of the existing therapeutics are potentially harmful to the normal tissues too and are neurotoxic in nature.

In the present work, to understand the complex differences in the metabolic behavior of astrocyte and glioblastoma, we develop a context-specific constraint-based model for astrocyte/glioblastoma metabolism, and analyze it using flux balance analysis (FBA). For specific comparison between the two scenarios, we have considered those pathways which are known to get deregulated in glioblastoma when compared to the normal astrocyte. Our model accommodates a total of 13 pathways, the abnormal functioning of which have been reported in glioblastoma literature. The model has 247 reactions, with 39 exchange reactions and 69 transport reactions associated with 147 genes. Analyzing this large network using flux balance analysis, the differences in the individual pathway response as a part of large metabolic network in astrocyte and glioblastoma scenarios were delineated. It further aims to capture the properties of the included pathways and metabolites in glioblastoma cells (which help in its growth), to understand the differences in the uptake and utilization of metabolites (which can be categorized as essential and non-essential) and release of overflow metabolites in the two scenarios, and to predict probable chemotherapeutic targets through *in silico* single and double reaction knockout analyses of the glioblastoma model.

The results generated from both astrocytic and glioblastoma scenarios corroborated qualitatively with the experimentally available information further validating its feasibility in predicting biologically reasonable phenomena. By analyzing the steady state flux profiles generated by flux balance analysis of the model, the fate of a few metabolites, their essentiality in glioblastoma growth and the path followed by them to contribute to the optimization of objective functions (mitochondrial ATP synthesis and glioblastoma growth) were interpreted. Single and double reaction knockout analyses were performed, to determine the essentiality of the reactions involved in the metabolic network, in governing the growth properties of

glioblastoma. Potential drug targets were identified from those set of essential reactions. To determine the extent of regulation that could be imposed on those drug targets and to analyze them quantitatively, they were further simulated for chemotherapeutic intervention scenarios with the motive of either reducing the glioblastoma growth to zero, or to reduce it to the growth rate of a normal astrocyte.

Thus, our simple but extensive modeling approach provides a deep insight into the consequences of glioblastoma metabolism substantiating the strength of suitable *in silico* approaches in understanding metabolic networks and predicting biologically reasonable disease scenarios. Additionally, the classification of reaction knockouts combined with simulation of chemotherapeutic interventions could largely predict reaction pairs as feasible drug targets, further supporting the large-scale applicability of constraint-based models in predicting reasonable chemotherapeutic target combinations.

Materials and methods

Model reconstruction

Information regarding the association of enzymes to crucial metabolic reactions, their appropriate subcellular locations, transports and exchanges were compiled using a variety of data sources. The basis of this reconstruction was to identify the gene–protein–reaction (GPR) network along with appropriate transports and exchanges. The GPR was reconstructed considering reactions that contribute to ATP synthesis and glioblastoma growth.

The reactions considered in the model and their corresponding Enzyme Commission Numbers (EC Numbers) were curated from ExPasy Enzyme (Bairoch 2000) and KEGG (Kanehisa et al. 2014). The genes to the enzymatic reactions considered in the model were obtained from NCBI Gene (Edgar et al. 2002). Molecular function of these reactions and their biological process was obtained from UniProt (Consortium 2014), KEGG (Kanehisa et al. 2014) and through literature survey. Information regarding the subcellular localization of the reactions was compiled through extensive literature search and those reactions, for which literature support for subcellular localization was limited or not available; cytosol was taken to be the default compartment of the reaction. A list of reactions, their corresponding genes, enzymes, UniProt ID and KEGG ID was compiled with appropriate literature support to gather evidences related to biological significance and subcellular localization of the reactions (Online Resource 1). Most of the internal reactions along with 12 transport reactions were associated with their corresponding genes, which accounted for 147 genes in the model. All the metabolites

and the corresponding reactions in which they were involved were distributed into five different compartments: *Extracellular space*, *Cytoplasm*, *Mitochondria*, *Mitochondrial intermembrane space* and *Nucleus*. All these information were organized in the rBioNet toolbox, a MATLAB extension of the COBRA Toolbox (Schellenberger et al. 2011), to reconstruct the constraint-based metabolic model. The reconstructed metabolic network consisted of 13 pathways that are significantly affected during the transformation from astrocyte to glioblastoma (see Table S1 of Online Resource 2). The detailed pathway diagram has been drawn in CellDesigner version 4.3 and has been provided in Fig. S1 of Online Resource 2.

Flux balance analysis (FBA)

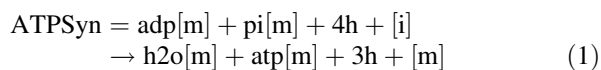
Flux balance analysis is a mathematical approach to analyze the flow of metabolites through a metabolic network, where the metabolic reactions are represented in a tabulated form of reaction matrix, of stoichiometric coefficients of each reaction. In our metabolic network, this relationship was established between the metabolites and the reactions in the form of an S-matrix which comprised of 159 metabolites and 247 reactions, building up the S-matrix of dimension '159 × 247'. The score assigned to each element of the S-matrix, S_{xy} , represented the stoichiometry of the metabolite 'x' in the reaction 'y'. A positive score signified the production of the metabolite and a negative score implied its consumption in the reaction. The column vector v had 247 fluxes, including 39 exchange reactions and 69 transport reactions. FBA formalizes the flux distribution through the whole metabolic network as the dot product of the S-matrix with the vector v . All the reactions in the model were organized in the rBioNet toolbox, where their fluxes were constrained between a lower bound v_{lb} and an upper bound v_{ub} . All the reversible reactions were bounded between $v_{lb} = -1000$ and $v_{ub} = 1000$. The irreversible reactions in the model were bounded either from 0 to 1000 or -1000 to 0 with respect to the substrate and products defined for that reaction as per available information from literature. The bounds to the exchange reactions were fixed as per the requirement of the system for uptake or release of the exchange metabolites. Those exchanges which were known to be taken in were bounded between $[-1000$ to $0]$ and those which were known to be released out were bounded between $[0$ to $1000]$. Rest of the exchanges was bounded between $[-1000$ to $1000]$ to analyze their role in the metabolism by simulating the model using FBA.

Selection of objective function

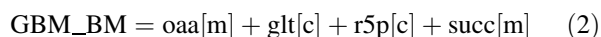
The metabolic requirement of the cancerous cells (glioblastoma, in the present case) is not completely

sufficed by diverting flux towards production of ATP through Oxidative Phosphorylation, which necessitates the requirement of an altered metabolism which can fulfill both the energy and metabolic requirement for the growth of the cells. Therefore, in our study, we defined two objective functions:

1. ATP synthesis through oxidative phosphorylation (ATPSyn)



2. a metabolic demand reaction that will dually fulfill the requirements of growth and ATP (GBM_BM). To define the metabolic requirement of the model ribose-5-phosphate, *r5p(c)*, oxaloacetate, *oaa(m)*, succinate, *succ(m)* and glutathione *glt(c)* were included as components of the objective function, selected on the basis of their contribution as (a) precursor to the nucleotide biosynthesis and synthesis of amino acids like valine, lysine, methionine, threonine, etc. (Lee et al. 2006), (b) intermediates for maintaining redox balance in different cellular compartments and biosynthesis of other cellular components required for cell growth (Covert et al. 2001; Pistollato et al. 2010), (c) preventing damage to cellular components caused by reactive oxygen species produced due to hypoxia or other cellular stress (Chung et al. 2005):



Creation and validation of astrocytic and glioblastoma scenario

Astrocytic brain tumors, commonly known as glioblastoma, are the most frequent human brain tumors, encompassing 50 % of the cases (Jellinger 1977). These emerge as manifestations of multiple alterations in the metabolic (Wolf et al. 2010) and signaling pathways (Kleihues and Ohgaki 2000) of astrocytes. Hence, in the model, selected pathways which were known to be deregulated in the astrocyte-derived glioblastoma (see Table S1 of Online Resource 2) were considered to define the metabolic differences between astrocyte and glioblastoma scenarios. Bounds to the flux through a few enzymes which defined the differences between the two scenarios were assigned on the basis of literature support. Both the objective functions were optimized for the two scenarios. Limited bounds were assigned to a few reactions to create the astrocyte scenario. The rest of the reactions fluxes were allowed to vary between a wide range of [−1000 to 1000] or [0 to 1000] or [−1000 to 0] as per the reversibility or irreversibility of the

reactions. The model was then simulated to obtain results that were in accordance with the experimentally available data defining the features of astrocyte (Mangia et al. 2009; Marrif and Juurlink 1999; Pellerin and Magistretti 1994). Bounds to the mitochondrial reactions—‘glutaminase’ [−50, 50], ‘glutamate dehydrogenase’ [−150, 150], ‘mitochondrial pyruvate carboxylase’ [−10, 10] and cytoplasmic reactions—‘acetyl-CoA carboxylase’ [0, 100], ‘L-carnitine O-palmitoyltransferase’ [0, 20], and ‘cytoplasmic malate dehydrogenase’ [−50, 50], were fixed and the model was analyzed using FBA to create the astrocytic scenario.

Perturbations were performed to the same astrocytic model by varying the lower and upper bounds to a few reactions that were experimentally found to be deregulated in glioblastoma, and then the model was simulated to create the glioblastoma scenario. Bounds were released to a few reactions, which were imposed in the astrocytic scenario: ‘glutaminase’ [−1000, 1000] and ‘acetyl-CoA carboxylase’ [0, 1000]. New bounds were assigned to another set of reactions to generate the glioblastoma scenario: ‘glutamate dehydrogenase’ [−200, 200], ‘Cytochrome c Oxidase (complex IV)’ [−10, 10], ‘Trans_Glutamate (ATP)’ [−90, 90] and ‘glycine exchange’ [−500, 500]. This model was analyzed using both ‘ATPSyn’ and ‘GBM_BM’ as objective function. This model was again validated with experimental data available for glioblastoma (Hertz and Zielke 2004; Wise et al. 2008; Ye et al. 1999). The effectiveness of GBM_BM in determining the growth properties of glioblastoma was verified with experimental evidence. The result has been provided in Fig. S2 of Online Resource 2.

In-silico prediction of minimal essential metabolite for glioblastoma growth

Glioblastoma cells are grown in commercially available MEM or DMEM media (Anton and Glod 2014; Guessous et al. 2013; Ye et al. 1999). However, due to lack of sufficient literature that report the essential metabolites required for glioblastoma growth even at glucose starved conditions, an in silico simulation was performed to check the fate of some key metabolites that contribute to the growth in the glioblastoma. The entry of each carbon source was considered in the model, one at a time and the corresponding solution of the GBM_BM objective function (growth) was computed. Also, the fate of the most essential metabolite with another input carbon source within the model was checked and the optimal solution of the GBM_BM objective was calculated. This was performed to identify the most important carbon sources required for enhancing glioblastoma growth.

Single and double reaction knockouts in glioblastoma

A reaction knockout strategy was chosen, instead of gene knockout approach, to completely nullify the functional effect of the reaction in the network. Reaction knockout predictions allowed the identification of reactions that could be targeted for either completely inhibiting or reducing the glioblastoma growth. Each of the 247 reactions in the metabolic network was knocked down individually to predict the mutations that could be lethal to the glioblastoma growth. For performing the knockout, flux through each reaction in the network was constrained to zero and solution of the GBM_BM objective function was computed for each knockout. Double reaction knockouts were also performed, with a combination of two reactions to be knocked down simultaneously. The single and double knockouts were classified on the basis of percentage reduction of flux through the objective function, GBM_BM, from its optimal value. The optimal value of the objective function for the astrocytic scenario in the model corresponded to the normal growth rate.

Simulation of chemotherapeutic interventions

Further, we filtered the results of double reaction knockouts for identifying feasible chemotherapeutic combinations to target glioblastoma growth. For performing *in silico* chemotherapeutic interventions, we divided the reactions into three groups as per their essentiality. We predicted the putative feasible ranges for each of these reaction combinations, in which chemotherapeutics can effectively target glioblastoma growth either for its complete inhibition or bring it back to the normal astrocytic growth rate.

Results

Properties of the model

The present context-specific model for glioblastoma metabolism has a total of 247 reactions, with 39 exchange reactions and 69 transport reactions. Most of the internal reactions along with a few transport reactions have been associated with their corresponding genes, which accounts for 147 genes in the model.

The present model for glioblastoma metabolism can be classified on the basis of the following four categories: (1) enzyme commission number, (2) gene non-gene association, (3) sub-cellular locations, and (4) metabolic processes (Fig. 1). A large number of the reactions in the model belonged to the class 1 category of enzyme classification i.e., the oxidoreductases (22 %). These set of enzymes catalyze the

oxidation of one chemical species and the simultaneous reduction of the other by transfer of electrons from one species to another. The other classes of enzymes in this classification scheme were the transferases (14 %) followed by lyases (10 %), hydrolases (4 %), isomerases (2 %), and ligases (2 %). Another 28 % of the reactions belonged to transport reactions and 16 % to extracellular exchange reactions, which occurred spontaneously in the system (Fig. 1a).

The reactions can also be classified on the basis of their association with genes to understand gene reaction associations (Fig. 1b). 60 % of the model reactions were gene-associated, out of which 6 % were transport reactions. The rest of the reactions were classified as: Non-Gene associated Exchange Reactions (16 %), Non-Gene associated Intracellular Reactions (2 %) and Non-Gene associated Transport Reactions (22 %).

In the classification shown in Fig. 1c, the cytosolic and mitochondrial reactions contributed to 54 % of the total reactions in the model. 2 % of the reactions belonged to the mitochondrial intermembrane space model compartment that specifically accounted for oxidative phosphorylation. The transport reactions were categorized according to the membrane to which it is associated. Transports accounted for 30 % of the total reactions: Mitochondrial membrane spanning (11 %), Nuclear membrane spanning (2 %) and Plasma Membrane spanning (17 %).

With reference to the metabolic processes, 23 % of the reactions belonged to fatty acid metabolism inclusive of both biosynthesis and beta oxidation of palmitic acid. The rest of the pathways contributed to 30 % of the total count of which 14 % belonged to Glycolytic, PPP, TCA cycle and Oxidative phosphorylation pathway and 2 % were contributed each by Glycine–Serine Metabolism, Cysteine Metabolism, Methionine Metabolism and Glutamate Metabolism, without taking into account the transport and exchange reactions. Another set of reactions, namely, cytosolic ATPase (ATPS), cytoplasmic malate dehydrogenase (MDH(Cyto)), Phosphoenolpyruvate carboxykinase (GTP) (PEP_CarbK_1), mitochondrial pyruvate carboxylase (Pyr_Carbm) which could not be assigned strictly under any particular pathway, were categorized as ‘Others’ which contributed 2 % of reactions to the (Fig. 1d).

Validation of astrocytic and glioblastoma model

The reconstructed metabolic model was validated for both the astrocytic and the glioblastoma scenarios, using mitochondrial ATP synthesis as the objective function. The astrocytic scenario was created first, by fixing bounds of a few reactions. Few known perturbations from experiments were introduced to the astrocytic scenario so as to create the glioblastoma scenario (See “[Materials and methods](#)” section for details).

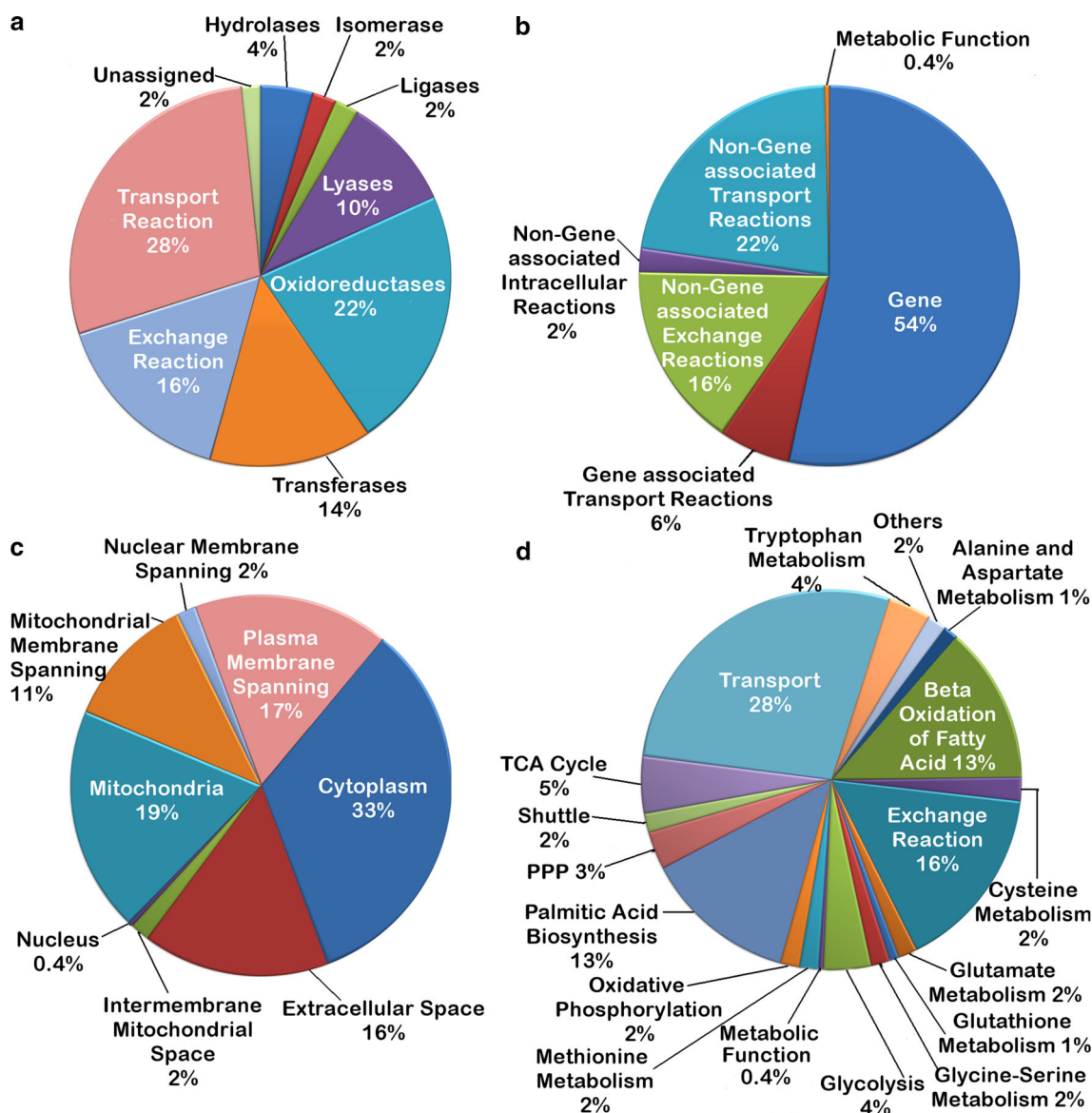


Fig. 1 Classification of the properties of reconstructed metabolic model. The model reconstruction has been classified on the basis of **a** enzyme commission number or E.C. number, **b** gene-non gene association, **c** cellular compartments, and **d** metabolic processes, respectively

Astrocyte

Required changes were made to the bounds of certain reactions during simulation of the astrocyte model and the optimal range of bounds within which it showed the properties of astrocyte was estimated (see “[Materials and methods](#)” section). The model astrocyte scenario was analyzed and validated, using mitochondrial ATP synthesis (ATPSyn) as the objective function. The astrocyte scenario was validated for a number of experimental observations, such as pyruvate recycling, lactate production and effect of glutamate.

Astrocytes prefer a glucose-dependent metabolism where glucose is catabolized to pyruvate that enters the

TCA cycle thereby leading to ATP synthesis (Mangia et al. 2009) and partly to the formation of lactate so as to suffice the neuronal requirement. This property was examined in the model astrocytic scenario by performing a robustness analysis of glucose uptake with increasing oxygen uptake. The default flux balance analysis (FBA) of model astrocytic scenario suggested an optimal flux of 160 for oxygen uptake from the environment. The uptake of oxygen was thus, varied up to its optimal flux and its effect on glucose uptake was observed. Increase in oxygen uptake led to linear but proportional increase in glucose uptake (Fig. 2a). This inferred the utilization of glucose to produce lactate by the astrocytes without affecting the mitochondrial respiratory chain. Further, a slight dip in the glucose uptake

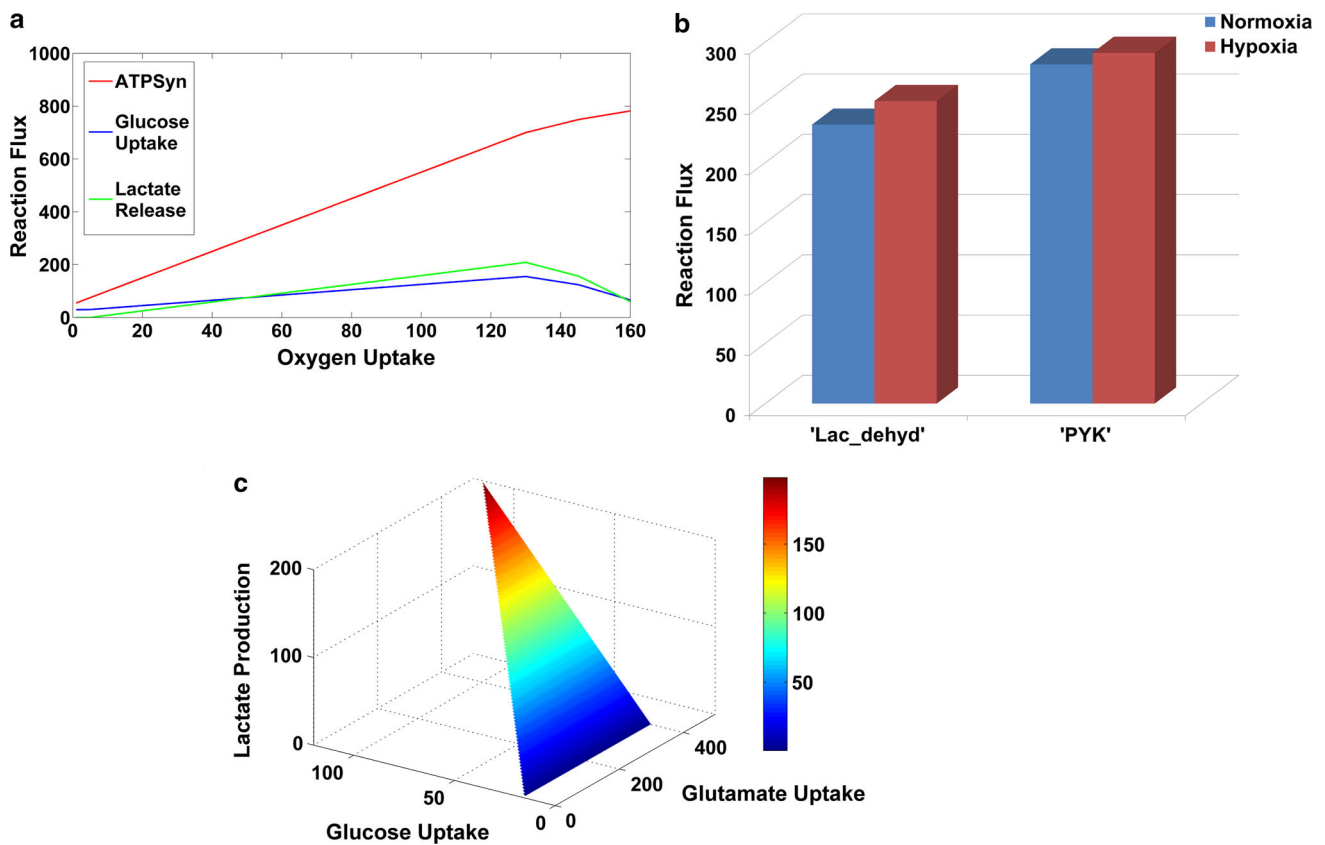


Fig. 2 Validation of astrocyte scenario. Properties of astrocyte: **a** increase in glucose uptake driven towards mitochondrial ATP synthesis and lactate production, **b** increase in the activity of lactate

dehydrogenase and pyruvate kinase in hypoxia conditions, **c** increase in glucose utilization and lactate production with increasing glutamate uptake

rate was observed when the flux through the oxygen uptake was more than 130. But simultaneously, flux through mitochondrial ATP synthesis continued to increase, signifying that the decrease in glucose uptake did not affect the ATP synthesis. The probable reason for this may be the recycling of pyruvate from the TCA cycle intermediates. Reports also suggest that one of the TCA cycle intermediates, citrate, may produce oxaloacetate, which is subsequently converted to pyruvate through the activity of malic enzyme or by the combined activity of PEP carboxykinase and pyruvate kinase (Sonnewald et al. 1996).

Similar to this, model simulations suggested recycling of pyruvate by utilization of TCA produced oxaloacetate through PEP carboxykinase and pyruvate kinase reactions. This resulted in a reduced dependence of pyruvate production on glucose uptake. The pyruvate so formed was catabolized into the TCA cycle and compensated for maintaining ATP production proportional to oxygen uptake.

The activity of lactate dehydrogenase and pyruvate kinase increased during anoxic conditions as compared to normoxic conditions in astrocytes (Marrif and Juurlink 1999). To verify this property, normoxic and hypoxic

conditions were created in the model by constraining the oxygen uptakes at the optimum (flux value = -120) and low (flux value = -2) values and ensuring sufficient glucose uptake in the model. It was observed qualitatively that the model is capable of capturing this feature of astrocytes (Fig. 2b). Although the actual experimental result was generated by incubating the astrocyte cells in a completely oxygen deprived anoxic condition for 6 h, creating such a situation in the in silico analysis would lead to zero ATP synthesis (objective function considered for validation) in the model due to its dependence on oxygen. Hence, the property was verified for hypoxic conditions only. Similar pathway-based down-regulation in activity of certain proteins under hypoxic stress has been reported earlier (Maity et al. 2000) but for the signaling pathways.

In astrocytes, the uptake of glucose increases with increase in glutamate uptake thus leading to increased lactate production (Pellerin and Magistretti 1994). This situation was created in the model by regulating the exchanges of glucose, glutamate, glutamine and oxygen. By varying the glutamate uptake from 0 to 450, a corresponding increase in glucose uptake and hence, lactate production was observed during model simulations.

Further, it was observed that highest lactate production was at a glutamate uptake flux of 450 (Fig. 2c).

Glioblastoma

In the model, the astrocytic scenario was further perturbed to create the glioblastoma scenario. To validate the glioblastoma scenario, steady state fluxes of certain reactions obtained by simulating for glioblastoma scenario was compared with that of the astrocyte scenario, while keeping all the nine inputs open to the system. The “Warburg effect”, which states a reduction of ATP production through mitochondrial respiration and an increase in glucose utilization to increase the flux towards aerobic glycolysis (Zhou et al. 2011), was observed in the glioblastoma scenario (Fig. 3a).

For further validation of this scenario, few experimental observations were replicated from the model. Glutaminolysis is a known property of glioblastoma cells, where the uptake and utilization of glutamine is favored over glutamate for compensating the loss of glutamate through cysteine–glutamate antiporter (Wise et al. 2008), which is a property that is exactly opposite to that of astrocytes (Hertz and Zielke 2004). Also, uptake of cystine increases in the glioblastoma cells due to enhanced activity of cysteine–glutamate antiporter (Ye et al. 1999). All these differences in the exchange properties of glioblastoma could be observed through our model, when the entry of all the input metabolites was allowed (Fig. 3b).

Validation of glioblastoma metabolic demand reaction (GBM_BM)

A separate metabolic demand reaction was also introduced in the model glioblastoma scenario so as to understand the

influence of different metabolites on glioblastoma growth. Considering this reaction as the cellular objective, the glioblastoma scenario was further studied for its metabolic properties. All the further analyses have been performed keeping the GBM_BM metabolic demand reaction as the objective function. For the verification of the objective function—‘GBM_BM’ in representing the properties of glioblastoma, a qualitative analysis was performed to compare the activity of certain reported reactions in the astrocytic and glioblastoma scenario. The fold change in activity from astrocytic to glioblastoma scenario as predicted from the model was compared to existing proteome data extracted from young glioblastoma patients (Deighton et al. 2014). The results of this comparison are listed in Table 1. Data was available as fold change in expression for eight reactions of the model. Out of the eight reactions, predicted activity for five reactions was qualitatively found to be in correspondence with the experimental observations.

Opposing roles of glycine and glutamate uptake in astrocytes

Evidences state that glycine content of neuronal cells was higher than that of glial cells (Roux and Supplisson 2000). Also, most of the CNS tissues sufficed their glycine requirement via the internal glycine–serine metabolism pathway derived from glucose via 3-phosphoglycerate (Nicklas and Browning 1978), even though astrocyte cultures fed with glycine were capable of utilizing it by maintaining intracellular levels of glutathione, serine and creatine (Dringen et al. 1998). Further, high uptake of glycine in astrocytes was observed to be tightly coupled with high secretion of Na^+ and Cl^- (Zafra and Gimenez

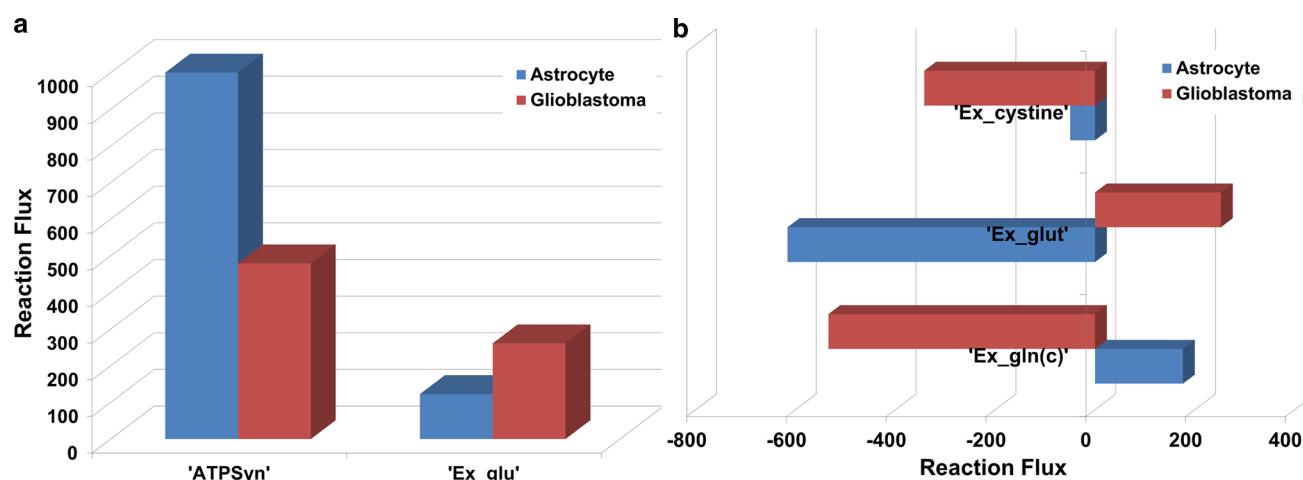


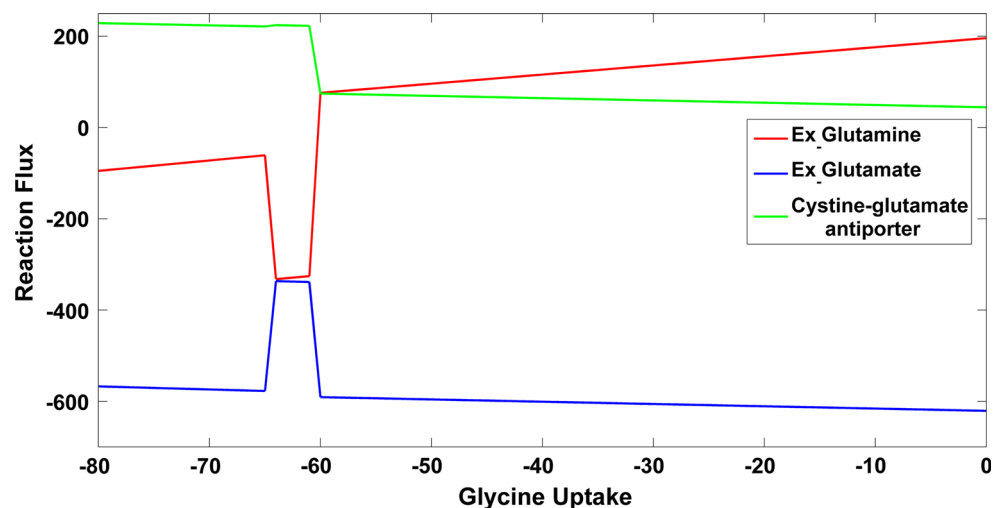
Fig. 3 Validation of glioblastoma scenario. Properties of glioblastoma: **a** reduced mitochondrial ATP synthesis and increased glucose utilization in glioblastoma scenario; **b** reversal in glutamate and glutamine utilization and increase in cystine uptake in glioblastoma scenario

Table 1 Comparison of model prediction with the data available for enzyme expression in young patients

Uniprot ID	Reaction name	Model abbreviation	Fold change	Model prediction	Gene abbreviation	Fold change	Experimental prediction
O43175	D-3-phosphoglycerate dehydrogenase	PGDH	0.9313	D	PHGDH	0.55	D
P04075	Fructose-bisphosphate aldolase A	FBA	0.9175	D	ALDOA	0.71	D
P50213	Isocitrate dehydrogenase [NAD] subunit alpha, mitochondrial	IDH	0.0000	D	IDH3A	0.48	D
P18669	Phosphoglycerate mutase 1	PGM	2.4046	U	PGAM1	1.6	U
Q9Y617	Phosphoserine aminotransferase	PST	0.9313	D	PSAT1	0.53	D
P00367	Glutamate dehydrogenase, mitochondrial	GlutDH	0.0000	D	GLUD1	1.4	U
P60174	Triosephosphate isomerase	TPI	0.7401	D	TPI1	2.1	U
P17174	Aspartate aminotransferase, cytoplasmic	ASPTc	1.0732	U	GOT1	0.53	D

N.B.: Regulation in enzymatic expression (up-regulation or 'U' and down-regulation or 'D') for eight reactions present in our model could be related to the enzymatic profile available for young glioblastoma patients

Fig. 4 Effect of glycine uptake on glutamate utilization by astrocyte. Change in the uptake and release of glutamate, glutamine and cystine–glutamate antiporter with increasing uptake of glycine in the astrocyte scenario. The uptake of glutamate reduces with increasing uptake of glycine and the glutamine exchange reverses its direction of flow of flux



1986). In the model, we have assumed the uptake of glycine to be a normal uptake devoid of its coupling with Na^+ and Cl^- . To simulate the effect of variation in extracellular Na^+ and Cl^- ions on glycine uptake, the bounds on glycine uptake in the astrocytic scenario was varied. Further, bounds on uptake of all the aforementioned input metabolites were released so as to allow their utilization within the model. It was observed that glycine uptake had a dominant influence on glutamate/glutamate uptake cycle of astrocytes. Glutamate taken in by the cell is catabolized through TCA, glutamine production and release, and release of glutamate through cystine–glutamate antiporter. Under low glycine uptake (flux value of glycine uptake < -60), most of the glutamate taken into the cell, forms glutamine and is released from the cell ensuring lower uptake of cystine and hence, less glutamate release through cystine–glutamate antiporter (Fig. 4). Whereas, increased glycine uptake is driven towards increased synthesis of glutathione. Simultaneously, an equal increase in flux through cystine uptake (cystine–glutamate antiporter) also

takes place. Cystine is then provided for cysteine biosynthesis, which combines with glycine for glutathione production. For increased uptake of cystine, an equal efflux of glutamate through the antiporter is also required. Glutamate required for this efflux is provided by its uptake through glutamate-ATP transporter. To compensate for the amount of glutamate lost through efflux, glutamine uptake increases and this glutamine leads to glutamate synthesis. This result suggests that the astrocyte prefers higher glycine uptake so as to combat oxidative stress whereas a lower uptake of glycine is preferred when there is a higher requirement of glutamine by the surrounding neurons.

Difference in pathway response between the astrocytic and glioblastoma scenarios

Cells tend to either maximize ATP synthesis or optimally use metabolites from the environment to satisfy their cellular demand for optimum growth. The choice of an objective function that can be used to capture actual

biological scenarios is a primary requirement for performing FBA. To understand the roles of the aforementioned cellular objectives, the model was simulated in both the astrocytic and glioblastoma scenarios for the two objective functions: mitochondrial ATP synthesis and GBM_BM metabolic demand reaction separately (See “Materials and methods” section).

Maximization of mitochondrial ATP synthesis

FBA simulations for maximization of ATP synthesis revealed a number of metabolic features of the glioblastoma scenario.

1. *Increase in glycolytic flux in glioblastoma* Simulations for ATP synthesis as the objective function demonstrated a significant increase in the flux through the glycolytic and pentose phosphate pathways in the glioblastoma scenario as compared to the astrocyte but a corresponding decrease in ATP synthesis (Fig. 5a, b). To create the glioblastoma scenario, a reduced activity of Complex IV of the electron transport chain was assumed (Chatterjee et al. 2006). ATP synthesis is largely dependent on Complex IV for redox balance. Hence, decreased ATP synthesis is observed. Under the reduced activity of Complex IV, the deficiency of electrons for ATP synthesis is partly met through Complex I and III of electron transport chain. This led to an increased synthesis of oxaloacetate from phosphoenolpyruvate through the PEP carboxykinase and aspartate aminotransferase reactions. Hence, flux through glycolysis is largely increased in the glioblastoma scenario for the provision of phosphoenolpyruvate. The glycolytic dependence of ATP synthesis is a unique feature of glioblastoma cells (when compared to astrocytes) that could be captured from the model (Vander Heiden et al. 2009). A comparison of the steady state flux profiles of astrocyte versus glioblastoma with ATPSyn as objective has been provided in Table S2 of Online Resource 2.
2. *Increased cystine uptake in glioblastoma* Simulations for ATP synthesis as the objective function also demonstrated an increased uptake of cystine (Fig. 5c). The total flux of cystine is distributed into cysteine biosynthesis which is then distributed towards a relatively low amount of glutathione biosynthesis (Fig. 5f) and largely towards production of pyruvate through the cysteine dioxygenase (CD), cysteine sulfinate transaminase (CST), and the spontaneous 3snpyr (SPON1) reactions. This pyruvate is utilized for acetyl coA synthesis and hence, the biosynthesis of fatty acids which are further released in the extracellular environment.

3. *Increased catabolism of glutamine in glioblastoma* Reactions belonging to glutamate metabolism showed a higher activity which was due to higher glutaminolysis in glioblastoma scenario (Wise et al. 2008). This was due to the uptake of glutamine by the glioblastoma cells, from external medium, which was converted to glutamate within the cell. The glutamate that was formed was mostly used by the cystine–glutamate antiporter (anti_cystine_glut) in order to uptake cystine. Cystine then is utilized in the cysteine metabolism pathway for pyruvate synthesis that enters TCA cycle (Fig. 5d).
4. *Decreased glycine–serine biosynthesis in glioblastoma* Simulations of the model for ATP synthesis as the objective function also demonstrated an increased uptake of glycine (Fig. 5e). It could be observed that in glioblastoma, glycine was preferred to be taken inside the cell whereas in contrary it is being synthesized within the astrocyte. This was because the glycolytic flux was completely utilized into TCA cycle for maximizing ATP production instead of being distributed into the mitochondrial TCA cycle and glycine–serine metabolism.

Maximization of the metabolic demand

Qualitatively, the same trend of pathway response was observed for the two scenarios while optimizing the model for the metabolic demand reaction ‘GBM_BM’. Although, a few more differences were further observed while considering the GBM_BM demand reaction.

1. *Increased flux through glycolysis and pentose-phosphate pathway in glioblastoma* Simulating the model for GBM_BM objective function in both the scenarios suggested an increased flux through the glycolysis and pentose-phosphate pathway (PPP) reactions (Fig. 6a, b). This increased flux is contributed by the glycine uptake through the phosphoglycerate dehydrogenase (PGDH) reactions into glycolysis and hence, PPP so as to provide for ribulose-5-phosphate present in the GBM_BM objective. Further, the lower part of glycolysis was observed to be more active as compared to the upper reactions as reported in a study (Oudard et al. 1996), where a low activity of hexokinase was observed due to the loss of chromosome 10. Apart from this, some amount of glycine is partly distributed through the phosphoenolpyruvate carboxykinase (PEP_CarbK_1) reaction for production of oxaloacetate and succinate which is part of the GBM_BM demand reaction. A comparison of the steady state flux profiles of astrocyte versus glioblastoma with GBM_BM as objective has been provided in Table S3 of Online Resource 2.

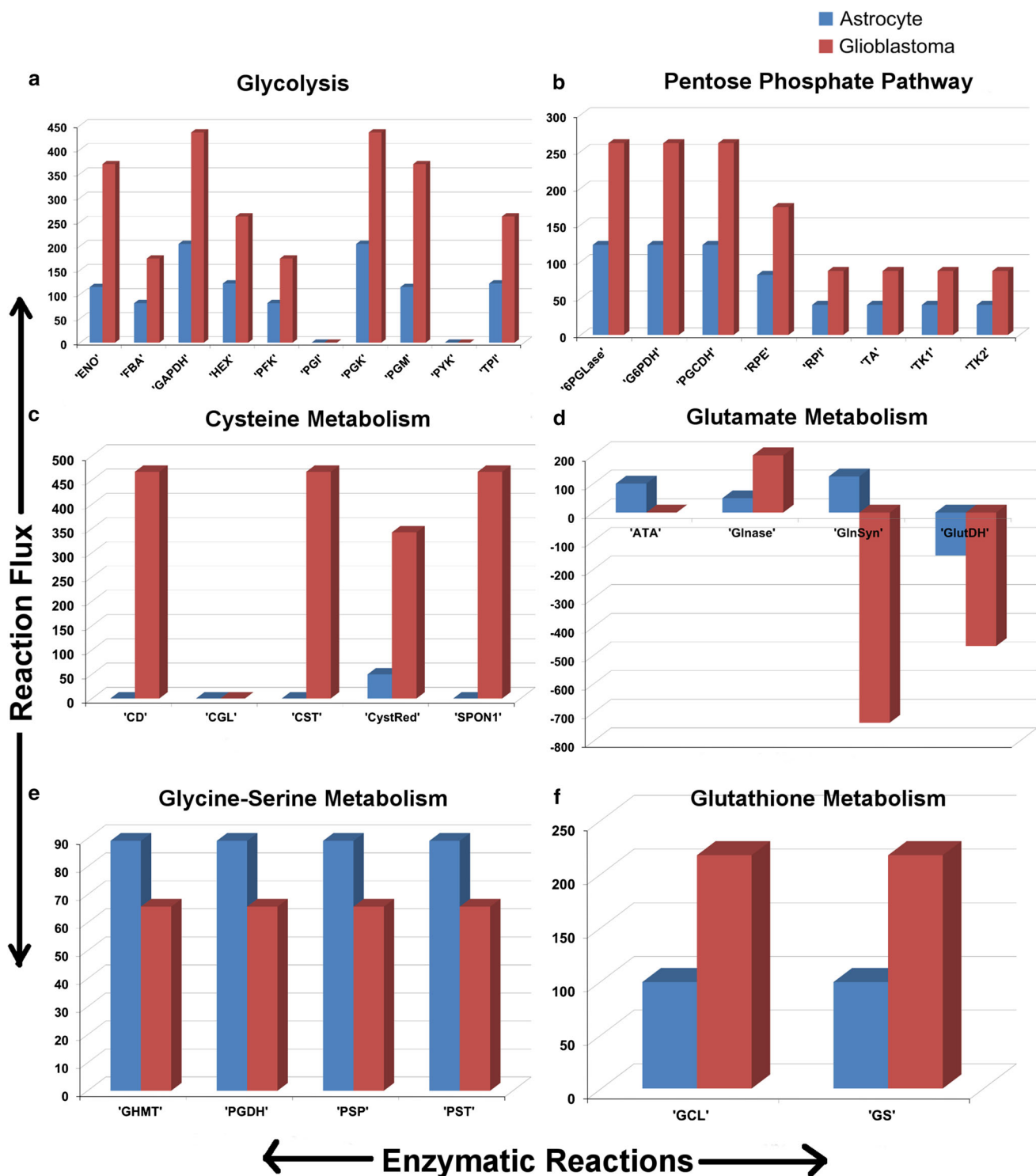


Fig. 5 Pathway response with maximization of mitochondrial ATP synthase, 'ATPSyn' as the objective. Flow of flux through the different reactions of **a** glycolysis, **b** pentose phosphate pathway,

c cysteine metabolism, **d** glutamate metabolism, **e** glycine-serine metabolism and **f** glutathione metabolism pathway while maximizing mitochondrial ATP synthesis

2. *Increased cystine uptake in glioblastoma* Simulating the model for GBM_BM objective function in both the scenarios further demonstrated a higher increase in

cystine uptake and its metabolism as compared to the model simulations using ATP synthesis as objective (Fig. 6c). This was because of the higher requirement

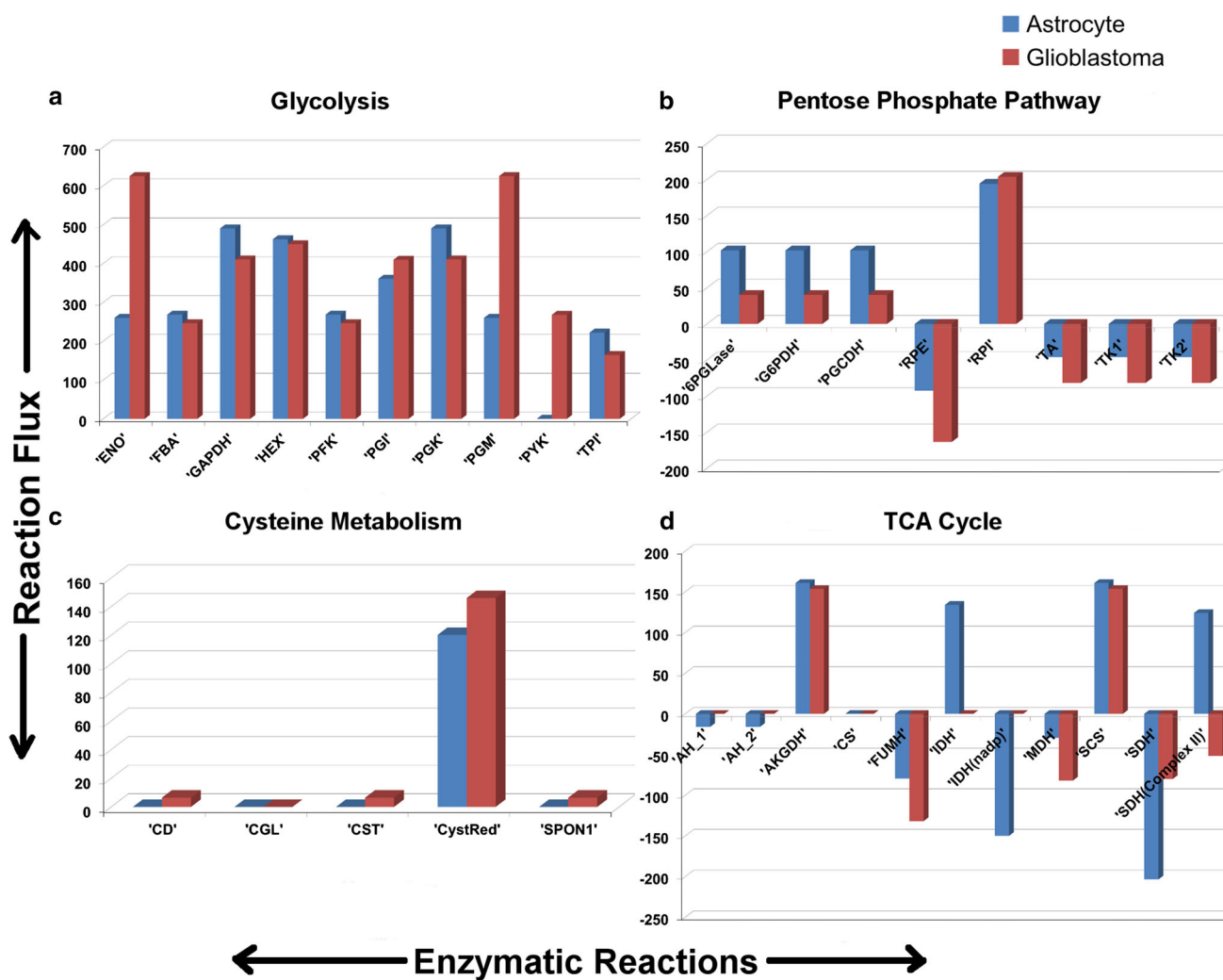


Fig. 6 Pathway response with maximization of metabolic function, 'GBM_BM' as the objective. Flow of flux through the different reactions of **a** glycolysis, **b** pentose phosphate pathway, **c** cysteine metabolism, **d** TCA cycle; while maximizing the metabolic function,

GBM_BM, for glioblastoma growth. A positive flux shows progression of reaction in forward direction and a negative flux implies flow of flux in reverse direction

of glutathione to meet the metabolic demand of glioblastoma cells to combat oxidative stress.

3. *Reversal of TCA cycle towards production of malate and fumarate in both scenarios* A back flux in TCA cycle, from oxaloacetate to fumarate was also observed in experiments, in both cultured astrocytes and in in vivo conditions, which was due to the activity of mitochondrial pyruvate carboxylase (Brekke et al. 2012). Through the model simulation, similar properties in the glioblastoma scenario were observed too (Fig. 6d). The flux through the fumarate hydratase (FUMH) and malate dehydrogenase (MDH) reactions was reversed and enhanced in the glioblastoma scenario. The reason for this reversal was to maximize succinate production through TCA cycle, which was an important component of the metabolic demand reaction.

Essentiality of metabolites and reactions in glioblastoma growth

The important metabolites that contributed significantly to glioblastoma growth were identified. Single and double reaction knockouts analyses were performed to identify the sets of reactions, which could significantly reduce glioblastoma growth. The analyses were performed using the GBM_BM objective function.

Determination of metabolites essential for glioblastoma growth

Glioblastoma cell lines can show extremely long survival under glucose starved conditions by undergoing physiological adaptations to utilize alternatives and thus, combat nutrient deprivation (Griguer et al. 2005). In order to

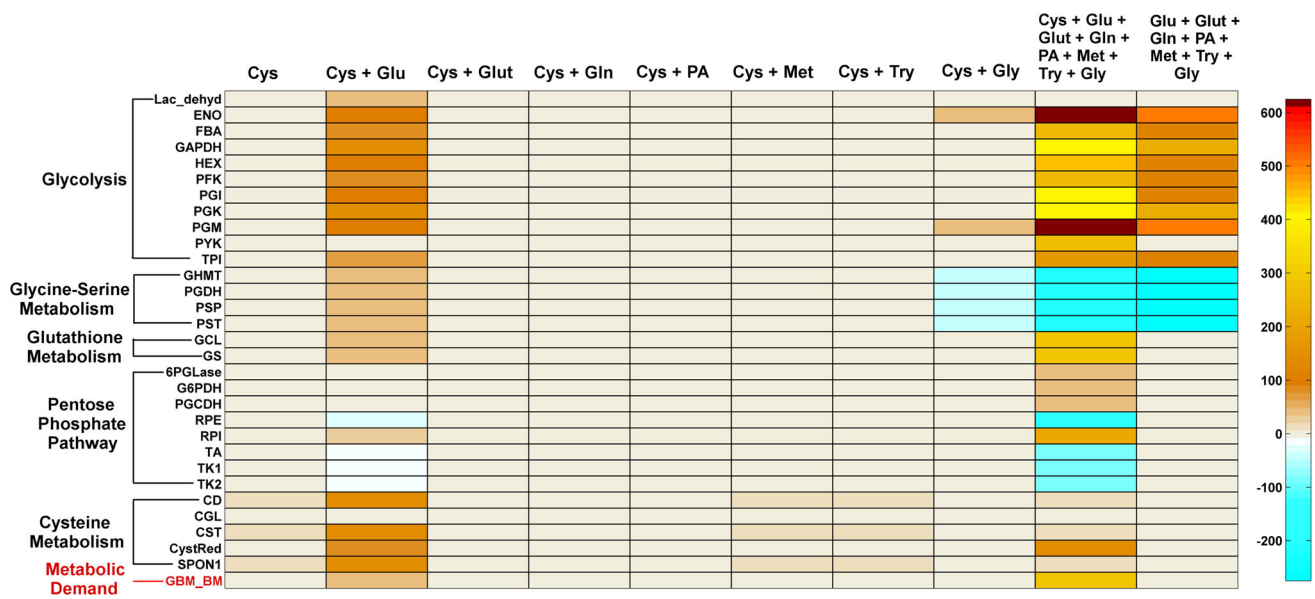


Fig. 7 Essentiality of metabolites in glioblastoma growth. Flux through different pathways and metabolic function in different input conditions to the glioblastoma scenario. Here flux through the different pathways and the metabolic function is maximum for cystine

and glucose as input. The metabolites have been abbreviated as: *Cys* cystine, *Glut* glutamate, *Glu* glucose, *Gln* glutamine, *Gly* glycine, *Met* methionine, *Try* tryptophan, *PA* palmitic acid

determine those metabolites which essentially contributed to glioblastoma survival, even at glucose starved conditions, the metabolic fate of eight carbon sources namely, glucose, cystine, methionine, tryptophan, palmitate, glutamate, glutamine, and glycine through the network, was investigated. From the simulation results, cystine was found to be an essential metabolite for glioblastoma growth, although glucose was largely required for satisfying the metabolic demand and increasing glioblastoma growth rate. A complete deprivation of glucose did not lead to zero growth although growth rate was largely reduced. Previous experimental findings have also suggested a large reduction in cell growth due to glycolytic blockade by glucose starvation (Griguer et al. 2005). Also, effect of glucose in combination with cystine was more pronounced in glioblastoma growth, instead of cystine alone as input (Fig. 7). The simultaneous uptake and utilization of cystine and glucose served as the minimal metabolite requirement that could drive all those pathways which lead to synthesis of objective function components [Eq. (2)]. The essential role of cystine is to produce glutathione that would be required to combat oxidative stress. This observation was in agreement with the available experimental evidences, where cystine uptake was proven to be essential (Chung et al. 2005) and cysteine metabolism was identified to be a novel pathway in the glioblastoma growth (Prabhu et al. 2014). And the role of glucose was to produce ribulose-5-phosphate, oxaloacetate and succinate through PPP and TCA cycle. Consequently, this minimal combination resulted in a solution higher than any other combination,

thereby accounting for optimal glioblastoma growth. Restricting the uptake of either of these metabolites led to either zero growth or a highly reduced growth rate (<20 % of the optimal value).

Predictions from single and double reaction knockouts

From the observations made in the previous section, cystine was found to be an important metabolite for glioblastoma survival. To further analyze the essentiality of the reactions involved in the metabolism of cystine, and also to find the other important reactions in the model, which could be targeted for reducing glioblastoma growth, single and double reaction knockout analyses were performed (Table 2 and Table S4 and Table S5 of Online Resource 2). All the single and double reaction knockout results were categorized as cases of lethal, trivial and non-trivial lethal and non-trivial solutions.

Glioblastoma cells can thrive on different metabolic pathways for survival and show great metabolic heterogeneity (Griguer et al. 2005). Similarly, it was observed that around 3 % (6 reactions) of the total single knockouts (208 reactions) and 6 % (1268 reactions) of the total double knockouts (21,528) were lethal to the glioblastoma scenario. A low number of lethal single knockouts suggested the robustness of metabolism in sustenance of the glioblastoma cells through alternative routes. Knockout analysis was performed on the network using GBM_BM as the objective function.

Table 2 Total number of single and double lethal reaction knockouts

Deletion	Lethal	Trivial lethal	Non-trivial lethal	Non-trivial total	Total cases
Single	6	NA	6	208	208
Double	1268	1227	41	20,301	21,528

N.B.: The lethal double reactions knockouts are categorized as trivial and non-trivial lethal. Those knockout combinations, of which at least one is involved in single lethal reaction knockout, are considered to be “trivial”. Those combinations in which neither of the reactions is involved in single lethal reaction knockout are considered to be “non-trivial”

NA not applicable

Knockout analysis identified ribulose phosphate isomerase (RPI), a part of the pentose phosphate pathway to govern a lethal phenotype. In many type of cancers, it has been experimentally observed that PPP drives the glycolytic flux for production of ribose-5-phosphate and NADPH that can be used by cancers cells for detoxification of reactive oxygen species (Boada et al. 2000). RPI represents a rate limiting-step for ribose-5-phosphate production in the PPP pathway. As ribose-5-phosphate is an essential component to meet the cellular metabolic demand, RPI was predicted to govern a lethal phenotype in the glioblastoma scenario. Also, in different types of cancers, high level of glutathione contents have been experimentally observed to combat with the oxidative stress experienced by the cancer cells (Ogunrinu and Sontheimer 2010). Glutamate–cysteine ligase (GCL), rate-limiting step for production of glutathione was predicted to govern a lethal phenotype as it is the penultimate step for glutathione production. Similarly, glutathione synthase (GS), the ultimate step of glutathione synthesis from glutamate and cysteine was also predicted to govern a lethal phenotype. The cystine–glutamate antiporter (Anti_cystine_glut) and cystine reductase (CystRed) reactions are involved in production of cysteine. In the previous results, it was demonstrated that cystine was sufficient for production of the components of the GBM_BM objective. Hence, both the reactions were predicted to demonstrate lethality when knocked out.

Of the 1268 lethal double knockout reactions, 41 were non-trivial, which included reactions from glycolytic, pentose phosphate, TCA cycle and glycine–serine metabolism pathway and a few transport reactions. The most typical observation of glioblastoma metabolism through experiments was the increased flux through glycolysis for a high production of ATP and corresponding reduction in glioblastoma growth under glucose starvation, even though their survival was maintained (Griguer et al. 2005). A combinatorial targeting of the glycolytic pathway with the PPP, TCA cycle and glycine–serine metabolic pathways was hence, found to be more effective in combating glioblastoma growth. Thus, the knockdown of a glycolytic pathway reaction in combination to a pentose phosphate

pathway reaction or a TCA cycle reaction hindered the production of r5p or oaa or succ. Consequently, the double knockouts proved to be lethal to the glioblastoma growth. The in silico results also yielded reactions belonging to glycine–serine metabolism as good targets in combination with each other. Glycine was necessarily required for glutathione production. When the availability of glycine was blocked through the knockdown of both the internal glycine–serine metabolism and the external source of glycine uptake, this paired knockout led to the inhibition of glutathione production, and hence proved lethal. Consequently, dual targeting the reactions of this pathway was effective in reducing the growth.

The knockouts reaction results were further classified as lethal, growth reducers and null reducers on the basis of percentage inhibition in the metabolic demand reaction rate in the glioblastoma scenario (Fig. 8). Knockouts which led to 100 % inhibition of metabolic demand reaction were considered to be “Lethal”. Reaction knockouts which caused a flux reduction of >80 % of the flux through the metabolic demand were considered to be “Partial growth reducers”. Those set of reaction knockouts which inhibited the flux of metabolic demand within 20–80 % of the default value, were considered as “Marginal growth reducers”. The class of ‘sub-marginal growth reducers’ was considered for those set of knockouts which could not bring effective reduction (0–20 % inhibition) through the objective function. Analysis of the double knockout showed that 48 % of the partial growth reducers belonged to the glycolytic pathway. The rest of the 52 % were mostly constituted by the reactions of TCA cycle, PPP, Oxidative phosphorylation and Glycine–serine metabolism. The larger fraction of both single and double reaction knockouts which belonged to sub-marginal growth reducers and null reducers which were indicative of the robust and redundant reactions of the glioblastoma metabolic network.

Chemotherapeutic interventions in glioblastoma scenario

The reaction knockout analyses could predict a subset of reactions, which were crucial in glioblastoma growth. To

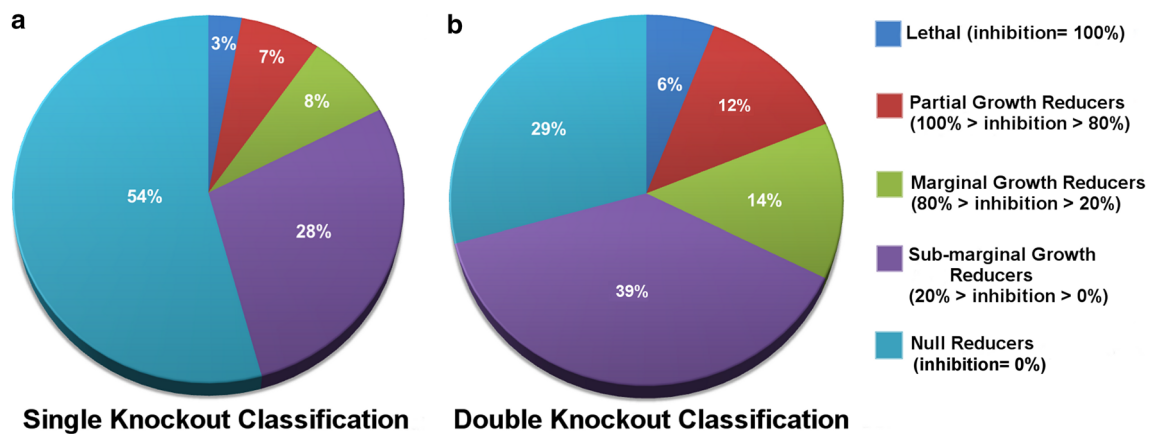


Fig. 8 Single and double reaction knockout predictions. The results of single and double reaction knockout predictions are summarized. **a**, **b** Single and double knockout reaction classifications, respectively. The predictions are classified in five categories: (1) lethal (inhibition = 100 %), (2) partial growth reducers

(100 % < inhibition < 80 %), (3) marginal growth reducers (80 % < inhibition < 20 %), (4) sub-marginal growth reducers (20 % < growth < 0 %), (5) null reducers (inhibition = 0 %), with the percentage inhibition imposed by them being indicated in the parentheses

identify the feasibility of targeting these reactions and their effectiveness, these reactions were simulated for their effect as chemotherapeutics for either inhibiting, or bringing down the growth rate of the glioblastoma cells to a normal range. For this analysis, the previously identified growth reducer reactions leading to reduced growth ($0 < \text{GBM_BM solution} < \text{glioblastoma optimum}$) were chosen.

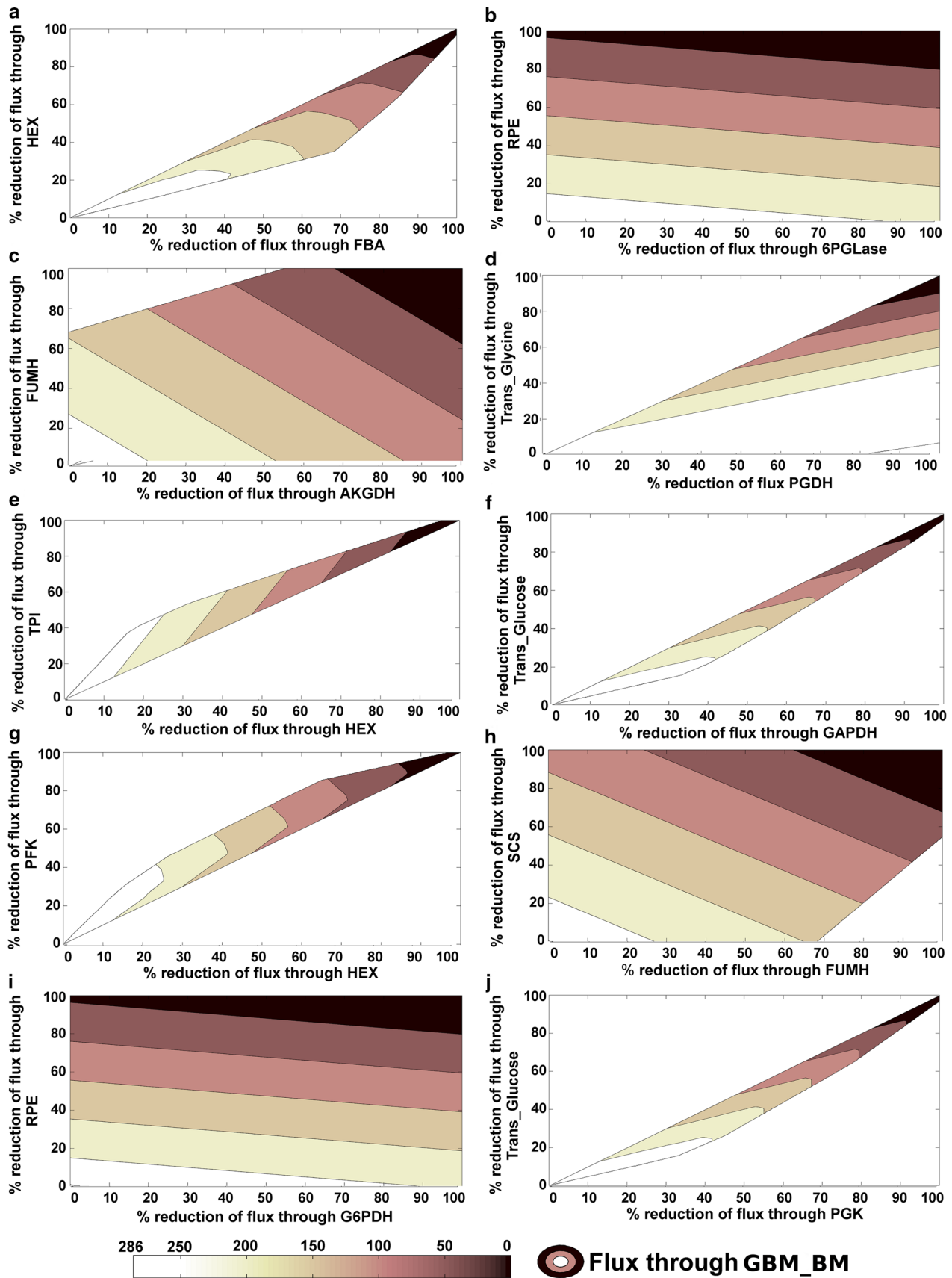
From the simulation studies it was observed that in order to completely reduce the flux through the metabolic function, targeting the lethal single knockout reactions required a complete reduction of flux through them. Whereas targeting the lethal double knockout reactions were more effective, as partial reduction of flux through those combinations brought a complete reduction of flux through the metabolic demand reaction. Recent experimental approaches also suggest that targeting a combination of proteins instead of each individual protein of the combination, could bring about a more pronounced anti-tumorigenic effect (Oliveira-Ferrer et al. 2013). As such, combinations from non-trivial lethal knockout reactions were simulated which could be targeted most effectively for efficient growth reduction.

Of the 41 non-trivial lethal double knockout predictions, 36 combinations were chosen for testing their chemotherapeutic intervening properties, which excluded a few transport reactions. Each reaction combination was simulated by varying the flux through individual reactions of the combination simultaneously, to obtain the effective reduction of flux through both of these reactions which reduced glioblastoma growth completely and to obtain a feasible flux range through both the reactions for which the growth rate was reduced to the normal level. The effective

reduction of flux was depicted in percentage, which was defined as percentage reduction of flux through any particular reaction. The simulation results for the 10 most effective combinations have been shown as contour plots in Fig. 9. A list of all the 36 chemotherapeutic combinations has been provided in Table S6 of Online Resource 2. The percentage reduction of flux value for complete reduction of growth and for Normal growth, for each reaction of the combinations has been listed in Table S7 of Online Resource 2.

Inhibitors to a few of these target reactions were already available (see Table S8 of Online Resource 1). In-silico study on the core metabolism in cancer cells showed that reactions of glycolytic, TCA cycle, oxidative phosphorylation and pentose phosphate pathway could be good targets to check cancer cell progression (Resendis-Antonio et al. 2010). Interestingly, our context-specific constraint based metabolic model specific to glioblastoma could identify reactions belonging to cysteine metabolism and reaction combinations of glycine–serine pathway to be potential targets for controlling glioblastoma growth.

These potent reaction pairs of the glycine–serine metabolism give way to discovery/formulation of combinatorial drugs that can inhibit them. Therapeutic agents to target the glycine receptors are already known. Inhibitors like Picrotoxin targeted the neuronal γ -aminobutyric acid and homomeric glycine receptors (Wang et al. 2006), whereas strychnine hydrochloride was found to be a potent antagonist specific to the glycine receptor (García-Colunga and Miledi 1999). These could be employed beneficially to understand the activity of the glycine transporters in glioblastoma too, as evidences state a correlation between the glycine transporter activities with the distribution of its



◀ **Fig. 9** Chemotherapeutic intervention scenarios and effective combination of target reactions. Percentage reduction of flux through combination of essential double knockout reactions **a** hexokinase (HEX) and fructose-1,6-bisphosphate aldolase (FBA), **b** ribulose phosphate-3 epimerase (RPE) and 6-phosphogluconolactonase (6PGLase), **c** fumarate hydratase (FUMH) and alpha ketoglutarate dehydrogenase (AKGDH), **d** glycine transport (Trans_glycine) and Phosphoglycerate dehydrogenase (PGDH), **e** hexokinase (HEX) and triose phosphate isomerase (TPI), **f** glucose transport (Trans_glucose) and glyceraldehyde-3-phosphate dehydrogenase (GAPDH), **g** phosphofructokinase (PFK) and Hexokinase (HEX), **h** succinyl-CoA synthetase (SCS) and fumarate hydratase (FUMH), **i** ribulose phosphate-3 epimerase (RPE) and glucose-6-phosphate dehydrogenase (G6PDH) and **j** glucose transport (Trans_glucose) and phosphoglycerate kinase (PGK), and its effect on the flux through the metabolic function, GBM_BM (different regions in the contour plots)

receptors (Jursky and Nelson 1995). In recent years, many pharmaceutical companies have also developed potent and selective inhibitors for glycine transporters. SSR 504734 and SSR 103800, a series of *N*-(2-aryl-cyclohexyl) substituted spiropiperidines and ORG 25935 are a few compounds, which showed promising results as inhibitors of glycine transporters (Hashimoto 2010).

Discussion

In the present work, a context specific metabolic network for astrocyte/glioblastoma has been developed, that studies the adaptation of complex metabolic reactions within the network under scenario-specific conditions to achieve specific biological goals like growth and maximization of ATP synthesis. Through this model, we tried to investigate the cumulative effect of a large scale metabolism on the metabolic functioning of glioblastoma, the effect of the mutual connectivity of the individual pathways within the metabolic network and the difference in response they show in the astrocytic and glioblastoma scenarios. Also, through the *in silico* approach, we tried to gain some insight into the alternative metabolic routes and metabolites which contributed to the metabolic heterogeneity of glioblastoma. The present model was capable of yielding results which were in correspondence to the experimentally proved phenomena of both astrocytes and glioblastoma (Deighton et al. 2014; Mangia et al. 2009; Marriif and Juurlink 1999; Pellerin and Magistretti 1994; Wise et al. 2008; Zhou et al. 2011).

From our study, specific pathways were observed to demonstrate a co-operative effect in the astrocyte and glioblastoma scenarios. In the model astrocyte scenario, dependence of glycolysis for mitochondrial ATP synthesis reduced with increased uptake and utilization of glutamate as energy source, due to coupling of both glutamate and glucose catabolism via TCA cycle (Fig. 2c). A similar phenomenon was reported in a previous experimental study

(Pellerin and Magistretti 1994). Similarly, in glioblastoma scenario, conversion of glutamine to glutamate and its extracellular release was coupled with cystine uptake and its catabolism to produce glutathione. Previously, through experiments, the cooperative effect of glutamate and cysteine metabolism was speculated and briefly studied in glioblastoma (Ye et al. 1999). Evidences stated that glycine content of neuronal cells was higher than that of glial cells (Roux and Supplisson 2000), and most of the CNS tissues sufficed their glycine requirement via the internal glycine-serine metabolism pathway derived from glucose via 3-phosphoglycerate (Nicklas and Browning 1978), even though astrocyte cultures fed with glycine were capable of utilizing it by maintaining intracellular levels of glutathione, serine and creatine (Dringen et al. 1998). Based on these literature evidences and predictions from the model, it was inferred that astrocytes take up glycine from external sources at a lower level and most of its requirement in the astrocytes was fulfilled by the internal glycine-serine metabolic pathway. Further, a higher uptake of glycine by astrocytes from external source resulted in a reduction in its glutamate uptake rate and an excess of glycine caused glutaminolysis in the astrocytes. On the contrary, glioblastoma showed an increased glycine uptake which was driven towards increased synthesis of glutathione. This increased production of glutathione was simultaneously accompanied with the increased uptake of cystine, which is taken in by the cystine-glutamate antiporter. Hence, a higher amount of glutamate was lost through efflux. This loss was compensated by glutamine uptake which is subsequently converted into glutamate within the cell.

Glioblastoma cell lines can show extremely long survival under glucose starved conditions, which are indicative to the fact that these cells undergo physiological adaptations to overcome nutrient deprivation (Griguer et al. 2005). From the model, it was predicted that cystine could be one essential metabolite that could serve to glioblastoma survival and growth, even at glucose starved conditions. The utilization of glucose was found to be coupled to the cystine uptake in the model. This was perhaps because of the choice of objective function. The objective function included ribulose-5-phosphate, oxaloacetate, succinate and glutathione, which were generated by glycolysis and cysteine metabolism pathways. Consequently, a minimal combination of cystine and glucose could drive a considerable amount of flux through the objective function, as compared to any other minimal combination.

In-silico study on the core metabolism in cancer cells showed that reactions of glycolytic, TCA cycle, oxidative phosphorylation and pentose phosphate pathway are essential for cancer cell progression (Resendis-Antonio et al. 2010) suggesting that central and highly connected

proteins (enzymes) can prove to be useful drug targets (Jeong et al. 2001). These enzymes belong to central carbon and energy metabolism that essentially meet the energy requirements of the cell and hence are important. However, the centrality of enzymes does not always imply lethality in complex protein networks (Raman et al. 2014). Similar to this observation, in our metabolic network, we identified some unique enzymatic reactions that did not belong to the aforementioned central metabolic pathways but still were deemed to be absolutely essential for glioblastoma growth. Pertaining to this, targeting the reactions belonging to cysteine metabolism ('Cystine glutamate antiporter', Anti_cystine_glut, and 'cystine reductase', CystRed) and dual targeting of the reactions belonging to glycine–serine metabolism along with glycine transporter could potentially suppress glioblastoma growth.

Thus to summarize the present study, the designed model could predict—that most of the astrocytic glycine requirement was fulfilled by the internal glycine–serine metabolism pathway, and excess glycine in the environment of growing astrocytes might have an effect on its glutamate metabolism. Further, it was observed that cystine and glucose were two vital metabolites, which could significantly contribute to glioblastoma growth. From model analysis for chemotherapeutic interventions, it was observed that reactions of cysteine metabolism and dual targeting of reactions belonging to glycine–serine metabolism could be potential chemotherapeutic targets for effective inhibition of glioblastoma growth.

The present metabolic model has both its advantages and limitations. The steady state assumption is a limitation to the model, which does not allow us to consider the intermediary dynamic changes in the flux profiles of the reactions. Even though, the present context-specific model suffices to achieve the biological goal of glioblastoma growth, considering only a subset of the whole genomic network might lead to results which deviate from the real biological scenario. In order to overcome such limitations, our predictions can further be validated through experiments, so as to help the chemists and biologists to discover small molecule inhibitors against brain cancer. An in vitro experimental approach, by treating the astrocyte-derived glioblastoma cell lines like LN-229 and U87MG with combinations of inhibitors/chemotherapeutic agents mentioned in Table S8 of Online Resource 2 for ensuring their synergy and selectivity to inhibit cell growth and proliferation (Lehár et al. 2009), can further validate the model predictions.

Therefore, our study not only contributes in understanding the complexities, differences and consequences of glioblastoma metabolism for predicting biologically reasonable disease scenarios, but also provides a deep insight into identification of important targets as well as chemotherapeutic interventions.

Acknowledgments We thank Council of Scientific and Industrial Research, XII Five Year Plan Project “GENESIS” (BSC0121) and Department of Biotechnology, Government of India (Project Code: BT/PR13689/BID/07/363/2010) for providing financial support to perform this work. Abhishek Subramanian acknowledges the research fellowship provided by DBT-BINC fellowship program.

References

- Anton K, Glod J (2014) An orchestrated response to tumor signals by macrophages and mesenchymal stem cells potentiates interleukin-6 secretion in glioblastoma. *Cell Death Ther* 1:2353–7817. doi:10.2478/cdth-2014-0001
- Bairoch A (2000) The ENZYME database in 2000. *Nucleic Acids Res* 28:304–305
- Banerji A (2013) An attempt to construct a (general) mathematical framework to model biological “context-dependence”. *Syst Synth Biol* 7:221–227
- Boada J, Roig T, Perez X, Gamez A, Bartrons R, Cascante M, Bermúdez J (2000) Cells overexpressing fructose-2, 6-bisphosphatase showed enhanced pentose phosphate pathway flux and resistance to oxidative stress. *FEBS Lett* 480:261–264
- Bouzier-Sore AK, Pellerin L (2013) Unraveling the complex metabolic nature of astrocytes. *Front Cell Neurosci* 7:179. doi:10.3389/fncel.2013.00179
- Brekke E, Walls AB, Norfeldt L, Schousboe A, Waagepetersen HS, Sonnewald U (2012) Direct measurement of backflux between oxaloacetate and fumarate following pyruvate carboxylation. *Glia* 60:147–158. doi:10.1002/glia.21265
- Burgess PK, Kulesa PM, Murray JD, Alvord EC Jr (1997) The interaction of growth rates and diffusion coefficients in a three-dimensional mathematical model of gliomas. *J Neuropathol Exp Neurol* 56:704–713
- Chatterjee A, Mambo E, Sidransky D (2006) Mitochondrial DNA mutations in human cancer. *Oncogene* 25:4663–4674
- Chinnaiyan P et al (2012) The metabolomic signature of malignant glioma reflects accelerated anabolic metabolism. *Cancer Res* 72:5878–5888
- Chung WJ, Lyons SA, Nelson GM, Hamza H, Gladson CL, Gillespie GY, Sontheimer H (2005) Inhibition of cystine uptake disrupts the growth of primary brain tumors. *J Neurosci* 25:7101–7110. doi:10.1523/JNEUROSCI.5258-04.2005
- Consortium U (2014) Activities at the universal protein resource (UniProt). *Nucleic Acids Res* 42:D191–D198
- Covert MW, Schilling CH, Palsson B (2001) Regulation of gene expression in flux balance models of metabolism. *J Theor Biol* 213:73–88
- Deighton RF et al (2014) The proteomic response in glioblastoma in young patients. *J Neurooncol* 119:79–89. doi:10.1007/s11060-014-1474-6
- Dringen R, Verleysdonk S, Hamprecht B, Willker W, Leibfritz D, Brand A (1998) Metabolism of glycine in primary astroglial cells: synthesis of creatine, serine, and glutathione. *J Neurochem* 70:835–840
- Edgar R, Domrachev M, Lash AE (2002) Gene expression omnibus: NCBI gene expression and hybridization array data repository. *Nucleic Acids Res* 30:207–210
- García-Colunga J, Mileti R (1999) Modulation of nicotinic acetylcholine receptors by strychnine. *Proc Natl Acad Sci* 96:4113–4118
- Griguer CE, Oliva CR, Gillespie GY (2005) Glucose metabolism heterogeneity in human and mouse malignant glioma cell lines. *J Neurooncol* 74:123–133. doi:10.1007/s11060-004-6404-6

- Guessous F et al (2013) Oncogenic effects of miR-10b in glioblastoma stem cells. *J Neurooncol* 112:153–163
- Hashimoto K (2010) Glycine transport inhibitors for the treatment of schizophrenia. *Open Med Chem* 4:10–19
- Hattingen E, Lanfermann H, Quick J, Franz K, Zanella FE, Pilatus U (2009) 1H MR spectroscopic imaging with short and long echo time to discriminate glycine in glial tumours. *Magn Reson Mater Phys, Biol Med* 22:33–41
- Hertz L, Zielke HR (2004) Astrocytic control of glutamatergic activity: astrocytes as stars of the show. *Trends Neurosci* 27:735–743. doi:10.1016/j.tins.2004.10.008
- Jellinger K (1977) Glioblastoma multiforme: morphology and biology. *Acta Neurochir* 42:5–32
- Jeong H, Mason SP, Barabási A-L, Oltvai ZN (2001) Lethality and centrality in protein networks. *Nature* 411:41–42
- Jursky F, Nelson N (1995) Localization of glycine neurotransmitter transporter (GLYT2) reveals correlation with the distribution of glycine receptor. *J Neurochem* 64:1026–1033
- Kanehisa M, Goto S, Sato Y, Kawashima M, Furumichi M, Tanabe M (2014) Data, information, knowledge and principle: back to metabolism in KEGG. *Nucleic Acids Res* 42:D199–D205
- Kleihues P, Ohgaki H (2000) Phenotype vs genotype in the evolution of astrocytic brain tumors. *Toxicol Pathol* 28:164–170
- Lee JM, Gianchandani EP, Papin JA (2006) Flux balance analysis in the era of metabolomics. *Brief Bioinform* 7:140–150
- Lehár J, Krueger AS, Avery W, Heilbut AM, Johansen LM, Price ER, Rickles RJ, Short GF 3rd, Staunton JE, Jin X, Lee MS, Zimmermann GR, Borisy AA (2009) Synergistic drug combinations tend to improve therapeutically relevant selectivity. *Nat Biotechnol* 27:659–666
- Maity A, Pore N, Lee J, Solomon D, O'Rourke DM (2000) Epidermal growth factor receptor transcriptionally up-regulates vascular endothelial growth factor expression in human glioblastoma cells via a pathway involving phosphatidylinositol 3'-kinase and distinct from that induced by hypoxia. *Cancer Res* 60:5879–5886
- Mandonnet E, Pallud J, Clatz O, Taillandier L, Konukoglu E, Duffau H, Capelle L (2008) Computational modeling of the WHO grade II glioma dynamics: principles and applications to management paradigm. *Neurosurg Rev* 31:263–269
- Mangia S, Simpson IA, Vannucci SJ, Carruthers A (2009) The in vivo neuron-to-astrocyte lactate shuttle in human brain: evidence from modeling of measured lactate levels during visual stimulation. *J Neurochem* 109(Suppl 1):55–62. doi:10.1111/j.1471-4159.2009.06003.x
- Marrif H, Juurlink BH (1999) Astrocytes respond to hypoxia by increasing glycolytic capacity. *J Neurosci Res* 57:255–260
- Nicklas WJ, Browning ET (1978) Amino acid metabolism in glial cells: homeostatic regulation of intra- and extracellular milieu by C-6 glioma cells. *J Neurochem* 30:955–963
- Ogunrinu TA, Sontheimer H (2010) Hypoxia increases the dependence of glioma cells on glutathione. *J Biol Chem* 285:37716–37724. doi:10.1074/jbc.M110.161190
- Oliveira-Ferrer L, Wellbrock J, Bartsch U, Penas EM, Hauschild J, Klokow M, Bokemeyer C, Fiedler W, Schuch G (2013) Combination therapy targeting integrins reduces glioblastoma tumor growth through antiangiogenic and direct antitumor activity and leads to activation of the pro-proliferative prolactin pathway. *Mol Cancer* 12:1–14
- Oudard S et al (1996) High glycolysis in gliomas despite low hexokinase transcription and activity correlated to chromosome 10 loss. *Br J Cancer* 74:839–845
- Pelicano H, Martin D, Xu R, Huang P (2006) Glycolysis inhibition for anticancer treatment. *Oncogene* 25:4633–4646
- Pellerin L, Magistretti PJ (1994) Glutamate uptake into astrocytes stimulates aerobic glycolysis: a mechanism coupling neuronal activity to glucose utilization. *Proc Natl Acad Sci* 91:10625–10629
- Pistollato F et al (2010) Hypoxia and succinate antagonize 2-deoxyglucose effects on glioblastoma. *Biochem Pharmacol* 80:1517–1527. doi:10.1016/j.bcp.2010.08.003
- Prabhu A, Sarcar B, Kahali S, Yuan Z, Johnson JJ, Adam KP, Kensicki E, Chinnaiyan P (2014) Cysteine catabolism: a novel metabolic pathway contributing to glioblastoma growth. *Cancer Res* 74:787–796
- Raman K, Damaraju N, Joshi GK (2014) The organisational structure of protein networks: revisiting the centrality–lethality hypothesis. *Syst Synth Biol* 8:73–81
- Resendis-Antonio O, Checa A, Encarnación S (2010) Modeling core metabolism in cancer cells: surveying the topology underlying the Warburg effect. *PLoS ONE* 5:e12383
- Roux MJ, Supplisson S (2000) Neuronal and glial glycine transporters have different stoichiometries. *Neuron* 25:373–383
- Sahm F et al (2013) The endogenous tryptophan metabolite and NAD⁺ precursor quinolinic acid confers resistance of gliomas to oxidative stress. *Cancer Res* 73:3225–3234. doi:10.1158/0008-5472.CAN-12-3831
- Schellenberger J et al (2011) Quantitative prediction of cellular metabolism with constraint-based models: the COBRA Toolbox v2.0. *Nat Protoc* 6:1290–1307
- Sonnwald U, Westergaard N, Jones P, Taylor A, Bachelard H, Schousboe A (1996) Metabolism of [U-13C5] glutamine in cultured astrocytes studied by NMR spectroscopy: first evidence of astrocytic pyruvate recycling. *J Neurochem* 67:2566–2572
- Swanson KR, Bridge C, Murray J, Alvord EC (2003) Virtual and real brain tumors: using mathematical modeling to quantify glioma growth and invasion. *J Neurosci* 23:1101–1110
- Tracqui P, Cruywagen G, Woodward D, Bartoo G, Murray J, Alvord E (1995) A mathematical model of glioma growth: the effect of chemotherapy on spatio-temporal growth. *Cell Prolif* 28:17–31
- Vander Heiden MG, Cantley LC, Thompson CB (2009) Understanding the Warburg effect: the metabolic requirements of cell proliferation. *Science* 324:1029–1103. doi:10.1126/science.1160809
- Wang D-S, Mangin J-M, Moonen G, Rigo J-M, Legendre P (2006) Mechanisms for picrotoxin block of $\alpha 2$ homomeric glycine receptors. *J Biol Chem* 281:3841–3855
- Warburg O (1956) On the origin of cancer cells. *Science* 123:309–314
- Wise DR et al (2008) Myc regulates a transcriptional program that stimulates mitochondrial glutaminolysis and leads to glutamine addiction. *Proc Natl Acad Sci USA* 105:18782–18787. doi:10.1073/pnas.0810199105
- Wolf A, Agnihotri S, Guha A (2010) Targeting metabolic remodeling in glioblastoma multiforme. *Oncotarget* 1:552–577
- Ye Z-C, Rothstein JD, Sontheimer H (1999) Compromised glutamate transport in human glioma cells: reduction–mislocalization of sodium-dependent glutamate transporters and enhanced activity of cystine–glutamate exchange. *J Neurosci* 19:10767–10777
- Zafra F, Gimenez C (1986) Characterization of glycine uptake in plasma membrane vesicles isolated from cultured glioblastoma cells. *Brain Res* 397:108–116
- Zhou Y et al (2011) Metabolic alterations in highly tumorigenic glioblastoma cells: preference for hypoxia and high dependency on glycolysis. *J Biol Chem* 286:32843–32853. doi:10.1074/jbc.M111.260935

RESEARCH ARTICLE

Differential suitability of reactive oxygen species and the role of glutathione in regulating paradoxical behavior in gliomas: A mathematical perspective

Rupa Bhowmick^{1,2}, Ram Rup Sarkar^{1,2*}

1 Chemical Engineering and Process Development Division, CSIR-National Chemical Laboratory, Pune, Maharashtra, India, **2** Academy of Scientific & Innovative Research (AcSIR), Ghaziabad, India

* rr.sarkar@ncl.res.in

OPEN ACCESS

Citation: Bhowmick R, Sarkar RR (2020) Differential suitability of reactive oxygen species and the role of glutathione in regulating paradoxical behavior in gliomas: A mathematical perspective. PLoS ONE 15(6): e0235204. <https://doi.org/10.1371/journal.pone.0235204>

Editor: Salvatore V. Pizzo, Duke University School of Medicine, UNITED STATES

Received: October 11, 2019

Accepted: June 10, 2020

Published: June 25, 2020

Peer Review History: PLOS recognizes the benefits of transparency in the peer review process; therefore, we enable the publication of all of the content of peer review and author responses alongside final, published articles. The editorial history of this article is available here: <https://doi.org/10.1371/journal.pone.0235204>

Copyright: © 2020 Bhowmick, Sarkar. This is an open access article distributed under the terms of the [Creative Commons Attribution License](https://creativecommons.org/licenses/by/4.0/), which permits unrestricted use, distribution, and reproduction in any medium, provided the original author and source are credited.

Data Availability Statement: All relevant data are within the manuscript and its Supporting Information files.

Abstract

Manipulative strategies of ROS in cancer are often exhibited as changes in the redox and thiol ratio of the cells. Cellular responses to oxidative insults are generated in response to these changes which are triggered due to the rerouting of the metabolic framework to maintain survival under stress. However, mechanisms of these metabolic re-routing are not clearly understood and remained debatable. In the present work, we have designed a context-based dynamic metabolic model to establish that the coordinated functioning of glutathione peroxidase (*GTHP*), glutathione oxidoreductase (*GTHO*) and NADPH oxidase (*NOX*) is crucial in determining cancerous transformation, specifically in gliomas. Further, we propose that the puzzling duality of ROS (represented by changes in h_2O_2 in the present model) in exhibiting varying cellular fates can be determined by considering simultaneous changes in $nadph/nadp^+$ and $gsh/gssg$ that occur during the reprogramming of metabolic reactions. This will be helpful in determining the pro-apoptotic or anti-apoptotic fate of gliomas and can be useful in designing effective pro-oxidant and/or anti-oxidant therapeutic approaches against gliomas.

1. Introduction

Reactive Oxygen Species (ROS) have been implicated in various disease conditions and are considered as a key driving factor in the process of aging and carcinogenesis. ROS is referred to possess a double-edged sword property having both tumor-promoting and a tumor-suppressing function [1]. An intricate balance between ROS and antioxidants and other ROS scavengers is maintained in a normal proliferating cell, which is a prerequisite for maintaining redox balance and proper functioning of the cell. Human cells generally tend to function in a reduced state (e.g. by maintaining high $gsh/gssg$ ratio [2] and high $nadph/nadp^+$ ratio [3]). However, exceptions are made when the cells need to maintain a slightly oxidative environment to aid various cellular processes like folding of nascent proteins in the endoplasmic reticulum, activation of gene transcription factors, etc. An increase in intracellular oxidative state

Funding: We thank SERB, Department of Science and Technology, Govt. of India (File No. EMR/2016/000516) and (DST/ICPS/EDA/2018), for providing financial support to Ram Rup Sarkar. Rupa Bhowmick acknowledges the Council of Scientific & Industrial Research (CSIR) for the Senior Research Fellowship. The funders had no role in study design, data collection and analysis, decision to publish, or preparation of the manuscript.

Competing interests: The authors have declared that no competing interests exist.

induces apoptosis, although too much oxidation helps to evade apoptosis by oxidizing and inactivating the caspase enzymes [4]. Thus the balance between oxidant and antioxidant activity becomes crucial, as a shift might facilitate apoptosis or might also suppress apoptosis rendering therapeutic approaches ineffective.

ROS are implicated as harmful byproducts of cellular metabolism, although they perform additional function as regulators of various intracellular signaling cascades [5–10]. Sequential reduction of oxygen results in the formation of superoxide, hydroxyl radical, hydrogen peroxide (H_2O_2), hydroxyl ion, etc. Most of these are converted into hydrogen peroxide by the activity of superoxide dismutase. H_2O_2 is one of the most stable ROS, which can penetrate membranes and quickly reach cellular targets affecting overall cellular functioning [11]. Responses of ROS differ under different experimental conditions; they can promote proliferation [12, 13] or can inhibit it [14] or can also induce apoptosis [15, 16]. These responses are governed by multiple cellular factors, anti-oxidant metabolism being the most crucial one. A constraint, however, is to obtain a holistic understanding of ROS and its regulatory mechanisms due to contextual [1, 17, 18] and experimental complexities [12, 14, 19, 20]. The use of computational approaches has been conducive in dealing with these limitations. Computational models allow observing the concurrent dynamics of many variables considered simultaneously, which are often challenging to assess experimentally [10, 21].

The differential suitability of ROS manipulation in tumor cells is explained by different theories. One of the most prevalent theories is the “Threshold concept for cancer therapy”. According to this theory, as the level of ROS within the cancer cell increases, the ratio of ROS and antioxidants reaches a balance, beyond which any further increase in ROS or decrease in antioxidant activity will lead to cell death or increased sensitivity of tumor cells to cytotoxic treatments [22]. According to an alternate threshold theory, when both tumor and normal cells are exposed to equal intensity of exogenous ROS-producing or stimulating agents, the intracellular ROS levels of tumor cells increase more easily than the normal cells to reach a threshold and to trigger death, due to higher basal level of ROS in tumors [23]. The changes induced during a cancerous transformation are readily reflected as a change in the redox status of the cells mostly triggering ROS production. The applicability and effectiveness of ROS promotion or ROS depletion strategies in cancer therapeutics depend on where the cell is in the sequence of events. Change in the thiol ratio of the cell is another important determinant of the cellular response towards an oxidative insult. Reportedly, changes in the $nadph/nadp^+$ ratio and $gsh/gssg$ ratio have been considered important in gaining a perspective towards the cellular response to such insults. $nadph/nadp^+$ ratio is indicative of the reducing potential of the cell, which is required to be maintained high to keep the overall redox pool at a significantly reduced state [24, 25]. Changes in $gsh/gssg$ ratio might induce the initiation of the induction phase of apoptosis [26, 27]. A decrease in $gsh/gssg$ ratio can induce apoptosis by causing Bcl-2 loss and activating caspase enzymes whereas an increase in the ratio may have an effect otherwise [28].

Thiol and redox ratios represent cumulative results of multiple changes in the metabolism and hence are considered as indicators of various diseased states. Although, the effect of ROS manipulation on these ratios and the metabolic re-routing that helps the cells to adapt to stressful conditions affect the redox and thiol status of the cell are not clearly understood. Another arguable topic of discussion is whether the redox and thiol statuses of the cell have any role in determining cellular fate during oxidative stress. The well-orchestrated metabolic processes related to these changes are re-routed, although the changes that govern the puzzling duality of ROS are yet not clearly understood. The role of the $gsh-gssg$ in determining the paradox is another aspect to be explored. Also, the changes in the metabolic network that affect the effectiveness of pro-oxidant or anti-oxidant approaches during cancer therapeutic design are

not well understood. In order to address these questions, we have designed a context-based dynamic metabolic model including the pathways which are known to be involved in regulating the oxidant-antioxidant mechanism.

In the present work, we have demonstrated the effect of redox and thiol status of the cell, and the antioxidants in maintaining ROS levels by considering h_2o_2 levels in particular in normal glial cells and gliomas. With the help of our simulations, we propose that the effectiveness of a therapeutic strategy depends on the target's ability to alter the redox states of the cell. We propose a set of sequential changes in metabolic events that determines the transformation from a normal glial to glioma condition that can be used for a pro-oxidative or anti-oxidative therapeutic approach. We have demonstrated these changes keeping in view the changes in $nadph/nadp^+$ and $gsh/gssg$ ratios with respect to the h_2o_2 levels in normal glial and glioma conditions. A holistic understanding of the changes in h_2o_2 levels along with changes in the redox and thiol statuses of the model provides convincing insight into the paradoxical behavior of ROS in gliomas and its cellular apoptotic fates. Also, understanding the effect of other enzymes that are not directly involved in ROS manipulation but affect the metabolic process by creating a distant regulation in the network can help augment the effect of proposed therapeutic strategies. In the future, this can be ventured to propose an effective design of pro-oxidant or anti-oxidant therapeutic approaches against glioma progression.

2. Materials and methods

2.1. Model setup

The present model (Fig 1) captures the dynamic changes in the metabolism regulating the interplay of glutathione and ROS (hydrogen peroxide) in normal glial cells and gliomas. The model is biologically motivated from a previous analysis in which a subset of metabolic reactions has been observed to be directed towards *gsh* production in gliomas [29]. A re-routing of the glycolytic, pentose phosphate, glycine-serine, glutamate, and cystine pathway was observed to be directed towards glutathione metabolism from the analysis. The present model has been designed considering these pathways, to understand the dynamics of this re-routing and their effect in determining the role of glutathione during ROS scavenging. ROS which typically show a paradoxical behavior in tumor progression and proliferation have been represented in the model with the inclusion of ROS production machinery. *gsh* is a tri-peptide composed of cystine (*cys*), glycine (*gly*) and glutamate (*glut*), is the prime anti-oxidant involved in ROS scavenging. The model essentially comprises of reactions required for the production of the components of tri-peptide units of *gsh*. A part of glycolytic pathways along with the glycine-serine metabolism has been included which directs the glucose metabolism towards glycine production. Cystine metabolism and a part of the glutamate metabolism have been incorporated to represent the metabolism of these two components into the complex- glutamyl-cysteine (*glucys*). The *gsh-gssg* cycle consisting of glutathione peroxidase (*GTHP*) and glutathione oxidoreductase (*GTHO*) has been included along with the ROS production machinery comprising of NADPH Oxidase (*NOX*) and Superoxide Dismutase (*SOD*). Although these enzymes are present as multiple isoforms, all the isoforms have been considered as one, as their basic mechanism and functioning remains the same. Other ROS scavenging machinery like the peroxiredoxin/thioredoxin systems, catalases, etc., have not been considered in the model for time being, as we intended to focus on the dynamics of glutathione during ROS scavenging and its role in determining the paradox. The scavenging of h_2o_2 (which has been considered as the ROS in the present model) by other mechanisms has been represented by the parameter dh_2o_2 , which is defined as the decay of intracellular hydrogen peroxide in other cellular processes. The model has been limited to two compartments only: extracellular matrix (e) and

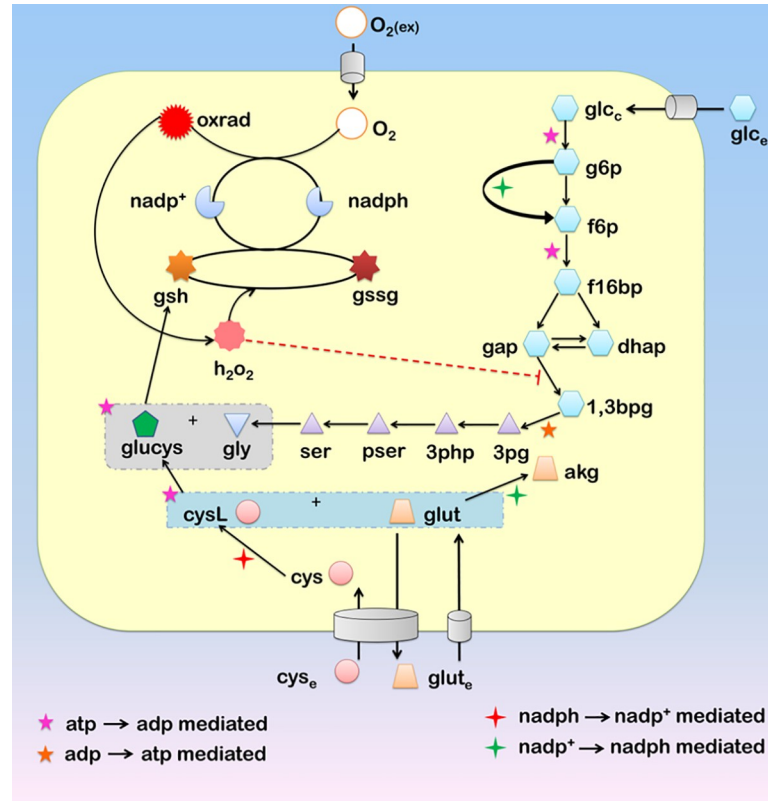


Fig 1. Diagrammatic representation of the metabolites belonging to different pathways directed towards the production of the glutathione along with the ROS generation machinery. The metabolites and the pathways to which they belong have been grouped into five groups viz.-(i) Central Carbon metabolism (*glc_e, glc_c, g6p, f6p, f16bp, gap, dhap, 1,3bpg, 3pg, akg*), (ii) Amino Acid metabolism (*3php, pser, ser, gly, cys_e, cys, cysL, glut_e, glut*), (iii) Thiol metabolism (*glucys, gsh, gssg*), (iv) *h₂O₂* production and metabolism (*O_{2(ex)}, O₂, oxrad, h₂O₂*) (v) Redox metabolism (*nadph, nadp⁺*). Descriptions to all the abbreviated forms have been provided in [S1 Text Section 4](#).

<https://doi.org/10.1371/journal.pone.0235204.g001>

cytosol (c) and intracellular compartments have not been considered as the availability of compartment-wise parameter remains a limitation and the introduction of intracellular compartments for such large ODE model would make it complex.

2.2. Model description

The model consists of 35 metabolite variables involved in 25 reactions required for the production of *gsh* and *h₂O₂* and for scavenging *h₂O₂*. All reactions have been provided in supporting information. As per the available information of the kinetics of these reactions, equations have been formulated as forms of uni-uni, bi-bi, bi-uni or ter-bi Michaelis-Menten kinetics. The equations have been written in Cleland Nomenclature. We have considered initial reaction kinetics with first-order reaction rates. All the rate equations, differential equations and parameter description along with the parameter values have been provided in [S1 Table of S1 Text](#).

The general form of the initial kinetics of reaction equations considered in the model is given below:

$$Uni - Uni/Uni - Bi : \frac{V_m^R \cdot a}{K_m^R + a}$$

$$Bi - Bi \text{ mechanism (Rapid equilibrium/Ordered)} : \frac{V_m^R(a,b)}{(k_{i(a)}^R \cdot k_b^R + k_b^R \cdot a + k_a^R \cdot b + a \cdot b)}$$

$$\text{Partial Rapid Equilibrium Random Bi - Bi mechanism} : \frac{V_m^R(a,b)}{(k_{i(a)}^R \cdot k_b^R + k_b^R \cdot a + a \cdot b)}$$

$$\text{Ordered Ter - Bi} : \frac{V_m^R(a,b,c)}{(k_{i(a)}^R \cdot k_{i(b)}^R \cdot k_c^R + k_{i(b)}^R \cdot k_c^R \cdot a + k_{i(a)}^R \cdot k_b^R \cdot c + k_c^R \cdot a \cdot b + k_b^R \cdot a \cdot c + k_a^R \cdot b \cdot c + a \cdot b \cdot c)}$$

Where R is the reaction, a , b and c represent the substrates, V_m^R the V_{\max} of the reaction, k_i^R the rate constant for dissociation of enzyme-substrate complex and $k_a^R/k_b^R/k_c^R$ represent the rate constant for the association of a substrate with the enzyme.

The motivation behind considering a larger metabolic network for dynamic analysis comes from the observed metabolic re-routing of these pathways which is directed towards glutathione production. In the present model, our main focus remains to understand the strategies of h_2o_2 manipulation within cells and its effect on cell proliferation or death. With this model, we also try to understand the effect of glutathione in scavenging h_2o_2 while considering the changes in the redox ratio depicted by $nadph/nadp^+$. The rationale behind considering the different pathways is specified hereunder.

Central carbon metabolism. The glycolytic pathway branches out to various other pathways which are precursors to the nucleotide, amino acid synthesis, and other important biosynthesis pathways. A part of the glycolytic pathway which branches to serine metabolism has been considered which allows the *de novo* synthesis of the amino acids serine and glycine within the cell. Also, the pentose phosphate pathway has been represented by the inclusion of G6PDH which is a major source of *nadph*.

Amino acid metabolism. All reactions belonging to serine and glycine metabolism has been considered in the model. This metabolism supports the generation of glutathione and maintains redox status of the cell. Serine and glycine can be produced *de novo* from glycolytic intermediate *3pg*, and this part of the metabolism has been considered in the model [30]. Glutamate metabolism has been considered partly. This forms another source of *nadph*, and glutamate supports the production of glutathione and also manages the uptake of cystine through the cystine-glutamate antiporter. Cysteine metabolism has also been considered. The initiation of the metabolism has been considered with the uptake of cystine which is metabolized to cysteine [31]. This reacts with glutamate to form glutamyl-cysteine (*glucys*), the precursor complex which reacts with glycine to produce glutathione [26].

Thiol metabolism. The thiol metabolism is represented by the glutathione metabolism itself. Two important enzymes that maintain the glutathione homeostasis i.e., glutathione peroxidase and glutathione oxidoreductase, have been considered [27]. Pertaining to the objective of looking into the glutathione and h_2o_2 dynamics, other thiol metabolisms like the peroxiredoxins, thioredoxins, and catalase systems have not been considered currently.

h_2o_2 production and metabolism. The model considers the activity of NADPH oxidase [32] and superoxide dismutase [33] as a part of h_2o_2 production. The formation of oxygen free radicals and their subsequent conversion into h_2o_2 is catalyzed by NADPH oxidase and superoxide dismutase respectively. The metabolism of h_2o_2 is linked to thiol metabolism. Other mechanisms through which h_2o_2 are scavenged is represented by the parameter dh_2o_2 , which is defined as the decay of intracellular hydrogen peroxide in other cellular processes.

Redox metabolism. $nadph-nadp^+$ has been considered as the prime redox balancer in the model. The homeostasis and metabolism of $nadph-nadp^+$ has been considered in reactions belonging to the earlier pathways where these function as cofactors to catalyze the reactions.

2.3. Model simulation

The system of differential equations was simulated using ODE15s in MATLAB 2017a. Calibration of the model was performed upon available experiment data on the change in *gsh* over a period of time in retinal Muller glial cells under normal and amino acid supplemented scenarios [34]. This was used to create the normal glial scenario, to which changes were introduced to create the hypoxic and glioma-like scenario. The basal parameters and initial values to the variables were considered within a biologically feasible range as obtained through literature search and are provided in S2 Table of S1 Text. Few of the parameters and initial values were assumed within a biologically feasible range as had been reported in the literature. A set of 23 parameters remained unknown which were determined using the parameter estimation technique. The model was ensured to reach a stable steady state with the basal parameter states and initial values. Also, the simulations performed using the above parameters indicate that at steady states the intracellular *gsh* concentration along with $nadph/nadp^+$ and atp/adp ratios resemble true biological concentrations as reported in the literature.

2.4. Parameter estimation

Parameter estimation of the unknown parameters was performed using Delayed Rejection Adaptive Metropolis (DRAM) algorithm of Markov Chain Monte Carlo (MCMC) Toolbox in MATLAB 2017a. The algorithm generates posterior distribution calibrated using the sample path of the MCMC chain to estimate unknown parameters for a known experimental result. In the present model, parameter estimation was performed using experimental data on the change in *gsh* in retinal Muller glial cells as has been specified in the earlier section (Fig 2A). Distributions plots and trace plots of all the 23 estimated parameters have been provided in S1 Fig of S1 Text. Values for the parameters V_m^{GLUTEX} and k_m^{GLUTEX} were estimated using an available data on glutamate exchange in astrocytes [35] (Fig 2B). Distributions plots and trace plots of the two estimated parameters have been provided in S2 Fig of S1 Text.

2.5. Model Validation with experimental data

In order to validate the model properties, we used available experimental data for comparison with model outcomes. Under normal physiological conditions, cells maintain a reduced redox state with a high $nadph/nadp^+$ ratio. $Nadp^+$ primarily acts as an electron donor in metabolic pathways, and a low $nadph/nadp^+$ depicts an enhanced oxidative state of the cell. A properly functional ROS machinery of a normal cell maintains a balanced $nadph-nadp^+$ pool, which is kept in a significantly reduced state by maintaining a high $nadph/nadp^+$ ratio [36]. As such, we validated the model with experimentally determined $nadph/nadp^+$ ratio [37], which ranged between 2.5–3 (Fig 3C). The average atp/adp ratio under functional glycolysis was also measured (Fig 3C). Non-proliferative cells maintain a very high cytosolic atp/adp ratio by metabolizing respiratory substrates, which essentially inhibits glycolysis [38]. However, with the initiation of cellular activity, glycolysis is initiated, which maintains an average cytosolic atp/adp ratio between 2.6–10 [39, 40] that has been captured through our simulation as well.

Furthermore, the model was simulated with an initial *gsh* concentration of 3.83mM, as has been reported in the case of glial cells [34]. Our simulations showed that the model was capable of maintaining h_2o_2 concentration within a biologically feasible range of $\sim 4\mu M$ while maintaining a value of $\sim 2.33mM$ of *gsh* at steady-state (Fig 3A), which is in agreement with the

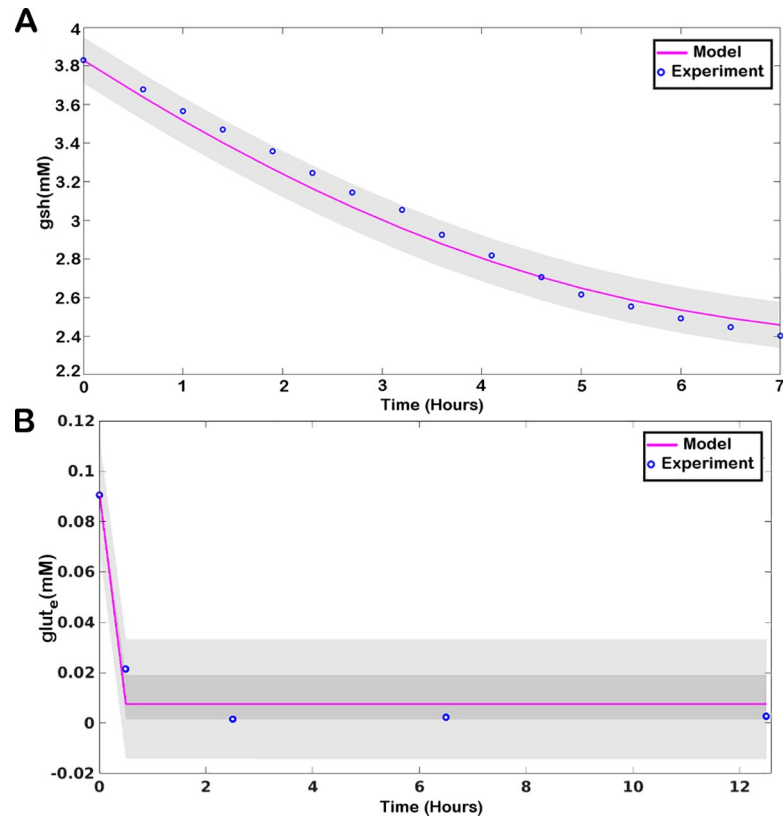


Fig 2. Predictive plot demonstrating of model fitting with experimental data: (A) for reduced glutathione (*gsh*) and (B) for extracellular glutamate (*glut_e*). The blue circles represent the data points obtained from experiments [34, 35] and the pink line represents the result obtained through model simulation.

<https://doi.org/10.1371/journal.pone.0235204.g002>

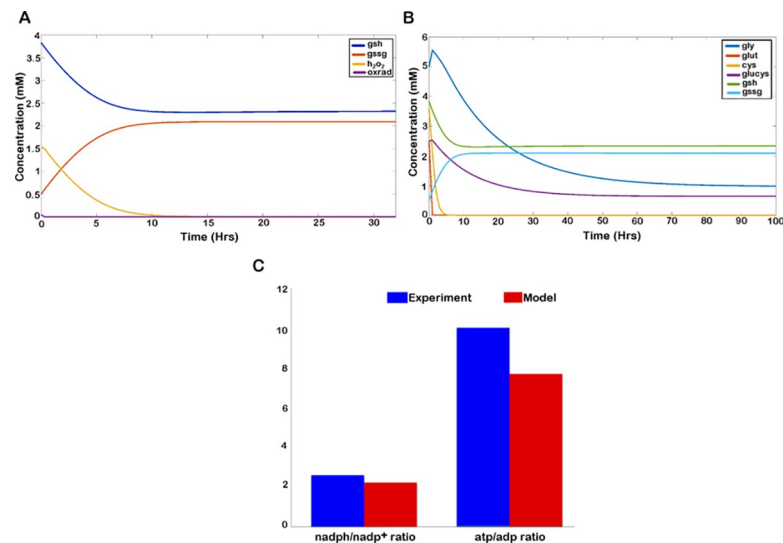


Fig 3. Model properties. A. The temporal plot of *gsh*, *gssg*, h_2O_2 , and *oxrad*. B. Temporal plot of the tri-peptides cystine (*cys*), glutamate (*glut*) and glycine (*gly*) and glutamyl-cysteine (*glucys*) along with changes in *gsh* and *gssg*. C. Comparison of experimentally obtained range of $nadph/nadp^+$ and atp/adp ratio with values obtained through model simulation.

<https://doi.org/10.1371/journal.pone.0235204.g003>

reported basal cytoplasmic concentration of *gsh* [41]. The *gsh* metabolizing cells maintain a negligibly small cytosolic pool of *cystine* which is readily reduced to *cysteine*, the rate limiting amino-acid of *gsh* biosynthesis [42]. This property has been captured in the model, where the *cystine* concentration is readily reduced to micromolar levels upon initiation of *gsh* metabolism (Fig 3B). Also, *cystine* import is coupled with *glutamate* through cystine-glutamate antiporter which allows the release of *glutamate* to extracellular matrix upon cystine uptake. Due to its role as a neurotransmitter, the extracellular concentration of *glutamate* in brain is tightly controlled and maintained at a micromolar concentration ranging between 2–9 μ M [43]. We could observe the diminished level of extracellular glutamate through our simulation (Fig 2B) based on temporal data available for astrocytes, which has been further used for parameter estimation of glutamate exchange reaction. Note that the following validations have been made under normal glial condition. High *nadph/nadp*⁺ and *atp/adp* ratios are characteristic of any normal proliferating cell, although the values for the ratios are specific to simulation conditions. The external glutamate concentration holds true for extracellular matrix of brain cells. The concentration of *gsh* is specific to glial cells and the concentration of all other metabolites upon simulation are also characteristic of glial cells.

2.6. Sensitivity analysis

Extended Fourier Amplified Sensitivity Test (eFAST) algorithm was used for identifying sensitive parameters to the system. The algorithm makes use of the variance decomposition method to predict the sensitivity of parameters in a nonlinear non-monotonic system. First-order sensitivity index S_i , and total order sensitivity index, S_{Ti} , were calculated for different transient time points and steady states of *gsh*, *gssg*, h_2o_2 and *oxrad*. Sensitivity plots of parameters with a p-value < 0.05 for *gsh* (reduced glutathione), *gssg* (oxidized glutathione), h_2o_2 (hydrogen peroxide) and *oxrad* (oxygen radical) are provided in S3 Fig of S1 Text. The analysis was repeated for high intracellular oxygen demand and multiple mutation conditions to check the sensitivity of parameters at different conditions.

2.7. Parameter variation

Parameter variation analyses for a single parameter and two parameters were performed to understand their effect on the respective variables. Parameters were varied over a feasible biological range at any given time point. For most of the instances, changes in the enzyme concentrations have been introduced by varying the V_{max} of the enzyme, as V_{max} is determined by the enzyme concentration and substrate availability. For two-parameter variation analysis, two parameters were simultaneously varied and the results were plotted as 3D surface plots to show their effect on the respective variable.

2.8. Changing oxygen demand: The creation of hypoxia situation

The oxygen uptake by cells is approximated by Michaelis-Menten kinetics in the model where V_{max} represents the rate of oxygen uptake by the cell and K_m represents the affinity of the cell for extracellular oxygen. Low K_m signifies a high affinity for oxygen. The value of K_m for extracellular oxygen had been varied to create low to high intracellular oxygen demand. A low K_m value created high oxygen demand within the cell which eventually created a hypoxic condition in the extracellular environment. Hence, a lower K_m value also represented a hypoxic condition.

To create the hypoxic scenario, oxygen uptake rates of the cell was enhanced by reducing the K_m of Oxygen ($k_m^{O_2}$). The initial K_m value for oxygen uptake was 164mM for the normal condition. This was reduced down a very low value of 1mM, which signifies a high affinity for

the substrate, which in the present model is the extracellular oxygen. The hypoxic condition which resulted was a consequence of the rapid uptake of oxygen by the cell. Hence, hypoxia was induced as a consequence of rapid metabolism of the cells.

2.9. Creation of glioma-like situation

In order to create a glioma like scenario in the model, we introduced changes in the values of multiple parameters to induce the change in activities of the respective enzymes. The selection of these parameters was made based on literature evidences of their malfunctioning in gliomas and also by the analysis of sensitive parameters. Differential regulations of the enzymes NADPH oxidase (NOX) [44, 45], glutathione peroxidase (GTHP) [33, 46] and glutathione oxidoreductase (GTHO) [47] have been reported in the literature. The sensitivity analysis further added to the understanding of the parameters which govern these changes. These include V_m^{NOX} , V_m^{GTHO} , V_m^{GTHP} and $k_m^{O_2}$ where $k_m^{O_2}$ has been considered to alter the oxygen demand of the cell as described in the earlier section. An increase in h_2o_2 concentration was considered as a signature to ensure that the model represents a glioma-like situation [48, 49].

3. Results

3.1. Dynamics of cells under normoxic conditions

We illustrate the temporal behavior of glutathione (reduced and oxidized), hydrogen peroxide (h_2o_2) and oxygen radicals (*oxrad*) over time in the normal scenario. The chemical kinetics of the enzyme GTHP has been included which uses h_2o_2 and *gsh* as the substrate to yield *gssg*. From simulations we observe that the model is capable of maintaining h_2o_2 concentration within a biologically feasible range of $\sim 4 \mu M$ which was initiated at a high h_2o_2 concentration of 1.5mM (Fig 3A), while there is a decrease in the *gsh* concentration (from 3.83mM to 2.33mM) and increase in the *gssg* concentration (from 0.5mM to 2.09mM) at steady state. Meanwhile, the oxygen radicals (*oxrad*) generated as an action of NADPH oxidase (NOX) is readily metabolized into h_2o_2 due to high activity of superoxide dismutase (SOD) as has been reported and considered in the model ($V_m^{SOD} = 11.4 \times 10^3 \text{ mM hr}^{-1}$). Hence, a consistent reduced level of *oxrad* is observed through our simulations.

The *nadph/nadp*⁺ and *atp/adp* ratios of the model have also been considered. As has been observed experimentally, a proliferating cell maintains a high *nadph/nadp*⁺ ratio to maintain its redox balances and high *atp/adp* ratio to suffice its proliferative requirements. In Fig 3C, we have compared the experimentally reported values of *nadph/nadp*⁺ [37] and average *atp/adp* [39, 40] ratios with the simulated values which are comparable. The dynamics of the components of tripeptide that result in the formation of *gsh* is dictated by the *gsh-gssg* cycle. Fig 3B shows the changes in the intracellular concentration of cystine (*cys*), glutamate (*glut*), glycine (*gly*) and glutamyl-cysteine (*glucys*) corresponding to changes in *gsh* and *gssg* over time. Simulation results show that in response to high oxidant (h_2o_2) concentration within the cell, available intracellular cystine and glutamate is used for the production of glutamyl-cysteine, which subsequently forms a complex with glycine to produce *gsh*. *gsh* then enters the *gsh-gssg* cycle where *gsh* and h_2o_2 are used as a substrate to produce *gssg*. As such, we observe a decline in the concentration of all other metabolites except for *gssg*, which is produced in response to nullify the high h_2o_2 concentration. The intracellular concentration of cystine and glutamate remain limiting in a normal scenario.

3.1.1. Parameter variation of sensitive parameters. Sensitivity analysis yielded a set of parameters crucial for determining the h_2o_2 level and the regulation of the *gsh-gssg* cycle. Enzymes GTHP, NOX and GTHO are observed to be most sensitive in determining model

properties. Changes in the uptake rate of oxygen also affected the model dynamics. Varying parameters for these enzymes show interesting results, which are discussed in the subsequent subsections.

V_{max} of Glutathione Peroxidase (V_m^{GTHP}):

The enzyme *GTHP* is crucial in neutralizing h_2o_2 with the help of *gsh* which itself converts to *gssg* converting h_2o_2 into h_2o . The V_{max} of the reaction is an important determinant of the rate of conversion of h_2o_2 . From our analysis, we could see that an increase in the V_m^{GTHP} (from 0.001 mM hr^{-1} to 1.5 mM hr^{-1}) resulted in a reduced level of h_2o_2 . Simulations were performed at different time points (6hrs, 12hrs, 18hrs, 24hrs, and 32 hrs) and a similar trend is observed for all time points. A sharp decrease is observed at a V_{max} value between 0.1 mM hr^{-1} to 0.3 mM hr^{-1} when the h_2o_2 concentration is maintained at micromolar concentration, which initiated at a millimolar concentration (Fig 4A). However, the corresponding *nadph/nadp*⁺ ratio remains unaltered which suggests that the redox balance of the system largely remains unaffected by the change in V_m^{GTHP} although the *gsh/gssg* ratio reduces significantly (Fig 4B and 4C). It is important to mention that the normal physiological expression of *GTHP* ranges between 0.2874 to 2.697 mM/hr (S1 Table of S1 Text) and interesting dynamics in h_2o_2 level, *nadph/nadp*⁺ and *gsh/gssg* ratios are only observable for a very low value of V_m^{GTHP} . By varying the value of V_m^{GTHP} from 0.001 mM hr^{-1} to 1.5 mM hr^{-1} we observe that high *GTHP* activity maintains a steady and low micromolar concentration of h_2o_2 , but h_2o_2 starts accumulating as the activity lowers, which might induce oxidative damage to the cell. This observation can be compared with the diminished level of *GTHP* in brain tumors [50] and can be interpreted as a characteristic for gliomas with a very low expression of *GTHP*.

V_{max} of NADPH Oxidase (V_m^{NOX}):

NADPH Oxidase catalyzes the production of oxygen free radicals from available oxygen using NADPH reduction. We could observe that an increase in the V_m^{NOX} (from $0.0001 \text{ mM hr}^{-1}$ to 1 mM hr^{-1}) results in an increase in the h_2o_2 concentration for the specified time points (6hrs, 12hrs, 18hrs, 24hrs and 32 hrs). A marked decrease in the *nadph/nadp*⁺ ratio and *gsh/gssg* ratio is observed at later time points (24hrs and 32hrs) with the increase in V_{max} value (Fig 4D, 4E and 4F). This could be interpreted as one of the important factors determining the cancerous transformation of the glial cells.

Two parameter variation of V_m^{GTHP} and V_m^{GTHO} :

We illustrate in (Fig 5A–5C), the effect of simultaneous change in V_m^{GTHP} and V_m^{GTHO} on h_2o_2 level, *nadph/nadp*⁺ and *gsh/gssg* ratios. The h_2o_2 level is reduced with increasing activity of V_m^{GTHP} , although change in the kinetics of *GTHO* does not affect (Fig 5A). When *nadph/nadp*⁺ is taken into account, we observe that at a very low V_m^{GTHO} , the effect of V_m^{GTHP} remains minimum. With a gradual increase in the V_m^{GTHO} there is a reduction in the *nadph/nadp*⁺ ratio, which furrows deeper at a higher value of V_m^{GTHP} . The enzyme *GTHO* facilitates the reduction of *gssg* into *gsh* in a *nadph-nadp*⁺ dependent manner and hence with an increasing enzyme availability and activity the *nadph/nadp*⁺ ratio reduces. Here we have considered the dynamics of *nadph/nadp*⁺ at 12hrs and could observe that the initial dynamics are dependent on V_m^{GTHO} . At high V_m^{GTHP} , with increasing value of V_m^{GTHO} there is a decrease in the ratio (Fig 5B) which is due to the active involvement of the enzyme in nullifying the persistent levels of the substrate, h_2o_2 . We observe the decrease in the ratio till V_m^{GTHO} reaches a value of 0.2 mM hr^{-1} at 12 hours. However, the decrease is compensated back with further increase in the V_{max} . As a high level of h_2o_2 is metabolized to a non-toxic micromolar level, we observe from our model simulation that a V_{max} of 0.2 mM hr^{-1} for the enzyme *GTHO* is sufficient to metabolize the persisting levels of h_2o_2 at 12 hours. At a V_{max} value lower than this the enzyme becomes the limiting factor and beyond this value, the activity of the enzyme is limited by the availability of the substrate

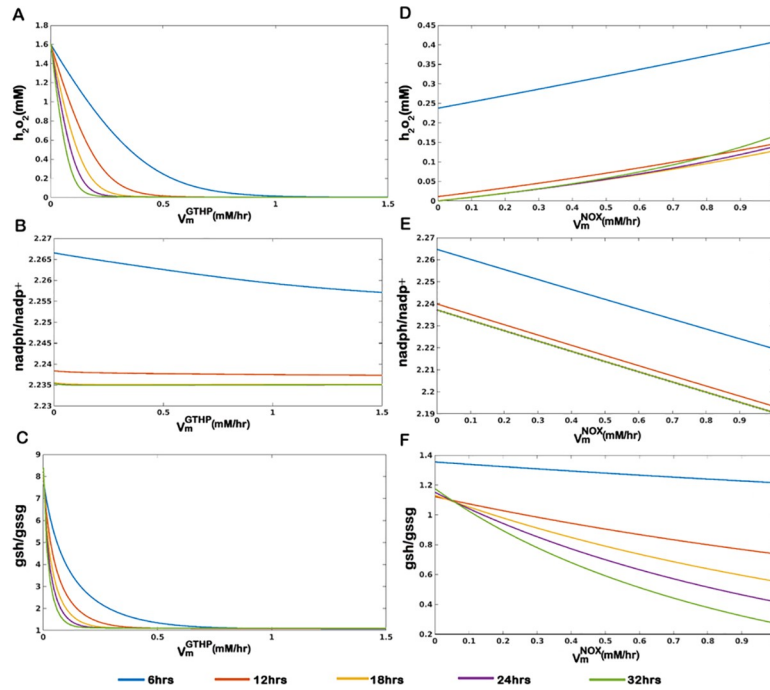


Fig 4. Parameter variation plot for (A-C) V_{max} of GTHP (V_m^{GTHP}) and (D-F) V_{max} of NOX (V_m^{NOX}) under the normal condition at different time points.

<https://doi.org/10.1371/journal.pone.0235204.g004>

(h_2o_2). Meanwhile, at lower values of V_m^{GTHP} ($<0.5 \text{ mM hr}^{-1}$), persisting level of h_2o_2 at 12hrs is higher due to the slow activity of GTHP (Fig 5B). The substrate remains available for GTHO activity which continues to metabolize the conversion (at higher V_m^{GTHO} which was limited by substrate concentration in the earlier case) and $nadph$ pool diminishes resulting into a reduction in $nadph/nadp^+$ ratio. The dip in the $nadph/nadp^+$ ratio is compensated by the action of other reactions that replenish $nadph$ pools represented in the model as l_{nadph} . Trends are similar for $gsh/gssg$ ratio which is dependent on the substrate availability (h_2o_2) except at a very low value of V_m^{GTHP} (0.001 mM hr^{-1}) which limits the conversion of gsh to $gssg$ thereby resulting in an accumulation of gsh and leading to very high $gsh/gssg$ ratios. h_2o_2 level persists in the sub-micromolar range ($\sim 0.045 \text{ mM}$) at a V_{max} of 0.5 mM hr^{-1} for GTHP, which is subsequently metabolized to micromolar levels (0.002 mM) with further increase in V_{max} (Fig 5A). This governs the change in $gsh/gssg$ ratio and an increase in both V_m^{GTHP} and V_m^{GTHO} coordinates to metabolize h_2o_2 till it reaches micromolar levels by cyclic production and consumption of gsh and $gssg$. As h_2o_2 reaches a micromolar level the activity of GTHP is limited due to h_2o_2 availability whereas gsh production continues by the action of GTHO till $gssg$ reaches a basal level. At this point we observe an increase in the $gsh/gssg$ ratio (Fig 5C).

3.2. Dynamics of cells under high oxygen demand: induction of hypoxia in the microenvironment

To mimic the high oxygen demand during cancerous transformation we tuned the model parameter $k_m^{O_2}$ which determines the affinity for the substrate. A decrease in the K_m value implies an increase in the affinity for the substrate. To represent an increased affinity of the cell for oxygen, lowering values of K_m is tried ($k_m^{O_2} = 164, 50, 10$ and 1 mM) and as the value lowers, the concentration of external oxygen reduces creating a mild to severe hypoxic

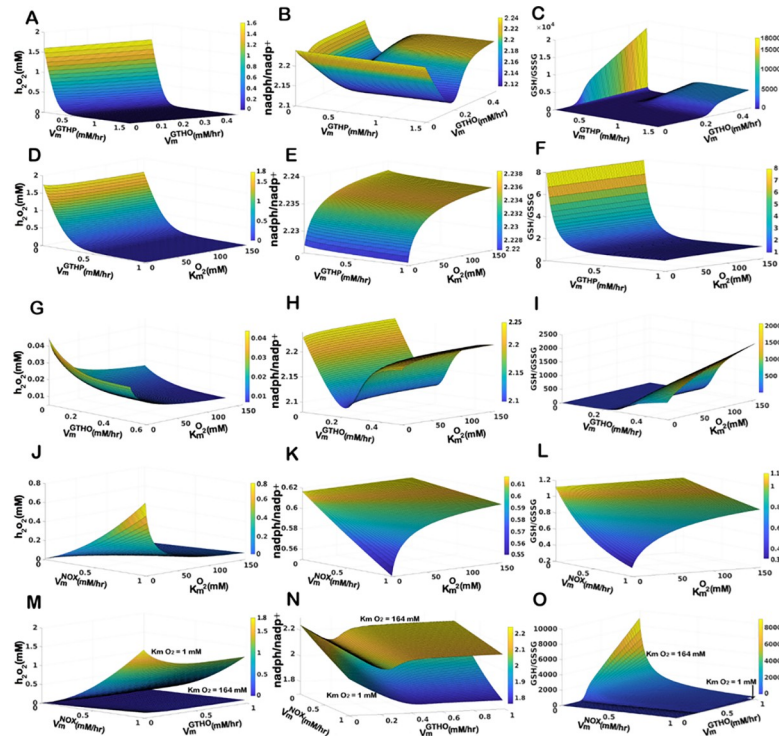


Fig 5. Surface plots of two parameter variation for the sensitive parameters on h_2O_2 level, $nadph/nadp^+$ ratio, and $gsh/gssg$ ratio. (A-C) Effect of variations in V_m^{GTHP} and V_m^{GTHO} under normoxic conditions ($k_m^{O_2} = 164mM$). (D-F) Effect of variation in V_m^{GTHP} under changing oxygen demand ($164mM \geq k_m^{O_2} \geq 1mM$). (G-I) Effect of variation in V_m^{GTHO} under changing oxygen demand ($164mM \geq k_m^{O_2} \geq 1mM$). (J-L) Effect of variation in V_m^{NOX} under changing oxygen demand ($164mM \geq k_m^{O_2} \geq 1mM$). (M-O) Combined effect of simultaneous variation in V_m^{NOX} and V_m^{GTHO} under $k_m^{O_2} = 164mM$ and $k_m^{O_2} = 1mM$.

<https://doi.org/10.1371/journal.pone.0235204.g005>

condition (S4 Fig of S1 Text). Parameter variation of sensitive parameters is tried for different affinities for oxygen and results are discussed below.

3.2.1. Effect of Changing Glutathione Peroxidase (GTHP) enzymatic activity. With the change in dynamics of h_2O_2 , $nadph/nadp^+$ and $gsh/gssg$ ratios with changing V_m^{GTHP} and $k_m^{O_2}$, we observe that h_2O_2 concentration (Fig 5D) and $gsh/gssg$ ratio (Fig 5F) primarily depends on V_m^{GTHP} and remain unaffected by the change in $k_m^{O_2}$. The enzyme *GTHP* metabolizes the conversion of h_2O_2 into water by oxidizing *gsh* to *gssg* and hence the enzyme concentration directly affects the h_2O_2 concentration and $gsh/gssg$ ratio. $nadph/nadp^+$ ratio however, depend on $k_m^{O_2}$ and remain unaltered with change in the V_m^{GTHP} (Fig 5E). We infer that high levels of oxidants created in response to increased uptake of oxygen (which eventually creates a hypoxic micro-environment for the cell) can be dealt with increased activity of *GTHP* within the cell, but at a cost of reduced $nadph/nadp^+$ and $gsh/gssg$ ratios.

3.2.2 Effect of Changing Glutathione Oxidoreductase (GTHO) enzymatic activity. At 12 hours, h_2O_2 is maintained between sub-micromolar to micromolar levels (0.045mM to 0.005mM) for varying levels of V_m^{GTHO} and $k_m^{O_2}$. The concentration of h_2O_2 reduces with increasing V_m^{GTHO} . Simultaneously with increasing $k_m^{O_2}$, a further reduction in h_2O_2 level is observed (Fig 5G). The $nadph/nadp^+$ ratio shows a dip at V_{max} value of 0.2 $mM\ hr^{-1}$ for GTHO which is compensated back with further increase in the V_{max} (Fig 5H). We plotted the temporal plots of varying V_m^{GTHO} at high oxygen demand ($k_m^{O_2} = 1mM$) and checked the $nadph/nadp^+$ ratios at different time points (S5 Fig of S1 Text). We infer from our model simulations that the $nadph/$

$nadp^+$ ratio in the model depends upon two factors: (i) concentration of the enzyme *GTHO* available to convert the *gssg* into *gsh* in order to maintain the *gsh-gssg* cycle necessary for neutralizing h_2o_2 levels (ii) the amount of oxidant (h_2o_2) concentration persisting at any point of time. The *gsh/gssg* ratio shows different patterns at different values of the two parameters (Fig 5I). At low values of V_m^{GTHO} , the enzymatic activity is limited and hence the conversion of *gssg* to *gsh* is slower. With a low V_m^{GTHO} ($< 0.2mM$), *gssg* accumulates and the difference in *gsh* and *gssg* concentration reduces resulting in low *gsh/gssg* ratio. As the V_{max} increases, the conversion of *gssg* to *gsh* enhances which adds to the *gsh* production pool and the difference in *gsh* and *gssg* concentration widens giving high values of *gsh/gssg* ratio. Adding to it is the effect of oxygen within the cell. As $k_m^{O_2}$ increases, the oxidant production is limited (due to limited substrate availability for *NOX* and *SOD*) and hence the conversion of *gsh* to *gssg* is reduced leading to further increase in the *gsh/gssg* ratio.

3.2.3 Effect of changing NADPH Oxidase (NOX) enzymatic activity. Characteristic changes in h_2o_2 , $nadph/nadp^+$ ratio and *gsh/gssg* ratio with changing V_m^{NOX} is observed under normoxic conditions. When we simulate the variation of the parameter over varying $k_m^{O_2}$, the concentration of h_2o_2 takes a leap as V_m^{NOX} increases and $k_m^{O_2}$ decreases (Fig 5J). At smaller K_m value, cellular uptake of oxygen increases and an increase in V_m^{NOX} ensures rapid metabolism of oxygen into free radicals. These free radicals are readily being metabolized into h_2o_2 due to the high V_m^{SOD} which catalyzes the conversion. Hence, with increasing activity of *NOX* the free radicals so formed are directed towards the production of h_2o_2 . An inverse pattern of $nadph/nadp^+$ and *gsh/gssg* ratio is observed in response to the changing h_2o_2 concentration (Fig 5) due to the activity of the *gsh-gssg* cycle (Fig 5K and 5L).

We infer from the above simulations that *GTHP* is an important determinant of h_2o_2 levels in the cell. An increase in the activity of *GTHP* is helpful in reducing the h_2o_2 levels to a feasible range without affecting the $nadph/nadp^+$ ratio much although it alters the *gsh/gssg* ratio. The effect of changing affinity for oxygen is nullified with a change in V_m^{GTHP} . We attempted varying the activity of *GTHP* with other sensitive parameters only to observe a reduction in the h_2o_2 while maintaining the redox balance of the cell within a feasible range. As such we propose here that an increase in the activity of *GTHP* is desirable for anti-oxidant therapy as it reduces the h_2o_2 levels irrespective of oxygen demand simultaneously lowering the *gsh/gssg* ratio which is considered an initiation factor in the induction of apoptosis.

While *GTHP* can be used for anti-oxidant therapy, analyses with *NOX* and *GTHO* suggest that they are favorable targets for pro-oxidant therapies. An increase in *NOX* activity at high oxygen demand clearly increases h_2o_2 production along with simultaneous lowering of $nadph/nadp^+$ and *gsh/gssg* ratio indicating cellular toxicity and initiation of apoptotic pathways. Changes in *GTHO* activity have differing patterns. Given the initial concentration of h_2o_2 in the model, a decrease in h_2o_2 concentration is observed with increasing *GTHO* activity. However, $nadph/nadp^+$ and *gsh/gssg* ratio at around a V_{max} value of $0.2 mM hr^{-1}$ of *GTHO* shows an ideal condition to initiate cellular toxicity. We further analyzed the effect of the two enzymes in reducing redox potential and *gsh/gssg* ratio of the cell at different oxygen demand of the cell.

An increase in *NOX* and *GTHO* activity has a synergistic effect in increasing the h_2o_2 concentration (Fig 5M) and lowering the $nadph/nadp^+$ ratio (Fig 5N) under high oxygen demand. *gsh/gssg* ratio, however, lowers down with increasing activity of *NOX*, which otherwise increases with increasing *GTHO* activity at low *NOX* activity ($< 0.3 mM hr^{-1}$) (Fig 5O).

3.3. Cellular behavior with multiple mutations

From the previous set of analyses, we observe that the system shows a characteristic change in its behavior for changes in sensitive parameters which are related to the oxidant and anti-

oxidant production. The system remained robust for most of the other parameter changes. The sensitivity of the h_2o_2 increased for *GTHO* during high oxygen demand which otherwise remains unaffected in normoxia conditions. Also, the sensitivity of h_2o_2 increased for *NOX* during high oxygen demand. Parameter values to V_m^{NOX} , V_m^{GTHO} , V_m^{GTHP} and $k_m^{O_2}$ were changed to $1mM\ hr^{-1}$, $0.2\ mM\ hr^{-1}$, $0.19\ mM\ hr^{-1}$ and $1\ mM$ from $0.0468\ mM\ hr^{-1}$, $0.5\ mM\ hr^{-1}$, $0.00216\ mM\ hr^{-1}$ and $164mM$ respectively to create the glioma scenario. Temporal plots generated for this model show an excess increase in h_2o_2 concentration due to limited regulation by *gsh* and *gssg*. A decline in $nadph/nadp^+$ and *gsh/gssg* ratio is also observed.

With an observable difference in the cellular redox status and the ROS level, we try to understand if the changes in $nadph/nadp^+$ and *gsh/gssg* ratios associated with the changes in h_2o_2 level in the glioma scenario can be used to determine the pro-apoptotic or anti-apoptotic fates of the cell. Temporal dynamics of the changes in h_2o_2 level and the two ratios for Normal, Hypoxia and Glioma conditions for a duration of 48hrs are shown in Fig 6. Under normal conditions, h_2o_2 levels are readily reduced to micromolar concentration ($4\mu M$) and the resulting values of $nadph/nadp^+$ and *gsh/gssg* ratios at steady state are 2.63 and 1.2 (Fig 6A). The values mostly remain unaltered during a shift to hypoxia except for a slight reduction in the *gsh/gssg* ratio over time (Fig 6B). Changes are however distinct in case of glioma. Reports suggest that different GBM cell lines have different level of *GTHO* expression and overexpression of *GTHO* mediates drug resistance in these cells. Whereas, *GTHO* knockdown resensitize *GTHO* overexpressed cells to drug treatment [47]. We corroborated this understanding to our model simulations to observe the effect of varying *GTHO* on the thiol and redox ratios and h_2o_2 concentration. We created both the conditions: high and low expression of *GTHO* in the model. We observe a characteristic difference in the *gsh/gssg* ratio and h_2o_2 level in the two scenarios. Under high *GTHO* expression ($V_m^{GTHO} = 0.19\ mM\ hr^{-1}$), the *gsh/gssg* ratio remains higher than the normal (Fig 6C) whereas, under low *GTHO* expression ($V_m^{GTHO} = 0.001\ mM\ hr^{-1}$) the ratio diminishes to a very low value of 0.01 with an abrupt increase in h_2o_2 level (Fig 6D). Through the simulations, we propose that at high values of V_m^{GTHO} , the increased level of *gsh/gssg* ratio helps the cell to evade programmed cell death which would otherwise lead to apoptosis by the induction of toxicity due to uncontrolled increase in h_2o_2 levels. However, at lower values of V_m^{GTHO} , a sharp decline in the *gsh/gssg* ratio drives the cell towards an apoptotic fate. As such employing an anti-oxidant approach at high V_m^{GTHO} and a pro-oxidant approach at low V_m^{GTHO} will provide a better surveillance strategy to eliminate cancer cell progression. We observe only a slight difference in the $nadph/nadp^+$ ratio under present simulation conditions. Regulation of $nadph/nadp^+$ ratio, however, can be employed to facilitate the pro- or anti-oxidant approach by modulating $nadph/nadp^+$ ratio either by inhibition or activation of NAD kinase, a potent regulator of the *nadph-nadp^+* pool within the cell [51, 52].

To identify parameters, which influence the cellular properties under these different conditions, sensitivity analyses are performed for the model with high oxygen demand (hypoxia scenario, by changing $k_m^{O_2}$) and for the model with multiple mutations (glioma scenario). A comparison of the sensitive parameters (p-value <0.05) for the variables h_2o_2 , *gsh* and *gssg* for the three conditions: normal, hypoxic and glioma show common and unique sensitive parameters for each scenario (Fig 7). The kinetics of the enzyme *GTHP* remains crucial in all three scenarios owing to its direct involvement in the production of *gsh*. Apart from the parameters which directly regulate the variables, a few indistinct parameters are found to be sensitive for the different scenarios. Analyses of these parameters show that the influence exerted by them on the variables is at micromolar and nanomolar concentrations for the present simulation conditions. The set of parameters which are unique and common to the three different simulation scenarios are shown in Fig 7 and the detail descriptions are provided in Table 1. We

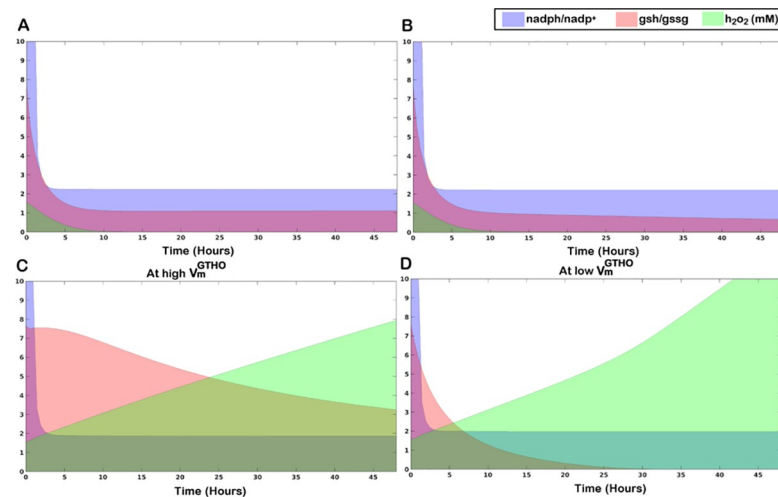


Fig 6. Temporal area plots of changing $nadph/nadp^+$ and $gsh/gssg$ ratios along with change in h_2o_2 concentration. A. Normal condition, B. Hypoxia, C. Glioma at high V_m^{GTHO} (0.19 mM hr^{-1}), D. Glioma at low V_m^{GTHO} (0.001 mM hr^{-1}).

<https://doi.org/10.1371/journal.pone.0235204.g006>

suggest that regulation of these parameters might help in facilitating pro- or anti-oxidant therapeutic strategies.

3.4. Identification of Combinatorial targets for pro- and anti- oxidant therapy

We have analyzed the influence of parameters sensitive in regulating h_2o_2 levels during the glioma scenario using the parameters listed in G11 in Table 1. These parameters do not necessarily have a role in regulating the ROS levels directly, yet show differences in the ROS levels along with changes in $gsh/gssg$ and $nadph/nadp^+$ ratios when varied individually or in combination. Enzymes and metabolites associated with a few of these parameters like methyltetrahydrofolate (*mlthf*) [53, 54], NADPH Oxidase (*NOX*) [32, 55, 56], cystine-glutamate antiporter (*xCT*) [57], etc., have already been implicated in having crucial role in regulating ROS levels in the cell. A few parameters associated with enzymes which do not directly regulate the ROS and glutathione production, like Phosphoglycerate Dehydrogenase (*PGCDH*), Cystine Reductase (*CR*) and Fructose Bis-phosphate Aldolase (*FBA*) have also been identified. These parameters do not necessarily show a significant difference in the ROS levels when varied individually but show a characteristic difference when varied in combinations. These changes can be utilized for designing pro-oxidant or anti-oxidant approaches for therapeutic targeting. A few of the combinations which bring distinct changes in the h_2o_2 level, $gsh/gssg$ and $nadph/nadp^+$ ratio during glioma scenario have been listed in Table 2. k_{nadph}^{CR} , a parameter that has been considered in the model, which catalyzes the conversion of cystine into L-cysteine subsequently using it for glutathione production, is found to have an effect on the h_2o_2 level, $gsh/gssg$ and $nadph/nadp^+$ ratio when varied in combination with other parameters. Availability of oxygen in the ECM for cellular uptake (L_{oxy}) when modulated in combination with k_{nadph}^{CR} show a significant change in level. Interestingly, a combinatorial variation of L_{oxy} with V_m^{FBA} cause a decline in the h_2o_2 level which can be utilized for anti-oxidant therapy, and a variation of k_{nadph}^{CR} with k_{glucys}^{GS} induces changes the h_2o_2 level which can possibly be used for pro-oxidant therapeutic design. Table 2 shows the possible utility of these combinations in pro- or anti-oxidant therapy

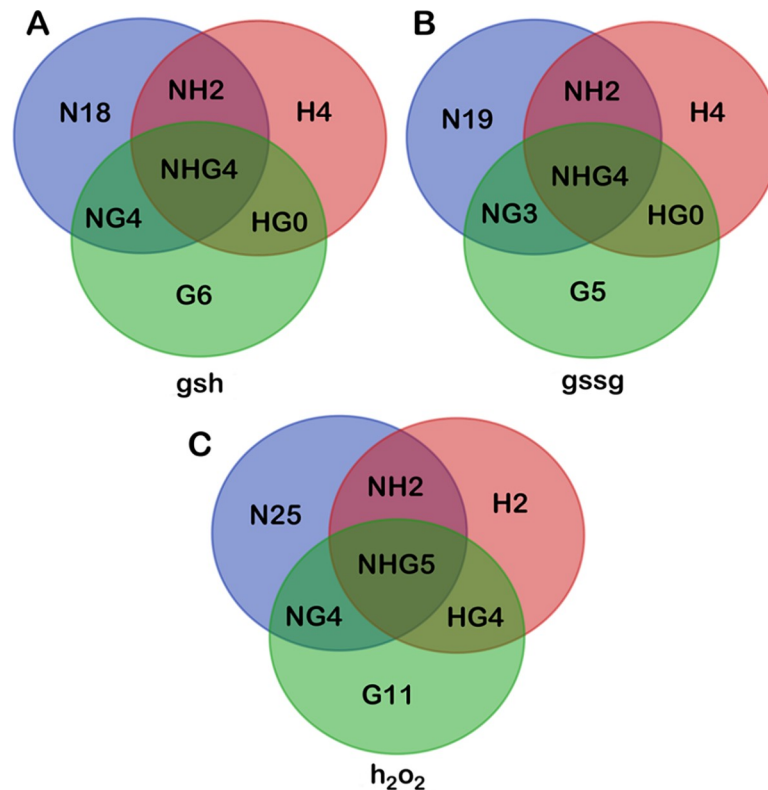


Fig 7. Comparison of sensitive parameters in Normal, Hypoxia and Gliomas for the variables *gsh*, *gssg* and *h₂O₂*. The abbreviations used here are **N**: Normal, **H**: Hypoxia, **G**: Gliomas, **NH**: Normal and Hypoxia, **NG**: Normal and Gliomas, **HG**: Hypoxia and Gliomas and **NHG**: Normal, Hypoxia and Gliomas. The sensitive parameters for each variable under each condition have been tabulated in Table 1.

<https://doi.org/10.1371/journal.pone.0235204.g007>

depending upon their influence on the *h₂O₂* level, *gsh/gssg* and *nadph/nadp⁺* ratio. The changes in *h₂O₂*, *gsh/gssg* and *nadph/nadp⁺* profiles due to these combinatorial variations in glioma scenario are shown in S6 Fig of S1 Text and the values for which the profiles are obtained have been listed in S3 Table of S1 Text. These combinations could be explored for their possible therapeutic abilities in the development of future therapeutic strategies. Altering the kinetic parameters like the V_{max} or k_m of an enzyme is challenging, though possible with the help of enzyme modulators and competitive and non-competitive inhibitors. Non-competitive inhibitors are capable of altering the V_{max} of an enzyme while keeping the k_m unaltered, while competitive inhibitors can alter the k_m of the enzyme [58]. A few of the inhibitors for the aforementioned enzymes have already been reported in literatures and have been tested in *in-vivo* experiments, which could be checked for their effectiveness in the present context. For e.g. iodoacetate, N-ethylmaleimide (NEM) and 5,5'-dithiobis-(2-nitrobenzoate) (DTNB) have been reported as potent inhibitors of glutathione synthase [59], and neopterin, magnolol, apocyanin and gliotoxin for NADPH oxidase [60]. However, the exact type of inhibition for these inhibitors i.e. competitive or non-competitive is not yet known and has to be understood. A context-based understanding of the involvement of these parameters in *h₂O₂* production or scavenging mechanism under different conditions has to be made through experiments in order to employ them for therapeutic strategies.

Table 1. List of sensitive parameters for *gsh*, *gssg* and h_2o_2 under normal, hypoxic and glioma scenarios.

<i>gsh</i>	
N18	$V_{PGI}, I_{3php}, k_{ap}^{GS}, K_{O_2}, k_{(3pg)}^{PGCDH}, k_{atp}^{GCL}, k_{i(cys)}^{CR}, V_{GHMT}, k_{cys}^{CR}, k_{f6p}^{PFK}, d_{oxy}, k_{i(glut)}^{PST}, V_{GLUTEX}, V_{PSP}, k_{i(gap)}^{GAPDH}, k_{gap}^{GAPDH}, k_{i(gly)}^{GS}, V_{PFK}$
H4	$k_{i(atp)}^{HK}, k_{oxrad}^{SOD}, k_{i(atp)}^{PFK}, K_{O_2}^{NOX}$
G6	$k_{i(gssg)}^{GTHO}, V_m^{NOX}, V_m^{GS}, I_{nadp}, I_{nadph}, d_{nadph}$
NH2	k_{adp}^{PGK}, V_m^{GCL}
HG0	-
NG4	$V_m^{GTHO}, k_{gssg}^{GTHO}, k_{i(atp)}^{GS}, k_{nadph}^{GTHO}$
NHG4	$k_{i(h_2o_2)}^{GTHP}, V_m^{GTHP}, k_{h_2o_2}^{GTHP}, k_{gsh}^{GTHP}$
<i>Gssg</i>	
N19	$V_{PGI}, I_{3php}, k_{ap}^{GS}, K_{O_2}, k_{(3pg)}^{PGCDH}, k_{atp}^{GCL}, k_{i(cys)}^{CR}, V_{GHMT}, k_{cys}^{CR}, k_{f6p}^{PFK}, d_{oxy}, k_{i(glut)}^{PST}, V_{GLUTEX}, V_{PSP}, k_{i(gap)}^{GAPDH}, k_{gap}^{GAPDH}, k_{i(atp)}^{GS}, V_{PFK}$
H4	$k_{i(atp)}^{HK}, k_{oxrad}^{SOD}, k_{i(atp)}^{PFK}, K_{O_2}^{NOX}$
G5	$k_{i(gssg)}^{GTHO}, V_m^{NOX}, I_{nadp}, I_{nadph}, d_{nadph}$
NH2	k_{adp}^{PGK}, V_m^{GCL}
HG0	-
NG3	$V_m^{GTHO}, k_{gssg}^{GTHO}, k_{nadph}^{GTHO}$
NHG4	$k_{i(h_2o_2)}^{GTHP}, V_m^{GTHP}, k_{h_2o_2}^{GTHP}, k_{gsh}^{GTHP}$
h_2o_2	
N25	$V_{PGI}, I_{3php}, k_{ap}^{GS}, K_{O_2}, k_{(3pg)}^{PGCDH}, d_{nadh}, k_{atp}^{GCL}, k_{i(cys)}^{CR}, V_{GHMT}, k_{cys}^{CR}, k_{f6p}^{PFK}, k_{i(glut)}^{PST}, V_{GLUTEX}, V_m^{GTHO}, V_{PSP}, k_{i(gap)}^{GAPDH}, k_{gssg}^{GTHO}, k_{gap}^{GAPDH}, d_{h_2o_2}, V_m^{GLYex}, k_{i(atp)}^{GS}, V_{PFK}, k_{i(glut)}^{GLUD}$
H2	$k_{i(atp)}^{HK}, k_{oxrad}^{SOD}$
G11	$d_{mlthf}, k_{3pg}^{PGCDH}, L_{oxy}, d_{ph}, k_{glut}^{XCT}, k_{i(nadph)}^{NOX}, k_{nadph}^{NOX}, V_m^{FBA}, k_{glucys}^{GS}, k_{nadph}^{CR}, I_{atp}$
NH2	$V_m^{GCL}, V_m^{O_2}$
HG4	$V_m^{NOX}, I_{nadph}, d_{in}, K_{O_2}^{NOX}$
NG4	$I_{glut}, k_{i(atp)}^{GCL}, I_{nadp}, d_{oxy}$
NHG5	$k_{adp}^{PGK}, k_{i(h_2o_2)}^{GTHP}, V_m^{GTHP}, k_{h_2o_2}^{GTHP}, k_{gsh}^{GTHP}$

<https://doi.org/10.1371/journal.pone.0235204.t001>

4. Discussion

ROS, produced as a byproduct of cellular metabolism, are often considered toxic to the cells. Nonetheless, in recent years, their functions as second messengers in signal transduction processes have been highly appreciated. In normal cells, any excess production of ROS is scavenged by the antioxidant machinery. ROS, however, exhibit a paradoxical behavior in augmenting or hindering tumor progression. It is described to have a “double-edged sword” property having both tumor-promoting and tumor-suppressing functions. Currently, both pro-oxidant and anti-oxidant approaches are employed as cancer therapeutics. However, owing to the paradoxical behavior, the employment and effectiveness of which strategy will suit a better therapeutic approach for any particular cancerous situation still remains unclear.

The oxidative status and functioning of anti-oxidant machinery have a crucial role to determine the proliferative fates of the cancer cells. The cellular $nadph/nadp^+$ ratio is a measure of the reducing potential of the cells which is usually maintained high for the proper cellular functioning [24, 25]. A decline in the $nadph/nadp^+$ ratio is observed in many cancer types [61, 62], although high $nadph/nadp^+$ ratio was observed to promote cancer cell growth and proliferation by stimulating anabolism and by protecting cancer cells against oxidative stress during nutrient limitation [63]. Thioli ratios are another important determinant of cellular apoptotic

Table 2. Combinatorial effect of sensitive parameters on gliomas.

Sr. No.	Parameter 1	Parameter 2	Variation of Parameter 1*	Variation of Parameter 2*	Effect
1.	$k_{i(nadph)}^{NOX}$	k_{nadph}^{CR}	Decrease	Increase	Pro-oxidant
2.	$k_{i(nadph)}^{NOX}$	k_{nadph}^{NOX}	Increase	Increase	Anti-oxidant
			Decrease	Decrease	Pro-oxidant
3.	L_{oxy}	k_{nadph}^{CR}	Increase	Increase	Pro-oxidant
4.	$k_{i(nadph)}^{NOX}$	l_{atp}	Decrease	Increase	Pro-oxidant
5.	V_m^{FBA}	L_{oxy}	Decrease	Decrease	Anti-oxidant
6.	k_{glucys}^{GS}	k_{nadph}^{CR}	Decrease	Decrease	Pro-oxidant

*Increase or decrease in the parameter value with respect to normal value.

<https://doi.org/10.1371/journal.pone.0235204.t002>

or anti-apoptotic fates. A high *gsh/gssg* ratio is maintained under normal conditions which often changes during cancerous transformations. A decline in *gsh/gssg* ratio induces the initiation of apoptosis while an increase might help the cells escape apoptosis. The puzzling duality of ROS in exhibiting varying cellular fates is determined by a coordinated response of these factors. To understand the effect of these factors cumulatively, under different cancerous scenarios is a challenge.

Motivated by these findings, we have designed a kinetic metabolic framework for glial cell, to trace the possible changes that might be occurring within them during their transformation into gliomas. The model takes into account the metabolic reactions involved in the production of the tri-peptide complex, glutathione and ROS producing machinery. A part of the glycolytic pathway which enters the glycine-serine metabolism has been considered along with cysteine and glutamate metabolism which result in the production of the components of the tri-peptide: glycine, cysteine and glutamate respectively. Herein, we considered the effect of these pathways on the anti-oxidant production machinery simultaneously looking for their effect on ROS production and scavenging and vice versa. To understand the effect of glutathione over ROS metabolism, reactions metabolizing the production of glutathione and ROS, along with the *gsh-gssg* cycle have been considered. Important reactions involving the *nadph-nadp⁺* conversions have been considered, to take into account the changes in *nadph/nadp⁺* ratio while manipulating *h₂O₂*-glutathione profiles. We postulate that the paradoxical behavior of ROS is governed by changes in the *nadph/nadp⁺* and *gsh/gssg* when considered together. An increase in *h₂O₂* along with a decline in both *gsh/gssg* and *nadph/nadp⁺* will disrupt the cellular redox status and drive the cell towards apoptosis by inducing toxicity due to accumulation of ROS.

Numerical simulations of the model provide us with a set of sensitive enzyme parameters, which are affected during a transition from normal glial conditions to hypoxia to the development of gliomas. Upon introducing variations into the parameters which are sensitive under normal glial conditions, interesting changes in the dynamics of *h₂O₂*, *nadph/nadp⁺* and *gsh/gssg* could be observed. The uptake of oxygen by the cells has been represented by the Michaelis-Menten equation form where $k_m^{O_2}$ determines the affinity of the cell for external oxygen. A decrease in $k_m^{O_2}$ results into a decline in the external oxygen concentration as the cellular affinity for external oxygen increases. This represents a condition with high cellular oxygen demand which is reflected as hypoxia in the external microenvironment.

GTHP is one of the important enzymes involved in the regulation of *gsh/gssg*, along with controlling the cellular content of *h₂O₂* and maintaining *nadph/nadp⁺*. Through our simulation on the glial cell model, we observe that with an increase in V_m^{GTHP} there is a considerable decline in the *h₂O₂* level and *gsh/gssg* ratio, although the effect on *nadph/nadp⁺* ratio is only trivial.

GTHO is another important enzyme, and the *GTHP-GTHO* duo completes the *gsh-gssg* cycle. Not much difference in *gsh/gssg* and *nadph/nadp⁺* could be observed for a change of *GTHO* alone keeping all other parameters fixed. However, simultaneously varying *GTHP* and *GTHO* result into interesting changes in *nadph/nadp⁺* and *gsh/gssg* with a decrease in h_2o_2 level. We interpret that at any given time point under normal condition there is a decline in the *nadph/nadp⁺* and *gsh/gssg* until the *gsh-gssg* cycle neutralizes h_2o_2 concentration to micromolar levels rendering it non-toxic to cellular processes, after which the cell regains a stable *nadph/nadp⁺* and *gsh/gssg* ratio. The involvement of NADPH Oxidase (*NOX*) is found to be crucial in the present simulation scenario. The activity of *NOX* determines the rate of production of free oxygen radicals which act as a substrate for superoxide dismutase (*SOD*) and is readily converted into h_2o_2 given V_m^{SOD} is sufficiently high. An increase in the *NOX* activity rapidly increases the h_2o_2 level decreasing both *nadph/nadp⁺* and *gsh/gssg* ratio.

While analyzing the dynamics of these parameters under changing affinity for oxygen, we observe that under hypoxic conditions increase in V_m^{GTHP} acts as the protective barrier against ROS by readily neutralizing h_2o_2 levels at the cost of reduced *gsh/gssg*, although the change in *nadph/nadp⁺* ratio remains trivial. A decrease in the V_m^{GTHP} can however help cancer development by causing h_2o_2 accumulation and inducing oncogenic signal transductions. The changes occurring due to an increase in activity of *NOX* and *GTHO* under hypoxia could also be interpreted as a condition initiating cancer development. While increasing *NOX* activity under hypoxia certainly disrupts cellular redox balance by reducing *gsh/gssg* and *nadph/nadp⁺*, the effect of changes in *GTHO* activity is minimal at a cost of sudden decrease in *nadph/nadp⁺* and *gsh/gssg* ratios with its effect being severe at lower values. When considered together, changes in *NOX* and *GTHO* activity under normal and hypoxic conditions show substantial differences suggesting their involvement in tumor initiation.

A decrease in V_m^{GTHP} and V_m^{GTHO} , and an increase in V_m^{NOX} along with a low $k_m^{O_2}$ were considered to create a situation under hypoxia with multiple mutations representing a glioma-like situation. Comparisons of sensitive parameters under normal, hypoxic and glioma-like situations provide an insight into the directly and distantly related parameters which affect the production of *gsh*, *gssg* and h_2o_2 . Through parameter variation analysis of sensitive parameters under the glioma-like scenario, it is observed that different values of V_m^{GTHO} has differing effect on the overall redox status of the cell. We interpret that differing *GTHO* activity during cancerous transformation can govern the pro-apoptotic or anti-apoptotic fate. This partially accounts for the paradoxical behavior of ROS and helps in therapeutic determination of pro-oxidant or anti-oxidant approach either by augmenting glioma cell death and clearance or by controlling it using anti-oxidant therapies. We propose that under high *GTHO* activity an anti-oxidative approach will be suitable to control glioma progression, whereas under low *GTHO* activity a pro-oxidative approach will be appropriate to induce apoptosis of the glioma cells.

Further analysis of the glioma scenario created *in-silico* in the model shows the involvement of non-trivial parameters in the regulation of *gsh*, *gssg* and h_2o_2 . It is interesting to note that a combinatorial parameter variation of enzymes belonging to glycolytic pathway (V_m^{FBA}) and cysteine metabolism (k_{nadph}^{CR}) could induce changes in the h_2o_2 level along with changes in *nadph/nadp⁺* and *gsh/gssg* profiles during glioma. Additionally, a combinatorial variation of a few other parameters like k_{glucys}^{GS} , L_{oxy} , I_{atp} and k_{nadph}^{NOX} which are not directly involved in ROS manipulation also show changes in h_2o_2 level. Combinatorial responses of these parameters have been captured which suggest the possibility of utilizing these combinations in designing pro- or anti-oxidant therapeutic approaches based on their effect on ROS manipulation. The present model has been tailored for glial and glioma conditions; however, the utility of the model can be extended to simulate the dynamics of antioxidant machinery for cells under oxidative stress

and to other tumor types exhibiting ROS manipulation. Since hypoxia and oxidative stress are characteristics of most tumors and antioxidant machinery plays a central role in maintaining redox balances in all cell types, this model can be used to simulate various scenarios related to redox imbalances in other types of cancers as well. Sensitive parameters for ROS manipulation under normal and cancerous conditions for different cancers can be obtained, and combinatorial targets for pro- and antioxidant therapy could be identified.

5. Conclusion

In the present work, we have demonstrated the effect of redox and thiol status of the cell and the antioxidants in maintaining ROS levels by considering h_2o_2 levels in particular, in normal glial cells and gliomas. *GTHP*, *GTHO*, and *NOX* are important in determining transition from normal glial to hypoxia to glioma situation and in regulating h_2o_2 levels with the cell. Additionally, changes in the redox and thiol status represented by *nadph/nadp⁺* and *gsh/gssg* respectively, along with changes in the enzymes can determine the pro-apoptotic or anti-apoptotic fate of the gliomas. The differing activity of *GTHO* during glioma development helps in understanding the paradoxical behavior of h_2o_2 in gliomas and hence is helpful in determining the selection of therapeutic strategies: pro-oxidant or anti-oxidant, against glioma progression. Also, the involvement of enzymes which are not directly involved in the regulation of h_2o_2 but affect the process by inducing effect distantly in the metabolic network are important in augmenting the effectiveness of the selected therapeutic approach. The effect of hypoxia in the model has been evaluated by the affinity of the cell for oxygen uptake. Further inclusion of the impact of endogenous factors like *HIF1 α* , the faulty oxidative phosphorylation, etc., inducing hypoxia can be insightful and will be considered in the future extension of the work. The understanding of these mechanisms and the identification of important enzymes that affect the ROS manipulation process can potentially build a better future prospect of developing effective and efficient therapeutic strategies for the treatment of gliomas.

Supporting information

S1 Text. Model parameters. The Supplementary Text contains the description of the equations, parameters and state variables used for the model simulations (Section 1, 2 and 4 and S1 and S2 Tables). S3 Table contains the values of parameters for which pro- and anti-oxidant effects are obtained in the glioma scenario. The text also contains 6 figures (S1-S6 Figs), descriptions of which are provided below.
(PDF)

Acknowledgments

The authors acknowledge Piyali Ganguli and Nabiha Sadique for their helpful suggestions.

Author Contributions

Conceptualization: Ram Rup Sarkar.

Data curation: Rupa Bhowmick.

Formal analysis: Rupa Bhowmick.

Funding acquisition: Ram Rup Sarkar.

Investigation: Rupa Bhowmick, Ram Rup Sarkar.

Methodology: Rupa Bhowmick.

Project administration: Ram Rup Sarkar.

Supervision: Ram Rup Sarkar.

Validation: Rupa Bhowmick.

Writing – original draft: Rupa Bhowmick.

Writing – review & editing: Ram Rup Sarkar.

References

1. Galadari S, Rahman A, Pallichankandy S, Thayyullathil F. Reactive oxygen species and cancer paradox: to promote or to suppress? *Free Radical Bio Med.* 2017; 104:144–64.
2. Zitka O, Skalickova S, Gumulec J, Masarik M, Adam V, Hubalek J, et al. Redox status expressed as GSH: GSSG ratio as a marker for oxidative stress in paediatric tumour patients. *Oncol Lett.* 2012; 4(6):1247–53. <https://doi.org/10.3892/ol.2012.931> PMID: 23205122
3. Hosios AM, Vander Heiden MG. The redox requirements of proliferating mammalian cells. *J Biol Chem.* 2018; 293(20):7490–8. <https://doi.org/10.1074/jbc.TM117.000239> PMID: 29339555
4. Halliwell B. The antioxidant paradox. *Lancet.* 2000; 355(9210):1179–80. [https://doi.org/10.1016/S0140-6736\(00\)02075-4](https://doi.org/10.1016/S0140-6736(00)02075-4) PMID: 10791396
5. Meier B, Radeke H, Selle S, Younes M, Sies H, Resch K, et al. Human fibroblasts release reactive oxygen species in response to interleukin-1 or tumour necrosis factor- α . *Biochem J.* 1989; 263(2):539–45. <https://doi.org/10.1042/bj2630539> PMID: 2556998
6. Haack F, Lemcke H, Ewald R, Rharass T, Uhrmacher AM. Spatio-temporal model of endogenous ROS and raft-dependent WNT/beta-catenin signaling driving cell fate commitment in human neural progenitor cells. *PLoS Comput Biol.* 2015; 11(3):e1004106. <https://doi.org/10.1371/journal.pcbi.1004106> PMID: 25793621
7. Dwivedi G, Gran MA, Bagchi P, Kemp ML. Dynamic redox regulation of IL-4 signaling. *PLoS Comput Biol.* 2015; 11(11):1004582.
8. Sharma P, Chakraborty R, Wang L, Min B, Tremblay ML, Kawahara T, et al. Redox regulation of interleukin-4 signaling. *Immunity.* 2008; 29(4):551–64. <https://doi.org/10.1016/j.immuni.2008.07.019> PMID: 18957266
9. Smith GR, Shanley DP. Computational modelling of the regulation of Insulin signalling by oxidative stress. *BMC Syst Biol.* 2013; 7(1):41.
10. Pereira EJ, Smolko CM, Janes KA. Computational models of reactive oxygen species as metabolic byproducts and signal-transduction modulators. *Front Pharmacol.* 2016; 7:457. <https://doi.org/10.3389/fphar.2016.00457> PMID: 27965578
11. Bienert GP, Schjoerring JK, Jahn TP. Membrane transport of hydrogen peroxide. *BBA-Biomembranes.* 2006; 1758(8):994–1003. <https://doi.org/10.1016/j.bbamem.2006.02.015> PMID: 16566894
12. Ruiz-Gines J, Lopez-Ongil S, Gonzalez-Rubio M, Gonzalez-Santiago L, Rodriguez-Puyol M, Rodriguez-Puyol D. Reactive oxygen species induce proliferation of bovine aortic endothelial cells. *J Cardiovasc Pharm.* 2000; 35(1):109–13.
13. Sauer H, Wartenberg M, Hescheler J. Reactive oxygen species as intracellular messengers during cell growth and differentiation. *Cell Physiol Biochem.* 2001; 11(4):173–86. <https://doi.org/10.1159/000047804> PMID: 11509825
14. Qu Y, Wang J, Ray PS, Guo H, Huang J, Shin-Sim M, et al. Thioredoxin-like 2 regulates human cancer cell growth and metastasis via redox homeostasis and NF- κ B signaling. *J Clin Invest.* 2011; 121(1):212–25. <https://doi.org/10.1172/JCI43144> PMID: 21123948
15. Simon H-U, Haj-Yehia A, Levi-Schaffer F. Role of reactive oxygen species (ROS) in apoptosis induction. *Apoptosis.* 2000; 5(5):415–8. <https://doi.org/10.1023/a:1009616228304> PMID: 11256882
16. Herrera B, Álvarez A M, Sánchez A, Fernández M, Roncero C, Benito M, et al. Reactive oxygen species (ROS) mediates the mitochondrial-dependent apoptosis induced by transforming growth factor β in fetal hepatocytes. *FASEB J.* 2001; 15(3):741–51. <https://doi.org/10.1096/fj.00-0267com> PMID: 11259392
17. Schumacker PT. Reactive oxygen species in cancer cells: live by the sword, die by the sword. *Cancer cell.* 2006; 10(3):175–6. <https://doi.org/10.1016/j.ccr.2006.08.015> PMID: 16959608
18. Martin K, Barrett J. Reactive oxygen species as double-edged swords in cellular processes: low-dose cell signaling versus high-dose toxicity. *Hum Exp Toxicol.* 2002; 21(2):71–5. <https://doi.org/10.1191/0960327102ht213oa> PMID: 12102499

19. Galanis A, Pappa A, Giannakakis A, Lanitis E, Dangaj D, Sandaltzopoulos R. Reactive oxygen species and HIF-1 signalling in cancer. *Cancer Lett.* 2008; 266(1):12–20. <https://doi.org/10.1016/j.canlet.2008.02.028> PMID: 18378391
20. Pierce GB, Parchment RE, Lewellyn AL. Hydrogen peroxide as a mediator of programmed cell death in the blastocyst. *Differentiation.* 1991; 46(3):181–6. <https://doi.org/10.1111/j.1432-0436.1991.tb00880.x> PMID: 1655543
21. Janes KA, Lauffenburger DA. Models of signalling networks—what cell biologists can gain from them and give to them. *J Cell Sci.* 2013; 126(9):1913–21.
22. Kong Q, Beel J, Lillehei K. A threshold concept for cancer therapy. *Med Hypotheses.* 2000; 55(1):29–35. <https://doi.org/10.1054/mehy.1999.0982> PMID: 11021322
23. Wang J, Yi J. Cancer cell killing via ROS: to increase or decrease, that is the question. *Cancer Biol Ther.* 2008; 7(12):1875–84. <https://doi.org/10.4161/cbt.7.12.7067> PMID: 18981733
24. Blacker TS, Duchon MR. Investigating mitochondrial redox state using NADH and NADPH autofluorescence. *Free Radical Bio Med.* 2016; 100:53–65.
25. Agledal L, Niere M, Ziegler M. The phosphate makes a difference: cellular functions of NADP. *Redox Rep.* 2010; 15(1):2–10. <https://doi.org/10.1179/174329210X12650506623122> PMID: 20196923
26. Aquilano K, Baldelli S, Ciriolo MR. Glutathione: new roles in redox signaling for an old antioxidant. *Front Pharmacol.* 2014; 5:196. <https://doi.org/10.3389/fphar.2014.00196> PMID: 25206336
27. Bansal A, Simon MC. Glutathione metabolism in cancer progression and treatment resistance. *J Cell Biol.* 2018; 217(7):2291–8. <https://doi.org/10.1083/jcb.201804161> PMID: 29915025
28. Aoyama K, Nakaki T. Impaired glutathione synthesis in neurodegeneration. *Int J Mol Sci.* 2013; 14(10):21021–44. <https://doi.org/10.3390/ijms141021021> PMID: 24145751
29. Bhowmick R, Subramanian A, Sarkar RR. Exploring the differences in metabolic behavior of astrocyte and glioblastoma: a flux balance analysis approach. *Syst Syst Biol.* 2015; 9(4):159–77.
30. Amelio I, Cutruzzolá F, Antonov A, Agostini M, Melino G. Serine and glycine metabolism in cancer. *Trends Biochem Sci.* 2014; 39(4):191–8. <https://doi.org/10.1016/j.tibs.2014.02.004> PMID: 24657017
31. Ye Z-C, Rothstein JD, Sontheimer H. Compromised glutamate transport in human glioma cells: reduction—mislocalization of sodium-dependent glutamate transporters and enhanced activity of cystine—glutamate exchange. *J Neurosci.* 1999; 19(24):10767–77. <https://doi.org/10.1523/JNEUROSCI.19-24-10767.1999> PMID: 10594060
32. Skonieczna M, Hejmo T, Poterala-Hejmo A, Cieslar-Pobuda A, Buldak RJ. NADPH oxidases: insights into selected functions and mechanisms of action in cancer and stem cells. *Oxid Med Cell Longev.* 2017; 2017.
33. Zhong W, Yan T, Lim R, Oberley LW. Expression of superoxide dismutases, catalase, and glutathione peroxidase in glioma cells. *Free Radical Bio Med.* 1999; 27(11–12):1334–45.
34. Huster D, Reichenbach A, Reichelt W. The glutathione content of retinal Müller (glial) cells: effect of pathological conditions. *Neurochem Int.* 2000; 36(4–5):461–9. [https://doi.org/10.1016/s0197-0186\(99\)00149-7](https://doi.org/10.1016/s0197-0186(99)00149-7) PMID: 10733014
35. Ye Z-C, Sontheimer H. Glioma cells release excitotoxic concentrations of glutamate. *Cancer Res.* 1999; 59(17):4383–91. PMID: 10485487
36. Pollak N, Dolle C, Ziegler M. The power to reduce: pyridine nucleotides—small molecules with a multitude of functions. *Biochem J.* 2007; 402(2):205–18. <https://doi.org/10.1042/BJ20061638> PMID: 17295611
37. Sheeran FL, Rydström J, Shakhparonov MI, Pestov NB, Pepe S. Diminished NADPH transhydrogenase activity and mitochondrial redox regulation in human failing myocardium. *BBA-Bioenergetics.* 2010; 1797(6–7):1138–48. <https://doi.org/10.1016/j.bbabi.2010.04.002> PMID: 20388492
38. Maldonado EN, Lemasters JJ. ATP/ADP ratio, the missed connection between mitochondria and the Warburg effect. *Mitochondrion.* 2014; 19(A):78–84.
39. Tantama M, Martínez-François JR, Mongeon R, Yellen G. Imaging energy status in live cells with a fluorescent biosensor of the intracellular ATP-to-ADP ratio. *Nature Comm.* 2013; 4:2550.
40. Mörikofer-Zwey S, Walter P. Binding of ADP to rat liver cytosolic proteins and its influence on the ratio of free ATP/free ADP. *Biochem J.* 1989; 259(1):117–24. <https://doi.org/10.1042/bj2590117> PMID: 2497727
41. Raftos JE, Whillier S, Kuchel PW. Glutathione synthesis and turnover in the human erythrocyte: alignment of a model based on detailed enzyme kinetics with experimental data. *J Biol Chem.* 2010; 285(31):23557–67. <https://doi.org/10.1074/jbc.M109.067017> PMID: 20498365
42. Gould RL, Pazdro R. Impact of Supplementary Amino Acids, Micronutrients, and Overall Diet on Glutathione Homeostasis. *Nutrients.* 2019; 11(5):1056.

43. Lewerenz J, Hewett SJ, Huang Y, Lambros M, Gout PW, Kalivas PW, et al. The cystine/glutamate antiporter system x(c)(-) in health and disease: from molecular mechanisms to novel therapeutic opportunities. *Antioxid Redox Signal*. 2013; 18(5):522–55. <https://doi.org/10.1089/ars.2011.4391> PMID: [22667998](https://pubmed.ncbi.nlm.nih.gov/22667998/)
44. Shono T, Yokoyama N, Uesaka T, Kuroda J, Takeya R, Yamasaki T, et al. Enhanced expression of NADPH oxidase Nox4 in human gliomas and its roles in cell proliferation and survival. *Int J Cancer*. 2008; 123(4):787–92. <https://doi.org/10.1002/ijc.23569> PMID: [18508317](https://pubmed.ncbi.nlm.nih.gov/18508317/)
45. Rinaldi M, Caffo M, Minutoli L, Marini H, Abbritti R, Squadrito F, et al. ROS and brain gliomas: an overview of potential and innovative therapeutic strategies. *Int J Mol Sci*. 2016; 17(6):984.
46. Dokic I, Hartmann C, Herold-Mende C, Régnier-Vigouroux A. Glutathione peroxidase 1 activity dictates the sensitivity of glioblastoma cells to oxidative stress. *Glia*. 2012; 60(11):1785–800. <https://doi.org/10.1002/glia.22397> PMID: [22951908](https://pubmed.ncbi.nlm.nih.gov/22951908/)
47. Zhu Z, Du S, Du Y, Ren J, Ying G, Yan Z. Glutathione reductase mediates drug resistance in glioblastoma cells by regulating redox homeostasis. *J Neurochem*. 2018; 144(1):93–104. <https://doi.org/10.1111/jnc.14250> PMID: [29105080](https://pubmed.ncbi.nlm.nih.gov/29105080/)
48. Szatrowski TP, Nathan CF. Production of large amounts of hydrogen peroxide by human tumor cells. *Cancer Res*. 1991; 51(3):794–8. PMID: [1846317](https://pubmed.ncbi.nlm.nih.gov/1846317/)
49. Zhang H, Kong X, Kang J, Su J, Li Y, Zhong J, et al. Oxidative stress induces parallel autophagy and mitochondria dysfunction in human glioma U251 cells. *Toxicol Sci*. 2009; 110(2):376–88. <https://doi.org/10.1093/toxsci/kfp101> PMID: [19451193](https://pubmed.ncbi.nlm.nih.gov/19451193/)
50. Rao GM, Rao AV, Raja A, Rao S, Rao A. Role of antioxidant enzymes in brain tumours. *Clin Chim Acta*. 2000; 296(1–2):203–12. [https://doi.org/10.1016/s0009-8981\(00\)00219-9](https://doi.org/10.1016/s0009-8981(00)00219-9) PMID: [10807983](https://pubmed.ncbi.nlm.nih.gov/10807983/)
51. Tedeschi PM, Bansal N, Kerrigan JE, Abali EE, Scotto KW, Bertino JR. NAD+ kinase as a therapeutic target in cancer. *Clin Cancer Res*. 2016; 22(21):5189–95. <https://doi.org/10.1158/1078-0432.CCR-16-1129> PMID: [27582489](https://pubmed.ncbi.nlm.nih.gov/27582489/)
52. Liao B, Gawienowski MC, Zielinski RE. Differential stimulation of NAD kinase and binding of peptide substrates by wild-type and mutant plant calmodulin isoforms. *Clin Cancer Res*. 1996; 327(1):53–60.
53. Aylett S-B, Neergheen V, Hargreaves IP, Eaton S, Land JM, Rahman S, et al. Levels of 5-methyltetrahydrofolate and ascorbic acid in cerebrospinal fluid are correlated: implications for the accelerated degradation of folate by reactive oxygen species. *Neurochem Int*. 2013; 63(8):750–5. <https://doi.org/10.1016/j.neuint.2013.10.002> PMID: [24140430](https://pubmed.ncbi.nlm.nih.gov/24140430/)
54. Stankova J, Lawrance A, Rozen R. Methylenetetrahydrofolate reductase (MTHFR): a novel target for cancer therapy. *Curr Pharm Design*. 2008; 14(11):1143–50.
55. Blanchetot C, Boonstra J. The ROS-NOX connection in cancer and angiogenesis. *Crit Rev Eukar Gene*. 2008;18(1).
56. Hole PS, Zabkiewicz J, Munje C, Newton Z, Pearn L, White P, et al. Overproduction of NOX-derived ROS in AML promotes proliferation and is associated with defective oxidative stress signaling. *Blood*. 2013; 122(19):3322–30. <https://doi.org/10.1182/blood-2013-04-491944> PMID: [24089327](https://pubmed.ncbi.nlm.nih.gov/24089327/)
57. Lim JK, Delaidelli A, Minaker SW, Zhang H-F, Colovic M, Yang H, et al. Cystine/glutamate antiporter xCT (SLC7A11) facilitates oncogenic RAS transformation by preserving intracellular redox balance. *P Natl Acad Sci*. 2019; 116(19):9433–42.
58. Blanco G, Blanco A. *Medical biochemistry*: Academic Press; 2017.
59. Philip G. Identification of an essential cysteine residue in human glutathione synthase. *Biochem J*. 1997; 321(1):207–10.
60. Borbély G, Szabadkai I, Horváth Z, Markó P, Varga Z, Breza N, et al. Small-molecule inhibitors of NADPH oxidase 4. *J Med Chem*. 2010; 53(18):6758–62. <https://doi.org/10.1021/jm1004368> PMID: [20731357](https://pubmed.ncbi.nlm.nih.gov/20731357/)
61. Wang Y-P, Zhou W, Wang J, Huang X, Zuo Y, Wang T-S, et al. Arginine methylation of MDH1 by CARM1 inhibits glutamine metabolism and suppresses pancreatic cancer. *Mol Cell*. 2016; 64(4):673–87. <https://doi.org/10.1016/j.molcel.2016.09.028> PMID: [27840030](https://pubmed.ncbi.nlm.nih.gov/27840030/)
62. Ren J-G, Seth P, Clish CB, Lorkiewicz PK, Higashi RM, Lane AN, et al. Knockdown of malic enzyme 2 suppresses lung tumor growth, induces differentiation and impacts PI3K/AKT signaling. *Sci Rep-UK*. 2014; 4:5414.
63. Jeon S-M, Chandel NS, Hay N. AMPK regulates NADPH homeostasis to promote tumour cell survival during energy stress. *Nature*. 2012; 485(7400):661. <https://doi.org/10.1038/nature11066> PMID: [22660331](https://pubmed.ncbi.nlm.nih.gov/22660331/)



T-Cell Activation and Differentiation: Role of Signaling and Metabolic Cross-Talk

6

Rupa Bhowmick, Piyali Ganguli, and Ram Rup Sarkar

Abstract

Different types of T effector cells function centrally in the immune-regulatory network, which acts as a line of defense for the body and elicits immune response during any diseased condition. At the molecular level, this functioning is maintained by an intricately designed network of signaling and metabolic pathways that function via multiple cross-talks to regulate complex immune responses during different antigenic challenges. These pathways regulate phenomena such as quiescence exit of naïve T cells, their activation, and differentiation into different effector T cells. Signaling properties of these T cells and their response to different cytokine signals have been well studied. Immune-metabolism is comparatively a new area of research that has been identified as driver for immune response. However, to gain a holistic understanding of the activation and differentiation of naïve T cells into the subtypes, the integration of signaling and metabolic pathway information is a prerequisite. The bidirectional mode of regulation between these cross-talking signaling and metabolic pathways governs the differentiation patterns. In this chapter, we review the activation and differentiation pattern of naïve T cells from both signaling and metabolic perspectives and also look into their cross-talk to understand their mutual regulation during differentiation into effector T cells.

R. Bhowmick · P. Ganguli · R. R. Sarkar (✉)
CSIR-National Chemical Laboratory, Pune, India

Academy of Scientific and Innovative Research (AcSIR), Ghaziabad, India
e-mail: rr.sarkar@ncl.res.in

© Springer Nature Singapore Pte Ltd. 2020
S. Singh (ed.), *Systems and Synthetic Immunology*,
https://doi.org/10.1007/978-981-15-3350-1_6

153

6.1 Introduction

The immune system forms the sentinel of the body that protects it from infectious disease and cancer. The adaptive immune system, composed mainly of the T and B lymphocytes, is responsible for maintaining this defense mechanism of the body as it helps to generate immune responses specific to the type of antigenic challenge that the body encounters [1]. The helper T cells (T_H) form the central orchestrators of the entire immune-regulatory network. They have been known to have an essential role in the recognition of the antigen when presented on the surface of the antigen-presenting cells and secrete cytokines that aid in the proliferation of the cytotoxic T cells and B cells, thereby playing an active role in stimulating both the humoral and the cell-mediated immunity [2]. The effector functions of these immune systems are mediated mainly by the cytokines and other microbicidal molecules secreted by them as a result of the activation of complex biochemical signaling pathways inside the immune cells. The T_H cells themselves produce a high amount of interferon and tumor necrosis factor via TCR and co-receptor mediated pathways that mediates apoptosis of infected and cancerous cells [3, 4].

The differentiation of the helper T cells is primarily influenced by the changes in the micro-environmental conditions that favor the proliferation of a certain subset of T cells that leads to disruption of the balance and ratio of the normal proportions of T-cell subsets present in a healthy individual [5, 6].

Naive T cells circulate in the body surveying for antigens. The metabolic activity of these cells is maintained low by allowing low uptake of glucose enough to fuel the TCA cycle and OXPHOS to produce ATP [7]. These cells are kept in a quiescent state that promotes their survival and persistence. On antigen stimulation, the metabolism of T cells is triggered via increased uptake of glucose, which allows quiescence exit and initiates clonal expansion and effector differentiation primarily by mTOR-mediated signaling responses [8]. Initially, the focus of studies remained on the immune receptors and transcriptional regulators involved in T-cell quiescence and activation, but recent findings highlight cell metabolism as a crucial regulator of these processes [9–12]. Receptor-induced signaling and metabolic networks in naïve T cells are mutually regulated by each other depending on the micro-environmental cues obtained by the cell that also influence quiescence exit. Here we will discuss the bidirectional communication of signaling and metabolic pathways that promotes proliferation, quiescence exit, and activation of naïve T cells and functioning of T cells upon activation. We will take into account the different signaling and metabolic events and their cross-talks that lead to differentiation of naïve T cells into T_{H1} , T_{H2} , T_{H17} , Treg, or Tfh effector cells. Understanding the cross-talks between T-cell signaling and metabolism under different environmental cues will be vital for understanding the differentiation patterns of naïve T cells during different pathogenic conditions. This will provide better prospects of developing novel approaches to modulate protective and pathological T-cell responses in human diseases.

6.2 Signaling and Metabolic Pathways Involved in Activation of Naïve T Cell

The activation of T_H cell is mediated by a complex chain of signaling events that involve the activation of distinct co-stimulators and co-inhibitors present on the surface of the lymphocyte. The interaction between the antigen-bound major histocompatibility complex (MHC) on the antigen-presenting cells (APCs) and the T-cell receptor (TCR) on T_H cells triggers the TCR-mediated signaling pathway. The phosphorylation of the LAT signalosome by LCK sends signal to three major cell-signaling pathways, viz. NF κ B, MAPK, and the calcium-mediated NFAT pathways [13]. Along with the TCR, the T cell also expresses several other co-receptor molecules that can be classified into two major functional groups. The first group consists of co-signaling receptors that have an immunoglobulin (Ig)-like fold in their ectodomains, such as CTLA-4, CD28, PD1, and BTLA [14]. The other co-signaling group belongs to the tumor necrosis factor receptor (TNFR) superfamily and includes DR3, OX40, 41BB, CD27, CD30, and HVEM [14]. Together with the TCR activation, a second signal from the co-stimulatory signal emanating from B7-CD28 interaction is also necessary for the T-cell activation. This is called the “two signal hypothesis” [13]. The B7 molecule present on the APC also binds with the CTLA-4 receptor of the T cell after the clearance of the antigen. This induces T-cell anergy after the antigen is cleared from the system and the T-cell activation is no longer required. The other co-receptor signaling pathway influences the type of cytokine expressed and regulates the T-cell differentiation pattern. Experimental studies have shown CD40-L, expressed on the surface of activated T cells, induces the APC to produce IL-12, thereby stimulating the T_H cells to differentiate into the T_{H1} cells [15, 16]. On the other hand, the TRAF2-mediated OX40 signaling pathway contributes to long-term survival of T_H cells [17]. OX40 has been implicated in the development of memory T cells, clonal expansion, and differentiation. It also mediates suppression of the Treg cells [17, 18]. The negative regulators of T-cell activation are required to maintain homeostasis and deactivate the T cells after the antigen is cleared out. This is mediated by the PD1-PDL axis that provides co-inhibitory signal to the T-cell activation. The T cell also expresses CD45, a phosphatase, that de-phosphorylates the carboxyl-terminal tyrosine of p56lck and p59fyn that aids T-cell activation [19]. Apart from these, the T cells express several other co-receptors that serve to regulate the cytokine expression and differentiation of the cell [20].

The calcium pathway also plays a major role in the proliferation of the T_H cell activation [21]. The influx of Ca^{2+} ions from the CRAC channels leads to the activation of the NFAT (Nuclear Factor of Activated T cell) transcription factor that acts as the master regulator of T-cell activation and T-cell anergy [22]. The activation of the calcium pathway in the T cell is initiated by the binding of the TCR with an antigenic peptide presented on MHC complexes of the APC that induces activation of PLC- γ that cleaves PIP2 into IP3 and DAG. This IP3 now activates the IP3-receptors located on the endoplasmic reticulum membranes inside the T cell, which causes the release

of intracellular stores of calcium, leading to a transient elevation in cytoplasmic calcium level. This activates the CRAC channels on the T-cell membrane that allows an inward flux of calcium from the extracellular environment. This triggers the calcium-mediated calmodulin-calcineurin pathway, which leads to the de-phosphorylation and nuclear translocation of NFAT proteins where it can cooperate with AP-1 complexes induced by co-stimulatory pathways. The NFAT/AP-1 complexes bind to the sites in the promoters of many cytokine genes to activate their transcription to mediate sustained T-cell activation and survival. In the absence of co-stimulation or in the presence of anergizing stimuli, sustained increases in intracellular calcium concentration activate NFAT proteins. However, in the absence of concomitant AP-1 activation, due to lack of co-stimulatory signals, NFAT proteins dimerize and translocate into the nucleus, inducing the expression of anergy-inducing genes that include E3-ubiquitin ligases, such as Itch, Grail, and Cbl-b that is known to ubiquitinate and inactivate the TCR signalosome and the co-stimulatory CD40-ligand, thereby destabilizing the immunological synapse in the anergic T cell. On the other hand, the calcium/NFAT-dependent activation of the Ikaros transcription factor in anergic T cells leads to the epigenetic changes in the IL-2 promoter by the recruitment of HDACs and other chromatin-modifying complexes, which results in stable silencing of the IL-2 gene expression [22].

Metabolic regulation of T cell is another aspect that determines activation and differentiation of naïve T cells and their functioning upon activation. Naïve T cells utilize glucose and glutamine metabolism for activation, and activation signals increase glucose and glutamine uptake by T cells through GLUT1 and ASCT2, respectively [23, 24]. Thus, both signaling and metabolism cooperate in a bidirectional manner to influence T-cell activation and differentiation. On encountering pathogenic antigens, a cascade of TCR signals and co-stimulatory signals are initiated, which leads to quiescence exit in naïve T cells. The first signal that initiates quiescence exit is the transduction of TCR signaling via PI3K/AKT/mTOR pathway, which induces glycolysis in the naïve T cells [25]. This initiation is marked by a trigger in the metabolism of T cells that suffices the increasing lipid, nucleotide, and amino acid requirement of differentiating cells. During quiescence exit, T cells produce lactate to sustain glycolysis. Lactate is also imported into cells through the monocarboxylate transporters and converted into pyruvate by lactate dehydrogenase A (LDHA). This reaction limits glycolytic programming and proliferation in T cells, potentially owing to the attenuated generation of glycolytic intermediates such as PEP that sustain glycolysis and biosynthesis reactions [26].

Glutamine metabolism regulates T-cell activation in different ways. It has an important role in determining differentiation to T_{H1} and T_{H17} cells. T_{H17} cells utilize both glucose and glutamine to fuel the TCA cycle and OXPHOS, which otherwise is optional for other T effector cells [27]. It regulates leucine uptake via regulation of LAT1-CD98 and together with leucine activates mTORC1 signaling [28]. Other amino acid metabolisms like tryptophan and arginine metabolism and their intermediate metabolites such as kynurenine and ornithine differentially regulate T-cell survival, apoptosis, and proliferation [29–31].

Glucose and glutamine metabolism also induce lipid metabolism via mTORC1-dependent regulation of AMPK [32]. These pathways are metabolically connected to the TCA cycle and OXPHOS, which also affect the redox and oxygen-sensing signals in T cells. The conversion of pyruvate to lactate via NAD⁺-NADH-dependent LDH reaction regulates redox signals, and impaired oxygen-sensing machinery of OXPHOS results in the formation of ROS, which induces ROS-dependent signaling that promotes IL-2 productions and induces T-cell proliferation by activating NFAT transcription factor [33].

6.3 T_H-Cell Differentiation and Diversity

The T_H cells display high plasticity that helps them to differentiate into specialized T_H cells according to the type of the antigenic challenge and the micro-environmental conditions (Fig. 6.1). The early events of the T-cell activation play a major role in the determination of the pattern of differentiation of the naïve T cell. The micro-environmental cues, in the form of cytokines, activate the signaling pathways of the T_H cells that eventually lead to the changes at the gene-regulatory levels [34]. The selective activation of specific transcription factors mediates the differentiation of the naïve cells into specialized CD4⁺ T_H effector cells, viz. T_{H1}, T_{H2}, T_{H17}, etc. (Table 6.1) [35]. Additionally, another type of CD4⁺ T_H cell called the regulatory T cells (iTreg) has a role in maintaining the T_H cell homeostasis.

The mechanism of T-cell differentiation is governed initially by the strength of the stimulus that the TCR receives from the APC. The strength of stimulus results in differential regulation of phosphatidylinositols that triggers different signaling

Fig. 6.1 Schematic diagram of signature signaling factors, cytokines, metabolites, and metabolic paths, which dictate T_H cell differentiation, proliferation, and effector function

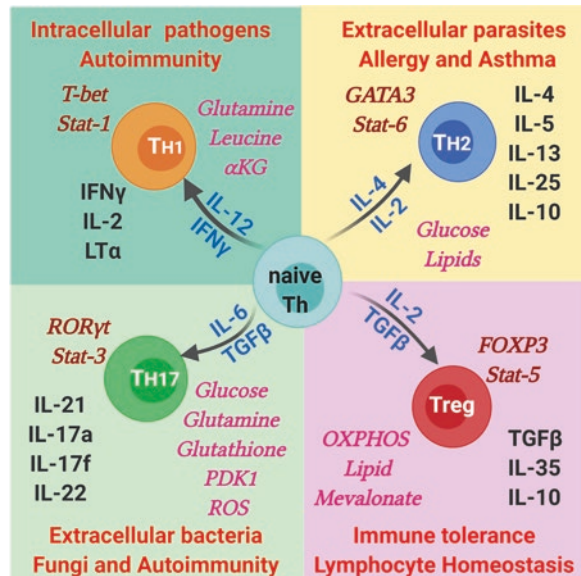


Table 6.1 Summary of T_H cell diversity, factors regulating T-cell plasticity and effector functions of each subtype

CD4 ⁺ subset	Polarizing cytokines	Transcription factors	Inhibitory transcription factors	Metabolic signature	Effector functions
T _{H1}	IL12, IFN γ	T bet, STAT1, STAT4, Runx 3, Eomes, Hlx	GATA3	Upregulated glycolysis, glutamine metabolism, leucine uptake, α KG production	Cell-mediated immunity against intracellular pathogens and phagocyte-dependent protective responses
T _{H2}	IL4, IL2	GATA3, STAT6, STAT5, STAT3, Gfi-1, c-Maf, IRF4	T-bet, Runx3	Downregulated glycolysis, upregulated lipid metabolism	Immune response against extracellular parasites, bacteria, allergens, and toxins. Help in activation and maintenance of humoral immune response and tissue repair
T _{H17}	IL6, IL 21, IL 23, TGF- β	ROR γ t, STAT3, ROR α , Runx1, Batf, IRF4, AHR	T-bet ⁺ Runx1, Smad3Runx1 ⁺ FOXP3	Uptake of both glucose and glutamine, glutathione production, upregulated PDK1 and ROS	Immune response against bacterial and fungal infection
T _H	IL6, IL21	Bcl6, STAT3	Not known	Not known	Help B cells produce antibody
iTreg	TGF- β , IL2	FOXP3, Smad2, Smad3, STAT5, NFAT	Not known	Inhibited glycolysis, upregulated OXPHOS, lipid and mevalonate metabolism	Suppression of immune response
T _{H9}	TGF- β , IL4	IRF4	Not known	Not known	Promotes mast cell and T-cell growth, stimulates mucous secretion to enhance innate immunity. Plays a role in allergic responses
T _H 1	IL27, IL10	c-Maf, Ahr	Not known	Not known	Suppression of T effector cells

pathways downstream. It has been observed that while a weak TCR signal generates a high level of PIP2 and lower levels of PIP3, which is required for the activation of the focal adhesion kinase and phosphorylation of AKT_{Thr308}, stronger signal favors the activation of mTORC2, and as a result, elevated level of PIP3 and reduced PIP2 are generated [36]. In vitro experiments have revealed that a stimulus of a lower strength induces the expression of the GATA-3 transcription factor, the master regulator of T_{H2} cells. Simultaneously, the expression of the IL-2 cytokine activates STAT5 that synergizes with GATA-3 to transcribe the IL-4 gene that eventually leads to the differentiation of the naïve cell into the T_{H2} subtype [37]. Recent advances in the field also divulged that during viral infection low TCR signals may also favor the formation of Tfh and memory T cells. On the other hand, a stronger stimulus favors the activation of the T-bet transcription factor that helps in the differentiation into the T_{H1} subtype and triggers the production of IFN- γ and IL12 cytokines. The differentiation of naïve CD4⁺ T cells into T_{H17} cells is induced by TGF- β /IL-6 in combination with TCR stimulation. This triggers the production of IL-23R, which induces the transcription factor ROR γ t, IL-17, and IL-21. The STAT-3 protein plays an important role in the production of the T_{H17} effector molecules and requires the activation of the ICOS co-stimulatory pathway. However, under the T_{H17}-inducing conditions, the presence of IL2/STAT5 induces the expression of the Foxp3 transcription factor that leads to the differentiation of the naïve cells into iTreg cells. The strength of TCR stimulus also plays a role in the T_{H17}/iTreg determination process, where it has been observed that a weak stimulus favors the differentiation into iTreg cells that is known to have a role in immune-suppression [37].

The effect of signaling in T_H cell differentiation is further augmented by the action of metabolism within these cells. On activation by the upstream TCR and co-stimulatory signals, metabolic pathways trigger the process of T-cell activation with the initiation of glycolysis in most of the cases [38]. The utilization of glucose is maintained nominal in naïve T cells, just to suffice ATP requirement enough to maintain survival during quiescence [39]. However, with the transduction of TCR signals via mTORC1/2 signaling, the rate of glucose utilization increases, leading to quiescence exit and activation of T_H cells [8, 38]. Upon activation, differentiation patterns are regulated by differential expression of metabolic pathways. For example, glutamine metabolism along with leucine induces proliferation and differentiation of T_{H1} and T_{H17} cells [27, 28]. In addition, α KG promotes initial programming in T_{H1} cells [40]. Further, glutaminolysis results in the formation of glutathione, which is required for T_{H17} differentiation [41]. An increase in glucose metabolism induces lipid metabolism to promote T_{H2} differentiation [42]. Inhibition of glycolysis and promotion of OXPHOS along with upregulated lipid and mevalonate metabolism induce Treg proliferation and differentiation [43, 44]. Intermediate metabolites of metabolic pathways, in return, regulate signaling processes as well. For example, tryptophan intermediate, kynurenine, and arginine intermediate ornithine regulate signaling processes in T cells, which have been discussed in the next section.

Each of the T_H sub-type has a specific effector function to perform [34, 35, 37, 45]. A balance between all the T_H cell subtypes is necessary for the proper functioning of the immune system. The effector molecules, in the form of interleukins,

interferons, tumor necrosis factor, etc., produced by these diverse groups of immune cells, maintain the integrity of the immune-regulatory network (Table 6.1). However, during any disease condition, this defense mechanism gets subdued. Changes in the micro-environmental conditions lead to alterations in the biochemical reaction network that disrupts the balance between the effector cell populations that favors the progression of the disease. This immune-suppression is observed very frequently in the cases of chronic infections (e.g., chronic *Leishmania* infection) and cancer.

6.4 Signaling and Metabolic Cross-Talk Mediated by mTOR Regulate Differentiation

Activation of naïve T cells is initiated with the tonic signals generated by T-cell receptor (TCR) on their interactions with self-peptides on MHC molecules. There is an intricate design of the signaling and metabolic interactions of these cells, which allow them to proliferate and produce effector molecules (Fig. 6.2). Sensitivity toward TCR signaling in the naïve T cells is partially mediated by the mechanistic target of Rapamycin complex (mTORC1 and mTORC2) [46]. Peripheral naïve T cells circulate in the blood and survey antigens. They maintain a low metabolic rate and import a small amount of glucose to fuel the TCA cycle and OXPHOS for ATP production [39]. Naïve T-cell homeostasis is disrupted by the activation of mTOR signaling [47]. The activation of mTORC1 signaling enhances glycolytic metabolism in these cells, inducing entry to cell cycle and cell growth. The naïve T cells, which otherwise remain in a quiescence state, are activated by the enhanced glycolytic pathway. Different regulators of mTORC affect the process of naïve T-cell activation [46].

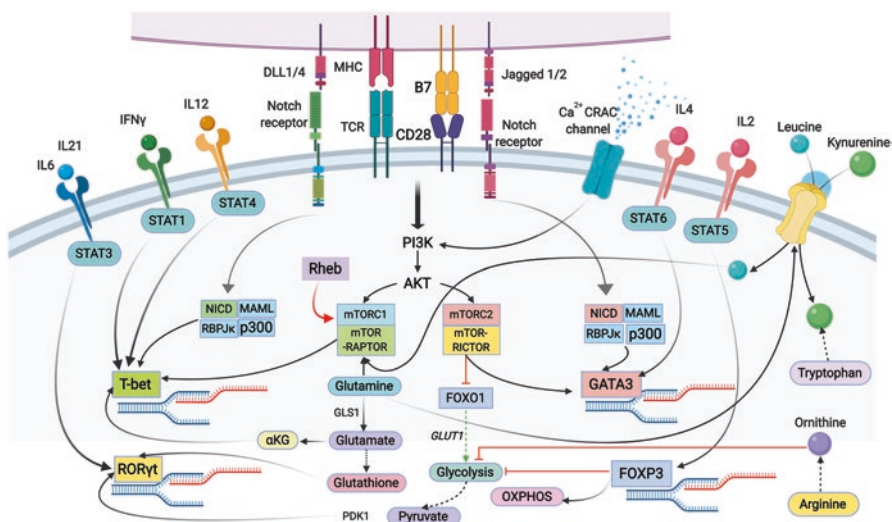


Fig. 6.2 Cross-talks of signaling and metabolic pathways regulating the activation of the T-bet, GATA3, ROR γ t, and FOXP3 transcription factors that mediate T-cell differentiation

mTOR signaling is regulated by a set of upstream signaling, which determines the formation of mTORC1 and mTORC2 and subsequent signaling. The signal induces upon activation of TCR and subsequently the PI3K/Akt pathway [48]. Raptor and rictor are the main components of mTORC1 and mTORC2 complexes, respectively. mTORC1 signaling is required for differentiation into T_{H1} and T_{H17} effector cells, and an inhibition of mTORC1 has been observed to induce T_{H2} differentiation and prevent T_{H1} and T_{H17} differentiation [25]. However, these observations differ according to the upstream signal received by the complex. Loss of tuberous sclerosis complex 1 (TSC1) results in mTORC1 activation [47]. The metabolic activity of naive T cells can also be enhanced by the exposure to IL-2 released by activated CD4⁺ effector cells [49]. Inhibition of mTORC1 by the TSC (Tuberous Sclerosis Complex) via Rheb inhibition leads to failure in differentiation into T_{H1} and T_{H17} effector cells [47].

mTORC1 is a master kinase that helps naive T cells to exit quiescence. TCR signaling along with costimulatory and IL-2 signals promote the activation of mTORC1 during quiescence exit. The magnitude and duration of mTORC1 activity likely determine quiescence exit. TCR signals must meet a certain threshold of activation to induce T-cell proliferation. This threshold is determined by the level of mTORC1 activation and expression of IRF4 and c-Myc [50, 51] that regulate anabolic and mitochondrial metabolism. mTORC1 also regulates sterol regulatory element-binding proteins (SREBPs) that has a role in metabolic reprogramming in naive T cells. Metabolism in turn regulates the activity of mTORC1. Leucine and glutamine coordinate with TCR and CD28 signaling to activate mTORC1 and sustain metabolic flux during quiescence exit [27, 28]. T-cell activation demands for the biosynthesis of lipids, cholesterol, nucleotides and amino acids in order to maintain the increase in metabolic rates of the activated cells. These increased demands are facilitated by the upregulation of hexokinase 2 (HK2), which is the rate-limiting enzyme for glycolysis [52, 53]. This induces increased utilization of glucose, which can also activate mTORC1 and inhibit the activation of AMP-activated protein kinase (AMPK) [32, 54]. AMPK induces lipid and cholesterol biosynthesis through the mTORC1-dependent upregulation of SREBP1 and SREBP2 [55]. mTORC1 forms a bridge between signaling and metabolic responses in T cells that senses metabolic cues and mediates signaling regulation over metabolic pathways and vice-versa. Thus, mTORC1-dependent responses are crucial in determining proliferation, activation, and functioning of T cells.

TCR signaling targets the transcription factor, c-Myc, in an mTORC1-dependent manner. It regulates the transcription of metabolic genes critical for T-cell activation. c-Myc induces the transcription factor AP4, which maintains the glycolytic transcriptional program initiated by c-Myc to support T-cell population expansion [50]. However, c-Myc expression is not continually sustained after T-cell activation [56].

Metabolites also influence T cells in an mTORC1-independent manner. For example, post-translational protein modifications by glycolytic, lipid, or mevalonate by-products allow receptors, enzymes, and scaffolding proteins to properly posit at their sites of activity [57, 58]. In T cells, extracellular ATP, glucose, and glutamine modulate AMPK activity to promote T-cell responses against bacteria and viruses

[54]. The glucose metabolite PEP regulates the activation of Ca^{2+} -calcineurin-NFAT signaling [59]. TCR signaling can be altered by cholesterol esters and cholesterol sulfate, which alter TCR clustering or affinity for antigens [60]. Also, N-glycans derived from the hexosamine pathway suppress TCR signaling [61].

mTORC2 also contributes to quiescence exit by enhancing glycolytic pathway. AKT/mTORC2 represses forkhead box protein O1 (FOXO1) function [62], which induces glucose transporter 1 (GLUT1) expression and enhances glycolytic flux [63]. Expression of glucose transporters contribute in determining naïve T-cell survival. IL-7-IL-7R signaling prevents degeneration of quiescent T cells by increasing glucose and amino acid catabolism [64]. Rate or quantity of glucose uptake via the GLUT1 receptor may have a role in determining quiescence versus quiescence exit as its expression is lower on naïve T cells than on activated T cells. During quiescence exit, cell growth and clonal proliferation are favored by glucose metabolism upon survival [51].

Duration and strength of TCR signaling mediate both quiescence and activation of T cells. However, based on the type of initiation of these signaling cascades, i.e., tonic or antigen-driven, TCR signals differ in both duration and strength. In antigen-activated T cells, CD28-mediated co-stimulation of TCR signaling induces GLUT1 expression to increase glucose uptake [65]. Expression of the glutamine transporter ASCT2 and of sodium-coupled neutral amino acid transporters (SNATs) increases on TCR and CD28 co-stimulation [23]. Upregulation of SNATs on T-cell activation suggests that they also modulate the rate or quantity of glutamine uptake.

Glutamine metabolism plays a crucial role in determining differentiation to $T_{\text{H}1}$ and $T_{\text{H}17}$ cells. Glutamine affects LAT1-CD98 activity, which promotes leucine uptake to induce the proliferation and differentiation of $T_{\text{H}1}$ cells, $T_{\text{H}17}$ cells, and effector $\text{CD}8^+$ T cells [23, 66]. Glutamine along with leucine activates mTORC1 and sustains metabolic flux during quiescence exit [28]. Further, utilization of glutamine to generate glutathione via glutaminolysis is essential for T-cell proliferation and differentiation into $T_{\text{H}17}$ cells [27]. Glutaminolysis also generates α -ketoglutarate (α -KG), which promotes initial programming of $T_{\text{H}1}$ cells. Glutaminolysis also affects IL-2 signaling, as it has been observed to suppress IL-2-induced mTORC1 activation during type 1 inflammation [27]. However, impaired glutaminolysis may promote abnormal leucine uptake to increase mTORC1 activation under such inflammatory conditions [23, 66]. Thus, glutamine and glutaminolysis have different roles during quiescence exit and upon T-cell activation.

During impaired glutaminolysis, the oxidation of pyruvate acts as a crucial checkpoint. The mitochondrial pyruvate carrier (MPC) transports pyruvate into the mitochondria to fuel the TCA cycle and OXPHOS and depletes it from the cytoplasm. The inhibition of MPC favors glycolysis over OXPHOS, particularly when glutaminolysis is also impaired. Downregulation of OXPHOS in T cells require inhibition of both MPC and glutaminase 1 (GLS 1) [67]. $T_{\text{H}17}$ cells suffice their nutrient requirement using both glucose and glutamine, which otherwise is optional for other activated T cells. The plausible explanation for this phenomenon is the high-level expression of pyruvate dehydrogenase kinase 1 (PDK1) in $T_{\text{H}17}$ cells, which prevents conversion of pyruvate to acetyl-CoA in mitochondria [53].

High expression of PDK1 diverts the pyruvate flux away from TCA in T_{H17} cells, and hence, the cell depends on glutamine to fuel the TCA cycle. The regulation of PDK1 is not well understood in T_{H17} cells; however, studies suggest that hypoxia-inducible factor 1 α (HIF1 α) might induce PDK1, promoting T_{H17} cell responses [53]. Also, lactate dehydrogenase A (LDHA), which catalyzes lactate formation from pyruvate, sustains glycolytic metabolism and promotes interferon- γ (IFN γ) expression in activated T cells [68].

Upon activation, amino acids play an important role in the functioning of activated T cells. Certain amino acids promote quiescence exit and proliferation of naïve T cells, whereas others might suppress proliferation and promote quiescence-like programs in naïve T cells. Majority of the biomass of activated T cells is made by amino acids. Uptake of essential amino acids such as leucine or conditionally essential amino acids such as glutamine are taken up by amino acid transporters, such as LAT1-CD98 or ASCT2 [23], but non-essential amino acids accumulate in T cells due to influx or de novo biosynthesis from glucose or glutamine. Accumulation of amino acid intermediates impact the functioning of activated T cells. Accumulation of kynurenine, an intermediate of tryptophan metabolism, suppresses T-cell proliferation [30]. Kynurenine accumulation might also result from its uptake through the LAT1-CD98 transporters [69]. Ornithine, an arginine intermediate, reduced glucose consumption via glycolysis. However, arginine supplementation increases serine biosynthesis and OXPHOS [31], which increases T-cell survival and promotes secondary effector responses.

Balanced redox reactions are one of the prerequisites for T-cell activation [70]. The NAD⁺-NADH-dependent conversion of pyruvate to lactate is a major redox balancer of T cells. An accumulation of NAD⁺ increases lysosome biogenesis, which can suppress T-cell activation. Mitochondrial reduction of NAD⁺ levels is utilized to promote aspartate synthesis, which is necessary for T-cell proliferation [70]. Both NAD⁺ and ATP cooperatively influence T-cell responses. Extracellular ATP augments quiescence exit and T-cell proliferation via the expression of purinergic receptor P2XY, which induces IL-2 production [71]. Conversely extracellular NAD⁺ promotes T-cell death by increasing the ART2-dependent activation of P2XY [72].

Oxygen sensing by T cells also regulates their effector functioning [73]. OXPHOS, which requires oxygen, is essential for both T-cell quiescence and activation [70, 74]. OXPHOS generates ROS, which stimulates IL-2 production and promotes T-cell proliferation by activating nuclear factor of activated T-cell (NFAT) transcription factors [75]. Under pathological conditions, increased levels of mitochondria-derived ROS can have antagonizing T-cell responses, including T_{H17} cell differentiation [27, 53].

FOXP3 is an important determinant of Treg differentiation and the Treg cell responses and regulated via the metabolic regulation exerted by FOXP3 [76]. It promotes OXPHOS and inhibits glycolysis in Treg cells. Survival and function of these cells are reduced by excessive PI3K or mTOR activity as it decreases FOXP3 expression and increases glycolytic metabolism [77]. Treg cells, upon activation, upregulate mTOR signaling, which induces lipid synthesis, mevalonate metabolism, and mitochondrial function [78, 79]. These pathways influence activation programs to regulate Treg cell function.

Mitochondria-derived metabolites like acetyl-Coa, succinate, α KG, and 2-hydroxyglutarate (2-HG) alter epigenetic programs. Acetyl-CoA induces histone acetylation, which is permissive for transcription. α -KG promotes the activity of demethylases that target DNA or histones, whereas 2-HG antagonizes demethylases [80]. Demethylation in turn allows changes in gene transcription associated with specific T-cell effector programs. 2-HG accumulation downstream of the von Hippel–Lindau disease tumor suppressor (VHL)–HIF1 α axis in T cells induces changes in DNA and histone methylation that increase CD8⁺ T-cell proliferation [80].

Thus, we observe metabolic regulation of T-cell activation and functioning at different levels. Mitochondria-derived metabolites affect the functioning and/or expression of various transcription factors through methylation–demythlation, acetylation processes or by mitochondria-derived ROS regulations. The effects of glucose metabolism in mTOR and c-Myc regulation have been implicated. Metabolites also regulate transcription factor activity. For example, transcriptional regulators BAZ1B, PSIP1 are activated by arginine and lipids or sterols regulate the activities of LXRs, PPARs, and SREBPs [81–83]. Further, metabolic processes also regulate processes at post-transcriptional and translational levels. For example, amino acid deprivation is sensed by GCN2 (or EIF2AK4) and leads to inhibition of protein translation by the EIF2 α pathway, which supposedly leads to suppression of T-cell proliferation [84]. Also, GAPDH produced by the glycolytic pathway has been observed to suppress protein translational processes [85]. Metabolites also affect the activity of activated T cells by the regulation of transporter proteins and complexes. Amino acids like leucine, glutamine, tryptophan, and arginine and the intermediate metabolites generated during the biogenesis or catabolism of these amino acids like kynurenine, ornithine, etc., affect the functioning of T cells upon activation via the regulation of transporter proteins like LAT1-CD98 or ASCT2. To summarize, metabolism can influence the processes of T-cell differentiation, activation, and functioning by regulating molecular processes at different levels starting from gene and transcription regulation.

6.5 Methodologies to Unwind the Regulations of the Immune Response

A comprehensive understanding of the complex regulations underlying the immune responses under different environmental conditions, antigenic challenges, strength of stimulus, and metabolic demands have challenged the implementation of successful immunotherapy. A need to unveil these regulatory mechanisms has driven experimental researchers as well as computational biologists to implement different omic studies and model the immunome under different antigenic stimulus. In the following section, we have taken up examples of the studies of T-cell responses and differentiation during infectious diseases (e.g., Leishmaniasis) and cancer that will give a clear insight of how the immune responses are altered under specific antigenic challenges.

6.5.1 Immunomics and Enrichment Analysis

Transcriptomic analysis, e.g., microarray, RNAseq, have opened up new avenues of research that allows the analysis of gene expression profile of several patient cohorts under various disease conditions. While microarray involves detection and quantification of gene expression based on the pairing of an mRNA transcript with its probe on a chip, RNA-Seq involves direct sequencing of gene transcripts by high-throughput sequencing technologies. This enables the RNAseq technique to detect novel transcripts as it does not require transcript specific probes as well as confers higher specificity and sensitivity for the detection of a wider range of differentially expressed genes, allowing detection of genes even with low expression. Following the identification of differentially expressed genes, gene ontology (GO) and pathway enrichment tools enable the identification of the biological processes (BP), molecular functions (MF), cellular component (CC), and biochemical pathways that are significantly enriched or over-represented in a given scenario. Various online tools and web-servers such as DAVID, GeneCodis, Gene Set Enrichment Analysis, and Reactome are available freely for performing enrichment analysis [86–90].

Researchers have exploited these techniques to unearth the immunome landscape in the microenvironment where the spatio-temporal dynamics of 28 different immune cell-types (immunome) have been studied using 105 human colorectal cancer patient data. Here the immunome was made up of mRNA transcripts specific for most innate and adaptive immune cell subpopulations. Using an integrative analysis, it has been elucidated that the densities of T follicular helper (Tfh) cells and innate cells increased, whereas most other T-cell densities decreased along with tumor progression. However, the Tfh and B cell numbers are inversely correlated with the disease progression and recurrence, and CXCL13 and IL21 genes are essential for the Tfh/B cell axis that is correlated with higher chances of survival of the patient [91, 92].

RNAseq analyses in the case of Leishmaniasis have been performed, that has revealed *Leishmania* species-specific differences in the expression of mammalian macrophage genes due to infection [93]. Such analyses have helped in the understanding of the changes in immune response generated during infection by unveiling the notable changes induced in the cytokine expression profiles during the *Leishmania* invasion. Experiments using microarray techniques have been used to assess the host cell genes and pathways in human dendritic cells associated with early *Leishmania major* infection. The study revealed 728 genes were significantly differentially expressed in the infected cells, and molecular signaling pathway revealed that the type I IFN pathway was significantly enriched. Here it was elucidated that *L. major* induces expression of IRF2, IRF7, and IFIT5, which indicates that the regulation of type I IFN-associated signaling pathways is responsible for the production of IL-12. However, this is not observed in the case of *L. donovani* [94].

6.5.2 Computational Methods for the Study of Immune Responses

The understanding of intra-cellular and inter-cellular signaling pathways involved in the generation of immune responses requires the study of a complex network of biochemical pathways under different disease-affected micro-environmental conditions. This is an extremely challenging task that can rarely be achieved using in vitro or in vivo experimental techniques. In order to gain insight into the immune-regulatory modules involved in T-cell functioning as well as study the immune-modulatory mechanisms employed by pathogen and the tumor cells, computational tools and mathematical modeling approaches have been extremely useful in obtaining a systems-level understanding. These have also helped the researchers and medical practitioners in the prediction of immunotherapeutic strategies and design of treatment protocols. Here we will throw light onto some of the most popular tools and techniques used for such studies and also explore a few of the mathematical models that have helped us unravel some of the intriguing problems in immunology.

6.5.2.1 Signaling and Metabolic Pathway Databases

The signaling pathway databases are important sources of information that collate pathway data from experimental studies regarding the intracellular signaling pathways in different immune cells [95, 96]. The KEGG provides information regarding the core TCR-mediated pathway along with a few co-receptor signaling pathways. The database also contains the pathways responsible for the T_{H1} , T_{H2} , and T_{H17} differentiation. Another popular database called Reactome provides detailed biochemical reactions involved in each step of the protein–protein interactions involved in the T-cell signaling pathway. It also enlists the pathway information related to CD28 and PD-1 co-signaling pathways. Simultaneously, Reactome forms a very important source for cytokine signaling pathways that includes different interleukin families, interferons, tumor necrosis factor, and a few growth hormones. A list of few of the available databases and the available information in each has been listed down in Table 6.2. However, the information regarding the intercellular cross-talks in the immune system is lacking in most of these databases that can be extracted through a thorough literature survey.

Few databases also provide data regarding the changes in the pathway during disease condition. The KEGG database has a sufficient amount of pathway information regarding the endocytosis of the *Leishmania* pathogen as well as the signaling events that occurs inside the infected macrophage. BioLegend database contains the cancer immune-editing network that consists of the intercellular signaling cross-talks governing the immune responses generated during cancer.

For the analysis of these biochemical pathways, the BIOPYDB database also provides an integrated platform for performing network analysis, logical steady-state analysis, knock-out analysis, etc. It contains detailed information regarding each protein involved in the immunological pathways as well as links them to the specific diseases associated with them. Apart from the TCR co-receptor-mediated

Table 6.2 List of a few signaling and metabolic pathway databases containing T-cell-specific pathway data and related cytokine pathways

Database	T-cell activation/differentiation pathways/network	Cytokine pathways	URL of database
Kyoto Encyclopedia of Genes and Genomes (KEGG)	T-cell receptor signaling pathway, T _{H1} and T _{H2} cell differentiation, T _{H17} cell differentiation	IL-17, TNF, calcium signaling pathway	http://www.genome.jp/kegg/
Reactome	TCR-mediated pathway, CD28 co-signaling pathway	IFN- α/β , IFN- γ , TNF- α , IL-1, IL-2, IL-3, IL-5, GM-CSF, IL-4, IL-13, IL-6, IL-7, IL-10, IL-12, IL-17, IL-20 family cytokines	https://reactome.org/
Wikipathways	TCR-mediated pathway, B7-CD28, B7-CTLA4, PDL- PD1 pathways	IL-2, IL4, IL-5, IL-7, IL-9, IL-11, Type-1 IFN, TNF- α pathways	http://www.wikipathways.org
NCI – Pathway Interaction Database (PID)	TCR signaling network in naïve CD4 cells, B7-CD28 signaling networks	IL-1, IL-2, IL-3, IL-4, IL-5, IL-6, IL-8, IL-12, IL-23, IL-27, TNF signaling networks	http://www.ndexbio.org
BioLegend	T-fh, T _{H1} , T _{H2} , T _{H17} , Treg, $\gamma\delta$ -T-cell signaling pathways	IL-1, IL-2, IL-4, IL-6, IL-10, IFN, TNF pathways and inter-cellular cytokine signaling network of immune cells	https://www.biolegend.com/pathways/
BIOPYDB	TCR-mediated pathway, co-receptor-mediated T-cell activation pathway	IL-1 α , IL- β , IL2, IL-4, IL-6, IL-12, IL-18, IL-36 α , IL-36 β , IL-36 γ , TNF α , TNF β , IFN α , IFN β , IFN γ , TGF β	http://biopydb.ncl.res.in/biopydb/index.php
HumanCyc	T _{H1} , T _{H2} , T _{H17} , Treg-associated processes and pathways	Cytokine pathways are not available separately, but integrated with the other immune processes	https://biocyc.org/HUMAN/
Brenda	T _{H1} , T _{H2} -related processes	IL-1, IL-3, IL-5, IL-6, IL-8, IL-12, IL-17, IL-18, IL-21, IL-33, IFN- α , IFN- β , IFN- γ , TNF- α , TNF- β ligands	https://www.brenda-enzymes.org/

and cytokine pathways, BIOPYDB also contains detailed information about the toll-like receptor (TLR) pathways that has an important role in the regulation of immune response [97].

With the realization of the importance of immune-metabolism as a decisive factor in eliciting immune responses, metabolic databases have started to incorporate such details into the database structure. Although the advent is very recent and

only a limited number of databases have included this information. Two of the popularly used metabolic databases, HumanCyc [98] and Brenda [99], include information about immune-metabolites that are linked to immune responses. HumanCyc is the *Homo sapiens*-specific repertoire of the metabolic database BioCyc, which enlists metabolism specific to human. The database enlists a range of “Biological Process” and “Proteins” related to immune system. The biological processes are linked to their “Gene Ontology” term. A few of the important immune processes listed are “leukocyte-mediated cytotoxicity,” “adaptive immune response,” “immune effector process,” “regulation of immune response,” and “immune system development.” The GO IDs of these processes link them to pathways and processes to which are linked/cross-linked, which are enlisted as “Parent Classes” and metabolites/proteins which are involved in these processes are enlisted under “Instances”. These metabolites/proteins are linked to their detailed descriptions along with reactions in which they are involved and the reaction mechanism [98]. Brenda also provides details of immune-metabolites. The database has a wide range of entries as search option. Upon search of immune processes, it provides a variety of immune-metabolites and proteins whose “Enzyme Nomenclature,” “Enzyme-Ligand Interactions,” “Diseases,” “Functional Parameters,” “Organism-related Information,” “General Information,” “Enzyme Structure,” “Molecular Properties,” “Applications,” and “References” are provided.

6.5.2.2 Graph Theoretical Analysis

The Graph Theory was initiated with Euler’s famous publication from 1736 on the Seven Bridges of Königsberg problem [100]. However, it was applied to biochemical networks much later with the advent of the concepts of small-world and scale-free networks in 1999 that describes the global architecture of any complex real-world network such as the network of biochemical reactions in a cell [101, 102]. Computational biologists have modeled biochemical pathways as network where each protein or metabolite has been considered a node and the reaction between any two such species have been denoted as an edge, thereby translating the entire reaction network as an interconnected mesh of nodes and edges. Various network parameters such as Degree (k), Betweenness Centrality, Closeness Centrality, Eccentricity, Edge Betweenness, and Clustering Coefficient are used to describe the topological properties of the network. These parameters help in the identification of important hubs, i.e., a highly connected node, and shortest paths in the biochemical reaction network that may have significant contribution in the functioning of the signaling or metabolic pathways. Tools such as Cytoscape, Gephi, Pajek are freely available for performing network analysis of large reaction network [103–105]. Cytoscape further offers downloadable plugins for identifying important motifs, extracting sub-networks, and performing enrichment analysis and a host of other functions required for visualizing and analyzing large biochemical reaction networks. These biochemical networks mostly follow the small-world property of a network that indicates a relatively short distance from any one node to another and a relatively high level of clustering. This network property, termed as scale-free property of a network, denotes a connectivity distribution that fits a power law

depicted in Eq. 6.1 where the value of γ lies in the range $2 < \gamma < 3$ [106]. It has been observed that networks following the scale-free property are generally resistant to perturbations and thus are highly robust:

$$P(k) = \alpha k^{-\gamma} \quad (6.1)$$

Graph Theory has successfully been applied to signaling pathway networks where the concept of shortest path has been used to hypothesize potential signaling mechanisms in Neuro2A cells downstream of CB1R receptors. Here the cells were stimulated with a CB1R agonist for the assessment of activity of transcription factors. This experiment revealed CB1R activation modulates the activity of 23 transcription factors [107]. Such methods are useful in the identification of important novel signaling routes between a cell-surface receptor and downstream transcription. In a recent study, Graph theoretic network analysis has been used to identify protein pathways responsible for cell death after neurotropic viral infection by Chandipura Virus (CHPV) [108]. Another important application of network analysis is that it can be used to identify important hub proteins that can be used as potential drug or immunotherapeutic target [109, 110].

6.5.2.3 Logic-Based Models

Logical modeling is gradually being recognized as a simple yet powerful tool in systems biology for the study of large and complex reaction networks. Here the information flow from one node to another in a network is determined by a combination of input nodes and their relation is specified using logic gates – AND, OR, NOT. It was first explained by Kauffmann where he modeled the gene as a binary device that can be either in the ‘ON’ or ‘OFF’ states signifying whether a gene expression is upregulated or downregulated, respectively [111]. Here he elucidated that a distinct advantage in this choice of a binary model for gene activity lies in the fact that the number of different possible rules by which a finite number (K) of inputs may affect the output behavior of a binary element is finite, i.e., 2^{2^K} . Figure 6.3a shows a simple toy model of three nodes interacting with one another. The reaction network can be represented using Boolean rules or equations (Eqs. 6.2, 6.3 and 6.4). The truth tables and the state transitions graphs of the reaction network show the temporal evolution of the states (0 or 1) of the nodes starting from different input combinations (Fig. 6.3a). Here, in this example we observe under the different input conditions the system tends to reach certain point steady-state attractors, i.e. 1–0–0 and 1–1–1 or cyclic attractor, i.e. 1–0–1 \leftrightarrow 1–1–0:

$$v1 = v1 \text{ OR } (\text{NOT } v3) \quad (6.2)$$

$$v2 = v1 \text{ AND } v3 \quad (6.3)$$

$$v3 = v2 \quad (6.4)$$

Several software packages such as BoolNet (R-based), BooleanNet (Python based), and CellNetAnalyzer (software with GUI) are available for performing logical steady-state analysis of large biochemical networks [112–114]. This concept

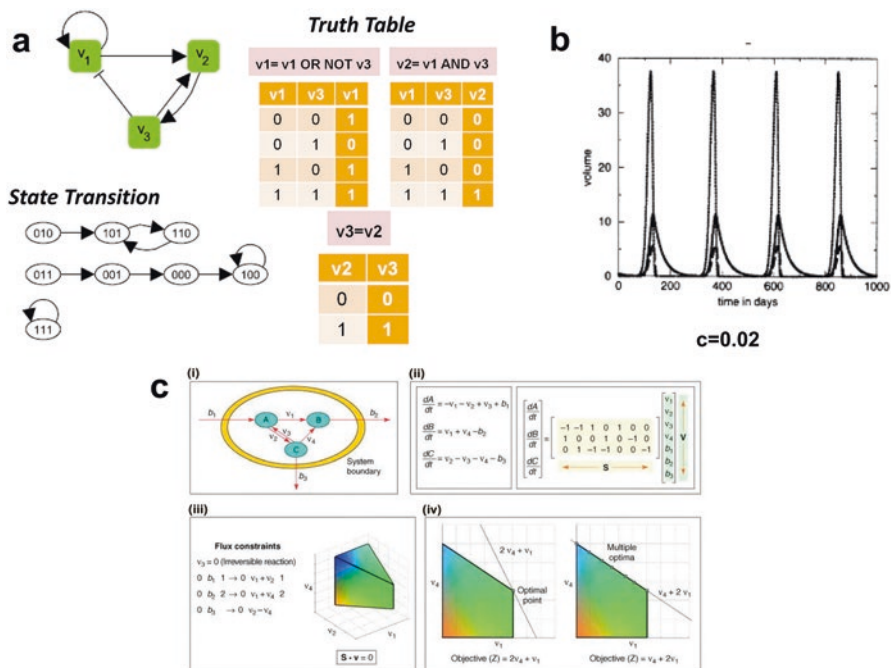


Fig. 6.3 Computational techniques used for study of large biochemical pathways. (a) Interaction Graph, Truth Table, and State Transition Graph for a Logic-Based Toy Model; (b) Temporal dynamics of Tumor, Effector cells, and IL-2 from an ODE-based model (adapted from Kirshner, et al. 1998 [150]); (c) A toy model describing (i) the flux distribution of metabolites A, B, and C through different reactions, (ii) the formation of stoichiometric matrix "S" and flux vector "v," (iii) defining constraints and (iv) defining objective and finding optimal solution within the solution space of linear optimization problem (Adapted from Kauffman et al. 2003 [157])

was later used by Huang and Ingber to model cell signaling networks for demonstrating that cellular phenotypes correspond to the dynamic steady states of the intracellular signaling molecules in a logic-based model. A key advantage of this strategy is that it does not require the knowledge of parameter values that is often not available for large biochemical networks. Later it has been extensively used for the study of cell signaling pathways and identification of drug targets for the treatment of cancer [109, 110]. Logical models have also been developed for the study of T-cell signaling pathways where the observations made from the *in silico* analysis were experimentally validated to establish the authenticity of their logic-based model. Using this model, the authors have predicted an alternative pathway of activation from CD28 to JNK that does not involve the canonical pathway involving LAT signalosome, nor does it involve the activation of PLC γ 1 or calcium flux, but depends on the activation of the nucleotide exchange factor Vav1, which activates MEKK1 via the small G-protein Rac1 [115]. A logical steady-state model that captures the effect of the co-receptor signaling pathway cross-talks has been developed that shows that simultaneous activation of the TCR:CD3, CRAC, and OX40

pathways are important for sustained T-cell proliferation. At the same time, it has been shown that the co-receptor CD27 and LTBR pathways are important for regulating the cytokine production [116]. A further extension of this work for the study of immune responses during Leishmaniasis explains how the differentiation of T cell is altered during infection [117]. Another model employing Boolean formalism has been used in the study of differentiation of naive cells into T_{H1} , T_{H2} , T_{H17} , and Treg subtypes under different environmental conditions [118]. This model provides evidences that $Foxp3^+$ Treg cells and T_{H17} cells are highly plastic and labile, whereas the T_{H1} and T_{H2} subtypes remain steady under different environmental conditions. However, this model also predicts the existence of hybrid states and cyclic attractors expressing markers characteristic of two or more canonical cell types under certain environmental conditions that lays the foundation for the oscillatory behavior of T-cell differentiation. This study further elucidates that under proper polarizing environments, the Treg cells may differentiate into T_{H1} or T_{H2} subtypes [118]. Later another model based on the Boolean formalism was developed to study the molecular mechanisms controlling the cytokine-driven T_H cell differentiation and plasticity. This model explained the role for peroxisome proliferator-activated receptor gamma (PPAR γ) in the regulation of T_{H17} to iTreg cell switching that gives promising cues for the prediction of therapeutic target for dysregulated immune responses and inflammation [119]. More recently, Probabilistic Boolean Control Network has also been employed for the study of T_H cell differentiation under varied environmental conditions. Here each input node is activated with a certain user-defined probability, which makes the system stochastic. Using this study, the authors have identified that the T-cell differentiation process is regulated by composition and dosage of signals that the cell receives from the environment. They have also predicted novel T-cell phenotypes using their model and have identified the specific environmental conditions that give rise to them [120].

6.5.2.4 Steady-State Metabolic Models

Immunometabolism has gained momentum in recent years as an emerging field of investigation at the interface between two highly discussed disciplines of immunology and metabolism [9, 10]. The idea of metabolism as a driver of the immune response [121] has been appreciated in recent years. However, capturing the bidirectional regulation of signaling and metabolism using a single computational platform is challenging. The mechanism of action of the two cascades is different, and the time scales in which the two processes occur also differ enormously. Mostly signaling cascades are faster than the metabolic reactions. This, along with the limitation of availability of information about how metabolism regulates immune cell responses and functioning, has limited the designing of immune-metabolic models to a small scale, mostly considering few parameters to design smaller dynamic models. An integrated systems-level computational model of immunometabolism is yet to be undertaken. Nevertheless, the currently employed computational approaches can be used to address immune-metabolism at a systems-level.

Genome-scale metabolic modeling (GSMM) is currently the most widely used systems-level modeling approach that accounts for whole-genome metabolism of

biological systems. It is a constraint-based mathematical modeling approach that assimilates biochemical, genetic, and genomic information within a single computational platform [122–126]. It allows the study of the metabolic genotype-phenotype relationship of an organism. Genome-scale metabolic models have been used in *in silico* metabolic engineering for the design of studies like defining essentiality of the reaction/gene [127, 128], the relevance of distant pathways [129] and overexpression or knockout analyses of metabolites, reactions, and metabolic pathways [130]. These are efficient tools for the prediction of growth in living cells/tissues exposed to different external conditions [131]. They have been used to predict conditional and absolute essentiality of metabolites and reactions in metabolic networks.

Flux balance analysis (FBA) is the most popularly used constraint-based approach in systems-level metabolic modeling, which works on the basic principles of linear optimization [132]. The technique assumes a steady-state approach, where all the metabolites of the network are considered to be in steady state; i.e., the rate of change of metabolites over time remains zero (Fig. 6.3c). This ensures that the rate of formation of a metabolite in the network is always equal to the rate of its consumption and hence a net difference in the metabolite concentration over time always remains zero. All reactions of the network work as constraints to the optimization problem. The reactions are bounded between a lower and an upper bound, which creates the constraint. The metabolites are connected to respective reactions in the form of a stoichiometric matrix, “ S ,” where the rows represent the metabolites (m) and the columns represent reactions (n). Thus, a “ $m \times n$ ” matrix is generated in which the involvement of a metabolite in a reaction is represented by its respective stoichiometry in that reaction. A positive stoichiometric value represents the formation of the metabolite and a negative stoichiometric value represents consumption. The flux through the reactions is represented in a separate flux matrix “ v ,” which is a “ $n \times 1$ ” matrix. The outcome of the optimization is obtained by matrix multiplication of “ $S \cdot v = 0$.” The matrix multiplication results in an optimized “ v ” matrix, which assigns an optimized flux to each of the reactions in the network. Generally, whole-genome models are large with a few hundreds of reactions and metabolites, which make it a multidimensional optimization problem. An objective is assigned to the model that depends on the biological question one wants to address. For example, if one wants to observe the behavior of the network when it tries to maximize ATP production, then one can assign ATP synthase (ATPS) reaction as the objective and try optimizing the model by maximizing the objective function. Thus, the model gets optimized a per the requirement of maximizing or minimizing the objective function.

A further extension of the modeling technique has been done to incorporate dynamic regulation of metabolic regulations by signaling pathways. This is popularly known as dynamic FBA (dFBA), where the initial activation of the metabolic FBA model depends on the output of signaling response generated by dynamic analysis. In yet another extension of FBA, the initial signaling response is analyzed using Boolean analysis. This is known as rFBA. The method that takes into account a combined FBA, Boolean regulatory, and ODE approach is known as integrative FBA (iFBA).

There are various tools available for performing these analyses. COBRA Toolbox is the most widely used platform for flux balance analysis [133]. This is a Matlab extension, which allows user-interface for ease in analysis. Other platforms are COBRAPy [134], PSAMM [135], OptFlux [136], FBASimVis [137], FluxViz [138], FlexFlux [139], FAME [140], and Escher-FBA [141].

6.5.2.5 Dynamic ODE-Based Immune Models

Several dynamic models have been developed for the study of immune responses for several diseases [142–146]. The study of immune responses during tumor formation using mathematical ODE-based models has helped clinicians in the prediction of tumor evolution and the determination of dosage schedules and treatment protocols [147–149]. A seminal work by Kirschner and Panetta has led to the development of many such similar models with further improvisations [150]. The model developed by them represents an ODE-based model of the tumor-immune interaction and the production of IL-2 that has important roles in the regulation of immune response generated during tumor progression (Eqs. 6.5, 6.6, and 6.7). The model considers that the proliferation of the effector immune cells increases proportional to the antigenicity of the tumor. The model equations comprise three variables, viz. tumor (T), effector cells (E), and IL2 (I_L), that interact among themselves, and 12 parameters that describe the rate at which these interactions occur. In this model the antigenicity, denoted with c , of the tumor has been considered as an essential parameter that regulates the dynamics of the effector cell population:

$$\frac{dE}{dt} = cT - \mu_2 E + \frac{p_1 E I_L}{g_1 + I_L} + s_1 \quad (6.5)$$

$$\frac{dT}{dt} = r_2 (1 - bT)T - \frac{aET}{g_2 + T} \quad (6.6)$$

$$\frac{dI_L}{dt} = \frac{p_2 ET}{g_3 + T} - \mu_3 I_L + s_2 \quad (6.7)$$

Figure 6.3b (adapted from Kirshner et al. 1998 [150]) shows the temporal evolution of the system and the oscillating steady state behavior of the variables when antigenicity parameter $c = 0.02$. This model explains short-term oscillations in tumor sizes as well as long-term tumor relapse. This model has been further used to explore the effects of adoptive cellular immunotherapy for the tumor elimination [150].

A more recent tumor-immune interaction model developed for understanding the dynamics of immune-mediated tumor rejection focuses mainly on the role of natural killer (NK) and CD8⁺ T cells in tumor surveillance. Here the techniques of parameter estimation and sensitivity analysis have been exploited for the model calibration and validation with experimental results. This study has revealed the variable to which the model is most sensitive is patient specific and that there exists a direct positive correlation between the patient-specific efficacy of the CD8⁺ T-cell response and the likelihood of a patient favorably responding to immunotherapy

treatments [151]. A more detailed model of immune responses during tumor progression has been developed using 13 variables and 71 parameters. The model considers cytokine feedbacks and five different immune cells present in the tumor microenvironment. This model is useful for optimizing combinatorial treatment dose and schedules for maximal tumor reduction using immunotherapy [152].

There is a range of ODE models that investigate various pathways involved in metabolism under different pathological conditions. Immune metabolic models are available for glucose metabolism [153], glutathione metabolism [154], folate-mediated one-carbon metabolism [154], and arsenic metabolism [155]. A composite review of these metabolic models is available in Nijhout et al.'s work [156]. The recent understanding from experimental research on the metabolic regulation of the immune response [9] will help to adapt these mathematical models to the reality of metabolic pathways inside immune cells.

6.6 Challenges and Future Directions

The immune-regulatory network forms a complex mesh of interacting cells and biochemical reactions that work in a coordinated fashion to eliminate the pathogen-infected cells and trigger the remission of any neoplastic growth inside the body. However, the intricacies of the immune signaling network are far from being completely understood, and the regulations governing the differential immune response of the T cells under varied antigenic challenges still remain elusive to immunologists. In this context, the knowledge regarding the signaling routes is essential to understand the mechanistic regulations such as the feedback and feed-forward loops and the alternative signaling pathways that govern the production of effector molecules from the lymphocytes. Hence, an in-depth study of the co-receptor signaling pathways and their cross-talks is essential that will provide valuable information regarding the pathways involved in the cytokine regulation and effector functions of the immune cells.

T-cell plasticity that determines their differentiation, de-differentiation, subtype specification, and T helper memory cell formation under different environmental conditions is yet another area that has remained very less explored. Although the recent developments in the field elucidate the process of T-cell differentiation with respect to changes in the cytokine milieu under *in vitro* conditions, the complex interactions in the human immunome needs to be studied using a holistic integrative approach in order to gain clear insights into the changes of immune responses due to changes in quality and quantity of the antigenic challenge, the strength of the stimulus, and the role of the other interacting immune cells. Such studies will throw light into the modulations of T-cell subtype ratios that has a substantial impact on the disease prognosis and response of a patient to an immunotherapeutic intervention.

Metabolic regulation of immune cell in determining T-cell activation, proliferation, and differentiation is a newer area of research; and studies are in progress to understand these processes. Many questions related to immune-metabolism still

remain unanswered. How metabolism alters during transition from quiescent T cells to activated effector T cells remains poorly understood. Although mTORC1 activity has been observed to be central to signaling and metabolic cross-talk and the master kinase in guiding quiescence exit of T cells, how nutrients tune mTORC1 activity remains to be explored further. Redox metabolism and oxygen sensing have been implicated in T-cell proliferation and activation; however, the exact mechanism of how they regulate T-cell quiescence and activation in different tissues remains unaddressed. Also, the cross-talks between signaling and metabolic pathways are only partially explored. A clear understanding of these mechanisms will help augment immune responses and pave way for immunotherapy under different pathogenic conditions.

References

1. Cruse JM, Lewis RE, Wang H (eds) (2004) Chapter 1 – Molecules, cells, and tissues of immunity. Immunology guidebook. Academic, San Diego, pp 1–15
2. Rabb H (2002) The T cell as a bridge between innate and adaptive immune systems: implications for the kidney. *Kidney Int* 61(6):1935–1946
3. Moticka EJ (2016) Chapter 20 – Activation of T lymphocytes and MHC restriction. A historical perspective on evidence-based immunology. Elsevier, Amsterdam, pp 169–179
4. Moticka EJ (2016) Chapter 37 – Tumor immunology. A historical perspective on evidence-based immunology. Elsevier, Amsterdam, pp 329–339
5. Kara EE, Comerford I, Fenix KA, Bastow CR, Gregor CE, McKenzie DR et al (2014) Tailored immune responses: novel effector helper T cell subsets in protective immunity. *PLoS Pathog* 10(2):e1003905
6. Moticka EJ (2016) Chapter 23 – T lymphocyte subpopulations. A historical perspective on evidence-based immunology. Elsevier, Amsterdam, pp 197–205
7. Pearce EL, Pearce EJ (2013) Metabolic pathways in immune cell activation and quiescence. *Immunity* 38(4):633–643
8. Zeng H, Chi H (2017) mTOR signaling in the differentiation and function of regulatory and effector T cells. *Curr Opin Immunol* 46:103–111
9. Ganeshan K, Chawla A (2014) Metabolic regulation of immune responses. *Annu Rev Immunol* 32:609–634
10. Assmann N, Finlay DK (2016) Metabolic regulation of immune responses: therapeutic opportunities. *J Clin Invest* 126(6):2031–2039
11. Patel CH, Leone RD, Horton MR, Powell JD (2019) Targeting metabolism to regulate immune responses in autoimmunity and cancer. *Nat Rev Drug Discov* 18(9):669–688
12. Jung J, Zeng H, Horng T (2019) Metabolism as a guiding force for immunity. *Nat Cell Biol* 21(1):85–93
13. Brownlie RJ, Zamojska R (2013) T cell receptor signalling networks: branched, diversified and bounded. *Nat Rev Immunol* 13:257
14. Ware CF (2008) Targeting lymphocyte activation through the lymphotoxin and LIGHT pathways. *Immunol Rev* 223:186–201
15. Elgueta R, Benson MJ, de Vries VC, Wasiuk A, Guo Y, Noelle RJ (2009) Molecular mechanism and function of CD40/CD40L engagement in the immune system. *Immunol Rev* 229(1):152–172
16. Munroe ME, Bishop GA (2007) A Costimulatory function for T cell CD40. *J Immunol* 178(2):671–682
17. Redmond WL, Ruby CE, Weinberg AD (2009) The role of OX40-mediated co-stimulation in T cell activation and survival. *Crit Rev Immunol* 29(3):187–201

18. Croft M, So T, Duan W, Soroosh P (2009) The significance of OX40 and OX40L to T-cell biology and immune disease. *Immunol Rev* 229(1):173–191
19. Ledbetter JA, Deans JP, Aruffo A, Grosmaire LS, Kanner SB, Bolen JB et al (1993) CD4, CD8 and the role of CD45 in T-cell activation. *Curr Opin Immunol* 5(3):334–340
20. Chen L, Flies DB (2013) Molecular mechanisms of T cell co-stimulation and co-inhibition. *Nat Rev Immunol* 13(4):227–242
21. Feske S (2007) Calcium signalling in lymphocyte activation and disease. *Nat Rev Immunol* 7:690
22. Baine I, Abe Brian T, Macian F (2009) Regulation of T-cell tolerance by calcium/NFAT signaling. *Immunol Rev* 231(1):225–240
23. Nakaya M, Xiao Y, Zhou X, Chang J-H, Chang M, Cheng X et al (2014) Inflammatory T cell responses rely on amino acid transporter ASCT2 facilitation of glutamine uptake and mTORC1 kinase activation. *Immunity* 40(5):692–705
24. Palmer CS, Ostrowski M, Balderson B, Christian N, Crowe SM (2015) Glucose metabolism regulates T cell activation, differentiation, and functions. *Front Immunol* 6:1
25. Chi H (2012) Regulation and function of mTOR signalling in T cell fate decisions. *Nat Rev Immunol* 12(5):325
26. Chapman NM, Boothby MR, Chi H (2020) Metabolic coordination of T cell quiescence and activation. *Nat Rev Immunol* 20:55–70
27. Johnson MO, Wolf MM, Madden MZ, Andrejeva G, Sugiura A, Contreras DC et al (2018) Distinct regulation of Th17 and Th1 cell differentiation by glutaminase-dependent metabolism. *Cell* 175(7):1780–95.e19
28. Dodd KM, Tee AR (2012) Leucine and mTORC1: a complex relationship. *Am J Physiol Endocrinol Metab* 302(11):E1329–42
29. Fallarino F, Grohmann U, Vacca C, Bianchi R, Orabona C, Spreca A et al (2002) T cell apoptosis by tryptophan catabolism. *Cell Death Differ* 9(10):1069
30. Fallarino F, Grohmann U, Hwang KW, Orabona C, Vacca C, Bianchi R et al (2003) Modulation of tryptophan catabolism by regulatory T cells. *Nat Immunol* 4(12):1206
31. Geiger R, Rieckmann JC, Wolf T, Basso C, Feng Y, Fuhrer T et al (2016) L-arginine modulates T cell metabolism and enhances survival and anti-tumor activity. *Cell* 167(3):829–42.e13
32. Zhao Y, Hu X, Liu Y, Dong S, Wen Z, He W et al (2017) ROS signaling under metabolic stress: cross-talk between AMPK and AKT pathway. *Mol Cancer* 16(1):79
33. Franchina DG, Dostert C, Brenner D (2018) Reactive oxygen species: involvement in T cell signaling and metabolism. *Trends Immunol* 39(6):489–502
34. Zhu J, Yamane H, Paul WE (2010) Differentiation of effector CD4 T cell populations. *Annu Rev Immunol* 28:445–489
35. Luckheeram RV, Zhou R, Verma AD, Xia B (2012) CD4+T cells: differentiation and functions. *Clin Dev Immunol* 2012:925135
36. Hawse WF, Cattle RT (2019) T cells transduce T-cell receptor signal strength by generating different phosphatidylinositols. *J Biol Chem* 294(13):4793–4805
37. Yamane H, Paul WE (2013) Early signaling events that underlie fate decisions of naive CD4(+) T cells towards distinct T-helper cell subsets. *Immunol Rev* 252(1):12–23
38. Peter C, Waldmann H, Cobbold SP (2010) mTOR signalling and metabolic regulation of T cell differentiation. *Curr Opin Immunol* 22(5):655–661
39. MacIver NJ, Michalek RD, Rathmell JC (2013) Metabolic regulation of T lymphocytes. *Annu Rev Immunol* 31:259–283
40. Klysz D, Tai X, Robert PA, Craveiro M, Cretenet G, Oburoglu L et al (2015) Glutamine-dependent α -ketoglutarate production regulates the balance between T helper 1 cell and regulatory T cell generation. *Sci Signal* 8(396):ra97
41. Mak TW, Grusdat M, Duncan GS, Dostert C, Nonnenmacher Y, Cox M et al (2017) Glutathione primes T cell metabolism for inflammation. *Immunity* 46(4):675–689
42. Stark JM, Tibbitt CA, Coquet JM (2019) The metabolic requirements of Th2 cell differentiation. *Front Immunol* 10:2318

43. Gerriets VA, Kishton RJ, Johnson MO, Cohen S, Siska PJ, Nichols AG et al (2016) Foxp3 and Toll-like receptor signaling balance T reg cell anabolic metabolism for suppression. *Nat Immunol* 17(12):1459
44. Angelin A, Gil-de-Gómez L, Dahiya S, Jiao J, Guo L, Levine MH et al (2017) Foxp3 reprograms T cell metabolism to function in low-glucose, high-lactate environments. *Nat Immunol* 25(6):1282–93.e7
45. Geginat J, Paroni M, Maglie S, Alfen JS, Kastirr I, Gruarin P et al (2014) Plasticity of human CD4 T cell subsets. *Front Immunol* 5:630
46. Pollizzi KN, Powell JD (2015) Regulation of T cells by mTOR: the known knowns and the known unknowns. *Trends Immunol* 36(1):13–20
47. Yang K, Neale G, Green DR, He W, Chi H (2011) The tumor suppressor Tsc1 enforces quiescence of naive T cells to promote immune homeostasis and function. *Nat Immunol* 12(9):888
48. Sauer S, Bruno L, Hertweck A, Finlay D, Leleu M, Spivakov M et al (2008) T cell receptor signaling controls Foxp3 expression via PI3K, Akt, and mTOR. *Proc Natl Acad Sci U S A* 105(22):7797–7802
49. Macintyre AN, Gerriets VA, Nichols AG, Michalek RD, Rudolph MC, Deoliveira D et al (2014) The glucose transporter Glut1 is selectively essential for CD4 T cell activation and effector function. *Cell Metab* 20(1):61–72
50. Wang R, Dillon CP, Shi LZ, Milasta S, Carter R, Finkelstein D et al (2011) The transcription factor Myc controls metabolic reprogramming upon T lymphocyte activation. *Immunity* 35(6):871–882
51. Yang K, Shrestha S, Zeng H, Karmaus PW, Neale G, Vogel P et al (2013) T cell exit from quiescence and differentiation into Th2 cells depend on Raptor-mTORC1-mediated metabolic reprogramming. *Immunity* 39(6):1043–1056
52. Tan H, Yang K, Li Y, Shaw TI, Wang Y, Blanco DB et al (2017) Integrative proteomics and phosphoproteomics profiling reveals dynamic signaling networks and bioenergetics pathways underlying T cell activation. *Immunity* 46(3):488–503
53. Gerriets VA, Kishton RJ, Nichols AG, Macintyre AN, Inoue M, Ilkayeva O et al (2015) Metabolic programming and PDHK1 control CD4+ T cell subsets and inflammation. *J Clin Invest* 125(1):194–207
54. Blagih J, Coulombe F, Vincent EE, Dupuy F, Galicia-Vázquez G, Yurchenko E et al (2015) The energy sensor AMPK regulates T cell metabolic adaptation and effector responses in vivo. *Immunity* 42(1):41–54
55. Mossmann D, Park S, Hall MN (2018) mTOR signalling and cellular metabolism are mutual determinants in cancer. *Nat Rev Cancer* 18(12):744–757
56. Buck MD, O'sullivan D, Pearce EL (2015) T cell metabolism drives immunity. *J Exp Med* 212(9):1345–1360
57. Mullen PJ, Yu R, Longo J, Archer MC, Penn LZ (2016) The interplay between cell signalling and the mevalonate pathway in cancer. *Nat Rev Cancer* 16(11):718
58. Doerig C, Rayner JC, Scherf A, Tobin AB (2015) Post-translational protein modifications in malaria parasites. *Nat Rev Microbiol* 13(3):160–172
59. Ho P-C, Bihuniak JD, Macintyre AN, Staron M, Liu X, Amezquita R et al (2015) Phosphoenolpyruvate is a metabolic checkpoint of anti-tumor T cell responses. *Cell* 162(6):1217–1228
60. Wang F, Beck-García K, Zorzin C, Schamel WW, Davis MM (2016) Inhibition of T cell receptor signaling by cholesterol sulfate, a naturally occurring derivative of membrane cholesterol. *Nat Immunol* 17(7):844–50
61. Demetriou M, Granovsky M, Quaggin S, Dennis JW (2001) Negative regulation of T-cell activation and autoimmunity by Mgat5N-glycosylation. *Nature* 409(6821):733–9
62. Lee K, Gudapati P, Dragovic S, Spencer C, Joyce S, Killeen N et al (2010) Mammalian target of rapamycin protein complex 2 regulates differentiation of Th1 and Th2 cell subsets via distinct signaling pathways. *Immunity* 32(6):743–753
63. Frauwirth KA, Riley JL, Harris MH, Parry RV, Rathmell JC, Plas DR et al (2002) The CD28 signaling pathway regulates glucose metabolism. *Immunity* 16(6):769–777

64. Kimura MY, Pobezinsky LA, Guinter TI, Thomas J, Adams A, Park J-H et al (2013) IL-7 signaling must be intermittent, not continuous, during CD8+ T cell homeostasis to promote cell survival instead of cell death. *Nat Immunol* 14(2):143–51
65. Jacobs SR, Herman CE, MacIver NJ, Wofford JA, Wieman HL, Hammen JJ et al (2008) Glucose uptake is limiting in T cell activation and requires CD28-mediated Akt-dependent and independent pathways. *J Immunol* 180(7):4476–4486
66. Sinclair LV, Rolf J, Emslie E, Shi Y-B, Taylor PM, Cantrell DA (2013) Control of amino-acid transport by antigen receptors coordinates the metabolic reprogramming essential for T cell differentiation. *Nat Immunol* 14(5):500
67. Bricker DK, Taylor EB, Schell JC, Orsak T, Boutron A, Chen Y-C et al (2012) A mitochondrial pyruvate carrier required for pyruvate uptake in yeast, *Drosophila*, and humans. *Science* 337(6090):96–100
68. Shi LZ, Wang R, Huang G, Vogel P, Neale G, Green DR et al (2011) HIF1 α -dependent glycolytic pathway orchestrates a metabolic checkpoint for the differentiation of TH17 and Treg cells. *J Exp Med* 208(7):1367–1376
69. Sinclair LV, Neyens D, Ramsay G, Taylor PM, Cantrell DA (2018) Single cell analysis of kynurenine and System L amino acid transport in T cells. *Nat Commun* 9(1):1981
70. Baixauli F, Acín-Pérez R, Villarroya-Beltrí C, Mazzeo C, Nuñez-Andrade N, Gabandé-Rodríguez E et al (2015) Mitochondrial respiration controls lysosomal function during inflammatory T cell responses. *Cell Metab* 22(3):485–498
71. Seman M, Adriouch S, Scheuplein F, Krebs C, Freese D, Glowacki G et al (2003) NAD-induced T cell death: ADP-ribosylation of cell surface proteins by ART2 activates the cytosolic P2X7 purinoceptor. *Immunity* 19(4):571–582
72. Adriouch S, Hubert S, Pechberty S, Koch-Nolte F, Haag F, Seman M (2007) NAD⁺ released during inflammation participates in T cell homeostasis by inducing ART2-mediated death of naive T cells in vivo. *J Immunol* 179(1):186–194
73. Clever D, Roychoudhuri R, Constantinides MG, Askenase MH, Sukumar M, Klebanoff CA et al (2016) Oxygen sensing by T cells establishes an immunologically tolerant metastatic niche. *Cell* 166(5):1117–31.e14
74. Tarasenko TN, Pacheco SE, Koenig MK, Gomez-Rodriguez J, Kapnick SM, Diaz F et al (2017) Cytochrome c oxidase activity is a metabolic checkpoint that regulates cell fate decisions during T cell activation and differentiation. *Cell Metab* 25(6):1254–68.e7
75. Sena LA, Li S, Jairaman A, Prakriya M, Ezponda T, Hildeman DA et al (2013) Mitochondria are required for antigen-specific T cell activation through reactive oxygen species signaling. *Immunity* 38(2):225–236
76. Chinen T, Kannan AK, Levine AG, Fan X, Klein U, Zheng Y et al (2016) An essential role for the IL-2 receptor in T reg cell function. *Nat Immunol* 17(11):1322
77. Yang K, Blanco DB, Neale G, Vogel P, Avila J, Clish CB et al (2017) Homeostatic control of metabolic and functional fitness of T reg cells by LKB1 signalling. *Nature* 548(7669):602
78. Zeiser R, Maas K, Youssef S, Dürr C, Steinman L, Negrin RSJI (2009) Regulation of different inflammatory diseases by impacting the mevalonate pathway. *Immunology* 127(1):18–25
79. Huynh A, DuPage M, Priyadharshini B, Sage PT, Quiros J, Borges CM et al (2015) Control of PI (3) kinase in T reg cells maintains homeostasis and lineage stability. *Nat Immunol* 16(2):188
80. Tyrakis PA, Palazon A, Macias D, Lee KL, Phan AT, Veliça P et al (2016) S-2-hydroxyglutarate regulates CD8+ T-lymphocyte fate. *Nature* 540(7632):236
81. Kidani Y, Elsaesser H, Hock MB, Vergnes L, Williams KJ, Argus JP et al (2013) Sterol regulatory element-binding proteins are essential for the metabolic programming of effector T cells and adaptive immunity. *Nat Immunol* 14(5):489
82. Bensinger SJ, Bradley MN, Joseph SB, Zelcer N, Janssen EM, Hausner MA et al (2008) LXR signaling couples sterol metabolism to proliferation in the acquired immune response. *Cell* 134(1):97–111
83. Angela M, Endo Y, Asou HK, Yamamoto T, Tumes DJ, Tokuyama H et al (2016) Fatty acid metabolic reprogramming via mTOR-mediated inductions of PPAR γ directs early activation of T cells. *Nat Commun* 7:13683

84. Munn DH, Sharma MD, Baban B, Harding HP, Zhang Y, Ron D et al (2005) GCN2 kinase in T cells mediates proliferative arrest and anergy induction in response to indoleamine 2, 3-dioxygenase. *Immunity* 22(5):633–642
85. Chang C-H, Curtis JD, Maggi LB Jr, Faubert B, Villarino AV, O'Sullivan D et al (2013) Posttranscriptional control of T cell effector function by aerobic glycolysis. *Cell* 153(6):1239–1251
86. Sherman BT, Lempicki RA (2009) Systematic and integrative analysis of large gene lists using DAVID bioinformatics resources. *Nat Protoc* 4(1):44–57
87. Huang DW, Sherman BT, Lempicki RA (2008) Bioinformatics enrichment tools: paths toward the comprehensive functional analysis of large gene lists. *Nucleic Acids Res* 37(1):1–13
88. Carmona-Saez P, Chagoyen M, Tirado F, Carazo JM, Pascual-Montano A (2007) GENECODIS: a web-based tool for finding significant concurrent annotations in gene lists. *Genome Biol* 8(1):R3
89. Subramanian A, Tamayo P, Mootha VK, Mukherjee S, Ebert BL, Gillette MA et al (2005) Gene set enrichment analysis: a knowledge-based approach for interpreting genome-wide expression profiles. *Proc Natl Acad Sci U S A* 102(43):15545–15550
90. Croft D, Mundo AF, Haw R, Milacic M, Weiser J, Wu G et al (2013) The Reactome pathway knowledgebase. *Nucleic Acids Res.* 42(D1):D472–D477
91. Bindea G, Mlecnik B, Tosolini M, Kirilovsky A, Waldner M, Obenauf Anna C et al (2013) Spatiotemporal dynamics of Intratumoral immune cells reveal the immune landscape in human cancer. *Immunity* 39(4):782–795
92. Fridman WH, Pagès F, Sautès-Fridman C, Galon J (2012) The immune contexture in human tumours: impact on clinical outcome. *Nat Rev Cancer* 12:298
93. Dillon LAL, Suresh R, Okrah K, Corrada Bravo H, Mosser DM, El-Sayed NM (2015) Simultaneous transcriptional profiling of *Leishmania* major and its murine macrophage host cell reveals insights into host-pathogen interactions. *BMC Genomics* 16:1108
94. Favila MA, Geraci NS, Zeng E, Harker B, Condon D, Cotton RN et al (2014) Human dendritic cells exhibit a pronounced type I IFN signature following *Leishmania* major infection that is required for IL-12 induction. *J Immunol* 192(12):5863–5872
95. Chowdhury S, Sarkar RR (2015) Comparison of human cell signaling pathway databases—evolution, drawbacks and challenges. *Database* 2015:bau126
96. Sherriff MR, Sarkar RR (2008) Computational approaches and modelling of signaling processes in immune system. *Proc Indian Natl Sci Acad* 74:187–200
97. Chowdhury S, Sinha N, Ganguli P, Bhowmick R, Singh V, Nandi S et al (2014) BIOPYDB: a dynamic human cell specific biochemical pathway database with advanced computational analyses platform. *J Integr Bioinform* 15(3):20170072
98. Trupp M, Altman T, Fulcher CA, Caspi R, Krummenacker M, Paley S et al (2010) Beyond the genome (BTG) is a (PGDB) pathway genome database: HumanCyc. *Genome Biol* 11(1):O12
99. Schomburg I, Chang A, Schomburg D (2002) BRENDA, enzyme data and metabolic information. *Nucleic Acids Res* 30(1):47–49
100. Euler L (1736) *Commentarii Academiae Scientiarum Imperialis Petropolitanae* 8:128
101. Watts DJ, Strogatz SH (1998) Collective dynamics of 'small-world' networks. *Nature* 393(6684):440
102. Barabási A-L, Albert R (1999) Emergence of scaling in random networks. *Science* 286(5439):509–512
103. Smoot ME, Ono K, Ruscheinski J, Wang P-L, Ideker T (2010) Cytoscape 2.8: new features for data integration and network visualization. *Bioinformatics* 27(3):431–432
104. Bastian M, Heymann S, Jacomy M (2009) Gephi: an open source software for exploring and manipulating networks. Third international AAAI conference on weblogs and social media.
105. Batagelj V, Mrvar A (1998) Pajek-program for large network analysis. *Connect* 21(2):47–57
106. Pavlopoulos GA, Secrier M, Moschopoulos CN, Soldatos TG, Kossida S, Aerts J et al (2011) Using graph theory to analyze biological networks. *BioData Min* 4(1):10
107. Bromberg KD, Ma'ayan A, Neves SR, Iyengar R (2008) Design logic of a cannabinoid receptor signaling network that triggers neurite outgrowth. *Science* 320(5878):903–909

108. Ghosh S, Kumar GV, Basu A, Banerjee A (2015) Graph theoretic network analysis reveals protein pathways underlying cell death following neurotropic viral infection. *Sci Rep* 5:14438
109. Chowdhury S, Pradhan RN, Sarkar RR (2013) Structural and logical analysis of a comprehensive hedgehog signaling pathway to identify alternative drug targets for glioma, colon and pancreatic cancer. *PLoS One* 8(7):e69132
110. Chowdhury S, Sarkar R (2013) Drug targets and biomarker identification from computational study of human notch signaling pathway. *Clin Exp Pharmacol* 3(137):2161–1459
111. Kauffman SA (1969) Metabolic stability and epigenesis in randomly constructed genetic nets. *J Theor Biol* 22(3):437–467
112. Müssel C, Hopfensitz M, Kestler HA (2010) BoolNet—an R package for generation, reconstruction and analysis of Boolean networks. *Bioinformatics* 26(10):1378–1380
113. Albert I, Thakar J, Li S, Zhang R, Albert R (2008) Boolean network simulations for life scientists. Source code for biology and medicine. *Source Code Biol Med* 3(1):16
114. Klamt S, Saez-Rodriguez J, Gilles ED (2007) Structural and functional analysis of cellular networks with CellNetAnalyzer. *BMC Syst Biol* 1(1):2
115. Saez-Rodriguez J, Simeoni L, Lindquist JA, Hemenway R, Bommhardt U, Arndt B et al (2007) A logical model provides insights into T cell receptor signaling. *PLoS Comp Biol* 3(8):e163
116. Ganguli P, Chowdhury S, Bhowmick R, Sarkar RR (2015) Temporal protein expression pattern in intracellular signalling cascade during T-cell activation: a computational study. *J Biosci* 40(4):769–789
117. Ganguli P, Chowdhury S, Sarkar RR (2015) Identification of Th1/Th2 regulatory switch to promote healing response during leishmaniasis: a computational approach. *EURASIP J Bioinform Syst Biol* 2015(1):13
118. Naldi A, Carneiro J, Chaouiya C, Thieffry D (2010) Diversity and plasticity of Th cell types predicted from regulatory network modelling. *PLoS Comp Biol* 6(9):e1000912
119. Carbo A, Hontecillas R, Kronsteiner B, Viladomiu M, Pedragosa M, Lu P et al (2013) Systems modeling of molecular mechanisms controlling cytokine-driven CD4+ T cell differentiation and phenotype plasticity. *PLoS Comp Biol* 9(4):e1003027
120. Puniya BL, Todd RG, Mohammed A, Brown DM, Barberis M, Helikar T (2018) A mechanistic computational model reveals that plasticity of CD4+ T cell differentiation is a function of cytokine composition and dosage. *Front Physiol* 9:878
121. Kelly PN (2019) Metabolism as a driver of immune response. *Science* 363(6423):137–139
122. Price ND, Reed JL, Palsson BØ (2004) Genome-scale models of microbial cells: evaluating the consequences of constraints. *Nat Rev Microbiol* 2(11):886
123. Blazier AS, Papin JA (2012) Integration of expression data in genome-scale metabolic network reconstructions. *Front Physiol* 3:299
124. Orth JD, Palsson BØ (2010) Systematizing the generation of missing metabolic knowledge. *Biotechnol Bioeng* 107(3):403–412
125. O'Brien EJ, Monk JM, Palsson BO (2015) Using genome-scale models to predict biological capabilities. *Cell* 161(5):971–987
126. Bordbar A, Monk JM, King ZA, Palsson BO (2014) Constraint-based models predict metabolic and associated cellular functions. *Nat Rev Genet* 15(2):107–120
127. Patil KR, Nielsen J (2005) Uncovering transcriptional regulation of metabolism by using metabolic network topology. *Proc Natl Acad Sci U S A* 102(8):2685–2689
128. AbuOun M, Suthers PF, Jones GI, Carter BR, Saunders MP, Maranas CD et al (2009) Genome scale reconstruction of a salmonella metabolic model comparison of similarity and differences with a commensal *Escherichia coli* strain. *J Biol Chem* 284(43):29480–29488
129. Pharkya P, Burgard AP, Maranas CD (2004) OptStrain: a computational framework for redesign of microbial production systems. *Genome Res* 14(11):2367–2376
130. Pharkya P, Maranas CD (2006) An optimization framework for identifying reaction activation/inhibition or elimination candidates for overproduction in microbial systems. *Metab Eng* 8(1):1–13

131. Förster J, Famili I, Fu P, Palsson BØ, Nielsen J (2003) Genome-scale reconstruction of the *Saccharomyces cerevisiae* metabolic network. *Genome Res* 13(2):244–253
132. Orth JD, Thiele I, Palsson BØ (2010) What is flux balance analysis? *Nat Biotechnol* 28(3):245
133. Becker SA, Feist AM, Mo ML, Hannum G, Palsson BØ, Herrgard MJ (2007) Quantitative prediction of cellular metabolism with constraint-based models: the COBRA Toolbox. *Nat Protoc* 2(3):727
134. Ebrahim A, Lerman JA, Palsson BO, Hyduke DR (2013) COBRApy: constraints-based reconstruction and analysis for python. *BMC Syst Biol* 7(1):74
135. Steffensen JL, Dufault-Thompson K, Zhang Y (2016) PSAMM: a portable system for the analysis of metabolic models. *PLoS Comput Biol* 12(2):e1004732
136. Rocha I, Maia P, Evangelista P, Vilaça P, Soares S, Pinto JP et al (2010) OptFlux: an open-source software platform for in silico metabolic engineering. *BMC Syst Biol* 4(1):45
137. Grafahrend-Belau E, Klukas C, Junker BH, Schreiber F (2009) FBA-SimVis: interactive visualization of constraint-based metabolic models. *Bioinformatics* 25(20):2755–2757
138. König M, Holzhütter H-G (2010) Fluxviz—Cytoscape plug-in for visualization of flux distributions in networks. *Genome Inform* 24:96–103
139. Marmiesse L, Peyraud R, Cottret L (2015) FlexFlux: combining metabolic flux and regulatory network analyses. *BMC Syst Biol* 9(1):93
140. Kirchmair J, Williamson MJ, Afzal AM, Tyzack JD, Choy AP, Howlett A et al (2013) FAMEtabolizer (FAME): a rapid and accurate predictor of sites of metabolism in multiple species by endogenous enzymes. *J Chem Inf Model* 53(11):2896–2907
141. Rowe E, Palsson BO, King ZA (2018) Escher-FBA: a web application for interactive flux balance analysis. *BMC Syst Biol* 12(1):84
142. Beerenwinkel N, Schwarz RF, Gerstung M, Markowetz F (2015) Cancer evolution: mathematical models and computational inference. *Syst Biol* 64(1):e1-25
143. Banerjee S, Sarkar RR (2008) Delay-induced model for tumor-immune interaction and control of malignant tumor growth. *Biosystems* 91(1):268–288
144. d’Onofrio A, Gatti F, Cerrai P, Freschi L (2010) Delay-induced oscillatory dynamics of tumour-immune system interaction. *Math Comput Model* 51(5–6):572–591
145. dePillis L, Caldwell T, Sarapata E, Williams H (2013) Mathematical modeling of regulatory T cell effects on renal cell carcinoma treatment. *Discrete Cont Dyn-B* 18(4):915–943
146. d’Onofrio A (2008) Metamodeling tumor-immune system interaction, tumor evasion and immunotherapy. *Math Comput Model* 47(5–6):614–637
147. Leder K, Pitter K, Laplant Q, Hambardzumyan D, Ross BD, Chan TA et al (2014) Mathematical modeling of PDGF-driven glioblastoma reveals optimized radiation dosing schedules. *Cell* 156(3):603–616
148. Robertson-Tessi M, El-Kareh A, Goriely A (2012) A mathematical model of tumor-immune interactions. *J Theor Biol* 294:56–73
149. Powathil GG, Adamson DJ, Chaplain MA (2013) Towards predicting the response of a solid tumour to chemotherapy and radiotherapy treatments: clinical insights from a computational model. *PLoS Comput Biol* 9(7):e1003120
150. Kirschner D, Panetta JC (1998) Modeling immunotherapy of the tumor-immune interaction. *JMB* 37(3):235–252
151. de Pillis LG, Radunskaya AE, Wiseman CL (2005) A validated mathematical model of cell-mediated immune response to tumor growth. *Cancer Res* 65(17):7950
152. Ganguli P, Sarkar RR (2018) Exploring immuno-regulatory mechanisms in the tumor microenvironment: model and design of protocols for cancer remission. *PLoS One* 13(9):e0203030
153. Chew YH, Shia YL, Lee CT, Majid FAA, Chua LS, Sarmidi MR et al (2009) Modeling of glucose regulation and insulin-signaling pathways. *Mol Cell Endocrinol* 303(1–2):13–24
154. Reed MC, Thomas RL, Pavisic J, James SJ, Ulrich CM, Nijhout HF et al (2008) A mathematical model of glutathione metabolism. *J Theor Biol* 5(1):8
155. Lawley SD, Yun J, Gamble MV, Hall MN, Reed MC, Nijhout HF et al (2014) Mathematical modeling of the effects of glutathione on arsenic methylation. *J Theor Biol* 11(1):20

-
156. Nijhout HF, Best JA, Reed MC (2015) Using mathematical models to understand metabolism, genes, and disease. *BMC Biol* 13(1):79
 157. Kauffman KJ, Prakash P, Edwards JS (2003) Advances in flux balance analysis. *J Coib* 14(5):491–496